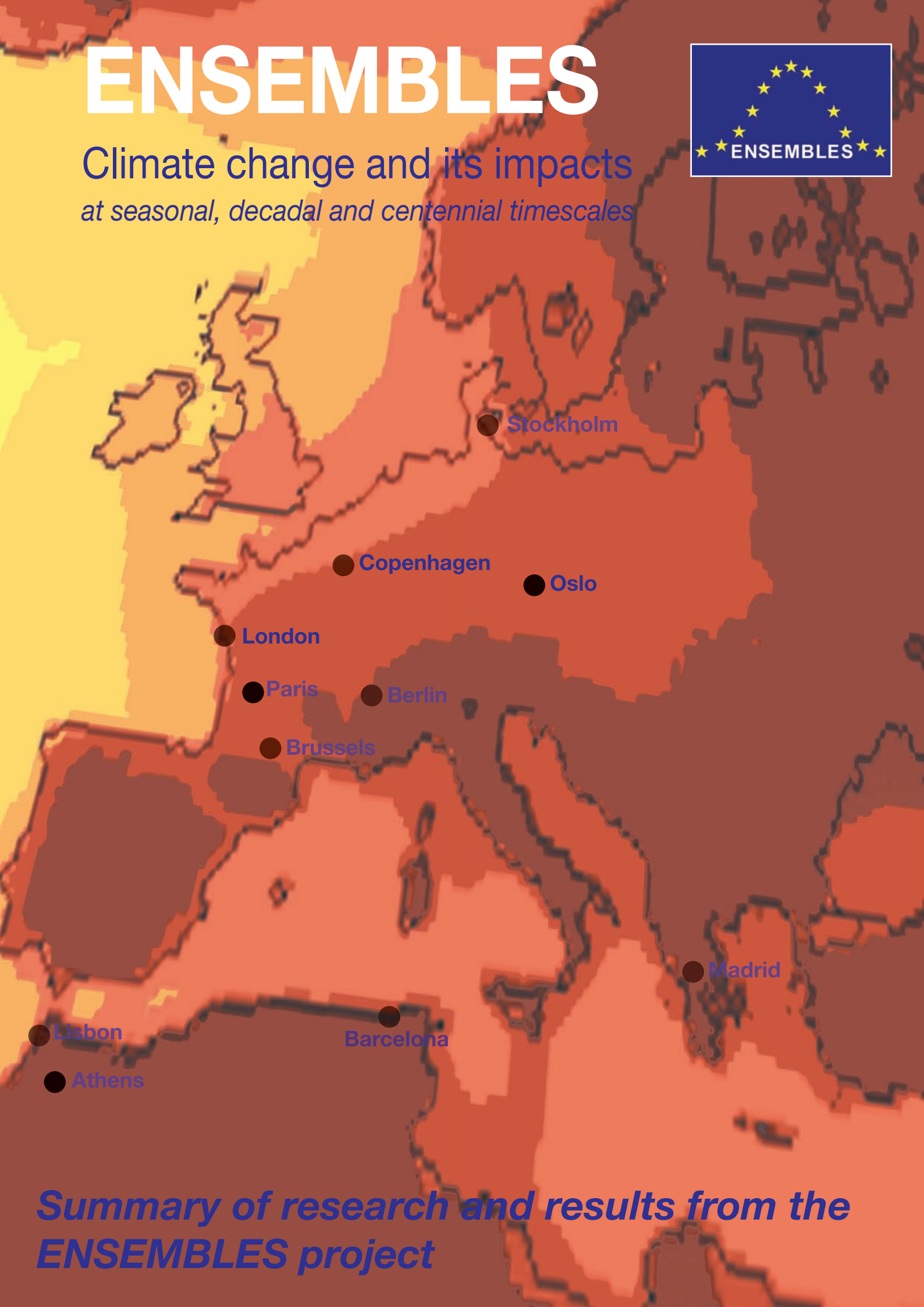


ENSEMBLES



Climate change and its impacts
at seasonal, decadal and centennial timescales



*Summary of research and results from the
ENSEMBLES project*

Project and Contact Information

ENSEMBLES is an integrated research project running from 2004 to 2009 and is coordinated by the Met Office Hadley Centre. It has produced probabilistic projections of climate for Europe to help inform researchers, decision makers, businesses and the public with climate information from the latest climate modelling and analysis tools.

ENSEMBLES is funded by the European Commission under the 6th Framework Programme Priority: Global Change and Ecosystems.

This report summarises the science research and results of the ENSEMBLES project. For more information please see www.ensembles-eu.org or contact us using the details below:

ENSEMBLES project office

Met Office Hadley Centre, FitzRoy Road, Exeter EX1 3PB, UK

Paul van der Linden
ENSEMBLES Director
+44 1392 884163

paul.vanderlinden@metoffice.gov.uk

Prof John F.B. Mitchell
ENSEMBLES Coordinator
+44 1392 884604

john.f.mitchell@metoffice.gov.uk

Pip Gilbert
ENSEMBLES Secretary
+44 1392 884603

ensemblesfp6@metoffice.gov.uk

European Commission

Climate Change and Environmental Risks Unit, General Directorate for Research, European Commission, CDMA 3/006, B-1049 Brussels, Belgium

Dr Philippe Tulkens

EC Project Officer

philippe.tulkens@ec.europa.eu

Editors

Paul van der Linden and John F.B. Mitchell of the Met Office Hadley Centre, FitzRoy Road, Exeter EX1 3PB, UK

Citation

Sections can be referenced by their title and authors, if citing the whole report please use:

van der Linden P., and J.F.B. Mitchell (eds.) 2009: ENSEMBLES: Climate Change and its Impacts: Summary of research and results from the ENSEMBLES project. Met Office Hadley Centre, FitzRoy Road, Exeter EX1 3PB, UK. 160pp.

Copyright and use of material and data

© 2009 ENSEMBLES

Material in this publication may be reproduced on condition that due credit is given, such as: "*The ENSEMBLES work reproduced here is from the EU-funded FP6 Integrated Project ENSEMBLES (Contract number 505539).*"

See the ENSEMBLES data policy for information about data use and its acknowledgement:

http://ensembles-eu.metoffice.com/docs/Ensembles_Data_Policy_261108.pdf

Contract number: GOCE-CT-2003-505539

Website: <http://www.ensembles-eu.org>

Project duration: 1 September 2004 to 31 December 2009

Full list of project partners is given on page 158

Credit and caption for cover picture:

The front cover of this report shows some European cities relocated to places where the current climate is the same as what the projected climate will be for that city in 2071–2100. The methodology involves running a multi-model ensemble of Regional Climate Models out to 2100 against a 1961–1990 climatological baseline and comparing the city climates between the two periods. The comparison takes into account temperature, precipitation and seasonal characteristics for each city. The cities are superimposed on a background of temperature anomaly for the 2071–2100 period of the ENSEMBLES multi-model average for Europe, Figure A1.13. Thanks go to the following people:

Stephane Hallegatte, Météo-France and CIRED, for developing the technique and producing the map,

Else van den Besselaar, KNMI, for providing the observed climate data,

Ole Christensen, DMI, for providing the temperature and rainfall projections for the end of the century.

Contents

1. Introduction to the ENSEMBLES project	3
2. Executive Summary	7
3. Development of ensemble prediction systems [Research Theme 1]	19
4. Production of seasonal to decadal hindcasts and climate change scenarios [Research Theme 2A]	35
5. Formulation of very-high-resolution regional climate model ensembles for Europe [Research Theme 3]	47
6. Downscaling methods, data and tools for input to impacts assessments [Research Theme 2B]	59
7. Understanding the processes governing climate variability and change, climate predictability and the probability of extreme events [Research Theme 4]	79
8. Evaluation of the ENSEMBLES Prediction System [Research Theme 5]	95
9. Assessments of impacts of climate change [Research Theme 6]	107
10. Scenarios and policy implications [Research Theme 7]	131

Appendices

1: Examples of ENSEMBLES climate descriptions and projections	139
2: ENSEMBLES datasets	155
3: ENSEMBLES partners and affiliates	158
4: Contributors	160

1 Introduction to the ENSEMBLES project

P. van der Linden (Met Office)

1.1 This report

This report is a summary of the research and results of the ENSEMBLES climate change project. The content preferentially includes findings that have not already been published and/or that are of greatest interest to the users of climate research. This approach is justified by the large size and long duration of the project, meaning that not every piece of work or every result can be reported in detail here. In this report, the balance between describing the methods and techniques developed during the course of the project and the results arising from the research is about equal.

This Introduction covers the aims, background and construction of the ENSEMBLES climate change project. It also acts as a 'road map' to the main body of the report, which is structured along the lines of the project's Research Themes, although the order in which they are presented follows the research development rather than the numerical order of the themes. The Executive Summary is written around the projects aims, which are described in Section 1.4.

A selection indicative of the type of spatial results for projected climate in Europe produced by the project can be found in Appendix 1; while a description of the datasets produced by the project is given in Appendix 2.

1.2 Climate change

Knowledge of climate and weather has always been important to society, as it is upon them that human activity and life on Earth depend. In the last century it was recognised that human activity is changing the composition of the atmosphere, and subsequently that the climate (both global and regional) is also changing. The global average temperature today is 0.7°C higher than in pre-industrial times and is the main measure of this change. Within the last decade the causal link between increasing concentrations of anthropogenic greenhouse gases in the atmosphere and the observed changes in temperature has been scientifically established.

Impacts from climate change on natural and human systems are now being observed both globally and regionally. Scenarios of possible futures indicate that these impacts may increase, especially if anthropogenic emissions of greenhouse gases continue to rise unchecked. Some of these future impacts are already unavoidable, due to the lifetime of emissions and the nature of the climate system. Thus there is interest in how to develop strategies for mitigating and adapting to climate

change. The European Union has the stated goal of keeping global anthropogenic warming at a level that is under 2°C above pre-industrial levels, while the UNFCCC aims to prevent dangerous anthropogenic interference with the climate system.

1.3 Climate research

Modelling climate and projected changes in climate is a resource-intensive research activity, usually involving supercomputers and a multidisciplinary approach. These disciplines range from socio-economics (scenarios), to computing, physics, chemistry (climate models) and Earth and life sciences (impact models), as well as statistics and probability (analysis). To set up and run a climate 'experiment', using a computer model to simulate 100 years of climate evolution on a global scale, can take weeks or months. Analysis of the results takes even longer.

In the European Union there are a finite number of institutes that conduct research into climate and climate change. Some institutes specialise in global modelling, while others focus on a regional approach. There are many more research centres which look at the potential impacts of climate change over a range of systems and sectors. There are also climate centres which study the observed historical climate, whose data are used to validate climate models. Finally there are the centres whose socio-economic research is used as the background for climate projections. The ENSEMBLES project represents the first occasion on which this spectrum of researchers was brought together to work with a single purpose.

1.4 Aims of the ENSEMBLES project

Against this background, the European Commission initiated the ENSEMBLES project to help inform researchers, decision makers, businesses and the public by providing them with climate information obtained through the use of the latest climate modelling and analysis tools. The value, and core, of the ENSEMBLES project is in running multiple climate models ('ensembles'); a method known to improve the accuracy and reliability of forecasts. The project output is a range of future predictions assessed to decide which of the outcomes are more likely (probable) than the others. This probabilistic information will assist policy makers, at all levels, in determining future strategies to address climate change.

The project's principal objective is to allow the uncertainty in climate projections to be measured, so that a clearer picture

of future climate can be formed. The specific aims leading from this are:

- to develop an ensemble prediction system for climate change based on the principal state-of-the-art, high-resolution, global and regional Earth system models developed in Europe, validated against quality-controlled, high-resolution gridded datasets for Europe, to produce for the first time an objective probabilistic estimate of uncertainty in future climate at the seasonal to decadal and longer time-scales;
- to quantify and reduce the uncertainty in the representation of physical, chemical, biological and human-related feedbacks in the Earth system (including water-resource, land-use and air-quality issues, and carbon cycle feedbacks);
- to maximise the exploitation of the results by linking the outputs of the ensemble prediction system to a range of applications, including agriculture, health, food security, energy, water resources, insurance and weather risk management.

1.5 Background to the ENSEMBLES project

The ENSEMBLES project is funded by the European Commission (EC), and runs from September 2004 to December 2009. ENSEMBLES is a flagship project of the EC's 6th Framework Programme (EC FP), an integrated project under the thematic sub-priority 'Global Change and Ecosystems' (contract number GOCE-CT-2003-505539).

The project is led by the UK Met Office and comprises a consortium of 66 institutes from 20 countries, mostly from Europe, although partners from across the world are also involved. In addition, 30 other organisations, mostly from Europe, have joined the project as affiliates. Affiliate status allows these organisations to engage with and contribute to the research programme, but without financial commitment. Lists of project partners and affiliated institutes are given in Appendix 3.

The EC has contributed €15 million of funding to the ENSEMBLES project. In addition, some partners were self-funding (receiving no money from the EC), either paying for their contribution themselves or being funded by governments outside the EC. A further 35 partners matched the funding that they received from the EC. The total amount spent on the project came to €22.8 million, which funded over 250 person-years of work.

The size, duration and budget of ENSEMBLES make it one of the biggest climate change research projects ever conducted. Although there are larger international programmes, these either assess or coordinate research but do not conduct any research themselves.

The ENSEMBLES work programme included coordination with bodies such as CMIP, NARCCAP, WCRP (CLIVAR, GEWEX), CFMIP, C4MIP, BALTEX and the IPCC. Collaboration with other EC FP projects was also an integral part of ENSEMBLES and, as this was built into the project at the design stage, it is described in the next section.

The work carried out in the ENSEMBLES project builds upon earlier EC projects such as PRUDENCE, STARDEX, MICE, and DEMETER, which can be considered as precursors of some of the components of the ENSEMBLES project.

1.6 Project construction

The ENSEMBLES project was designed by the partners in the consortium, who then went on to conduct the work. The construction of the project plan was top-down and driven by the science. This method was used to achieve a fully integrated research programme across the full range of disciplines and topics included in the project.

The project is constructed around ten Research Themes (RTs) which are summarised by name and purpose as follows:

- RT0 Project integration, management and promotion
- RT1 Development of the ENSEMBLES Prediction System (EPS)
- RT2A Production of seasonal to decadal hindcasts and climate change scenarios: 'Model Engine Part 1'
- RT3 Formulation of very-high-resolution Regional Climate Model ensembles for Europe
- RT2B Production of regional scenarios for impact assessment: 'Model Engine Part 2'
- RT4 Understanding the processes governing climate variability and change, climate predictability, and the probability of extreme events
- RT5 Independent comprehensive evaluation of the ENSEMBLES simulation–prediction system against observations/analyses
- RT6 Assessments of impacts of climate change
- RT7 Scenarios and policy implications
- RT8 Outreach, education and training

Figure 1.1 shows the relationships and linkages between the ten Research Themes. The project structure worked well, even when the project methods were changed part way through the programme. For example, RT1 developed an alternative to the Ensemble Prediction System, known as the 'perturbed physics ensemble'; a method whose results were incorporated into the existing flow of information through the RTs to add an extra set of results.

At the core of the ENSEMBLES integrated project was the development of the first global, high-resolution, ensemble-based, modelling system for the prediction of climate change and its impacts. The Earth system models were combined into a multi-model ensemble system, with common output, for seasonal, decadal and centennial time-scales. This work was carried out in RT1.

The purpose of RT2A was to produce sets of climate simulations with several models and to provide the multi-model results needed for the other Research Themes. The results from RT2A were used for validation (RT5), studies of feedbacks in the Earth system (RT4), as well as boundary conditions and forcing fields for regional model simulations (RT3/RT2B). The simulations covered time-scales ranging from seasons to decades and centuries. Two streams of Global

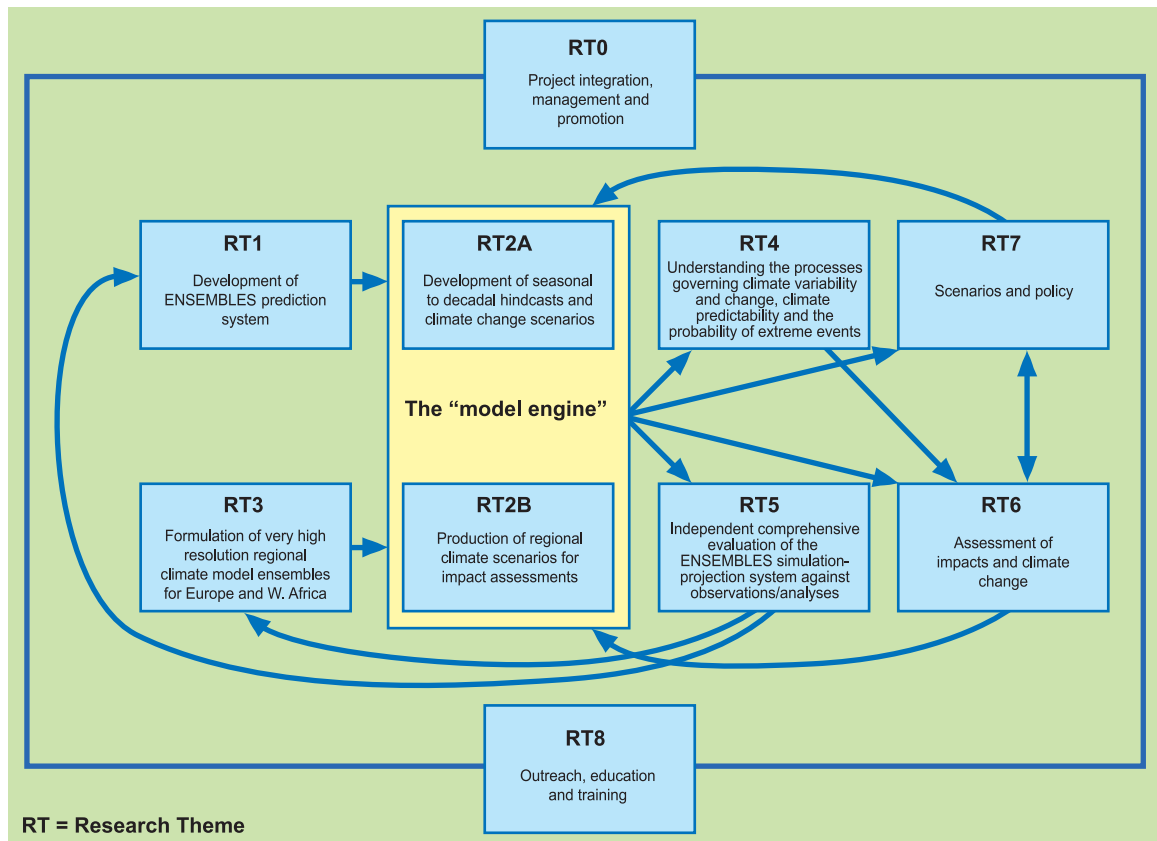


Figure 1.1: The relationships and linkages between the Research Themes in ENSEMBLES.

Climate Model (GCM) runs were produced: the first for the ensemble prediction system and the second using later models incorporating new features such as carbon cycle feedbacks. The development and running of the E1 stabilisation scenario was led by RT2A.

RT3 had responsibility for providing improved climate model tools developed in regional models, at spatial scales of 25 and 50 km on a Europe-wide scale. Analogous to RT1, and using boundary conditions from RT2A, RT3 produced a multi-model ensemble-based system for regional climate prediction at multi-decadal time-scales to be applied in RT2B.

Along with RT2A, RT2B provided the 'model engine' of the ENSEMBLES project. RT2B constructed probabilistic high-resolution regional climate scenarios using dynamical and statistical downscaling methods in order to add value to the model output from RT1 and RT2A and to exploit the full potential of the Regional Climate Models (RCMs) developed in RT3. The outputs are in formats appropriate for input to the RT6 assessments of the impacts of climate change as well as for more general end-users and stakeholders.

The purpose of RT4 was to advance understanding of the basic science issues at the heart of the ENSEMBLES project. Using the outputs of RT2A and RT2B, the work focused on the key processes that govern climate variability and change, and the predictability of climate on time-scales of seasons, decades and beyond. Particular attention was given to understanding feedbacks in the climate system that may lead to climate 'surprises' and extreme events. The improved scientific

knowledge gained in RT4 was fed back into further development of the models used in RT1 and RT3.

The development of the ensemble-based prediction system and the production of regional climate scenarios were subjected to rigorous evaluation. RT5 carried out a comprehensive and independent evaluation of the performance of the ENSEMBLES Prediction System developed in RT1 and RT3 and run through the model engines of RT2A and RT2B, against analyses/observations. This included the production of the high-resolution observational datasets necessary to perform this task.

RT6 used the output from the ensemble-based prediction system developed in RT1 and RT3, and run through the model engines of RT2A and RT2B, to carry out impacts assessments. Its primary objective was to simulate the potential impacts of future climate change during the 21st century on natural systems and human activities at different scales under alternative scenarios of future climate. This included, for example, the integration of process models of impacts on the natural and managed global environment into Earth system models, the results from which were fed back into the model development in RT1. However, the main output from RT6 was aimed at the public and stakeholder community, and was disseminated through RT8.

The main aim of RT7 was to take the first step towards the integration of the human dimension into Earth system models. This was done by including the feedback of climate change, as produced by the ensemble-based prediction system developed in RT1 and RT3 and run through the model engines of RT2A

and RT2B, on the emissions scenarios driving the climate models. RT7 also provided RT1 with ensembles of emissions and land-use scenarios with and without mitigation policies, as well as scenarios of adaptive capacity.

The two remaining themes, RT0 and RT8, were concerned with the management and outreach of the project, respectively. The former included, in addition to management, ensuring that the project was integrated both internally and with external research bodies and programmes. RT0 was also responsible for promoting the project, so that the research and results were publicised and made available to the scientific research community, policy makers, users of climate information, and other stakeholders. RT8 ran a programme of education and training using ENSEMBLES research, implemented through seminars, workshops, summer schools, publications, and courses for PhD students.

The Research Themes were divided into Work Packages (WPs), indicating the level at which the work targets and responsibilities lie. Some partners were involved in more than one WP, which also helped to keep the flow of information and results moving. The linkages also allowed for feedbacks and checks between WPs to ensure the quality and timeliness of the research. This structure was supported by an annual

project plenary, frequent inter- and intra-RT meetings, plus joint meetings between WPs and other organisations for specific goals. There were also many electronic communication tools employed to facilitate knowledge transfer within the project (e.g., web pages, Wiki pages, newsletters, email groups, telephone conferences). The management and outreach aspects of the project were RTs in their own right, which ensured that they had suitable weight and integration in the project.

Strong research links between ENSEMBLES and other EC FP6 projects were also built into the plan. The following projects had shared goals: AMMA, CECILIA, CIRCE, CLAVIER and DYNAMITE, which were helped in many cases by certain institutes being involved in both projects. Of these, the AMMA project had the best-defined interactions with ENSEMBLES, with a common region for modelling and observational verification. See Section 5.3.3 for more information.

Lastly, the institutional composition of the ENSEMBLES project includes organisations from the private sector and international arenas. Gender equality was actively promoted at all levels within the project, and there was a successful mentoring scheme for young scientists.

2 Executive Summary

P. van der Linden (Met Office), J.F.B. Mitchell (Met Office)

The climate projections generated in ENSEMBLES describe the world and Europe experiencing tangible, measurable climate change. As the century progresses the projected climate moves increasingly farther away from its current state, so that by 2100 the climate of Europe will be very different from today. Even under a mitigation scenario, the climate of Europe during the next few decades is still calculated to depart significantly from that of the present.

ENSEMBLES results show how the impacts resulting from these climate changes, including changes in climate mean, variability and extremes, affect all the systems and sectors studied. Adverse impacts increase in magnitude through time often exceeding critical system thresholds. Examples include impacts on health, water resources, agriculture, energy supply and demand, and fire and pest risks to forests.

Many of these new results reinforce the conclusions of earlier studies of climate change projections and impacts. What is new about the ENSEMBLES results is that they describe in far greater detail how the climate is expected to change under standard scenarios of future emissions. They also include, for the first time, multi-model climate projections for a greenhouse gas mitigation scenario leading to emissions and temperature stabilisation in line with European policy aims. The results have been used as a basis for a set of new tools and datasets for informing potential users about present and future climate, and have been linked to new techniques for assessing the impacts of climate change in Europe in terms of risk.

This ‘added value’ in the ENSEMBLES results comes from using improved models, developing new and better techniques to analyse and disseminate projections of climate change and their uncertainties, and demonstrating how this information can be applied in policy-relevant impact assessments. The improvements for example, add skill to seasonal forecasting while multi-decadal models, for the first time, have produced probabilistic climate change projections for Europe.

2.1 Introduction

The ENSEMBLES project is large and covers almost the entire spectrum of climate change sciences. It brought together researchers from different, but connected disciplines to work on a common goal – to construct an end-to-end climate prediction system for the first time. This summary is written around the aims of the project (Section 1.4) as these are the threads that run through the project providing the common purpose. In brief, the project’s aims are to:

- develop an ensemble climate prediction system on seasonal to centennial time-scales
- quantify and reduce the uncertainty in modelling climate
- link the outputs of the ensemble prediction system to a range of applications.

The summary ends with a description of the key features of the E1 mitigation scenario presented in a case study. Brackets at the end of the paragraphs refer to the sections of this report in which more detail can be found.

2.2 The ensemble prediction system

2.2.1 Introduction

The ENSEMBLES project fulfilled its first aim of ‘developing an ensemble prediction system for climate change’, and in addition investigated other complementary modelling techniques for producing more reliable climate projections. Significant advances were made in model performance, and this is seen

especially at the seasonal to decadal timescale with verification against observations and analyses. To couple the climate projections to impact models – the third aim of the project – a cascading system of links was constructed, see Figure 2.1. These links went from global climate models (GCM), to regional climate models (RCM) and statistical downscaling methods and then to climate change impact models. The exploratory nature of the work meant that techniques were often tried in parallel, for example GCM data were often statistically downscaled directly, and climate change impact models used probabilistic, regional climate or statistically downscaled data as their input. Significant steps towards constructing an end-to-end system were made and future research directions to fulfil this long-term aim were identified. [Section 3]

2.2.2 The GCM component of the ensemble prediction system

Seasonal to decadal timescales

Ensemble climate forecasts on seasonal to decadal time-scales can be verified against observations or analyses, making them a powerful tool for quantifying and reducing modelling uncertainty. Three different approaches to address model uncertainty in coupled ocean-atmosphere circulation models were developed and assessed: The multi-model ensemble builds on the experience of previous projects where it has been shown to be a successful method to improve the skill of seasonal forecasts from individual models. The perturbed parameter approach reflects uncertainty in physical model parameters, while the newly developed stochastic physics methodology represents uncertainty due to inherent errors in model parameterisations and to the unavoidably finite resolution of the models. [Section 3]

Results from a large set of seasonal hindcasts show that significant progress has been made in reducing systematic model errors compared with previous generations of models. A detailed comparison of the probabilistic forecast performance of the different approaches to model uncertainty has been carried out. The multi-model ensemble has a high standard of forecast skill, see Figure 2.2a. It was found that the two new schemes to represent model uncertainty also provide forecasts competitive with the multi-model approach, for climate forecasts on seasonal time-scales. The relative performance for the three methodologies for forecasting temperature and precipitation over a set of standard land regions around the globe up to seven months ahead is summarised in Figures 2.2b and c. The complementary benefits of the different approaches provide future potential to address model uncertainty more comprehensively in climate predictions across seasonal to decadal and longer time-scales. [Section 3]

The potential of decadal ensemble forecasting using fully initialised coupled GCMs was explored. ENSEMBLES provided a first and pioneering opportunity to assess the benefits of combining projections from different models in a coordinated experiment, following initial studies carried out with individual climate models. The existence of simulation biases in the models used for the decadal hindcasts necessitates the use of strategies to account for these systematic errors when comparing forecasts against observations. These results illustrate that initialised decadal forecasts have the potential to provide im-

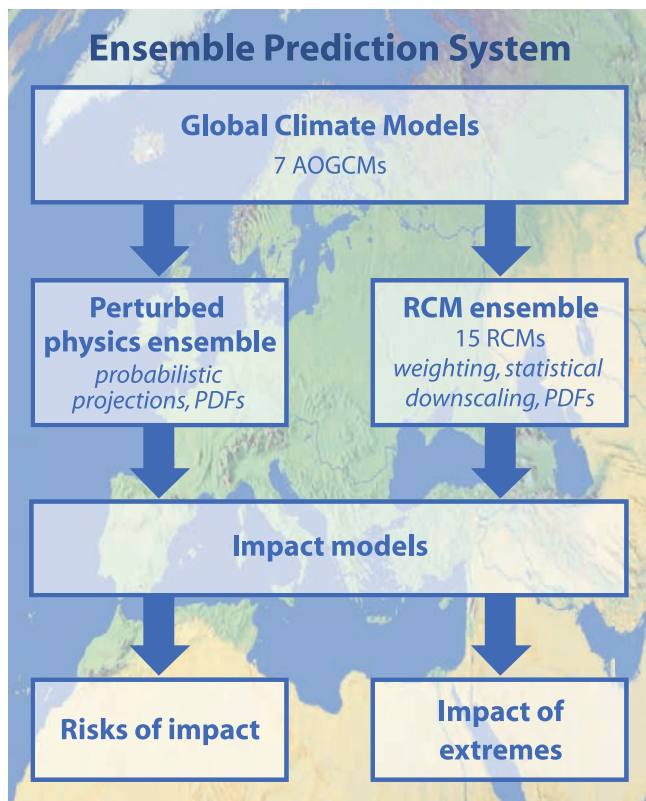


Figure 2.1: Linkages between the modelling components of the ensemble prediction system (EPS), as developed for use at multi-decadal to centennial timescales, and the methods of impact assessment using outputs from the system.

proved information compared with traditional climate change projections, but the optimal strategy for building improved decadal prediction systems in the presence of model biases remains an open question for future work. [Sections 3 and 4]

Multi-decadal to centennial timescales

The ENSEMBLES project built ensemble prediction systems based on global climate models to generate projections of future climate on seasonal, decadal and multi-decadal time-scales. The scope included the assembly and testing of new global climate models, development and implementation of methods to represent the effects of uncertainties in the modelling of key physical, biological and chemical processes (‘modelling uncertainties’), and the use of observations to initialise and constrain the projections. There was also an improvement in the quantification of uncertainties arising from model imperfections, as well as from internal climate variability. [Sections 3,4,7 and 8]

Seven European climate modelling centres ran GCMs under historic and four different scenario forcings (B1, A1B, A2, 1%CO₂). All centres ran several realisations to create multi-simulation ensembles of most scenarios, which together contributed to the multi-model ensemble developed in the project. The GCM output was then used for boundary conditions to drive Regional Climate Models for a European domain. [Sections 3,4,5 and 6]

In addition, probability distributions (PDFs) of future temperature and precipitation changes for regions of Europe were produced. These were derived from a large ensemble of GCM projections designed to sample uncertainties in key Earth system processes through a perturbed parameter approach, combined with results

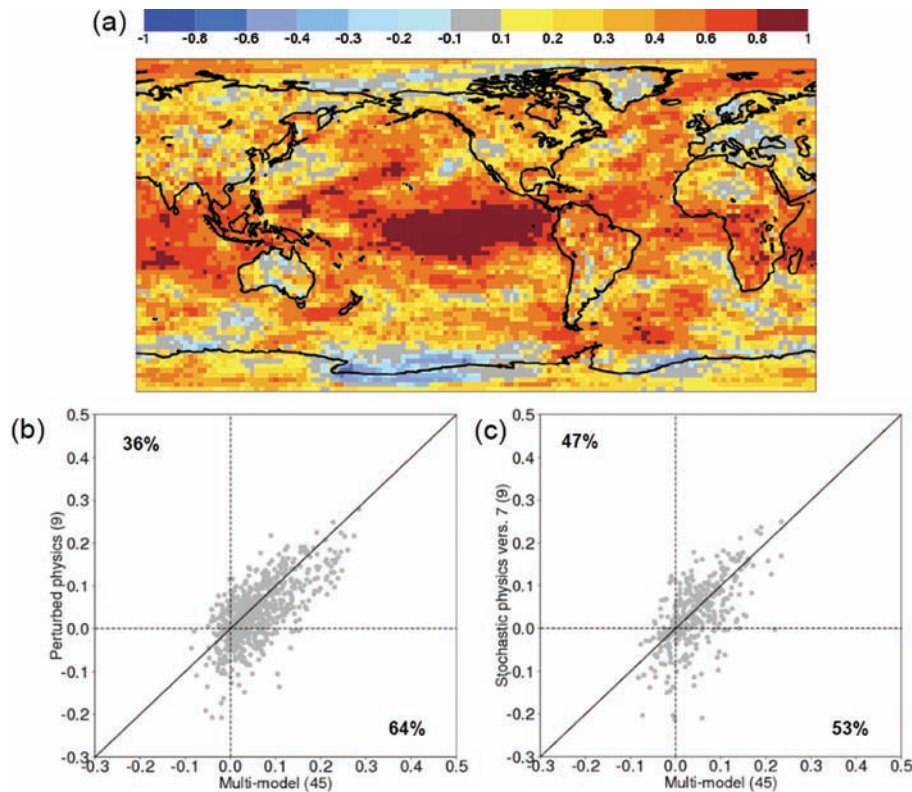


Figure 2.2: (a) Probabilistic forecast skill score (relative operating characteristics, ROC) of the multi-model ensemble for DJF warm temperature seasonal anomalies from re-forecasts started every year on the 1st of November over the period 1960-2005. (b) Scatter plot of Brier Skill scores for the perturbed parameter and multi-model forecasting systems for the standard land-regions for temperature and precipitation. See Figure 3.3 for more details. The inset numbers indicate the percentage of wins for each system. (c) As in (b), but for the stochastic physics re-forecasts versus the multi-model ensemble. [Section 3]

from alternative climate models and a multivariate set of observational constraints measuring the relative performance of alternative model variants in simulating a variety of aspects of present day climate and historical climate change. This comprehensive approach supports the specification of a spread of plausible outcomes for future change consistent with current climate modelling technology and understanding of the driving feedback processes, and expressed through PDFs of multidecadal mean changes in surface temperature and precipitation (Figure 2.3). The PDFs have also been sampled to produce a large set of individual estimates of seasonal or annual mean temperature and precipitation changes for individual GCM grid boxes across Europe, and also for a set of aggregated regions. The left column in Figure 2.3 shows the 10, 50 and 90% percentiles for projected summer temperature change in Europe for the 20 year period 2080-2099 relative to 1961-1990, where the median case shows up to 7°C warming in Southern Europe and 5°C in Northern Europe. [Section 3]

2.2.3 The RCM component of the ensemble prediction system

Fifteen institutes ran their RCMs at 25km spatial resolution, with boundary conditions from five different GCMs, all using the A1B emissions scenario, creating a GCM/RCM matrix filled with 25 runs. It was never planned to fill the matrix entirely with the full combination of possible GCM/RCM runs, however ways of inflating it artificially through pattern scaling could be investigated. The driving GCMs of the matrix were not weighted although this possibility was explored. A weighting scheme for the RCMs based on different performance criteria was con-

structed so that variations in model performance can be accounted for when calculating best-estimate projections and associated uncertainties from ensemble mean and spread diagnostics. This refines the interpretation of the model runs in an ensemble result. The weighting system developed is pioneering in nature and represents a first step in developing this type of methodology. Uncertainty investigation meant that RCM performance was measured by means of hindcast runs driven by ERA-40 reanalysis data and compared against the new ENSEMBLES gridded climate observation data set. These analyses also contributed to investigating RCM uncertainties, together with an examination of the relation between the role of RCMs and the GCM driving boundary conditions for the regional projection results. Projected changes in climate from the RCM simulations can, for comparative purposes, also be displayed alongside the GCM probabilistic output. The RCM projections provide plausible scenarios of detailed regional change, consistent with larger-scale changes lying within the wider uncertainty envelope defined by the GCM projections, as demonstrated in Section 2.3.3. [Sections 5,6,7 and 8]

2.2.4 Adding conditional probabilistic information to ensemble regional output

Regional output was provided from both GCM and RCM ensembles, and from statistical downscaling mostly to point locations. These different outputs were subject to further processing including the construction of conditional probability density functions (PDFs). A number of different methods of producing conditional PDFs were developed. One of these is

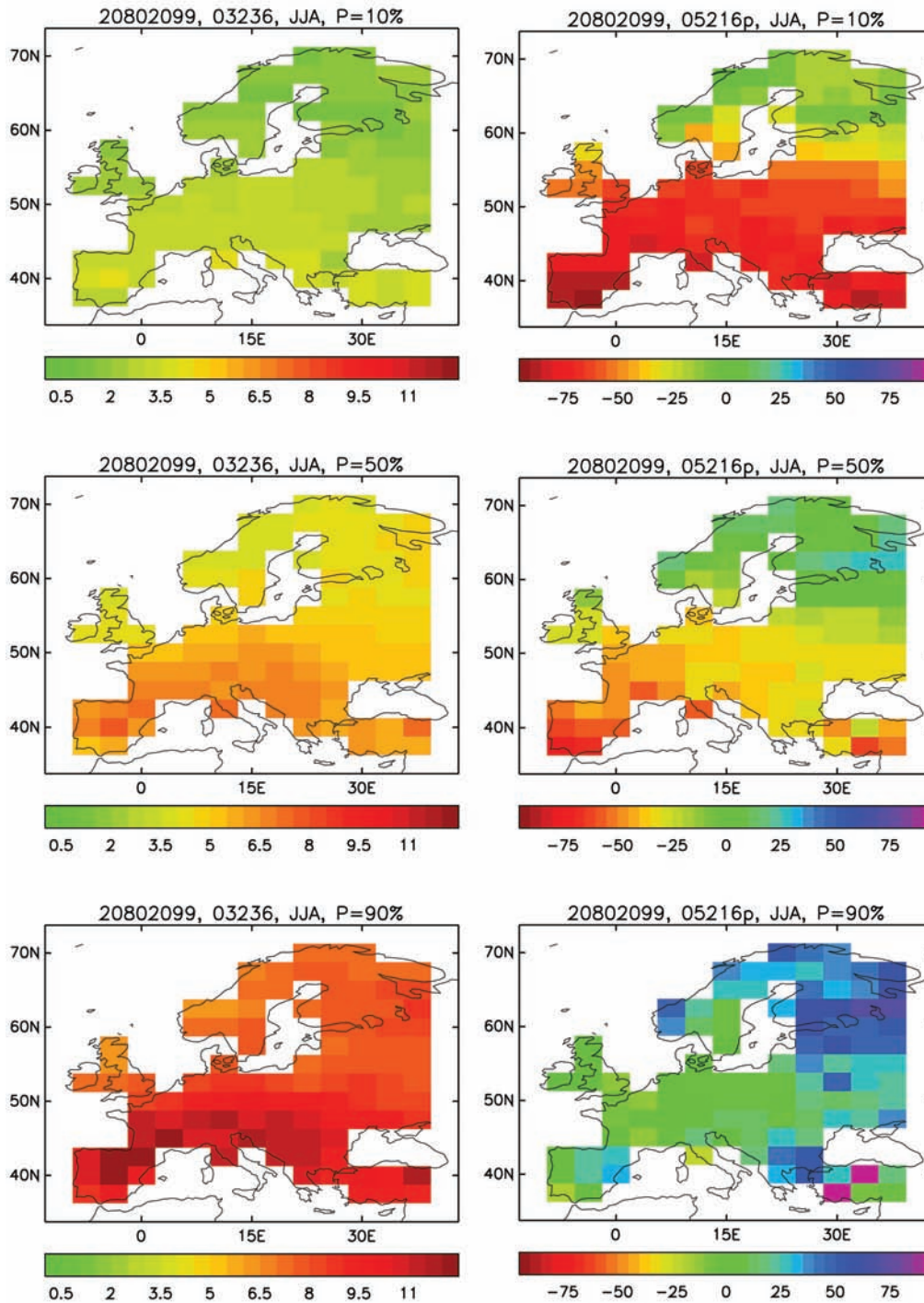


Figure 2.3: ENSEMBLES probabilistic projections for Europe under the A1B emission scenario produced by the perturbed physics parameter approach. The maps show the 10%, 50% (median) and 90% percentiles of (left column) European surface temperature change and (right column) European percentage precipitation change, for the summer season for the period 2080-2099 relative to the 1961-1990 baseline period. [Figure 3.11]

modified Reliability Ensemble Averaging (REA), which was applied to GCM output for European regions, another method used the ENSEMBLES RCM ensemble and weighting scheme. A weighting scheme for use with statistical downscaling was also developed. These techniques can produce either single or joint conditional PDFs, the latter usually as changes in temperature and precipitation - see Figure 2.4 for an example from a European city. The conditional PDFs produced are subjective in the sense that they do not encompass the entire range of upstream or downscaling uncertainties. [Section 6]

In general results indicate that statistical downscaling, generally (but not always) brings additional skill. Other statistical down-

scaling work includes downscaling for seasonal indices of temperature (see Figure 2.5 for an example from Northern Italy) and precipitation extremes, and developing a conditional stochastic weather generator to construct projections for daily precipitation, including extremes. A web-based tool for statistical downscaling was developed and is available at: <http://grupos.unican.es/ai/meteo/ensembles/>. [Section 6]

Climate change impact models took their inputs from any of these stages in the EPS (i.e., from GCM, RCM and statistically downscaled output – either in probabilistic formats or as time series data). A description of the climate impact models and their input from the EPS is given in Section 9.2.

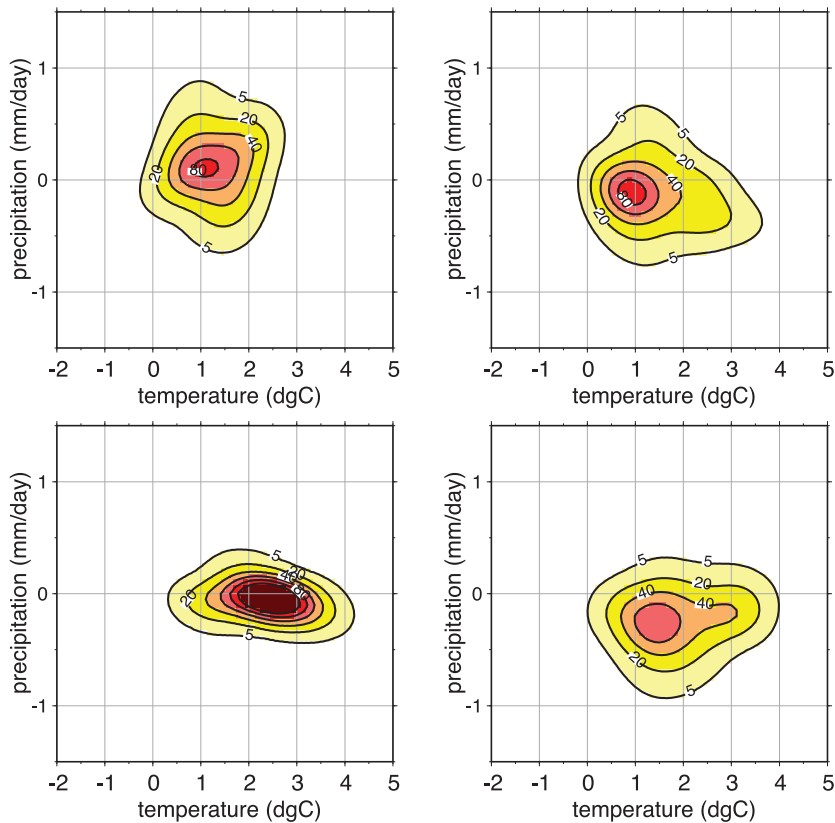


Figure 2.4: Bivariate conditional PDFs for temperature and precipitation response (2021-2050 minus 1961-1990, A1B scenario) in Madrid for DJF (top left), MAM (top right), JJA (bottom left), SON (bottom right). Contours indicating densities are plotted for 5, 20, 40, 60, 80 and 100 of 10-2°C-1mm-1day. Calculated from scaled and weighted RCM data using the gaussian kernel method. [Figure 6.14]

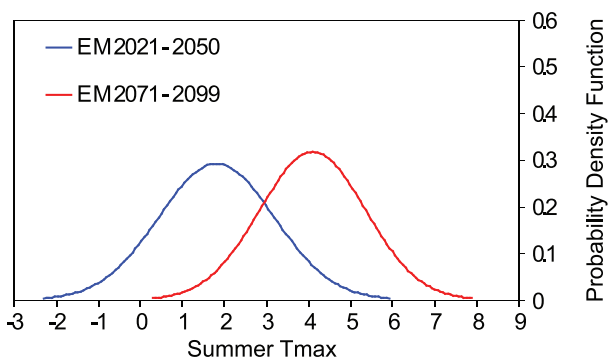


Figure 2.5: Statistical downscaling applied to six GCM runs to construct conditional PDFs of changes in temperature extremes over Northern Italy. Large increases in maximum temperature extremes are indicated. [Section 6]

2.3 Quantifying and reducing uncertainty in climate models

2.3.1 Introduction

The quantification and reduction of uncertainty was a major theme throughout the project, and was represented in every Research Theme. The following is a list of the major sources of uncertainty which were identified so as to better quantify and reduce them:

- (1) Uncertainties associated with different classes of model error, including structural modelling uncertainty (inherent in basic model construction), uncertainty in model parameters controlling the best-estimate outputs of parameterisations of sub-grid-scale processes (for example cloud physics), and stochastic uncertainties arising from coupling between unresolved sub-grid-scale variability and the resolved grid-scale flow;
- (2) Initial model state (for example, from ocean temperature);
- (3) Dynamical downscaling between GCMs and RCMs (for example; in the driving GCM boundary conditions, the choice of GCM/RCM pair) and from RCMs and impact models;

- (4) Statistical downscaling, typically from GCM to point-scale (for example, choice of predictors, stationarity);
- (5) Uncertainties associated with climate observations (the way climate observations are constructed and applied) including distribution pattern of atmospheric constituents (for example the concentration distribution of ozone, or distribution of aerosols);
- (6) Translating greenhouse gas emissions to atmospheric concentrations;
- (7) Translating atmospheric concentrations of greenhouse gases to radiative forcing;
- (8) The socio-economics upon which emissions scenarios are based (for example technological development, land use, carbon taxation);
- (9) Feedbacks from changes in the climate system on socio-economic systems and then on anthropogenic emissions back into the climate system.

In the rest of this section reference is made to the uncertainty sources described above given as a number in brackets e.g. (3) refers to the uncertainty arising from dynamical downscaling.

2.3.2 Quantifying and reducing uncertainty

The construction of the EPS was in itself the biggest step toward reducing uncertainty in model projections as it allowed, up to a point, the quantification and linking of the components of uncertainty within the EPS production chain. However, along with the new areas of research it also had to describe new areas of uncertainty, for example, matrix downscaling from GCMs to RCMs and weighting the output was the first time that such an uncertainty space has been constructed, sampled and described. [Sections 3,4,5 and 6]

Global Climate Models

Describing the uncertainty space intrinsic to within GCMs, given in point 1 in the list above, at seasonal to decadal time-scales was addressed by the three complementary modelling approaches: multi-model ensemble; perturbed physics, and stochastic physics. The multi-model approach samples structural variations among a range of models by combining climate models that have been developed quasi-independently in an ad hoc way without systematically exploring individual sources of uncertainty. The perturbed parameter approach aims at sampling uncertainties in the relationship between grid-box model variables and the effects of parameterised sub-grid-scale processes in a single model, when these are represented by deterministic bulk formulae (as is currently typical in climate models). The stochastic physics approach addresses an additional aspect of parameterisation uncertainty (also in a single model), associated with uncertainties arising from how alternative (but unresolved) organisations of sub-grid-scale variability within a model grid box might couple with and influence the resolved scales of the model. The last two methods can be seen as complementary ways to account for model error and begin to outperform the more traditional approach of the multi-model. For example, the probabilistic skill of predicting anomalous rainfall over Europe 2–4 months in advance was found to be improved by each of these two new schemes over the multi-model ensemble. [Section 3]

At the centennial time-scale the multi-model ensemble and perturbed parameter approaches were used. The former provides input for the dynamic downscaling, while the latter (in combination with multi-model projections and observational constraints) produced probabilistic projections based on a more comprehensive approach to the specification of the spread of plausible future changes than previously attempted. The probabilistic projections (see Figure 2.3) can show a range of up to 10°C for the 10 to 90 percentiles and this comes from many different sources of uncertainty, with no one source being dominant. The multi-model ensemble results confirm the large spread in the projected changes of the water cycle, the climate variability and the extreme events. It has been shown that atmospheric processes such as cloud physics, convection or coupling with the surface are at the heart of these major uncertainties. Strategies have been developed and proposed to improve and better assess the models. (1) In discussing uncertainty it is also useful to look at model agreement and in projections of regional precipitation change with patterns of summer Mediterranean drying and winter Northern European wetting the agreement between models indicates a robust result, with little uncertainty. [Sections 3,4 and 7]

The uncertainty associated with the carbon cycle feedbacks was investigated with dynamic global vegetation models that include land use, plant processes, vegetation types, fire and runoff (1). In general, the response including carbon cycle feedbacks was found to be as large as that associated with climate change, even when a perturbed physics model was used to scope the range of uncertainty of changes in the climate component of the model. [Section 9]

Initialisation strategies for seasonal to decadal forecasts were investigated and improved, through developments of ocean data assimilation systems by participating modelling groups, the production and use of an updated dataset of observed temperature and salinity values to produce ocean re-analyses for the initialisation and verification of hindcasts, and the implementation of approaches to account for uncertainties in the initial conditions, especially those associated with sea surface temperatures and surface exchanges (2). Improvements in characterising the factors governing non-linear feedbacks and extreme events in climate models have helped reduce uncertainty in seasonal to decadal predictions (1). This included results from an experiment with six atmospheric GCMs forced by a common sea surface temperature which examined model uncertainty instead of scenario or initial condition uncertainty. A better understanding of the global hydrological cycle has been developed, especially about its origins in the tropics and its relation to large interannual fluctuations in tropical precipitation. [Sections 3 and 7]

The global projections out to 2100 all used a common forcing from the A1B scenario (6,7,8), with its underlying socio-economics and emissions distributions. The global simulations were run over a historic time period (1860-2000) again, with all using an identical forcing for this historic period. This allowed the definition of a statistical distribution of the climate response and an assessment of the probability of climate change including the uncertainty as models were weighted to climate observations (5). The use of a common set of forcings in the project meant that the uncertainty associated with emissions and concentrations was not introduced (7). Work was also done on the impacts of climate change affecting socio-economic behaviour, which would then affect emissions. This magnitude of this feedback was calculated to be smaller than the climate change signal (9). [Sections 4 and 10]

Regional Climate Models and downscaling

The process of dynamical downscaling was investigated using RCMs nested in GCMs. For this experiment a number of participating GCMs and RCMs were set up in a matrix (Table 5.1), although it was never planned to run all possible combinations. Twenty-five RCM runs were subsequently made. The RCMs were run on 25 km resolution, a scale that was largely untested at the start of the project. Prior knowledge about model performance and bias was unknown, thus running them first at 50km resolution, as in earlier projects, and then across a spread of several GCMs helped identify these sources of uncertainty (1). A driving GCM run with different climate sensitivities was also used and these showed very different climate responses with the same RCM. Uncertainty related to simulated natural variability (2) was of importance in the first part of the century but for the end part other sources become more important. [Sections 5 and 6]

A common forcing from the A1B scenario was used for the RCM modelling. Uncertainty in future emissions was not explicitly studied, in part because the basic length of the regional projections was to extend only to 2050, a time horizon for which the emission scenario uncertainty is less relevant (7,8). [Sections 5 and 6]

A weighting methodology for RCMs was developed as no single model is best at representing all climate processes and variables. Performance-based model weights applied to a combination of simulations from different models should have enhanced projection skill (1,3). The weighting methodology is relevant to both robustness and uncertainty in model performance, but cannot be used to find the best – or worst – overall model. Impacts assessment using RCM output should ideally use at least two or more RCMs forced by two or more GCMs and consider their output in the context of the full matrix output to ensure that they do not under sample uncertainty (3). [Section 5]

A weighting scheme was also developed for use with statistical downscaling and the uncertainties inherent to this approach were explored (4). For example, the assumption of predictor-predictand stationarity was investigated using RCM output as pseudo-observations. [Section 6]

An evaluation of robustness in the regional RCM projections shows the mid-century signal for the multi-model mean temperature is one of warming in all of Europe and is much larger than the inter-model standard deviation. For precipitation the signal shows agreement in direction, projecting an increase in precipitation in the north and a decrease in the south, with all models agreeing in the north and twelve out of sixteen models agreeing in the south. [Section 6]

Next was an examination of the sources of uncertainty within the GCM/RCM pairing experiment, of which three were identified: choice of GCM, choice of RCM, and interannual variability. All available simulations within the GCM-RCM matrix were examined, and the results showed regional and seasonal variation over whether the GCMs or the RCMs had the dominant influence. The choice of GCM/RCM pair showed that large-scale seasonal mean changes were dependent on the GCM, while many of the differences between RCMs could be explained more by simulated natural variability, for the first half of the century. Beyond that it was found that with a higher climate change signal, the more important the GCM spread and the lower the signal, the more important the RCM. However, it is clear from this and other work that uncertainties in both global and regional processes contribute significantly to the total spread of plausible responses at both decadal and centennial lead times. Therefore comprehensive sampling of both is needed in order to provide a set of projections suitable to inform risk assessments for adaptation (1,3). The extent and design of the ENSEMBLES GCM/RCM matrix gives users the opportunity to test the effects of different sampling strategies, with future testing of unfilled pairs being a goal for future work. [Sections 5 and 6]

Downstream use of projections

The next step in representing the sources of uncertainty, was to construct probabilistic projections for downstream users, based on both dynamical and statistical downscaling approaches. Many

statistical downscaling methods were used, including regression, neural networks, canonical correlation analysis and analogue methods. Conditional PDFs, which encompass the sampled uncertainty, were constructed from the statistically and dynamically downscaled output (and from GCM output) for temperature and/or precipitation for a number of areas and points. These are, however, qualitative constructions (3,4). Alternative approaches were used for constructing PDFs including the gaussian kernel method and REA. [Section 6]

Modellers of climate change impacts were provided with this suite of probabilistic climate information to use as a starting point for their work. (Work was also done using large ensembles of time-series data.) They applied the climate data for their area of impact research, including the uncertainty information cascaded down to them, ranging from risk surfaces or PDFs to more subjective outputs (3,4). To this could be added the uncertainty inherent in their projections, and to try to address this a technique for ensemble modelling of crop yields at seasonal timescales was developed. [Section 9]

Evaluation of climate models against observations

The ENSEMBLES gridded observations data set was used along with other datasets to verify and calibrate both global and regional models, and also to assess the uncertainties in model response to anthropogenic forcing. The gridded dataset was constructed so that descriptions of current climate (e.g., extremes) could be compared with model output. The gridded observations were constructed on the same grid as the RCMs so that interpolation was not needed. (5) [Section 8]

The E1 scenario

E1 is a mitigation scenario in which atmospheric concentrations of greenhouse gases are stabilised at 450ppm CO₂-equivalent. It was developed using a reverse-engineered approach with a starting point of atmospheric concentrations/forcings, instead of the usual emissions. This meant that the forward calculation from emissions to concentrations was avoided and therefore too the uncertainty arising from it (6,7). This technique is being developed for the IPCC Fifth Assessment Report (AR5) as the Representative Concentration Pathways. The scenario was run on the latest European GCMs, some including carbon cycle feedbacks (1), which again helps quantify the uncertainty in the global climate projections. An overview of the E1 mitigation scenario is given in Section 2.6. [Sections 4 and 7]

2.3.3 ENSEMBLES model projections in the context of wider uncertainties

As a final approach for locating the model simulation results from ENSEMBLES in the context of wider uncertainties, Figure 2.6 has been constructed to compare projections of mean annual temperature and precipitation change over northern Europe (48N-75N 10W-40E) and the Mediterranean Basin (30N-48N 10W-40E) for the mid-term (2030-2050) and long-term (2080-2100) future. Using these plots, it is possible to compare the GCM-based (Section 2.2.2) and RCM-based (Section 2.2.3) projections generated specifically

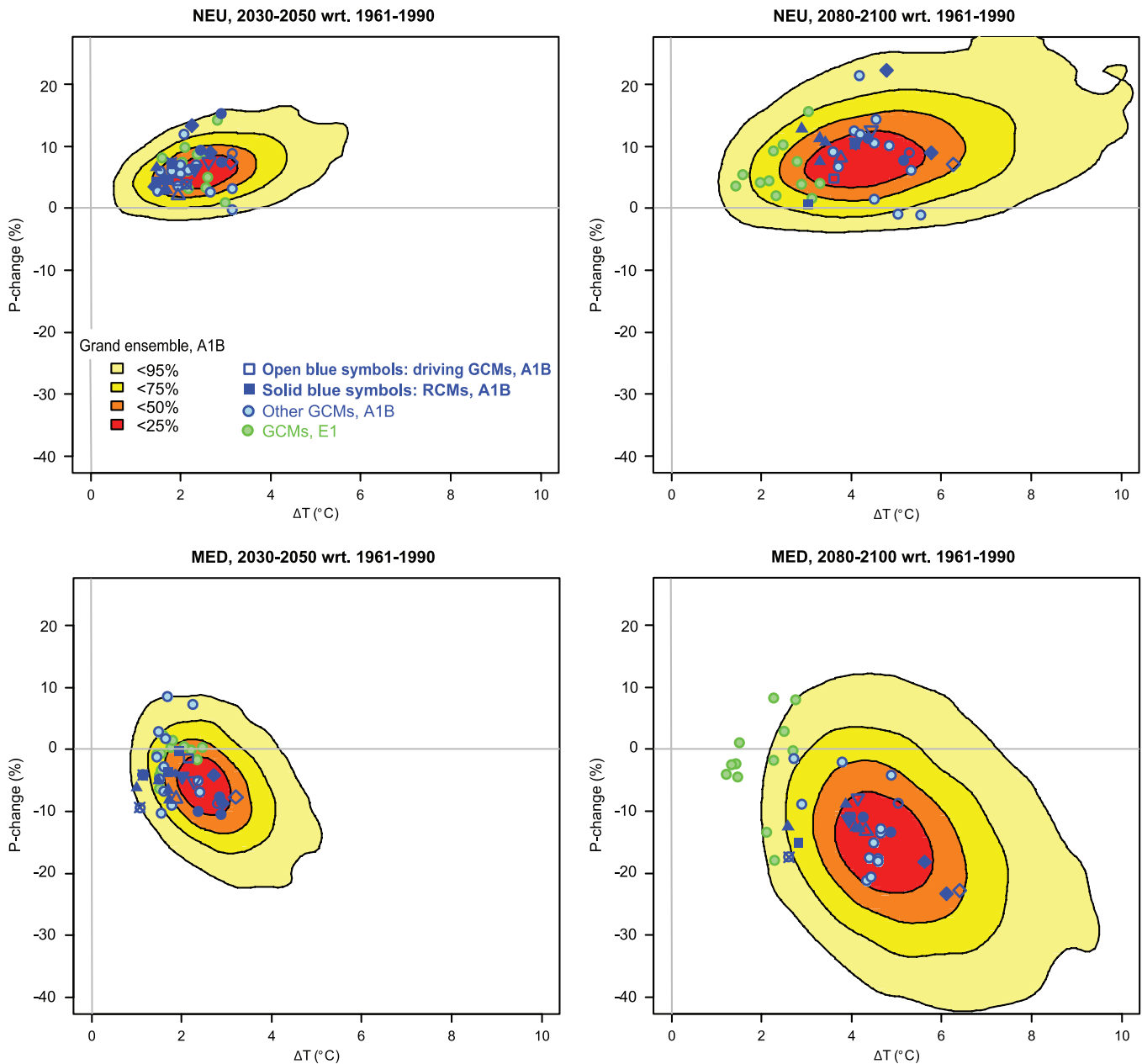


Figure 2.6: Annual changes in temperature (T) and precipitation (P) in northern Europe (NEU, top panels) and the Mediterranean Basin (MED, bottom panels) by the periods 2030-2050 (left) and 2080-2100 (right) relative to 1961-1990. Coloured areas depict probabilistic projection percentiles based on a statistical emulation of various sources of uncertainty from models and observations for the A1B scenario. Dark blue symbols are projections from RCM (closed) and their driving GCM (open) simulations for the A1B scenario (atmospheric concentration of ~ 700 ppm CO_2 only in 2100); light blue symbols are other GCM simulations for A1B; green symbols are GCM simulations for the E1 mitigation scenario (stabilisation at 450ppm CO_2 -equivalent after 2100).

in ENSEMBLES for the A1B (medium, non-mitigation) emissions scenario with probabilistic projections based on multiple sources of information for the same emissions scenario (cf. Figure 2.3). In addition, Figure 2.6 also depicts the ENSEMBLES GCM-based projections of climate change under the E1 mitigation scenario (cf. Section 2.6). Comparison of the green (E1) with the blue (A1B) symbols indicates clearly how the effects of mitigation become apparent only towards the end of the 21st century. The depiction of uncertainty in future projections using bivariate PDFs such as those shown as coloured zones in Figure 2.6 has been carried forward in the next section into impact assessments, where probabilities of future climate outcomes have been translated into estimates of impact risk. [Sections 3,4,5,6 and 9]

2.4 Exploiting the results of the ensemble prediction system

The ensemble climate projections and the probabilistic projections were used to assess climate change impacts across a number of systems and sectors. These assessments were for Europe apart from one study on seasonal malaria forecasts in West Africa. Around twenty large studies into projected impacts were conducted in the insurance, energy, health, water, agriculture, and natural environment sectors, plus many smaller ones. These studies cover a range of time-scales (from seasonal to centennial), different countries and European regions and diverse aspects within each sector. For example the agricultural impacts work includes potato, wheat and kiwi fruit yields, nitrogen leaching and Bluetongue disease. The work also covers

projections to changes in mean climate, climate variability and climate extremes. [Section 9]

Ten examples are given in Section 9 of this report illustrating the type of work done in the project. Now that probabilistic projections are available to climate change impacts modellers new techniques are being employed to exploit them, such as the impact response surface. This is where changes in climate variables (e.g., temperature and precipitation) are given and system thresholds (e.g., in river flow, or crop yield) plotted on the climate variables to make a response surface. The probabilistic climate projection is then superimposed and it can be seen whether, and by how much, an impact threshold is exceeded. See Figure 2.7 for an illustrative example of this method for operational water levels in Lake Mälaren in Sweden projected for 2031-2050. [Section 9]

Time-series climate projections direct from the weighted output of the RCM ensemble were also used directly in impact models, which in addition to providing information about mean future climate also provides characterisations of future extremes and variability. [Section 9]

Ensemble model projections at seasonal timescales were linked to application models through seasonal hindcasts to develop forecast models for seasonal events such as crop yield and electricity demand. A seasonal application model was linked to downscaled RCM projections to include climate dynamics which was shown to add skill. This was malaria modelling in West Africa using the Liverpool malaria Model. [Section 9]

The impact assessment work shows that climate change affects all the systems and sectors studied. The impacts were noticeable in the near future (2020s to 2050s) becoming more severe by the

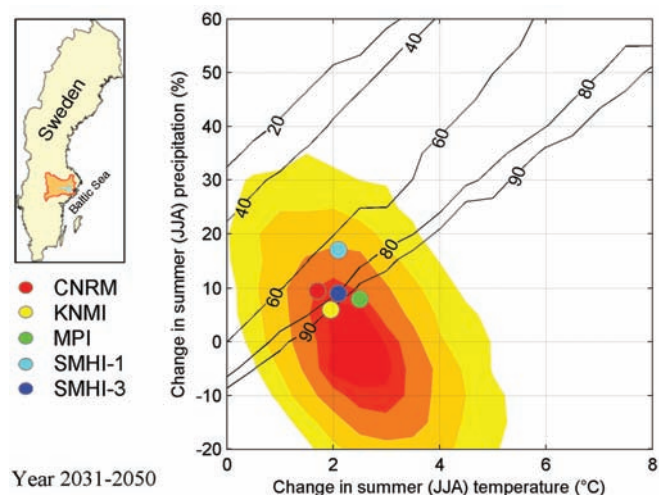


Figure 2.7: Impact response surface for Lake Mälaren in Sweden. Diagonal black lines are the likelihood in percent of summer water level below the target operating threshold for a consecutive period of 50 days for the change in summer temperature/precipitation. Climate projections are depicted as probability density plots for the period 2031-2050 based on probabilistic projections from the perturbed physics ensemble. The coloured area encloses approximately 90% of all projected outcomes. Also shown are projections from five RCM simulations (coloured dots). The impact response surface was created from some 300 simulations using the HBV (Hydrologiska Byråns Vattenbalansavdelning) hydrological model. [Figure 9.20 part]

end of the century. In many sectors, especially in the last thirty years of the century, critical impact thresholds are exceeded implying that damages will be incurred by climate change. [Section 9]

The ENSEMBLES datasets are just beginning to be exploited by the wider climate impacts community and there is still a great scope for their further exploitation of them in climate impacts research. All datasets are publicly available for the international research community to explore their wider scientific potential. The statistical downscaling web portal will also continue to provide additional new datasets for researchers derived from existing regional projections.

2.5 Extreme weather events in climate projections

The impacts from extreme weather events (heavy rainfall, drought, severe cold, heatwaves and storms) under current climate are damaging and costly in both economic and human terms. Extreme events are, by definition rare, but because of their high impact any changes in frequency and/or intensity under future projected climate are of interest. Knowledge of future changes in extreme events is also needed for constructing adaptation strategies.

Model simulations of extremes in RCMs have been compared with the ENSEMBLES gridded observations dataset using descriptive indices of extremes as well as Generalized Extreme Value distribution for estimating return levels of extreme events. Many observed characteristics of extremes are well simulated by the models, although differences in model performance exist. In addition to model biases, the consistency of projected changes in extremes has been evaluated. For the precipitation extremes in the Rhine basin, some interesting common tendencies have been identified. For the summer season, there is hardly any change in the daily amounts for short return periods (every 2 years), but there is a considerable increase in the daily amounts for longer return periods (every 50 years). For the winter season, the reverse occurs with larger changes in the 5-day amounts for short return periods and almost no change in the 5-day amounts for the longer return periods, despite the clear increase in mean winter precipitation in most RCM simulations. [Section 8]

Three RCMs were evaluated in the Mediterranean region against the gridded observations, then extreme climate indices were calculated and their trends analysed over the period of 1961-2050. All models show extremes of high temperatures increasing in the future and an increase in summer low temperatures. For the precipitation indices, the models present similar current and future spatial patterns of the extreme precipitation amounts in winter, with the most extreme precipitation observed along the western borders of all peninsulas of the northern Mediterranean. [Section 7]

Projections in extreme events from transient climate simulations were configured for studies at regional and smaller scales. Case studies, some of which involved statistical downscaling, include extreme precipitation events in Romania and Spain, drought in Germany, river flow extremes in the Rhine and Danube, and temperature extremes over the Mediterranean. [Section 6]

The effects of projected changes in extreme events in different systems were investigated: property damage due to windstorms in western and central Europe, effects of temperature changes on energy demand in the Mediterranean, forest fire risk in Fennoscandia, forest damage due to low temperature and pests in Sweden and effects on crop yields, water resources and health in Poland. All show significant, mostly negative, impacts. [Section 9]

2.6 Case study: The E1 mitigation scenario

The E1 mitigation scenario, developed in ENSEMBLES, is the first mitigation scenario run using an ensemble of GCMs. It stabilises atmospheric CO₂ at 450 ppm equivalent by 2140, while emissions peak at about 12 gigatonnes of carbon in 2010. The E1 scenario was constructed using the IPCC AR5 methodology of starting at concentrations/forcings and running forward calculations for climate projections, and reverse calculations for emissions and socio-economics. The scenario is based on the IPCC A1B scenario and uses the PBL Integrated Assessment Model (IAM) to simulate energy, land use and carbon cycle. The A1B scenario was also run through IAM and the GCMs to use for comparison. Ten European GCMs were run using E1, five of which include carbon cycle feedbacks. Results show that the global mean temperature rise for most models, relative to pre-industrial, stays below 2°C (Figure 2.8). The spatial pattern for the global mean temperature anomaly (Figure 2.9) shows regional variations, while bi-variate projections for temperature and precipitation for Northern and Mediterranean European regions at mid and end century from a number of GCMs are shown in Figure 2.4. [Sections 4 and 10]

The five GCMs which model carbon cycles feedbacks were used to back-calculate anthropogenic CO₂ emissions from land/ocean/atmosphere carbon fluxes. They show that implied emissions of CO₂ to the atmosphere at the end of the century fall close to zero, or in the case of one model (HadCM3C) below zero, implying carbon sequestration exceeding emissions (Figure 2.10). [Sections 4 and 10]

Further work on the E1 scenario could include an end to end analysis, including risks, on possible future impacts. It would also be informative to examine the pathway leading to future potential impacts to have a better picture of their onset, incidence and magnitude. Lastly, knowing the damages avoided by stabilising greenhouse gases at E1 scenario levels would be informative for policy makers. It could also provide information about levels of adaptation to avoid impacts under mitigation.

2.7 Conclusions

The ENSEMBLES project was built upon foundations laid by many earlier EC funded projects (DEMETER, PRUDENCE, STARDEX, MICE). The new techniques pioneered in ENSEMBLES include a coordinated approach to seasonal to decadal prediction, probabilistic climate change projections, development and assessment of alternative approaches to the sampling of modelling uncertainties, use of a GCM/RCM matrix to provide an ensemble of plausible realisations of detailed regional climate change, improved estimates of regional climate impacts and their uncertainties through a systematic and integrated approach to climate and impacts modelling. These innovations have opened up new areas of research that have the potential to provide insight to many of today’s unanswered questions about future climate change.

Through these developments, ENSEMBLES represents a significant step towards a seamless climate prediction system that addresses climate changes and their impacts at the fullest possible range of temporal and spatial scales. The seamless paradigm has allowed the transfer of knowledge and innovative methodologies across different components of the ENSEMBLES prediction system. The legacy of ENSEMBLES will in part reflect the extent to which its key contribution to the current state of the art is translated into future progress in the understanding and prediction of climate variability and change.

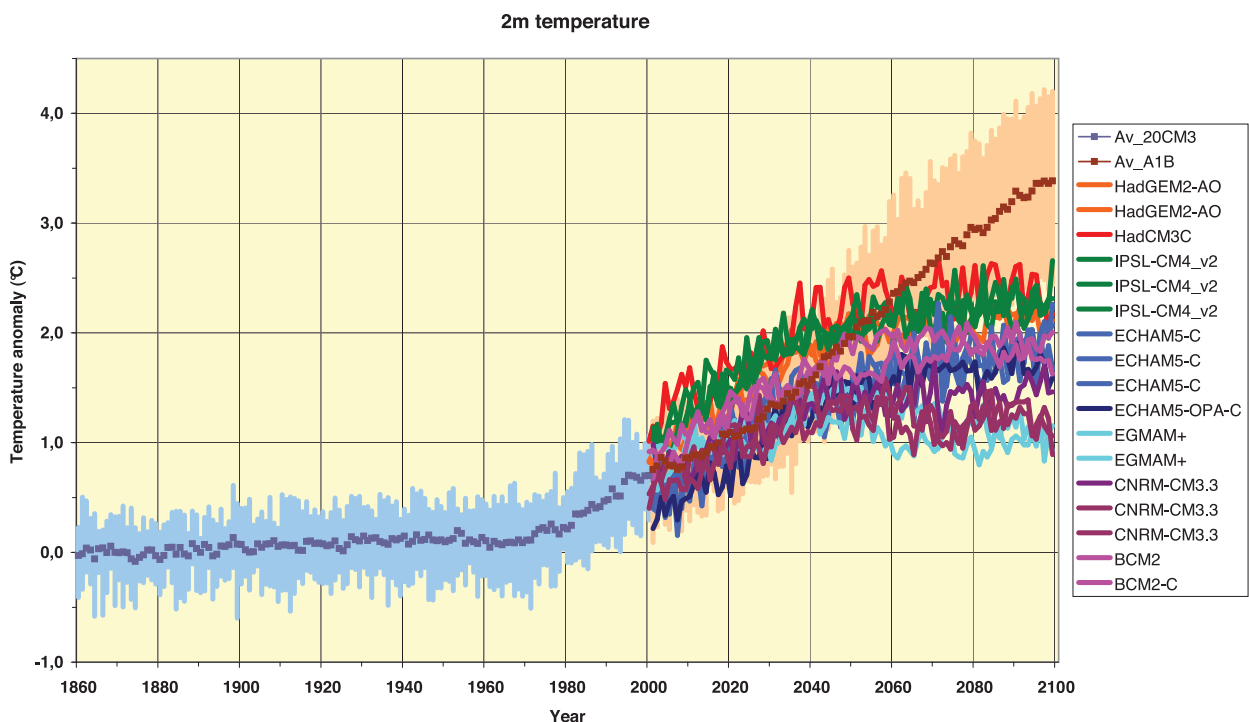


Figure 2.8: Global average temperature projected by a range of models for E1 in the 21st century. [Figure 4.6]

ENSEMBLE2 MEAN ANN ΔT E1 (2070/99) – 20C3M (1961/90)

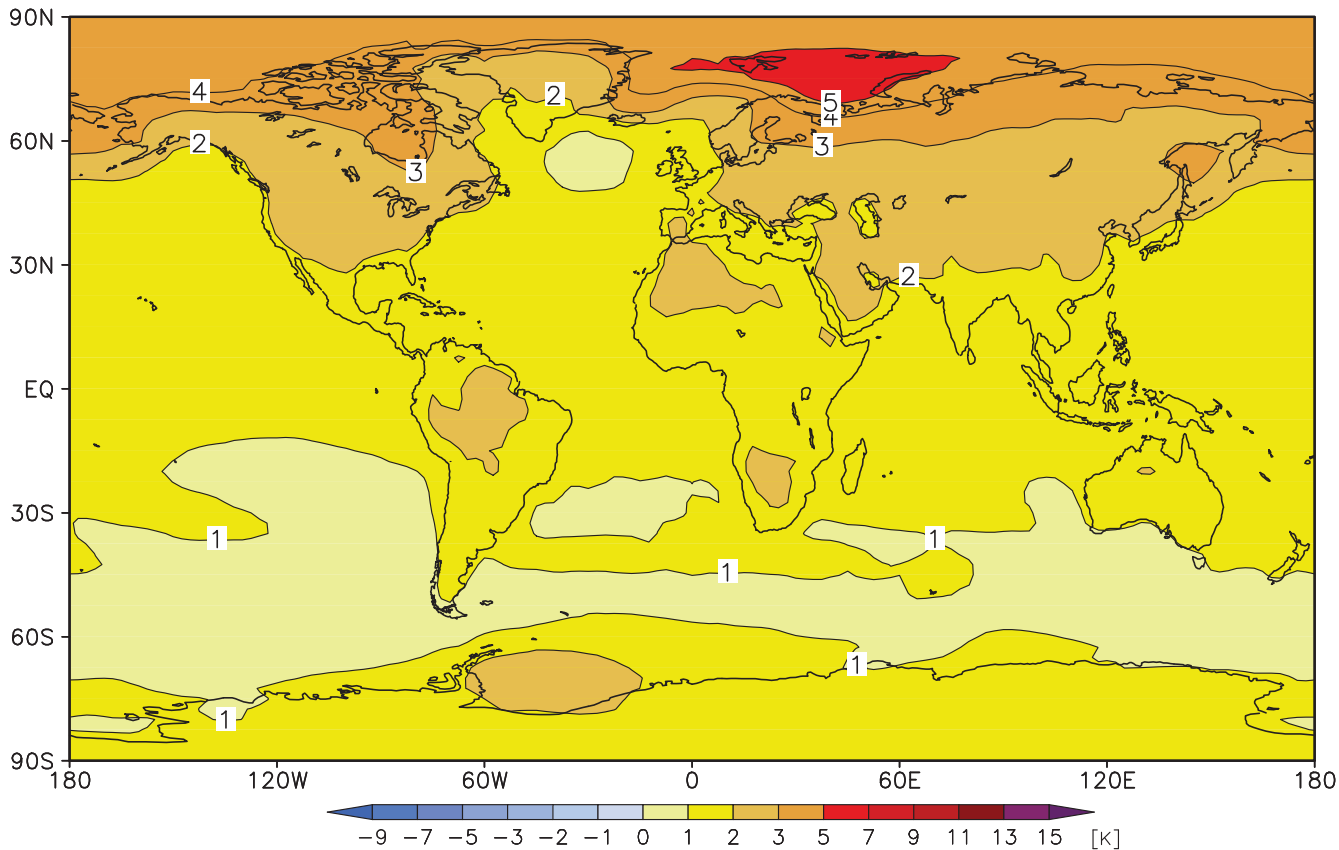


Figure 2.9: Annual mean temperature anomaly 2070-99 in E1 relative to 1961-90 as an average of 10 GCMs. [Section 4, Figure Appendix 1 A1.6 part]

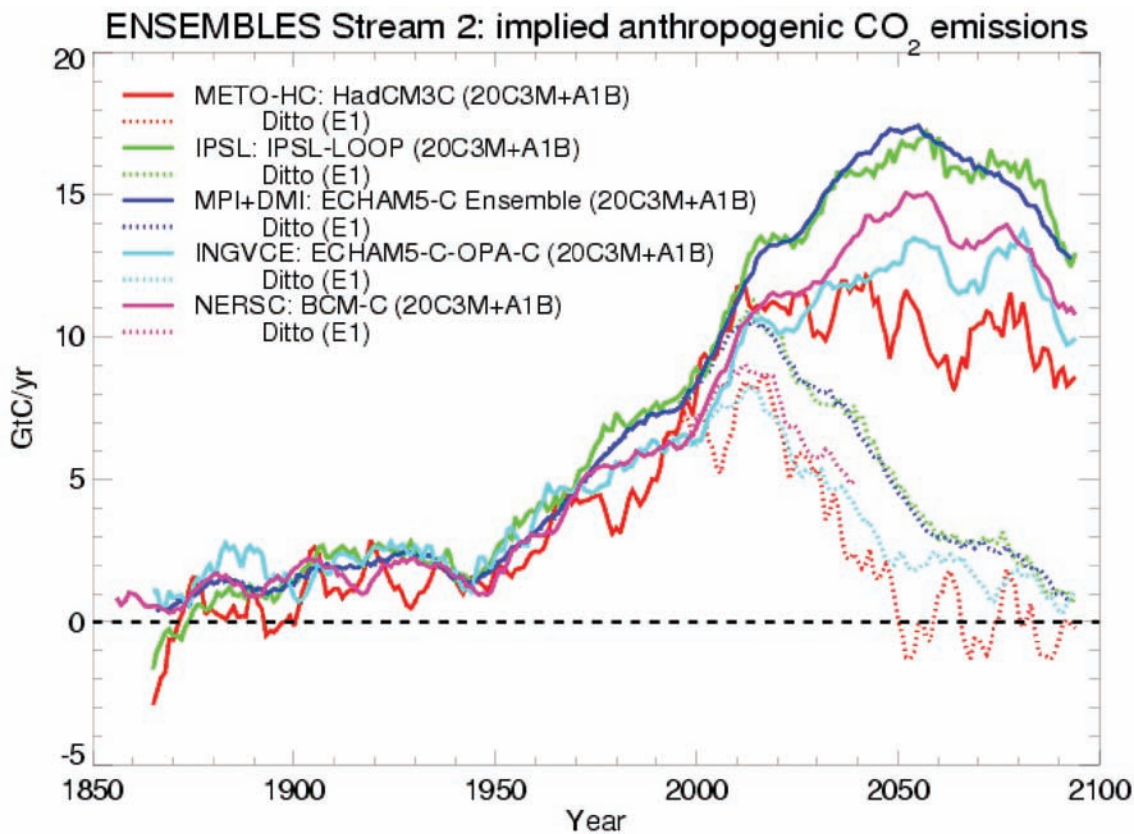


Figure 2.10: Implied (“permitted”) anthropogenic net carbon dioxide emissions to the atmosphere (Gt C/yr) in A1B and E1 20th and 21st century from modeled net carbon flux exchanges for the atmosphere. [Figure 4.8 part]

3 Development of ensemble prediction systems

[Research Theme 1]

J. Murphy (Met Office), M. Collins (Met Office), F. Doblas-Reyes (ECMWF), T. Palmer (ECMWF)

3.1 Introduction

The purpose of RT1 was to build ensemble prediction systems based on global climate or Earth system models for use in generating projections of future climate on seasonal, decadal and multi-decadal time-scales. The scope included the assembly and testing of new Earth system models, development and implementation of methods to represent the effects of uncertainties in the modelling of key physical, biological and chemical processes (hereafter termed ‘modelling uncertainties’), and the use of observations to initialise and constrain the projections.

Recognising the emergence of pioneering work in decadal prediction at the start of the project, and building on a proven multi-model approach to seasonal prediction deployed in a previous EU project (DEMETER; see Palmer et al., 2004), RT1 included a substantial effort to develop a coordinated system for seasonal to decadal (s2d) prediction, assessed via a comprehensive set of retrospective forecasts for past cases (‘hindcasts’) started from dates covering the period 1960–2005. In addition to an updated multi-model ensemble, two new approaches to the characterisation of modelling uncertainties were considered, both based on systematic perturbation strategies applied to a single model. One involved adding stochastic elements (Berner et al., 2008) to model parameterisations of sub-grid-scale physical processes (which are otherwise assumed to be deterministic in climate models); the other involved sampling uncertainties in poorly constrained parameters which control the deterministic outputs themselves. These systems were used to produce a large set of hindcasts, carried out as a coherent joint programme between RT1 and RT2A – the results from both RTs being presented together in Section 3.2. The decadal projections provide a forerunner to the worldwide near-term climate projection experiment planned for the next IPCC assessment (see Meehl et al., 2009), and results from the seasonal and decadal hindcasts are available for use by the climate research and impact communities via a public database developed in RT2A (see Section 4.5 and Appendix 2).

The perturbed parameter approach (often referred to as ‘perturbed physics’ in the climate change literature) also formed the central element of work on decadal–centennial climate prediction in RT1, encompassing several projects building on earlier studies (e.g., Murphy et al., 2004; Stainforth et al., 2005; Collins et al., 2006), and described in Section 3.3. This focus arose from the recognition that while multi-model ensembles are a valuable tool for the projection of long-term climate change (Meehl et al., 2007), they are typically assembled on an opportunity basis, and are not

designed to sample systematically the spread of possible outcomes consistent with our current understanding of climate feedback processes. Attempts to generate probabilistic estimates of climate change from multi-model projections require substantial assumptions, and different methods therefore generate significantly different results (Tebaldi and Knutti, 2007). RT1 therefore developed a new modelling system specifically designed for probabilistic projections, based on perturbed parameter ensembles of a family of configurations of a single climate model (HadCM3), but also including results from alternative models in order to take account of uncertainties arising from basic structural choices which cannot be varied within a single model. This system was used to provide probabilities for multi-decadal changes in European surface temperature and precipitation during the 21st century, based on a medium non-mitigation emissions scenario (SRES A1B) and available at a spatial resolution of about $300 \times 300 \text{ km}^2$. These results provide a much-improved basis for the assessment of climate-related risks in adaptation planning, and has been used extensively for assessments of climate impacts by RT6. The envelope of possible outcomes defined by these projections also supplies context for the more detailed multi-model projections available from regional climate models within ENSEMBLES, developed by RT3 and produced by RT2B.

In addition, RT1 included a Work Package to assemble and test a new generation of Earth system models. Results from these are reported by RT2A, in which they were used to provide updated multi-model projections of global change, investigating, in particular, the carbon emissions required to replicate greenhouse gas concentration pathways available from the A1B scenario, and also from a new mitigation scenario (E1) developed by RT7.

3.2 Seasonal to decadal prediction system

Here we summarise the work done on the seasonal–decadal prediction system in ENSEMBLES, carried out jointly by RT1 and RT2A.

Climate predictions on seasonal time-scales are now made routinely at a number of operational meteorological centres around the world, in many cases using comprehensive coupled dynamical models of the atmosphere, oceans and land surface. The non-linear nature of the climate system makes dynamical climate forecasts sensitive to uncertainty in both the initial state and the model used for their formulation. Uncertainties in the initial conditions are accounted for by generating an

ensemble from slightly different atmospheric and ocean analyses. Uncertainty in model formulation arises due to the inability of dynamical models of climate to simulate every single aspect of the climate system with arbitrary detail. Climate models have limited spatial and temporal resolution, so that physical processes that are active at smaller scales (e.g., convection, orographic wave drag, cloud physics, mixing) must be parameterised using semi-empirical relationships.

In ENSEMBLES, three approaches to address model uncertainty in seasonal–decadal predictions have been explored.

1. The multi-model method empirically samples errors that occur due to structural inadequacy in individual climate models by using models with different formulations and parameterisations (Palmer et al., 2004). This approach relies on the fact that global climate models have been developed somewhat independently at different climate institutes, using different numerical schemes to represent the dynamics, and applying different parameterisations of physical processes.
2. Given that some of the most important model uncertainties are in the specification of the parameters that are used in the physical parameterisations (Murphy et al., 2004; Stainforth et al., 2005), the perturbed parameter approach (see also Section 3.3) samples model uncertainty by creating ensembles of alternative variants of a single model in which multiple uncertain parameters are perturbed.
3. Due to the finite spatial resolution of climate models, the representation of processes on spatial scales smaller than the truncation scales, and their feedback onto larger scales, remains subject to considerable uncertainty. The impact of unresolved scales can be approximated by stochastic physics elements that act either as perturbations to the physical tendencies or via energy backscatter processes from the sub-grid scales to the resolved scales (Palmer, 2001; Berner et al., 2008).

Two streams of coordinated seasonal–decadal experiments were carried out during the project:

Stream 1 covered the 1991–2001 hindcast period for seasonal to annual range with 7-month-long hindcasts started every May and November. The November start dates were extended to 14 months in order to cover a full calendar year. Each of the groups contributing to the multi-model ensemble ran nine-member ensembles sampling uncertainties in the observed initial conditions (see Section 3.2.1). In addition, further nine-member ensembles were run to assess the stochastic physics and perturbed parameter approaches to sampling modelling

uncertainties, using the IFS/HOPE and DePreSys systems, respectively. Papers documenting the results have been written (Berner et al., 2008; Doblas-Reyes et al., 2009). The perturbed parameter hindcasts were also tested in decadal prediction mode by extending the hindcasts for all 22 start dates. Partners contributing to the multi-model ensemble also carried out test decadal projections for two start dates (November 1965 and November 1994), using the results to inform the design of the subsequent stream 2 hindcasts.

Stream 2 hindcasts consisted of a comprehensive set of seasonal, annual and decadal integrations. The seasonal (7-month long) and annual (14-month long) hindcasts were performed over the 46-year hindcast period 1960–2005, with start dates every 4 months (February, May, August and November). This gave a total of 184 seasonal hindcasts. Ten multi-model decadal hindcasts were carried out over the same hindcast period, starting every 5 years (1960, 1965, 1970, ..., 2005) in November. The 2005 start date also provides a future prediction for 2010–2014 (see Section 3.2.3). The seasonal–annual hindcasts again consisted of nine ensemble members per model, whereas the decadal runs were done with three members per model. Table 3.1 summarises the contribution from each partner to the s2d stream 2 hindcasts.

The DePreSys system was used to create a large set of decadal hindcasts, initialised every November during 1960–2005. The ensemble hindcasts consisted of the HadCM3 model variant with standard parameter settings plus eight variants distinguished by multiple parameter perturbations. These formed a subset of the model variants used in the multi-decadal climate change projections of Section 3.3, and were chosen to span a wide range of model behaviour in terms of climate sensitivity and ENSO amplitude.

A revised version of the stochastic physics approach (Palmer et al., 2008) has been used in test mode for a subset of stream 2 seasonal hindcasts. The revised scheme includes the latest developments for the stochastically perturbed parameterisation tendencies (SPPT) and the spectral stochastic backscatter (SPBS) schemes. SPPT is based on univariate perturbations of the wind, temperature and humidity tendencies, using a spectral pattern generator with a synoptic and a seasonal time-scale. SPBS uses stochastic backscatter to perturb the streamfunction forcing based on dissipation rates calculated from numerical, convective and orographically induced dissipation. Preliminary hindcasts for the May and November start dates over the 1991–2008 period have been completed at the time of writing.

Table 3.1: Overview of coupled models used in the stream 2 seasonal–decadal hindcasts.

Partner	Model	Atmosphere	A-Resolution	A-Levels	Ocean	O-Resolution	O-Levels	Contribution
ECMWF	IFS/HOPE	IFS	T159	62	HOPE	0.3–1.4°	29	Multi-model, Stochastic physics
METO-HC	HadCM	HadAM3	2.5×3.75°	38	HadOM	1°	40	Perturbed parameter
IfM	ECHAM5/MPI-OM	ECHAM5	T63	31	MPI-OM	1.5°	40	Multi-model
METO-HC	HadGEM2-AO	HadGAM2	N96	38	HadGOM2	0.33–1°	20	Multi-model
CNRM+CERFACS	ARPEGE/OPA	ARPEGE4.6	T63	19	OPA8.2	0.5–2°	31	Multi-model
INGV	ECHAM5/OPA	ECHAM5	T63	19	OPA8.2	0.5–2°	31	Multi-model

3.2.1 Initialisation strategies

Building on work done in the previous European projects, DEMETER and ENACT, a substantial effort on the ocean initialisation for seasonal–decadal climate prediction was carried out. The work can be summarised as follows.

1. Improvement of existing assimilation systems, particularly those developed previously in ENACT, in order to facilitate production of multi-decadal reanalyses (see ENSEMBLES report D1.3: http://ensembles-eu.metoffice.com/project_reporting/year2reporting/public_completed_milestones_deliverables_13_24/D1.3_NewD_Asystems.pdf). Several partners then pursued further developments of their data assimilation systems in order to prepare the ENSEMBLES stream 2 experiments. This involved, for example, better calibration of the systems, introduction of new datasets, and better covariance models for the representation of the remote effects of available observations.
2. Improvement of the common EN3 database of observed temperature and salinity profiles: recent data were included, historical records were updated with data from the recent World Ocean Database, and the quality control was improved (Ingleby and Huddleston, 2007).
3. Definition of an approach to deal with uncertainties in estimates of the observed state of the ocean: the approach chosen by most of the groups was to produce sets of surface forcing perturbations and apply them to ocean models and assimilation systems in order to generate ensembles of ocean reanalyses and/or initial conditions. In particular, a set of perturbations for sea surface temperature (SST), wind stress, and freshwater flux were produced and made available by ECMWF. Although usage of these perturbations differs somewhat from one system to another, they constitute a coordinated method for dealing with ocean uncertainty.
4. Final production of ensembles of multi-decadal ocean reanalyses, for both ocean state estimation and coupled seasonal–decadal hindcast initialisation.

A project report (ENSEMBLES report D2A.1: http://ensembles-eu.metoffice.com/project_reporting/year2reporting/public_completed_milestones_deliverables_13_24/D2A.1_OceanAnalyses.pdf, also appearing as Weisheimer et al., 2007) summarises the choices made.

All these developments fed directly into the production of seasonal–decadal stream 2 hindcasts by providing ocean initial conditions. Additionally, some products have been made available to the project, as well as to the public, to stimulate research studies within the community. These are:

- The Met Office quality-controlled oceanographic database EN3, which includes temperature and salinity profile data. Documentation appears in Ingleby and Huddleston (2007).
- A database of ensembles of ocean reanalyses available from the ENSEMBLES seasonal–decadal public data server at <http://ensembles.ecmwf.int/download/ocean/>. The database contains a set of ocean variables, using the common NetCDF data format, interpolated on a common grid. Data are available from five groups: namely ECMWF, INGV, Met Office, IfM Kiel and CERFACS, amounting to about 23 realisations for the period 1960–2005.

Figure 3.1 presents an illustration of the reanalyses database. It shows the multi-decadal evolution of the upper ocean heat content (or, equivalently, the averaged temperature) for ensembles of ocean reanalyses from ECMWF, INGV, the Met Office and CERFACS. The results show substantial decadal variability in the reanalyses, whereas some recent observation-only estimates (e.g., Domingues et al., 2008) show a much less pronounced decadal variability, especially during 1975–1985. This is because the database of Ingleby and Huddleston (2007) contains some historical data, mostly from expendable bathythermographs (XBTs), that have been diagnosed as being affected by a wrong correction (see Wijffels et al., 2008). In addition, there are differences in the heat content tendency from different reanalyses, probably due to differences in the strategies for restoration towards climatology. Furthermore, there appears to be a clustering of the ensembles of reanalyses issued from the same system, implying that the application of our perturbation strategy to any single reanalysis system might not be sufficient to sample fully the true uncertainty in the observed ocean state, in the decadal prediction context. In this regard, the ‘multi-analysis spread’ may provide a more realistic estimate of the uncertainty.

AVERAGED TEMPERATURE (0–300m) 1960–2005
Global mean (80S–80N)

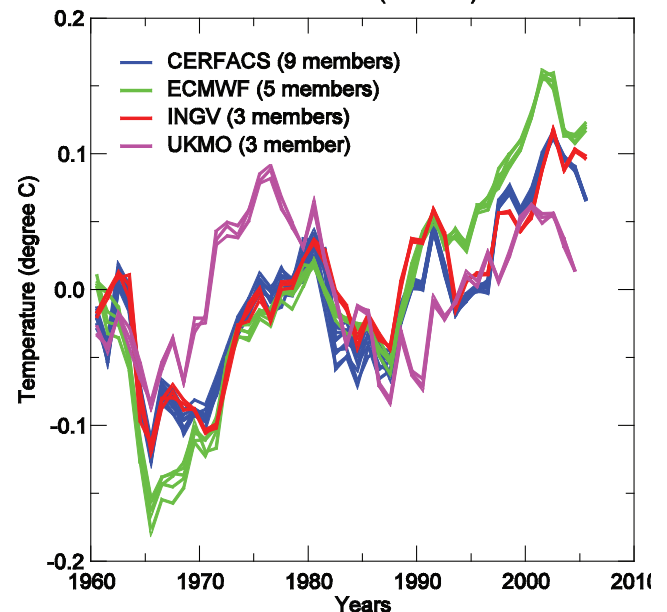


Figure 3.1: Global (80°S–80°N) annual mean upper (0–300 m) ocean averaged temperature anomalies (with respect to the average for 1960–2005) in 20 ENSEMBLES ocean reanalyses.

3.2.2 Results of the seasonal to annual hindcasts

The forecast quality of the different approaches to model uncertainty on the seasonal–annual time-scale has been carefully analysed and assessed in terms of different aspects of deterministic and probabilistic forecast performance.

For tropical Pacific SSTs, the multi-model ensemble was shown to outperform any of the perturbed initial condition ensembles from the participating individual models, demonstrated by reduced RMS errors and enhanced ensemble dispersion at all lead times (Weisheimer et al., 2009). A

considerable reduction in systematic error compared with a previous multi-model ensemble from the DEMETER project was also found. Probabilistic forecast skill scores indicated that the new ENSEMBLES multi-model ensemble is, on average, more skilful than DEMETER in the 4–6 month forecast range. The degree of these improvements depends on the region, season and event of interest. The combination of ENSEMBLES and DEMETER into a grand multi-model ensemble did not improve the seasonal forecast skill further.

Table 3.2 shows a summary of probabilistic seasonal skill scores of the ENSEMBLES multi-model stream 2 hindcasts for 21 standard land regions around the globe. The events considered are cold/warm seasonal mean temperature and dry/wet seasons, for 2–4 months ahead. Positive (negative) scores are indicated as green (red) cells and indicate more (less) skilful probabilistic hindcasts than issuing a forecast solely based on a knowledge of climatology. Strong bold colours denote statistically significant scores. In general, the forecast skill is positive for most areas and events. Surface air temperature is, on average, more predictable than precipitation. The level of skill depends strongly on the region: whereas some land areas such as the Amazon Basin (AMZ) and South East Asia (SEA) have positive scores for all events considered; other geographical areas are more difficult to predict (e.g., Central North America, CNA, or Northern Europe, NEU).

For this wider set of regions, comparison with the DEMETER results shows that the hindcast skill of the two multi-model systems is generally comparable. However, it is also found that

a combination of the DEMETER and ENSEMBLES results generally leads to improved skill compared with either system alone. This is in contrast with the result found for tropical Pacific SSTs (see above).

Preliminary simulations with the new stochastic physics scheme showed that this approach is capable of reducing systematic errors in the system and improving forecast scores over the control model version (Palmer et al., 2008). The new scheme increases the ensemble spread without adversely affecting the magnitude of forecast errors, thus successfully reducing the overconfidence in seasonal predictions. This is reflected in a better match between the ensemble spread and the root mean square error (RMSE) in the ensemble mean, and also in improved reliability when hindcasts are expressed in probabilistic form. Further tests of the scheme are under way.

An intercomparison was performed to highlight the relative merits of the three systems in the stream 1 seasonal and annual hindcasts (Doblas-Reyes et al., 2009). It was found that the three methods to account for model error performed with comparable levels of skill overall. For lead times up to 4 months, however, the multi-model hindcasts indicated slightly higher scores on average, whereas for longer lead times the perturbed parameter hindcasts gave slightly better results on average.

Results from the stream 2 simulations are shown in Figure 3.2, for ensemble average hindcasts of surface air temperature spatially averaged over the entire Northern Hemisphere

Table 3.2: Overview of the forecast quality of the stream 2 seasonal multi-model hindcasts for 2–4 months ahead. The quantity shown is the Brier skill score (BSS)*100, with values above zero indicating positive skill compared with a climatological reference forecast. Positive BSS is shown in green, negative BSS in red. Significantly positive (negative) BSS are indicated in strong green (red). The events summarised in the table are warm and cold 2 m temperature (T2m) and wet and dry conditions (precipitation) for the JJA and DJF seasons. The definition of these events is based on model terciles. For verification, ERA-40 was used in the case of T2m, and GPCP for precipitation. The regions shown are the standard land regions, following Giorgi and Francisco (2000).

	Surface air temperature (T2m)				Precipitation			
	JJA		DJF		JJA		DJF	
	lower	upper	lower	upper	lower	upper	lower	upper
AUS	14.0	11.2	-2.1	-1.7	0.9	-1.9	-3.4	-3.2
AMZ	14.3	14.1	26.0	26.6	5.2	4.3	11.9	11.2
SSA	9.9	9.0	3.3	3.7	9.0	7.9	-0.8	-1.0
CAM	14.9	12.2	12.1	7.1	6.1	7.6	9.6	12.9
WNA	10.6	10.5	1.1	3.3	2.0	2.7	3.0	2.8
CNA	-3.0	-5.5	-10.2	1.3	-3.4	-3.1	1.9	4.0
ENA	4.5	5.2	-3.2	6.5	-3.0	-2.5	6.1	4.4
ALA	3.1	0.1	-3.1	0.2	-0.1	-1.3	1.5	-1.2
GRL	6.0	6.9	4.9	2.4	-0.3	-1.1	-2.5	-2.3
MED	10.9	14.3	4.3	4.8	-2.6	0.1	1.3	-0.4
NEU	2.9	-4.0	5.6	0.7	-3.6	-0.3	-1.9	-4.4
WAF	10.4	11.3	16.9	18.4	-7.0	-4.8	-5.0	-0.7
EAF	14.4	5.2	12.9	7.2	-5.9	-2.5	-1.2	-1.9
SAF	8.7	3.5	14.0	14.7	1.5	1.4	7.0	3.0
SAH	9.7	8.5	7.9	7.6	-6.3	-7.4	0.1	1.2
SEA	13.5	12.5	15.4	21.9	14.9	10.7	5.9	3.9
EAS	7.8	11.0	5.2	7.9	-1.6	-3.4	1.0	-0.5
SAS	8.9	17.0	9.5	5.9	-4.8	-4.1	0.6	1.1
CAS	5.8	6.6	2.8	3.0	0.3	1.3	4.2	3.2
TIB	14.6	17.2	4.0	2.4	0.4	0.0	2.7	-0.6
NAS	3.4	2.5	3.8	4.6	-0.9	-1.4	-1.9	-3.2

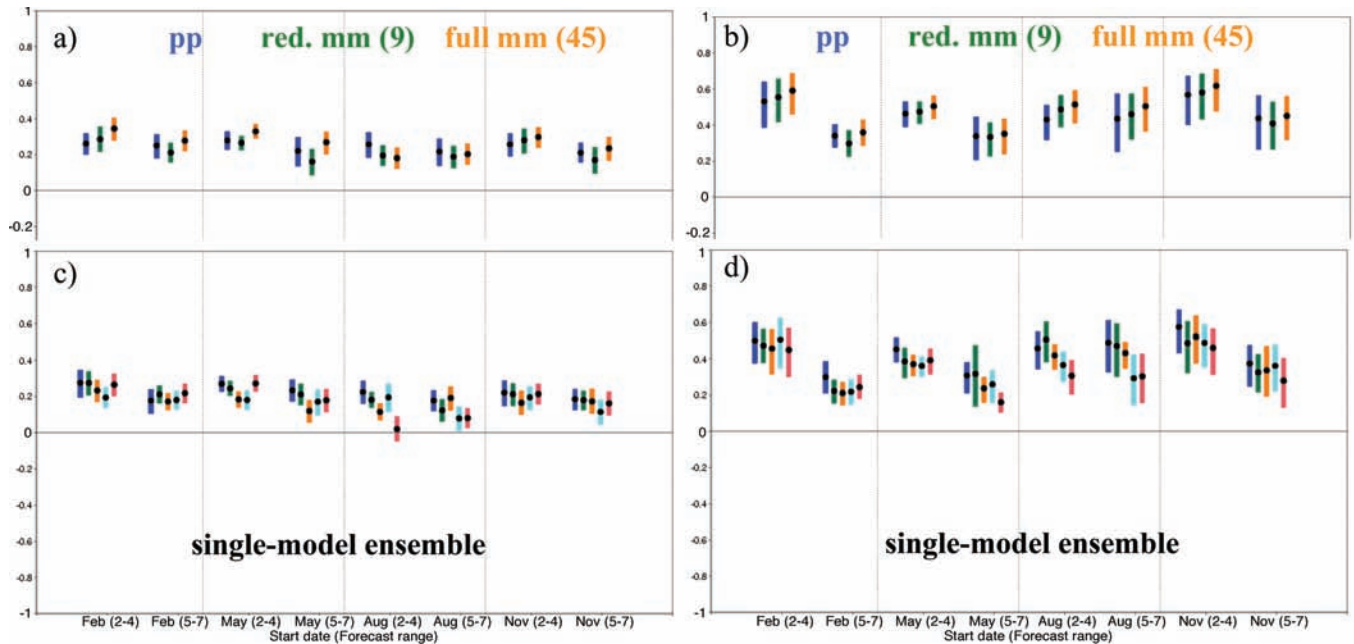


Figure 3.2: Anomaly correlation for T2m spatially averaged over the Northern Hemisphere extratropics (left), and precipitation averaged over the tropics (right), as a function of start date and lead time estimated over the period 1960–2005. The top row shows results for the perturbed parameter ensemble (blue) and for two versions of the multi-model (green – reduced ensemble with nine ENSEMBLE members; orange – full ensemble with 45 ENSEMBLE members). The reduced multi-model ensemble is constructed by selecting randomly from the 45 members, ensuring that at least one member is selected from each participating model. The bottom row shows the individual models contributing to the multi-model ensemble (blue – ECMWF, green – Météo France, orange – INGV, cyan – IfM Kiel, red – Met Office). Scores are grouped according to the four start dates per year. For each start date, correlations for forecast lead times of 2–4 months and 5–7 months are displayed separately.

extratropics, and precipitation averaged over the tropics. In both cases, the multi-model ensemble shows a higher anomaly correlation than any of its constituent individual models. When considering ensembles of equal size (nine members), the perturbed parameter ensemble displays similar skill to the multi-model ensemble, and in general the two methods also give similar estimates of the spread of possible outcomes. The skill of the multi-model ensemble improves somewhat when all 45 of its members are pooled in order to provide a better combined sample of initial state and model uncertainties.

Figure 3.3 gives a further comparison between the multi-model and perturbed parameter approaches, for hindcasts up to 7 months ahead. This is based on a probabilistic measure of skill which credits both the ability to discriminate between different events, and to forecast probabilities which are reliable, in the sense that an event predicted $x\%$ of the time should occur in practice $x\%$ of the time. Here, the multi-model ensemble gives slightly better results than the perturbed parameter ensemble on average, although the relative performance varies according to the region, variable, and lead time considered. Figure 3.4 shows that the new stochastic physics results provide a level of skill comparable to that of the multi-model ensemble on average, based on a similar comparison. Overall, we find that the multi-model ensemble gives seasonal predictions competitive with (and in some respects better than) those obtained in previous projects, while the stochastic and perturbed parameter techniques provide promising indications that a similar level of performance can potentially be achieved through the application of systematic techniques for the sampling of uncertainties in a single-model system.

In ENSEMBLES, coordinated multi-model hindcasts on the annual time range have been performed for the first time. Four

of the participating modelling groups (Table 3.1) extended the length of the stream 2 hindcasts for the November start dates beyond seasonal time-scales up to 14 months. An approximately linear growth of tropical Pacific SST RMSE and ensemble spread for the multi-model was found (Weisheimer et al., 2009). The SST anomaly correlation reached a level of about 0.5 around forecast month 9 and stayed relatively constant thereafter.

3.2.3 Results of the decadal hindcasts

The basis for investigating decadal prediction rests on evidence from observed low-frequency climate variations around the world, results from idealised modelling studies, and evidence that forced climate change can also provide skill (for a recent review, see Meehl et al., 2009). The ENSEMBLES stream 2 decadal hindcasts provided a first opportunity to assess the benefits of combining projections from different models in a coordinated experiment, following initial studies carried out with individual climate models (Smith et al., 2007; Keenlyside et al., 2008; Pohlmann et al., 2009). The inevitable existence of simulation biases in the models used for the decadal hindcasts necessitates (as in seasonal prediction) the use of strategies to account for these systematic errors when comparing forecasts against observations. This was achieved by expressing each hindcast as anomalies relative to either a long-term model climatology (if available), or to the average of other hindcasts. Some groups also adopted a strategy of initialising their hindcasts using observed anomalies added to a model climatology in order to reduce model drift during hindcasts, whereas others initialised using full observed fields in order to provide starting conditions as close as possible to the real climate system. The optimal strategy for forecast production in the presence of model biases remains an open question for future work.

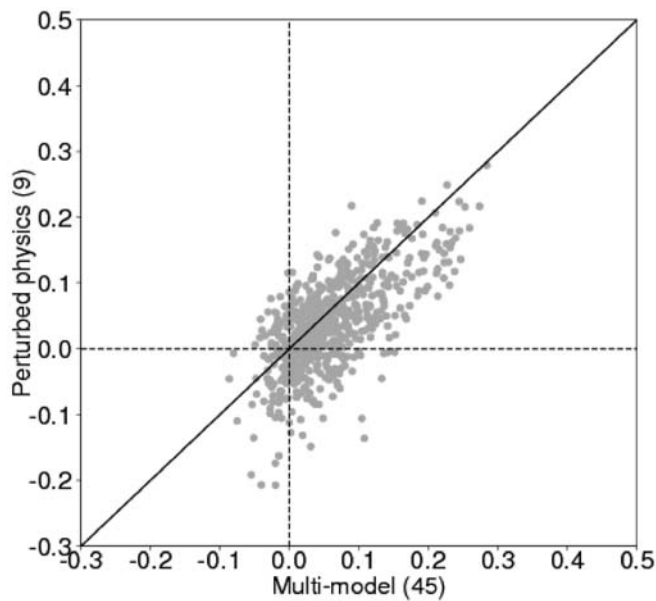


Figure 3.3: Scatter plot of Brier skill scores (BSS) for the multi-model and perturbed parameter forecasting systems. The dots represent the BSS estimated for the standard land regions of Giorgi and Francisco (2000), for T2m and precipitation and for the two events ‘anomalies in lower or upper terciles’. Results are from the stream 2 hindcasts for lead times of 2–4 months and 5–7 months ahead, calculated from all available start dates. The multi-model results are based on all 45 members, compared with nine for the perturbed parameter hindcasts; however, the BSS scores were adjusted using the technique of Ferro (2007) to remove the effects of differing ensemble size.

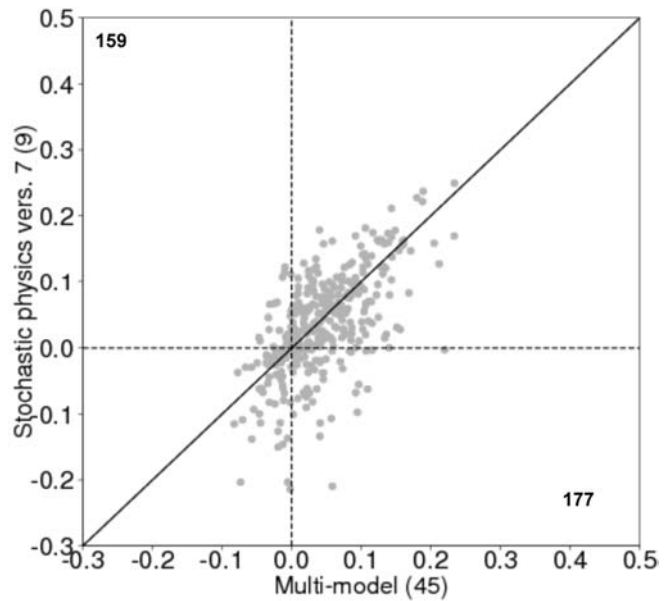


Figure 3.4: As for Figure 3.3, but comparing the multi-model and stochastic perturbed parameter forecasting systems. Results are for a subset of the stream 2 hindcasts covering the May and November start dates from 1991–2005, for lead times of 2–4 months and 5–7 months ahead. The multi-model results are based on all 45 members, compared with nine for the stochastic physics hindcasts; however, the BSS scores were adjusted to remove the effects of differing ensemble size, as in Figure 3.3.

Figure 3.5 shows that each of the models contributing to the multi-model ensemble achieves modest skill in projections of surface temperature anomalies averaged over the Northern Hemisphere extratropics. The skill increases for longer lead times, being larger for 6–10 years ahead than for 3–14 months or 2–5 years ahead. This is because the forced climate change signal, the sign of which is highly predictable, is greater at longer lead times. Encouragingly, the multi-model ensemble mean, which consists of the average of twelve individual projections, gives somewhat higher scores than any of the individual models, whose projections are derived from three members with perturbed initial conditions.

The perturbed parameter hindcasts also show improved skill when results from the individual model variants are averaged to form an ensemble mean (in this case there is a single hindcast from each variant, so the ensemble mean is made from nine members). Figure 3.6 shows an example, plotting a time-series of global pattern correlations for 9-year average hindcasts of surface temperature throughout the stream 2 period. While individual ensemble members sometimes give better results than the ensemble mean (data not shown), the average skill of individual members is consistently lower (compare dashed and solid red curves). The results also show that the skill increases for more recent hindcasts. In order to diagnose sources of skill, the blue curve of Figure 3.6 shows ensemble mean results from a parallel ensemble of ‘NoAssim’ hindcasts containing the same external forcing from greenhouse gases, sulphate aerosols, volcanoes and solar variations, but initialised from randomly selected model states rather than analyses of observations. The results replicate the trend in skill found in the initialised hindcasts, showing that this arises mainly from the strengthening influence of external forcing, particularly that due to anthro-

pogenic greenhouse gases. However, the average correlation skill is slightly smaller in the NoAssim hindcasts (0.25 versus 0.30), indicating that initialisation provides a modest increase in average skill.

As an example of the effects of initialisation, Figure 3.7 shows ensemble mean surface temperature anomalies for December 2005–November 2008 from three projections initialised from November 2005. These consist of the ENSEMBLES multi-

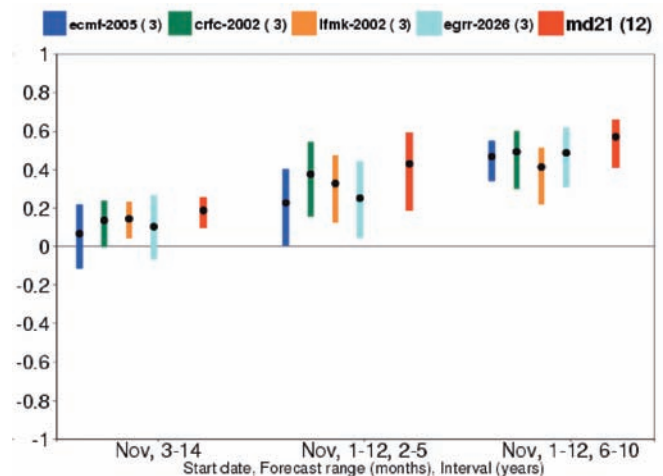


Figure 3.5: Anomaly correlation coefficient for near-surface temperature over the NH extratropics from the ENSEMBLES decadal hindcasts over the period 1960–1995. The three groups of bars stand for lead times of 3–14 months, i.e., the first forecast year (left), for lead times of 2–5 years (middle), and lead times of 6–10 years (right). The vertical bars indicate the uncertainty range based on a bootstrap resampling. Colour code: blue – ECMWF, green – CERFACS, orange – IfM Kiel, cyan – Met Office HadGEM2, red – multi-model ensemble.

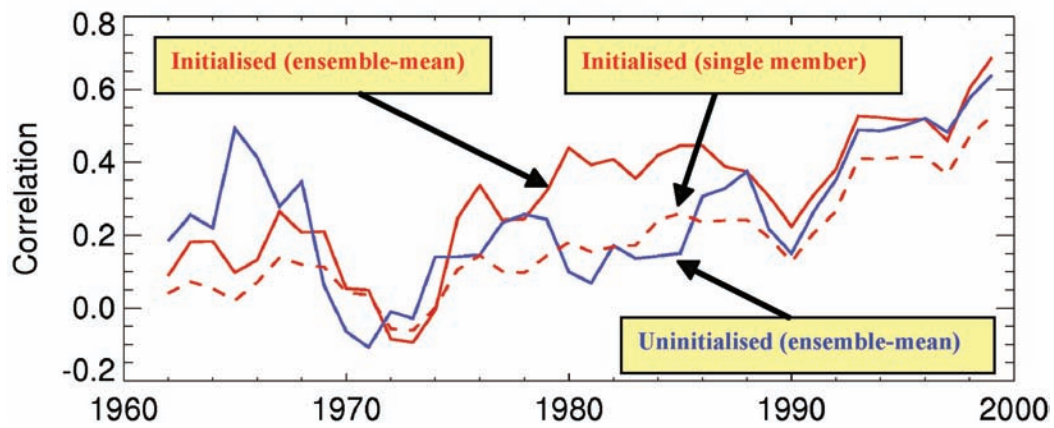


Figure 3.6: Time-series of correlations between hindcast and observed global patterns of near-surface temperature anomalies, for hindcasts of nine-year means during the stream 2 period. The red dashed curve shows average scores for individual variants of HadCM3 included in the DePreSys perturbed parameter ensemble, and the solid red line shows scores for the ensemble mean of the nine constituent variants. The blue curve shows scores for the ensemble mean of a corresponding 'NoAssim' perturbed parameter ensemble in which hindcasts are driven by the same time-dependent specification of external radiative forcing anomalies, but lacking the initialisation from analyses of atmosphere and ocean observations used in the DePreSys hindcasts. Time-dependent forcing anomalies arise from anthropogenic greenhouse gases and sulphate aerosols from the SRES A1B scenario, and projected natural forcing from volcanoes and solar variation, assuming no prior knowledge of volcanic eruptions after the initialisation date.

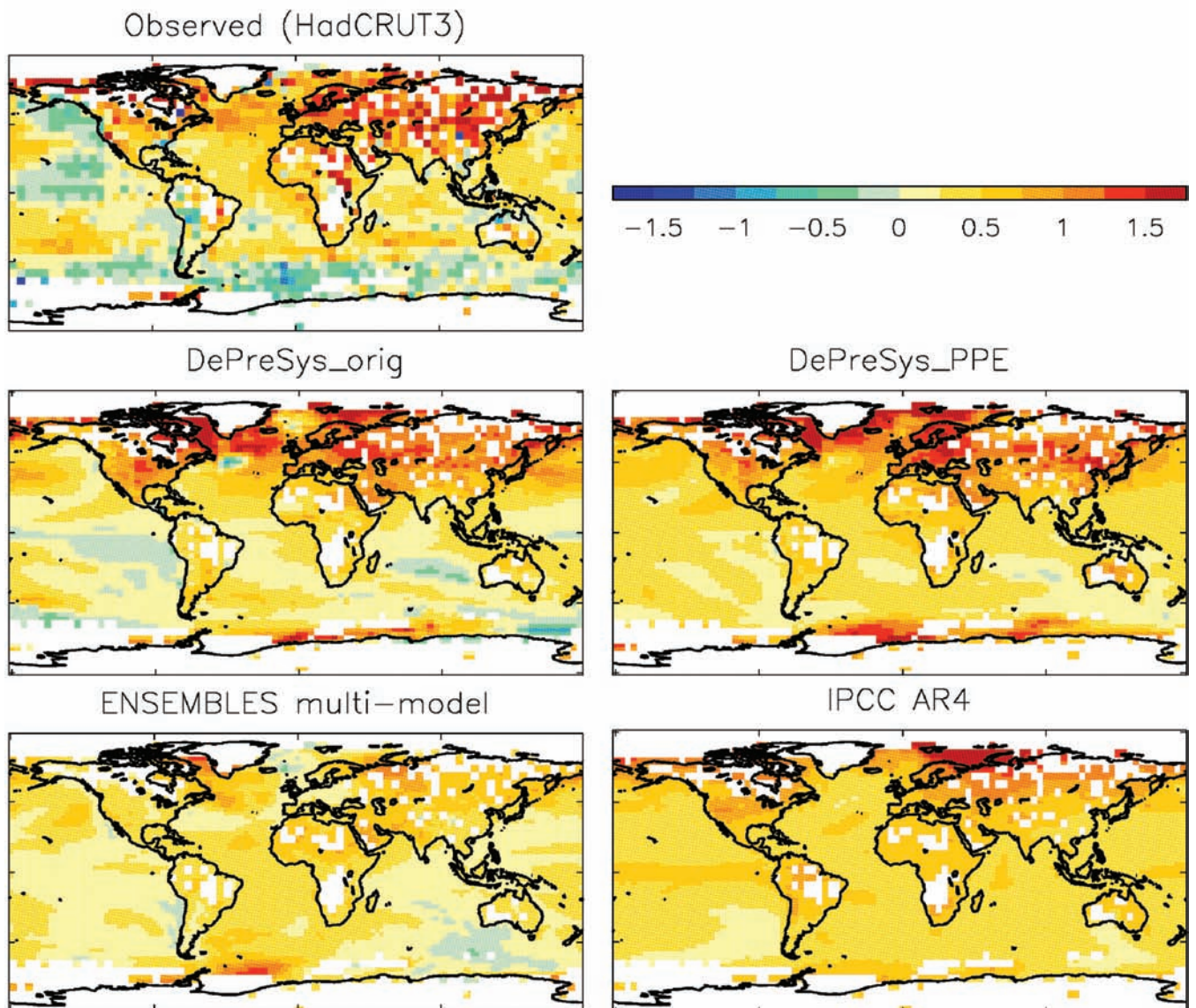


Figure 3.7: Surface temperature anomalies ($^{\circ}\text{C}$) for December 2005–November 2008, relative to 1961–2001. Verifying observations were compared against initialised ensemble mean projections from the DePreSys perturbed parameter and multi-model forecasts started from November 2005 in ENSEMBLES, a further initialised projection from the original DePreSys single-model system of Smith et al. (2007), and also against uninitialised climate change projections from the IPCC AR4 assessment. The ensemble means were created from 9, 12, 10 and 22 simulations, respectively.

model and perturbed parameter experiments, plus a projection from the original DePreSys system of Smith et al. (2007), based on ten simulations with a single model sampling initial state perturbations. These were compared against verifying observations (top panel), and also against the ensemble mean of the set of uninitialised climate change simulations available from the IPCC AR4 (bottom right). All the initialised projections show enhanced warming in the North Atlantic compared with the IPCC projections, in better agreement with observations; and the original and perturbed parameter DePreSys projections also capture the enhanced warming observed over the Eurasian landmass. The IPCC simulations and the initialised perturbed parameter experiments overestimate the observed global mean warming by about 0.2°C, while the ENSEMBLES multi-model projection gives a global mean change consistent with observations. None of the initialised projections capture the observed cool anomalies found in northern tropical regions of the Pacific Ocean (partly due to overestimation of the global mean warming); however, they do capture the spatial pattern of anomalies in the Pacific (relatively warm anomalies at northern mid-latitudes compared with the tropics) to some extent, which is not the case in the IPCC simulations. These results illustrate that initialised decadal forecasts have the potential to provide better information than traditional climate change projections; however, the differences between the alternative systems shown in Figure 3.7 (see also Appendix 1) also illustrate the research challenges associated with building improved decadal prediction systems in future, informed by the pioneering studies performed in ENSEMBLES.

3.3 Decadal to centennial prediction system

An overarching aim of the ENSEMBLES project has been to produce projections of climate in which sources of uncertainty are quantified and projections are expressed in terms of probability distribution functions (PDFs). Uncertainty in decadal–centennial projections arises from uncertainties in future emissions of greenhouse gases and other forcing agents, unforced natural (‘internal’) variability in climate, and uncertainties in formulation of models (see Section 3.2).

As explained in the Introduction, the principal tool used to quantify both internal variability and modelling uncertainties in our long-term climate projections was the ‘perturbed parameter’ approach, whereby uncertainties in global climate model parameters which determine the magnitude of climate feedbacks associated with physical, chemical and biological processes are systematically explored. Developments in this area are reported in Section 3.3.1, while a method to convert some of our perturbed parameter ensemble results into probabilistic climate change projections is described in Section 3.3.2. In these projections, uncertainties due to internal variability were included via the use of long model simulations spun up from initial conditions statistically independent of recent observed conditions (as is currently typical in long-term climate projections). A topic for future work is to assess the prospects for constraining some aspects of internal variability in projections beyond a decade ahead, by initialising the model with observations, as in Section 3.2. Finally, in Section 3.3.3

we describe work using a simple climate model to explore the implications of uncertainties in the global response of physical and carbon cycle climate feedbacks for the setting of policy-relevant carbon emissions targets.

3.3.1 Sampling uncertainties in future climate change using perturbed parameter ensembles

A version of the HadCM3 climate model was adapted to run on personal computers by Oxford University, under the climateprediction.net initiative. The model was distributed to members of the general public to run multi-thousand-member ensembles exploring the sensitivity of the model to perturbations of model parameters (Murphy et al., 2004). This highly successful project, which allowed over 300,000 people to participate directly in ensemble climate modelling, was taken up by the BBC and made the subject of two television documentaries, winning the 2007 Prix Europa Internet Project of the Year award. The key early result of this project (Stainforth et al., 2005) related to climate sensitivity, the equilibrium warming on stabilising greenhouse gas levels at, for example, 550 ppm CO₂-equivalent. It was found that perturbations to model parameters were much more likely to substantially increase the climate sensitivity of this model than to substantially reduce it, reflecting in a complex general circulation model the asymmetric uncertainty in climate sensitivity consistently found in observational estimates based on simple models (Allen et al., 2006)

This result is illustrated, and updated, in Figure 3.8, which shows the relative likelihood of the control climates of several thousand members of the initial climateprediction.net ensemble, consisting of simulations using HadCM3 coupled to a simple mixed-layer ocean (the ‘slab’ model configuration, HadSM3). The likelihood measure is based on a simple goodness-of-fit to observed surface pressure, temperature and rainfall (more complex likelihood measures give similar results), plotted against the equilibrium climate sensitivities of the different model variants. Points are coloured according to the values assigned to one of the parameters of the model, the ‘entrainment coefficient’, which controls the mixing between ascending plumes and the surrounding environment in the HadCM3 parameterisation of convection. This parameter was found to have the largest impact on sensitivity. The highest sensitivities, in excess of 10°C, are associated with low values of this parameter (red symbols) which consistently give unrealistic control climates. The distribution of model variants with the standard value (green symbols), however, also displays this characteristic asymmetry, with a tail of not-particularly-unlikely model variants extending over 7°C. Increasing the entrainment coefficient (blue symbols) also displaces the distribution of sensitivities in models with plausible control climates upwards. This illustrates the importance of non-linear interactions between parameters in perturbed parameter ensembles, because sensitivity is reduced if the entrainment coefficient is increased on its own (Murphy et al., 2004).

Figure 3.9 highlights a further suite of perturbed physics ensembles performed at the Met Office Hadley Centre (MOHC), projecting time-dependent climate change using the configuration of HadCM3 including a full dynamical ocean component (climateprediction.net also carried out ensembles of this type). In this set of experiments, parameters in one of the

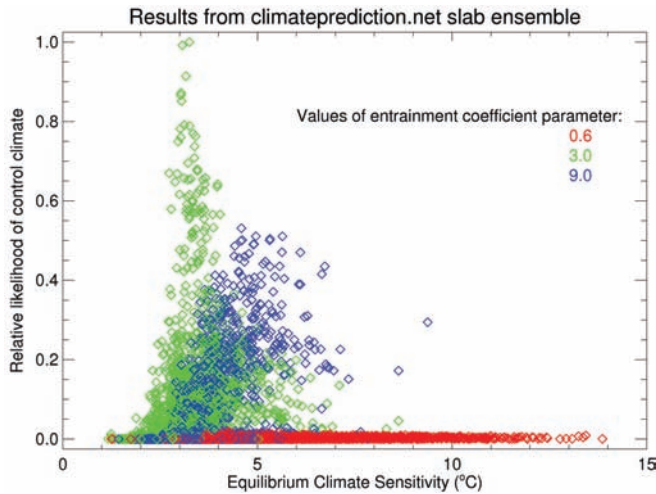


Figure 3.8: Climate sensitivity versus an estimate of the relative likelihood of different model variants, selected from a multi-thousand-member perturbed parameter ensemble of the atmosphere-mixed layer ('slab') ocean configuration of the HadCM3 climate model. The different colours denote different values for the convective entrainment parameter in the different model variants.

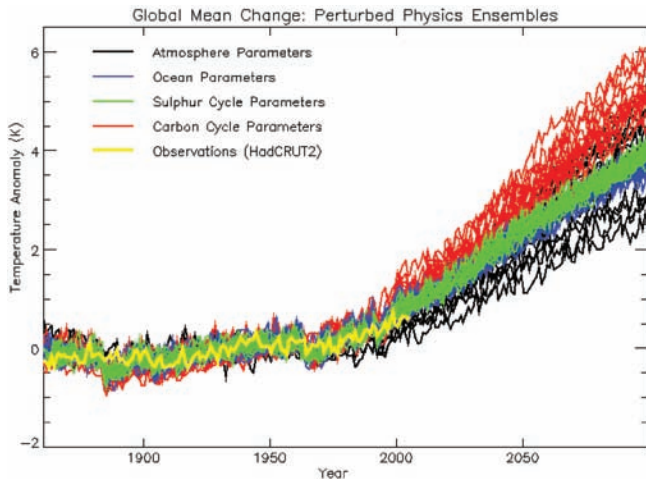


Figure 3.9: Global-mean temperature anomalies from 1860–2100 in perturbed parameter HadCM3 experiments forced by historically observed changes in anthropogenic and natural forcing agents and future greenhouse gas and sulphate aerosol emissions under the SRES A1B scenario, compared with observations to 2000. The different colours indicate ensembles with perturbations to parameters in different model components (as indicated in the legend), while keeping parameters in the other components fixed.

model components (atmosphere, ocean, sulphur-cycle and terrestrial carbon cycle) were varied, while parameters in the other components were held fixed. For global mean surface temperature, uncertainties in atmosphere parameters have a relatively important impact on the ensemble spread via differences in the surface and atmospheric physical feedbacks (black lines in Figure 3.9). Feedbacks associated with clouds are the dominant source of uncertainty, but other feedback processes also contribute to the spread of projected outcomes (Webb et al., 2006; Collins et al., 2009; Yokohata et al., 2009). Uncertainties in the parameters in the terrestrial carbon cycle of the model have a similarly important effect on the global mean (red lines in Figure 3.9) via differences in feedbacks associated with the changing balance of carbon sinks and sources (Booth

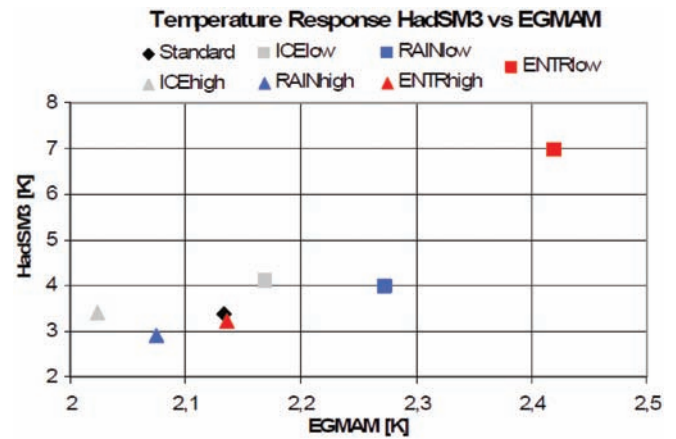


Figure 3.10: A comparison of perturbed parameter experiments performed with different ENSEMBLES models. The figure shows global mean temperature responses of perturbed variants of HadSM3 and EGMAM models for low (squares) and high (triangles) values for the convective entrainment rate (red), the rainout efficiency of cloud droplets (blue), and the cloud ice fall speed (grey) parameters. The standard model variants are shown in black. Note the differences in the scale of the axes, which is due to the different experimental set-up for each ensemble (see text).

et al., 2009). Ocean-component and sulphur-cycle-component parameter uncertainties have a smaller effect on the global mean temperature response (Collins et al., 2007; Brierley et al. 2009a, 2009b).

While the RT1 system for probabilistic projections uses perturbed parameter ensembles based on HadCM3, the effects of some of the parameters were compared with corresponding perturbations applied in another model (the Freie Universität Berlin EGMAM model). Figure 3.10 shows a comparison of the effects of perturbing three key cloud and convection parameters in the two models. The magnitudes of the changes are different due to different experimental set-ups: the results show equilibrium responses to doubled CO_2 in simulations employing the slab ocean configuration of HadCM3, whereas the EGMAM simulations show smaller changes, because a full dynamical ocean component was used to simulate the early stages of the transient response to an instantaneous change in CO_2 . Nevertheless, the results show that the global mean temperature response of the two sets of experiments is highly correlated. Further analysis of the components of the feedbacks associated with the global temperature response is discussed in Niehörster (2009). This comparison gives further evidence that perturbing the parameters within a climate model is a useful way of systematically exploring uncertainty, and thus provides a suitable technique for producing probabilistic projections of climate change.

3.3.2 Construction of probabilistic climate change projections

Given a suite of perturbed parameter ensembles, there are further steps required to produce probabilistic projections expressed in terms of PDFs. An overview of the approach is given by Murphy et al. (2007), the detailed implementation of which follows that used in probabilistic projections recently issued for the UK

(Murphy et al., 2009) except that the RT1 projections (Harris et al., 2009) do not include downscaling beyond the scale of global climate model grid boxes. In ENSEMBLES, finer-scale projections are provided by RT2B, using an ensemble of regional climate model simulations designed in RT3. The steps involved in producing the RT1 probabilistic projections were as follows.

- Production of an ensemble of around 300 equilibrium $1\times\text{CO}_2$ and $2\times\text{CO}_2$ simulations using HadSM3. Each pair of simulations was carried out using a variant of the model distinguished by different perturbations to a set of 31 parameters controlling surface, atmospheric and sea-ice processes. Some variants sampled perturbations to a single parameter (Murphy et al., 2004), whereas many sampled multiple perturbations (Webb et al., 2006; Collins et al., 2009). This ensemble was run on the Met Office supercomputer, being necessarily smaller than the corresponding distributed computing ensemble produced by climateprediction.net (Figure 3.8), but also allowing the archiving of a detailed set of regional climate diagnostics to provide a basis for the probabilistic projections described below.
- Construction of a statistical emulator allowing the historical climate and the response to doubled CO_2 of HadSM3 to be rapidly estimated for any combination of input parameter values. This allowed large numbers of estimated results to be produced, making it possible to sample the entire parameter space of the model defined from expert-specified prior distributions.
- Production of smaller ensembles using the atmosphere component of HadCM3 coupled to a full dynamical ocean component. These ensembles (described above and shown in Figure 3.9) simulate transient climate change in response to historical and future changes in forcing, and allow us to sample uncertainties in additional Earth system processes.
- Implementation of a time-scaling approach which maps equilibrium changes in climate variables at a regional level to transient climate changes under specified emissions scenarios. This allows transient changes to be estimated for any point in the model parameter space, providing a basis for the generation of probabilistic estimates of regional, time-dependent climate change. The time-scaling combines a method for inferring transient patterns of change from equilibrium patterns (calibrated using equilibrium and transient model simulations with corresponding parameter settings) with projections of global mean temperature obtained from a simple climate model. The simple model uses input parameters fitted to the HadCM3 ensemble output in order to sample uncertainties due to the main global-scale feedbacks accounted for in Figure 3.9. The method is based on Harris et al. (2006), with updates summarised by Murphy et al. (2009).
- Estimated climate changes are converted into probabilistic projections using a general Bayesian statistical framework designed to support inference of real world information from complex but imperfect models (Goldstein and Rougier, 2004; Rougier, 2007). Probabilities are obtained by integrating changes sampled at different points in the model parameter space, accounting for relationships between different variables and weighting each point in parameter space (i.e., each possible variant of HadCM3) according to the likelihood of each variant. Likelihood estimates are based on the ability to reproduce observed

spatial patterns of seasonal-mean climate for sea surface temperature, land surface air temperature, precipitation, pressure at mean sea level, short-wave and long-wave radiation at the top of the atmosphere, short-wave and long-wave cloud radiative forcing, total cloud amount, surface fluxes of sensible and latent heat, and latitude-height distributions of zonally averaged atmospheric relative humidity. The ability of the scaled transient projections to reproduce historical trends in large-scale temperature variables also contributes to the likelihood weights. The likelihood is calculated in a reduced dimension state space and takes into account covariances between different variables.

- The calculation includes an estimate of the additional effects of structural modelling uncertainties, necessary because some simulation errors in HadCM3 (as in any model) arise from basic choices made when building the model in the first place (see also Section 3.2), and cannot be resolved by varying the model parameters. The effects of structural errors in surface and atmospheric processes are estimated by using the emulator to find points in the parameter space of HadCM3 which best represent the behaviour of alternative coupled atmosphere-mixed layer ocean models in the CMIP3 archive used by the IPCC AR4 (Meehl et al., 2007). Due to structural differences between HadCM3 and the other models, this calculation fails to replicate perfectly the projections of the latter, and the results are used to inflate the variance and adjust the mean of the future PDFs. This calculation assumes that structural differences between models are reasonable proxy estimates for the effects of structural errors in HadCM3 relative to the real world, and cannot account for the effects of biases common to all models. The methodology does not support the treatment of structural errors in ocean transport and carbon cycle processes to the same degree; however, a simpler ad hoc allowance is made for these, by including results from multi-model ensembles (Friedlingstein et al., 2006; Meehl et al., 2007) alongside those of Figure 3.9 when sampling possible settings for global mean feedback values in step (4) above.

There are various ways of presenting the spatio-temporal information contained within the PDFs. Figure 3.11 shows European maps of the 20-year 10th, 50th and 90th percentiles of surface air temperature and precipitation changes under the SRES A1B scenario at the end of the 21st century expressed as anomalies with respect to a 1961–1990 baseline. Median temperature changes vary substantially with location, and are largest in the Mediterranean region in summer and in north-east Europe in winter. The uncertainty, as measured by the 10–90% range, is large for this time period – as much as 10 degrees Celsius in some locations. This is due to a combination of factors; parameter uncertainty in HadCM3, structural uncertainty from the CMIP3 ensemble, carbon cycle feedback uncertainty, internal variability, and time-scaling uncertainty. No single source of uncertainty dominates. For the projections of changes in precipitation, the canonical signals of summer Mediterranean drying and winter northern Europe wetting are evident, but again the uncertainty range is wide. For many grid boxes there are significant probabilities of both drier and wetter future climates, and this may be important for impacts studies.

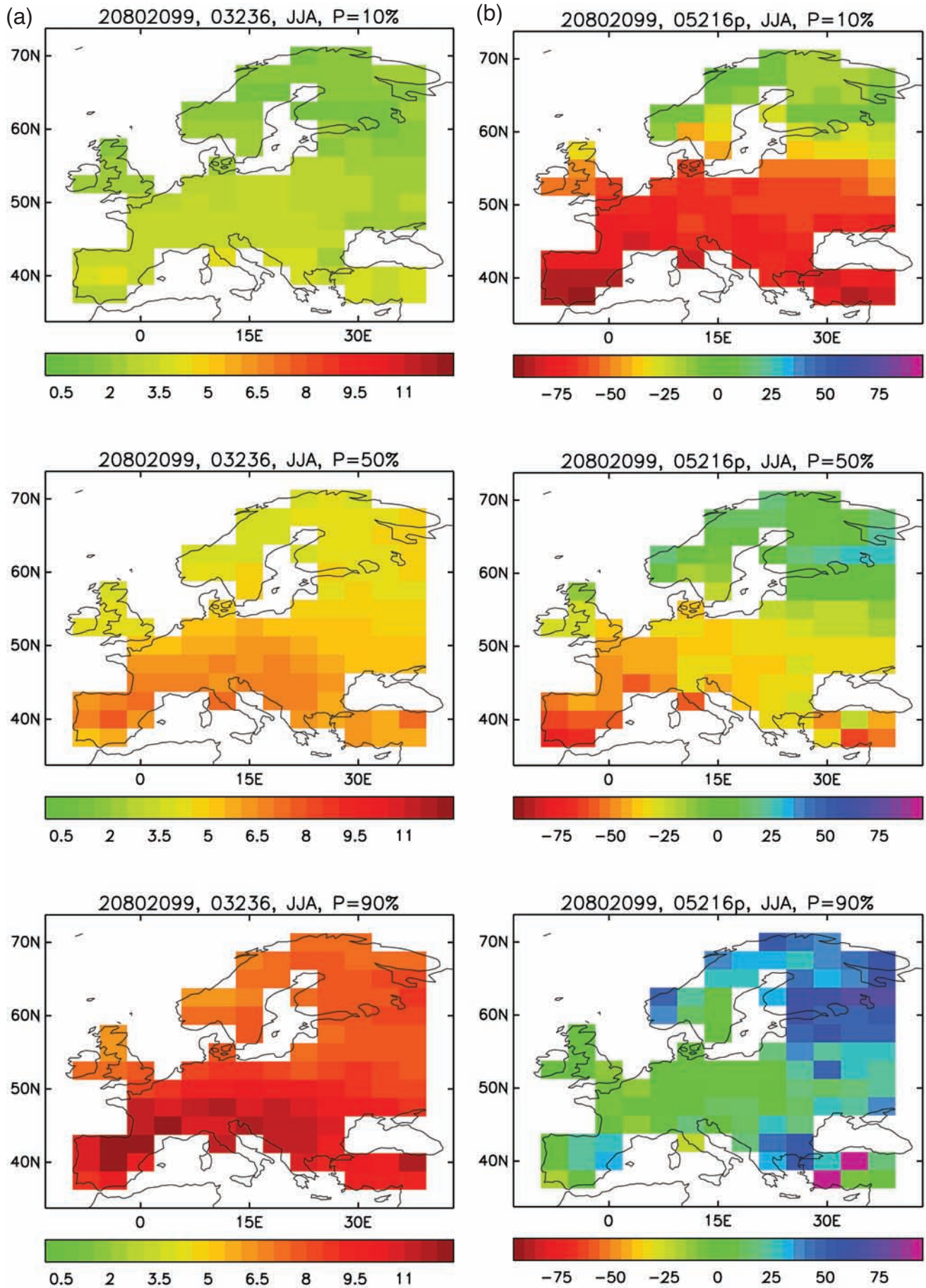


Figure 3.11: The ENSEMBLES probabilistic projections for Europe under the A1B emissions scenario. The maps show the 10% (top row), 50% (median; middle row) and 90% (bottom row) percentiles of (a) European surface temperature change and (b) European percentage precipitation change, for the summer season for the period 2080–2099 relative to the 1961–1990 baseline period.

Figure 3.12 shows alternative formats in which PDFs can be presented; in this case the distributions are for the Gulf of Finland grid box. Plumes show changes in temperature and precipitation through the 21st century under the A1B scenario. The data underlying these figures are supplied in numerical form in terms of 10,000 distribution sample points per grid box and can be presented as a contour plot in order to highlight potential relationships between variables. The data are available from http://ensembles-eu.metoffice.com/secure/RT6_data_230609/data_for_RT6.html.

3.3.3 Development of methodologies for interpreting ensembles using simple climate models

While ensembles of global climate model projections are needed to assess the effects of uncertainties in detailed Earth system processes, simpler models, constrained by observations and by the results of more complex models, have an important role to play in interpreting the implications of the results. Step (4) of Section 3.3.2 provides one such example. Oxford University carried out another study of this type, highlighting the difficulty of using climate sensitivity as the focal benchmark for climate policy. The non-linear relationship between climate sensitivity and any quantity that can be observed directly raises fundamental issues in the statistical interpretation of ensembles (Frame et al., 2005). The ENSEMBLES project has helped to elucidate these methodological issues, but many questions remain open.

This naturally raises the question of whether alternative benchmarks of climate system response might be more tractable: Allen et al. (2009) concluded that the peak warming response to a given total injection of carbon into the atmosphere was better constrained by observable quantities than the equilibrium response to a stabilisation scenario, and remarkably insensitive to the timing of carbon dioxide emissions. This is illustrated by Figure 3.13, which shows the warming induced by three CO₂ emission profiles, each of which involves a total cumulative emission of one trillion tonnes of carbon (the integrals under the three emission curves on the left are the same). The best-fit temperature responses (coloured lines in the right panel) are almost indistinguishable, dwarfed by the uncertainty in the response (grey shading). This raises the prospect of using cumulative carbon emissions as a policy benchmark; a highly policy-relevant output of ENSEMBLES research that has fed directly into the UNFCCC negotiations.

3.4 Summary

Research Theme 1 developed, assessed and applied new systems for seasonal–decadal forecasting, and for multi-decadal projections of climate change. Substantial effort has resulted in the production of improved climate and Earth system models, an improved database of ocean observations, and better methods of using these and other observations to initialise the models for near-term climate forecasts. In addition, there has been a major focus on methods for improved quantification of the inevitable uncertainties arising from model imperfections, as well as from internal climate variability.

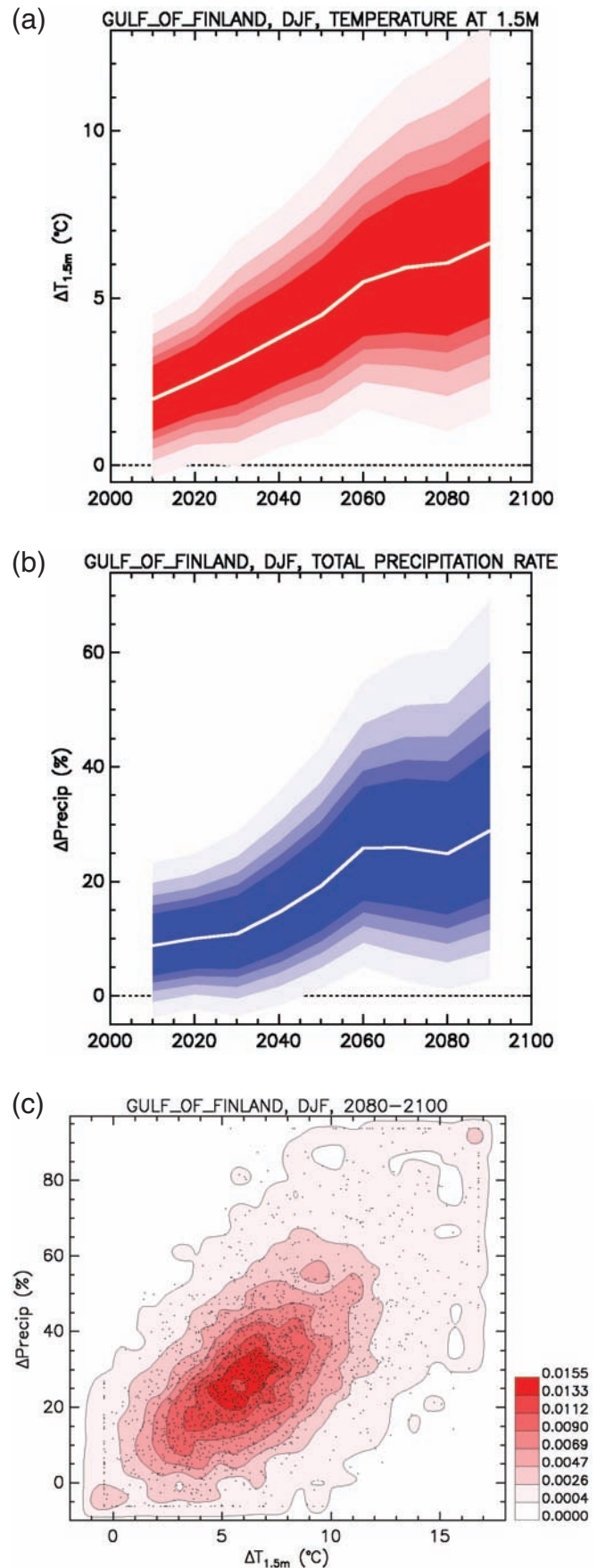


Figure 3.12: Evolution of the median (white curve) and the 50, 60, 70, 80 and 90% confidence ranges for: (a) 20-year mean winter surface temperature change for the Gulf of Finland grid point; (b) percentage change in 20-year mean winter precipitation for the Gulf of Finland; (c) contours of the Winsorised sampled joint probability distribution function for surface temperature change and percentage precipitation change for the winter season for the Gulf of Finland, for the period 2080–2099 relative to the 1961–1990 baseline period.

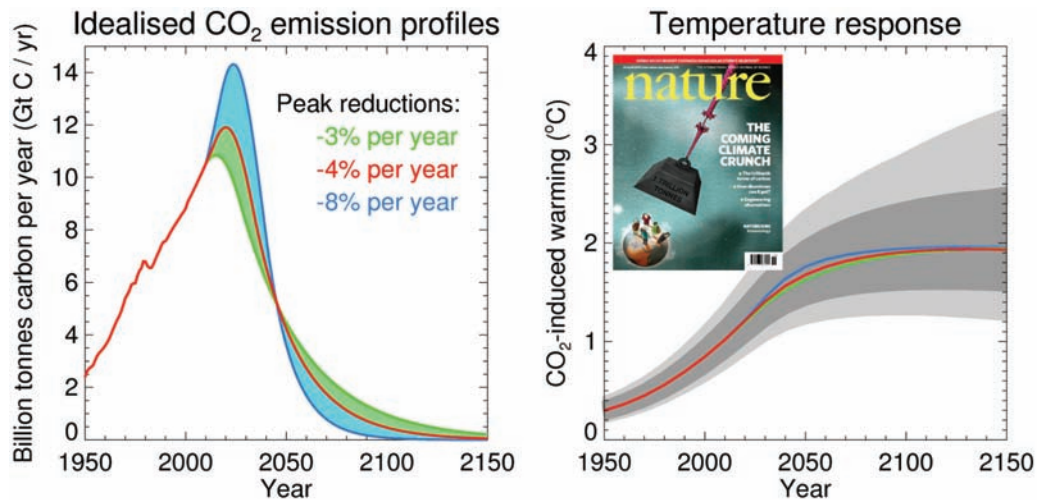


Figure 3.13: Warming (right panel) induced by three CO_2 emission profiles (left panel), each of which involves total cumulative emissions of one trillion tonnes of carbon (Allen et al., 2009).

As a result, ENSEMBLES has delivered three approaches for seasonal–decadal prediction, consisting of an updated method based on a multi-model ensemble of models drawn from different European modelling centres, plus two novel methodologies applying either stochastic or sustained perturbations to the outputs of physical parameterisation schemes in the atmospheric component of a single model. For seasonal–annual forecasts, the multi-model ensemble results demonstrate performance competitive with, and in some aspects superior to, the previous European system from DEMETER. The multi-model results also provide levels of hindcast skill and estimates of the associated uncertainties comparable to or (in some aspects) slightly better than those of the new methodologies. However, our demonstration that the stochastic physics and perturbed parameter methods can provide results of similar utility to multi-model hindcasts is itself a significant result, as there is the potential to optimise the design of such systems to improve performance in future; something that has not been attempted during ENSEMBLES. We also stress that care is needed in interpreting our results. The skill of different systems depends not just on the technique for sampling model uncertainty, but also on the baseline skill of the participating models, and the quality of the initialisation. For example, some of the improvements found in multi-model ensembles could arise from improved sampling of initial state uncertainties when different single-model ensembles are combined (Figure 3.1), as well as from better sampling of modelling uncertainties per se. Also, the three techniques for sampling modelling uncertainty are essentially complementary to one another, so should not be seen as competing alternatives: the multi-model approach samples structural variations in model formulation, but does not systematically explore parameter uncertainties for a given set of structural choices, whereas the perturbed parameter approach does the reverse. The stochastic physics approach recognises the uncertainty inherent in inferring the effects of parameterised processes from grid box average variables which cannot account for unresolved sub-grid-scale organisations in the modelled flow, whereas the other methods do not. There is likely to be scope to develop better prediction systems in future by combining aspects of the separate systems considered in ENSEMBLES.

The decadal hindcasts build on pioneering studies with individual models by several ENSEMBLES partners (Smith et al., 2007; Keenlyside et al., 2008; Pohlmann et al., 2009), and constitute the first coordinated international experiment in this area. Skill is found in projections of surface temperature at large regional scales, for multi-year averages out to a decade ahead. The skill is found to be greater for hindcasts started from more recent dates (1990s and later) compared with the 1960s–1980s, due mainly to the emerging climate change signal. Combining hindcasts from different model versions, in either multi-model or perturbed parameter ensembles, is found to increase skill, as is also the case in the seasonal–annual hindcasts. The added value of initialising hindcasts from observations was also assessed, finding evidence of a modest but potentially useful enhancement to the skill arising from forced climate change. A decadal forecast started from late 2005 shows enhanced warming in the Northern Hemisphere compared with uninitialised climate change projections; a feature supported by verification against observations for the period 2006–2009. The ENSEMBLES effort places European groups in the vanguard of emerging worldwide efforts to provide better information on climate variability and change for the decadal time-scale (Meehl et al., 2009), and this new arm of climate research is likely to develop significantly in future.

For decadal–centennial projections, a series of perturbed parameter ensembles were designed and run to sample uncertainties in key processes, sampling carbon cycle feedbacks in addition to uncertainties arising from surface and atmospheric feedbacks, ocean transport, and human-caused forcing from sulphate aerosols. The model simulations were processed using an advanced statistical framework designed to support the inference of probabilistic projections of real world systems from complex but imperfect models of those systems (Goldstein and Rougier, 2004; Rougier, 2007). The methodology allows us to produce thousands of plausible outcomes for 20-year average temperature and precipitation changes during the 21st century for Europe. The effects of structural model errors in atmospheric processes are accounted for by using the perturbed parameter ensembles to ‘predict’ the results of an ensemble of alternative

international climate models from the CMIP3 archive used in the IPCC AR4 assessment (Meehl et al., 2007), and the projections are also constrained by a multivariate set of observations of historical climate, consisting of time-averaged seasonal patterns of several key climate variables, plus historical changes in large-scale surface temperature patterns during the 20th century. This allows us to present changes at spatial scales resolved by global climate models (Figure 3.10), noting that the same methodology with an additional downscaling procedure has recently been used to provide probabilistic projections at 25 km resolution for the UK (Murphy et al., 2009). The projections should be interpreted as an attempt to quantify the relative probability of different future outcomes, consistent with climate modelling technology, physical understanding and observational evidence currently available. Inevitably they cannot account for errors common to all current climate models, or feedback processes yet to be discovered or not yet included in models (e.g., methane cycle processes). The results also depend on the chosen methodology, which includes expert choices such as the assumed prior distributions of plausible values for uncertain model parameters.

The probabilistic projections provide a much more comprehensive specification of uncertainties in future European climate than has been possible hitherto. However, there remains considerable scope to improve them in future. Ideally, several alternative methodologies of similar scope but different construction should be produced, to test further the robustness of the results. For example, RT1 included a limited comparison of perturbed parameter ensembles with different models (Figure

3.9); however, further work is needed in this area. The extension of initialised projections may offer possibilities to predict some aspects of internal climate variability beyond the seasonal–decadal time-scale considered in ENSEMBLES. Also, there is scope to extend the use of observational constraints to improve the techniques used to weight model projections. For example, Palmer et al. (2008) suggested that seasonal prediction errors could be used to calibrate long-term climate projections. This depends on the strength of the relationships between seasonal and longer-term prediction errors (a preliminary investigation in RT1 suggests that a limited relationship may exist), and the extent to which new information like this can provide constraints which add independent information to those already accounted for in projections such as those of Figure 3.10. More detailed evaluation of models at a process-based level (see Section 7) could also be exploited to provide additional constraints on physical climate feedbacks, while work is urgently needed to find methods of constraining the range of carbon cycle feedbacks. There is also clear potential for projections to change as a result of anticipated developments in the climate models themselves, for instance through the emergence of additional mechanisms of regional change from better resolution of processes such as stratosphere–troposphere interactions (Huebener et al., 2007). While the RT1 projections of future climate change provide a state-of-the-art expression of uncertainties based on current knowledge, it is nevertheless vital that users maintain an active dialogue with climate scientists to keep the results under review, and also that updated projections are developed in future to take account of improved models and methods.

References

ENSEMBLES publications are highlighted as bold text.

- Allen, M., N. Andronova, B. Booth, S. Dessai, D. Frame, C. Forest, J. Gregory, G. Hegerl, R. Knutti, C. Piani, D. Sexton and D. Stainforth (2006): Observational constraints on climate sensitivity. In: *Avoiding dangerous climate change* [Schellnhuber, H.J., et al. (eds.)]. Cambridge University Press, New York, NY, pp. 391–427.
- Allen MR, Frame DJ, Huntingford C, Jones CD, Lowe JA, Meinshausen M, Meinshausen N, 2009. Warming caused by cumulative carbon emissions towards the trillionth tonne. *Nature* 458, 1163–1166.**
- Berner J, Doblas-Reyes FJ, Palmer TN, Shutts G, Weisheimer A, 2008. Impact of a quasi-stochastic cellular automaton backscatter scheme on the systematic error and seasonal prediction skill of a global climate model. *Philosophical Transactions of the Royal Society A* 366, 2561–2579.**
- Booth BBB, Jones CD, Collins M, Totterdell IJ, Cox PM, Sitch S, Huntingford C, Betts R. 2009. Global warming uncertainties due to carbon cycle feedbacks exceed those due to CO₂ emissions. *Nature* submitted
- Brierley CM, Collins M, Thorpe AJ, 2009b. The impact of perturbations to ocean–model parameters on climate and climate change in a coupled model. *Climate Dynamics*, doi:10.1007/s00382-008-0486-3.**
- Brierley CM, Thorpe AJ, Collins M, 2009a. An example of the dependence of the transient climate response on the temperature of the modelled climate state. *Atmospheric Science Letters* 10, 23–28.**
- Collins M, Booth BBB, Bhaskaran B, Harris GR, Murphy JM, Sexton DMH, Webb MJ, 2009. Climate model errors, feedbacks and forcings: a comparison of perturbed physics and multi-model ensembles. In preparation.**
- Collins M, Booth BBB, Harris GR, Murphy JM, Sexton DMH, Webb MJ, 2006. Towards quantifying uncertainty in transient climate change. *Climate Dynamics* 27, 127–147.
- Collins M, Brierley CM, MacVean M, Booth BBB, Harris GR, 2007. The sensitivity of the rate of transient climate change to ocean physics perturbations. *Journal of Climate* 20, 2315–2320.**
- Doblas-Reyes FJ, Weisheimer A, Déqué M, Keenlyside N, McVean M, Murphy JM, Rogel P, Smith D, Palmer TN, 2009. Addressing model uncertainty in seasonal and annual dynamical ensemble forecasts. *Quarterly Journal of the Royal Meteorological Society* 135, 1538–1559.**
- Domingues CM, Church JA, White NJ, Gleckler PJ, Wijffels SE, Barker PM, Dunn JR, 2008. Improved estimates of upper-ocean warming and multi-decadal sea-level rise. *Nature* 453, 1090–1094.
- Ferro CAT, 2007. Comparing probabilistic forecasting systems with the Brier score. *Weather Forecasting* 22, 1076–1088.
- Frame DJ, Booth BBB, Kettleborough JA, Stainforth DA, Gregory JM, Collins M, Allen MR, 2005. Constraining climate forecasts: the role of prior assumptions. *Geophysical Research Letters* 32, L09702, doi:10.1029/2004gl022241.**
- Friedlingstein P, Cox P, Betts R, Bopp L, von Bloh W, Brovkin V, Cadule P, Doney S, Eby M, Fung I, Bala G, John J, Jones C, Joos F, Kato T, Kawamiya M, Knorr W, Lindsay K, Matthews HD, Raddatz T, Rayner P, Reick C, Roeckner E, Schnitzler K-

- G, Schnur R, Strassmann K, Weaver AJ, Yoshikawa C, Zeng N, 2006. Climate carbon cycle feedback analysis: results from the C4MIP model intercomparison. *Journal of Climatology* 19, 3337–3353.
- Giorgi F, Francisco R, 2000. Uncertainties in regional climate change prediction: a regional analysis of ensemble simulations with the HADCM2 coupled AOGCM, *Climate Dynamics* 16, 169–182.
- Goldstein M, Rougier JC, 2004. Probabilistic formulations for transferring inferences from mathematical models to physical systems. *SIAM Journal of the Science of Computing* 26, 467–487.
- Harris GR, Collins M, Sexton DMH, Murphy JM, 2009. Probabilistic Predictions for 21st Century European Climate. ENSEMBLES Deliverable D1.15.**
- Harris GR, Sexton DMH, Booth BBB, Collins M, Murphy JM, Webb MJ, 2006. Frequency distributions of transient regional climate change from perturbed physics ensembles of General Circulation Model simulations. *Climate Dynamics* 27, 357–375.**
- Huebener H, Cubasch U, Langematz U, Spanghel T, Niehorster F, Fast I, Kunze M, 2007. Ensemble climate simulations using a fully coupled ocean–troposphere–stratosphere general circulation model. *Philosophical Transactions of the Royal Society A* 365, 2089–2101.
- Ingleby B, Huddleston M, 2007. Quality control of ocean temperature and salinity profiles: historical and real-time data. *Journal of Marine Systems* 65, 148–175.**
- Keenlyside NS, Latif M, Jungclaus J, Kornblueh L, Roeckner E, 2008. Advancing decadal-scale climate prediction in the North Atlantic sector. *Nature* 453, 84–88.**
- Meehl GA, Stocker TF, Collins WD, Friedlingstein P, Gaye AT, Gregory JM, Kitoh A, Knutti R, Murphy JM, Noda A, Raper SCB, Watterson IG, Weaver AJ, Zhao Z-C, 2007. Global climate projections. In: *Climate Change 2007: The Physical Science Basis. Contribution of Working Group I to the Fourth Assessment Report of the Intergovernmental Panel on Climate Change* (S Solomon, D Qin, M Manning, Z Chen, M Marquis, KB Averyt, M Tignor, HL Miller, eds). Cambridge University Press, Cambridge UK and New York, 747–845.
- Meehl, GA, Goddard L, Murphy J, Stouffer RJ, Boer G, Danabasoglu G, Dixon K, Giorgetta MA, Greene AM, Hawkins E, Hegerl G, Karoly D, Keenlyside N, Kimoto M, Kirtman B, Navarra A, Pulwarty R, Smith D, Stammer D, Stockdale T, 2009. Decadal prediction: can it be skillful? *Bulletin of the American Meteorological Society*, doi:10.1175/2009 BAMS 2778.1.
- Murphy JM, Booth BBB, Collins M, Harris GR, Sexton DMH, Webb MJ, 2007. A methodology for probabilistic predictions of regional climate change from perturbed physics ensembles. *Philosophical Transactions of the Royal Society A* 365, 1993–2028.**
- Murphy JM, Sexton DMH, Barnett DN, Jones GS, Webb MJ, Collins M, Stainforth DA, 2004. Quantification of modelling uncertainties in a large ensemble of climate change simulations. *Nature* 430, 768–772.
- Murphy JM, Sexton DMH, Jenkins GJ, Boorman PM, Booth BBB, Brown CC, Clark RT, Collins M, Harris GR, Kendon EJ, Betts RA, Brown SJ, Howard TP, Humphrey KA, McCarthy MP, McDonald RE, Stephens A, Wallace C, Warren R, Wilby R, Wood RA, 2009. UK Climate Projections Science Report: Climate Change Projections. Met Office Hadley Centre, Exeter, UK.
- Niehorster F, 2009. PhD Thesis. Unsicherheiten in Rueckkopplungsmechanismen in Klimaaenderungsprojektionen (Uncertainty in Feedback Mechanisms in Climate Change Projections). Freie Universität Berlin.**
- Palmer TN and co-authors, 2004. Development of a European multi-model ensemble system for seasonal—to interannual prediction (DEMETER). *Bulletin of the American Meteorological Society* 85, 853–872.
- Palmer TN, 2001. A nonlinear dynamical perspective on model error: a proposal for non-local stochastic–dynamic parametrisation in weather and climate prediction. *Quarterly Journal of the Royal Meteorological Society* 127, 279–304.
- Palmer TN, Doblas-Reyes FJ, Weisheimer A, Rodwell MJ, 2008. Toward seamless prediction: calibration of climate change projections using seasonal forecasts. *Bulletin of the American Meteorological Society* 89, 459–470.**
- Pohlmann H, Jungclaus JH, Köhl A, Stammer D, Marotzke J, 2009. Initializing decadal climate predictions with the GECCO oceanic synthesis: effects on the North Atlantic. *Journal of Climate* 22, 3926–3938.
- Rougier JC, 2007. Probabilistic inference for future climate using an ensemble of climate model evaluations. *Climate Change* 81, 247–264.
- Smith DM, Cusack S, Colman AW, Folland CK, Harris GR, Murphy JM, 2007. Improved surface temperature prediction for the coming decade from a global climate model. *Science* 317, 796–799.
- Stainforth DA, Aina T, Christensen C, Collins M, Faull N, Frame DJ, Kettleborough JA, Knight S, Martin A, Murphy JM, C. Piani, D. Sexton, L. A. Smith, R.A. Spicer, A. J. Thorpe, M. R. Allen 2005. Uncertainty in predictions of the climate response to rising levels of greenhouse gases. *Nature* 433, 403–406.
- Tebaldi C, Knutti R, 2007. The use of multi-model ensembles in probabilistic climate projections. *Philosophical Transactions of the Royal Society A* 365, 2053–2076.
- Webb MJ, Senior CA, Sexton DMH, Ingram WJ, Williams KD, Ringer MA, McAvaney BJ, Colman R, Soden BJ, Gudgel R, Knutson T, Emori S, Ogura T, Tsushima Y, Andronova N, Li B, Musat I, Bony S, Taylor KE, 2006. On the contribution of local feedback mechanisms to the range of climate sensitivity in two GCM ensembles. *Climate Dynamics* 27, 17–38.**
- Weisheimer A, Doblas-Reyes F, Rogel P, Da Costa E, Keenlyside N, Balmaseda M, Murphy J, Smith D, Collins M, Bhaskaran B, Palmer T, 2007. Initialisation Strategies for Decadal Hindcasts for the 1960–2005 Period within the ENSEMBLES Project. ECMWF Technical Memorandum 521.**
- Weisheimer A, Doblas-Reyes FJ, Palmer TN, Alessandri A, Arribas A, Déqué M, Keenlyside N, MacVean M, Navarra A, Rogel P, 2009. ENSEMBLES – a new multi-model ensemble for seasonal-to-annual predictions: skill and progress beyond DEMETER in forecasting tropical Pacific SSTs. *Geophysical Research Letters*, submitted.**
- Wijffels SE, Willis J, Domingues CM, Barker P, White NJ, Gronell A, Ridgway K, Church JA, 2008. Changing expendable bathythermograph fallrates and their impact on estimates of thermosteric sea level rise. *Journal of Climate* 21, 5657–5672.
- Yokohata T, Webb MJ, Collins M, Williams KD, Yoshimori M, Hargreaves JC, Annan JD, 2009. Structural similarities and differences in climate responses to CO₂ increase between two perturbed physics ensembles. *Journal of Climate*, submitted.**

4 Production of seasonal to decadal hindcasts and climate change scenarios [Research Theme 2A]

J-F. Royer (CNRM), E. Roeckner (MPIMET), U. Cubasch (FUB), F. Doblas-Reyes (ECMWF), H-D. Hollweg (MPIMET-MD), T. Johns (Met Office), W. May (DMI), D. van Vuuren (PBL)

4.1 Introduction

4.1.1 Background and linkages

One of the prerequisites for all studies of climate change and its consequences is the existence of climate simulations at the global scale from which coherent atmospheric, oceanic or surface field time-series can be extracted for further modelling or statistical studies. Though such global simulations are produced for assessment by the IPCC, the constraints of such a wide international exercise do not allow the flexibility and interaction in the choice of scenarios and the storage of datasets featured in the ENSEMBLES project. Therefore the production of a coordinated new set of global climate simulations with all the most advanced European climate models was considered to be an essential part of the ENSEMBLES project. This production was then defined as the main and central task of a dedicated Research Theme 2A (RT2A). Such global simulations have direct interactions with several of the other Research Themes, since their results are needed as lateral boundary conditions and forcing fields for driving the regional model simulations (RT2B and RT3), in validation studies (RT5), studies of feedbacks in the Earth system (RT4), or climate change impact studies (RT6). An ambitious objective of the project was to develop, in collaboration with RT7, a new stabilisation scenario corresponding to the European climate policy (called the E1 scenario) and then apply it in the second stream of simulations using the improved versions of the Earth system models developed in RT1. However, this objective could only be planned for the end of the project, since it needed input from two other Research Themes (RT1 and RT7). In order to be able to provide results for use by the other Research Themes, a first set of simulations (Stream 1) was performed during the first two years of the project, based on the then available versions of the climate model and using the IPCC scenarios and methodology.

4.1.2 Work completed

The European global modelling groups contributing to ENSEMBLES all developed global climate models coupling the key components of the climate system (atmosphere, ocean, sea ice), which participated in the assessment of climate simulations by the IPCC for its Fourth Assessment Report (AR4). Some also developed additional model components, such as carbon cycle or aerosol transport. The ENSEMBLES project first offered the opportunity to better coordinate the European participation to the AR4, and then to extend the modelling effort beyond the AR4 by carrying out a second set of simulations (Stream 2) using

improved models and also by defining a new stabilisation scenario. The coordination of the simulations allowed a detailed definition of the set of simulations and the forcings to be used by the European models in the AR4. Effort was made in complementing the data storage at the IPCC database at PCMDI, by identifying further high-resolution datasets that would be most useful for subsequent analyses of the climate processes, and for potential impact studies by various user groups. The high volume of the datasets required storage at established and reliable database centres such as ECMWF for the seasonal simulations, and CERA for the climate scenarios. Furthermore a very significant effort was needed from the modelling groups in terms of further data processing of their simulations to extract the required fields and convert them to the common format appropriate for the databases.

Initially all time-scales from seasonal to centennial were included in the RT2A Research Theme. However, a large part of the new developments for the seasonal to decadal prediction have been made in the framework of another Work Package (RT1), and although the production of the bulk of the seasonal to decadal simulations were part of the modelling effort of RT2A, they have also been defined in close collaboration with RT1, and their results have been regrouped and reported in the RT1 description of a ‘seasonal–decadal prediction system’ (see Section 3.2). Only the storage of the resulting dataset will be reported here. This section therefore deals essentially with the centennial simulations.

The global multi-decadal simulations were divided into two separate Work Packages according to time and the type of forcings to be used. The first Work Package was for the historical simulations using observed forcings. The second Work Package was for future simulations using forcings from a few selected projections based on socio-economic scenarios. The most straightforward approach to estimating the uncertainties due to current model formulations in climate simulations is simply to run a set of simulations with different state-of-the-art models using the same experimental set-up and identical forcings. This multi-model approach has produced a coherent set of climate simulations which can be further processed in various ways to define statistical distributions of the climate response and apply different statistical methods to assess the probability of climate changes. In order to reduce the other possible sources of differences between the simulations, a particular effort was made to carefully define the experiments to be performed and the forcings to be used by the climate models, so that the difference between the results could be fully attributable to differences in the models themselves, so as to allow an estimation of model uncertainties.

4.2 Description of the forcings used in the ENSEMBLES multi-decadal simulations

4.2.1 Design of forcings

The design of the experiments was made in such a way as to avoid the so-called ‘cold start’ problem which may arise when the coupled models start from an initial condition in which the atmosphere and ocean are not satisfactorily balanced, which usually leads to a climate drift of several decades until a new quasi-equilibrium has been reached. This drift period has to be removed from the actual climate simulations as it could interfere with the climate change one wants to simulate. In order to eliminate this problem, a careful methodology has been devised for the ENSEMBLES global simulations. Each model started the simulations from a condition of constant atmospheric concentrations for greenhouse gases corresponding to a pre-industrial state for which a climate equilibrium can be assumed. The interest of a control pre-industrial simulation is to provide a reference on the simulated climate regime in the absence of anthropogenic interference, and to provide balanced initial conditions from which to start historical simulations with the observed changes in the external forcings. The observed values of the forcing corresponding to the year 1860 were chosen as boundary conditions for the pre-industrial control simulation.

The external forcings that have been considered are of two different kinds.

- The natural forcings that result from solar and volcanic variability. These forcings can be specified for the past based on suitable observations; however, there is currently no generally accepted method to predict their future evolution.
- The anthropogenic forcings due to the emission of greenhouse gases and sulphate aerosols, and optionally those due to land-use changes. For simulations of the future climate, the usual procedure that has been applied in previous IPCC assessments is to compute the future changes with the help of so-called integrated impact assessment models for predefined economic development scenarios. The economic scenarios retained by the IPCC AR4 for the CMIP3 modelling experiments were the SRES marker scenarios A2, A1B and B1 (see Nakicenovic and Swart, 2000). These scenarios have been applied for the Stream 1 simulations in ENSEMBLES so that they could contribute to the IPCC CMIP3 simulations.

Over the period 1860–2000, two different simulations have been performed using the observed forcings.

- *A first simulation* with only the anthropogenic forcings. This simulation has been used as a starting point for the future climate scenarios, in order to have a continuous simulation for the past and the future, without any discontinuity or inhomogeneity. Care was taken in defining the concentration series for the main greenhouse gases with a smooth annual interpolation between the observed values for the past years and the future values specified for the different IPCC scenarios. The series of carbon dioxide (CO₂), methane (CH₄), nitrogen oxide (N₂O) and chlorofluorocarbon CFC-12 have been interpolated at annual resolution. The radiative forcing resulting from all the other halogenated species except CFC-12 has been converted into the CFC-11 concentration giving the same radiative forcing.

- *A second simulation* using, in addition to the anthropogenic forcings of the first simulation, the observed natural forcings due to solar and volcanic variability. This simulation was mainly used to assess the effect of natural forcings and for comparison with observed climate series, and extended up to the year 2000. The natural forcings were specified according to the solar irradiance proposed by Solanki and Krivova (2003), and an updated version of Sato et al. (1993) for volcanic forcing.

In order to provide a contribution to the IPCC CMIP3 simulations for the AR4, all the ENSEMBLES Stream 1 simulations were run over 2000–2100 with the recommended SRES scenarios (A2, A1B, B1). In addition, other optional simulations in CMIP3 (1%/year CO₂ increase until 2×CO₂ and 4×CO₂, committed simulation with constant 2000 concentration, continuation of the scenarios A1B and B1 with constant concentrations beyond 2100) were also performed with most of the models.

4.2.2 Stream 2 forcings

The same methodology was used for the ENSEMBLES Stream 2 simulations, in which the models with a carbon cycle were also driven by the atmospheric CO₂ concentrations (observed and specified in the different scenarios) and the carbon cycle computations used to diagnose the implied fluxes between the different carbon reservoirs. The main differences were mainly from changes in the models, the introduction in most of the models of the land-use changes in Stream 2 (versus a single model in Stream 1), and the choice of different scenarios.

In Stream 2 only two main scenarios were considered. First, a rehearsal of the A1B scenario with new versions of the models in order to extend the size of simulations for this scenario, which is considered the most likely in the absence of a climate policy. Secondly, a new stabilisation scenario based on climate policy measures to limit the radiative forcing to that equivalent to 450 ppm of CO₂ (scenario E1). The construction of this scenario is described in more detail later.

The different scenarios considered in ENSEMBLES span a large variety of greenhouse gas concentration evolution trajectories for the future and illustrate the large uncertainties due to different possible options to be considered in future development paths (Figure 4.1).

Besides the well-mixed greenhouse gas concentration, other forcings maps were provided for the distribution of ozone concentrations, sulphate aerosols, and land use.

4.3 Production and results of the Stream 1 IPCC simulations

The modelling groups involved (CNRM, DMI, IPSL, METOHC, MPIMET, NERSC and FUB) performed the Stream 1 simulations using the common set of agreed forcings for the historical simulations over the period 1860–2000, and for the three recommended IPCC scenarios A2, A1B and B1 over the

21st century. Some simulations were extended beyond the year 2100 with constant atmospheric concentrations from the B1 and A1B scenarios. Additional simulations with a 1% increase of CO₂ per year with stabilisation at 2×CO₂ and 4×CO₂ were also performed.

A summary of the different atmosphere–ocean model combinations used in the RT2A Stream 1 simulations is shown in Table 4.1. Table 4.2 gives an overview of the availability of the Stream 1 simulations that contributed to the multi-model ensemble developed in the project.

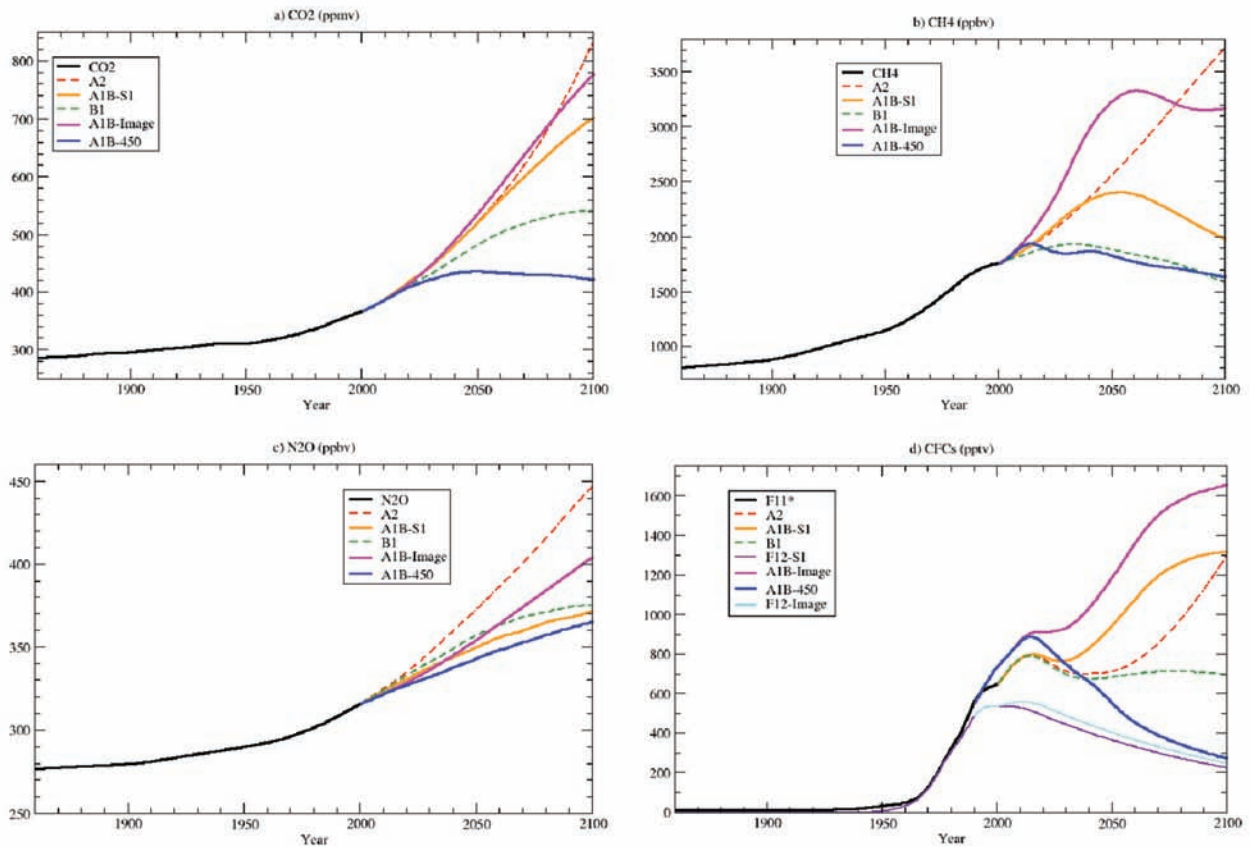


Figure 4.1: Evolution of the greenhouse gas concentrations for the historical period 1860–2000 and for the different scenarios: A2, A1B-S1 and B1 are the IPCC SRES marker scenarios used in Stream 1; A1B-Image and A1B-450 (E1) are the new Stream 2 scenarios with emissions produced by the IMAGE integrated assessment model.

Table 4.1: Summary of the main features of the models used in Stream 1.

Partner	Model	Atmosphere	Resolution l	Levels	Ocean	Resolution	Levels
METO-HC	HadCM3	HadAM3	2.5×3.75°	19	HadGOM1	1.25×1.25	20
	HadGEM1	HadGAM1	1.25×1.875°	38			
IPSL+UCL-ASTR	IPSL-CM4	LMDZ-4	2.5×3.75°	19	OPA8.1	0.5–2°	31
MPIMET+DMI	ECHAM5/MPI-OM	ECHAM5	T63	31	MPI-OM	1.5°	40
INGV-SX	INGV-CMCC	ECHAM4.6	T106	19	OPA8.2	0.5–2°	31
FUB	EGMAM	ECHAM4-MA	T30	19/39	HOPE-G	0.5–2.8°	20
CNRM	CNRM-CM3	ARPEGE V3	T63	45	OPA8	0.5–2°	31
NERSC	BCM2	ARPEGE V3	T63	31	MICOM 2.8 (modified)	1.5°	35

Table 4.2: The multi-model simulations performed in ENSEMBLES Stream 1. The symbol • denotes an available simulation, and the figure after it denotes the size of the ensemble in case an ensemble of several similar simulations is available. The columns are: GA – historical forcing by GHGs and aerosols; +SV – the addition of solar and volcanic forcing, ‘other’ – other combinations of forcings; B1, A1B and A2 – the SRES 2000–2100 scenarios; 1% CO₂ are the simulations with 1%/year increase in CO₂ up until two or four times its pre-industrial concentration.

Models	1860–2000 (20CM3)			SRES Scenarios			1%/year CO ₂	
	GA	GA+SV	other	B1	A1B	A2	2×CO ₂	4×CO ₂
HadGEM1	•3	•3	•2	•	•	•	•	•
IPSL-CM4	•	•	•	•	•	••	•	•
ECHAM5+DMI	•3	•2	•3	•3	•3	•3	•	•
EGMAM	•3	•	•	•3	•3	•3	•	•
INGV-CMCC	•				•	•	•	•
CNRM-CM3	•	•		•	•	•	•	•
BCM2	•	•		•	•	•	•	•

ANN ΔT A1B (2070/99) – 20C3M (1961/90)

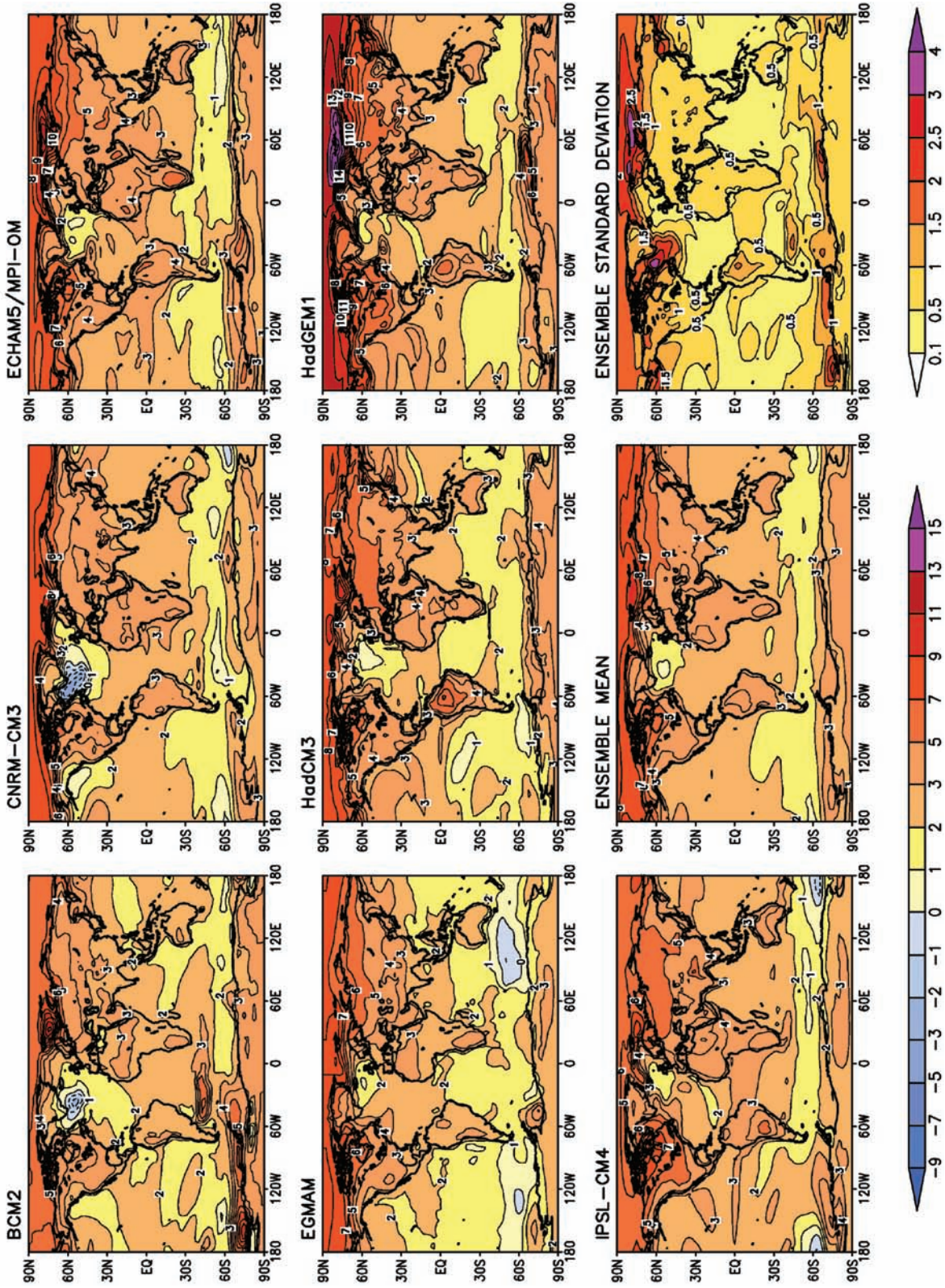


Figure 4.2: Annual mean surface air temperature change (K) for the ‘medium emission’ scenario A1B and the time period 2070–2099 relative to the 1961–1990 mean for individual models as well as the multi-model ensemble mean and inter-model standard deviation of projected changes as a measure of ensemble spread. The ECHAM5/MPI-OM and EGMAM modelled temperature change averaged over three realisations is shown. The left colour bar refers to the temperature anomalies, the right colour bar refers to the standard deviation.

4.3.1 Results of the Stream 1 simulations

The Stream 1 ENSEMBLES simulations have provided a major contribution of the European modelling groups to the IPCC AR4 assessment. These simulations are generally of high quality and can be used as a representative basis for studying the climate response to increasing greenhouse gases. Some basic results for the temperature and precipitation are provided as an illustration of the projected changes.

4.3.2 Temperature projections

A robust picture of temperature changes among the contributing models was found, with the largest temperature increase occurring over the Arctic in boreal winter, little warming over the Southern Ocean, and larger warming over land than over ocean (Figure 4.2). In boreal summer the warming is more confined to continents and sea-ice-covered areas of the Southern Ocean. The patterns of change were found to be similar for different scenarios, with the most pronounced warming in A2.

4.3.3 Precipitation projections

All models simulate a global mean precipitation rise, but with a weaker signal-to-noise ratio than for the temperature signal. As an example of the larger uncertainty in precipitation response, Figure 4.3 shows the geographical distribution of the number of models with simulated precipitation increase. In general, precipitation increases along the intertropical convergence zone (ITCZ) and decreases in the subtropics. A robust feature across all models is the mid- to high-latitude precipitation increase (which is most pronounced during winter in each hemisphere) associated with increased water-holding capacity of the warmer atmosphere and poleward moisture transport. In winter (DJF), precipitation is reduced over Central America, North Africa and the Mediterranean. In summer (JJA), the precipitation reduction over continents is more widespread. The drying in the Mediterranean extends further northward and eastward. A large precipitation reduction is seen over the Caribbean Sea and parts of North America. The monsoon in South and East Asia intensifies.

4.3.4 Other results

Higher-resolution simulations for particular time-slices were also produced. A 30-year time-slice experiment over the periods 1961–1990 and 2071–2100 for the A1B scenario was carried out at DMI at an enhanced horizontal resolution (T159) using their DKCM-A GCM with the dynamical core from the ARPEGE and the physical parameterisations from the ECHAM5 model. A multi-decadal simulation was performed at the University of Reading with a high-resolution version of the Hadley Centre’s coupled model, (HiGEM: atmosphere 1° resolution, ocean 1/3°). A version of the model with even higher resolution in the atmosphere (NUGEM, 0.6°) has been developed on the Earth simulator. The results have confirmed that resolution in both the atmosphere and the ocean is important for capturing important phenomena such as El Niño.

The results of the Stream 1 simulations were provided to the CMIP3 database at PCMDI, and their analyses in a large number of diagnostic sub-projects provided an essential contribution to the IPCC Fourth Assessment reports, in particular to the Working Group I Report entitled ‘The Physical Science Basis’ (IPCC, 2007).

The models and simulations have been presented in a number of publications by the different modelling groups: METO-HC (Johns et al., 2006; Martin et al., 2006; Ringer et al., 2006; Stott et al., 2006), MPIMET (Brasseur and Roeckner, 2005; Roeckner et al., 2006; Hagemann et al., 2009), DMI (May, 2008), IPSL (Dufresne et al., 2005), FUB (Huebener et al., 2006), CNRM (Salas y Mélia et al., 2005). The Stream 1 simulations have also been analysed with regard to different research topics: Sea-ice cover (Arzel et al., 2006; McLaren et al., 2006), radiation budget at high northern latitudes (Sorteberg et al., 2007), evolution of the Arctic freshwater balance (Guemas and Salas-Mélia, 2008a, 2008b), ENSO teleconnections (Müller and Roeckner, 2006, 2008; Joly and Voltaire, 2009), influence of Eurasian snow cover on Indian monsoon (Peings and Douville, 2009), storm tracks (Bengtsson et al., 2006), response of precipitation over land (Douville, 2006; Douville et al., 2006), precipitation trend analysis (Good and Lowe, 2006), extreme events (Chauvin and Denvil, 2007; Sillmann and Roeckner, 2008; Royer et al., 2008), carbon cycle and sulphate aerosol effects and feedbacks (Brasseur and Roeckner, 2005; Crueger et al., 2007). Further analyses of these simulations are reported in other sections, especially for RT4 and RT5.

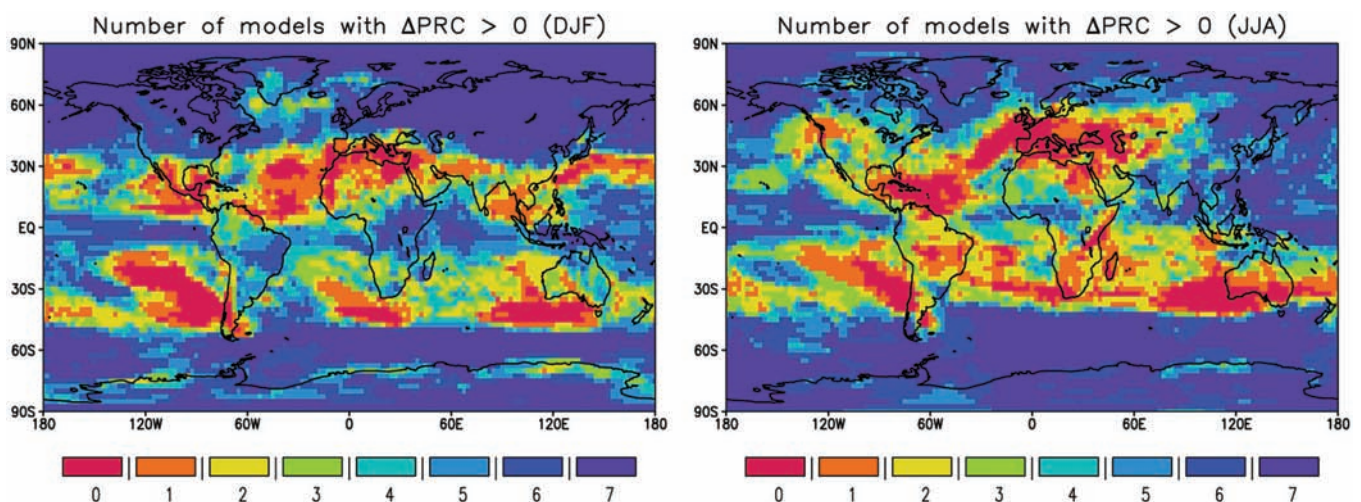


Figure 4.3: The number of models (0='none', 7='all') that simulate a precipitation increase for 2070–2099 in comparison with 1961–1990 for the SRES A1B scenario in winter (DJF, left) and summer (JJA, right).

4.4 The E1 greenhouse gas emissions scenario

4.4.1 Introduction

The IPCC SRES (Special Report on Emissions Scenarios) scenarios (Nakicenovic and Swart, 2000) have been extensively used for climate and impacts modelling. These scenarios, however, do not include climate policy. Recently, attention has focused on scenarios that aim to reach radiative forcing targets below 3 W/m^2 in 2100 (van Vuuren et al., 2007). Such scenarios would be able to keep global mean temperature increase below 2°C with a probability higher than 50%. A stated aim of the EC is to keep anthropogenic warming below 2°C by 2100, and the ENSEMBLES project included the development of a stabilisation scenario to help investigate this area of climate research.

Method for developing the E1 scenario

For the ENSEMBLES project, a scenario based on the SRES A1B scenario but aiming for 2.9 W/m^2 in 2100 was developed, called E1 (Lowe et al., 2009). The E1 scenario has an emissions peak around 2010 and eventually stabilises at 450 ppm CO_2 -equivalent in the 22nd century. Low stabilisation targets are mostly reached via so-called overshoot emission profiles – based on cost considerations (den Elzen and van Vuuren, 2007). The E1 scenario was developed using the IMAGE 2.4 Integrated Assessment Model, which simulates in detail the energy system, land use and carbon cycle (MNP, 2006; van Vuuren et al., 2007). Emissions and the energy system are described for seventeen world regions. Land use is modelled at 0.5×0.5 degrees. Emission reduction comes from changes to the energy system, non- CO_2 gases and carbon plantations. The modelling framework determines which emission reduction options are used on the basis of minimising abatement costs. An increase in agricultural productivity, slowing down of deforestation rates, and allowing greater bioenergy production was also included. The E1 scenario starting point was concentrations/forcings which were then reverse-engineered for emissions

and forward-modelled to temperatures. This methodology can help reduce uncertainty from more traditional linear approaches to scenarios and modelling. This is the same as the methodology currently being developed by the IPCC for its Fifth Assessment Report, and the work done in ENSEMBLES should help inform the work of the IPCC.

In order to meet a 2.9 W/m^2 target in 2100, CO_2 emissions peak in 2010 and then decline to almost zero by the end of the century (Figure 4.4). Implementing such large-scale emission reductions is only likely to occur through a large-scale political consensus. The largest contribution to reducing radiative forcing comes from reducing CO_2 emission from energy production. This is mainly reduced through the introduction of carbon capture and storage (CCS), energy efficiency, and the use of bioenergy.

Information for the climate models

The results of the E1 scenario have been made available for the climate modelling community. Specifically, information was forwarded on concentrations of well-mixed greenhouse gases, gridded information on air pollutants, and land-use maps (both at $0.5 \times 0.5^\circ$). Historical reconstructions for cropland (Ramankutty and Foley, 1999) and pasture from the HYDE dataset (Klein Goldewijk, 2001) have been used to produce maps of the proportion of grid-cells covered by cropland and pasture on a $0.5 \times 0.5^\circ$ global grid until 1992, and harmonised afterwards with the changes in land-use computed by the IMAGE scenario in order to ensure consistency between past and future changes.

For ozone and aerosol concentrations (as opposed to precursor emissions), some additional offline chemical transport modelling work has been required to generate the forcing datasets. Ozone data have been computed at UiO from the Oslo-CTM2 chemical transport model (Søvde et al., 2008) (horizontal resolution T21; vertical resolution L60; upper bound at 0.1 hPa) as monthly mean global-gridded three-dimensional files for emissions of ozone depleting substances of the years 1850, 1900, 1950, 1980, 2000,

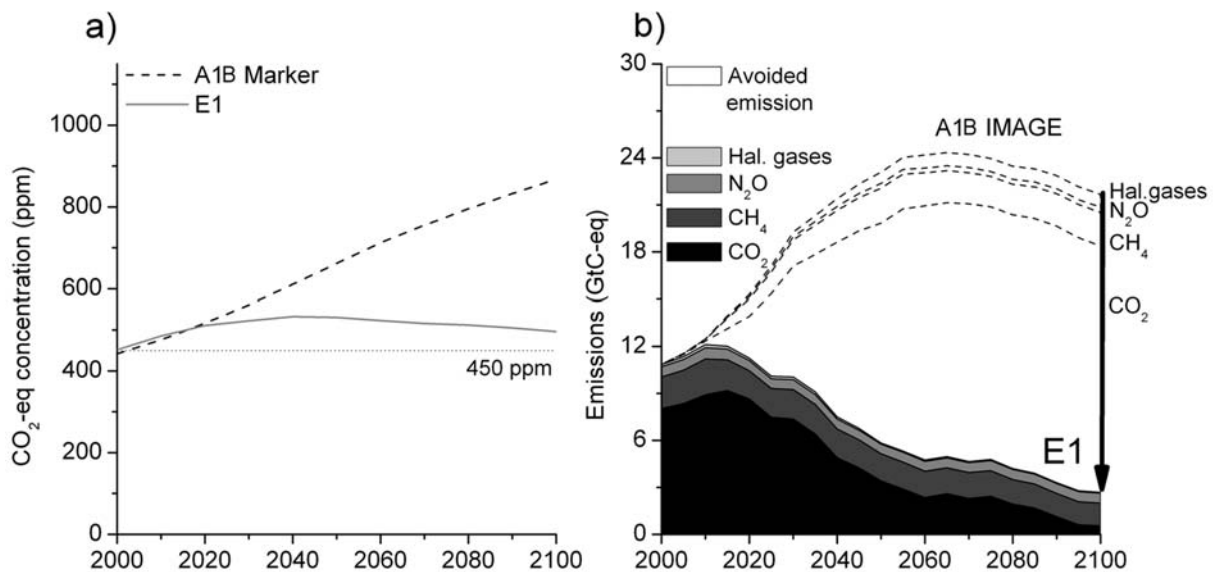


Figure 4.4: The CO_2 equivalent concentration pathways (based on Kyoto gases) (a) and the emissions and emission reductions (b) in the A1B and E1 scenarios. The A1B-SRES-marker scenario has been run in ENSEMBLES for consistency with earlier runs. The recent IMAGE A1B implementation (against which the E1 scenario was developed) has higher emissions, due – among other reasons – to a higher carbon intensity of GDP (associated with uncertainty in technology development).

and for the SRES A1B and the E1 scenarios at 2050 and 2100. Using the gridded emissions of black carbon and precursors of sulphates from the IMAGE scenarios, the same chemical transport model as used for IPCC (Boucher and Pham, 2002) has been used to compute the 3-D sulphate aerosol concentration maps.

4.4.2 Models for Stream 2 simulations

Stream 2 simulations make use of improved coupled atmosphere ocean models, as developed in Work Package 1.1 of RT1. A major difference consists in the coupling of an interactive carbon cycle in five Earth system models (Table 4.3), so that the net CO₂ fluxes between atmosphere and ocean, and atmosphere and land can be computed interactively, depending on the prescribed atmospheric CO₂ concentrations, as proposed by Hibbard et al. (2007). The carbon cycle model components generally describe the carbon storage in different pools related to vegetation and soils, and the carbon uptake and cycling in the oceans.

Eight of the models can be forced with land cover changes. Land cover changes influence the physical properties of land surfaces, and imply carbon emissions in models including land carbon pools for vegetation and soils, e.g. when deforestation takes place. Aerosol and/or chemistry models were introduced in three models. Further improvements concerning details of the model formulations have also been included, so that the new set of Earth system models represents a considerable step forward towards future models with prognostic treatment of all major greenhouse gases. Several models used here represent prototypes of Earth system models that will be used for CMIP5 simulations, in support of the Fifth Assessment Report of IPCC.

4.4.3 Results of the Stream 2 simulations

In total, eight modelling groups have used ten different models to construct the stream 2 simulations. The participating models are generally improved or extended versions of models contributing to IPCC AR4 (through improvements to core physical schemes, and the inclusion or improvement of aerosol,

carbon cycle and variable vegetation cover components). The Earth system models including the carbon cycle have been driven by CO₂ concentrations rather than emissions, following an approach similar to that suggested by Hibbard et al. (2007) for the AR5. The key features of the different models and the simulations performed are listed in Table 4.3.

All GCMs in the study, initialised for pre-industrial conditions (approx. 1860), have simulated climate change driven up to the present day, with 19th and 20th century reconstructed climate forcings and 21st century forcings extending up to at least 2100 for two core scenarios – A1B and E1. In many models, land-use change due to human activity is included, although this could not be done with every model, due to the technical challenge of representing it in GCMs that include carbon cycle components. Some simulations additionally include natural (solar and volcanic) forcings, as previously modelled in Stream 1.

Taken collectively, the models are able to reproduce rather realistically the observed warming trend over the 20th century (Figure 4.5).

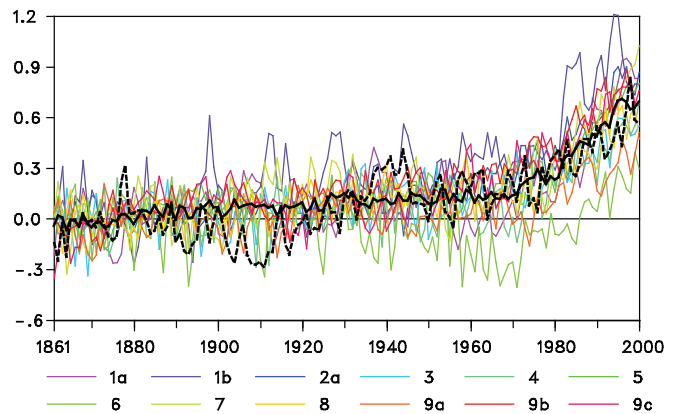


Figure 4.5: Anomalies of the globally averaged annual mean near-surface temperature over the period 1861–2000 with respect to the period 1861–1890 for the twelve hindcasts in GA. The solid black curve indicates the multi-model mean values (giving equal weight to the different models) and the dashed black curve the observational values (HadCRUT3). The numbers indicate the different models/simulations from the different modelling groups. Units are °C.

Table 4.3: ENSEMBLES Stream 2 multi-model ensemble summary (CC = carbon cycle component; AT = aerosol chemical transport component; LU = transient land-use change component) and core simulations (CTL = pre-industrial forcing control; GA = historical forcing by GHGs, aerosols, and land-use changes if represented; +SV = plus solar and volcanic forcing; A1B and E1 = future forcing scenarios for SRES A1B baseline and ENSEMBLES low-stabilisation cases). • = model component included and simulation (or multiple simulations indicated by a number) performed.

Multi-model ensemble members		Model components			Generic resolution		Simulations				
Group	Model name(s)	CC	AT	LU	Atmosphere	Ocean	CTL	1860–2000		2000–2100	
								GA	GA+SV	A1B	E1
METO-HC	HadGEM2-AO HadCM3C	•	•	•	N96L38	1°L40	•	•		•2	•2
					N48L38	1.25°L20				•	•
IPSL	IPSL-CM4_v2 IPSL-CM4-LOOP	•		•	N48L19	2°L31	•	•3	•3	•3	•3
					N48L19	2°L31				•	•
MPI+DMI	ECHAM5-C	•		•	T31L19	3°L40	•	•5	•5	•5	•5
FUB	EGMAM+		•	•	T30L39	T42 L20	•	•2		•	•2
INGV	ECHAM5-OPA-C	•			T31L19	2° L31	•	•		•	•
CNRM+DMI	CNRM-CM3.3			•	T63L31	2° L31	•	•3	•	•	•3
NERSC	BCM2 BCM2-C	•		•	T63L31	2.4°L35	•	•		•	•
										•	•

Figure 4.5 shows time-series of the anomalies of the globally averaged annual mean near-surface temperature over the period 1861–2000 based on the twelve hindcasts in GA provided by the different modelling groups. In those cases, where ensembles of simulations are available, the ensemble mean values are shown. In accordance with observations, most models show a marked warming over the last 30 years of the 20th century, although in one of the hindcasts the marked warming does not start before the mid-1980s. When the solar and volcanic forcing is also considered (in GA+SV), the hindcasts are able to capture the observed cooling in the 1880s and give a slightly weaker warming in the last 40 years of the 20th century, compared with the hindcasts considering the greenhouse gas forcing only.

Over the 21st century, all models simulate a similar global mean surface temperature warming for the E1 scenario and the A1B scenario until the middle of this century. After that the projections for the A1B scenario are higher than for the E1 scenario because the temperature stays almost constant for the E1 scenario for the remainder of the century. In four models (CNRM, ECHAM5, EGMAM, INGV) the temperature increase for the year 2100, with respect to the 1970-1999 average, is lower than 2°C. For the IPSL and the HadGEM-AO models, the temperature rise is above 2°C, but below 3°C. The ensemble mean stays below 2°C (see Figure 4.6). The precipitation changes at the end of this century are smaller in the E1 scenario than in the A1B scenario, while in the middle of this century no difference can be detected (Figure 4.7) The geographical distri-

bution of the precipitation response is broadly similar to the pattern obtained in the Stream 1 simulations (see Appendix 1).

The second key part of the experimental design was for the subset of models that include the carbon cycle to diagnose the net flux of carbon into the atmosphere needed to achieve the prescribed target concentration profiles.

4.4.4 Diagnoses of carbon fluxes

The implied anthropogenic carbon emissions in the ENSEMBLES Stream 2 experiment from four different global models that include an interactive carbon cycle is illustrated in Figure 4.8 for the historical industrial period and A1B and E1 scenarios. The experimental design dictates that the models are driven with atmospheric greenhouse gas concentrations (specifically CO₂), rather than emissions. The concentrations profile is thus a controlled variable – i.e., the same for all model simulations of a given scenario – and global mean anthropogenic permitted emissions consistent with those which can be diagnosed as a residual term from the difference between the imposed rate of change of atmospheric CO₂ (shown as the black curves in Figure 4.8) and the modelled net sinks (sum of air-to-ocean plus air-to-land surface carbon fluxes – not shown).

To reduce interannual noise, an 11-year mean smoothing was applied to each model’s implied emissions (and to the atmospheric CO₂ change, for consistency). In one case (MPI:

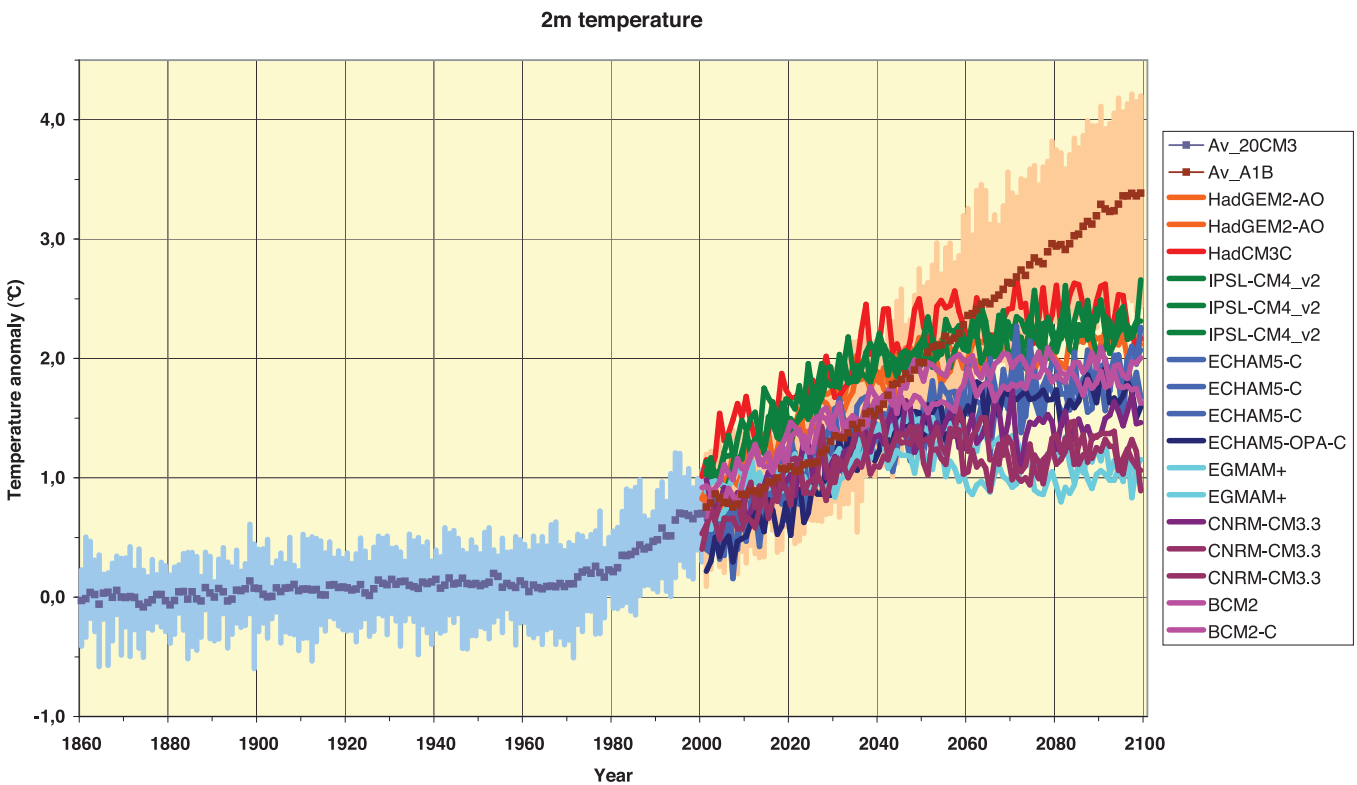


Figure 4.6: The global annual mean surface air temperature in 20C3M, A1B and E1 for the Stream 2 simulations (deviation from 1861–1890 mean). For 20C3M and A1B only, the average and range (minimum and maximum of all models for each year) of the simulations are displayed, and for E1 the individual model runs (as identified in Table 4.3).

ECHAM5-C) the results shown also represent an ensemble mean of five simulations for each scenario, which further reduces the noise. Considerable (unforced) variability nonetheless exists in the implied emissions, particularly in the case of METO-HC model results.

For the 20C3M simulation there is a generally consistent behaviour across the model ensemble – a rising trend with anthropogenic emissions reaching between 6 and 9 GtC/yr in 2000 – reasonably consistent with the consensus estimate of around 8 GtC/yr (see, e.g., Fig. SPM-3 of Nakicenovic and Swart, 2000). All models agree that the combined carbon sinks remove about half of the net anthropogenic emissions from the atmosphere at 2000.

In the future projections there is a much greater spread within the model ensemble. Remarkably, two models (IPSL and MPI) agree consistently not just in the historical period but also throughout both the A1B and E1 scenarios, despite differences in model formulation (for instance, one includes land-use carbon emissions explicitly while the other does not). This suggests that the representation of the carbon cycle response in terms of net sinks is very similar in these models. There is some overlap between the multi-model ensemble implied emissions for A1B and E1 in the early 21st century, but a clear separation occurs by 2030. A pattern emerges in which the two consistent models (IPSL and MPI) predict the largest net sinks and hence imply the highest permitted anthropogenic emissions (peaking at around 17 GtC/yr in 2050 and falling to ~12 GtC/yr in 2100 for A1B), while the METO-HC model implies the lowest permitted emis-

sions (only ~10 GtC/yr in 2050, falling to ~8 GtC/yr in 2100 for A1B), with the INGVCE model falling somewhere in between (closer to METO-HC). The same model ordering is seen in the E1 scenario results, but in this case the range of permitted emissions at 2050 is from +4 GtC/yr to near zero in the case of the METO-HC model, in which the net carbon uptake by the land and ocean reduces considerably as the atmospheric carbon dioxide concentration stabilises. A key result is that all models imply that by 2100 permitted anthropogenic emissions must fall close to zero, or even become slightly negative, to achieve the E1 scenario concentrations pathway (see Figure 4.8, top panel).

The magnitude of the land carbon source/sink term covers a considerable range, and most models also exhibit considerable interannual to decadal variability in that term (Figure 4.8, middle panel). However, the ocean shows a more consistent and smoother behaviour, remaining consistently a carbon sink in both scenarios across all models (Figure 4.8, bottom panel). One conclusion arising from the large decadal variability in model carbon sinks is that, assuming this is a realistic characteristic of the real climate system, forcing models with specified observed CO₂ concentrations may in fact impose an undesirable partly non-anthropogenic forcing (e.g., the dip in implied anthropogenic emissions which emerges as a common signal in this experiment around 1940 may simply reflect a natural variation in the real land carbon sink rather than be interpreted as a reduction in actual anthropogenic emissions). We therefore suggest that the experimental design – although a step forward – could still be improved.

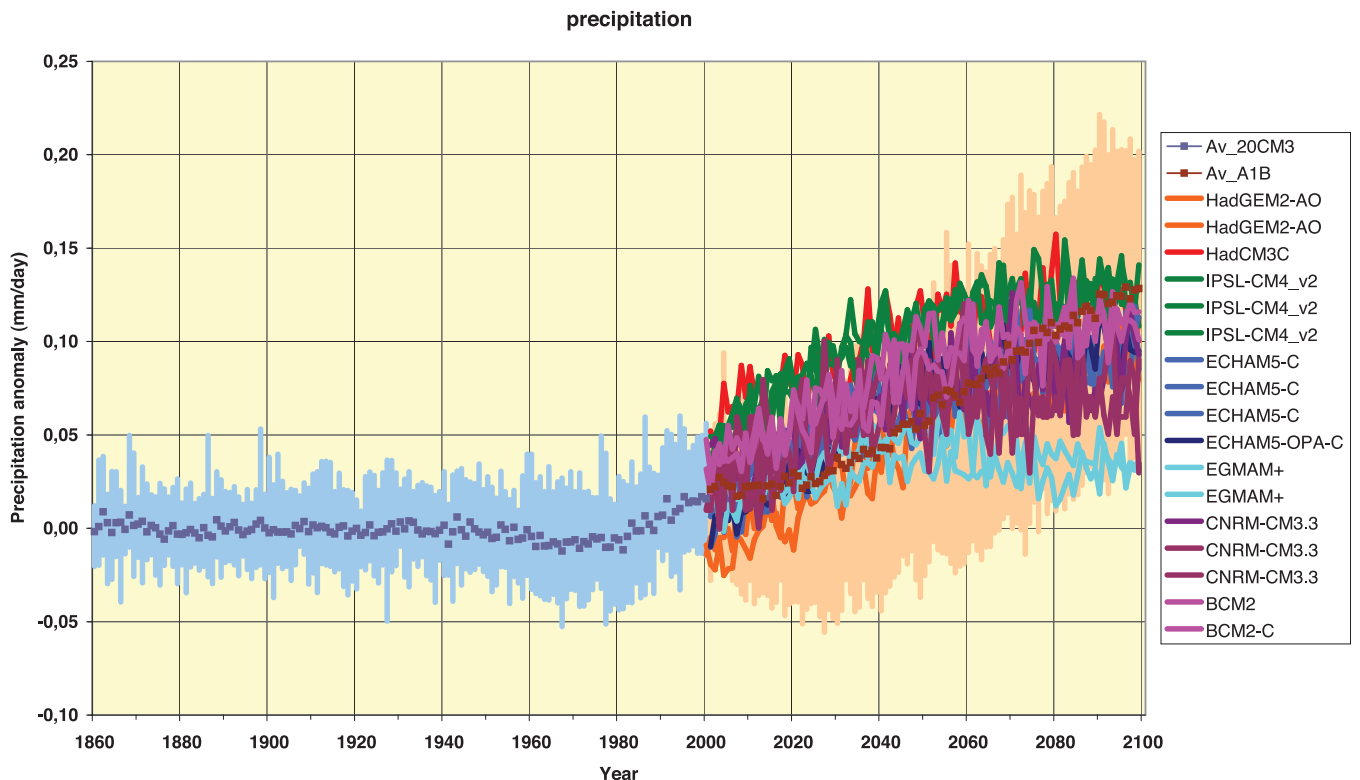


Figure 4.7: The global annual mean precipitation in 20C3M, A1B and E1 for the Stream 2 simulations (deviation from 1861–1890 mean). For 20C3M and A1B only, the average and range (minimum and maximum of all models for each year) of the simulations are displayed, and for E1 the individual model runs (as identified in Table 4.3).

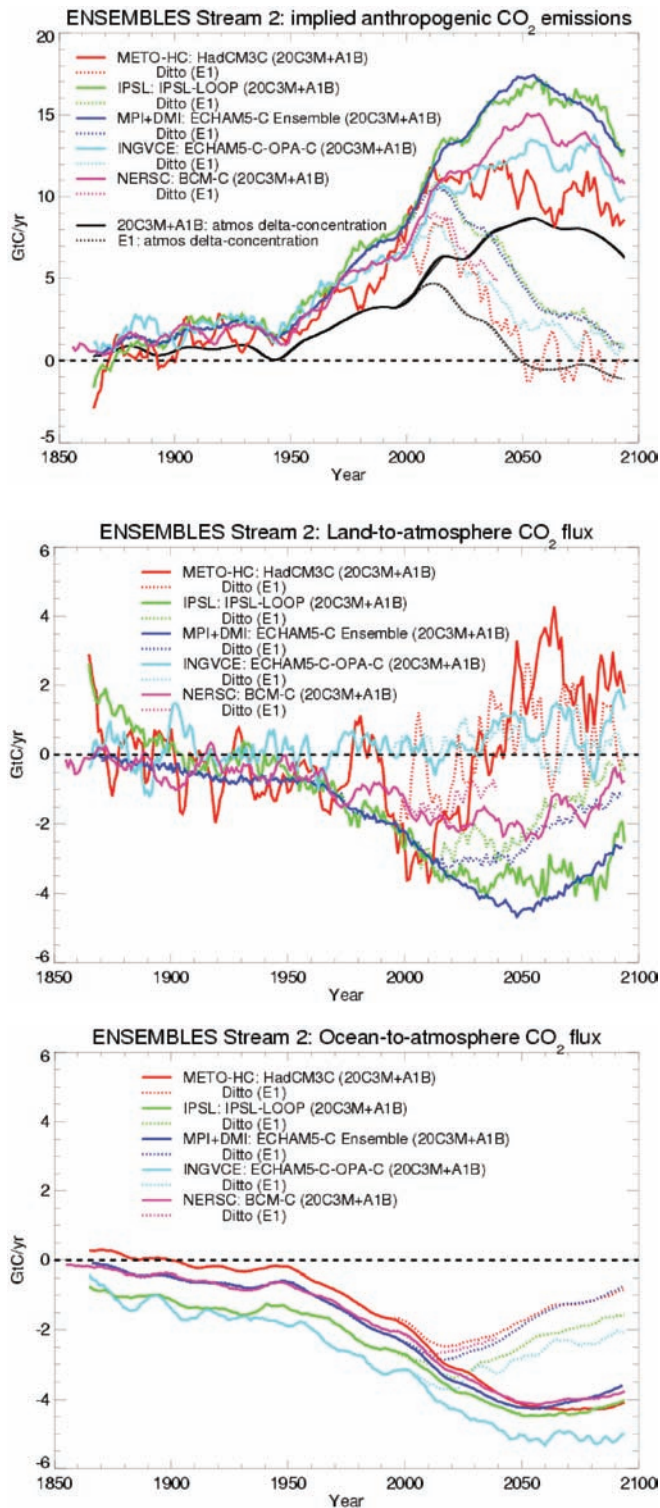


Figure 4.8: Implied ('permitted') anthropogenic net carbon dioxide emissions to the atmosphere (Gt C/yr) in ENSEMBLES RT2A Stream 2 runs for the 20th and 21st century (top panel) as diagnosed from the imposed change in atmospheric concentrations (black curves) and the modelled net carbon flux exchange between the atmosphere and the land surface (middle panel) and ocean (bottom panel). Note that an 11-year mean smoothing has been applied to all curves (including delta-concentrations) and that MPI+DMI: ECHAM5-C results show ensemble means of eight (20C3M+A1B) and five (E1) independent simulations, tending to smooth those results compared with other models.

4.5 Databases of global model results

The aim was to develop a database system in a common format, allowing easy access by all the partners to selected results of the global ensemble simulations. Typically, an atmosphere–ocean coupled simulation can generate about half a terabyte of data for a 100-year simulation if daily fields are stored. A similar amount is found in ensemble seasonal simulations. The model results are stored in the MARS storage system of ECMWF, and of the Climate and Environmental Retrieval and Archive (CERA) database system at the World Data Centre for Climate hosted by the Model and Data Group in Hamburg (MPIMET-MD). Common lists of variables and the need for a common format were outlined in the early stages of the project, depending on the requirements of the scientific community taking part in the other Research Themes. Project data will still be updated and available online after the project has ended.

ECMWF public data server

A large set of atmosphere and ocean variables from the multi-model, stochastic physics and perturbed parameter experiments s2d (seasonal to decadal) integrations are centrally stored at ECMWF for quality control, basic forecast quality assessment, and dissemination. The atmospheric variables are archived on ECMWF's Meteorological Archival and Retrieval System (MARS) in GRIB (gridded binary) format. The fields are stored following a set of atmospheric conventions, based on the experience gained in DEMETER (Palmer et al., 2004) and the operational European multi-model seasonal forecasts. The encoding of the ocean variables is carried out using rules based on newly developed conventions, with storage of CF-compliant NetCDF files into the ECFS server.

A subset of the data is being publicly disseminated. The list of atmospheric variables includes daily data for temperature, wind, humidity and geopotential at four pressure levels and a selection of the most common surface data and fluxes. Monthly mean data are also available. The ocean output includes monthly means of the ocean analyses and forecasts. They comprise 3-D fields (temperature, salinity and velocity) and a limited number of 2-D fields (e.g., sea level, mixed layer depth, 20°C isotherm depth). For a full list of atmospheric and oceanic variables see: http://www.ecmwf.int/research/EU_projects/ENSEMBLES/data/comm_on_variables.html.

The ENSEMBLES s2d data have been made available over the internet without charge for use in research, education and commercial work. Two dissemination systems, one based on MARS and another one based on the Open-source Project for a Network Data Access Protocol (OPeNDAP), have been developed to help users to access the ENSEMBLES data in the most efficient way for their specific requirements.

The MARS-based system uses the technology developed for the ECMWF public data server and offers a quick and easy way to interactively download the data from a user-friendly front page. From that page the user can retrieve daily and monthly mean data in both GRIB and NetCDF formats, as well as plot the required fields. This system is expected to be of use to scientists interested in relatively small samples or needing interactive access to the dataset.

The OPeNDAP-based tool allows remote application clients to access the ENSEMBLES dataset. This is a powerful tool to provide automatic access to clients for a variety of tasks. The OPeNDAP serves data in both ASCII and CF-compliant NetCDF formats. The NetCDF format used in the OPeNDAP system is one of the main novelties of this service: it provides product standardisation through a new set of encoding rules for multi-forecast system ensemble simulations (Doblas-Reyes et al., 2007).

CERA database at MPI

MPIMET.MD has established a website to enable easy access to the ENSEMBLES-related multi-decadal simulations. After providing the necessary information to the data-providing centres, metadata for most experiments have been completed. The website is continually kept up-to-date to include in the CERA database the datasets provided by the modelling groups.

ENSEMBLES data are archived in the Climate and Environmental Retrieval and Archive (CERA) of the World Data Center System for Climate (WDCC) run by the Model and Data group. Access is given by <http://ensembles.wdc-climate.de>. The web page provides links to ENSEMBLES RT2A and the CERA database, and asks users to read and take note of the ENSEMBLES Data Policy document before using the data. The experiments for Stream 1 and Stream 2 are briefly described and access is given to each scenario variable of each contributing institute.

Alternatively, the CERA database may be browsed directly using the CERA portal (<http://cera-www.dkrz.de/WDCC/ui/Browse-Experiments.jsp>), which is subdivided into three frames: which if ENSEMBLES is selected in the upper right-hand frame, the lower frame then displays all the ENSEMBLES experiments according to model, scenario and time interval. The list of experiments may further be reduced by selecting a key-word from the upper-left frame. Finally, after the selection of an experiment, the buttons below the lower frame give further information about a particular experiment and lead to the entries (variables). The database covers about 300 ENSEMBLES experiments (where experiment means a single multi-decadal simulation performed

with one of the contributing models), of which 160 are for Stream 1. Overall there are more than 25,000 entries (an entry is defined as a two-dimensional field for a variable at a given vertical level). By mid-2009, about 140 visitors had accessed 55,000 CERA entries and downloaded around 17 terabytes of information; demonstrating a lively interest in ENSEMBLES data. First-time users should look at <http://cera-www.dkrz.de/CERA/> for more information on CERA and instructions for setting up an account.

4.6 Conclusions and perspectives

The first phase (Stream 1) of ENSEMBLES has provided an important contribution to the Intergovernmental Panel on Climate Change (IPCC) Fourth Assessment Report (AR4) by providing coordinated European climate model simulations corresponding to the IPCC SRES A1B, A2 and B1 emissions scenarios. The next phase (Stream 2) of ENSEMBLES has provided the first opportunity to test simulations with a new set of improved climate models, including some with integrated carbon cycle components or aerosol transport, using two future scenarios specified in terms of global greenhouse gas (GHG) concentration pathways. Two pathways considered are a baseline without climate mitigation policy (SRES A1B) and an aggressive mitigation pathway which aims eventually to stabilise the additional anthropogenic radiative forcing to that equivalent to a carbon dioxide concentration (CO₂-e) at around 450 ppm during the 22nd century. The results for this second scenario have shown that the simulations for this stabilisation scenario were generally able to match the European Union target of keeping global anthropogenic warming below 2°C above pre-industrial levels. It is expected that the high-time-resolution results permanently stored in the CERA database will be used beyond the end of the project for further analyses of the climate response and the resulting impacts. As some other modelling groups have already expressed their interest in performing the ENSEMBLES RT2A Stream 2 simulations, the forcing fields necessary for running the scenarios have been put on the RT2A web server in a directory that is publicly accessible: http://www.cnrm.meteo.fr/ensembles/public/model_simulation.html.

References

ENSEMBLES publications are highlighted as bold text.

- Arzel O, Fichefet T, Goosse H, 2006. Sea ice evolution over the 20th and 21st centuries as simulated by current AOGCMs. *Ocean Modelling* 12, 412–427.
- Bengtsson L, Hodges KI, Roeckner E, 2006. Storm tracks and climate change. *Journal of Climate* 19, 3518–3543.
- Boucher O, Pham M, 2002. History of sulfate aerosol radiative forcings. *Geophysical Research Letters* 29, 1308.
- Brasseur GP, Roeckner E, 2005. Impact of improved air quality on the future evolution of climate. *Geophysical Research Letters* 32, L23704, doi:10.1029/2005GL023902.
- Chauvin F, Denvil S, 2007. Changes in severe indices as simulated by two French coupled global climate models. *Global and Planetary Change* 57, 96–117.
- Crueger T, Roeckner E, Raddatz T, Schnur R, Wetzell P, 2007. Ocean dynamics determine the response of oceanic CO₂ uptake to climate change. *Climate Dynamics* 31, 151–168.
- den Elzen MGJ, van Vuuren DP, 2007. Peaking profiles for achieving long-term temperature targets with more likelihood at lower costs. *Proceedings of the National Academy of Sciences of the USA* 104, 17931–17936.
- Doblas-Reyes FJ, Valiente C, Fuentes M, 2007. ENSEMBLES public data dissemination. *ECMWF Newsletter* 113, 4.
- Douville H, 2006. Detection-attribution of global warming at the regional scale: how to deal with precipitation variability? *Geophysical Research Letters* 33, L02701, doi:10.1029/2005GL024967.
- Douville H, Salas-Méla D, Tyteca S, 2006. On the tropical origin of uncertainties in the global land precipitation response to global warming. *Climate Dynamics* 26, 367–385.
- Dufresne J-L, Quaas J, Boucher O, Denvil S, Fairhead L, 2005. Contrasts in the effects on climate of anthropogenic sulfate aerosols between the 20th and the 21st century. *Geophysical Research Letters* 32, L21703, doi:10.1029/2005GL023619.
- Good P, Lowe JA, 2006. Emergent behaviour and uncertainty in multi-model climate projections of precipitation trends at

- small spatial scales. *Journal of Climate* 19, 5554–5569.
- Guemas V, Salas-Méla D, 2008a. Simulation of the Atlantic meridional overturning circulation in an atmosphere–ocean global coupled model. Part I. A mechanism governing the variability of ocean convection in a preindustrial experiment. *Climate Dynamics* 31, 29–48.
- Guemas V, Salas-Méla D, 2008b. Simulation of the Atlantic meridional overturning circulation in an atmosphere–ocean global coupled model. Part II. Weakening in a climate change experiment: a feedback mechanism. *Climate Dynamics* 30, 831–844.
- Hagemann S, Göttel H, Jacob D, Lorenz P, Roeckner E, 2009. Improved regional scale processes reflected in projected hydrological changes over large European catchments. *Climate Dynamics* 32, 767–781.
- Hibbard KA, Meehl GA, Cox PM, Friedlingstein P, 2007. A strategy for climate change stabilization experiments. *EOS Transactions of the American Geophysical Union* 88(20), 217–221.
- Huebener H, Cubasch U, Langematz U, Spanghel T, Niehoerster F, Fast I, Kunze M, 2006. Ensemble climate simulations using a fully coupled ocean–troposphere–stratosphere GCM. *Philosophical Transactions of the Royal Society A*, 365, 2089–2101.
- IPCC, 2007. *Climate Change 2007: The Physical Science Basis*. Contribution of Working Group I to the Fourth Assessment Report of the Intergovernmental Panel on Climate Change (S Solomon, D Qin, M Manning, eds). Cambridge University Press, Cambridge UK and New York, 996 pp.
- Johns TC, Durman CF, Banks HT, Roberts MJ, McLaren AJ, Ridley JK, Senior CA, Williams KD, Jones A, Rickard GJ, Cusack S, Ingram WJ, Crucifix M, Sexton DMH, Joshi MM, Dong B-W, Spencer H, Hill RSR, Gregory JM, Keen AB, Pardaens AK, Lowe JA, Bodas-Salcedo A, Stark S, Searl Y, 2006. The New Hadley Centre Climate Model (HadGEM1): evaluation of coupled simulations. *Journal of Climate* 19, 1327–1353.
- Joly M, Voldoire A, 2009. Influence of ENSO on the West African monsoon: temporal aspects and atmospheric processes. *Journal of Climate* 22, 3193–3210.
- Klein Goldewijk K, 2001. Estimating global land use change over the past 300 years: the HYDE database. *Global Biogeochemical Cycles* 15, 417–433.
- Lowe JA, Hewitt CD, van Vuuren DP, Johns TC, Stehfest E, Royer J-F, van der Linden PJ, 2009. New study for climate modeling, analyses, and scenarios. *EOS Transactions of the American Geophysical Union* 90, 181–182.
- Martin GM, Ringer MA, Pope VD, Jones A, Dearden C, Hinton TJ, 2006. The physical properties of the atmosphere in the new Hadley Centre Global Environmental Model (HadGEM1). Part I. Model description and global climatology. *Journal of Climate* 19, 1274–1301.
- May W, 2008. Climatic changes associated with a global ‘2°C-stabilization’ scenario simulated by the ECHAM5/MPI-OM coupled climate model. *Climate Dynamics* 31, 283–313.
- McLaren AJ, Banks HT, Durman CF, Gregory JM, Johns TC, Keen AB, Ridley JK, Roberts MJ, Lipscomb WH, Connolley WM, Laxon SW, 2006. Evaluation of the sea ice simulation in a new coupled atmosphere–ocean climate model (HadGEM1). *Journal of Geophysical Research* 111, C12014.
- MNP, 2006. *Integrated Modelling of Global Environmental Change: An Overview of IMAGE 2.4*. Netherlands Environmental Assessment Agency, Bilthoven, The Netherlands.
- Müller WA, Roeckner E, 2006. ENSO impact on mid-latitude circulation patterns in future climate change projections. *Geophysical Research Letters* 33, L05711, doi:10.1029/2005GL025032.
- Müller WA, Roeckner E, 2008. ENSO teleconnections in projections of future climate in ECHAM5/MPI-OM. *Climate Dynamics* 31, 533–549.
- Nakicenovic N, Swart R (eds), 2000. *Special Report on Emissions Scenarios*. Intergovernmental Panel on Climate Change, Cambridge University Press, Cambridge, UK.
- Palmer TN, et al., 2004. Development of a European multi-model ensemble system for seasonal-to-interannual prediction (DEMETER). *Bulletin of the American Meteorological Soc.* 85, 853–872.
- Peings Y, Douville H, 2009. Influence of the Eurasian snow cover on the Indian summer monsoon variability in observed climatologies and CMIP3 simulations. *Climate Dynamics*, doi:10.1007/s00382-009-0565-0.
- Ramankutty N, Foley JA, 1999. Estimating historical changes in global land cover: croplands from 1700 to 1992. *Global Biogeochemical Cycles* 13, 997–1027.
- Ringer MA, Martin GM, Greeves CZ, Hinton TJ, James PM, Pope VD, Scaife AA, Stratton RA, Inness PM, Slingo JM, Yang G-Y, 2006. The physical properties of the atmosphere in the new Hadley Centre Global Environmental Model (HadGEM1). Part II. Aspects of variability and regional climate. *Journal of Climate* 19, 1302–1326.
- Roeckner E, Stier P, Feichter J, Kloster S, Esch M, Fischer-Bruns I, 2006. Impact of carbonaceous aerosol emissions on regional climate change. *Climate Dynamics* 27, 553–571.
- Royer J-F, Chauvin F, Biaou A, Schertzer D, Lovejoy S, 2008. Multifractal analysis of the evolution of simulated precipitation over France in a climate scenario. *Comptes Rendus Geoscience* 340, 431–440.
- Salas y Méla D, Chauvin F, Déqué M, Douville H, Guérémy JF, Marquet P, Planton S, Royer JF, Tyteca S, 2005. *Description and Validation of CNRM-CM3 Global Coupled Model*. CNRM Working Note 103 [available at: http://www.cnrm.meteo.fr/scenario2004/paper_cm3.pdf].
- Sato M, Hansen JE, McCormick MP, Pollack JB, 1993. Stratospheric aerosol optical depth, 1850–1990. *Journal of Geophysical Research* 98, 22987–22994.
- Sillmann J, Roeckner E, 2008. Indices for extreme events in projections of anthropogenic climate change. *Climatic Change* 86, 83–104.
- Solanki SK, Krivova NA, 2003. Can solar variability explain global warming since 1970? *Journal of Geophysical Research* 108(A5), 1200, doi:10.1029/2002JA009753.
- Sorteberg A, Kattsov V, Walsh J, Pavlova T, 2007. The Arctic surface energy budget as simulated with the IPCC AR4 AOGCMs. *Climate Dynamics* 29, 131–156.
- Søvde OA, Gauss M, Smyshlyaev SP, Isaksen ISA, 2008. Evaluation of the chemical transport model Oslo CTM2 with focus on Arctic winter ozone depletion. *Journal of Geophysical Research – Atmosphere* 113, D09304.
- Stott PA, Jones GS, Lowe JA, Thorne PW, Durman CF, Johns TC, Thelen J-C, 2006. Transient simulations with the HadGEM1 climate model: causes of past warming and future climate change. *Journal of Climate* 19, 2763–2782.
- van Vuuren DP, den Elzen MGJ, Lucas PL, Eickhout B, Strengers BJ, van Ruijven B, Wonink S, van Houdt R, 2007. Stabilizing greenhouse gas concentrations at low levels: an assessment of reduction strategies and costs. *Climatic Change* 81, 119–159.

5 Formulation of very-high-resolution regional climate model ensembles for Europe

[Research Theme 3]

J.H. Christensen (DMI), M. Rummukainen (SMHI), G. Lenderink (KNMI)

5.1 Introduction

RT3 was the ENSEMBLES Research Theme responsible for regional climate modelling research. It provided advances in regional climate modelling science and had significant exchanges with the other RTs: the new gridded observations of RT5 were employed in Regional Climate Model (RCM) evaluation, RT3 received input from RT2A (GCM data) and provided input to statistical downscaling, studies on extreme events, and impact studies in RT2B, RT5 and RT6. In particular, RT3 provided the regional climate modelling system put into use in RT2B. Finally, RT3 studies addressed West Africa, providing added value for the AMMA project (Redelsperger et al., 2006).

RT3 had a more extensive agenda than other coordinated regional climate modelling projects, such as NARCCAP, CLARIS and RMIP, as well as the earlier European PRUDENCE project (e.g., Christensen et al., 2007). Specifically, within ENSEMBLES:

- performance-based weighting of RCMs was considered;
- an extensive set of RCMs was employed with a thoroughly coordinated experimental design;
- two regions were studied, with different climate characteristics;
- compared with earlier and other joint RCM studies, the ENSEMBLES runs were much longer and made on a higher resolution (25 km).

The RT3 coordination extended to simulation set-up, evaluation and systematic exploration of model biases, as well as the exploration of model weighting, as means for combining results in a more skilled sense than simple ensemble means and spreads.

5.2 Coordinating RCM experimentation

5.2.1 Common Regional Climate Model domains

An important facet of the coordination was the definition of common Regional Climate Model (RCM) domains (Figure 5.1), model resolution and output. The majority of the RCMs employed a rotated latitude–longitude grid, which allowed for identical and overlapping grids and subsequent comparison without the need for interpolation. The RT5 observation-based grid was defined accordingly (see Section 8).

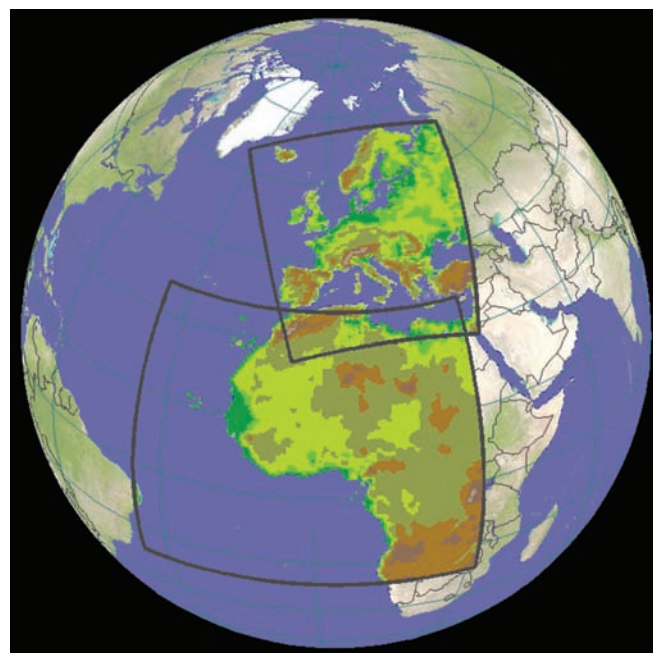


Figure 5.1: The two RCM domains in the ENSEMBLES RT3 simulations.

5.2.2 The RCM simulation streams

There were two RCM simulation streams. The first enabled model evaluation and work on performance-based RCM weights for the European region. The period for this was 1958–2002, with boundary conditions from the observation-based ERA-40 reanalysis, first on 50 km and then on 25 km resolution. The second stream included ERA-Interim reanalysis-driven simulations for the period 1989–2005 over a domain encompassing the West Africa region at 50 km grid resolution (see Section 5.3.2).

5.2.3 Common – and extensive – output

Given the anticipated use of RT3 results within RT2B, RT5 and RT6, as well as in climate impact and extreme event studies outside ENSEMBLES, coordination included an extensive dialogue on common model output. The list of output variables increased due to a wide range of demands. Some of the output was stored at a sub-daily resolution, successively collected into

a joint data archive at DMI. The archive had an OpenDAP interface for the retrieval of geographical sub-windows, sub-periods and strides. The archive has been public since January 2009 at <http://ensemblesrt3.dmi.dk/>, collecting the ENSEMBLES RCM data from RT3/RT2B (see also Section 6.6). Information on sub-daily extremes of wind maxima and precipitation intensity allows better estimates of climate impacts and can be significantly different from those obtained from daily changes (Lenderink and van Meijgaard, 2008).

5.2.4 Improved regional climate modelling

ENSEMBLES brought various improvements to the state-of-the-art of regional climate modelling into being. The coordination mentioned above was one such important development, along with the increase in model resolution from earlier ~ 50 km to 25 km. The latter had, of course, been attempted earlier, but more as an exception than common practice. Consequently, many groups had the opportunity to test how their models fared with increasing resolution. Indeed, high resolution is one key advantage of RCMs compared with GCMs, especially in regions with variable land forms or characteristics (see Figure 5.2).

Comparison of lower and higher resolution RCM runs showed that a move to higher resolution can require some model refinements. Although, in general, the simulations improved with higher resolution, some model biases nevertheless became larger in certain regions and seasons (see, e.g., Jaeger et al., 2008; Rauscher et al., 2009). For example, at higher resolution almost all of the ENSEMBLES RCMs tended to simulate more precipitation (Rauscher et al., 2009), which over some regions resulted in an increased wet bias. However, the results also show that higher resolution leads to a general improvement in the simulation of precipitation extremes. Moving one step further to cloud-resolving scales of ~ 2 km and applying an explicit treatment of convection can substantially improve the timing of

convective precipitation and the simulation of land–atmosphere feedbacks (Hohenegger et al., 2008, 2009). The ENSEMBLES experiments, however, clearly indicated that the increase in model resolution needs to be approached carefully.

Another major advance in regional modelling produced by ENSEMBLES was the completion of century-long RCM simulations (as part of RT2B; see Jacob et al., 2009) using a system provided by RT3. Such simulations were extremely rare before ENSEMBLES. This unprecedented dataset of transient runs allows analyses of trends and regime shifts simulated by the RCMs, with important implications for regional-scale detection, attribution, impact and adaptation work for Europe.

Some examples of the specific evaluations and improvements explored include a detailed comparison of the regional-scale components of the water budget in the Baltic Sea drainage basin for one of the RCMs (Lind and Kjellström, 2009) and testing the role of the spectral nudging technique to improve the large-scale and small-scale skills of an RCM (Radu et al., 2008). The impact of RCM domain size was also explored (Farda et al., 2009) as well as the ability to represent extreme temperature events (Kostopoulou et al., 2009). The capacity of the ERA40-driven RCM simulations to follow the large scales of their driving models was assessed by Sanchez-Gomez et al. (2009a), and the RCMs' capacity to simulate the heat and water budget of the Mediterranean Sea is reported by Sanchez-Gomez et al. (2009b).

Owing to the length of the ERA40-driven evaluation runs and coordinated experimentation in ENSEMBLES, it became feasible to conduct extensive exploration of systematic biases in RCMs. The new ENSEMBLES gridded observational data (see Section 8) was very useful as a common reference for model bias studies, including the utilisation of daily data for looking at extreme events (e.g., Pall et al., 2009). All in all, substantial new insights were gained on systematic RCM biases using data from the ERA40-driven simulations (Christensen et al., 2008). An example is shown in Figure 5.3.

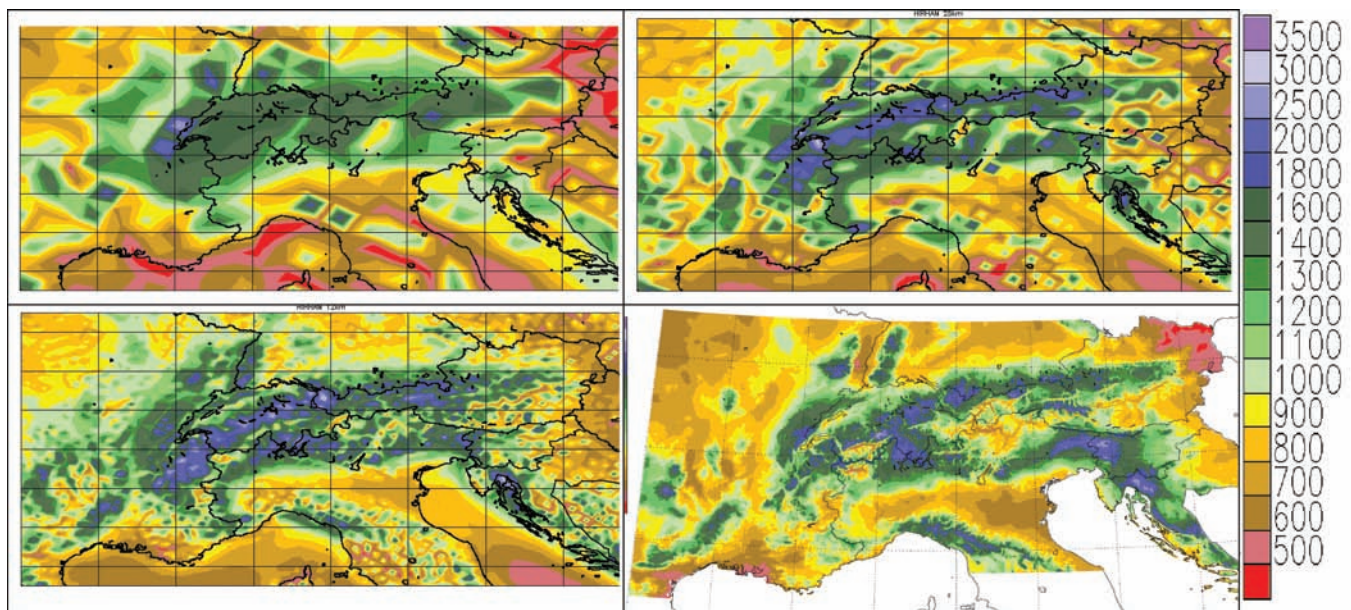


Figure 5.2: Annual precipitation over the Alpine region (mm/yr) as simulated at 50 km resolution (top left), 25 km, (top right) and 12 km (bottom left). Observations adapted from Frei and Schär (1998) are in the bottom right panel.

Some RCMs have systematic biases, and also a clear tendency to enhance these in more extremely cold or warm conditions. Others have no evident systematic bias. Such an analysis of individual RCM bias characteristics, in principle, allows for projection of model biases under climate change conditions.

An attempt to use this simple bias information to correct projections of climate change information was suggested by Boberg et al. (2009). Figure 5.4 shows how RCM temperature projections might be corrected using a simple second-order polynomial fit to the bias depicted in Figure 5.3.

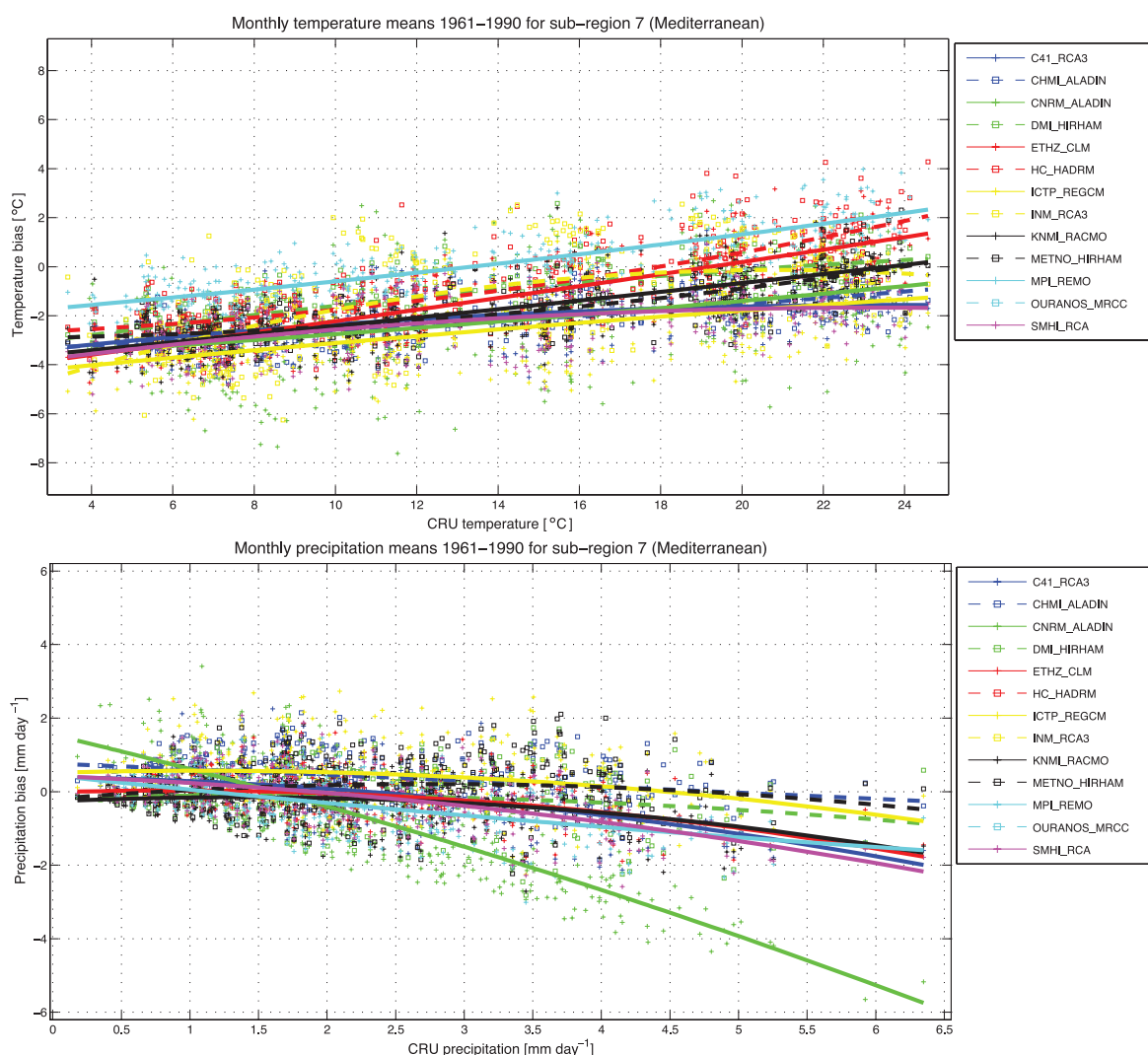


Figure 5.3: RCMs' bias dependency per temperature (top) and precipitation (bottom) regime, here for a Mediterranean region. Each symbol represents one month in the period 1961–1990. The curves are second-order polynomial fits.

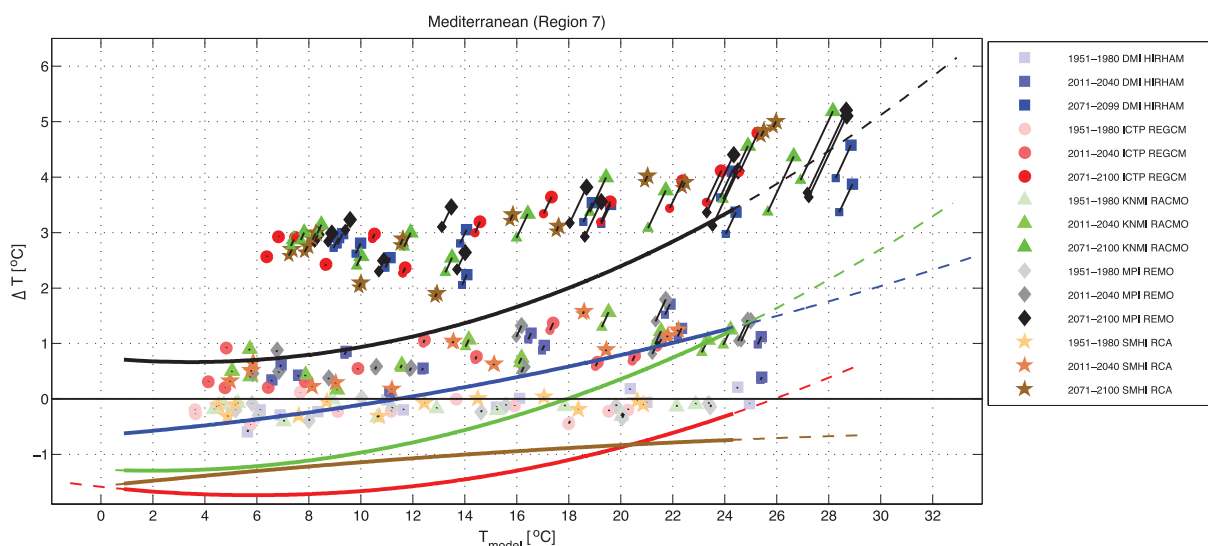


Figure 5.4: Illustration of a simple monthly mean bias correction for three of the ENSEMBLES RCMs which were run all the way to 2100. Larger symbols show model results and smaller symbols corrected values for 30-year time-slices.

The most obvious result is the reduction of the warming signal during summer and the reduced spread of projected changes. The corrected results are more in agreement than the raw data. The basis for these kinds of corrections still needs further investigation. Nevertheless, it is clear that systematic model biases can result in unwanted uncertainty regarding projected climate change signals.

5.2.5 Metrics, weighting and RCM ensemble

At the heart of ENSEMBLES was the construction of a system for probabilistic global and regional climate change projections. Concerning RCMs, this included exploration of performance-based model weights that allow the combination of individual model simulations in a more skilled sense than just taking each model as being equally good (or their results as equally likely) and providing arithmetic model averages and simple model spreads.

Past experience with RCMs has shown that no single model is best for all climate variables and statistics (Christensen and Christensen, 2007; Jacob et al., 2007). Thus, multi-model information has value, which can be enhanced with a performance-based weighting of the contributing models. Work along these lines for GCMs was conducted within ENSEMBLES (see Section 3). For RCMs, an exploratory set of metrics for a derivation of RCM weights was designed using the 25 km ERA40-driven RCM simulations and the RT5 gridded observations (Haylock et al., 2008). Given the preliminary nature of the methodology, different ways of combining the metrics were explored in order to study the robustness of the methodology. Indeed, there is a considerable degree of subjectivity regarding both the choice of metrics and how they are combined into weights. This does not mean that weighting, however exploratory, would be without meaning. Rather, it stresses that the underlying assumptions and choices need to be recognised and taken into account.

The evaluation metrics were selected to specifically target aspects of RCM performance relevant to their added value in producing climate change projections. These included large-scale regimes and meso-scale climate features, variability, extremes, trends and the seasonal cycle (Kjellström et al., 2009):

- f1: Large-scale circulation and weather regimes
- f2: Temperature and precipitation meso-scale signal
- f3: PDFs of daily precipitation and temperature (Sanchez et al., 2009)
- f4: Temperature and precipitation extremes
- f5: Temperature trends
- f6: Temperature and precipitation annual cycle.

The last five of these metrics were defined for both the full European continent and some of its sub-regions, and on both an annual and a seasonal basis. The general philosophy behind combining the metrics into weights is that a ‘good’ model should perform well in all metrics considered. This helps to avoid the counterbalancing effects of systematic biases affecting some, but not all, of the considered measures.

Combined metrics

All the individual metrics have a value between 0 and 1. A straightforward method for combining them is multiplication, i.e.:

$$W_{RCM} = \prod_{i=1}^6 f_i^{n_i}$$

If some metrics are to be considered more relevant than others, or if some of the metrics have an overlap of some kind, the exponents in the equation above can be varied. Note that a value of 0 for the exponent implies equal weighting of the RCMs and, in essence, that information carried by the metrics is not used. A value of 1 for the exponent implies that each metric is considered equally important. Given the exploratory nature of these studies, it is important to study how such choices affect the result (see Figure 5.5).

‘Normalisation’ obtained by constraining the ratio between the highest and lowest assigned weight is an additional option. Formally, this can be established by taking a value of n_i different from 1. Yet another method is to rank all models according to their order of performance in terms of each of the metrics, sum these ranks, and then transform this rank sum into a model weight which is obtained by dividing the sum of the rank sums by the rank sum of each model and then normalising it so the total sum of weights is equal to 1.

These efforts were an important step in quantifying RCM behaviour. However, due to the exploratory nature of these metrics, and how they were combined, these weights are not sufficient to identify ‘good’ or ‘bad’ models. Furthermore, the metrics are conditional on the quality of the underlying driving and observational data, which is an issue in particular for extremes. Finally, these weights do not necessarily quantify the quality of the representation of the underlying physics in the models.

The weighting methodology presented here is a first attempt (Christensen et al., 2009). We are, however, encouraged by these results as they seem to have the ability to emphasise both

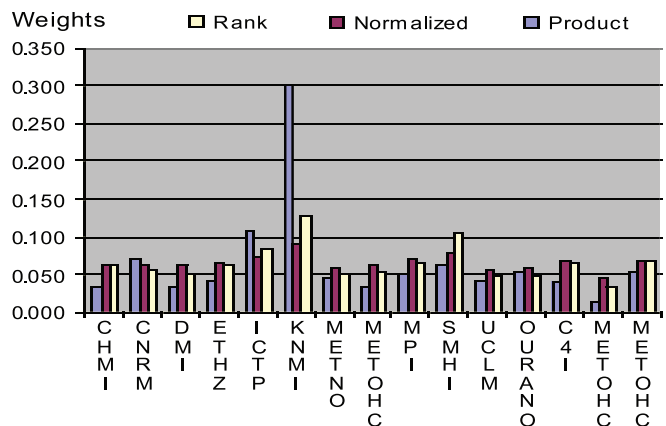


Figure 5.5: Straightforward multiplication has the severest differentiating impact on the RCMs when the performance-based weights defined here are applied. The other explored methods retain the same overall order of the RCMs, but with an attenuated variation within the set.

similarities and differences in the RCMs' capabilities. Indeed, performance-based analysis can bring out both robust and uncertain aspects and consequently can assist in designing model development and efforts on observational data. Subsequently, this can lead to a more knowledge-based use of regional climate change information in climate impacts analysis and adaptation efforts.

To summarise, for users who employ time-series to force impact modelling, choosing a subset of the available RCMs based on the weights is not necessarily the best strategy. It might lead to an undersampling of uncertainty. The minimum requirement would seem to be to use results based on two or more Regional Climate Models that are forced by at least two Global Climate Models (see Christensen and Christensen, 2007). The full GCM-RCM matrix should furthermore be used as supporting information on how the chosen case(s) (GCM-RCM pair[s]) relate to the other cases.

5.2.6 Construction of the RCM climate change projection matrix

Whereas the RCM climate change projections were part of the RT2B's remit, the planning of these was a joint undertaking. One of the main tasks in RT3 was to design an experiment strategy for use in the regional climate change projection ensemble in RT2B. In addition to providing the contributing RCMs (see above) and exploratory weighting options, the work involved a design of the so-called GCM-RCM matrix, i.e., the pairing of available GCM runs and RCMs. (The total possible number of combinations was considerably larger than what in practice could be accommodated, due to limited computing resources.)

In order to pursue probabilistic climate change scenarios, as much of the uncertainty as possible should be covered. The RT3/RT2B subsampling mainly addressed the uncertainty in (1) boundary conditions (choice of GCM) and (2) RCM model formulation. Uncertainties in future emissions were not explicitly studied, in part because the main body of the regional projections was to extend only up to 2050, a time horizon for which the emission scenario uncertainty is less relevant. Neither was initial condition uncertainty sampled. Some groups, however, made available additional simulations looking into this at a coarser horizontal resolution. Also, recent work within the ENSEMBLES project (Kendon et al., 2009; see also Section 6.3.4) has considered the role of natural variability in explaining RCM differences.

Uncertainty in boundary conditions

Differences between climate projection results from different GCMs relate to different model resolution, model dynamics and physical parameterisations, along with scenario assumptions and, to some degree, initialisation details. As is well known, ensembles of GCM simulations provide a number of comparable climate change signals, not least on a large scale. Even regional climate changes as simulated in global models are similar in a number of respects. In the case of Europe, regional differences between GCMs seem to depend to a large extent on differences in the large-scale circulation response to global warming (van Ulden and van Oldenborgh, 2006; van Ulden et al., 2007). Many of these differences are imported to the RCMs, sometimes leading to large local/regional differences

(Räisänen et al., 2004). Indeed, an important conclusion from the previous PRUDENCE project was that the uncertainty due to the boundary conditions (choice of GCM) is generally larger than the choice of RCM (Déqué et al., 2007), at least for large-scale seasonal mean changes towards the end of the 21st century (see also Section 6.2.1).

From a total number of six ENSEMBLES (RT2A) GCMs, results from those five that were run with a reasonably high resolution were employed in the RCM climate change simulation matrix (Table 5.1). As the ENSEMBLES GCMs projected a smaller range in global mean warming than the 'IPCC AR4 GCMs' (Meehl et al., 2007), also GCM runs within the METO-HC GCM perturbed physics ensemble were employed. In particular, a HadCM3 'reference' simulation, one with low climate sensitivity and one with high climate sensitivity were employed. These members of HadCM3 are considered different for the purposes here, as they show very different climate responses (Collins et al., 2006). Thus, the number of different global models considered in RT2B was eight. In addition to those also a Canadian GCM was downscaled by one of the ENSEMBLES affiliates.

Uncertainty in RCM model formulation

Another main result of the previous PRUDENCE project was that many local features and aspects of extremes varied with the choice of RCM (Kjellström et al., 2007). This suggested the need to explore uncertainty due to regional model formulation, which in part led to the ENSEMBLES experimentation set-up (Table 5.1). Also, inasmuch as one particular RCM may amplify climate change signals in some GCM, another RCM may weaken the same. In this sense, RCMs are not readily interchangeable. Subsampling could thus artificially inflate or downplay uncertainty.

At the start of ENSEMBLES, most of the RCMs were either new versions or otherwise untried for the ENSEMBLES set-up. Thus, there was no *a priori* information on which models might amplify or weaken the GCM climate change signals. Consequently, efforts were spread over the available models to the degree possible in terms of available computational resources. (Quite a few additional runs were provided in the end, adding to the runs stipulated by the project contract.)

Uncertainty in radiative forcing

All the RT2B regional climate projection runs extended over the period 1951–2050, with many continuing all the way to 2100. The choice of the emission scenario is of less importance for the early decades of the 21st century than for the later ones. Consequently, one emission scenario was chosen for use in the runs, so as to be in a better position to explore uncertainties due to the choice of boundary conditions (i.e., the GCM) and model formulation (i.e., the RCM). After joint considerations with RT1 and RT6, the SRES A1B scenario was chosen.

Uncertainty due to initial conditions

As concluded in the PRUDENCE project, the uncertainty due to initial conditions is of less importance than the other uncertainties (Déqué et al., 2007) towards the end of the 21st

century. However, this uncertainty is relatively larger in the first few decades, as the climate change signal is not large for this period of time (Kjellström et al., 2009). Also, higher-order variability may be more sensitive to the choice of sampling than changes in seasonal and annual averages, as shown for interannual variability. Kendon et al. (2008) have shown that internal variability significantly affects our ability to measure robust signals of extreme precipitation change, with multi-annual variability contributing significantly to the overall uncertainty.

The resulting GCM-RCM matrix

The final GCM-RCM matrix is shown in Table 5.1. These runs provided input for regional climate change and impact analyses in RT2B and RT6. The matrix is foreseen to leave a legacy after ENSEMBLES, such as prompting further additional simulations to add to the ensemble.

Inflating the matrix

Although this GCM-RCM matrix was large and better populated than what had been achieved in other projects, such as PRUDENCE, it still has many empty cells. To ‘fill in the blanks’ requires an estimation of the GCM-RCM pairs’ climate change signals that have not been explicitly run. For this, both a pattern-scaling approach and a method based on the analysis of variance (ANOVA) were used in the joint RT3/RT2B work. The local pattern-scaling approach is outlined in Section 6.3.4. Here we only note briefly that local scaling using the large-scale change in the GCM as a predictor of the local-scale climate response in the

RCM was found to have some skill in estimating local changes for different driving GCMs and hence for filling the matrix.

In Déqué et al. (2007) the missing cells in the PRUDENCE matrix were filled in with a method based on ANOVA. This method has been refined within ENSEMBLES (Déqué et al., 2009) based on weather regime decomposition (see Vautard, 1990). Thus the method now also accounts for the GCM providing large-scale forcing on the RCM. A clustering of the daily 500 hPa height values over the North Atlantic–Europe domain leads to large-scale patterns that can be linked to weather in Europe (Robertson and Ghil, 1999); the most commonly studied being the positive and negative phases of the North Atlantic Oscillation. Here, clustering in four regimes, such as in Michelangeli et al. (1995), is applied.

The method assumes that the way the RCM behaves under a given regime only depends on the RCM. The matrix completion was tested by removing an RCM-GCM pair and comparing its reconstruction with the original response. This could be done only for the RCMs that were run with two GCMs. For these runs the reconstructed results showed reasonable skill for temperature, but demonstrated only little skill for precipitation. Table 5.2 shows the RCM-based winter (DJF) temperature changes averaged over Europe. The results reconstructed as described above are shaded. It is worth mentioning that the reconstructed responses may be well outside the range of the explicitly simulated responses. The average of the seventeen original responses is little changed when considering the full matrix of 98 responses: on average over Europe, the

Table 5.1: The ENSEMBLES RCM simulations at 25 km resolution. Those simulations and institutions marked with an asterisk (*) are outside of the contractual runs. For the METO-HC GCM, there are standard (std), low, and high sensitivity runs.

RCM	GCM	ERA40	METO-HC, Std	METO-HC, Low	METO-HC, High	MPIMET	IPSL	CNRM	NERSC	CGCM3	Total
METO-HC HadRM	1961–2002	1951–2100	1951–2100*	1951–2100*	1951–2100						4
MPIMET REMO	1961–2002				1951–2100	1951–2050*					2
CNRM ALADIN	1961–2002							1951–2050			1
DMI HIRHAM	1961–2002				1951–2100*			1951–2100	1951–2100*		3
ETH CLM	1961–2002	1951–2100									1
KNMI RACMO	1961–2002				1951–2100						1
ICTP RegCM	1961–2002				1951–2100						1
SMHI RCA3	1961–2002		1951–2100*		1951–2100*				1951–2100		3
UCLM PROMES	1961–2002	1951–2050	1951–2050								1
C4I RCA3	1961–2002				1951–2100*	1951–2050*					2
GKSS CLM	1961–2002						1951–2050*				1
Met.No HIRHAM	1961–2002	1951–2050							1951–2050*		1
CHMI ALADIN	1961–2002							1951–2050*			1
OURANOS* CRCM	1961–2002									1951–2050*	1
EC* GEMLAM	1961–2002										
VMGO* VMGO			1951–2050*								1
Total			3	3	2	7	2	3	3	1	25

Table 5.2: RCM-GCM response for DJF temperature (°C) over Europe, by 2021–2050, compared with 1961–1990.

RCM \ GCM	NERSC	CGCM3	CNRM	METO-HC,Low	METO-HC,Std	METO-HC,High	MPIMET
C4I	1.82	1.80	2.13	2.72	2.82	2.18	1.67
CNRM	0.95	0.94	1.38	1.86	1.96	1.93	0.83
DMI	1.08	1.02	1.84	1.98	2.09	2.03	1.07
ETHZ	1.86	1.66	2.12	2.70	2.22	2.76	1.69
HC-lo	1.91	1.79	2.20	2.29	2.89	2.85	1.75
HC-med	2.05	1.90	2.32	2.90	2.44	2.96	1.87
HC-hi	1.99	1.86	2.26	2.85	2.96	2.34	1.82
ICTP	0.74	0.74	1.05	1.64	1.74	1.69	1.13
KNMI	0.85	0.74	1.13	1.72	1.84	1.79	1.22
METN	1.44	0.58	1.16	1.72	1.85	1.77	0.69
MPI	0.81	0.77	1.09	1.70	1.81	1.76	1.21
OURANOS	1.33	1.21	1.59	2.14	2.27	2.18	1.11
SMHI	1.22	0.98	1.38	2.11	2.07	2.02	1.18
UCLM	1.93	1.77	2.19	2.77	2.28	2.84	1.75

temperature response increases by 0.1 K (in winter, but also in summer). The precipitation response, on the other hand, decreases by 0.02 mm/day.

The efforts on the RCM-GCM matrix were further extended into studies on sampling strategies, i.e., how to produce a design of runs that is as optimal as possible. On one hand, the number of models to consider and runs to conduct should be as small as possible in order to reduce the computational demand. On the other hand, the matrix should be sufficient to provide reasonable sampling of uncertainties.

Work assessing the optimal design for RCM-GCM experimental matrices (Kendon et al., 2009) suggests that priority should be given to sampling different driving GCMs, whereas a reduced set of RCMs could be enough if the interest lies in temperature and precipitation changes in the latter half of the century. The ANOVA results (Déqué et al., 2009) show that, for mid-century and 25 km resolution, several RCMs per GCM are warranted because the way that local ‘weather’ is linked to a large-scale regime is strongly RCM-dependent.

5.3 Applications

5.3.1 Climate projection based on the ENSEMBLES Regional Climate Model ensemble

The final RT3 RCM system consisted of the RCMs evaluated in RT3, the GCM-RCM pairing strategy and the studies on performance-based weighting. The system was consequently applied by RT2B to create a set of transient regional climate change projections for Europe (see Section 6). The ‘present-day’ part of these simulations that nominally overlaps the RT3 evaluation simulation period (the period 1958–2002) was studied by both RT2B and RT3.

For example, application of the RT3-derived weights to the RT2B-runs’ present-day component did not lead to significant improvements of the multi-model temperature or precipitation results compared with an unweighted multi-model mean (see Figure 5.6) when averaged over the entire European region. Other examples are shown in Section 6. Another result was that the multi-model GCM-forced RCM runs show less interannual

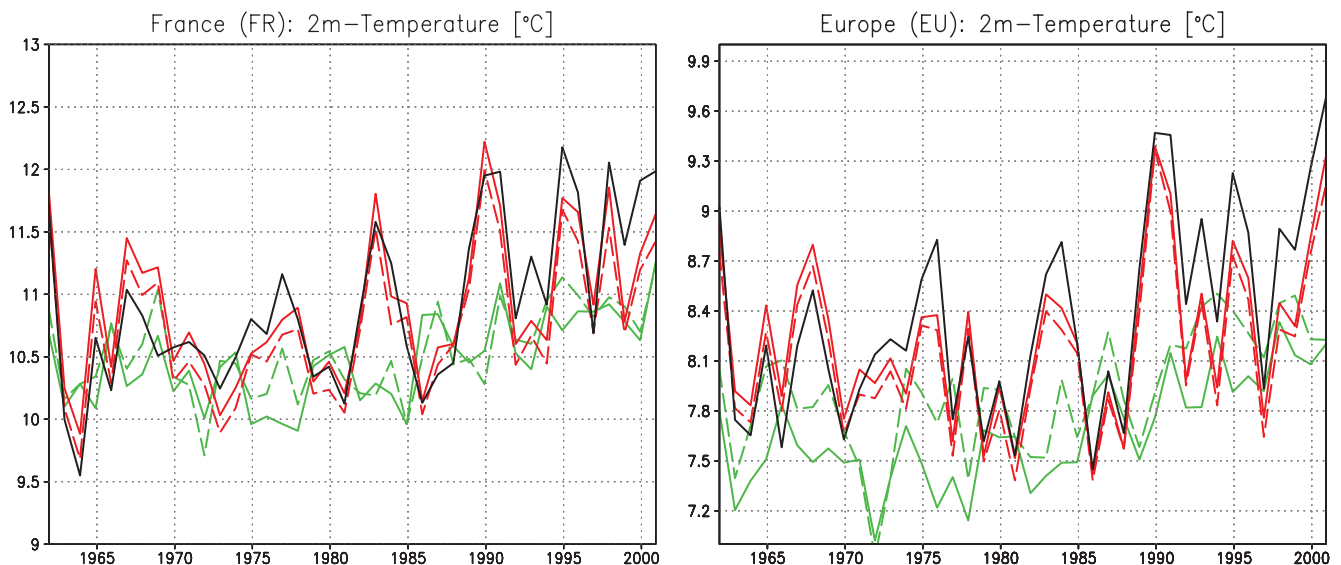


Figure 5.6: Evolution of annual 2 m temperature (°C): RT5 observational dataset (black line), the ERA40-driven RT3 RCM runs (red), the control period of the RT2B transient climate change projections (green). Solid lines show the equal-weighted multi-model RCM mean. Dashed lines depict a weighted (using a simple multiplication of the metrics) multi-model mean. The results on the left are for one European region (France) and the results on the right are for the European land region.

variability than the ERA40-driven runs. In the former, the simulated interannual variability is different depending on the driving GCM and tends to average out. In the latter the synoptic course is the same for all RCMs. The respective warming trend over the last few decades was, by and large, the same in the RCM runs and the observations – albeit slightly smaller in the former (Lorenz and Jacob, in preparation).

For additional applications of the RT3/RT2B RCM runs in ENSEMBLES impact studies, please refer to Section 9.

5.3.2 Regional Climate Model ensemble investigation for West Africa

Introduction

RT3 included a study of West African climate (Rummukainen et al., 2009), leading to a close collaboration with the AMMA project (Redelsperger et al., 2006). On one hand, regional climate modelling provided input to the process and impact studies by AMMA. On the other, AMMA made available observational data for RCM evaluation. For RT3, the benefit was that European RCMs could be tested for another climate regime. The region in question has strong climatic gradients from the Gulf of Guinea in the south, to the Sahara in the north, and these are not adequately resolved by present-day GCMs. Consequently, it was interesting to investigate whether higher-resolution RCMs could play a role in reducing uncertainties and hence provide more reliable estimates of future change.

As for the European region, the RCM runs were coordinated, data archiving was discussed with users, and both evaluation and climate projection runs were made. The results were imported to the same RCM data archive at DMI that hosted the European data. There also were some differences from the European region RCM set-up: the total number of RCMs and runs was smaller, the evaluation runs were forced by the so-called ERA-Interim (rather than ERA-40) data, which also

meant that only the period since 1989 could be covered. The ERA-Interim dataset was used because it has been shown to significantly improve the simulation of the hydrological cycle over tropical regions.

The first stream West Africa simulations (see Table 5.3), driven by the ERA-Interim reanalysis (Uppala et al., 2008), show to what extent the RCMs differ from one another and also give insight into the regional dynamics of this region's climate. The second stream involved runs at 50 km for 1991–2050, with forcing according to SRES A1B and three different GCMs.

Analysing ENSEMBLES Regional Climate Model performance for West Africa

Although independent RCM studies have been undertaken in the past, the RCM simulations produced by ENSEMBLES for the West African domain provide an unprecedented resource for climate research in this region. These coordinated experiments allow for an evaluation of model uncertainty in this tropical region, in a similar manner to what has been undertaken for the European domain. Not least, intraseasonal and interannual characteristics of the West African Monsoon (WAM) are of particular interest, as well as land–atmosphere interactions (van den Hurk and van Meijgaard, 2009). The results indicate promising skill in the models' ability to represent the dominant spatial features and the seasonal cycle of WAM rainfall. In Figure 5.7, the mean seasonal evolution of rainfall over the Guinea Coast and Sahelian zones for five of the RCMs is compared with observations.

All models distinctly capture the three phases of the monsoon, but with varying degrees of accuracy in the magnitude and timing of these phases. For example, the HIRHAM RCM greatly overestimates rainfall amounts along the coast (~6°N), but reasonably captures the Sahel rainy season. RCA represents the coastal rainfall well, but has a premature onset of the Sahel rainy season.

By the end of the ENSEMBLES project, several studies were under way. One of these was on land–atmosphere coupling, focusing on regions and seasons of strong coupling as defined by significant correlations (1) between soil moisture and evaporation and (2) between soil moisture and the precipitation recycling ratio. Areas where both correlations are positive are shown in Figure 5.8 for one RCM. They are concentrated at the boundaries of the migrating wet season. A surprisingly small coherence was found, probably because the atmosphere is often too dry to generate precipitation, and perhaps also because alternating dry and wet conditions may promote advection.

In areas with strong land–atmosphere interactions, clear seasonal cycles of soil moisture and atmospheric humidity introduce asymmetries. This suggests that phasing of atmospheric properties plays an important role in land–atmosphere feedback in most regions of West Africa.

Regional climate change ensemble application

The second stream Regional Climate Model simulations provided transient projections of future climate change, again for the A1B scenario and with different GCM boundary forcing.

Table 5.3: The RT3 RCM simulations for West Africa.

GCM RCM	ERA-Interim	METO-HC Std	MPIMET	CNRM
METO-HC HadRM	1990–2007	1990–2050		
MPIMET REMO	1990–2007		1990–2050	
DMI HIRHAM	1990–2007		1990–2050	
KNMI RACMO	1990–2007		1990–2050	
ICTP RegCM	1990–2007		1990–2050	
SMHI RCA3	1990–2007	1990–2050		
UCLM PROMES	1990–2007	1990–2050		
GKSS CLM	1990–2007			
Met.No HIRHAM	1990–2007	1990–2050		
CHMI ALADIN	1990–2007			1990–2050
INM RCA3	1990–2007	1990–2050		
Total	11	5	4	1

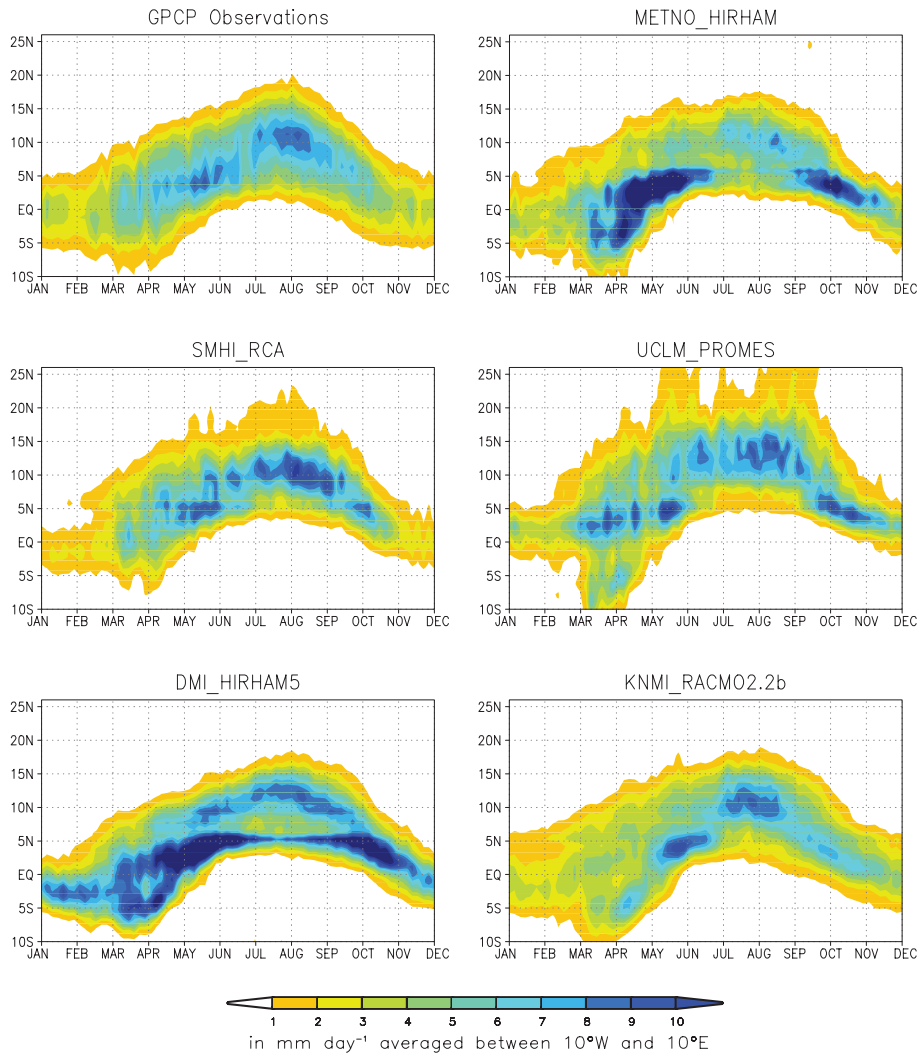


Figure 5.7: Mean seasonal cycle (pentad composites for 1989–2007) of rainfall over West Africa for the Global Precipitation Climatology Project (GPCP) and five RCMs driven by ERA-Interim reanalysis.

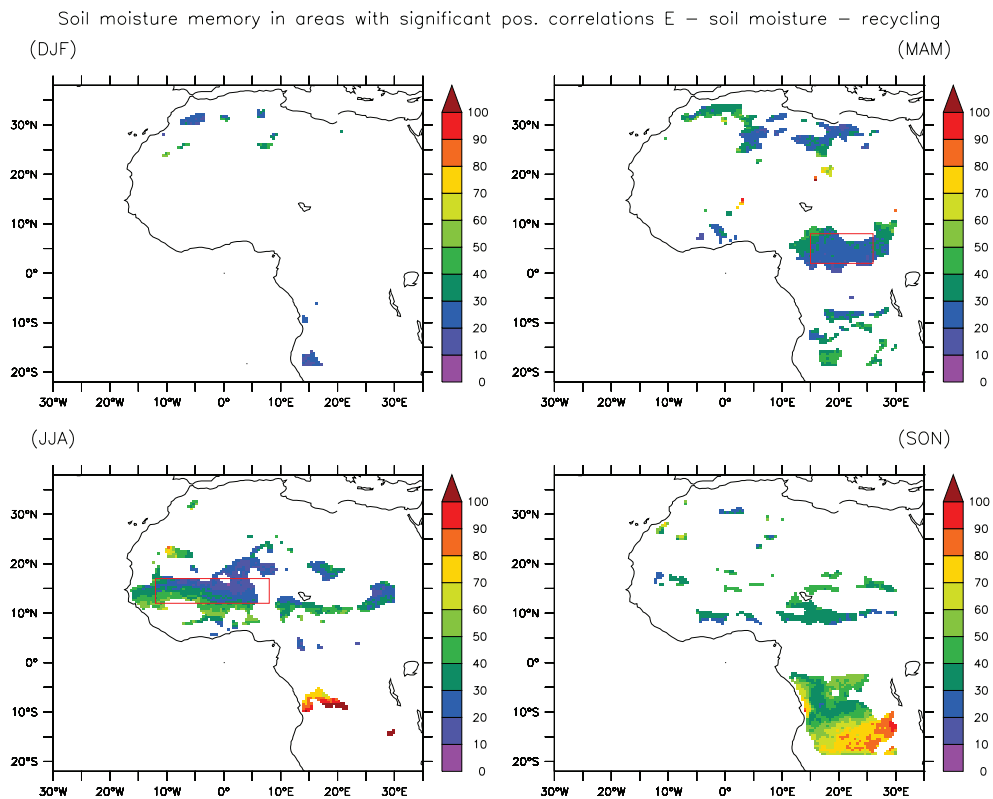


Figure 5.8: Soil memory (days) per season in areas with positive correlations.

This represents the first comprehensive source of information for assessing likely regional climate changes over West Africa, and associated uncertainties, which can feed directly into impacts and adaptation studies (Figure 5.9)

At the time of the writing of this report, the ENSEMBLES RCM climate change projections for West Africa are under analysis.

5.3.3 Regional studies facilitated by ENSEMBLES

AMMA (Redelsperger et al. 2006) partners currently use these RCM simulations for process and impact studies for Western Africa. Some examples of these studies are:

- Regional evaluation of the seasonal cycle of rainfall for the 2000-2003 period is made by ENEA. The RCMs have so far been found to show large differences in their ability to reproduce the onset and retreat of the monsoon on the Guinean coast and the Sahel zone. Further analysis and in particular a comparison with the spread of GCMs in their ability to simulate these characteristics of the monsoon rainfall is foreseen. The objective is to quantify the added value of using regional models forced by re-analysis compared to GCMs for reproducing rain fields.
- The University of Cotonou uses the detailed rainfall observations obtained during the AMMA field campaign

(2005-2007) over the upper Ouémé site to evaluate the quality of simulated rainfall. This analysis concentrates on smaller spatial scales and synoptic variability. One of the questions to be answered is the ability of RCMs to capture the main features of the large convective systems which produce most of the rain in the region.

- 2iE in Ouagadougou and UPCT in Cartagena concentrate on the regional climate change simulations. They look at the projected evolution of the dry spells which occur during the rainy season and how the intra-seasonal characteristics of the monsoon might evolve in a warmer climate. Also water resources impact studies are made for the upper Volta basin (The Nakambé) for estimates of water resources until 2050.
- IPSL examines the potential of RCM simulations to drive the crop yield models developed within AMMA. This entails testing the ability of these simulations to reproduce realistic inter-annual variations of crop yield. Once this is established then the impact of climate change is examined. The large number of simulations available will allow to test the climate related uncertainty and compare it to those linked to farming practices or market evolutions.

It is expected that other studies will be forthcoming over the next few years, contributing to the overall outcome and legacy of the ENSEMBLES project.

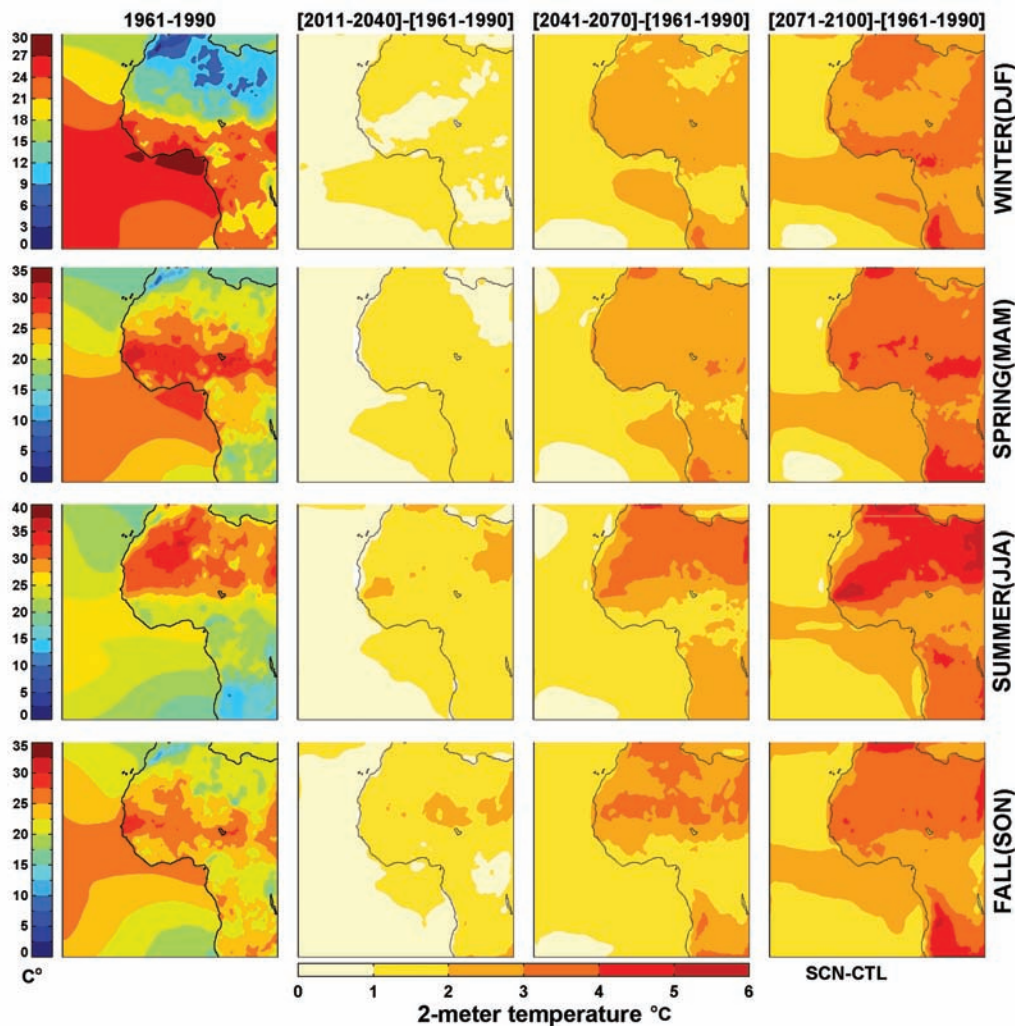


Figure 5.9: An example of ENSEMBLES RCM climate change projections for West Africa (following Rummukainen et al., 2009). From top to bottom, results for three-month seasons of DJF, MAM, JJA and SON.

References

ENSEMBLES publications are highlighted as bold text.

Boberg F, Christensen JH, Lucas-Picher O, Christensen OM, 2009. Bias corrected climate change projections over Europe: exploring an ensemble of regional climate models. In preparation

Christensen JH, Carter TR, Rummukainen M, Amanatidis G, 2007. Evaluating the performance and utility of regional climate models: the PRUDENCE project. *Climatic Change* 81(Supplement 1), 1–6.

Christensen JH, Christensen OB, 2007. A summary of the PRUDENCE model projections of changes in European climate by the end of this century. *Climatic Change* 81(Supplement 1), 7–30.

Christensen JH, Giorgi F, Rummukainen M, 2009. Weighting models based on several RCM-specific metrics: does it work? Climate Research, to be submitted.

Christensen, H, Boberg F, Christensen OB, Lucas-Picher P, 2008. On the need for bias correction of regional climate change projections of temperature and precipitation. Geophysical Research Letters 35, L20709, doi:10.1029/2008GL035694.

Collins M, Booth BBB, Harris GR, Murphy JM, Sexton DMH, Webb MJ, 2006. Towards quantifying uncertainty in transient climate change. *Climate Dynamics* 27, 127–147.

Déqué M, Rowell DP, Lüthi D, Giorgi F, Christensen JH, Rockel B, Jacob D, Kjellström E, Castro M, van den Hurk B, 2007. An intercomparison of regional climate simulations for Europe: assessing uncertainties in model projections. *Climatic Change* 81(Supplement 1), 53–70.

Déqué M, Somot S, Sanchez-Gomez E, Goodess CM, Jacob D, Lenderink G, Christensen OB, 2009. The spread amongst ENSEMBLES regional scenarios: regional climate models, driving general circulation models and interannual variability. Climate Dynamics, submitted.

Farda A, Déqué M, Somot S, Horanyi A, Spiridonov V, Toth H, 2009. The ALADIN model as a regional climate model for Central and Eastern Europe. Studia Geophysica et Geodaetica, submitted.

Frei C, Schär C, 1998. A precipitation climatology of the Alps from high-resolution rain-gauge observations. *International Journal of Climatology* 18, 873–900.

Haylock MR, Hofstra N, Klein Tank AMG, Klok EJ, Jones PD, New M, 2008. A European daily high-resolution gridded dataset of surface temperature and precipitation. Journal of Geophysical Research 113, D20119, doi:10.1029/2008JD10201.

Hohenegger C, Brockhaus P, Bretherton CS, Schär C, 2009. The soil moisture-precipitation feedback in simulations with explicit and parameterized convection. Journal of Climate, in press.

Hohenegger C, Brockhaus P, Schär D, 2008. Towards climate simulations at cloud-resolving scales. Meteorologische Zeitschrift 17, 383–394.

Jacob D, Bärring L, Christensen OB, Christensen JH, de Castro M, Déqué M, Giorgi F, Hagemann S, Hirschi M, Jones R, Kjellström E, Lenderink G, Rockel B, Sánchez E, Schär C, Seneviratne SI, Somot S, van Ulden A, van den Hurk B, 2007. An intercomparison of regional climate models for Europe: model performance in present-day climate. *Climatic Change* 81(Supplement 1), 31–52.

Jacob D, et al., 2009. An ensemble of high resolution regional climate change projections for EUROPE: datasets for impact research and adaptation strategies. In preparation

Jaeger EB, Anders I, Lüthi D, Rockel B, Schär C, Seneviratne S, 2008. Analysis of ERA40-driven CLM simulations for Europe. Meteorologische Zeitschrift 17, 349–367.

Kendon EJ, Jones RG, Kjellström E, Murphy JM, 2009. Using and designing GCM-RCM ensemble regional climate projections. Journal of Climate, to be submitted.

Kendon EJ, Rowell DP, Jones RG, Buonomo E, 2008. Robustness of future changes in local precipitation extremes. Journal of Climate 21, 4280–4297.

Kjellström E, Bärring L, Jacob D, Jones R, Lenderink G, Schär C, 2007. Modelling daily temperature extremes: recent climate and future changes over Europe. *Climatic Change* 81(Supplement 1), 249–265.

Kjellström E, Giorgi F, Rummukainen M, Lenderink G, 2009. Evaluation of an ensemble of regional climate model simulations for the ERA40-period. Climate Research, to be submitted.

Kostopoulou E., Tolika K, Tegoulas I, Giannakopoulos C, Somot S, Anagnostopoulou C, Maheras P, 2009. Evaluation of a regional climate model using in-situ temperature observations over the Balkan Peninsula. Tellus A 61, 357–370.

Lenderink G, van Meijgaard E, 2008. Increase in hourly precipitation extremes beyond expectations from temperature changes. Nature Geoscience 1, 511–514.

Lind P, Kjellström E, 2009. Water budget in the Baltic Sea drainage basin: evaluation of simulated fluxes in a regional climate model. Boreal Environment Research 14, 56–67.

Lorenz P, Jacob D, in preparation. Validation of temperature trends in the ENSEMBLES RCM runs driven by ERA40. To be submitted to Climate Research, special issue on Regional Climate Model Evaluation and Weighting.

Meehl GA, Stocker TF, Collins WD, Friedlingstein P, Gaye AT, Gregory JM, Kitoh A, Knutti R, Murphy JM, Noda A, Raper SCB, Watterson IG, Weaver AJ, Zhao ZC, 2007. Global climate projections. In: *Climate Change, 2007: The Physical Science Basis. Contribution of Working Group I to the Fourth Assessment Report of the Intergovernmental Panel on Climate Change* (S Solomon, D Qin, M Manning, Z Chen, M Marquis, KB Averyt, M Tignor, HL Miller, eds). Cambridge University Press, Cambridge, UK and New York.

Michelangeli P, Vautard R, Legras B, 1995. Weather regimes: recurrence and quasi stationarity. *Journal of Climate* 52, 1237–1256.

Pall P, Arnold J, Kotlarski S, Bosshard T, Schär C, 2009. Evaluation of heavy Alpine precipitation in ENSEMBLES regional climate models. In preparation.

Radu R, Déqué M, Somot S, 2008. Spectral nudging in a spectral regional climate model. Tellus A 60, 885–897.

Räisänen J, Hansson U, Ullerstig A, Döscher R, Graham LP, Jones C, Meier HEM, Samuelsson P, Willén U, 2004. European climate in the late twenty-first century: regional simulations with two driving global models and two forcing scenarios. *Climate Dynamics* 22, 13–31.

Rauscher SA, Coppola E, Piani C, Giorgi, F, 2009. Resolution effects on regional climate model simulations of sea-

- sonal precipitation over Europe. *Climate Dynamics*, doi:10.1007/s00382-009-0607-7.
- Redelsperger J-L, Thorncroft CD, Diedhiou A, Lebel T, Parker DJ, Polcher J, 2006. African Monsoon Multidisciplinary Analysis (AMMA): an international research project and field campaign. *Bulletin of the American Meteorological Society* 87, 1739–1746.
- Robertson AW, Ghil M, 1999. Large-scale weather regimes and local climate over the western United States. *Journal of Climate* 12, 1796–1813.
- Rummukainen M, Giorgi F, the ENSEMBLES RT3 participants, 2009. ENSEMBLES regional climate model simulations for Western Africa (the ‘AMMA’ region). In: Second International Lund RCM workshop ‘21st Century Challenges in Regional-scale Climate Modelling’, 4–8 May, 2009: Workshop Proceedings (B Rockel, L Bärring, M Reckermann, eds). International BALTEX Secretariat Publication No. 41, 213–214.**
- Sanchez E, Romera R, Gaertner MA, Gallardo C, Castro M, 2009. A weighting proposal for an ensemble of regional climate models over Europe driven by 1961–2000 ERA40 based on monthly precipitation probability density functions. *Atmospheric Science Letters*, doi:10.1002/asl.230.**
- Sanchez-Gomez E, Somot S, Déqué M, 2009a. Ability of an ensemble of regional climate models to reproduce weather regimes over Europe–Atlantic during the period 1961–2000. *Climate Dynamics* 33, 723–736.**
- Sanchez-Gomez E, Somot S, Elguindi N, Josey S, Déqué M, 2009b. Evaluation of the Mediterranean Sea water and heat budgets as simulated by an ensemble of high-resolution regional climate models. *Journal of Geophysical Research – Ocean*, submitted.**
- Uppala S, Dee D, Kobayashi S, Berrisford P, Simmons A, 2008. Towards a climate adapt assimilation system: status update of ERA-Interim. *ECMWF Newsletter* 115, 12–18.
- van den Hurk BJM, van Meijgaard E, 2009. Diagnosing land–atmosphere interaction from a regional climate model simulation over West Africa. *Journal of Hydrometeorology*, submitted.
- van Ulden AP, Lenderink G, van den Hurk B, van Meijgaard E, 2007. Circulation statistics and climate change in Central Europe: PRUDENCE simulations and observations. *Climatic Change* 81(Supplement 1), 179–182.
- van Ulden AP, van Oldenborgh GJ, 2006. Large-scale atmospheric circulation biases and changes in global climate model simulations and their importance for climate change in Central Europe. *Atmospheric Chemistry and Physics* 6, 683–881.
- Vautard R, 1990. Multiple weather regimes over the north Atlantic: analysis of precursors and successors. *Journal of Climate* 118, 2056–2081.

6 Downscaling methods, data and tools for input to impacts assessments

[Research Theme 2B]

C.M. Goodess (UEA), D. Jacob (MPI), M. Déqué (Météo-France), J.M. Gutiérrez (University of Cantabria), R. Huth (CAS), E. Kendon (Met Office), G.C. Leckebusch (FUB), P. Lorenz (MPI), V. Pavan (ARPA-SIMC)

6.1 Introduction

RT2B provided the regional component of the ENSEMBLES climate model engine, drawing on the regional modelling system developed in RT3. The main task for RT2B was to provide relevant and – if possible – robust information on regional climate change as input data for climate change impact assessments, in particular those undertaken in RT6.

The starting point for this work was the PRUDENCE, STARDEX, MICE and DEMETER projects. As in these earlier projects, two different downscaling approaches (dynamical and statistical) were used, but the emphasis of work has shifted to reflect the scientific objectives of ENSEMBLES and the aim of maximising exploitation of the results. This shift of emphasis is demonstrated by the five key issues which are highlighted in this section.

- The adaptation of existing downscaling methods for probabilistic projections.
- The synergistic use of dynamical and statistical downscaling.
- The integration of downscaling work on climate change and seasonal-forecasting time-scales.
- The shift of emphasis to tools.
- Meeting user needs.

6.2 Adapting methods for probabilistic projections

Exploration of uncertainty is central to ENSEMBLES work. The downscaling step is centrally embedded in the cascade of uncertainty and thus needs to take account of ‘upstream’ uncertainty (in the case of ENSEMBLES, the information provided by RT1, RT2A and RT7), as well as accounting for the downscaling uncertainties themselves (information from RT2B and RT3), before passing on accessible and relevant information to ‘downstream’ users (such as RT6). See Figure 1.1 for an illustration of this flow of information.

While the earlier PRUDENCE, STARDEX and DEMETER projects undertook some preliminary analyses of downscaling uncertainty, these were not extensive and, at least in the case of climate change projections, information was not presented in a probabilistic way. Thus, adapting downscaling methods for probabilistic climate change projections has been a major challenge for the regional work in ENSEMBLES.

The emphasis of this work has been on uncertainties associated with the boundary conditions driving the downscaling models and the downscaling uncertainties themselves. For both science and policy reasons, it makes sense to consider these uncertainties separately from the emissions scenarios uncertainties, particularly for users whose main concern is changes over the first part of the century, where the choice of emissions scenario is less important. Thus the RT2B climate change work has focused on the A1B emissions scenario, using outputs from the RT2A stream 1 simulations.

6.2.1 Sampling and ‘quantifying’ the uncertainties

Dynamical downscaling

One of the major achievements and legacies of ENSEMBLES is the production of a large ensemble of transient RCM runs for Europe at 25 km resolution for the A1B scenario (Jacob et al., 2009). All runs cover the time period 1950–2050 (the period of greatest interest to most applications users and stakeholders), with many of them extending to 2100 (when the signal-to-noise ratio is highest). This ensemble was designed jointly by RT3 and RT2B partners, and the construction of the GCM-RCM matrix is described in Section 5.2.6. Project resources did not permit this matrix to be completely filled, although this is an issue for ongoing discussion in the European RCM community. Statistical techniques for extending the matrix are discussed in Sections 6.3 and 5.2.6. Nonetheless, the ENSEMBLES RCM ensemble is the largest available for any region of the world and is readily accessible to users (see Section 6.6).

A so-called ‘quick-look’ analysis was undertaken in order to monitor the progress and quality of the simulations (important for the project team), and to provide first results at an early stage (important for users). The analysis focused on near-surface temperature, precipitation and evaporation and used the eight PRUDENCE regions. Figure 6.1 shows, as an example, the temporal evolution of annual near-surface temperature for the ‘Scandinavia’ region, while Figure 6.2 shows the annual precipitation totals.

In Scandinavia, temperatures show an increasing trend throughout the entire 21st century (Figure 6.1). This is typical of the behaviour for all European regions; only the strengths

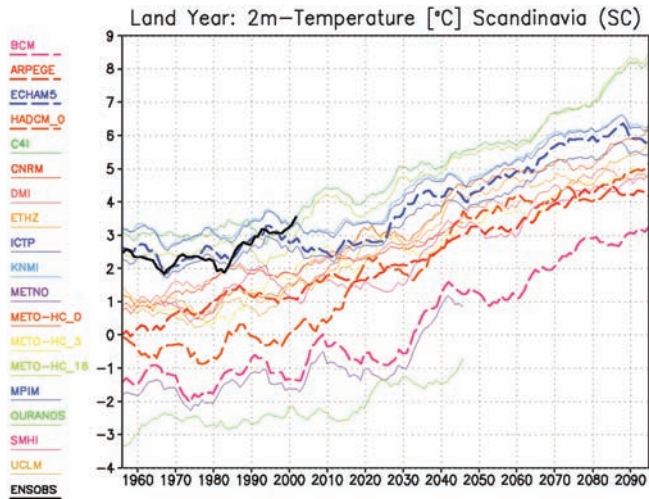


Figure 6.1: Time-series (running 10-year mean) of annual mean near-surface (2 m) temperature ($^{\circ}\text{C}$) for the land fraction of the PRUDENCE region 'Scandinavia'. Dashed thick lines show the driving GCMs, thin lines the ENSEMBLES RCMs, and the black line the ENSEMBLES RT5 gridded observational dataset.

of the temperature increases vary from region to region. Compared with observations (black line in Figure 6.1), three of the four shown GCMs and several RCMs start from a clear cold bias during the 20th century. The increase in temperature is, however, clearly visible in all simulations.

Less obvious is the trend in precipitation for Scandinavia (Figure 6.2). For some models, almost no trend is visible, whereas others show only a small trend. The overestimation of observed precipitation in all simulations is striking (see also Section 5.2.4). This can only partly be explained by the observations being too low due to undercatch of precipitation drifting around rain gauges. The overestimation could be caused either by deficiencies in model formulation or by too much moisture being transported into the domain from the GCM boundary information. One study of the RCA3-simulated water budget for the Baltic Sea drainage basin shows that part of the overestimated precipitation in this region is due to poor boundary conditions, but the wet bias in the global model is reinforced by the RCM (Kjellström and Lind, 2009).

For the annual precipitation trends, there is no clear signal across all regions. While there is some indication of an increasing trend for Scandinavia, there are other regions with nearly no change, or with moderate decreasing trends. However, for the seasonal trends in precipitation (not shown), there are – for most regions – clear decreasing trends in summer (JJA) over the 21st century, which are strongest in the southern regions, and clear increasing trends for winter (DJF), which are strongest in the northern regions.

Analyses have also been undertaken of more 'applied' variables. For example, changes in the Mediterranean Sea water budget have been explored (Sanchez-Gomez et al., 2009). Compared with the IPCC AR4 GCMs (Mariotti et al., 2008), the RCMs give major improvements in aspects such as runoff and Black Sea discharge terms. The transient RCM runs show the emergence of significant changes from 2050, with a

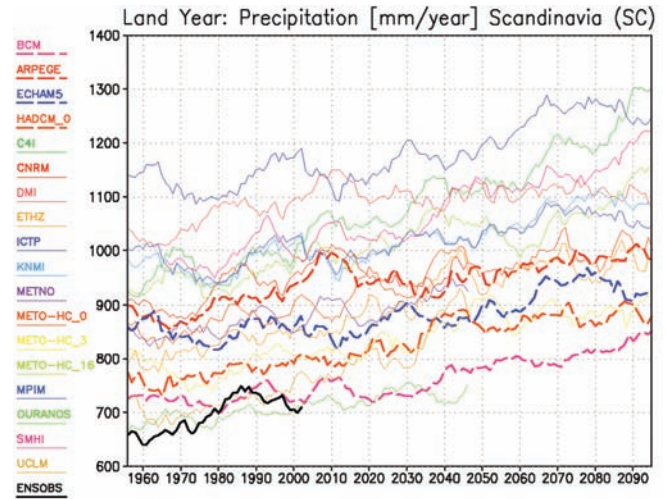


Figure 6.2: Time-series (running 10-year mean) of annual precipitation totals (mm/yr) for the land fraction of the PRUDENCE region 'Scandinavia'. Dashed thick lines show the driving GCMs, thin lines the ENSEMBLES RCMs, and the black line the ENSEMBLES RT5 gridded observational dataset.

large increase of +40% in the Mediterranean fresh water deficit from 1950–1999 to 2070–2099.

Robustness of RCM results

The uncertainties embedded in the development of the climate systems models and estimation of possible changes are very large and only partly quantifiable (see Section 5). Nonetheless, adaptation to climate change requires robust information about possible regional changes. Thus, preliminary steps to analysing the robustness of the ENSEMBLES RCM annual climate-change signals are shown in Figures 6.3–6.6 (based on results from sixteen RCMs). For near-surface temperature, the signal of the multi-model mean is positive in all parts of Europe (Figure 6.3) and is much larger than the standard deviation (Figure 6.4). This increase in temperature can therefore be interpreted as a robust signal.

For precipitation, Europe can clearly be divided into two regimes, with increased precipitation in the north and decreased precipitation in the south (Figure 6.5). This pattern can also be interpreted as a robust one, since the number of models agreeing on an increasing precipitation signal reaches sixteen out of sixteen for the northern increase, and only two to four out of sixteen disagree with the decrease in the south.

These findings are in general agreement with earlier studies from the PRUDENCE project. However, since the ENSEMBLES results are based on a larger GCM-RCM matrix, a somewhat lower emissions scenario (A1B rather than A2) and a closer to present-day period (2021–2050 rather than 2071–2100), they provide stronger evidence of the robustness of these climate-change signals.

In addition, the robustness of seasonal changes in precipitation is shown in Figure 6.7. Here, a new approach based on weather regimes has been used to estimate changes for missing cells in the GCM-RCM matrix (see Section 5), allowing statistical significance to be assessed. In large parts of Europe, significant

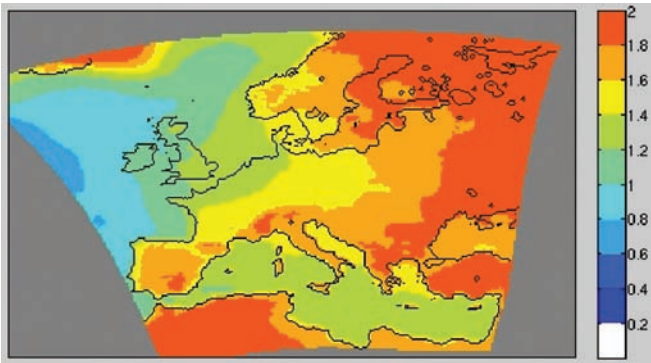


Figure 6.3: Climate-change signal (2021–2050 minus 1961–1990) for annual near-surface (2 m) temperature (°C) for the multi-model mean of the ENSEMBLES RCMs.

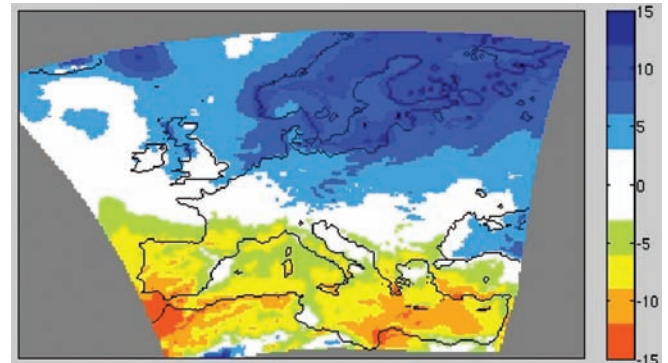


Figure 6.5: Climate-change signal (2021–2050 relative to 1961–1990) for annual precipitation total (%) for the multi-model mean of the ENSEMBLES RCMs.

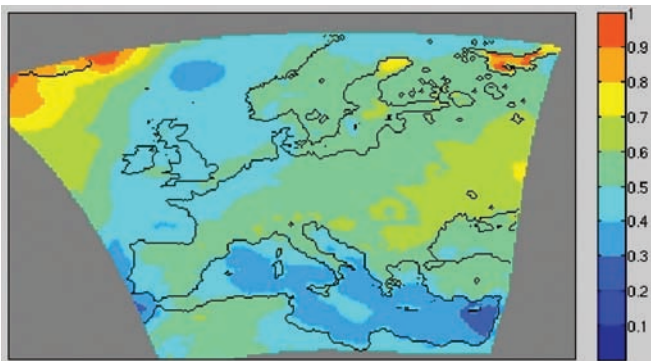


Figure 6.4: Inter-model standard deviation of the climate-change signal (2021–2050 minus 1961–1990) for annual near-surface (2 m) temperatures (°C) for the ENSEMBLES RCMs.

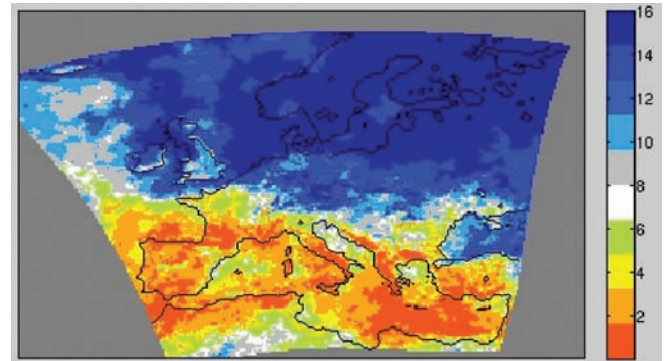


Figure 6.6: Number of RCMs which show an increase in precipitation (2021–2050 relative to 1961–1990) for the ENSEMBLES RCMs.

and spatially coherent patterns in winter and summer precipitation trends are visible, although there are also quite extensive areas with no significant patterns. These results are in general agreement with those coming directly from the ENSEMBLES GCMs (Figures 3.11 and 4.3), but the added regional detail is of utmost importance for downstream impact assessments. For Scandinavia, the signal of increasing precipitation is robust for both winter and summer, while for the UK the winter precipitation increase is robust but there is no summer signal, and for much of southern Europe the only clear signal is the summer decrease. At the same time, there are areas such as the south-east Iberian Peninsula, the Alps and parts of central Europe with no clear signal in either season. Complementary ENSEMBLES work (Kendon et al., 2009a) analysing the underlying mechanisms has shown that model agreement in precipitation change across Europe generally reflects the dominance of mechanisms in which we have high confidence. In particular, increases in precipitation across northern Europe in winter are dominated by increasing atmospheric moisture with warming; whilst, in summer, warming combined with reduced soil moisture drives decreases in precipitation across southern Europe.

As well as considering the coherence and consistency of the climate-change signal as a component of robustness, issues related to model performance and ensemble size are also relevant. The topic of the different possibilities for ensemble construction and the resulting performance has been examined with respect to wind storms (see Section 6.6.3) in order to estimate the effect of the partly arbitrary model selection for

multi-model ensemble studies (e.g., due to the availability of model simulations). Based on the ten ENSEMBLES RCMs available at the time of the study, there are in total 1,023 possible combinations containing between one and ten models. The results indicate a higher consistency of the (sub-)ensemble performance for large ensembles containing many models, even if the more weakly performing models are included (Donat et al., 2009c; see Figure 6.8). This provides support for the ensembles strategy and indicates that users should work with the full ensemble wherever possible.

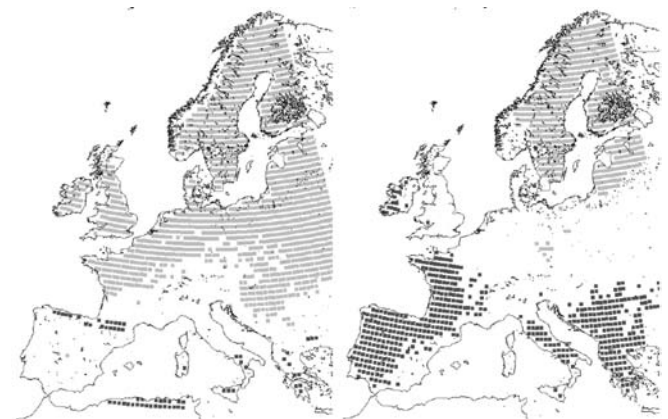


Figure 6.7: Location of points with a significant positive (light grey) or negative (dark grey) change in total precipitation (2021–2050 minus 1961–1990) in winter (left panel) and summer (right panel).

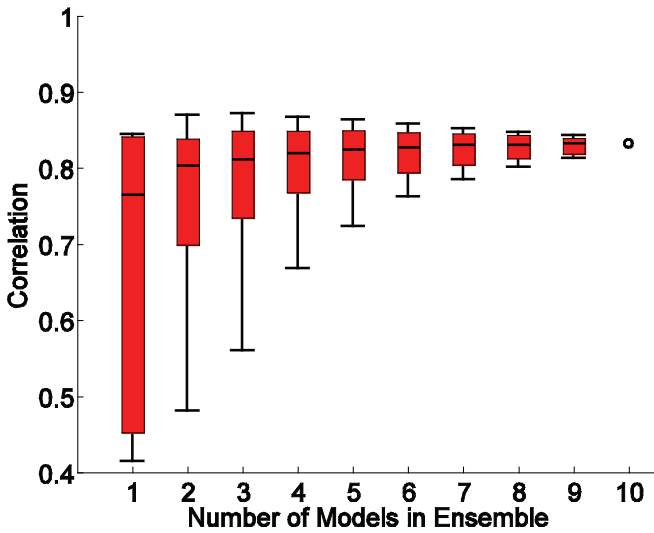


Figure 6.8: Correlations of annual wind storm losses in Germany calculated from all possible model combinations in comparison with insurance loss data. For each group of sub-ensembles consisting of between one and ten models (x axis) the range of correlation values (y axis) is indicated. The black vertical ticks at the top (bottom) of the range show the highest (lowest) correlation value from all sub-ensembles in each group consisting of N models. The red boxes indicate the range between the 10th and the 90th percentile of all correlations, the black horizontal line in the centre corresponds to the median.

Partitioning of uncertainty in the RCM simulations

A Monte Carlo variance partitioning approach was used to quantify three sources of uncertainty (choice of GCM, choice of RCM, and interannual variability) in the seasonal temperature and precipitation changes projected by the ENSEMBLES RCMs (Déqué et al., 2009). As well as using the ANOVA approach used in PRUDENCE (Déqué et al., 2007), a new, weather-regime-based, matrix-filling technique has been developed to complete the GCM-RCM matrix (see Section 5.2.6). The application of this technique is demonstrated in Figure 6.9, which shows the partitioning of GCM and RCM uncertainties (and their interaction) for the eight European PRUDENCE (or Rockel) regions.

This analysis (Déqué et al., 2009) indicates that for precipitation the first cause of model spread in summer is the choice of RCM, with the second being the choice of GCM (Figure 6.9). In winter (as for temperature in both seasons), both components contribute fairly equally, although the GCM choice dominates in western Europe. The finding that the relative strength of different uncertainties varies from region to region, variable to variable, and season to season confirms earlier findings from the PRUDENCE project. The third cause of spread (not shown) is interannual variability.

Another ENSEMBLES study has demonstrated the importance of considering intra- as well as inter-RCM variability (Kjellström et al., 2009). This study shows that differences in the climate-change signal are sometimes as large, or larger, between the three RCA3–ECHAM5–A1B simulations than between the corresponding RCA3–other GCM–A1B simulations. Also, the three-member perturbed physics ensemble (RCA3 downscaling HadCM3Q1 [reference], Q3 [low climate sensitivity] and Q16 [high sensitivity]) shows that natural variability is important

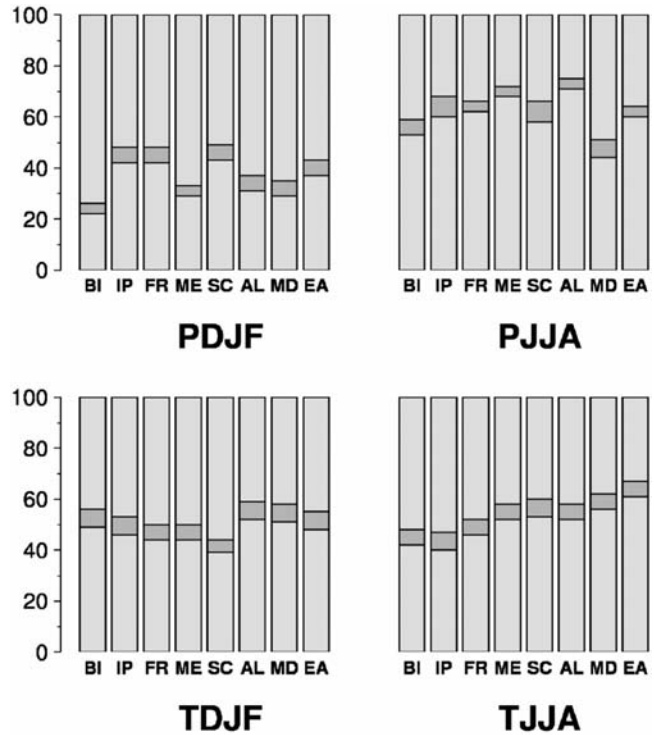


Figure 6.9: Fraction of variance (%) explained by the RCM (lower part of bars), the GCM (top part of bars) and their interaction term (middle part of bars) for 2021–2050 minus 1961–1990 changes in temperature (T) and precipitation (P) in winter (DJF) and summer (JJA), and for eight regions: British Isles (BI), Iberian Peninsula (IP), France (FR), Mid-Europe (ME), Scandinavia (SC), Alps (AL), Mediterranean (MD) and Eastern Europe (EA).

(here, the low-sensitivity simulation shows a much larger climate-change signal for wintertime temperature in the 2011–2040 period than the high-sensitivity simulation – also a result of natural variability).

It should be stressed that these results are based on changes up to the middle of the century (2021–2050 and 2011–2040). Work focusing on the end of the 21st century (the 2080s) suggests a somewhat different balance of uncertainty, with a stronger emphasis on GCM uncertainty (see Sections 5.2.6 and 6.3.4). The general message emerging from the new ENSEMBLES studies, and the earlier PRUDENCE work, can be summarised as: the higher the climate-change signal, the more important the GCM spread; the lower the signal, the more important the RCM. This implies that, for the end of the century, it is important to fully sample the range of GCM uncertainty, whereas for periods closer to the present day, more RCMs should be sampled. The design of the ENSEMBLES GCM-RCM matrix gives users the opportunity to adopt such different sampling strategies.

The ENSEMBLES work has, however, raised some interesting questions concerning how ‘interannual’ and ‘natural’ variability are defined and the extent to which they are encompassed by inter- and intra-RCM variability. It has been shown, for example, that there is a significant contribution to natural variability on at least multi-annual time-scales and potentially up to multi-decadal time-scales (Kendon et al., 2008). But it is difficult to determine whether longer time-scale natural variability is included in, for example, the ‘RCM uncertainty’ component of the Déqué et al. (2009) analysis discussed above.

Statistical downscaling

As a starting point for the modification of statistical downscaling methods for probabilistic projections, ENSEMBLES first considered the issues from a theoretical perspective – dividing the uncertainties into three groups, as follows.

1. Uncertainties ‘previous’ to downscaling, encompassing uncertainties in the large-scale forcing – which can be expressed as: What will be the low-resolution atmospheric configuration in the future (not for a specific date in the future, but the frequency of occurrence of each configuration)?
2. Uncertainties related to downscaling itself, expressed by the question: If the low-resolution atmospheric configuration for a day is a ‘certain one’, what will be the high-resolution surface effects? In this case the uncertainties are related to issues such as forcings not considered; stationarity; overfitting; range of applicability; overall underlying skill; and spatial resolution of predictands.
3. ‘Downstream’ uncertainties, expressed as: What will be the impacts of the projected changes on human and natural systems? (see Section 9).

In order to quantify the second set of uncertainties, a number of partners have contributed to a common experimental framework using daily maximum and minimum temperature for ten European stations, a set of standard predictors from one GCM, from which different combinations of predictor fields are chosen for individual models, and several different downscaling methods and their variants: regression (stepwise, PCs, stratified by circulation pattern), neural networks, canonical correlation analysis, and a two-step analogue method. For the construction of the PDFs (probability density functions), a Gaussian kernel estimate with a window width of 0.25°C is employed. An example of the effect of weighting the PDF is shown in Section 6.2.2. Once completed, this work will provide an indication of the relative importance of the different sources of statistical downscaling uncertainty.

While the use of inputs from a single GCM allows exploration of the downscaling uncertainties, work has also been done using multiple GCM inputs. For example, a conditional stochastic weather generator (CWG) has been developed and used to construct daily precipitation projections for stations in Romania. The CWG first estimates the model parameters from large-scale predictors using canonical correlation analysis. Daily precipitation is then generated in 1,000 runs of the stochastic model for each set of boundary conditions – allowing calculation of the ensemble mean for ten precipitation indices (including six extremes) and associated 90% confidence intervals – a novel way of presenting statistical downscaled outputs. Currently, the CWG has been applied to seven ENSEMBLES GCM runs to produce probabilistic projections for the 2080s.

The ENSEMBLES work has shown that statistical downscaling methods can successfully be modified and used to construct probabilistic regional projections. Further methodological issues relating to statistical downscaling are discussed in Sections 6.2.2 and 6.3.

6.2.2 Development and application of model weighting schemes

The development and application of model weighting schemes is one of the cross-cutting issues that has been addressed in many of the ENSEMBLES Research Themes. A number of critical questions were identified in the early stages of the project and have informed the downscaling-related work, although it has not been possible to answer all of them (Table 6.1).

The weighting methodology developed for the ENSEMBLES RCM simulations (i.e., for dynamical downscaling) is described in Section 5.2.5. Independently of this work, consideration was given to the components that should be included in weighting schemes for statistical downscaling. The following five criteria were identified.

1. Statistical downscaling model performance (i.e., conventional metrics such as correlation, bias and RMSE calculated over an independent validation period).
2. Reproduction of trends and climate states.
3. Performance of driving-model predictors (i.e., ability of forcing GCMs to reproduce the predictors used for statistical downscaling).
4. Stability of predictor–predictand relationships.
5. Correction for multiplicity of statistical downscaling models.

Of these five, criteria (1) and (2) have been implemented to date. An example is provided in Figure 6.10, based on a set of 39 statistical downscaling models. It displays the effect of two weights; one related to criterion (1), in this case, the variance explained. For criterion (2), the weight is constructed so that it (a) equals one for the exact reproduction of a trend; (b) equals zero for a zero trend; (c) equals zero for trends equal to double

Table 6.1: Questions on model weighting and answers from the downscaling perspective.

Question	Answer from the RT2B downscaling perspective
<i>Is weighting a necessary and appropriate technique?</i>	In theory yes – see Section 5.2.5. In practice, weighting is always used (e.g., equal weighting with all weights = 1; or 1 (for models used) and 0 (for models not used).
<i>How should weights be calculated?</i>	See Section 5.2.5 and below.
<i>How should weights be used to construct PDFs and other forms of probabilistic projections?</i>	See Section 6.2.3 for examples.
<i>How can the performance of a weighted prediction be compared with an unweighted one?</i>	See below, Figure 6.11 and Figure 5.6.
<i>Should the weights be assigned to the RCMs and GCMs separately or to the RCM-GCM combination?</i>	This question has not been addressed – only the first approach has been followed – see discussion below.

the value of the observed trend; (d) is linearly interpolated between these three values; and (e) equals zero outside these values. A trend here means the slope of a regression line for temperature against time. One can see that the probability of a temperature change being small decreases considerably when the model outputs are weighted. The models producing low temperature changes tend to explain less variance, i.e., tend to be less reliable. The effect of a correct estimation of trends is smaller, mainly because of the short independent validation period on which this example is based (10 years).

Criterion (3) has been considered through the comparison of observed (from ERA-40) and GCM control period EOF (empirical orthogonal function) patterns – which could be quantified as a single metric using anomaly correlation coefficients and root mean square errors. For the moment it is unclear how to quantify criterion (5), multiplicity, since it is unclear how to quantify the (dis)similarity between the statistical models themselves (which is fundamentally different from the (dis)similarity between their outputs).

This set of criteria can be compared with that selected for dynamical downscaling (see Section 5.2.5). In both cases, the metrics extend beyond simple measures of mean climate. Both sets include the reproduction of trends, for example, based on the argument that the ability to capture observed temporal trends implies that a model is capturing some of the processes associated with anthropogenic warming. This relates to the views expressed by ENSEMBLES scientists in workshop discussions that a climate model is more likely to be credible if

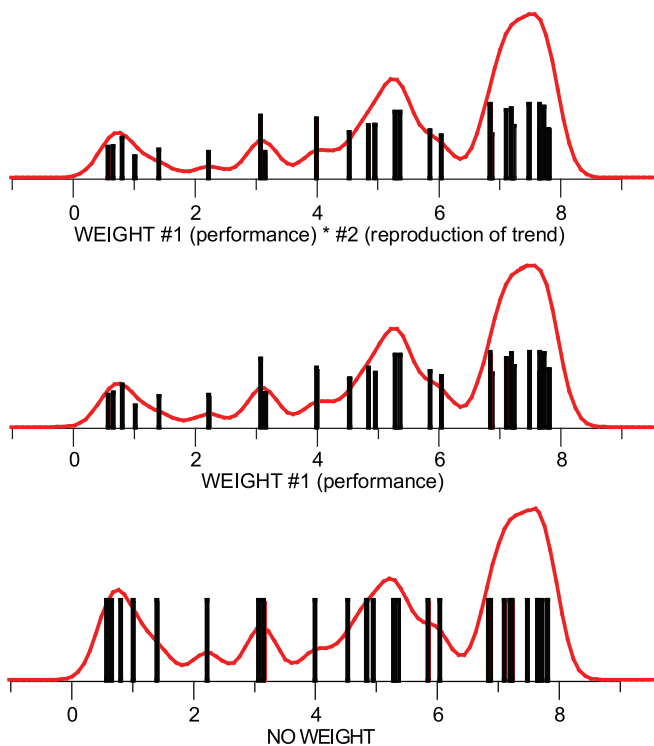


Figure 6.10: PDFs of daily maximum temperature from 39 statistical downscaling models, winter, Strážnice, Czech Republic. Horizontal axis = temperature change (°C); vertical axis = probability; black bars = weights of individual downscaling models, horizontally positioned by their temperature change; red line = estimated PDF of temperature change. Bottom = without weighting; centre = weighted by criterion (1); top = weighted by the product of criteria (1) and (2).

the climate physics and processes are well represented than simply if the simulated mean control climate for the important variables is close to the mean observations. The latter is a ‘necessary but not sufficient’ condition with respect to future performance. However, while other ENSEMBLES Research Themes have explored these process issues thoroughly (see Sections 7 and 8), it has not been possible to incorporate this work or qualitative expert knowledge into the quantitative weighting metrics.

The weighting schemes developed for both statistical and dynamical downscaling should be viewed as first and partial attempts. A number of issues still need to be resolved; in particular, how to combine regional weights with those from global models (see Table 6.1). One potential approach would be to calculate the RCM weights using the GCM-forced control runs (the current weights are based on ERA40-forced runs). An analysis of 50 km resolution simulations performed with the RCA RCM indicates that the biases are generally larger when RCA is forced by GCMs compared with ERA-40 and that the biases are very different, given different GCMs (Kjellström et al., 2009). For statistical downscaling, one strategy would be to incorporate metric three above. How to apply separate weighting schemes for the GCM and downscaling, without any ‘double-counting’, is a more problematic issue. Another issue which has not been fully addressed is the extent to which the weighting schemes are considered relevant by applications users.

Mindful of their preliminary nature, the statistical and dynamical downscaling ENSEMBLES weighting schemes have been used to construct PDFs (Figures 6.10 and 6.11) and to explore the sensitivity of the PDFs to weighting. Figure 6.11 shows PDFs of changes in daily mean temperature and precipitation for Heathrow, UK. The PDFs are constructed using ‘climate change factors’ from seventeen ENSEMBLES RCM runs to perturb the parameters of a weather generator trained on station data (Goodess et al., 2007). The weather generator is stochastic and is run 100 times for each set of change factors (i.e., 17×100 runs). The RT3 product-based weighting scheme (Figure 5.5) is used to sample from the outputs: sampling future minus present-day changes more frequently from the higher-ranked models (selecting or skipping runs randomly). This approach has been applied for thirteen European stations. In general, as Figure 6.11 illustrates, the RCM-based weighting scheme does not have a major impact on the PDFs. The effect does, however, appear to be somewhat greater for temperature (particularly in winter) than for precipitation, tending to shift the mode towards smaller temperature changes and, in some cases, to slightly narrow the width of the PDF.

However, these findings may be a reflection of the particular methodology used (for example, the noise produced by the weather generator or because the GCMs are not equally sampled; twelve of the RCM runs are driven by two GCMs), although a similar conclusion is reached through a comparison of weighted and unweighted multi-model means (see Figure 5.6). Further comparison of weighted and unweighted (or, more accurately, equally weighted) PDFs using different PDF construction techniques is needed. It may also be the case that incorporating GCM weights would increase the sensitivity to weighting. An alternative approach for constructing future

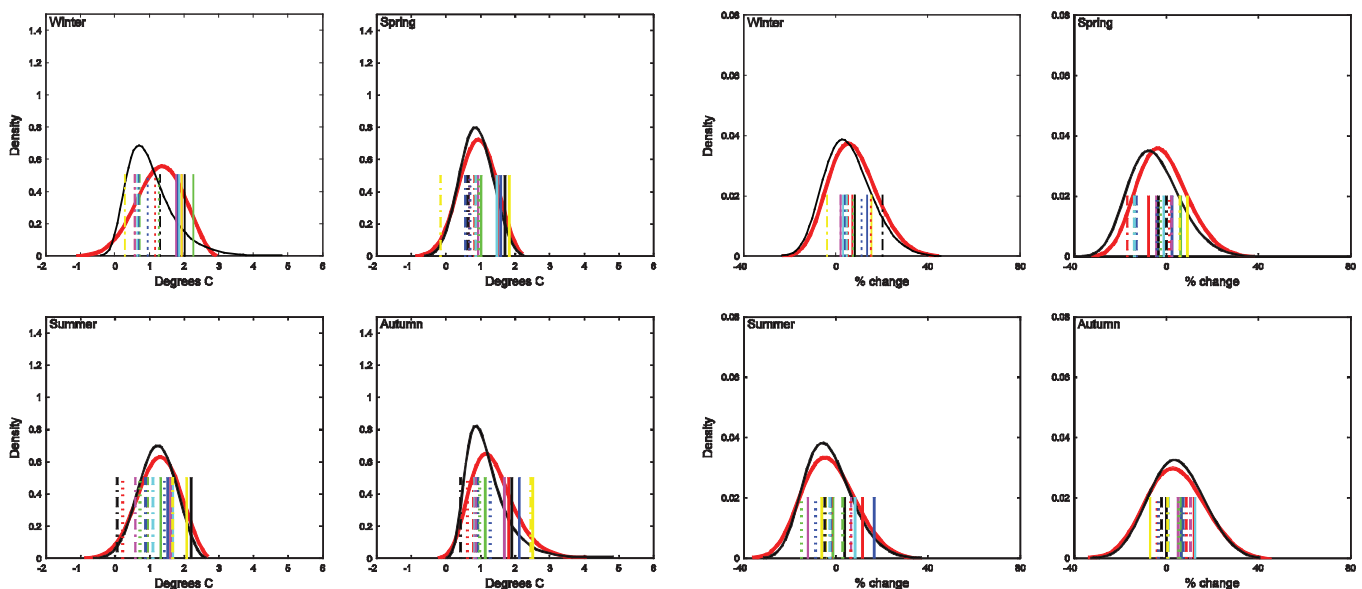


Figure 6.11: Probability density of getting a certain change in mean temperature (left side) and precipitation (right side) for Heathrow, UK (2021–2050 minus 1961–1990; A1B scenario). Red curve = unweighted (equal weighting); black curve = weighted using RT3 product-based scheme; coloured vertical bars = changes calculated directly from the seventeen RCMs.

PDFs, applying an implicit weighting, has been presented by Buser et al. (2009). This method is based on a Bayesian statistical model and allows for a time-dependent estimation and correction of model biases. In addition, it includes an estimation of changes in interannual variability.

Weighting of downscaled outputs is a new research area. The ENSEMBLES work has shown that this is a complex topic, from both a theoretical and a practical viewpoint. While it has not been possible to answer all the questions (Table 6.1), the first examples of weighted regional PDFs have successfully been produced (see also Sections 6.2.3 and 6.6.2).

6.2.3 Constructing PDFs

Probability density functions (PDFs) are one of the most common and useful ways of presenting probabilistic climate change information (see Section 6.6). At the start of the ENSEMBLES project, a number of groups had produced PDFs of global temperature change, but PDFs of regional change were almost non-existent. Thus the development of methods for producing regional PDFs from Global and Regional Climate Model output, as well as from statistical downscaling (Figures 6.10 and 6.11) has been an important part of RT2B work. Here, two examples are presented: the first uses a refined version developed in ENSEMBLES (Xu et al., 2009) of the reliability ensemble averaging (REA) approach (Giorgi and Mearns, 2002, 2003) applied to CMIP3 GCM output (which includes the ENSEMBLES stream 1 climate change simulations; see Section 4), while the second uses the ENSEMBLES RT3 weighting scheme and the RT2B transient RCM runs.

Figures 6.12 and 6.13 show PDFs of seasonal temperature and precipitation change at 2021–2050 for the eight European PRUDENCE/Rockel regions and the A1B scenario, based on output from eighteen CMIP3 GCM runs. In the refined REA

method, the PDFs are constructed by first calculating weights for each model based on their temperature and precipitation biases, errors in temperature and precipitation variability, and sea level pressure correlations (Xu et al., 2009). After the weights are calculated, the probability of the change being greater than a specific threshold is given by the sum of the models that exceed that threshold – each multiplied by its weight and normalized by the sum of the weights. For example, if the weights are all $1/N$ (where N = number of models), this is simply the proportion of models above that threshold (similar to the approach used in unweighted seasonal prediction). This procedure produces a cumulative distribution function (CDF). A numerical derivative of the CDF is then taken to obtain the PDF. Finally, everything is normalized.

Even at 2021–2050, some clear changes are evident in the PDFs, particularly for temperature. The temperature PDFs for the different regions largely overlap, though there are clear seasonal differences, with the greatest warming indicated for the Scandinavia region in autumn and winter, and for the Iberian Peninsula in summer (Figure 6.12). The peaks of the precipitation PDFs (Figure 6.13) cluster closer to zero, with quite a large spread either side, but there is indication of the north/south, summer/winter differences in signal previously identified in Section 6.2.1. PDFs have also been constructed for 2071–2100 (not shown). As expected, these indicate larger changes and even greater spread. In a few cases (e.g., spring rainfall changes for the Iberian Peninsula 2021–2050, and autumn rainfall changes for the Mediterranean 2071–2100), the distributions are bimodal.

Figure 6.14 shows an example, for Madrid, of a joint (bivariate) PDF for seasonal changes in temperature and precipitation (Déqué, 2009). Similar plots, along with single variable PDFs and bivariate cumulated distribution plots, have been produced for the RCM grid-box locations closest to 35 European capitals using output from sixteen of the ENSEMBLES transient RCM runs and the RT3 rescaled weights (see Section 5.2.5). Rather than using a

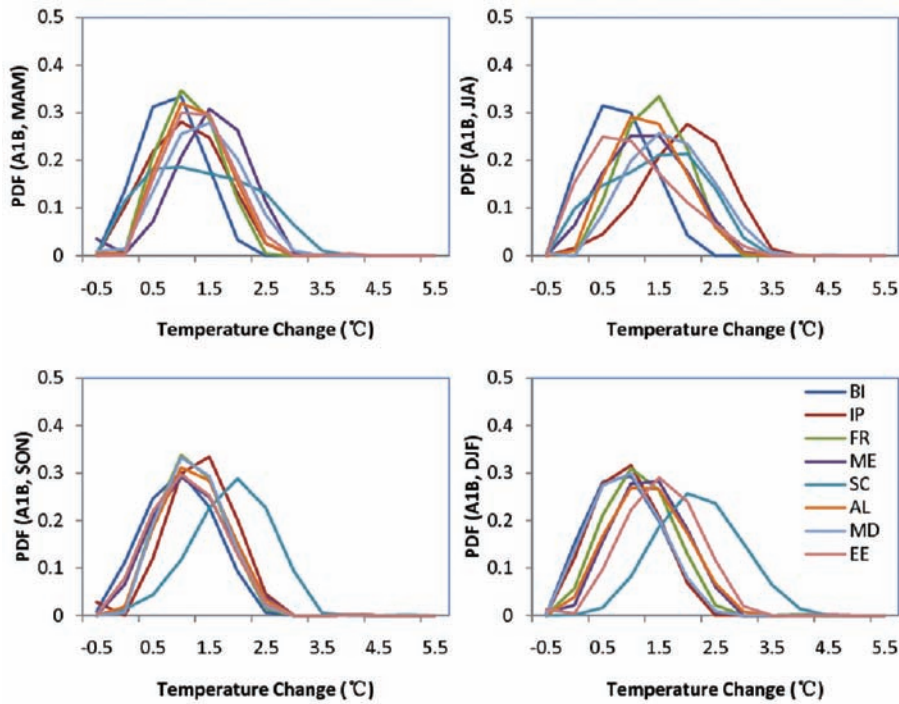


Figure 6.12: PDFs of seasonal temperature change (2021–2050 minus 1961–1990; A1B scenario) constructed using the revised REA method applied to eighteen CMIP3 GCM runs. British Isles (BI), Iberian Peninsula (IP), France (FR), Mid-Europe (ME), Scandinavia (SC), Alps (AL), Mediterranean (MD), Eastern Europe (EE).

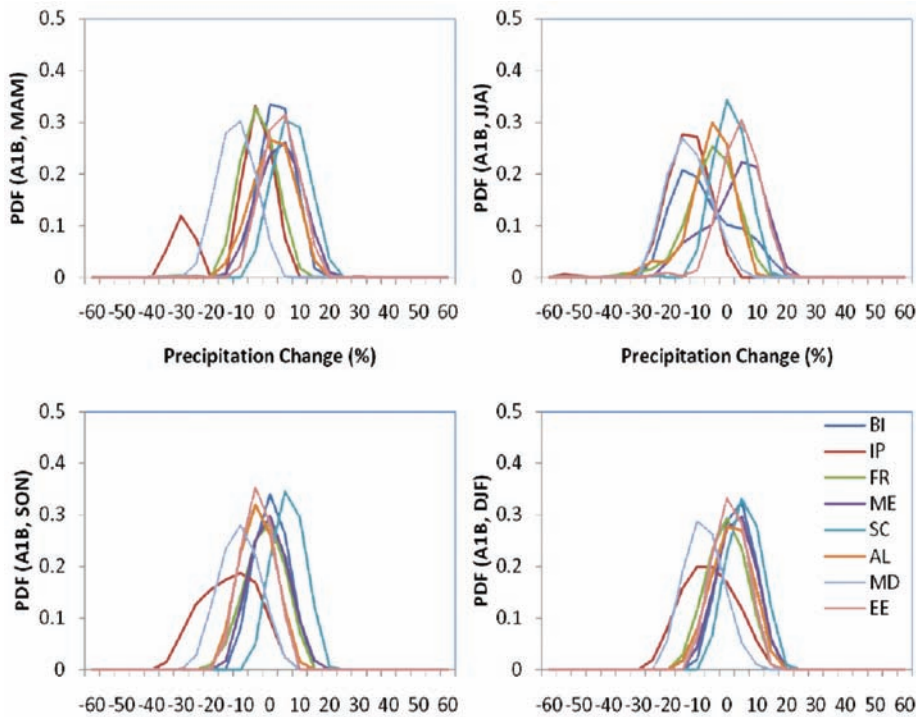


Figure 6.13: PDFs of seasonal precipitation change (2021–2050 minus 1961–1990; A1B scenario) constructed using the revised REA method applied to eighteen CMIP3 GCM runs. British Isles (BI), Iberian Peninsula (IP), France (FR), Mid-Europe (ME), Scandinavia (SC), Alps (AL), Mediterranean (MD), Eastern Europe (EE).

computationally complex continuous distribution, 200 bins are considered for each variable. A Gaussian filter (known as the Gaussian kernel method) is applied. The probability (frequency) in each bin is replaced by a Gaussian distribution with the mean as the centre of the bin and standard deviation values adjusted to cancel out as far as possible any multimodal effects, but to avoid over-smoothing of the distribution.

The PDFs for Madrid (not shown), for example, indicate a mean precipitation increase in winter at 2021–2050 of 0.1 mm/day, with decreases in other seasons (a maximum of 0.22 mm/day in autumn). The maximum warming is in summer (2.3°C). As illustrated by Figure 6.14, the spread is quite large. And while the temperature changes are nearly always positive, the precipitation distributions always span a negative to positive

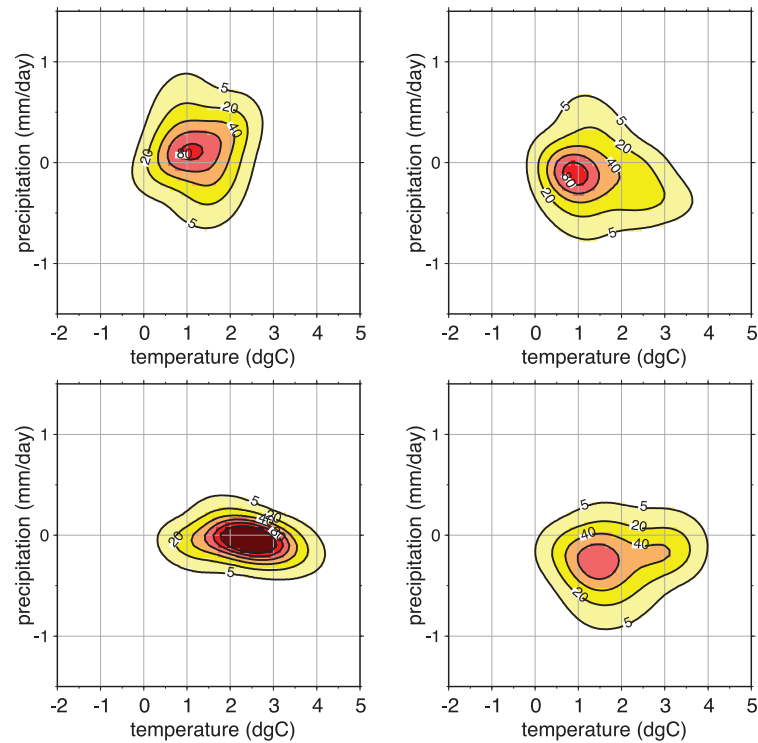


Figure 6.14: Bivariate PDFs for temperature and precipitation response (2021–2050 minus 1961–1990; A1B scenario) in Madrid for DJF (top left), MAM (top right), JJA (bottom left) and SON (bottom right). Contours indicating densities are plotted for 5, 20, 40, 60, 80 and 100 of $10^{-2} \text{°C}^{-1} \text{mm}^{-1}$ per day.

range. In fact, there is always at least 10% probability that the sign of precipitation response is negative and at least 10% that it is positive, whatever the capital or season. Thus the PDFs provide a valuable graphical representation of the different spread of uncertainties for temperature (more certainty) compared with precipitation (less certainty).

6.3 Synergistic use of dynamical and statistical downscaling

6.3.1 Introduction

There has been a tendency to view dynamical and statistical methods as mutually exclusive and even competing approaches to downscaling. A rather different view has been taken in ENSEMBLES, where the potential for using the two approaches in a complementary, synergistic way has been explored, as well as undertaking some direct comparisons of performance.

6.3.2 Forcing statistical downscaling models with RCM output

The ENSEMBLES RCMs provide grid-box information at 25 km resolution (which generally has added value compared with coarser resolutions – see Section 5.2.4), while one of the benefits of statistical downscaling is the potential to provide information at station/point locations. The usual approach is to drive statistical models with GCM output, but ENSEMBLES has also used RCM forcing. Figure 6.11, for example, shows PDFs for Heathrow constructed by perturbing a stochastic weather generator with output from the ENSEMBLES transient RCMs.

In another ENSEMBLES study, predictors from the ERA40-forced RCM runs have been used to downscale seasonal indices of temperature and precipitation extremes for four Irish stations, using multiple linear regression. Preliminary results for one RCM indicate that statistical downscaling brings additional skill for most investigated indices if examining the root mean square error and the correlation. However, regressions for the precipitation indices are generally too ‘flat’, resulting in an underestimation of the most extreme values of the indices. Therefore a bias correction method has been developed which corrects daily values of 2 m temperature and precipitation towards the observed distribution. This method has to be further tested with other RCMs, but it is promising, as it seems to result in a better representation of the most extreme values of the precipitation indices than the direct model output.

6.3.3 Direct comparison of dynamical and statistical downscaling

The availability of the E-OBS gridded dataset at 25 km resolution (Section 8) has facilitated the direct, like-with-like (i.e., grid box vs grid box rather than point vs grid box) comparison of the two downscaling approaches. E-OBS data have been used as predictands in a two-step analogue downscaling model and the results compared with those from the ERA-40 RCM runs. Results for trends in the Tmax 95th percentile are shown in Figure 6.15. The statistical method displays consistently higher correlations than the RCMs, but the standard deviations of spatial variability across the European domain are consistently low – lower than the worst of the RCMs in the majority of cases. Overall, however, the statistical model results lie somewhat closer to the ‘perfect point’ than those of the RCMs.

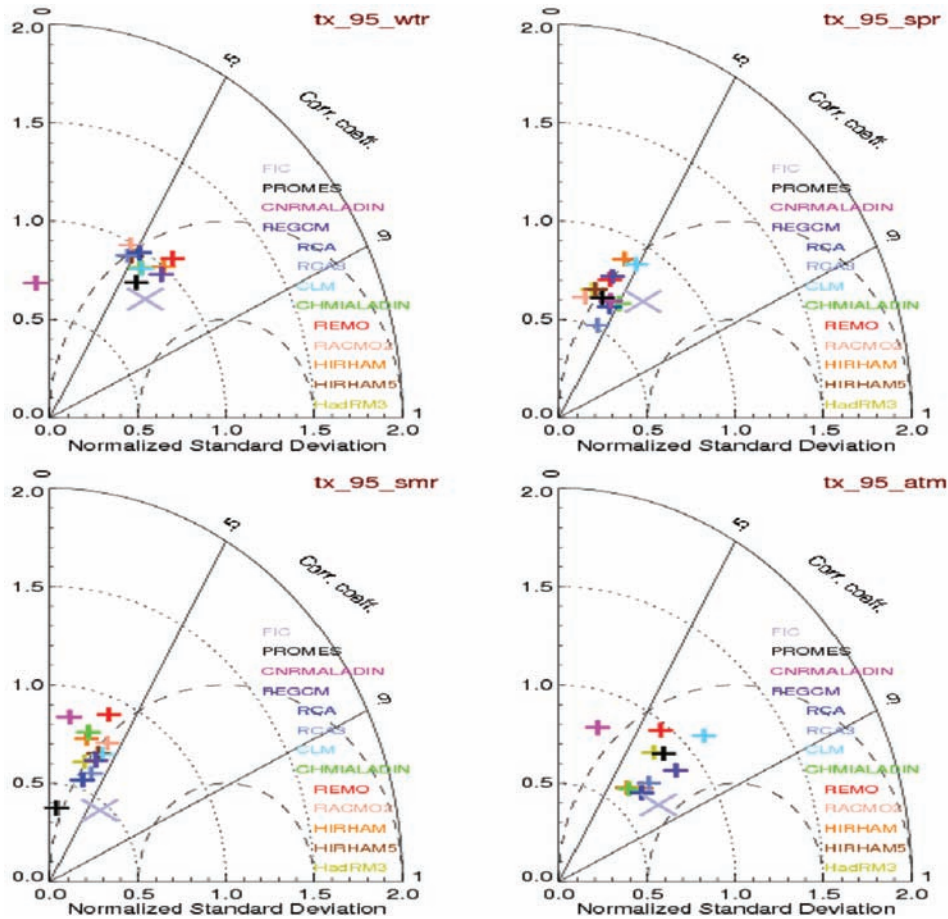


Figure 6.15: Taylor diagram for trends in the 95th percentile of T_{max} in winter (top left), spring (top right), summer (bottom left) and autumn (bottom right). All models are forced with ERA-40. Small crosses = RCMs; large cross = two-step analogue method. The 'perfect point' is located at 1.0 on the horizontal axis, 0.0 on the vertical axis.

6.3.4 Matrix filling and pattern scaling

As noted in Section 5.2.6, one of the techniques for filling the GCM-RCM matrix evaluated in ENSEMBLES is a pattern-scaling approach. The conventional approach is to estimate the local climate response using global mean temperature change as the scalar, and this has been shown to be skilful for temperature but not for precipitation (Mitchell et al., 1999). In ENSEMBLES, a new local scaling approach has been developed, using the large-scale GCM change as a predictor of the 2080s RCM response. Initial results suggest that this may be skilful for different driving GCMs (i.e., the RCM response can be predicted for untested GCM-RCM pairs) and is therefore skilful for filling the GCM-RCM matrix (Kendon et al., 2009b). In particular, it performs well for precipitation (mean, variance and extremes) across much of Europe in winter; and for temperature (mean and extremes) in summer and winter, with the exception of central Europe in summer (Figure 6.16). Internal variability may, however, lead to a substantial apparent reduction in scaling skill for precipitation, with scaling relationships only being reliable where the local change is robust compared with internal variability. By comparing scaling skill for different driving GCMs with different RCMs (Figure 6.16), this work also provides guidance on how to prioritise RCM simulations for the 2080s. In particular it suggests that, for this period, priority should generally be given to sampling different driving GCMs rather than different RCMs (see Section 5.2.6).

6.3.5 Evaluating stationarity

The problem of stationarity – i.e., the assessment of whether the statistical relationships between large-scale GCM fields (predictors) and local observations (predictands) derived from present climate data are still valid under future climate conditions – remains a concern for statistical downscaling. The ENSEMBLES downscaling portal (see Section 6.5.2) has been used to analyse this problem in the northern Iberian Peninsula, a homogeneous climatic region with mostly frontal activity. Predictors (geopotential, temperature and humidity fields at 1,000, 850 and 500 mb) were taken from the ECHAM5 GCM, using as pseudo-observations daily surface temperature and precipitation from the RACM02 RCM coupled to present and future (A1B) ECHAM5 projections. Different statistical downscaling methods were tested: M1 – a standard analogue method; M2 – a linear regression model based on the first ten circulation patterns; and M3 – linear regression conditioned on fifteen weather types. The present climate scenario (1961–2000) was used to train the models, which were then applied to the A1B time-slices 2011–2040, 2041–2070 and 2071–2100. RMSE errors for temperature for these future periods are shown in Table 6.2. The statistical methods are generally able to reproduce the RCM simulations of future climate periods – implying stationarity – with only small relative increments in RMSE over time. The only exception is the analogue downscaling method, which exhibits large increases in error for summer temperature in

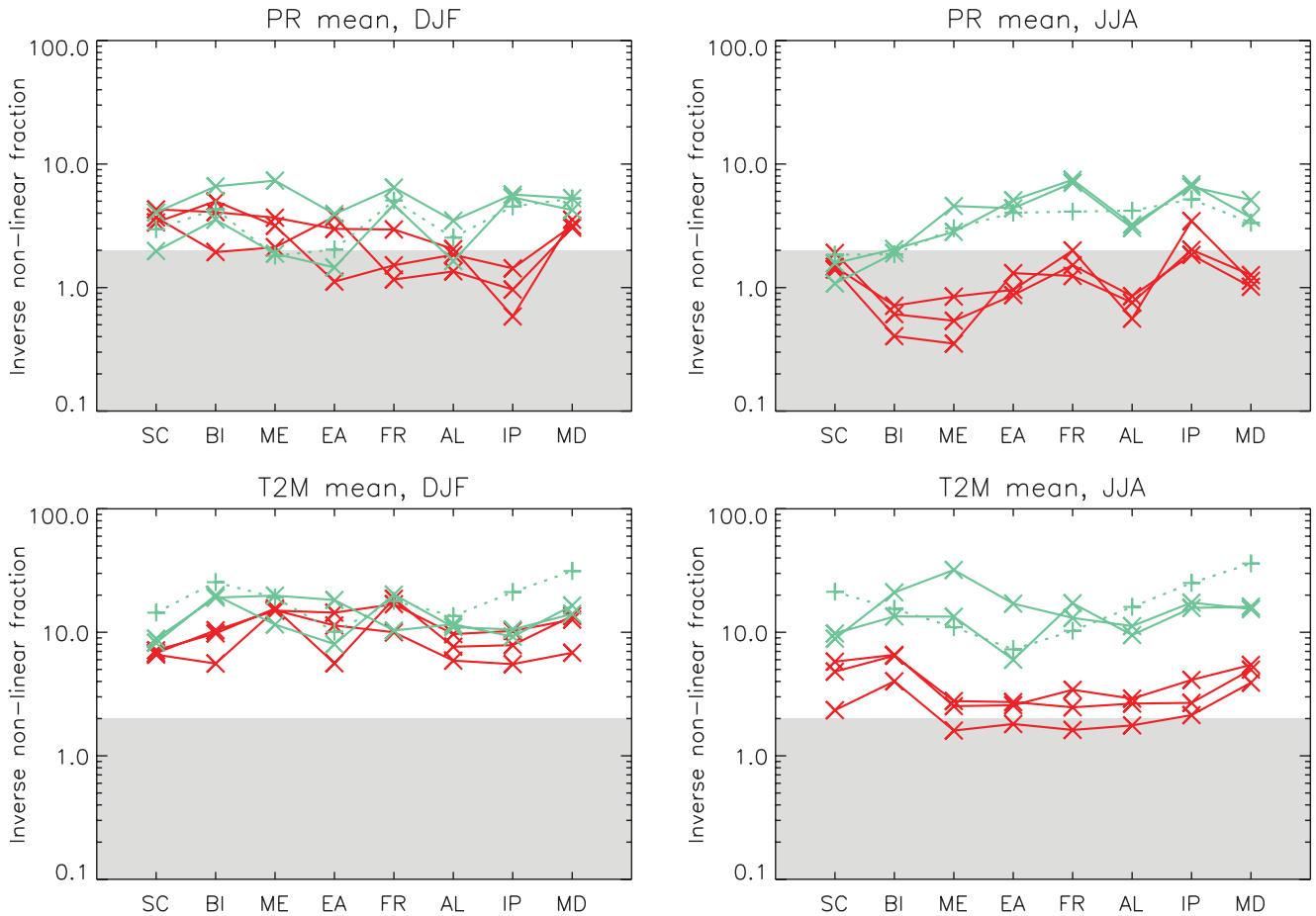


Figure 6.16: Comparison of local scaling skill in estimating local changes for the 2080s for different driving GCMs (red) with that for different RCMs (green). Only grid cells where the local change is robust compared with natural variability are included in the analysis. SC Scandinavia, BI British Isles, ME Mid-Europe, EA Eastern Europe, FR France, AL Alps, IP Iberian Peninsula, MD Mediterranean. Values lying above the shaded area are considered to be skilful.

the final period. As well as providing insight into the stationarity issue (along with an analysis where M1, M2 and M3 are alternately trained/validated on cold/warm periods), these results indicate that statistical downscaling can be an appropriate technique for matrix filling and increasing the ensemble size (see Section 6.3.4).

Table 6.2: Root mean square error (RMSE) for three different statistical downscaling methods (M1, M2, M3) applied to the RACMO temperature pseudo-observations, using as predictors the output from the ECHAM5 A1B scenario for different seasons and future time-slices.

	Period	M1: Analogues	M2: Regression CPs	M3: Regression WTs
Winter	2011–2040	1.234	0.844	0.613
	2041–2070	1.251	1.09	0.743
	2071–2100	1.381	1.178	0.88
Summer	2011–2040	0.965	0.837	0.626
	2041–2070	1.404	0.944	0.79
	2071–2100	2.303	1.148	0.966
Spring	2011–2040	0.68	0.703	0.592
	2041–2070	0.698	0.626	0.579
	2071–2100	0.864	0.702	0.649
Autumn	2011–2040	1.247	0.997	0.736
	2041–2070	1.457	0.99	0.919
	2071–2100	1.85	1.184	1.255

6.4 Integration of climate change and seasonal forecasting time-scales

One of the novel aspects of ENSEMBLES has been the focus on both climate change and seasonal forecasting time-scales. This has provided the opportunity for new interactions and discussions between the two research communities, which has been particularly valuable in the context of downscaling issues. For example, theoretical and practical comparisons have been made of the Perfect Prog approach to statistical downscaling (in which the statistical models are calibrated using observations), typically used by the climate change community, with the Model Output Statistics (MOS) approach used by the seasonal community. Here, work on the ENSEMBLES stream 2 seasonal hindcasts (see Section 3) is presented.

Validation of the stream 2 seasonal multi-model prediction dataset has been undertaken, focusing on winter precipitation forecasts over Europe for the whole period (1961–2005). The validation method consists in evaluating the ROC skill area (RSA) for the three terciles: dry, normal and wet (Sordo et al., 2008). Although, in general, there is little skill in the winter precipitation forecast over Europe, if the same validation is done conditioned to ENSO events (e.g., La Niña events), then some areas of skill appear (Figure 6.17). This indicates that at least the ENSO-driven portion of precipitation over Europe is predicted with some skill (Frías et al., 2009).

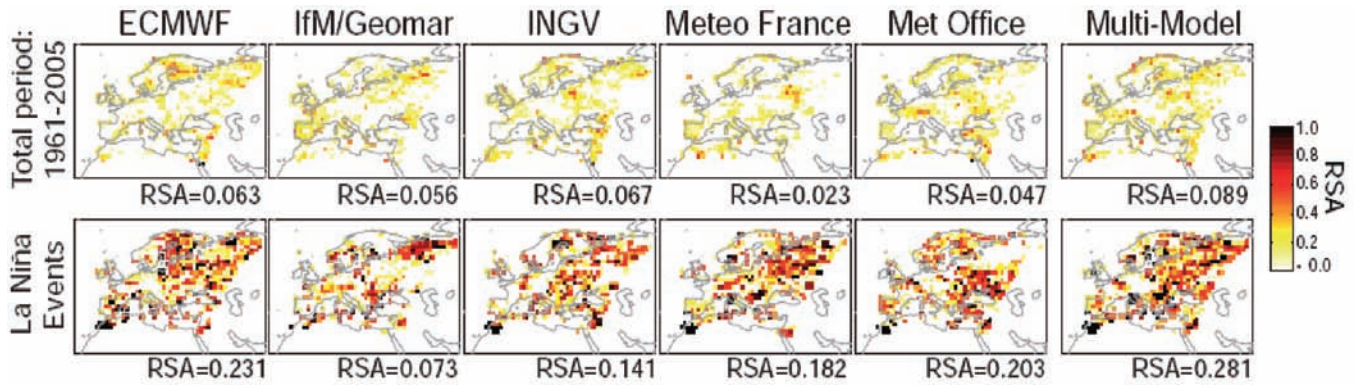


Figure 6.17: ROC skill area (RSA) for winter dry events (lower tercile) for all stream 2 multi-model hindcasts over Europe (upper row), and conditioned to La Niña events (lower row). The higher RSA scores in the lower row indicate greater predictive skill under La Niña conditions.

In addition, the Rossby Centre RCA regional climate model has been applied to dynamically downscale the ECMWF stream 2 seasonal simulations in the European-Atlantic domain for the period 1981–2001 and five ensemble members (Diez et al., 2009). The 1-month lead time global and regional precipitation predictions were evaluated in Spain focusing on autumn, since some skill has already been found for this period. A robust tercile-based probabilistic validation approach was applied to compare the forecasts obtained from the global and regional models. For the low tercile, the skill of an ensemble combining the five members of the regional model ensemble and six members from the global model not used to provide the boundaries in the downscaling process is higher than that of the driving global model over a relatively large area covering the southern half of peninsular Spain. Moreover, the five-member regional model ensemble competes with, and occasionally surpasses, the skill of the full ensemble of eleven members provided by ECMWF’s operational System3.

Finally, the multi-model stream 2 summer (JJA) predictions have been calibrated using a Model Output Statistics scheme so as to produce summer averaged multi-model ensemble predictions of Tmax over Italy for the period 1971–2005. Figure 6.18 shows the time-series of the box plot of the

calibrated ensemble prediction for the first principal component (PC1) of Tmax over Italy, together with the observed value and the median for each model ensemble. Results show the presence of some skill in the calibrated forecasts (the correlation between the multi-model ensemble median and observations is 0.86 and the Brier skill score for positive events of PC1 is 0.34) and an analysis has been done to investigate the sources of predictability in the system. The statistical calibration technique has also been applied to produce seasonal predictions which are used as input to an impact model chain consisting of a weather generator, a surface water balance model, and a crop yield model in order to produce predictions of wheat yield and kiwi fruit irrigation water requirement (see Section 9).

6.5 Shift of emphasis to tools

6.5.1 Introduction

End-user applications for impact studies require accessing and post-processing huge amounts of information (reanalysis, GCM projections, etc.) over particular regions of interest. This information is typically distributed in different repositories,

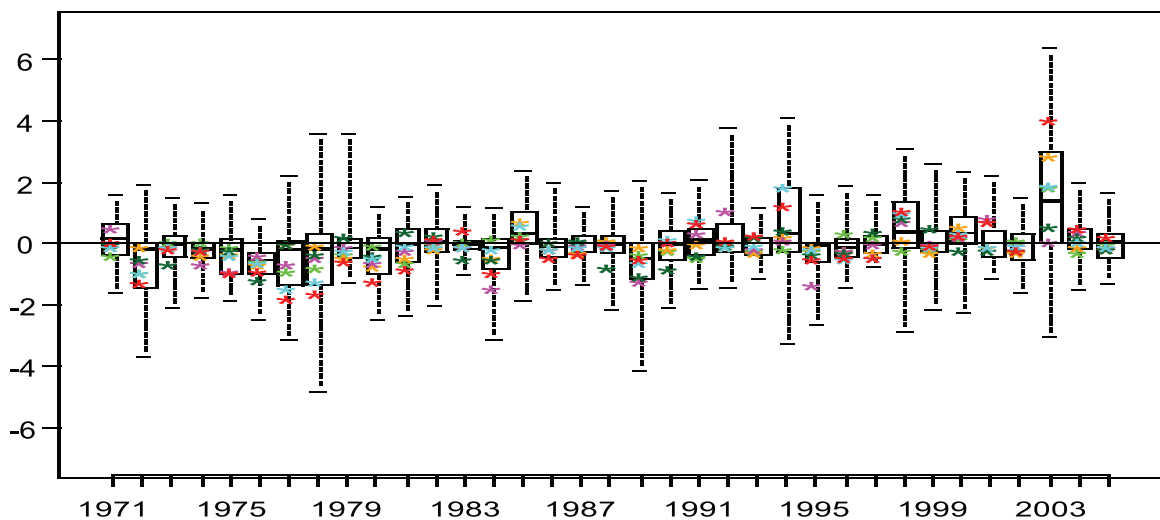


Figure 6.18: Time-series of box plots of calibrated ensemble predictions of the first principal component (PC1) (dimensionless units) of JJA averaged Tmax over Italy compared with observations (red stars). In the majority of cases, the observations lie reasonably close to the median (solid horizontal line at the centre of each box plot) for each model ensemble, and only in a few cases lie outside the quantile range (boxes). Other colour stars indicate single model ensemble median, namely: green - ECMF ensemble median; orange - EGRR ensemble median; magenta - LFPW ensemble median; dark green - INGV ensemble median; cyan - IFMK ensemble median

which use different formats, data conventions and storage systems. Moreover, different post-processing algorithms (bias removal, interpolation, calibration with observations, etc.) are typically applied to the accessed data before using the resulting time-series to feed the impact models. User-friendly data access and analysis tools, such as the climate explorer portal (climexp.knmi.nl), are becoming increasingly popular among end-users in order to facilitate this work. These tools provide homogeneous access to local and remote (e.g., through OPeNDAP) climate data, allowing the application of different post-processing algorithms and delivery of the results in simple formats (e.g., graphics or text files).

6.5.2 The ENSEMBLES downscaling portal

A key ENSEMBLES aim is to maximize the exploitation of results by linking the outputs of the ensemble prediction system to a range of applications, including agriculture and energy. Thus the ENSEMBLES Downscaling Portal (www.meteo.un-ican.es/ensembles; Cofiño et al., 2007; San-Martín et al., 2009) has been developed following an end-to-end approach to fill the gap between the coarse-resolution model outputs and the high-resolution/local needs of end-users. The portal is based on internet and GRID technologies allowing the transparent use of distributed resources, both for data and computation – thus connecting data providers and end-users in a web-based transparent way.

The downscaling portal provides user-friendly homogeneous access to a subset of ENSEMBLES GCM (both seasonal predictions and climate change projections) and RCM outputs, allowing local interpolation or downscaling to the region/location of interest and bias removal. Users can also upload their own observed grids or networks and interactively downscale the model outputs testing several statistical downscaling methods (including regression, neural networks, analogues and weather typing).

6.5.3 Applications

As well as being freely available to all external users, the ENSEMBLES downscaling portal has been applied in a variety of studies within the project. In particular, it has been intensively tested and used by two of the partners in impact studies. Feedback from these partners and other users has helped to shape the development of the portal and the accompanying user guidance.

Electricité de France (EDF) has assessed the skill of seasonal forecasts over France in order to forecast electric power consumption (maximum and minimum temperatures for 26 French cities were considered), and hydropower production (precipitation and temperature in nine watersheds). The portal allowed the testing of different large-scale predictors, areas, and statistical downscaling methods. The analogue methods turned out to be the best compromise (easy and fast to implement). When using ERA-40 data, downscaling outperformed the direct model outputs, and adding extra predictors always improves the skill. However, when considering DEMETER and ENSEMBLES hindcasts (Figure 6.20), the picture is much more complicated and results depend on season and the local parameter being forecast. In particular, the best predictor for a given target variable is not the same for all seasons.

The Joint Research Centre (JRC) has tested the skill of statistical downscaling techniques (as compared with other alternatives) and produced regional climate change scenarios on a grid (the 50 km JRC grid) suitable for modelling crop yield production (see Section 9).

The ENSEMBLES downscaling portal has also been used to run sensitivity studies focusing on specific scientific issues, such as the robustness and stationarity of statistical downscaling methods (see Section 6.3.5). It is also being used to downscale the E-OBS dataset (Section 8) for the whole European domain, allowing further direct comparison of statistical and dynamical downscaling (see Section 6.3.3).

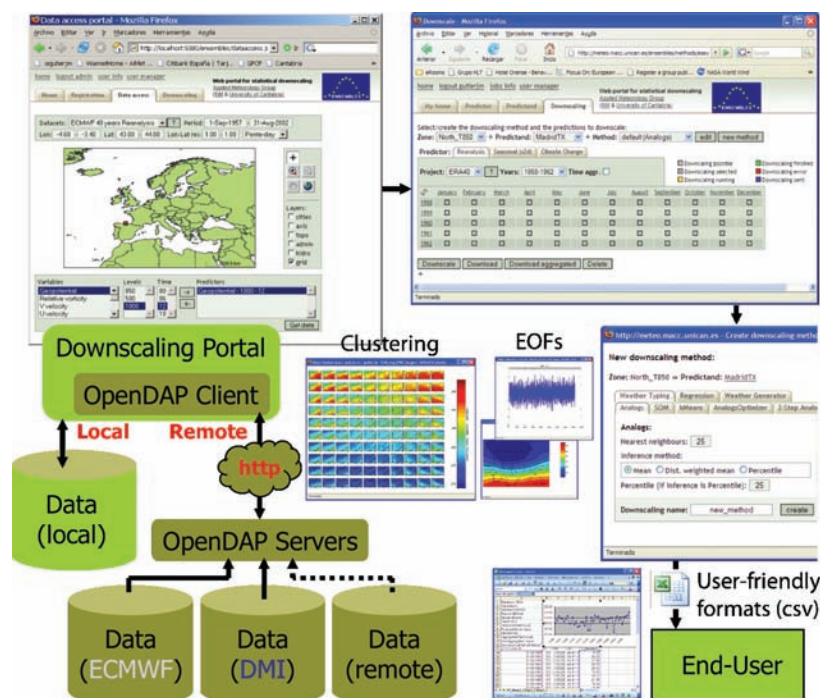


Figure 6.19: The ENSEMBLES downscaling portal.

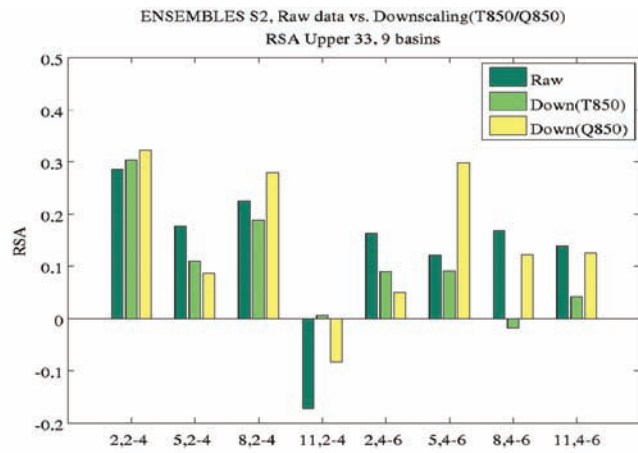


Figure 6.20: Comparison of the skill of raw model (dark green) and statistically downscaled values (using two different upper-air predictors: temperature (T) and specific humidity (Q) at 850 hPa) of temperature and precipitation for nine French watersheds. Raw values are from the ENSEMBLES stream 2 seasonal hindcasts (see Section 6.4). The skill metric is the ROC skill area (RSA) for the upper terciles – higher positive values indicate greater skill. The horizontal axis shows the (initialization month, initial–final lead months). Thus, for initialization in February and 2–4 lead months (first set of bars), downscaling improves the forecast skill, with specific humidity slightly more skillful than temperature as a downscaling predictor. For the second set of results, however, downscaling actually reduces the forecast skill.

6.6 Meeting user needs

6.6.1 Introduction

The RT2B task of providing information on regional climate change as input for impact assessments, together with the central position of RT2B in ENSEMBLES (see Figure 1.1), means that two-way communication with users (particularly those in RT6 – see Section 9) was vital. It was achieved through various formal and informal means, including a questionnaire on the ‘tailoring of ENSEMBLES regional climate scenario outputs to user needs’.

The responses to this questionnaire reflected some of the communication and technical difficulties in the move towards probabilistic projections – in some cases raising issues that some users had not yet had an opportunity to think through. And while it indicated that many users were willing to explore the potential of using probabilistic outputs such as PDFs, CDFs and climate response surfaces, it also demonstrated a continuing need to provide time-series inputs to impacts models (see Section 9.2.2). Thus, outputs from RT2B are available as daily time-series as well as in probabilistic formats. Provision of documentation, recommendations and guidance is also an important outcome of the regional work in ENSEMBLES and is the focus of increased attention in the closing stages of the project.

Access to RT2B regional data, deliverables and other documentation is provided through three portals.

- The Regional Scenario Web Portal – <http://www.cru.uea.ac.uk/projects/ensembles/ScenariosPortal/>
- The ENSEMBLES downscaling portal – <http://www.meteo.unican.es/ensembles/> (see Section 6.5.2)
- The DMI RCM data archive – <http://ensemblestr3.dmi.dk/> (see Section 5.2.3).

6.6.2 Provision of information at different spatial scales

It is evident, from the previous sections of this report, that the ENSEMBLES work on downscaling has been very diverse, drawing on different types of input data, using a number of different methodologies, and working at a number of different spatial scales. Thus the outputs reflect this diversity, as well as the diverse requirements of users (see Section 6.6.1).

This diversity is demonstrated in the four sets of PDFs of temperature and precipitation changes at 2021–2050 shown below for the Middle European location of Prague. PDFs 1 represent changes over the Middle Europe sub-region and are based entirely on GCM output – in this case sampling from a large part of the CMIP3 range (eighteen GCMs). PDFs 2 also represent areal changes, although this time for a 25 km grid box. In this case, only three GCMs are sampled, but sixteen RCM runs are used. PDFs 3 and 4 are both representative of point locations, since the statistical models are trained on station data for Prague. However, they sample different types of uncertainty: PDFs 3 focus on GCM-RCM uncertainty, together with some representation of natural variability coming from the stochastic character of the weather generator; while PDFs 4 focus on uncertainty arising from the choice of statistical downscaling model.

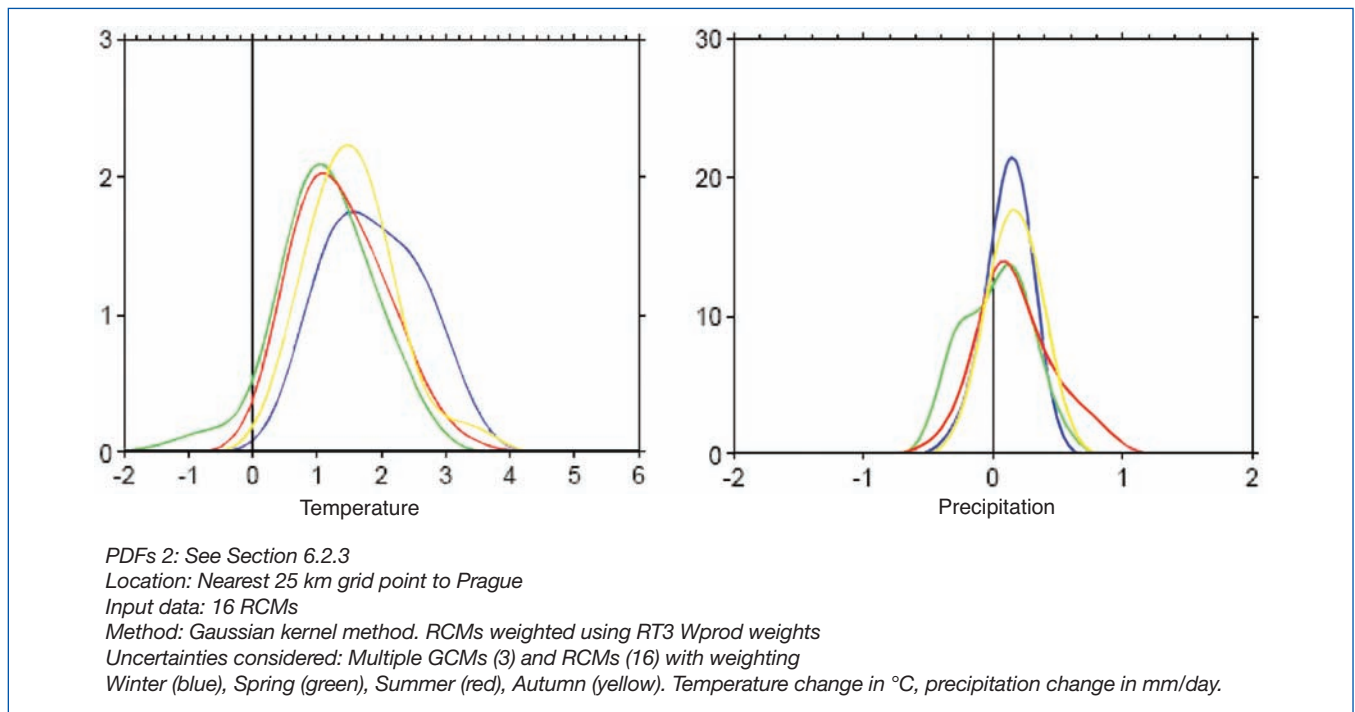
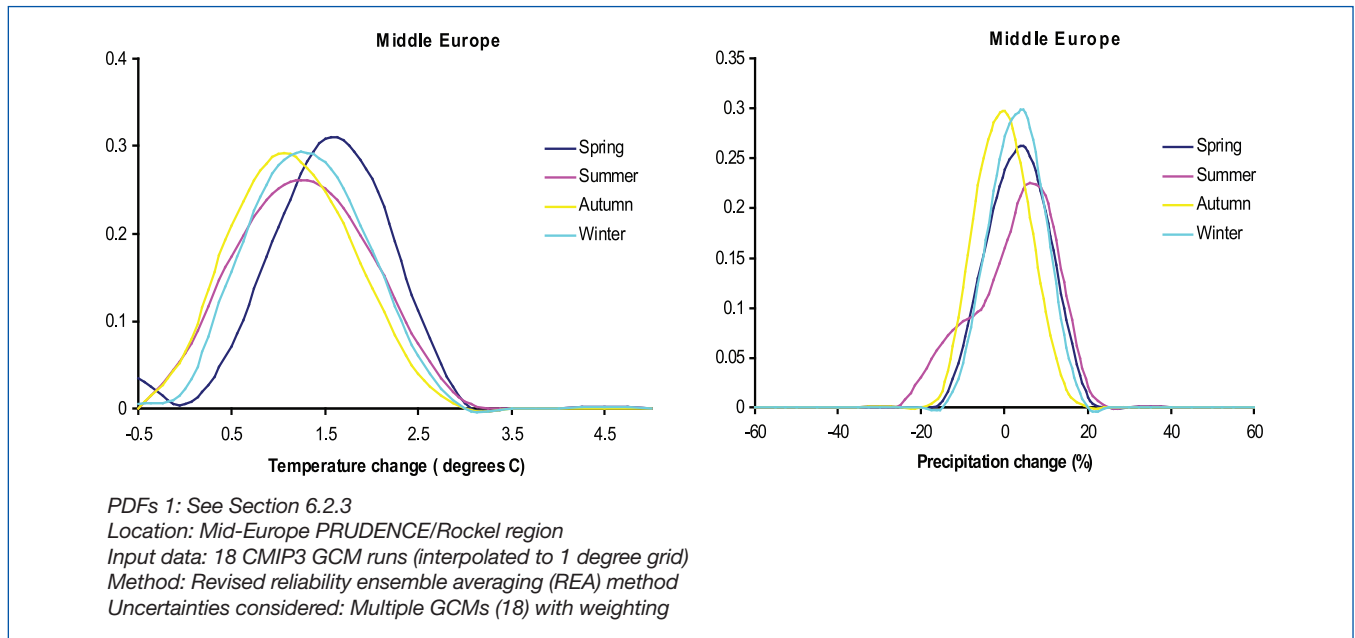
Given these different approaches, it is not surprising that the changes indicated by the different PDFs differ in some respects, although some common characteristics are evident. The mode of all temperature distributions, for example, is positive – and all extend slightly into the negative range in at least some seasons. The temperature changes tend, however, to be somewhat larger for PDFs 2–4 (which include downscaling) than for PDF 1 (based only on GCMs), and largest where statistical downscaling is used (PDFs 3 and 4). For precipitation, the modes of most distributions are slightly positive (with the exception of spring PDF 3), but there are differences in the shapes of the distributions, particularly in summer. PDF 1, for example, is negatively skewed (with a long left-hand tail) in summer, while PDF 2 is positively skewed (with a longer right-hand tail). In general, the precipitation PDFs reflect the location of Prague – close to the boundary between increased precipitation over northern Europe and decreased precipitation to the south (see, for example, Figure 6.5). Hence there is relatively little difference in the precipitation PDFs for different seasons and the modes of the distributions lie closer to zero than they would for regions with stronger and more robust signals.

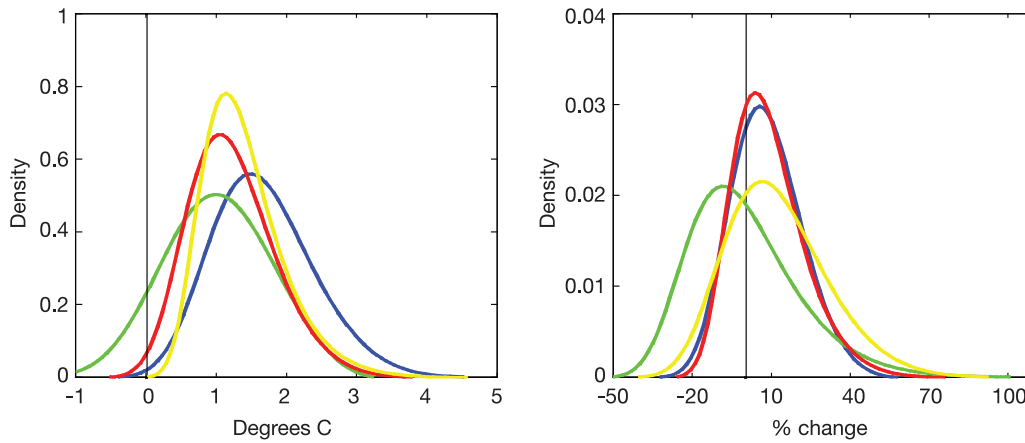
It is clear that none of the PDFs shown here sample the full range of upstream or downscaling uncertainties (see Section 6.2). Thus they should all be considered as ‘subjective’ rather than ‘objective’ (as in the case of probabilities associated with dice throwing) probabilities, and it is important for any user to know the underlying inputs, assumptions and methods. In this context, it should also be stressed that all the PDFs shown here are conditional on the A1B emissions scenario. The ENSEMBLES work has demonstrated the benefit of using probabilistic approaches to explore the uncertainties (and certainties) in regional climate change projections.

Nonetheless, there is a potential danger in that the underlying assumptions tend to be harder to explain and understand than in the case of single deterministic scenarios. Just because a PDF appears wide, for example, does not mean that all the

uncertainties have been extensively or uniformly sampled. Therefore good communication and user guidance are essential in ensuring that such projections are used appropriately.

PDFs for change in temperature (left) and precipitation (right) for 2021–2050 minus 1961–1990





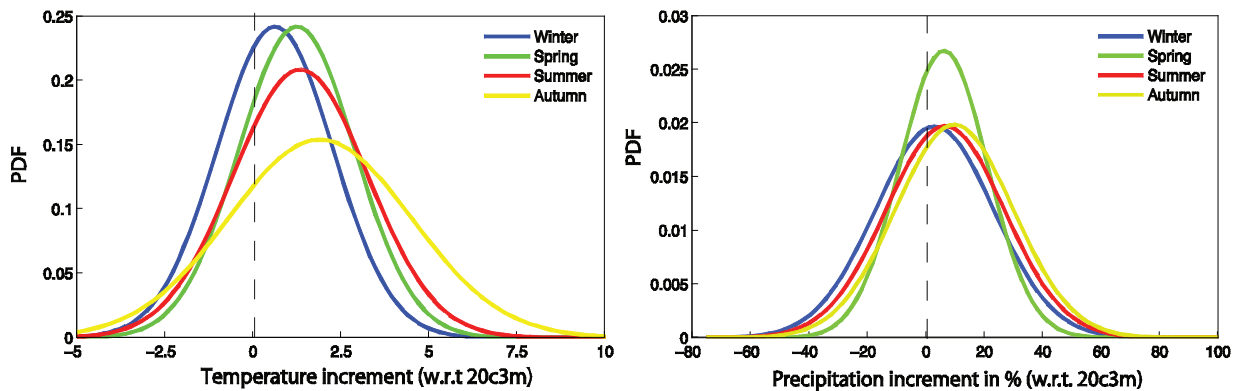
PDFs 3: See Section 6.2.2

Location: Prague, weather generator trained on station data; RCM change factors from nearest 25 km grid box

Input data: 17 RCMs

Method: Stochastic weather generator with change factors from 17 RCMs, with RT3 Wprod weighting

Uncertainties considered: Multiple GCMs (5) and RCMs (17) with weighting and one statistical downscaling method with natural variability
Winter (blue), Spring (green), Summer (red), Autumn (yellow).



PDFs 4

Location: Prague, models trained on station data

Input data: Predictors from ECHAM5 GCM

Method: Three statistical downscaling methods (analogues, regression with circulation patterns and regression with weather types) run using the ENSEMBLES downscaling portal (see Section 6.5.2) Gaussian distribution fitted to outputs to produce PDFs

Uncertainties considered: Multiple (3) downscaling methods

6.6.3 Case studies and applications

Statistically and dynamically downscaled outputs have been used in a number of RT2B regional case studies, many focusing on specific impact sectors and applications and with local stakeholder involvement. These case studies are summarised in Section 6.6.4 – more detailed results and descriptions of the techniques used are available from the Regional Scenario Web Portal (see Section 6.6.1).

Work has also been undertaken for Europe as a whole. For example, future changes in heat-wave characteristics have been analysed based on the ENSEMBLES RCM results (Fischer and Schär, 2009b). Different RCMs driven by different GCMs yield qualitatively consistent results, which are also in line with those from PRUDENCE (Fischer and Schär, 2009a). The results indicate pronounced increases in temperature variability on all time-scales (interannual, seasonal, subseasonal, diurnal) in south-central Europe. Important increases in heat-wave amplitude, frequency and duration are found in large parts of

the study area, especially in southern Europe (Figure 6.21). An analysis of health-specific indicators suggests a strong need for adaptation measures by the year 2050, particularly in low-altitude Mediterranean river basins.

Work has also been undertaken on deep cyclones and wind storms. For example, the characteristics of large-scale flow associated with the occurrence of wind storms based on circulation weather type (CWT) cyclone tracking approaches have been analysed with reanalysis (Donat et al., 2009a) and multi-model (Donat et al., 2009b) data. For central Europe, the majority of the storm days are connected with westerly flow. The ENSEMBLES GCM ensemble reproduces the observed class frequencies reasonably well, although overestimating the occurrence of westerly flow and underestimating anticyclonic situations (Donat et al., 2009b). For the future under the A1B scenario, a significantly increased frequency of westerly flow and also of storm days is indicated. Frequencies of cyclonic and easterly flow are decreased in the climate projections for the end of the 21st century (Figure 6.22).

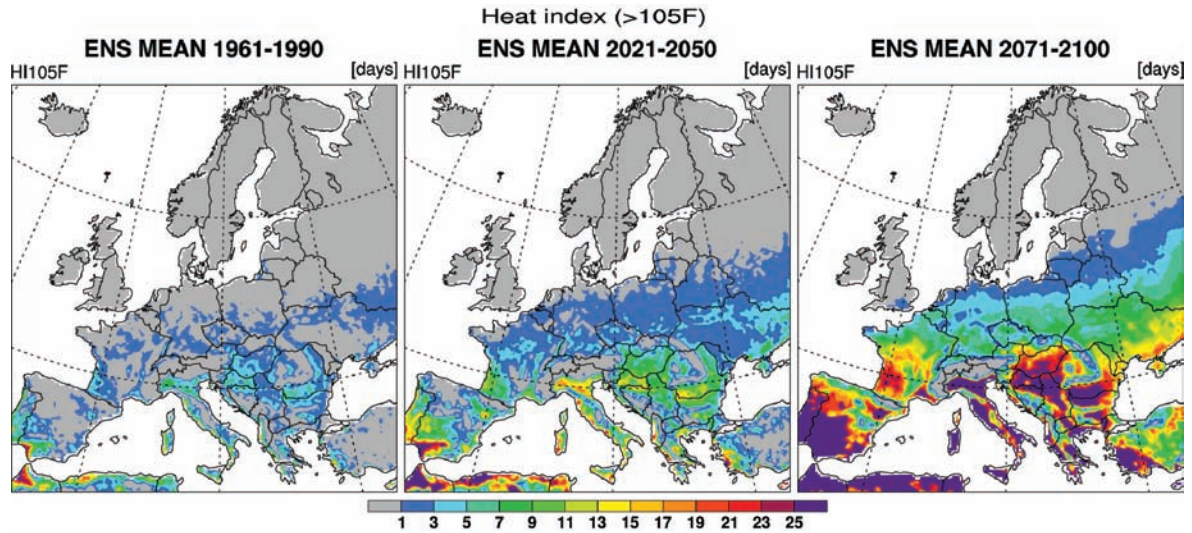


Figure 6.21: Projected average number of summer days exceeding the apparent temperature (heat index) threshold of 40.7°C (105°F). Ensemble mean summer (JJA) days as simulated by five ENSEMBLES RCM runs (MPI, KNMI, HC, ETH, C4I) are shown.

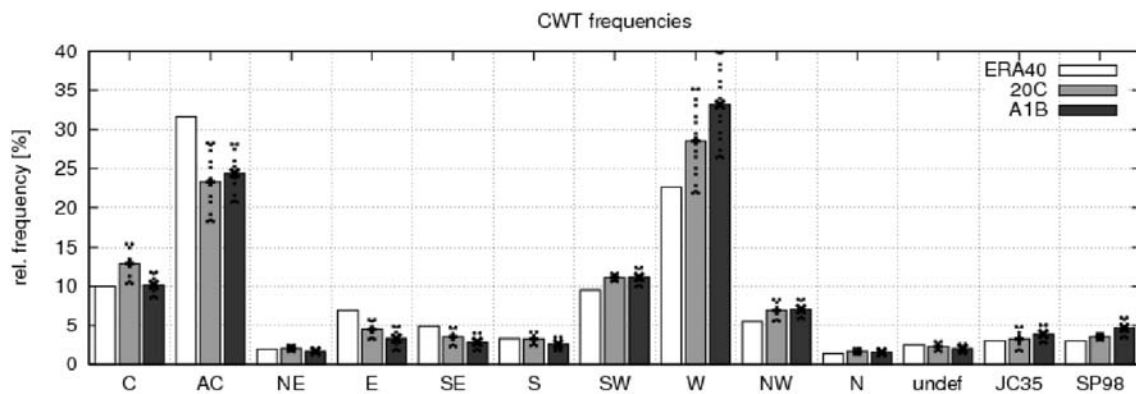


Figure 6.22: Relative frequency of circulation weather types in ERA-40 and ENSEMBLES 20th century and A1B GCM simulations.

(a) ENSEMBLE A1B-20C, all systems

(b) ENSEMBLE A1B-20C, extreme systems

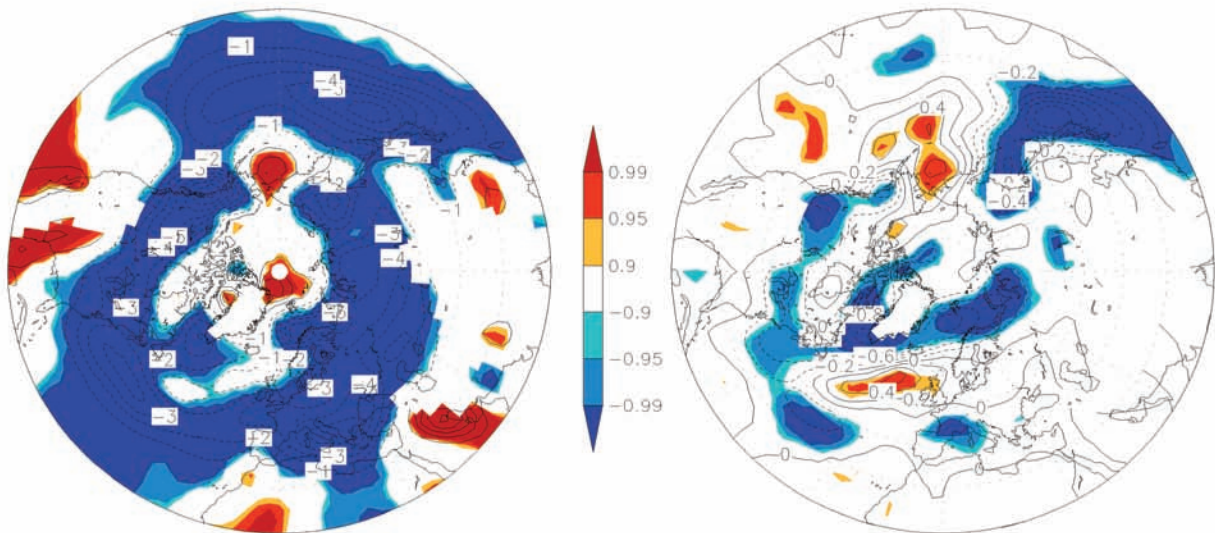


Figure 6.23: Changes in winter (ONDJFM) cyclone track density at the end the century for (a) all systems and (b) extreme systems. Contours show the frequency change and coloured shading indicates the statistical significance level.

Analysis of Northern Hemisphere cyclone track densities reveals a decreased total number of cyclone systems. Considering only extreme cyclones (i.e., the 5% strongest in terms of Laplacian pressure), hot-spots of increased activity are found over the eastern North Atlantic and eastern North Pacific (Leckebusch et al., 2008). The significance of this signal can be increased by weighting the different GCMs according to their ability to reproduce the observed climatology of cyclone tracks (Figure 6.23).

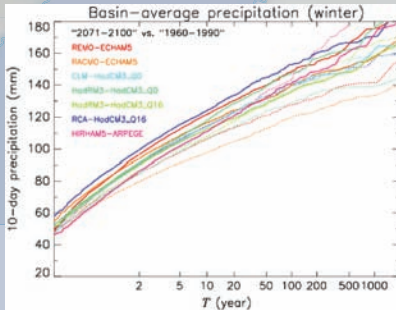
Extreme wind speeds and related loss potentials have been calculated based on the ENSEMBLES GCM and RCM simulations. In addition to an estimation of changed risk of storm losses under future climate conditions, in particular, the effects of dynamical downscaling on the storm loss calculations were investigated. The results from these applied analyses are presented in Section 9.

6.6.4: Illustrative examples of case studies in Research Theme 2B: Downscaling methods, data and tools for

For more details on the RT2B case studies see: <http://www.cru.uea.ac.uk/projects/ensembles/ScenariosPortal/>

Changes in return levels of extreme precipitation events in the Rhine basin

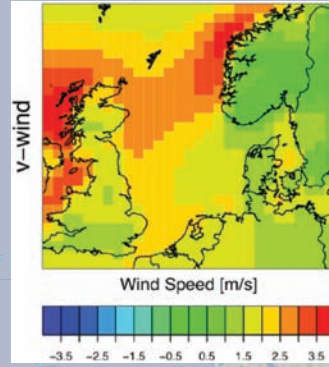
For the design of river dykes in the Netherlands return periods of 1,000 years or more are needed. These are obtained from 3,000-year series of daily precipitation and temperature for the Rhine basin simulated by time series resampling of the output from the ENSEMBLES RCMs. There seems to be a tendency for the larger quantiles to increase relatively more than the smaller quantiles. Leander and Buishand, 2007.



Return level plots of the annual maxima (winter half year) of 10-day precipitation sums in the Rhine basin in 3,000-year resampled series for seven RCM runs for 2071-2100 (1961-1990 reference period denoted by dotted lines).

Statistical modelling of North Sea winds

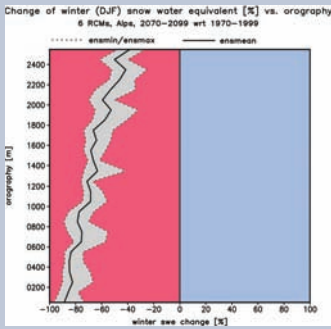
High-resolution information about changes in marine winds is needed for offshore wind farms and other marine constructions, but fitting of statistical models is difficult because of the lack of marine observations. Thus a new approach has been developed where 'pseudo-observations' from the ENSEMBLES ERA-40 forced runs are used in a two-step downscaling approach.



V-wind speed component for January 1961-1990 used in a two-step statistical downscaling approach applied to the ECHO-G GCM.

Changes in snow cover over the Alps

The ENSEMBLES RCMs indicate that by 2100 snow cover is reduced all over Europe and will have almost completely disappeared in southern and western Europe. In the Alps, the decrease is much smaller above 2000 m. Kotlarski et al., 2009.



Change of mean winter snow water equivalent in the European Alps (2070-2099 minus 1970-1999) versus orography from an ensemble of six RCMs.

Changes in phytoclimatic indices in Castilla Leon

Work is being undertaken with the Environmental Ministry of Castilla and Leon Autonomous Community to investigate changes in phytoclimatic indices. Preliminary results indicate that by 2040 the currently dominant Quercus species (Quercus faginea) may be taken over by a 'drier' species (Quercus ballota) as the dominant species.



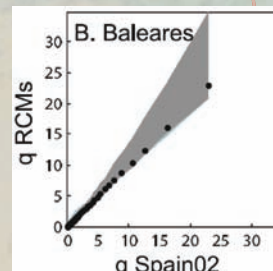
Projected changes in suitability index for Quercus faginea (pink line) and Quercus ballota (yellow line).

Changes in bioclimatic and drought indices in Andalusia

Work is being undertaken with the Environmental Ministry of Andalusia to explore changes in bioclimatic and drought indices.



Percentage changes in four bioclimatic types in Andalusia, showing a shift towards generally 'drier' types.

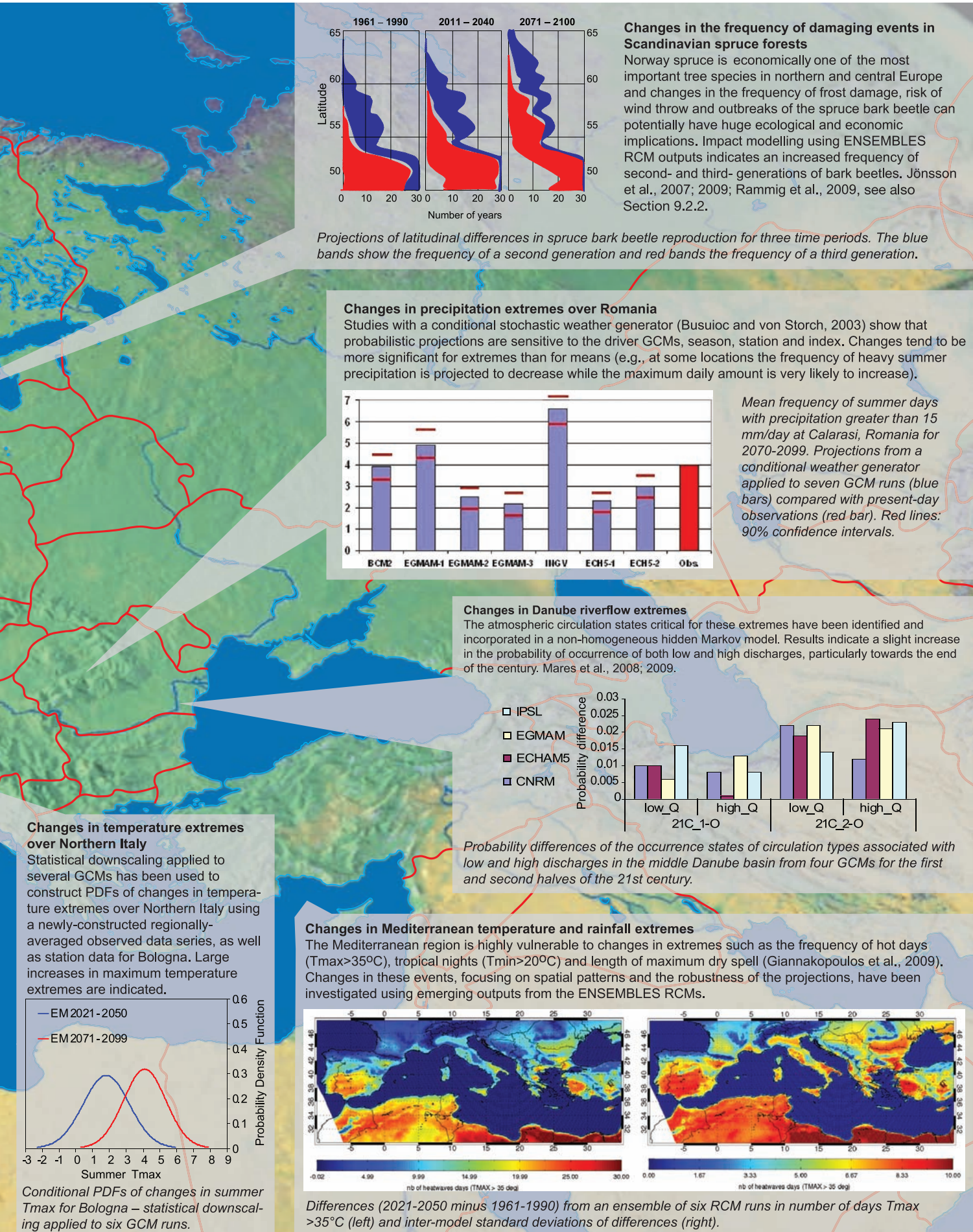


Quantile-quantile (q-q) plot of simulated (using an ensemble of five ERA-40 forced RCMs) and observed (dots) spatially-averaged precipitation for the Balearic Islands.

Changes in precipitation extremes over Spain

The skill of different ENSEMBLES RCMs to reproduce the mean and extreme precipitation regimes occurring in the different Spanish hydrological basins has been evaluated. The results will be used in the Spanish Coordinated Programme for Regional Climate Change Scenarios, funded by the Spanish Ministry of Medio Ambiente and Medio Rural y Marino. Herrera et al., 2009.

input to impacts assessments



References

ENSEMBLES publications are highlighted as bold text.

- Buser CM, Künsch HR, Lüthi D, Wild M, Schär C, 2009. **Bayesian multi-model projection of climate: bias assumptions and interannual variability.** *Climate Dynamics* 33, 849–868.
- Busuioc A, von Storch H, 2003. Conditional stochastic model for generating daily precipitation time series, *Climate Research* 24, 181–195.
- Cofiño AS, San-Martín D, Gutiérrez JM, 2007. A web portal for regional projection of weather forecast using GRID middleware. *Lecture Notes in Computer Science* 4489, 82–89.
- Déqué M, 2009. **Temperature and Precipitation Probability Density Functions in ENSEMBLES Regional Scenarios.** ENSEMBLES Technical Report 5 [available from <http://www.ensembles-eu.org/>].
- Déqué M, Rowell DP, Lüthi D, Giorgi F, Christensen JH, Rockel B, Jacob D, Kjellström E, Castro M, van den Hurk B, 2007. An intercomparison of regional climate simulations for Europe: assessing uncertainties in model projections. *Climatic Change* 81, 53–70.
- Déqué M, Somot S, Sanchez-Gomez E, Goodess CM, Jacob D, Lenderink G, Christensen OB, 2009. **The spread amongst ENSEMBLES regional scenarios: Regional Climate Models, driving General Circulation Models and interannual variability.** *Climate Dynamics*, submitted.
- Diez E, Orfila B, Frias MD, Fernandez J, Cofiño AS, Gutierrez JM, 2009. **Dynamical downscaling of seasonal precipitation forecasts over Spain using ECMWF-System3 and RCA models.** *Geophysical Research Letters*, submitted.
- Donat MG, Leckebusch GC, Pinto JG, Ulbrich U, 2009a. Examination of wind storms over Central Europe with respect to circulation weather types and NAO phases. *International Journal of Climatology* doi:10.1002/joc.1982.
- Donat MG, Leckebusch GC, Pinto JG, Ulbrich U, 2009b. **European storminess and associated atmospheric circulation: future changes in a multi-model ensemble of GCMs.** *Climate Research*, to be submitted.
- Donat MG, Leckebusch GC, Wild S, Ulbrich U, 2009c. **The benefit of multi-model RCM simulations for storm loss calculations.** *Climate Research*, to be submitted.
- Fischer EM, Schär C, 2009a. Future changes in daily summer temperature variability: driving processes and role for temperature extremes. *Climate Dynamics*, doi:10.1007/s00382-008-0473-8.
- Fischer EM, Schär C, 2009b. **High-impact European heatwaves in a changing climate.** *Geophysical Research Letters*, submitted.
- Frias MD, Herrera S, Cofiño AS, Gutiérrez JM, 2009. **Assessing the skill of precipitation and temperature seasonal forecasts in Spain: windows of opportunity related to ENSO events.** *Journal of Climate*, doi:10.1175/2009JCLI2824.1.
- Giannakopoulos C, Le Sager P, Bindi M, Moriondo M, Kostopoulou E, Goodess CM, 2009. **Climatic changes and associated impacts in the Mediterranean resulting from a 2°C global warming.** *Global and Planetary Change* 68, 209–224.
- Giorgi F, Mearns LO, 2002. Calculation of average, uncertainty range, and reliability of regional climate changes from AOGCM simulations via the ‘reliability ensemble averaging’ (REA) method. *Journal of Climate* 15, 1141–1158.
- Giorgi F, Mearns LO, 2003. Probability of regional climate change based on the reliability ensemble averaging (REA) method. *Geophysical Research Letters* 30, 1629.
- Goodess CM, Hall J, Best M, Betts R, Cabantous L, Jones PD, Kilsby CG, Pearman A, Wallace CJ, 2007. Climate scenarios and decision making under uncertainty. *Built Environment* 33 (1: Climate Change and Cities), 10–30.
- Herrera S, Fita L, Fernández J, Gutiérrez JM, 2009. **Evaluation of the mean and extreme precipitation regimes in the ENSEMBLES RCM multi-model dataset over Spain.** *Journal of Geophysical Research*, to be submitted.
- Jacob D, et al., 2009. **An ensemble of high-resolution regional climate change projections for Europe: datasets for impact research and adaptation strategies.** In preparation.
- Jönsson AM, Appelberg G, Harding S, Barring L, 2009. **Spatio-temporal impact of climate change on the activity and voltinism of the spruce bark beetle, *Ips typographus*.** *Global Change Biology* 15, 486–499.
- Jönsson AM, Harding S, Barring L, Ravn HP, 2007. **Impact of climate change on the population dynamics of *Ips typographus* in southern Sweden.** *Agricultural and Forest Meteorology* 146, 70–81.
- Kendon EJ, Jones RG, Kjellström E, Murphy JM, 2009b. **Using and designing GCM-RCM ensemble regional climate projections.** *Journal of Climate*, submitted.
- Kendon EJ, Rowell DP, Jones RG, 2009a. **Mechanisms and reliability of future projected changes in daily precipitation.** *Climate Dynamics*, doi:10.1007/s00382-009-0639-z.
- Kendon EJ, Rowell DP, Jones RG, Buonomo E, 2008. **Robustness of future changes in local precipitation extremes.** *Journal of Climate* 21, 4280–4297.
- Kjellström E, Lind P, 2009. **Changes in the water budget in the Baltic Sea drainage basin in future warmer climates as simulated by the regional climate model RCA3.** *Boreal Environment Research* 14, 114–124.
- Kjellström E, Nikulin G, Barring L, Hansson U, Strandberg G, Ullerstig A, 2009. **An ensemble of regional climate change simulations.** In: *Proceedings of WCRP Workshop on Regional Climate Modelling*, Lund, Sweden 4–8 May 2009 (B Rockel, L Barring, M Reckermann, eds). International BALTEX Secretariat Publication No. 41.
- Kotlarski S, Lüthi D, Schär C, 2009. **Future changes of European snow cover as simulated by an ensemble of regional climate models.** In preparation.
- Leander R, Buishand TA, 2007. **Resampling of regional climate model output for the simulation of extreme river flows.** *Journal of Hydrology* 332, 487–496.
- Leckebusch GC, Donat M, Ulbrich U, Pinto JG, 2008. **Mid-latitude cyclones and storms in an ensemble of European AOGCMs under ACC.** *CLIVAR Exchanges* 13(3), July 2008.
- Mares C, Mares I, Mihailescu M, Hübener H, Cubasch U, Stanciu P, 2008. **21st century discharge estimation in the Danube lower basin with predictors simulated through EGMAM model.** *Revue Roumaine de Géophysique* 52.
- Mares C., Mares I, Stanciu A, 2009. **Extreme value analysis in the Danube lower basin discharge time series in the twentieth century.** *Theoretical and Applied Climatology* 95, 223–233.
- Mariotti A, Zeng N, Yoon J-H, Artale V, Navarra A, Alpert P, Li LZ, 2008. **Mediterranean water cycle changes: transition to drier 21st century conditions in observations and CMIP3 simulations.** *Environmental Research Letters* 3, 044001, doi:10.1088/1748-9326/3/044001.
- Mitchell JFB, Johns TC, Eagles M, Ingram WJ, Davis RA, 1999. **Towards the construction of climate change scenarios.** *Climatic Change* 41, 547–581.
- Rammig A, Jönsson AM, Hickler T, Smith B, Barring L, Sykes MT, 2009. **Impacts of changing frost regimes on Swedish forests: incorporating cold hardiness in a regional ecosystem model.** *Ecological Modelling*, doi:10.1016/j.ecolmodel.2009.05.014.
- Sanchez-Gomez E, Somot S, Mariotti A, 2009. **Future changes in the Mediterranean water budget projected by an ensemble of Regional Climate Models.** *Geophysical Research Letters*, in press.
- San-Martín D, Cofiño AS, Herrera S, Gutiérrez JM, 2009. **The ENSEMBLES statistical downscaling portal: an end-to-end tool for regional impact studies.** *Environmental Modelling and Software*, submitted.
- Sordo C, Frias MD, Herrera S, Cofiño AS, Gutiérrez JM, 2008. **Interval-based statistical validation of operational seasonal forecasts in Spain conditioned to ENSO events.** *Journal of Geophysical Research* 113, 17121, doi:10.1029/2007JD009536.
- Xu Y, Gao X, Giorgi F, 2009. **Upgrades to the REA method for producing probabilistic climate change predictions.** *Climate Research*, submitted.

7 Understanding the processes governing climate variability and change, climate predictability and the probability of extreme events

[Research Theme 4]

B. Dong (Reading University), J-L. Dufresne (LMD/IPSL), S. Gualdi (INGV/CMCC), P. Friedlingstein (IPSL), N. Keenlyside (IfM), P. Maheras (AUTH), D. Salas (CNRM), R. Sutton (Reading University), L. Terray (CERFACS)

7.0 Introduction

The purpose of Research Theme 4 (RT4) was to advance understanding of the basic science issues at the heart of the ENSEMBLES project, focusing on the key processes that govern climate variability and change, and that determine the predictability of climate. Particular attention was given to understanding linear and non-linear feedbacks that may lead to climate ‘surprises’, and to understanding the factors that govern the probability of extreme events. Improved understanding of these issues will contribute significantly to the quantification and reduction of uncertainty in seasonal to decadal predictions and projections of climate change.

RT4 exploited the ENSEMBLES integrations (stream 1) performed in RT2A as well as undertaking its own experimentation to explore key processes within the climate system. It was working at the cutting edge of problems related to climate feedbacks, the interaction between climate variability and climate change – especially how climate change pertains to extreme events, and the predictability of the climate system on a range of time-scales. The statistical methodologies developed for extreme event analysis are new and state-of-the-art. The RT4-coordinated experiments, which have been conducted with six different atmospheric GCMs forced by common time-invariant sea surface temperature (SST) and sea-ice fields (removing some sources of inter-model variability), are designed to help to understand model uncertainty (rather than scenario or initial condition uncertainty) in predictions of the response to greenhouse-gas-induced warming. RT4 links strongly with RT5 on the evaluation of the ENSEMBLES prediction system and feeds back its results to RT1 to guide improvements in the Earth system models and, through its research on predictability, to steer the development of methods for initialising the ensembles.

7.1 Feedbacks and climate surprises

7.1.1 Radiative feedbacks

Radiative feedbacks are known to make a major contribution to global temperature change in response to an external forcing, but how much the different feedback processes contribute to the temperature change estimate and to its spread was not quantified. A method was proposed to quantify the contribution of the different radiative feedbacks to the equilibrium or

transient temperature change, and this was applied to the simulation results of twelve coupled GCMs (Dufresne and Bony, 2008). Results showed that the water vapour plus lapse rate (WV+LR) feedback had the largest contribution to the multi-model mean of the temperature increase, while the cloud feedbacks constituted by far the primary source of spread of both equilibrium and transient climate responses simulated by GCMs (Figure 7.1). Surprising for such an idealised experiment was the quite large contribution of the forcing to the spread. Another important result was that the ratio between the temperature increase due to each feedback and the global temperature increase was the same for both equilibrium and transient runs. The origin of the large spread due to cloud feedback has been identified: it is mainly due to low-level clouds that cover the largest part of the ocean (Bony and Dufresne, 2005; Bony et al., 2006; Webb et al., 2006).

In order to reduce the spread of climate feedback estimated by GCMs, and therefore in climate change projections, a strategy

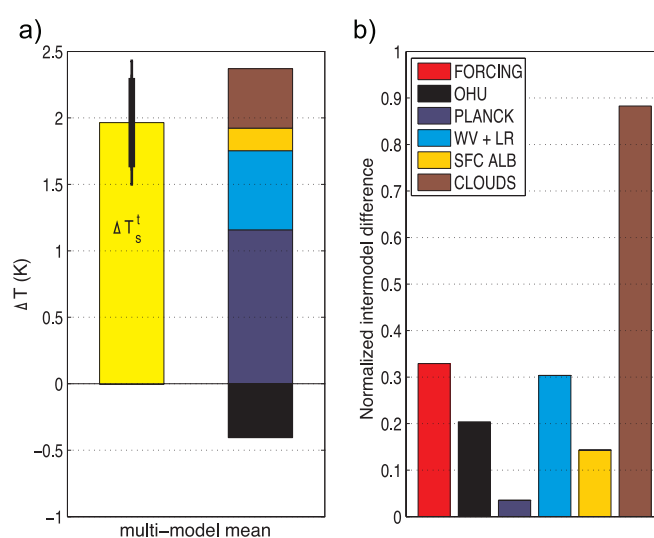


Figure 7.1: For simulations where CO_2 increases by 1%/yr, at the time of CO_2 doubling, (a) multi-model mean ± 1 standard deviation (thick line) and 5–95% interval (thin line) of the equilibrium temperature change (ΔT_s), and contributions to this temperature change associated with the Planck response, combined water vapour and lapse rate (WV+LR) feedback, surface albedo feedback, cloud feedback and ocean heat uptake; (b) inter-model standard deviation of the temperature change estimates associated with the radiative forcing, the Planck response and the various feedbacks normalised by the inter-model standard deviation of the equilibrium temperature change ΔT_s shown in (a).

was developed on how to constrain water vapour and cloud feedback processes using observations and process studies. This main objective, in common with the Cloud Feedback Model Intercomparison Project (from WGCM/WCRP) and the ENSEMBLES project, gives significant inputs to the CFMIP phase 2 plans; for instance through the organisation of a joint CFMIP/ENSEMBLES workshop held in Paris in April, 2007. Within this framework, the importance of developing specific tools to make quantitative comparisons between model results and satellite observations was highlighted. A CFMIP Observational Simulator Package (COSP) has been developed, which currently includes five satellite instruments. The ENSEMBLES project contributes to two of them – the Calipso and Parosol simulators (Chepfer et al., 2008). To ensure the consistency between the outputs of the Calipso simulators and the measurements of the Calipso satellite, a specific ‘GCM-Oriented Calipso Cloud Product’ (GOCCP) has been developed (Chepfer et al., 2009). This COSP simulator will be used by climate models when running the simulations recommended by the CMIP-5 project to support the preparation of the IPCC Fifth Assessment Report. This work was done in close collaboration with RT5.

7.1.2 Climate-carbon feedbacks

Global models of the coupled climate-carbon system have shown that climate change induces a reduction in the capacity of both land and ocean to absorb atmospheric CO₂ (e.g., Cox et al., 2000; Friedlingstein et al., 2001; Dufresne et al., 2002). Consequently, these reduced sinks act to further build up atmospheric CO₂ concentrations, by an estimated 20–220 ppm by 2100 (from the Coupled Climate-Carbon Cycle Model Intercomparison Project, ‘C4MIP’; Friedlingstein et al., 2006), which corresponds to an additional climate warming of 0.1–1.5°C. This has major policy implications for climate change mitigation and reduces the ‘permissible’ emissions to achieve CO₂ stabilisation (Jones et al., 2006).

Most C4MIP models attribute their carbon-climate change response to (1) reductions in land carbon uptake in the tropics and a widespread, climate-driven, loss of soil carbon, and (2) a decreased CO₂ uptake by the oceans, caused both by ocean warming and by a shrinking volume of the surface mixed layer. Nevertheless, the broad range in carbon cycle–climate feedback

among models reflects divergences in model representations of basic carbon cycle processes and their interactions (e.g., Le Quéré et al., 2005; Sitch et al., 2008).

Cadule et al. (2009) defines new metrics based on various characteristics of atmospheric CO₂ at three different time-scales:

1. *the long-term trend of atmospheric CO₂* (TR), which informs on the model’s ability to simulate realistic land and ocean carbon sinks over the historical period;
2. *the modelled atmospheric CO₂ seasonal cycle* (SC), which, particularly at Northern Hemisphere atmospheric CO₂ stations, constrains the model’s simulation of the seasonal activity of continental fluxes: vegetation growth in spring and summer, and vegetation decay in autumn;
3. *the interannual variability of the atmospheric CO₂* (IAV) as a constraint on the model’s capability to simulate realistic ENSO climate patterns and impacts on land and ocean carbon fluxes. For the seasonal and interannual variability, Cadule et al. (2009) evaluated the model’s capability to represent the CO₂ signal, and then evaluated the sensitivity of the atmospheric CO₂ to climatic fluctuations for these two time-scales.

These new metrics were applied to three C4MIP models: HadCM3LC, IPSL-CM2-C and IPSL-CM4-LOOP (Figure 7.2). Results confirm that multiple time-scales are needed to evaluate models, e.g., because the best model on seasonal scales did not outperform the others on the interannual time-scale. A further advantage of defining single metrics is that it allows for testing future structural improvements of models and the inclusion of new processes in the same rigorously defined framework. Indeed, Cadule et al. (2009) demonstrated how the new-generation IPSL model (IPSL-CM4-LOOP) outperforms the older IPSL-CM2-C on all metrics.

7.1.3 Interactions between Atlantic meridional overturning circulation, sea ice and climate

Detailed analysis has been performed on ENSEMBLES stream 1 climate change simulations performed with the third version of the CNRM (Centre National de Recherches Météorologiques) and the fourth version of the Institut Pierre-Simon Laplace (IPSL-CM4) global atmosphere–ocean–sea ice coupled models. Most state-of-the art global coupled models

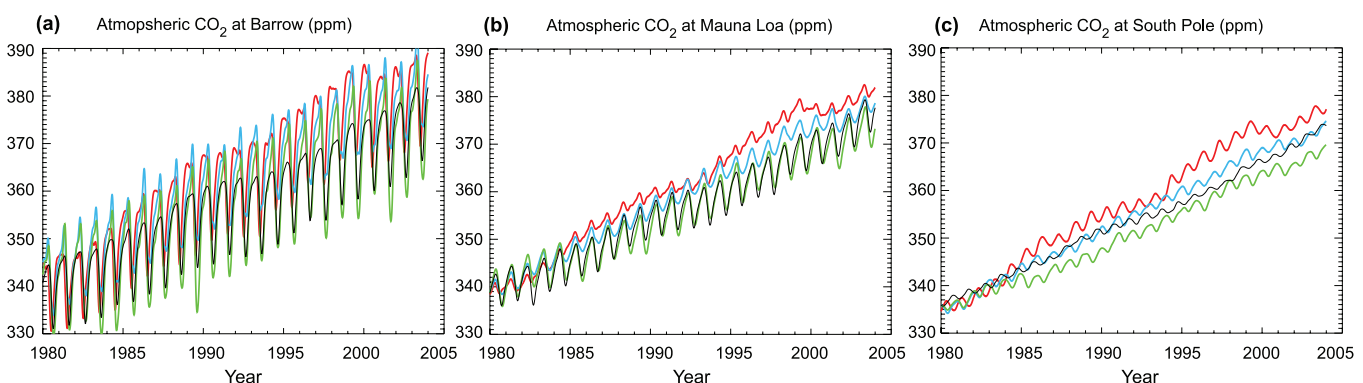


Figure 7.2: (a) Atmospheric CO₂ concentration at Point Barrow (BRW), Alaska, simulated by the three coupled models: HadCM3LC (red), IPSL-CM2-C (blue) and IPSL-CM4-LOOP (green). Observed CO₂ concentration is shown in black. (b), (c) Same as (a) for Hawaii, and the South Pole (SPO), respectively.

simulate a weakening of the Atlantic meridional overturning circulation (MOC) in climate change scenarios, but the mechanisms leading to this weakening are still being debated. The analysis of the A1B scenario experiment run with CNRM-CM shows that global warming leads to a slowdown of North Atlantic deep ocean convection and thermohaline circulation south of Iceland. This slowdown is triggered by a freshening of the Arctic Ocean and an increase in freshwater outflow through Fram Strait. Sea-ice melting in the Barents Sea induces a local amplification of the surface warming, which enhances the cyclonic atmospheric circulation around Spitzberg. This anticlockwise circulation forces an increase in Fram Strait outflow and a simultaneous increase in ocean transport of warm waters toward the Barents Sea, favouring further sea-ice melting and surface warming in the Barents Sea. Additionally, the retreat of sea ice allows more deepwater formation north of Iceland, and the thermohaline circulation strengthens there. The transport of warm and saline waters towards the Barents Sea is further enhanced, which constitutes a second positive feedback. The whole mechanism is summarised in Figure 7.3.

The mechanisms influencing the Arctic freshwater balance in response to anthropogenic greenhouse gas forcing were investigated in 20th and 21st century climate simulations run with IPSL-CM4. In these simulations, the Fram Strait outflow, which is an important source of freshwater for the northern North Atlantic, experiences a rapid and strong transition from a weak state towards a relatively strong state during 1990–2010 (see Figure 7.4). Arzel et al. (2008) suggest that this climate shift is triggered by the retreat of sea ice in the Barents Sea during the late 20th century. In agreement with CNRM-CM simulations, sea-ice reduction initiates a positive feedback in the atmosphere–sea ice–ocean system that alters both the atmospheric and oceanic circulations in the Greenland–Iceland–Norwegian (GIN) Barents Sea sector. Around the year 2080, the model simulates a second transition threshold beyond which the Fram Strait outflow is restored to its original weak value (see Figure 7.4). The long-term freshening of the GIN Seas is invoked to explain this rapid transition. It is further found that the mechanism of interannual changes in deep mixing differ

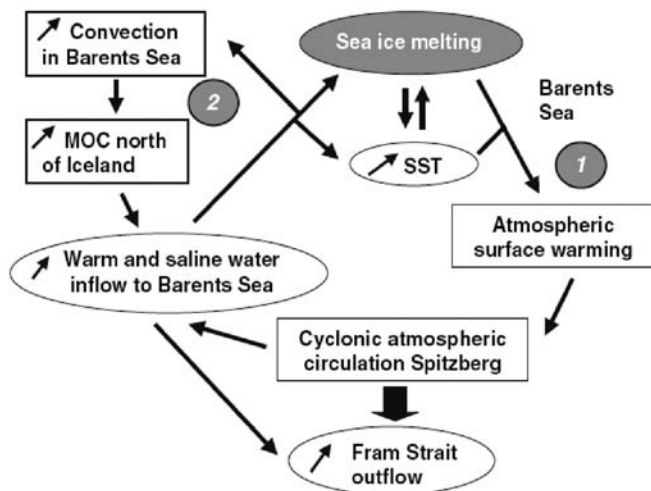


Figure 7.3: Summary of the feedback loop mechanism suggested by the analysis of the ENSEMBLES stream 1 SRES-A1B scenario run with CNRM-CM (Fig. 16 from Guemas and Salas-Méla, 2008a).

fundamentally between the 20th and 21st centuries. This difference is caused by the dominant influence of freshwater over the 21st century. In the GIN Seas, the interannual changes in the liquid freshwater export from the Arctic Ocean through Fram Strait combined with the interannual changes in the liquid freshwater import from the North Atlantic are shown to have a major influence in driving the interannual variability of the deep convection during the 21st century. South of Iceland, which is the other region of deepwater renewal in the model, changes in freshwater import from the North Atlantic constitute the dominant forcing of deep convection on interannual time-scales over the 21st century.

7.2 Natural variability and regional climate

7.2.1 Understanding the land–sea warming contrast, and changes in the global hydrological cycle in response to increasing greenhouse gases

Climate model simulations consistently show that, in response to greenhouse gas forcing, surface air temperature over land increases more rapidly than over sea. Analysis of the IPCC/CMIP3 model integrations shows a land–sea warming ratio ranging from 1.36 to 1.84 (Sutton et al., 2007). Understanding

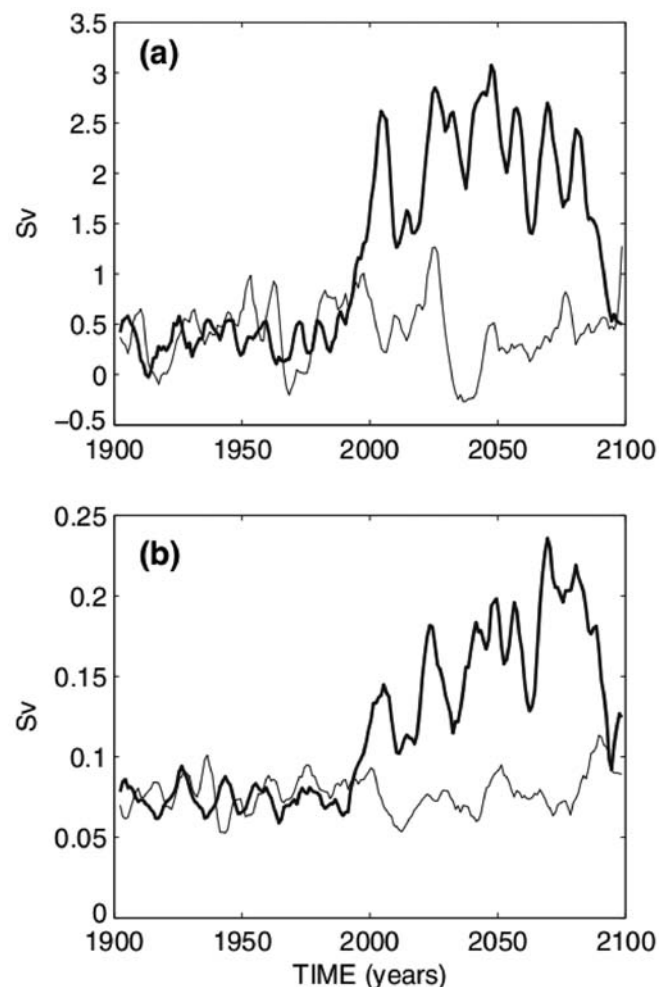


Figure 7.4: Time-series of (a) Fram Strait volume flux and (b) liquid freshwater export at Fram Strait in the pre-industrial experiment (thin line) and in the experiment covering the 20th century and the SRES A1B scenario over the 21st century (thick line) run with IPSL-CM4. A 5-year running mean has been applied (Fig. 6 from Arzel et al., 2008).

the factors that govern this warming contrast is an important issue for climate projections, both because of the direct impacts of regional warming, and because of interactions between the land–sea warming contrast and atmospheric circulation on local and regional scales. The mechanisms responsible for enhanced land surface warming in the response to increased CO₂ concentration have been elucidated using the HadAM3 model (Figure 7.5). Results indicate that warming over land may be viewed partly as a direct response to CO₂ change, and partly as an indirect response to warming of the sea. The processes responsible for the land surface warming in response to different forcings involve a local positive feedback between warming, relative humidity and cloud cover. The reduction of cloud cover enhances land surface warming in response to both CO₂ change and imposed SST change through its effect on surface short-wave radiation. In addition to the land surface warming induced by the CO₂ radiative effect, the CO₂-induced stomatal response inhibits evapotranspiration, favouring near-surface warming, especially in summer when evapotranspiration is strongest. The increased net downward short-wave radiation due to cloud changes further amplifies this near-surface warming. Results imply that the change in stomatal resistance in land surface schemes among different models in response to CO₂ change is one factor that might be responsible for the uncertainty of the land–sea warming ratio seen in IPCC/CMIP3 models. Analysis of warming ratios in the RT4-coordinated experiments shows that the range of warming ratios (1.54–1.78) is smaller than that obtained from IPCC/CMIP3 models. This indicates that the uncertainty of the

land–sea warming ratio is reduced in the atmospheric models forced by the same SST change, implying that another factor responsible for the spread of the land–sea warming ratio in response to greenhouse gas changes in IPCC/CMIP3 models is the uncertainty of the magnitude and spatial pattern of SST change. (See ENSEMBLES Deliverable 4.2.3 available at: <http://www.ensembles-eu.org/deliverables.html>.)

Understanding the response of the global hydrological cycle to recent and future anthropogenic emissions of greenhouse gases and aerosols is a major challenge for the climate modelling community. Using eight IPCC/CMIP3 models, it has been shown that the main uncertainties of the global hydrological changes originate from the tropics, where even the sign of the zonal mean precipitation change remains uncertain over land (Douville et al., 2006). Given the large interannual fluctuations of tropical precipitation, it is then suggested that the ENSO variability can be used as a surrogate of climate change in order to better constrain the model response. The study indicates that uncertainties in the 21st century evolution of these teleconnections represent an important contribution to the model spread, thus emphasising the need to improve the simulation of the tropical Pacific variability so as to provide more reliable scenarios of the global hydrological cycle. It also suggests that validating the mean present-day climate is not sufficient for assessing the reliability of climate projections, and that interannual variability is another suitable – and possibly more useful – candidate for constraining the model response.

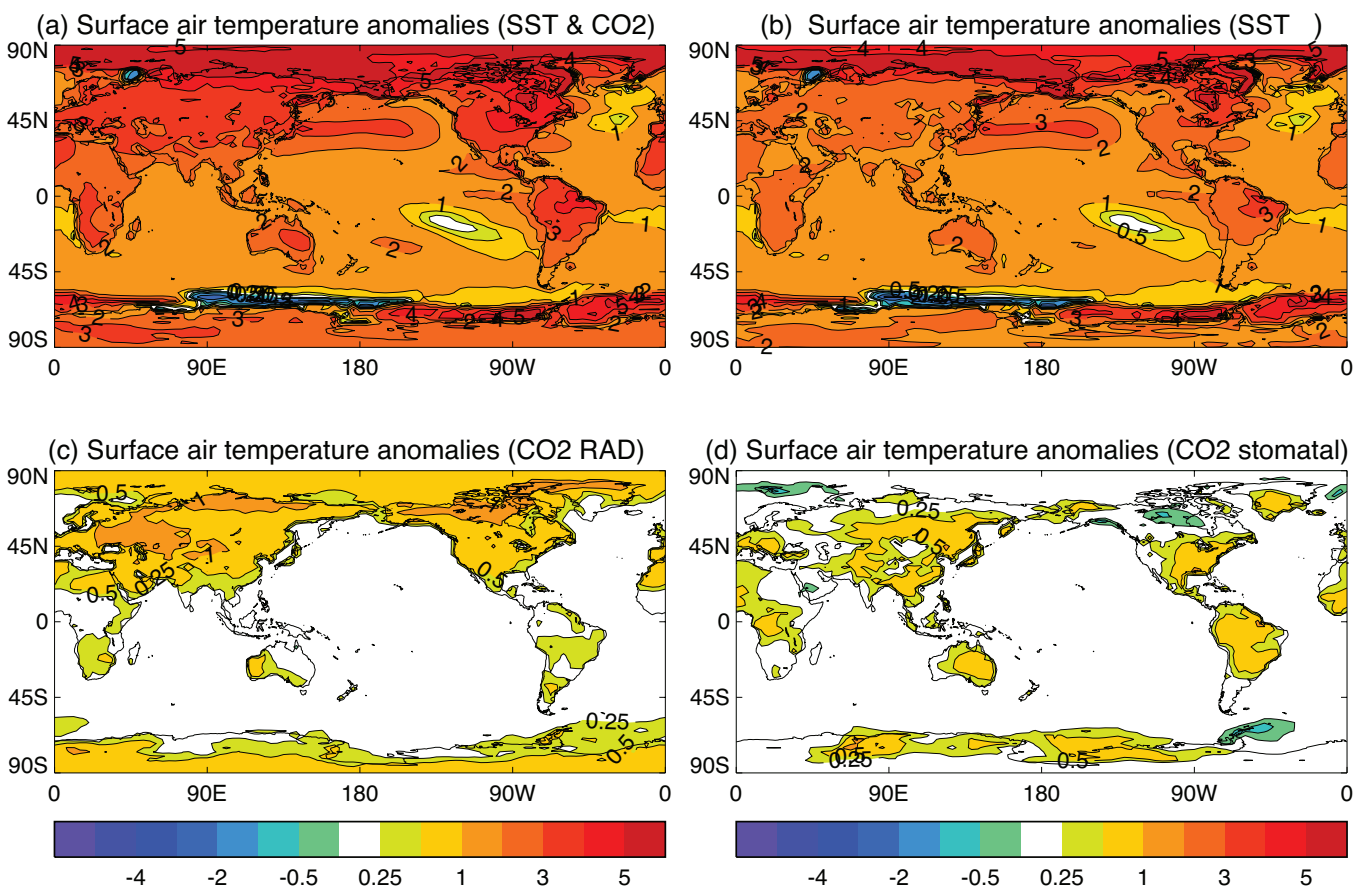


Figure 7.5: Annual mean surface air temperature changes in HadAM3 in response to (a) SST+CO₂ change, (b) SST change, (c) CO₂ radiative forcing change, and (d) the change in stomatal resistance in response to doubled CO₂ (Dong et al., 2009a, 2009b). The response to SST+CO₂ change reproduces many features of the land–sea warming contrast seen in the coupled model (a). A land–sea warming ratio of 1.34 with SST forcing only (b) suggests that direct CO₂ forcing is not necessary for enhanced land warming. (c) and (d) show that the purely radiative effects of CO₂ change and the reduction in stomatal resistance both contribute to warming over land.

7.2.2 Tropical climate variability, dynamics of monsoons, and their response to greenhouse gas forcing

Firstly attention was devoted to the effects of the model resolution on the simulations of the El Niño–Southern Oscillation (ENSO) and its interaction with Asian monsoons. It has been demonstrated that simulations of the MJO, ENSO, and the ENSO–monsoon interaction are significantly improved in a high-resolution model (Cherchi and Navarra, 2007; Navarra et al., 2008) and it has been suggested that, at high resolution, a good simulation of tropical instability waves in the cold tongue region of the East Pacific has led to better ocean mixing as well as a stronger coupled response in the atmosphere (Figure 7.6). As a result, the east–west temperature gradient is better simulated and the seasonal cycle of the East Pacific is much improved. Both aspects have direct consequences for the representation of the MJO and El Niño in the model. The implication of all these results is that high resolution coupled simulations do provide significant improvements in model performance, both with respect to the mean climatology and modes of variability.

The response of El Niño to climate change has also been investigated (Latif and Keenlyside, 2008; Guilyardi et al.,

2009). It has been concluded that there is no consensus among the current IPCC/CMIP3 models on the sense of future changes in ENSO, although no models exhibit large changes in ENSO behaviour (Guilyardi et al., 2009). These studies have provided a good basic set of diagnostics for characterising El Niño in coupled models, and its response to climate change, and have concluded that there is an urgent need to better constrain ENSO feedbacks in models in order to provide reliable climate projections. The teleconnection between ENSO and Indian summer monsoons remains robust in response to external forcing (Turner et al., 2007).

The teleconnections between the West African monsoon and the tropical sea surface temperature at the interannual to multi-decadal time-scales have been assessed based on twelve IPCC/CMIP3 models (Joly et al., 2007; Joly and Voldoire, 2009). The simulations of the 20th and 21st centuries do not show any significant change in the pattern of the teleconnections, but the dominant ENSO teleconnection exhibits a significant strengthening.

It has been identified that the southern tropical Atlantic Ocean SST anomalies are the main driver of deviations in the Indian monsoon rainfall (IMR) from the (linearly) ENSO-forced component (Kucharski et al., 2007, 2009). This finding also has important implications for seasonal predictions of IMR. Using a subset of the IPCC/CMIP3 20th century integrations, it has been further shown that the increase in greenhouse gases in the 20th century has had little influence on the decadal IMR variability (Kucharski et al., 2008).

The possible influence of the winter/spring Eurasian snow cover on the subsequent Indian summer precipitation has been revisited using both observations and a subset of CMIP3 simulations (Peings and Douville, 2009; Turner and Slingo, 2009c). Observations suggest a link between an east–west snow dipole over Eurasia and the Indian summer monsoon precipitation. However, this relationship is neither statistically significant nor stationary over the last 40 years. The maximum covariance analysis of the 20th century, CMIP3, indicates that some models (including HadCM3) do show an apparent influence of the Eurasian snow cover on the Indian summer monsoon precipitation, but the patterns are not the same as in the observations. Moreover, the apparent snow–monsoon relationship generally suggests a too strong El Niño–Southern Oscillation teleconnection with both winter snow cover and summer monsoon rainfall rather than a direct influence of the Eurasian snow cover on the Indian monsoon. Further analysis of the HadCM3 control simulation shows that this model is capable of simulating weakened monsoon conditions in the absence of ENSO, following heavy snow over either north/west Eurasia or the Himalaya/Tibetan Plateau (Turner and Slingo, 2009c). Idealised spring snow forcing conditions are tested separately for north/west Eurasia and the Himalaya/Tibetan Plateau regions in the HadAM3 model forced with climatological SST. In the HadAM3 model, forcing from the Himalaya region is found to dominate, in support of the Blanford hypothesis, whereby delayed snow melt leads to a reduction in surface sensible heating and consequently a reduction in the strength of the tropospheric temperature gradient. Thus Indian rainfall suffers, particularly during the early part of the summer season.

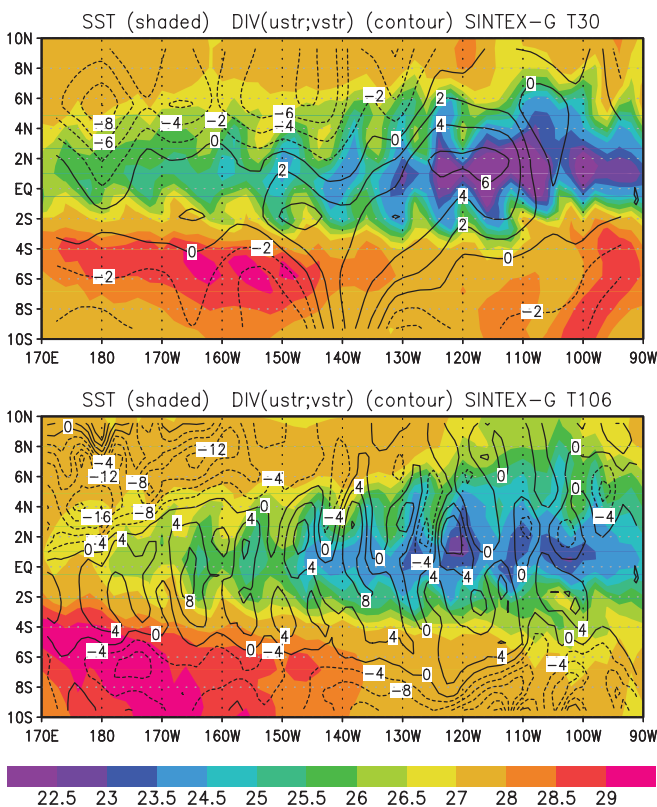


Figure 7.6: Snapshot of the SST (shaded) and the divergence of the surface stresses (contours) for pentads. Upper panel: low-resolution model (T30). Lower panel: high-resolution model (T106). The ocean model readily produces tropical instability waves in both models at T30 and at T106; however, the results show that the atmosphere reacts to the tropical instability waves (TIW) only at T106. The low-resolution model is effectively decoupled from the atmosphere at this spatial scale and there is no signature of the TIW in the atmosphere. The T106 shows the typical signature for the TIW in an area close to the equator, between 5N and 5S. A consequence of the coupling at the scale of the TIW is that the average surface stress over an area, such as the NINO3 area, is decreased by the coupling (after Navarra et al., 2008).

The effect of climate change on subseasonal precipitation extremes and active-break cycles of the Indian monsoon in a coupled GCM has also been investigated (Turner and Slingo, 2009a). The results suggest an increased probability of subseasonal extremes of rainfall over India, and changes in magnitude beyond changes in the mean alone. Active-break cycles of monsoon rainfall are found to intensify against the climatological seasonal cycle, although there is little evidence that break events are of longer duration, more frequent, or more severe in absolute terms (Figure 7.7). The analysis of the change in spatial distribution and magnitude of the heaviest extremes of daily monsoon rainfall over India in response to climate change using IPCC/CMIP3 models suggests that convection schemes are likely to play an important role for the uncertainties in the projected extreme precipitation change (Turner and Slingo, 2009b).

7.2.3 Extratropical climate variability and its response to greenhouse gas forcing

The North Atlantic Oscillation (NAO) is the primary variability mode of the North Atlantic sector. The NAO variability not only influences the mean winter climate over Europe but also influences climate extremes (e.g., Scaife et al., 2008) and ocean circulation (Bellucci et al., 2008). The possible changes at the end of the 21st century in the North Atlantic European winter large-

scale atmospheric circulation due to anthropogenic influence have been analysed using IPCC/CMIP3 simulations (Ensembles Milestone 4.2.3: available at: <http://www.ensembles-eu.org>). Most models show a significant increase in the occurrence frequency of the NAO+ and Atlantic Ridge weather regimes and a decrease in the NAO- regime while changes in blocking occurrence vary strongly between models (Figure 7.8). Results also suggest that changes in circulation (as represented by weather regimes) can explain a large proportion of the winter precipitation changes as simulated by the IPCC/CMIP3 multi-model ensemble mean (strong increase over northern Europe and Scandinavia in particular, decrease over the Mediterranean area).

The stratosphere and troposphere influence each other via propagating temperature and wind signals (e.g., Andrews et al., 1987). Modelling studies show that the strength of the stratospheric circulation influences the long-term variability of the NAO (Scaife et al., 2005), emphasising the need to reproduce stratospheric variability to fully simulate surface climate in the North Atlantic sector. The role of representation of the stratosphere on the changes in extratropical circulation and storm tracks in response to climate change has been investigated (Huebener et al., 2007). Results highlight the need to use stratosphere-resolved models to project climate change and variability, since simulated sudden stratospheric warmings are improved in the stratosphere-resolved model (Huebener et al., 2007).

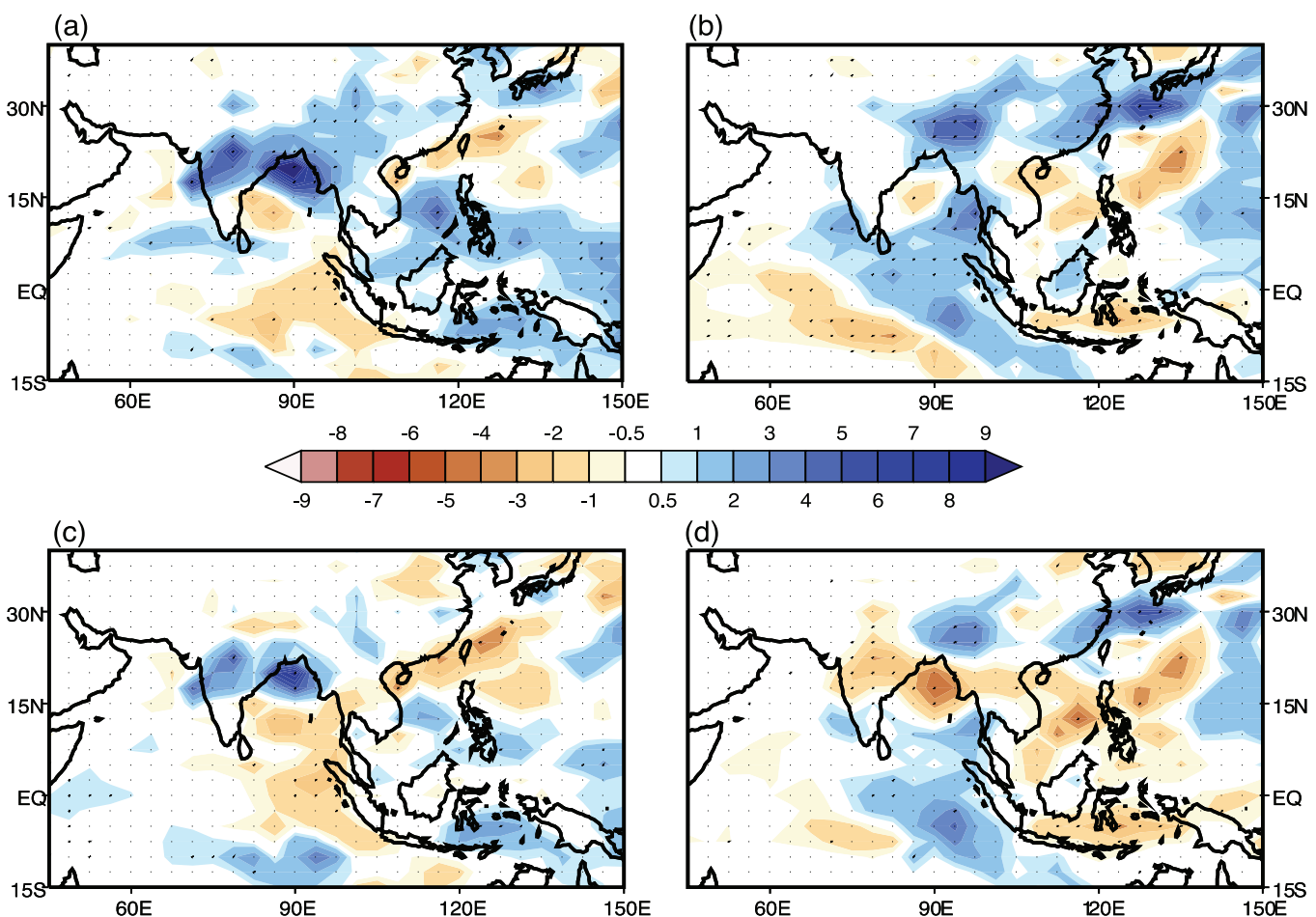


Figure 7.7: (a), (b) The differences ($2\times\text{CO}_2$ minus $1\times\text{CO}_2$) in precipitation associated with active-break cycles in HadCM3; (c) and (d) the anomalies with the change in seasonal cycle removed. Units are mm/day. In the difference plots, stippling indicates significance at the 95% level using Student's *t*-test. Results (c) and (d) indicate that flooding and drought associated with the active-break cycle of Indian summer monsoon will become more intense in response to the increase in greenhouse gas concentrations.

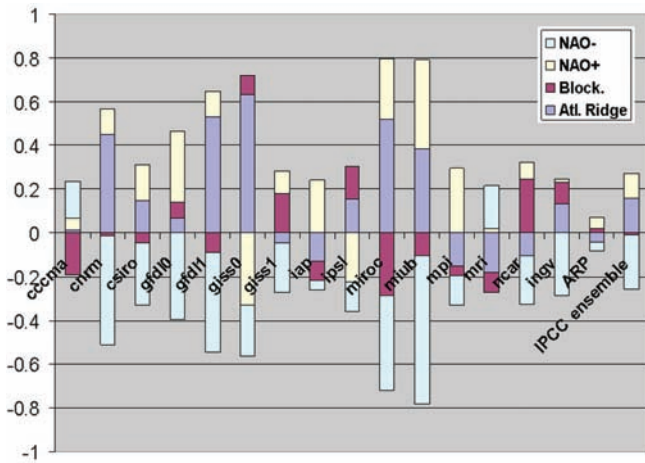


Figure 7.8: Change in the occurrence of the standard winter weather regimes for the North Atlantic European sector (units are in days). Each bar represents an individual model (with the bar labelled “IPCC ensemble” being the multi-model mean). Each colour represents a different weather regime. Most models show a significant increase in the occurrence frequency of the NAO+ and Atlantic Ridge weather regimes and a decrease in the NAO– regime, while changes in blocking occurrence vary strongly between models.

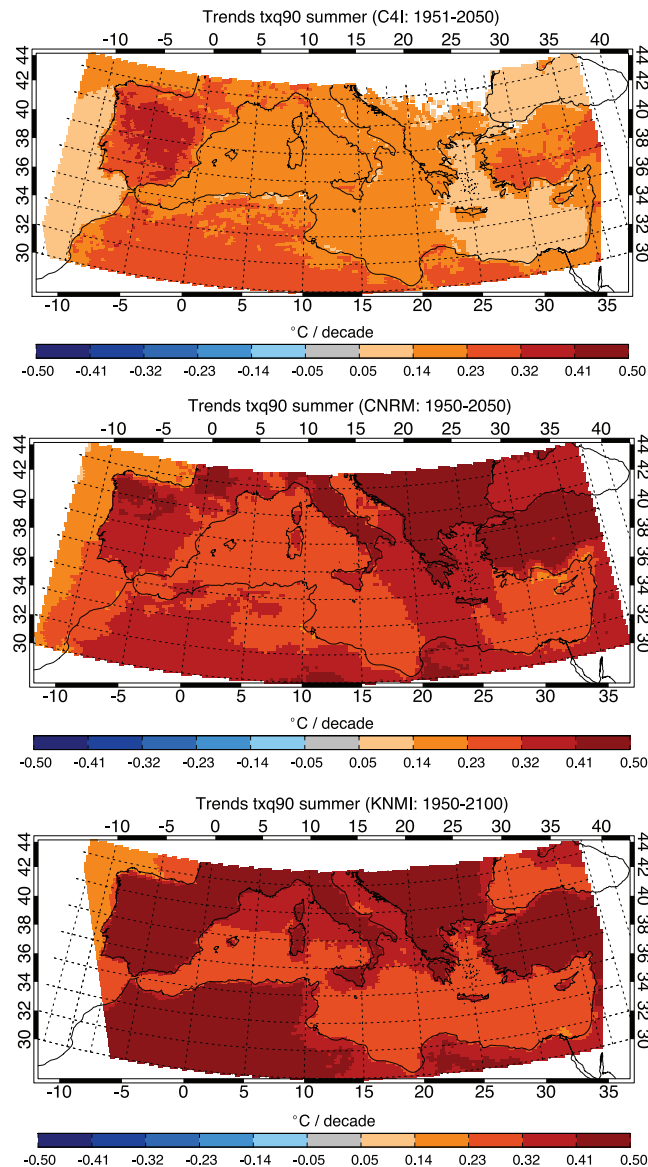


Figure 7.9: Statistically significant trends of the 90th percentile for maximum temperature (TXQ90) for summer as estimated by the three examined models (trends are statistically significant at the 0.05 level of significance).

7.3 Extreme weather and climate events

7.3.1 Warm extremes and heat waves

The occurrence of specific climate extremes in the Mediterranean region as well as the relationships with large-scale circulation have been studied using three transient ENSEMBLES regional climate model (RCM) simulations (Tolika et al., 2009). The RCMs are first evaluated against observations for the control period 1961–1990, then seven extreme climate indices are calculated, and finally their trends are analysed over the entire time period, which is 1961–2050 for two models and 1961–2100 for the third model. All models marked a shift towards warmer climate, with the high temperatures getting warmer in the future (Figure 7.9). The models also indicated an increase in summer low temperatures. With respect to precipitation indices, the models show similar present and future spatial patterns of the extreme precipitation amounts in winter, with the most extreme precipitation observed along the western borders of all peninsulas of the northern Mediterranean. All three models compare better and are better evaluated for temperature extremes, while showing less clear results for precipitation extremes.

Extreme climate events over north-west Europe and Eurasia are typically related to the occurrence of blocking situations, and specific methodologies have been developed and tested to study these relationships (e.g., Carril et al., 2008). The intraseasonal variability of those patterns is related to the amplitude of the blocking, the relative location of the action centre, and the wavetrain of anomalies downstream or upstream of the blocking. During June and July, blocking situations which give extremely hot climate conditions over north-west Europe are also associated with cold conditions over the eastern Mediterranean sector. The Euro-Mediterranean region is a transition area in which extratropical and tropical systems compete, influencing the occurrence of climate events: blockings tend to be related to extremely hot months during June, while baroclinic anomalies dominate the variability of the climate events in July and August. Climate model simulations are able to capture the extreme-related variability in July, and climate change projections indicate that the most sensitive location for changes in extremes is north-west Europe.

A methodology to diagnose the relationship between large-scale circulation anomalies and the occurrence of local weather regimes has also been developed (Panja and Selten, 2007). The method, referred to as extreme associated functions (EAF), was applied to present (1958–2000) observed and simulated local daily summer temperature time-series in Europe to validate the model, and to future (2050–2100) simulated time-series to assess the effect of changes in the circulation on the temperature extremes. To illustrate the methodology, Figure 7.10 shows results for the Netherlands. The EAF pattern is characterised by a high-pressure anomaly slightly to the north of the Netherlands and summarises flow patterns, with advection of warm air from the south-east as well as flow patterns without advection but subsidence conditions in clear, sunny skies. The model results compare very well with observations. The scatter plot shows a strong relation between the amplitude of this pattern and the local temperature. This relation changes in the future; the same pattern amplitude in future is associated with warmer temperature extremes primarily due to a decrease in the latent heat flux as soil water availability is

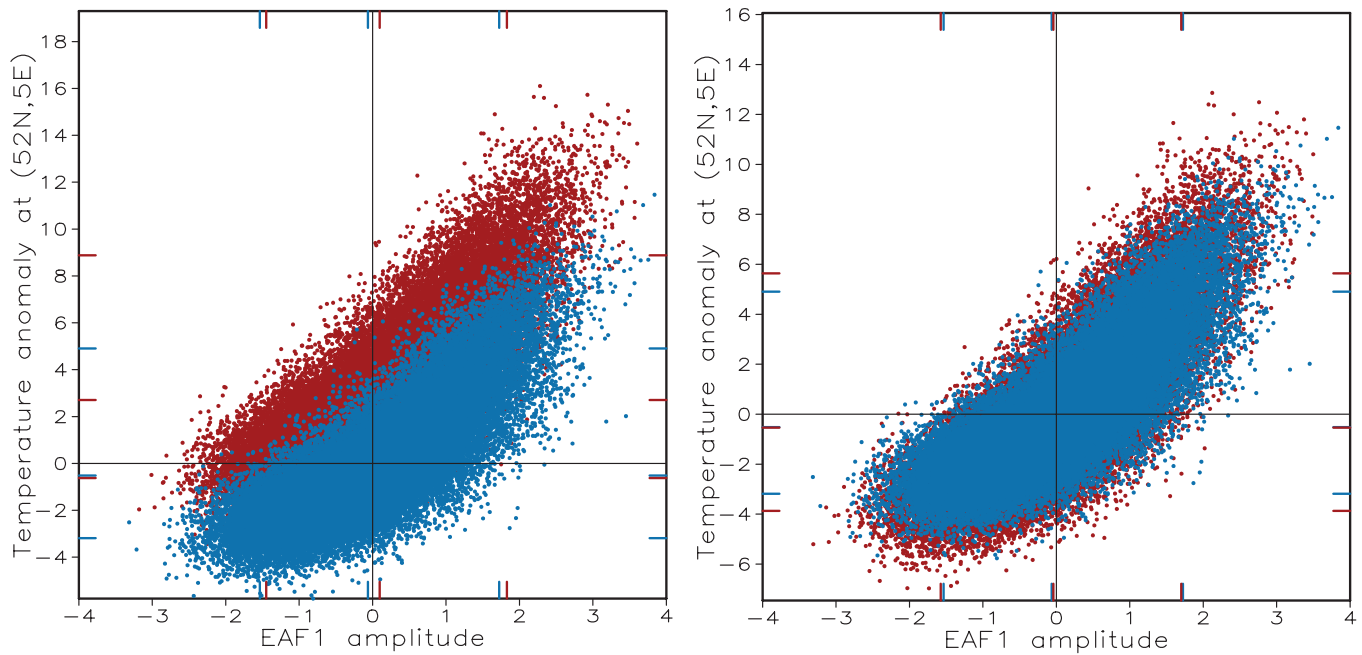


Figure 7.10: Left panel: scatter plots of the temperature anomaly versus the dominant EAF amplitude for the historical period (blue) and the future period 2050–2100 (red) under the SRESA1B scenario. Right panel: the same but with removal of the mean change. The coloured stripes on the axis indicate the 5% quantile, the median and the 95% quantile, again with blue for the historical period, and red for the future.

reduced. The pattern itself, as well as its probability distribution, does not change much. Larger simulated changes in the EAFs are found for locations in southern Europe.

7.3.2 Tropical cyclones

Tropical cyclones (TC) are one of the most important sources of extreme weather in the tropics, and understanding how extreme weather events will change under future climate changes is of great importance to society. How the characteristics - intensity, frequency, and duration - of TCs will change under future climate change was investigated by analyzing coupled model simulations and performing high-resolution (60 km) atmospheric model simulations.

There has been significant debate on the impact of global warming on tropical cyclones. Much of this has been stimulated by the anomalously strong hurricane activity in the Atlantic sector during recent years. Several studies in ENSEMBLES have investigated different aspects of how TC will respond to global warming, including the role of natural internal climate variability (Bengtsson et al., 2007; Latif et al., 2007; Gualdi et al., 2008; Royer et al., 2009). These studies indicate, in agreement with other recently published studies, that under global warming there will be an overall decrease in the frequency of TC, resulting from the increase in static stability and reduced vertical circulation. A clear increase in the number of intense tropical storms was found in the high-resolution simulations. This is due to the increase in temperature and water vapour, which provide more energy for the storms once they have developed. There is disagreement over the predicted regional changes, likely due to uncertainties in the tropical SST response to global warming.

Royer et al. (2009) analysed TC genesis in fifteen coupled climate models running the IPCC CMIP3 simulations for the 20th century and for scenario A2, among which were the climate models used

in ENSEMBLES stream 1 simulations. They showed that most of the models simulate rather realistic patterns of cyclogenesis for the current climate. The cyclogenesis index shows inter-decadal fluctuations and long-term trends. In scenario A2 the patterns of response of cyclogenesis at the end of the 21st century differ according to the ocean basins and models. While, in a few ocean basins, such as the Indian Ocean, the majority of models compute an increasing trend in TC genesis, the response is less coherent in other basins, where some models give a decreasing trend. The lack of coherence of the TC genesis response to future climate change can be associated with the different response patterns of the ocean sea surface temperatures (SST) simulated by the coupled models, particularly over the equatorial Pacific (discussed in Section 7.2.2).

The impact of non-local SST changes on TC was highlighted in the study of Latif et al. (2007). This study showed that the temperature difference between the tropical North Atlantic and the tropical Indian and Pacific Oceans (Indo-Pacific) is a key parameter in controlling the vertical wind shear over the Atlantic; an important quantity for hurricane activity. This is illustrated by the close relationships between the accumulated cyclone energy (ACE) index (a measure of hurricane activity), vertical wind shear over the hurricane main development region, and the difference in SST between the tropical North Atlantic and the Indo-Pacific region (Figure 7.11). The stronger warming of the tropical North Atlantic relative to that of the Indo-Pacific during the most recent years drove reduced vertical wind shear over the Atlantic and is thus responsible, at least in part, for the strong hurricane activity observed. In 2006, however, the temperature difference between the tropical North Atlantic and the tropical Indian and Pacific Oceans was much reduced, consistent with the relatively weak hurricane season.

The possible changes that greenhouse global warming might generate in the characteristics of tropical cyclones (TCs) was investigated in more detail using scenario climate simulations carried out with a fully coupled high-resolution global general circulation model (Gualdi et al., 2008). The results from the

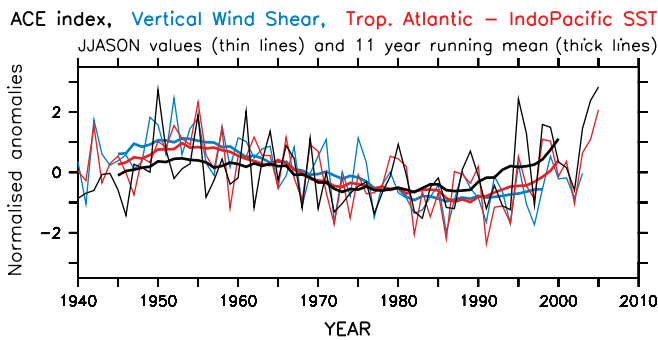


Figure 7.11: ACE index (black), inverted simulated vertical wind shear (blue), and tropical North Atlantic/Indo-Pacific SST difference (red). Results are shown from 1940 onwards, since observations are most reliable for this period. The data were normalised with respect to their individual long-term standard deviations to ease comparison. The thin lines are the raw JJASON values. The thick lines denote the low-pass filtered (applying a 11-year running mean) values.

climate scenarios reveal a substantial general reduction of TC frequency when the atmospheric CO_2 concentration is doubled and quadrupled (Figure 7.12). The reduction appears particularly evident for the tropical western North Pacific (WNP) and North Atlantic (ATL). In the WNP the weaker TC activity seems to be associated with reduced convective instabilities. In the ATL region the weaker TC activity seems to be due to both the increased stability of the atmosphere and a stronger vertical wind shear. Despite the generally reduced TC activity, there is evidence of increased rainfall associated with the simulated cyclones. Finally, the action of the TCs remains well confined to the tropical region and the peak of TC number remains equatorwards of 20° latitude in both hemispheres, notwithstanding the overall warming of the tropical upper ocean and the expansion polewards of warm SSTs.

The sensitivity of the results to atmospheric model resolution was also assessed (Bengtsson et al., 2007, 2009). In particular, TCs under different climatic conditions in the Northern Hemisphere have been investigated with the Max Planck Institute (MPI) coupled (ECHAM5/MPI-OM) and atmosphere (ECHAM5) climate models. The intensity and size of the TC depend crucially on resolution with higher wind speed, and smaller scales at the higher resolutions. The typical size of the TC is reduced by a factor of 2.3 from T63 (≈ 200 km) to T319 (≈ 40 km) using the distance of the maximum wind speed from the centre of the storm as a measure. The full three-dimensional structure of the storms becomes increasingly more realistic as the resolution is increased.

For the T63 resolution, three ensemble runs were explored for the period 1860–2100, using the IPCC SRES scenario A1B and evaluated for three 30-year periods at the end of the 19th, 20th and 21st centuries. While there is no significant change between the 19th and the 20th century, there is a considerable reduction in the number of TCs by around 20% in the 21st century, but no change in the number of more intense storms. The reduction in the number of storms occurs in all regions. A single additional experiment at T213 resolution was run for the two latter 30-year periods. The T213 is an atmospheric only experiment using the transient sea surface temperatures (SST) of the T63 resolution experiment. Also, in this case, there is a reduction by about 10% in the number of simulated TCs in the 21st century compared with the 20th century but a marked increase in the number of intense storms (Figure 7.13). The number of storms with maximum wind speeds greater than 50 m s^{-1} increases by one-third. Most of the intensification takes place in the eastern Pacific and in the Atlantic, where the number of storms stays more or less the same.

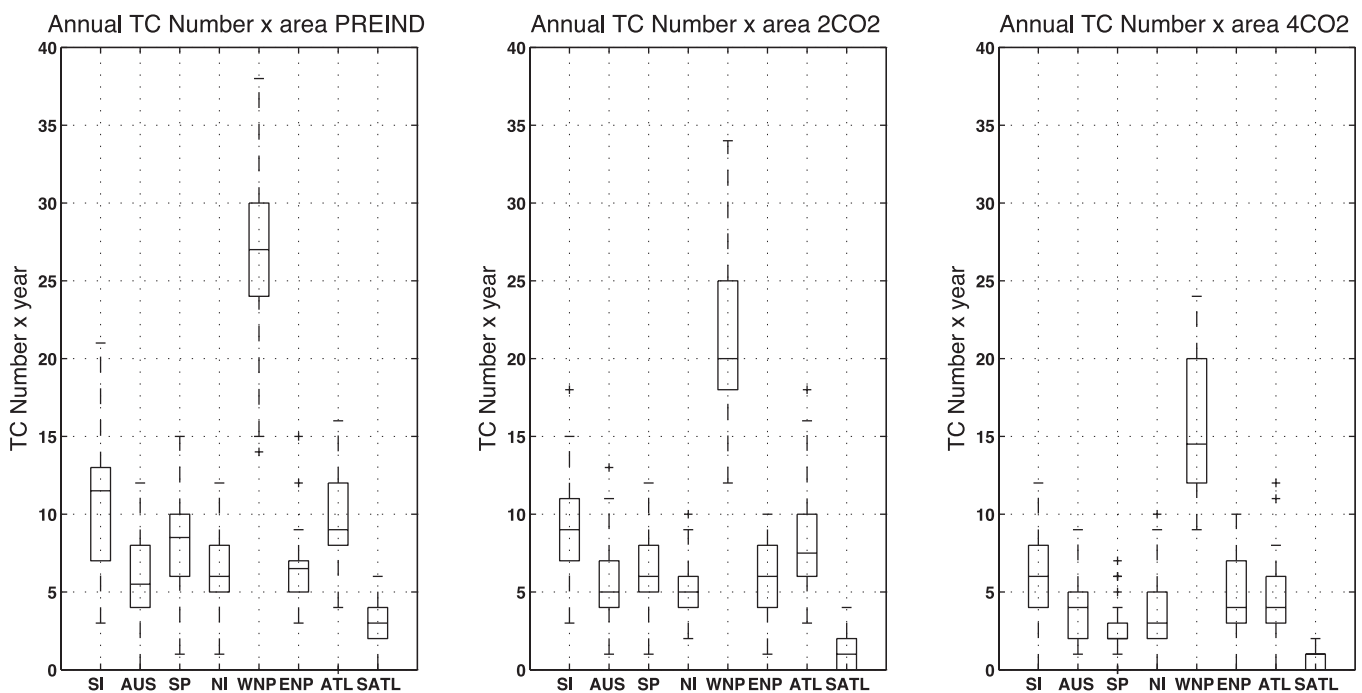


Figure 7.12: Box plots of the number of TCs per year for the (left) pre-industrial period, (middle) $2\times\text{CO}_2$ scenario and (right) model simulation. The number of TCs (y axis) is plotted for each area of TC genesis (x axis). The horizontal lines within the box are the median. The vertical dashed lines indicate the range of the non-outliers. The values indicated with crosses are the outliers. Regions are northern Indian Ocean (NI), western North Pacific (WNP), eastern North Pacific (ENP), North Atlantic (ATL), South Atlantic (SATL), southern Indian Ocean (SI), the ocean north of Australia (AUS), and the southern Pacific (SP).

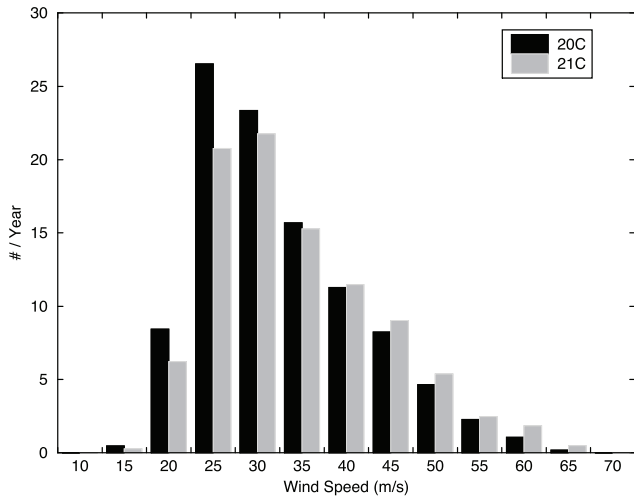


Figure 7.13: Distribution of maximum wind speeds at 925 hPa for the Northern Hemisphere tropical cyclones for the last 30 years of the 20th (20C) and 21st (21C) centuries as computed by a high-resolution (T213) version of the ECHAM5 atmospheric model. Bin widths are 5 m s⁻¹.

7.3.3 Extratropical storms

Little evidence was found for significant changes in the number of Northern Hemisphere extratropical storms in the future in either the high- or low-resolution simulations (Löptien et al., 2008; Bengtsson et al., 2009). Nor were there any significant changes found in the intensities of storms. One reason for this may be that, in contrast to tropical storms, diabatic heating is not a central process in extratropical storms. There are larger regional changes, in agreement with previous studies. The largest changes found are in total and extreme precipitation (Figure 7.14), where significant increases are seen. Cumulative precipitation along the tracks of the cyclones increases by some 11% per track, or about twice the increase in global precipitation, while the extreme precipitation is close to the globally averaged increase in column water vapour (around 27%). Regionally, changes in extreme precipitation are even higher because of changes in the storm tracks.

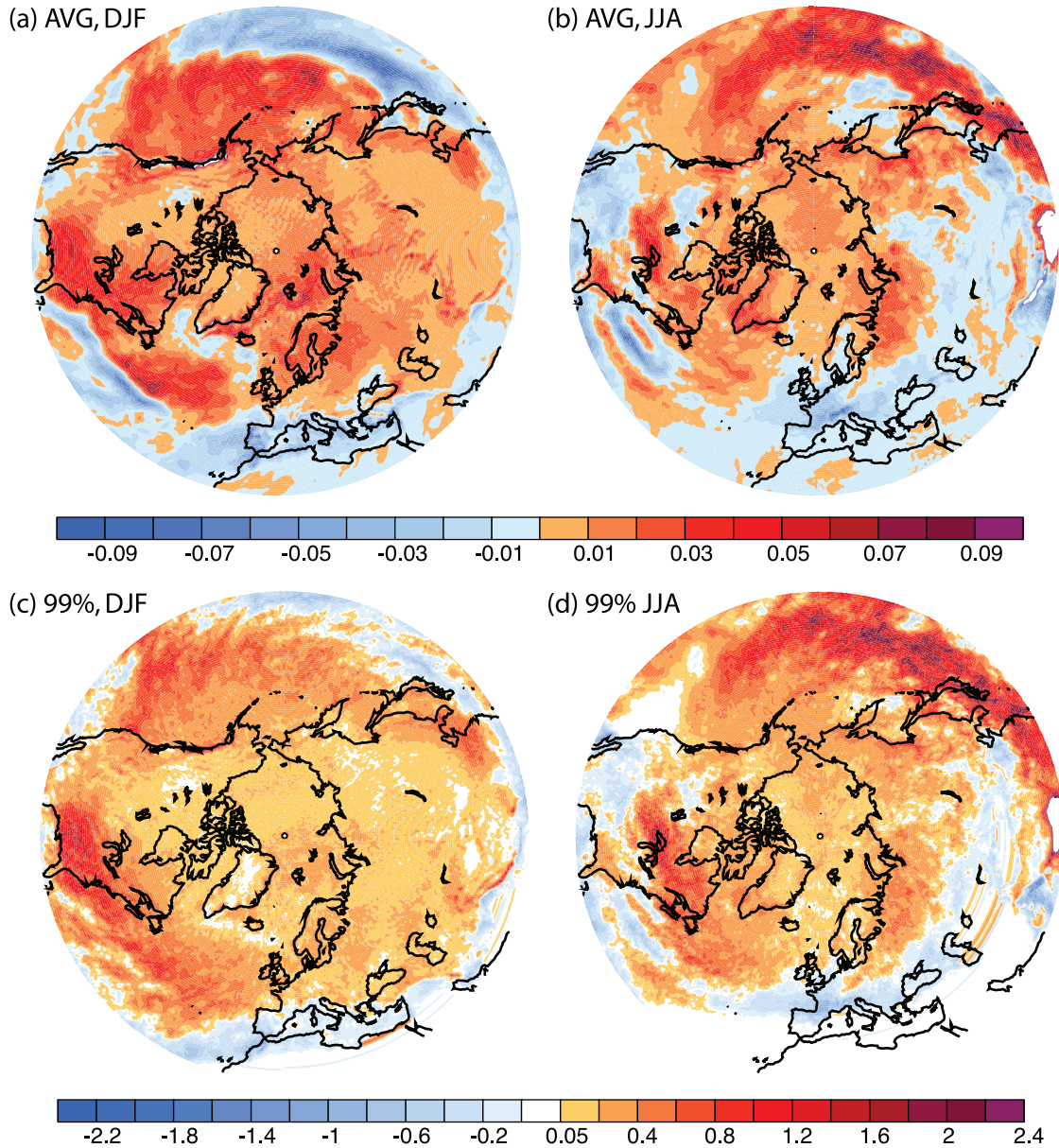


Figure 7.14: The geographical distribution of changes in average (a, b) and extreme (c, d) precipitation (mm/hr) for the Northern Hemisphere between 21st century (2069–2100) and 20th century (1959–90) from the ECHAM5 atmosphere model at T213 with 31 vertical levels, using IPCC scenario A1B with the time-slice method. SST and sea-ice fraction data are from one of the T63 ECHAM5OM coupled model integrations. (a) DJF time mean, (b) JJA time mean, (c) DJF 99th percentile, and (d) JJA 99th percentile.

7.4 Sources of predictability in current and future climate

7.4.1 Predictability on intraseasonal time-scales and its impact on seasonal predictability

A significant impact of tropical intraseasonal variability on the phase of the NAO was identified in observations. This presents a previously overlooked source of predictability for extended-range weather forecasts in the North Atlantic sector. Evidence was found that the main tropical climate intraseasonal oscillation, MJO, controls part of the distribution and sequences of North Atlantic-European daily weather regimes in winter (Cassou, 2008). Regimes associated with the NAO are the most affected, allowing for medium-range predictability of their phase far exceeding the usually quoted 1-week limit. Using a very simple statistical model, the correct sign of NAO regimes could be successfully forecast in ~70% of the cases based solely on knowledge of the MJO during the previous 12 days (Figure 7.15). This promising skill could be of great importance, as weather regimes are closely linked with both mean conditions and extreme temperature and precipitation events over Europe.

The organisation of convection plays an important role in the intraseasonal predictability of the monsoon. A detailed assessment of the Asian summer monsoon intraseasonal variability (ISV), based on DEMETER seasonal hindcasts, indicates that current climate models do not simulate this organisation of convection

well (Xavier et al., 2008). The periods of ISV events are shorter and the event-to-event pattern similarity, or the reproducibility of the convective events, is poor in the models. These findings point to a problem in the convective parameterisation of climate models. Analysis of the air–sea interaction processes associated with the ISV reveals that the models produce systematic phase relationships between atmospheric convection, the surface winds, and the sea surface temperature (SST) and weak SST variability. In reality, this relation is variable, depending on atmospheric heat fluxes, the oceanic mixed layer depth, and mixing and entrainment processes at the bottom of this mixed layer. This highlights the need to represent two essential factors for improved SST variability in the models; namely, the diurnal warm layer of SST and the variations of the oceanic mixed layer depth (Klingaman et al., 2009).

7.4.2 Predictability on seasonal and interannual time-scales

Land surface hydrology (LSH) is a potential source of long-range atmospheric predictability that has received less attention than sea surface temperature (SST). Results from the ensemble atmospheric simulations driven by observed or climatological SST in which the LSH is either interactive or nudged towards a global monthly reanalysis highlight the influence of soil moisture boundary conditions in the summer mid-latitudes and the role of snow boundary conditions in the northern high latitudes

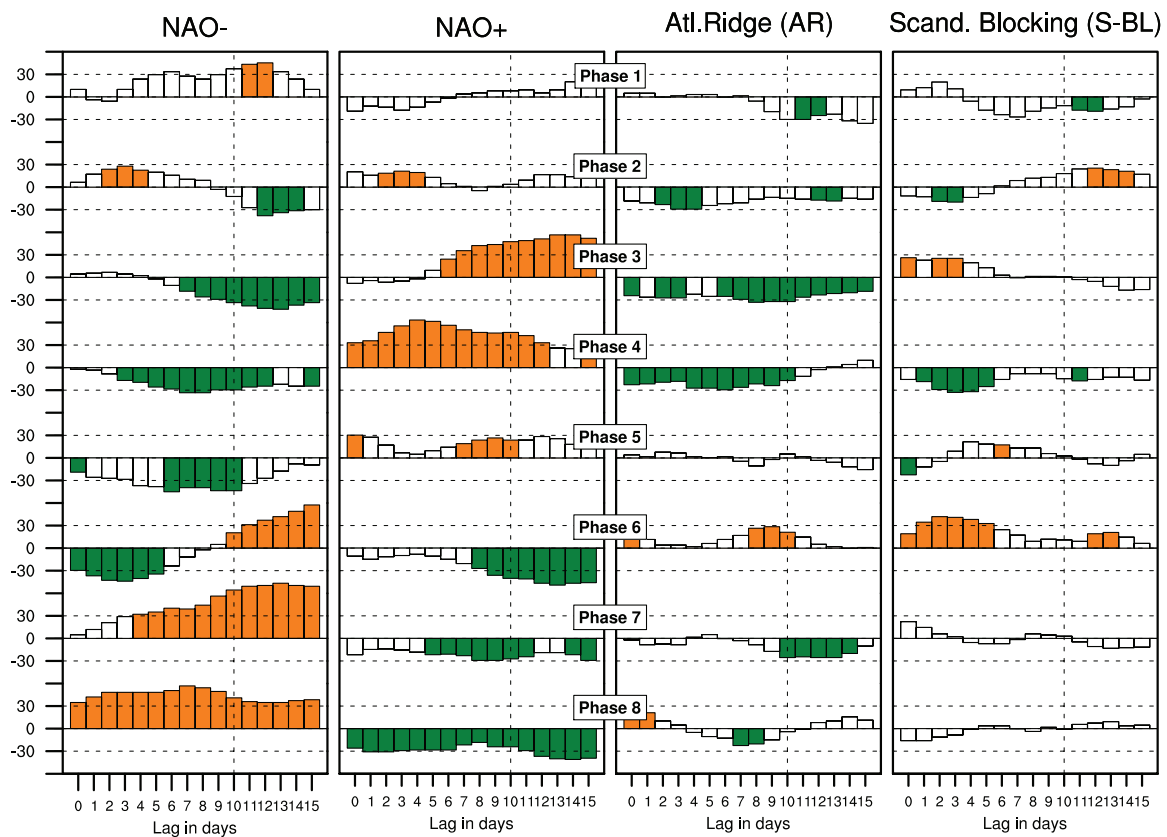


Figure 7.15: Table of contingency between the MJO phases and the North Atlantic weather regimes. For each MJO phase, the anomalous percentage occurrence of a given regime is plotted as a function of lag in days (with regimes lagging MJO phases). The 0% value means that the MJO phase is not discriminative for the regime whose occurrence is climatological. A 100% value would mean that this regime occurs twice as frequently as its climatological mean; –100% means no occurrence of this regime. The presence of a slope as a function of lag is suggestive of MJO forcing. For white bars, either the change in the distribution between the four regimes is not significant at the 99% significance level, or the individual anomalous frequency of occurrence is lower than the minimum significant threshold tested at 95% using Gaussian distribution. For the orange (green) bars, the regimes occur significantly more (less) frequently than their climatological occurrence (after Cassou, 2008).

(Douville, 2009) (Figure 7.16). In addition to the nudged experiments, ensembles of seasonal hindcasts in which the relaxation is switched off at the end of spring or winter have been conducted in order to evaluate the impact of soil moisture or snow mass initialisation. Land surface hydrology appears as an effective source of surface air temperature and precipitation predictability over Eurasia (as well as North America), which is at least as important as SST in spring and summer. Cloud feedbacks and large-scale dynamics contribute to amplify the regional temperature response, which is, however, mainly found at the lowest model levels and only represents a small fraction of the observed variability in the upper troposphere.

The role of variable greenhouse gas concentrations in improving seasonal forecasts/hindcasts has been demonstrated (Doblas-Reyes et al., 2006; Liniger et al., 2007). An experiment to determine the relevance for seasonal predictions of the increase in greenhouse gas concentration recorded in the last 50 years has been carried out. Results show that there is a substantial increase in the predictability of global average air temperature after the first month of the integration. In addition, probabilistic skill scores for the Northern Hemisphere, Southern Hemisphere and tropics are systematically better during boreal summer with regard to a control experiment with constant greenhouse gas concentration (Figure 7.17).

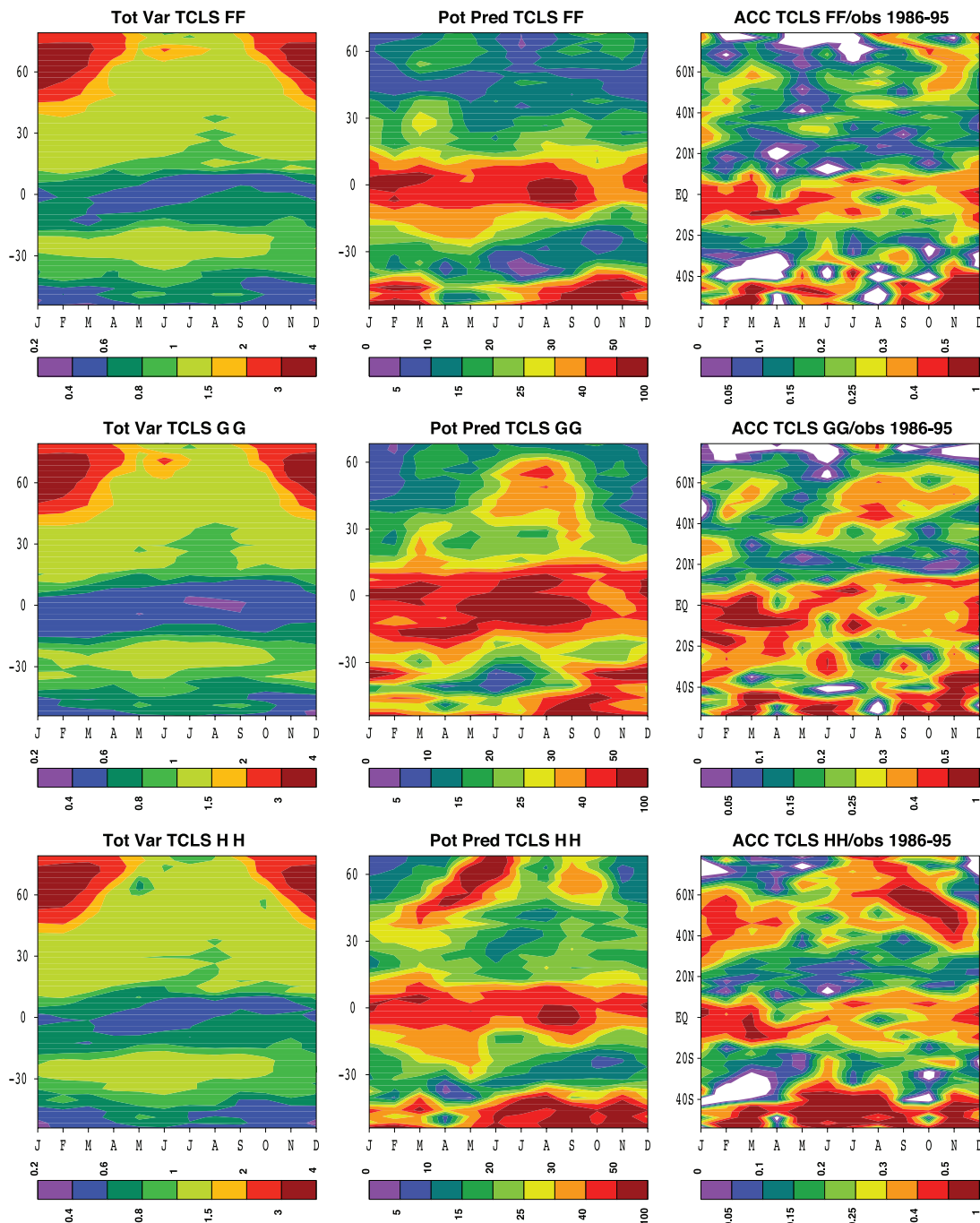


Figure 7.16: Zonal mean annual cycle of land surface air temperature: interannual standard deviation (left column, in K), potential predictability defined as the ratio between explained variance and total variance (central column, in %), and effective predictability defined as the anomaly correlation coefficient with the observed anomalies derived from the CRU2 climatology (right column, dimensionless). FF, GG and HH experiments are ensembles of 10-year simulations driven by observed monthly mean SSTs. GG (HH) also includes a nudging towards a soil moisture (snow mass) reanalysis. Including soil moisture initialisation improves both potential and effective predictability, especially over northern mid-high latitudes in summer and autumn. The improvement due to snow nudging occurs over high latitudes, especially in winter, spring and autumn.

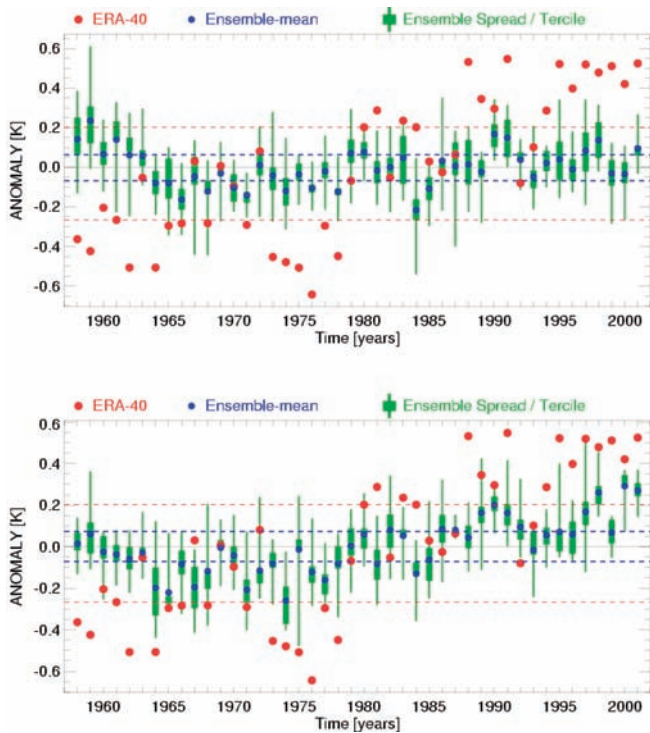


Figure 7.17: ECMWF 3-month lead time hindcasts of global 2 m temperature for August–October without (upper panel) and with (lower panel) time-varying anthropogenic greenhouse gases (GHG). In the upper panel the correlation between the ensemble mean and the observations is only 0.29, whereas this increases to 0.68 with variable GHGs, indicating that including variable greenhouse gas concentrations improves the seasonal forecast/hindcast skill of global mean surface air temperature (after Doblas-Reyes et al., 2006).

7.4.3 Decadal–multi-decadal climate variability and predictability associated with Atlantic meridional overturning circulation (MOC)

The mechanisms that govern the variability and predictability of the Atlantic sector climate on decadal time-scales have been studied (Latif et al., 2006; Guemas and Salas-Méla, 2008a, 2008b; Hawkins and Sutton, 2008 and ENSEMBLES Deliverable 4.2.2 available at: <http://www.ensembles-eu.org/deliverables.html>). It has been shown that changes in the Atlantic meridional overturning circulation (MOC) have significant and widespread climate impacts, which are potentially predictable a few years ahead. In particular, a rapid increase in the Atlantic MOC leads to large-scale warming of the Northern Hemisphere. A simple initialisation scheme, which consists of relaxing SST anomalies of the coupled general circulation models to observations, has been proposed (Figure 7.18; Keenlyside et al., 2008). Using this initialisation scheme, it has been forecast that global surface temperature may not increase over the next decade, as natural climate variations in the North Atlantic and tropical Pacific temporarily offset the projected anthropogenic warming. The results highlight the importance of initialising ocean conditions for the decadal forecast.

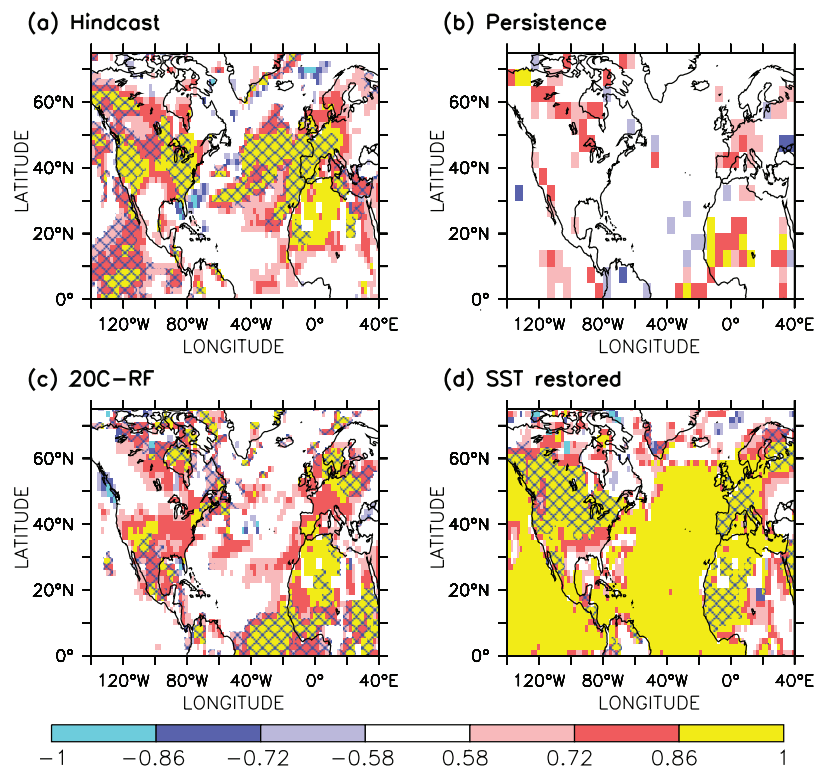


Figure 7.18: (a) Skill of nine 10-year predictions, evenly distributed over the period 1955–2005, made with a climate model initialised using ocean (SST) observations and run with projected changes in radiative forcing; (b) as in (a) but given by persistence; (c) as in (a) but not initialised using ocean observations and with radiative forcing following observations; (d) as in (c) but with model SST relaxed to observations between 60°S and 60°N. Correlations exceeding 0.58 are significant at the 5% level. Regions where initialisation results in a significant enhancement or reduction in skill compared with radiative-forcing-only simulations are indicated by blue cross-hatching in (a) and (c), respectively. Land regions where restoring to observed SST anomalies provides a significant enhancement in skill relative to radiative-forcing-only simulations are indicated by blue cross-hatching in (d). Correlations in (a) and (c) are field-significant at close to the 0% level, while those in (b) pass the field significance test at the 1% level (after Keenlyside et al., 2008).

References

ENSEMBLES publications are highlighted as bold text.

- Andrews DG, Holton JR, Leovy CB, 1987. *Middle Atmosphere Dynamics*. Academic Press, San Diego, CA.
- Arzel O, Fichefet T, Goosse H, Dufresne J-L, 2008. Causes and impacts of changes in the Arctic freshwater budget during the twentieth and twenty-first centuries in an AOGCM. *Climate Dynamics* 30, 37–58.
- Bellucci A, Gualdi S, Scoccimarro E, Navarra A, 2008. NAO–ocean circulation interactions in a coupled general circulation model. *Climate Dynamics* 31, 759–777.
- Bengtsson L, Hodges KI, Esch M, Keenlyside NS, Kornbluh L, Luo J-J, Yamagata T, 2007. How may tropical cyclones change in a warmer climate? *Tellus* 59A, 539–561.
- Bengtsson L, Hodges KI, Keenlyside N, 2009. Will extra-tropical storms intensify in a warmer climate? *Journal of Climate* 22, 2276–2301.
- Bony B, Dufresne J-L, 2005. Marine boundary layer clouds at the heart of cloud feedback uncertainties in climate models. *Geophysical Research Letters* 32, L20806, doi:10.1029/2005GL023851.
- Bony S, Colman R, Kattsov V, Allan R, Bretherton C, Dufresne J-L, Hall A, Hallegatte S, Holland M, Ingram W, Randall D, Soden B, Tselioudis G, Webb M, 2006. How well do we understand and evaluate climate change feedback processes? *Journal of Climate* 19, 3445–3482.
- Cadule P, Friedlingstein P, Bopp L, Sitch S, Jones CD, Ciais P, Piao SL, Peylin P, 2009. Benchmarking coupled carbon-climate models against long-term atmospheric CO₂ measurements. *Global Biogeochemical Cycles*, submitted.
- Carril A, Gualdi S, Cherchi A, Navarra A, 2008. Heatwaves in Europe: areas of homogeneous variability and links with the regional to large-scale atmospheric and SSTs anomalies. *Climate Dynamics* 30, 77–98.
- Cassou C, 2008. Intraseasonal interaction between the Madden–Julian Oscillation and the North Atlantic Oscillation. *Nature* 455, 523–527.
- Chepfer H, Bony S, Winker D, Cesana G, Dufresne J-L, Minnis P, Stubenrauch CJ, Zeng S, 2009. The GCM Oriented Calipso Cloud Product (CALIPSO-GOCCP). *Journal of Geophysical Research*, in press, doi:10.1029/2008JE003276.
- Chepfer H, Bony S, Winker D, Chiriac M, Dufresne J-L, Sèze G, 2008. Use of CALIPSO lidar observations to evaluate the cloudiness simulated by a climate model. *Geophysical Research Letters* 35, L15704, doi:10.1029/2008GL034207.
- Cherchi A, Navarra A, 2007. Sensitivity of the Asian summer monsoon to the horizontal resolution: differences between AMIP-type and coupled model experiments. *Climate Dynamics* 28, 273–290.
- Cox PM, Betts RA, Jones CD, Spall SA, Totterdell IJ, 2000. Acceleration of global warming due to carbon-cycle feedbacks in a coupled climate model. *Nature* 408, 184–187.
- Doblas-Reyes FJ, Hagedorn R, Palmer TN, Morcrette J-J, 2006. Impact of increasing greenhouse gas concentrations in seasonal ensemble forecasts. *Geophysical Research Letters* 33, L07708, doi:10.1029/2005GL025061.
- Dong B-W, Gregory JM, Sutton RT, 2009a. Understanding land–sea warming contrast in response to increasing greenhouse gases. Part I. Transient adjustment. *Journal of Climate* 22, 3079–3097.
- Dong B-W, R Sutton T, Gregory JM, 2009b. Understanding land–sea warming contrast in response to increasing greenhouse gases. Part II. Equilibrium responses. *Journal of Climate*, to be submitted.
- Douville H, 2009. Relative contribution of soil moisture and snow mass to seasonal climate predictability: a pilot study. *Climate Dynamics*, doi:10.1007/s00382-008-0508-1.
- Douville H, Salas-Mélia D, Tyteca S, 2006. On the tropical origin of uncertainties in the global land precipitation response to global warming. *Climate Dynamics* 26, 367–385.
- Dufresne J-L, Bony S, 2008. An assessment of the primary sources of spread of global warming estimates from coupled atmosphere–ocean models. *Journal of Climate* 21, 5135–5144.
- Dufresne J-L, Fairhead L, Le Treut H, Berthelot M, Bopp L, Ciais P, Friedlingstein P, Monfray P, 2002. On the magnitude of positive feedback between future climate change and the carbon cycle. *Geophysical Research Letters* 29, 1405, doi:10.1029/2001GL013777.
- Friedlingstein P, Bopp L, Ciais P, Dufresne J-L, Fairhead L, Le Treut H, Monfray P, Orr J, 2001. Positive feedback between future climate change and the carbon cycle. *Geophysical Research Letters* 28, 1543–1546.
- Friedlingstein P, Cox P, Betts R, Bopp L, von Bloh W, Brovkin V, Cadule P, Doney S, Eby M, Fung I, Bala G, John J, Jones C, Joos F, Kato T, Kawamiya M, Knorr W, Lindsay K, Matthews HD, Raddatz T, Rayner P, Reick C, Roeckner E, Schnitzler K-G, Schnur R, Strassmann K, Weaver AJ, Yoshikawa C, Zeng N, 2006. Climate–carbon cycle feedback analysis: results from the C4MIP model intercomparison. *Journal of Climate* 19, 3337–3353.
- Gualdi S, Scoccimarro E, Navarra A, 2008. Changes in tropical cyclone activity due to global warming: results from a high-resolution coupled general circulation model. *Journal of Climate* 21, 5204–5228.
- Guemas V, Salas-Mélia D, 2008a. Simulation of the Atlantic meridional overturning circulation in an atmosphere–ocean global coupled model. Part I. A mechanism governing the variability of ocean convection in a preindustrial experiment. *Climate Dynamics* 31, 29–48.
- Guemas V, Salas-Mélia D, 2008b. Simulation of the Atlantic meridional overturning circulation in an atmosphere–ocean global coupled model. Part II. Weakening in a climate change experiment: a feedback mechanism. *Climate Dynamics* 30, 831–844.
- Guilyardi E, Wittenberg A, Fedorov A, Collins M, Wang C, Capotondi A, van Oldenborgh GJ, 2009. Understanding El Niño in ocean–atmosphere general circulation models: progress and challenges. *Bulletin of the American Meteorological Society* 90, 325–340.
- Hawkins E, Sutton RT, 2008. Potential predictability of rapid changes in the Atlantic meridional overturning circulation. *Geophysical Research Letters* 35, L11603, doi:10.1029/2008GL034057.
- Huebener H, Cubasch U, Langematz U, Spanghel T, Nierhorster F, Fast I, Kunze M, 2007. Ensemble climate simulations using a fully coupled ocean–troposphere–stratosphere general circulation model. *Philosophical Transactions of the Royal Society A* 365, 2089–2101.
- Joly M, Voldoire A, 2009. Influence of ENSO on the West African monsoon: temporal aspects and atmospheric processes. *Journal of Climate* 22, 3193–3210.

- Joly M, Voldoire A, Douville H, Terray P, Royer J-F, 2007. African monsoon teleconnections with tropical SSTs: validation and evolution in a set of IPCC4 simulations. *Climate Dynamics* 29, 1–20.
- Jones CD, Cox PM, Huntingford C, 2006. Climate–carbon cycle feedbacks under stabilization: uncertainty and observational constraints. *Tellus B* 58, 603–613.
- Keenlyside NS, Latif M, Jungclauss J, Kornbluh L, Roeckner E, 2008. Advancing decadal-scale climate prediction in the North Atlantic sector. *Nature* 453, 84–88.
- Klingaman NP, Weller H, Woolnough SJ, Inness PM, Slingo JM, 2009. Coupled simulations of the Indian monsoon intraseasonal oscillation using a fine-resolution mixed-layer ocean model. In: Proceedings of the ECMWF Workshop on Ocean–Atmosphere Interaction, 195–205.
- Kucharski F and the C20C Team, 2008. The CLIVAR C20C project: skill of simulating Indian monsoon rainfall on interannual to decadal timescales – does GHG forcing play a role? *Climate Dynamics* 33, 615–627.
- Kucharski F, Bracco A, Yoo J-H, Molteni F, 2007. Low-frequency variability of the Indian monsoon–ENSO relation and the tropical Atlantic: the ‘weakening’ of the ‘80s and ‘90s. *Journal of Climate* 20, 4255–4266.
- Kucharski F, Bracco A, Yoo JH, Tompkins A, Feudale L, Ruti P, Dell’Aquila A, 2009. A Gill–Matsuno-type mechanism explains the tropical Atlantic influence on African and Indian monsoon rainfall. *Quarterly Journal of the Royal Meteorological Society* 135, 569–577.
- Latif M, Collins M, Pohlmann H, Keenlyside NS, 2006. A review of predictability studies of Atlantic sector climate on decadal time-scales. *Journal of Climate* 19, 5971–5987.
- Latif M, Keenlyside N, 2008. El Niño/Southern Oscillation response to global warming. Proceedings of the National Academy of Sciences of the USA, doi:10.1073/pnas.0710860105.
- Latif M, Keenlyside N, Bader J, 2007. Tropical sea surface temperature, vertical wind shear, and hurricane development. *Geophysical Research Letters* 34, L01710, doi:10.1029/2006GL027967.
- Le Quéré C, Harrison SP, Prentice IC, Buitenhuis ET, Aumont O, Bopp L, Claustre H, Cotrim da Cunha L, Geider R, Giraud X, Klaas C, Kohfeld KE, Legendre L, Manizza M, Platt T, Rivkin RB, Sathyendranath S, Uitz J, Watson AJ, Wolf-Gladrow D, 2005. Ecosystem dynamics based on plankton functional types for global ocean biogeochemistry models. *Global Change Biology* 11, 2016–2040.
- Liniger MA, Mathis H, Appenzeller C, Doblas-Reyes FJ, 2007. Realistic greenhouse gas forcing and seasonal forecasts. *Geophysical Research Letters* 34, L04705, doi:10.1029/2006GL028335.
- Löptien U, Zolina O, Gulev S, Latif M, Soloviev V, 2008. Cyclone life cycle characteristics over the Northern Hemisphere in coupled GCMs. *Climate Dynamics* 31, 507–532.
- Navarra A, Gualdi S, Masina S, Behera S, Luo JJ, Masson S, Guilyardi E, Delecluse P, Yamagata T, 2008. Atmospheric horizontal resolution affects tropical climate variability in coupled models. *Journal of Climate* 21, 730–750.
- Panja D., Selten FM, 2007. Extreme associated functions: optimally linking local extremes to large-scale atmospheric circulation structures. *Atmospheric Chemistry and Physics Discussions* 7, 14433–14460.
- Peings Y, Douville H, 2009. Influence of the Eurasian snow cover on the Indian summer monsoon variability in observations and CMIP3 simulations. *Climate Dynamics*, doi:10.1007/s00382-009-0565-0.
- Royer JF, Chauvin F, 2009. Response of tropical cyclogenesis to global warming in an IPCC AR-4 scenario assessed by a modified yearly genesis parameter. ‘Hurricanes and Climate Change’, J. B. Elsner and T. H. Jagger (Eds.), Springer, ISBN: 978-0-387-09409-0, pp 213–234.
- Scaife AA, Folland CK, Alexander LV, Moberg A, Knight JR, 2008. European climate extremes and the North Atlantic Oscillation. *Journal of Climate* 21, 72–83.
- Scaife AA, Knight JR, Vallis GK, Folland CK, 2005. A stratospheric influence on the winter NAO and North Atlantic surface climate. *Geophysical Research Letters* 32, L18715, doi:10.1029/2005GL023226.
- Sitch S, Huntingford C, Gedney N, Levy PE, Lomas M, Piao SL, Betts R, Ciais P, Cox P, Friedlingstein P, Jones CD, Prentice IC, Woodward FI, 2008. Evaluation of the terrestrial carbon cycle, future plant geography and climate–carbon cycle feedbacks using five dynamic global vegetation models (DGVMs). *Global Change Biology* 14, 2015–2039.
- Sutton RT, Dong B-W, Gregory JM, 2007. Land/sea warming ratio in response to climate change: IPCC AR4 model results and comparison with observations. *Geophysical Research Letters* 34, L02701, doi:10.1029/2006GL028164.
- Tolika K, Maheras P, Tegoulas I, 2009. Extreme temperatures in Greece during 2007: could this be a ‘return to the future’. *Geophysical Research Letters* 36, L10813, doi:10.1029/2009GL038538.
- Turner AG, Inness PM, Slingo JM, 2007. The effect of doubled CO₂ and model basic state biases on the monsoon–ENSO system. I. Mean response and interannual variability. *Quarterly Journal of the Royal Meteorological Society* 133, 1143–1157.
- Turner AG, Slingo JM, 2009a. Subseasonal extremes of precipitation and active-break cycles of the Indian summer monsoon in a climate-change scenario. *Quarterly Journal of the Royal Meteorological Society* 135, 549–567.
- Turner AG, Slingo JM, 2009b. Uncertainties in future projections of extreme precipitation in the Indian monsoon region. *Atmospheric Science Letters* 10, 152–158.
- Turner AG, Slingo JM, 2009c. Snow–monsoon teleconnections: testing competing mechanisms in the HadAM3 GCM. *Climate Dynamics*, to be submitted.
- Webb MJ, Senior CA, Sexton DMH, Ingram WJ, Williams KD, Ringer MA, McAvaney BJ, Colman R, Soden BJ, Gudgel R, Knutson T, Emori S, Ogura T, Tsushima Y, Andronova N, Li B, Musat I, Bony S, Taylor KE, 2006. On the contribution of local feedback mechanisms to the range of climate sensitivity in two GCM ensembles. *Climate Dynamics* 27, 17–38.
- Xavier PK, Duvel JP, Doblas-Reyes FJ, 2008. Boreal summer intraseasonal variability in coupled seasonal hindcasts. *Journal of Climate* 21, 4477–4497.

8 Evaluation of the ENSEMBLES Prediction System

[Research Theme 5]

A.M.G. Klein Tank (KNMI), E. Manzini (INGV), P. Braconnot (IPSL), F. Doblas-Reyes (ECMWF), T.A. Buishand (KNMI), A. Morse (Liverpool University)

8.1 Introduction

To assess the quality of the ensemble prediction system for climate change, a comprehensive and independent evaluation was performed against analyses/observations. The evaluation included seasonal to decadal as well as climate change time-scales and all spatial scales. The focus has been on:

- the representation of key phenomena and processes causing variability in Global Climate Model (GCM) simulations;
- the actual and potential seasonal to decadal forecast quality;
- the amount of change in the occurrence of extremes in Regional Climate Model (RCM) simulations compared with gridded observational data;
- the quality of impact models when forced with downscaled reanalysis data and hindcasts.

To facilitate this work, a new, quality-controlled and high-resolution, gridded observational dataset for Europe was developed as part of the project.

8.2 Relevance to decision makers

The quality of the probabilistic predictions by the ensemble prediction system depends critically on the ability of the Global and Regional Climate Models to simulate key processes and to reproduce the statistics of present-day weather and climate variability. For impact studies and adaptation strategies in European countries, in particular the representation of extremes in Regional Climate Models, is important. But high-resolution regional modelling only makes sense if the global models that provide the boundaries for the regional models have sufficient quality. The comparison of GCM and RCM simulations against observations, as performed in this Research Theme, provides insights into the extent that climate models can be used for climate prediction. The evaluation also helps in assessing the uncertainties in the response of models to anthropogenic forcing.

8.3 The E-OBS daily gridded dataset for Europe

A new daily observational dataset has been developed for surface climate variables. The dataset covers Europe, for the greater part with a resolution high enough to capture extreme weather and climate events. The dataset includes associated information on uncertainty due to sampling and interpolation.

The ENSEMBLES gridded observational dataset (E-OBS) is a European land-only daily high-resolution dataset for precipitation and minimum, mean and maximum surface temperature for the period from 1950 to the present. This dataset improves on other products in its spatial resolution and extent, time period, number of contributing stations, and research into finding the most appropriate method for spatial interpolation of daily climate observations (Hofstra et al., 2008). A full description can be found in Haylock et al. (2008). The underlying station data are from the quality-controlled daily observations of the European Climate Assessment and Dataset project (ECA&D – <http://eca.knmi.nl>; see Klok and Klein Tank, 2008).

The E-OBS dataset is publicly available from <http://eca.knmi.nl/ensembles>, strictly for use in non-commercial research and non-commercial education projects only. The gridded dataset is made available on two regular latitude–longitude grids (resolutions 0.25 and 0.50 degrees) and on two rotated pole grids (resolutions 0.22 and 0.44 degrees) with the North Pole at 39.25 N, 162 W. It covers the area between 25 N to 75 N and 40 W to 75 E. The regular grid is the same as that for the monthly datasets available from the Climatic Research Unit (CRU) and the rotated grid is the same as that used in many ENSEMBLES Regional Climate Models (RCMs). The interpolation method has been designed to provide the best estimate of grid-box averages rather than point values. This enables direct comparison with RCM simulations. In addition to the ‘best estimate’ values, daily standard errors (as a measure of interpolation uncertainty) and surface elevation are also provided. The dataset will continue to be maintained and updated beyond the project’s duration. As an illustration of the dataset, Figure 8.1 shows the 0.25 degree regular temperature grid for the day with the record high maximum temperature averaged over Europe (30.3°C compared with the 1961–1990 summer mean of 22.4°C). This day was 29 July 2002.

Homogeneity tests by Begert et al. (2008) reveal that many of the underlying station series are subject to potential inhomogeneities (Figure 8.2), for instance as a result of changes in observation practices. This affects, in particular, the understanding of extremes, because changes in extremes are often more sensitive to inhomogeneous climate monitoring practices than changes in the mean. In addition, there are limitations in the ability of the interpolation method to estimate grid values from the underlying station network. Hofstra et al. (2009a, 2009b) found that, in areas where relatively few stations

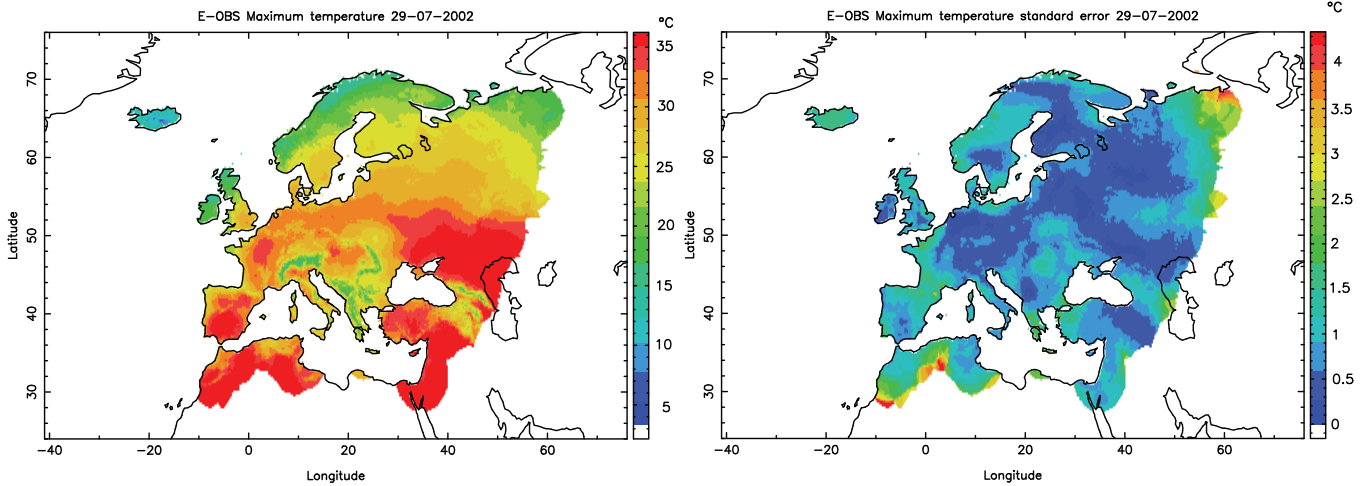


Figure 8.1: Example of E-OBS showing the maximum temperature (left) plus standard error (right) on the hottest day in Europe since 1950: 29 July 2002. The box defines the extent of the dataset. White land areas indicate not enough station data for interpolation.

have been used for the interpolation, both precipitation and temperature are ‘oversmoothed’. This leads to reduced interpolated values relative to the ‘true’ area averages, in particular for extremes. As a result, care has to be taken when using the E-OBS dataset, even though E-OBS is the only daily gridded dataset currently available.

8.4 Representation of key variability phenomena and processes

Systematic errors in the simulation of climate variability have been evaluated by considering whether GCMs are capable of reproducing correctly the intensity, frequency and distribution of the major teleconnection patterns in the tropics and extratropics (such as PNA, ENSO, NAO, Monsoon-Mediterranean, etc.).

The aim was to identify and understand model biases and to provide diagnostics and metrics that help to evaluate aspects of climate models that are critical to assess the response of different models to anthropogenic forcing. This was done firstly by developing diagnostics that were applied to the stream 1 simulations and secondly by sensitivity experiments. The latter serve either to develop new diagnostics or to test the role of particular aspects of model formulation, such as clouds, surface fluxes, or vertical and horizontal resolution. The evaluation focused on the global climate and tropical regions, but tropical–extratropical teleconnections were also considered. Some examples of key phenomena and processes are provided below.

8.4.1 Climate sensitivity and clouds

The analyses of climate sensitivity show that there is a strong relationship between the response of clouds in subsiding regions in the tropics and the magnitude of the temperature change (Dufresne and Bony, 2008; Webb et al., 2006). A first diagnosis (Bony et al., 2006) proposes sorting the atmospheric circulation into convective regimes in the tropical regions. Heat fluxes and cloud radiative forcing can then be compared with satellite data, in a way that clearly identifies the major differences between models that are linked to the convection scheme. In addition, the sensitivity of these fluxes to the SST at the interannual time-scale and the comparison with data has been proposed in order to assess the changes in cloud forcing between different simulations, and to explore the reasons for the range of climate sensitivity found between different models (see also IPCC, 2007).

8.4.2 The east Pacific and the El Niño–Southern Oscillation

The regime-sorted analyses were further extended at a more regional scale to understand the double-ITCZ (Intertropical Convergence Zone) structure produced in most coupled models in the east Pacific (Figure 8.3; Bellucci et al., 2009). The proposed diagnostics show that the double-ITCZ structure results from a too frequent onset of deep convection south of the equator triggered by the convection SST threshold in the models. A major

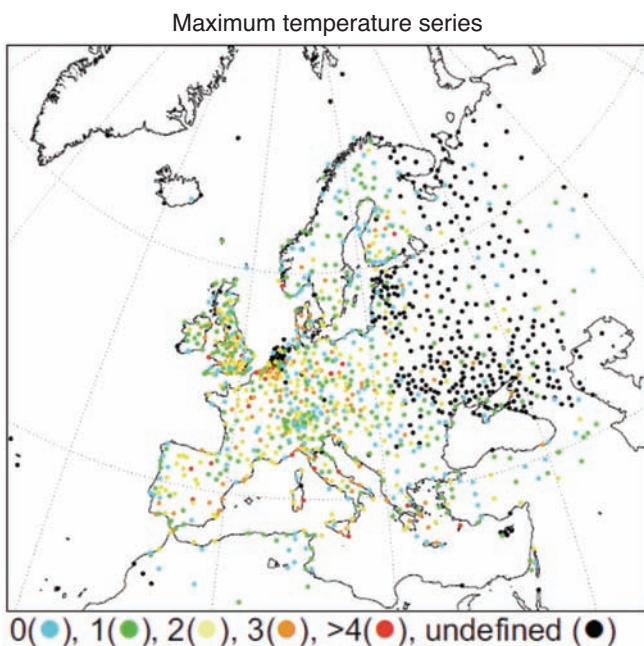


Figure 8.2: Potential number of breakpoints detected using the VERHOM methodology for statistical homogeneity testing of station series (Begert et al., 2008).

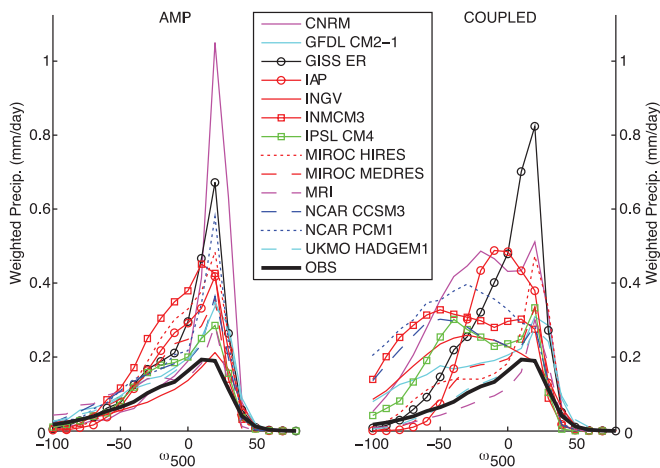


Figure 8.3: Regime-sorted precipitation (mm/day) weighted by the PDF of ω_{500} for AMIP (left) and the corresponding coupled AR4 models (right) for the region 100 W–150 W, 20 S–0 (Bellucci et al., 2009). Part of the model difference is already found in the atmosphere-only simulation (AMIP), whereas the coupling with the ocean (coupled) and the changes in SST further trigger too deep convection and precipitation, which favour the development of the double-ITCZ structure.

outcome of this work is the identification of two distinct sources for the double-ITCZ error; namely (1) an error in the frequency of the occurrence of deep convection (associated with the ocean–atmosphere coupled interactions), and (2) an error in the magnitude of precipitation for an individual convective event (which can be ascribed to the atmospheric GCM only).

The east Pacific is the core region for the development of the El Niño–Southern Oscillation (ENSO), and the double-ITCZ structure has some implications for the development of the seasonal cycle of SST along the equator and on the characteristics of the interannual variability. The relationship between land and ocean convection has been identified as an important player in the east Pacific, from sensitivity experiments with the IPSL-CM4 coupled model differing only in the convection scheme (Braconnot et al., 2007). Increased resolution is needed to better represent coastal upwelling and the frequency of the Pacific ENSO (Navarra et al., 2008). However a change in model physics (such as convection) has greater implications for model results than a change in resolution. A metric is proposed to characterise the behaviour of ENSO in climate models considering the dynamical and the heat fluxes coupling between the ocean and the atmosphere. Comparing the behaviour of two different convection schemes in the IPSL model, the method clearly shows that the dynamical feedback is underestimated in both versions of the model, whereas the thermodynamic feedback explains why the ENSO has a correct magnitude in one version but is damped in the other version (Guilyardi et al., 2009). This evaluation approach has been extended to all ENSEMBLES stream 1 simulations.

8.4.3 Indian and west Pacific Oceans

Several evaluation studies have considered the Indian Ocean, the west Pacific and the Indian and East Asian monsoon. A diagnostic tool is proposed in order to extract the climatic interannual signals from the non-stationary fields in the

simulations and observations. It has been applied to the analyses of the stream 1 simulations. The statistical method allows estimation of the 20th century trends, as well as the relationship between the Indian summer monsoon and the development of ENSO. Relatively cold (warm) SSTs in the central-eastern Pacific are associated with a strong (weak) monsoon during boreal summer in the observations. Results of the analyses show that almost all simulations fail to reproduce this relationship. Sensitivity experiments have been performed to understand the wind–evaporation and the wind–thermocline feedbacks in the east Indian Ocean and to explain why they became a highly significant precursor of ENSO during recent decades. This was done through a sensitivity experiment where SST was altered by $\pm 1^\circ\text{C}$ in the south-east Indian Ocean. The results confirm the important role of this region and the need to reproduce it accurately in climate simulations (Terray and Dominiak, 2005). Specific attention has also been devoted to the modelling of the Asian summer monsoon and the effects of horizontal model resolution, air–sea coupling and improved physics on the simulation of this phenomenon (Alessandri et al., 2007; Cherchi and Navarra, 2007).

Intraseasonal variability (ISV) is also strongly connected with the development of active and break phases of the Indian monsoon. SST warming may affect the characteristics of ISV in the future. A new metric is proposed to assess the representation of the ISV in the climate models. This work was done in close collaboration with the seasonal prediction evaluations to address both the DEMETER and the IPCC class models. The diagnosis uses the local mode analyses proposed by Goulet and Duvel (2000), which was extended by Xavier et al. (2009). The method allows us to detect and to characterise in a simple mathematical form the main events of an intermittent phenomenon. It provides a pattern and statistics for each intraseasonal event that can be combined to assess the simulated ISV with observations. The results show that, for the summer ISV over the Indian Ocean, the DEMETER versions of the climate models produce more reproducible but less realistic ISV patterns compared with the IPCC versions of the models (Figure 8.4). The metric bears a significant relationship with the high frequency variability and the accuracy of the simulated summer monsoon climate. This implies that a correct representation of internal atmospheric processes such as the synoptic weather variability and ISV is required in order to reduce uncertainties in monsoon climate projections (Xavier et al., 2009).

The importance of synoptic weather variability and ISV was further highlighted by analysing the relationship between surface temperature warming over the northern Indian Ocean (the local climate sensitivity) and changes in the strength of the heaviest monsoon rainfall events during boreal summer in climate projections (Turner and Slingo, 2009a,b). This revealed two major subsets among the models: one in which the strengthening of the heaviest monsoon rainfall events is entirely consistent with thermodynamic arguments (the degree of surface warming and available moisture through the Clausius–Clapeyron relation); and another in which the increases include some additional dynamic component. This suggests that the type of convective parameterisation may influence the response of monsoon extremes in the CMIP3 models. Those models with bulk mass-flux-type convection are strongly tied to changes in surface properties and thus have (predominantly) predictable increases

in extremes. Other models, with Arakawa–Schubert type convection, tend to show increases in monsoon extremes far beyond thermodynamic predictions.

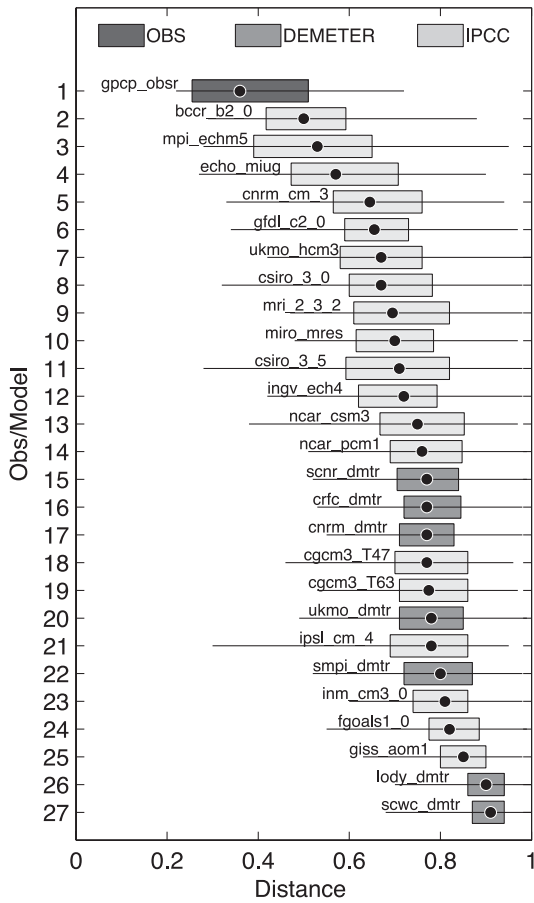


Figure 8.4: Distribution of distances between individual intraseasonal variability (ISV) events to the observed average summer ISV pattern in the observations and models. The bars range from the 25th percentile to the 75th percentile value. The line represents the range of values. The median (50th percentile) values are denoted by the black dots. Models are arranged according to the median distance.

8.4.4 The role of the stratosphere

The effect of systematic biases in the stratosphere on the troposphere climate has been investigated using the ECHAM5 atmospheric model (Giorgetta et al., 2006). The results show how the model representation of the stratosphere has positive effects on the mean state of temperature and wind in the troposphere (Roeckner et al., 2006). It is also shown that these effects are more pronounced when the atmosphere is coupled to the ocean. In addition, changes in the horizontal diffusion scheme are needed, as a direct consequence of the vertical discretisation, to represent properly the dynamics of the stratosphere and the wave-mean flow interaction. These changes affect the Brewer–Dobson circulation as well as the Hadley circulation, and have a positive impact on climate teleconnections between ENSO and the North Atlantic European regions (Cagnazzo and Manzini, 2009). These studies therefore recommend the use of climate models that resolve the stratosphere for climate studies.

8.5 Seasonal to decadal forecast quality

A thorough forecast quality assessment of the seasonal and annual GCM simulations was carried out. Several tools have been made available which help scientists (including those from outside ENSEMBLES) to access and analyse the data. Significant progress has been made with assessing the predictability for the North Atlantic sector and in answering the question why, and under what conditions, a multi-model can outperform the best participating single model.

8.5.1 Forecast quality assessment

A preliminary set of forecast quality results for the seasonal hindcasts over the period 1970–2005 has been published on the website: http://www.ecmwf.int/research/EU_projects/ENSEMBLES. Different aspects of the forecast quality are available for all the single-model systems, as well as for the multi-model. This comparison takes into account the larger ensemble size of the multi-model and thus introduces a reduced multi-model for the comparison with the perturbed-parameter ensemble. A comprehensive assessment of the perturbed-parameter decadal hindcasts suggests that there is a small increase in forecast quality of temperature and precipitation when the predictions are initialised. The increase in forecast quality is found in the first couple of years.

8.5.2 ECMWF seasonal to decadal (s2d) public data server

The capabilities of the ECMWF seasonal–decadal OPeNDAP server have been further enhanced to allow others to perform analyses on the stream 1 seasonal-to-decadal hindcasts. Also, a set of general-purpose forecast-quality assessment tools has been developed for working with the data. In addition, the public data server at ECMWF has been linked to the KNMI Climate Explorer.

8.5.3 KNMI Climate Explorer (<http://climexp.knmi.nl>)

The KNMI Climate Explorer is a tool which allows anyone to correlate station data, climate indices, observations, reanalysis fields, past seasonal forecasts and climate change experiments. A large number of datasets (both climate model data and observations) have been brought together on a server at KNMI. For the ENSEMBLES project, additional functionality has been added to the Climate Explorer. A set of seasonal forecast verification measures has been added in collaboration with the University of Reading, and links to the seasonal–decadal archive at ECMWF and the RCM archive at DMI have been constructed. As a result, most datasets generated in ENSEMBLES are now also available for analysis in the Climate Explorer. Figure 8.5 illustrates the seamless integration that has been made between the KNMI Climate Explorer and the s2d public data server at ECMWF in a seasonal forecast verification setting.

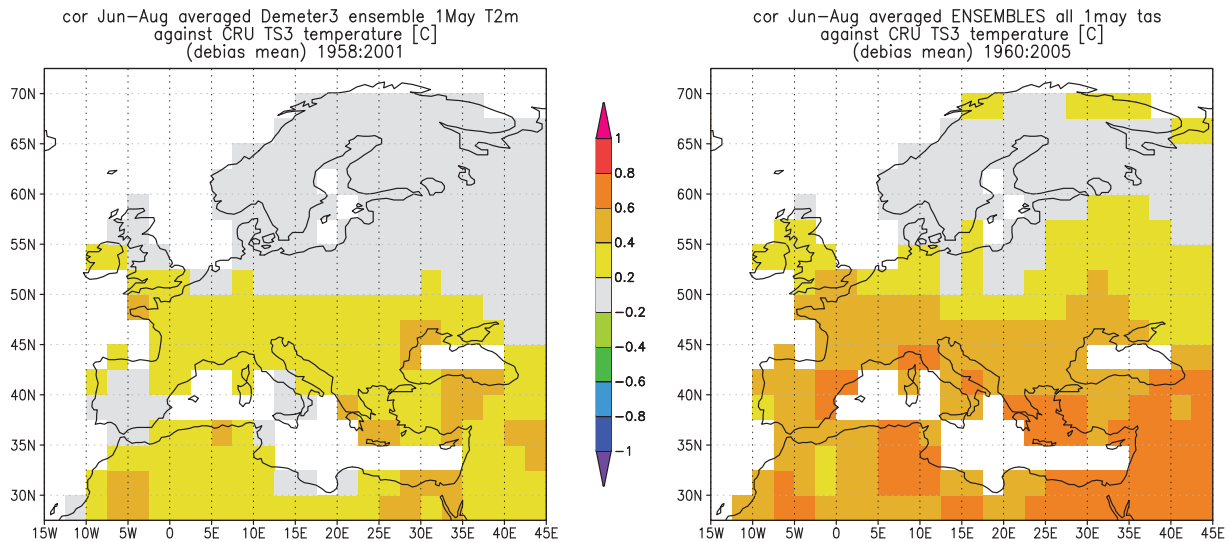


Figure 8.5: Comparison of the point-correlation of summer seasonal predictions of near-surface air temperature started on 1 May of each year against observations for DEMETER (left) and ENSEMBLES stream 2 (right). There is a gain in skill over the Mediterranean area, and over part of Britain; probably as a consequence of the better representation of global warming in the ENSEMBLES experiments. Anybody with internet access can reproduce these plots using the KNMI Climate Explorer linked to the s2d public data server at ECMWF.

8.5.4 North Atlantic sector

Perfect predictability analysis of high-resolution simulations on seasonal to decadal time-scales has been performed for the North Atlantic sector. This focused on assessing the predictability of mid-latitude storms, tropical storms, and weather extremes on these time-scales. Predictability is much higher for the tropical regions, reaching a minimum over central western North America, Greenland and northern Europe.

8.5.5 Mechanics of multi-model combination

Multi-model ensemble combination has become a standard technique to improve ensemble forecasts on all time-scales, including those that are relevant for the ENSEMBLES project. While the success of multi-model combination has been demonstrated in many studies, the underlying mechanisms have so far not been properly understood. The question of why, and under what conditions, a multi-model can outperform the best participating single model has been addressed (Weigel et al., 2008, 2009). The answer is that multi-model ensembles can indeed locally outperform a best-model approach, but only if the single-model ensembles are overconfident (Figure 8.6). The reason is that multi-model combination reduces overconfidence, i.e., ensemble spread is widened while average ensemble-mean error is reduced. This implies a net gain in prediction skill, because probabilistic skill scores penalise overconfidence. Under these conditions, even the addition of an objectively poor model can improve multi-model skill. It seems that simple ensemble inflation methods cannot yield the same skill improvement.

8.6 Extremes in Regional Climate Model simulations

The evaluation of the representation of extremes in RCMs has focused on the European region, with special case studies for the Rhine Basin, the Alps, and the eastern Mediterranean. Both RCM simulations nested within the ERA-40 reanalysis and nested within transient ESM simulations were considered.

8.6.1 Extreme indices in ERA40-driven runs and observations

Maximum (TX) and minimum (TN) temperatures from the CNRM ALADIN RCM simulation were assessed in detail for the Balkan Peninsula using observations from 53 stations (Kostopoulou et al., 2009a). The model performance was first evaluated by calculating the correlation coefficients between the seasonal mean values from the model and the observations. The result for TN is shown in Figure 8.7. The map for the winter season reveals low correlations (<0.4) in the north-western part of the domain in the vicinity of the Dinaric Alps. An area of low

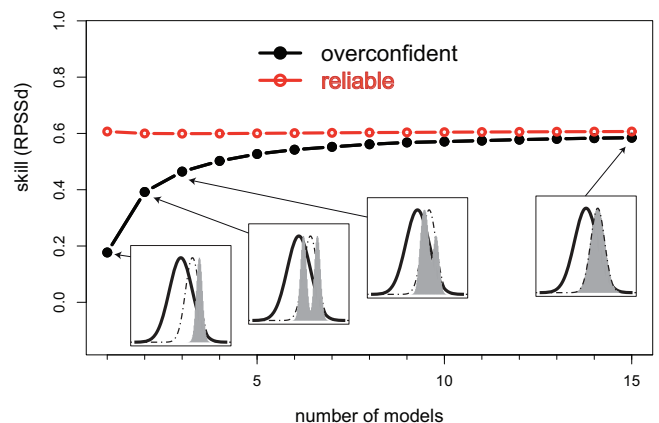


Figure 8.6: Expected skill of multi-model ensemble forecasts as a function of the number of participating single model ensembles. The red line indicates well-calibrated reliable ensembles and the black line represents highly overconfident ensembles. The ensembles have been generated from synthetic toy model simulations. It can be seen that only in the latter case does model combination truly enhance prediction skill, because multi-model combination of overconfident single model ensembles widens the spread. The underlying 'mechanics' of multi-model combination is illustrated by the four small panels at the bottom of the plot: the combination of more and more overconfident single model ensembles (shown as grey shading) successively widens the ensemble spread and reduces the ensemble overconfidence until eventually the entire predictable signal is correctly sampled and forecasts are reliable.

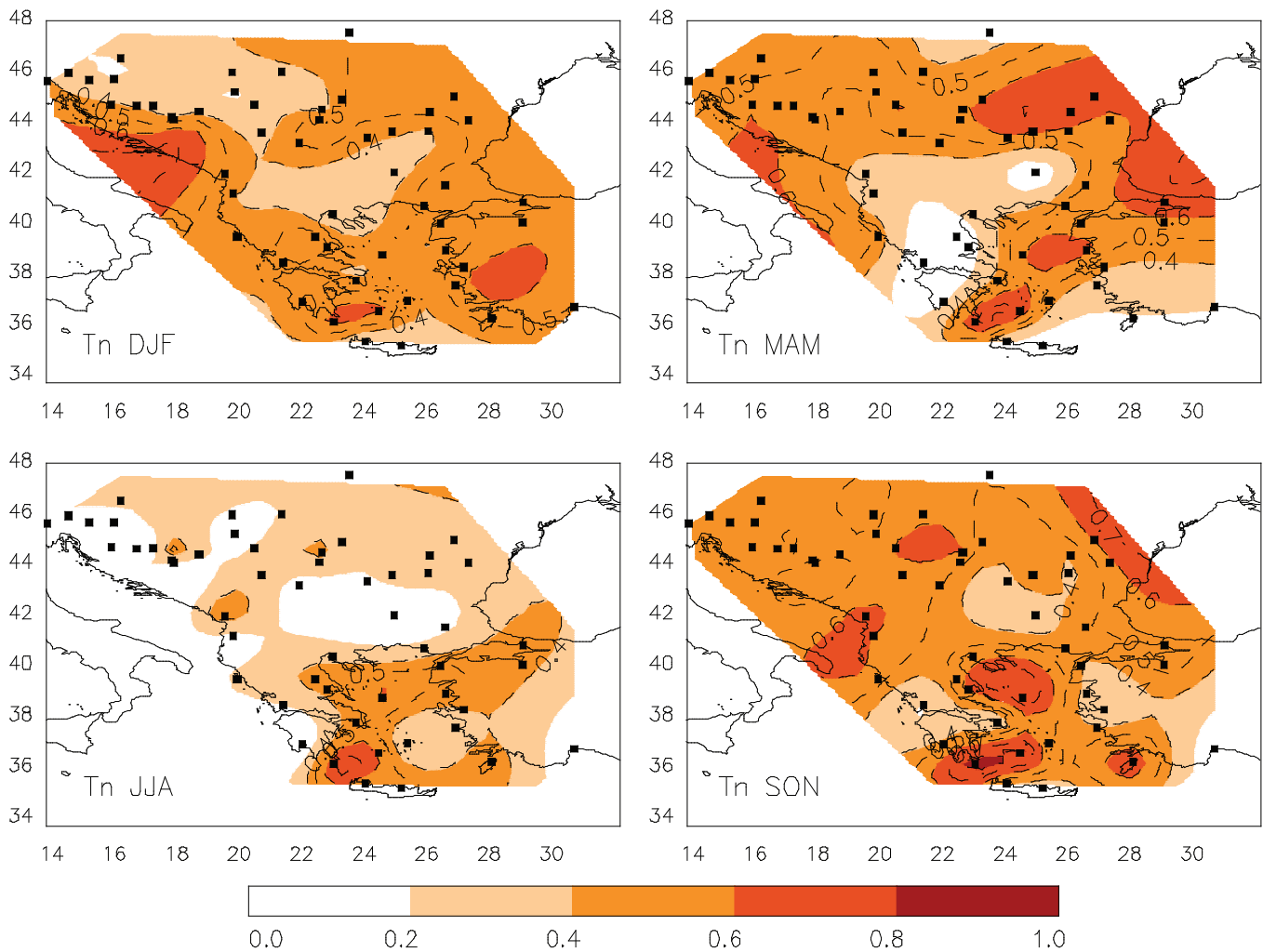


Figure 8.7: Correlations between seasonal mean values of TN from the ERA40-driven CNRM ALADIN RCM simulation and station observations.

correlations is also evident in northern Greece. These low correlations may be attributed to the surface snow scheme of the RCM. In the three other seasons, relatively high correlations are found around the Aegean Sea. Correlations are weak and statistically not significant in summer in the northern part of the domain. A further analysis showed that cold spells (sequences of 5 days or longer below the 10th percentile of TN) were better reproduced than warm spells (sequences of 5 days or longer above the 90th percentile of TN). However, poor results for cold spells were obtained for stations located in the north-western part of the study region, which is consistent with the low correlations in Figure 8.7.

Extreme precipitation events in the Alpine region have been analysed within the ERA40-driven RCM experiments (Pall et al., 2009). Model simulations from fifteen RCMs have been compared to the E-OBS dataset for the baseline 1961–1990 period, using precipitation indices as well as the generalised extreme value (GEV) distribution for estimating return levels of extreme events. Focusing on the 90th percentile of wet days as a simple index of extremes reveals that the models are generally too wet around the southern Alpine rim, and too dry around the Po Valley, though large differences in model performance occur. This is illustrated in Figure 8.8 for autumn, which is climatologically the wettest Alpine season due to moist and weakly stratified southerly airflows (Frei et al., 2006).

8.6.2 Evaluation of trends in extremes in ERA40-driven RCM simulations

Trends in the extremes indices and quantiles of temperatures and precipitation in the ERA40-driven RCM simulations have been compared with those in the E-OBS data for the period 1961–2000 (Lister and Jones, 2009). An example of extreme minimum temperatures is given in Figure 8.9. A salient feature is the strong negative trend in the eastern part of the domain in the autumn season, which is well reproduced by the CHMI-ALADIN RCM simulation. Kostopoulou et al. (2009a) obtained a similar result for the trend in observed extreme minimum temperatures in the autumn season at stations across the Balkan Peninsula and those simulated by the CNRM-ALADIN RCM. By contrast, the RCM simulation in Figure 8.9 is unable to reproduce the trends in the winter extremes in the E-OBS data.

8.6.3 Evaluation of extremes in transient RCM simulations

Hanel and Buishand (2009a) analysed the 1-day summer and 5-day winter precipitation extremes over the Rhine Basin in fifteen RCM simulations (Figure 8.10). For this purpose, the index-flood method has been extended for application to transient climate model simulations (Hanel et al., 2009). The Rhine Basin was

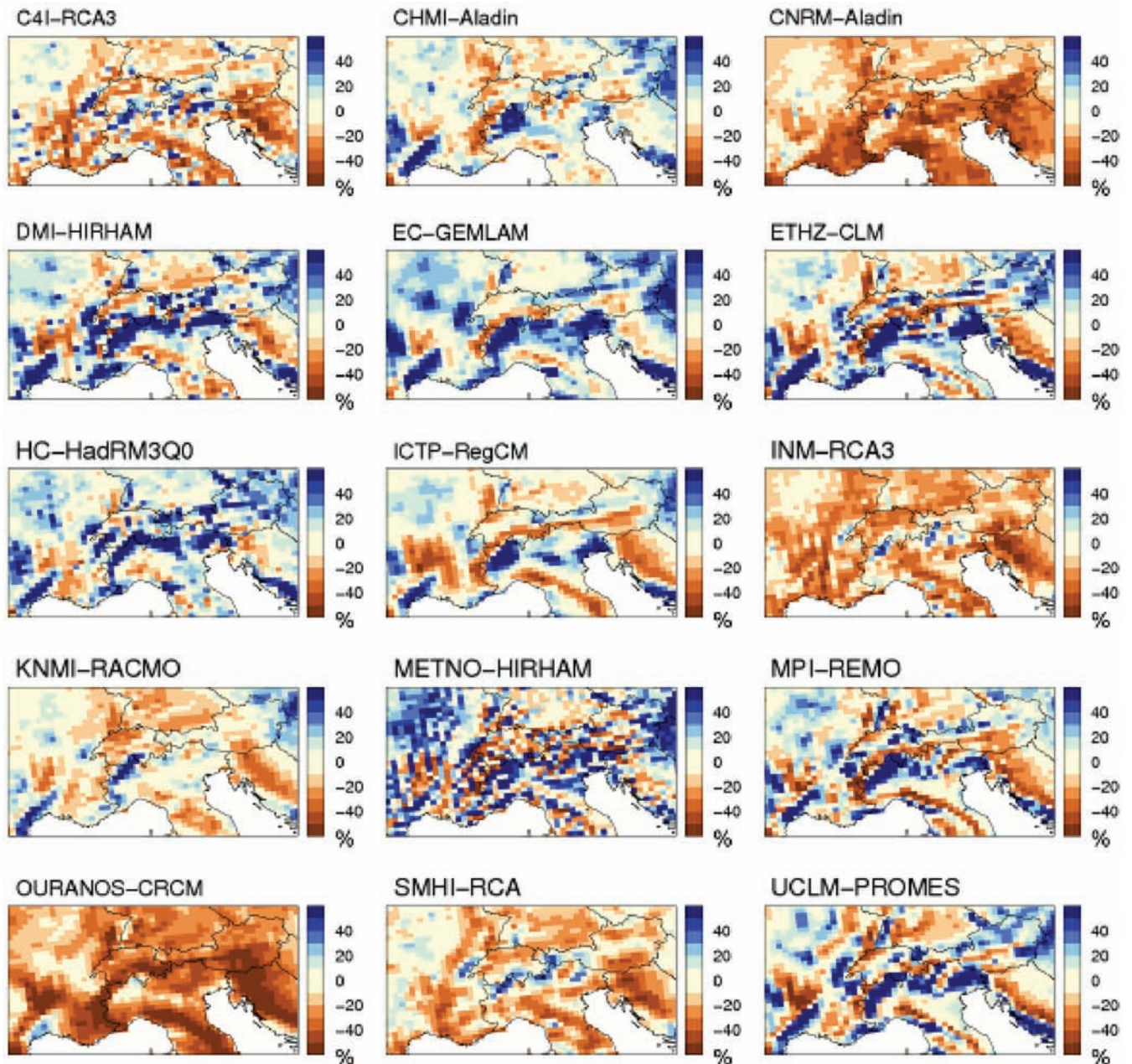


Figure 8.8: Relative bias of the 90th percentile of wet days (>1 mm/day) for all autumn seasons (SON) in the period 1961–1990 (Pall et al., 2009). Shown are the biases in fifteen different ERA40-driven RCMs relative to the E-OBS dataset, on the 0.22 degree (~25 km) rotated grid for the Alpine domain.

divided into five regions. For each region a non-stationary GEV model was fitted. This model assumes that the GEV location parameter varies over the region, while the dispersion coefficient (the ratio between the GEV location and scale parameters) and the shape parameter are constant within the region. All these parameters are allowed to vary with time. Seasonal global temperature anomalies were used as a time-dependent covariate. The estimated GEV parameters for the period 1961–1990 were, for most RCM simulations in the summer season, larger than those from the E-OBS data. These biases could in large part be ascribed to the small number of stations used for gridding the observations. For the winter season, the majority of the RCM simulations considerably overestimated the GEV location parameter and underestimated the dispersion coefficient.

In addition to the model biases, the consistency of projected changes in extremes has also been evaluated. Figure 8.11 shows the projected changes between the periods 1961–1990 and 2070–

2099 for the twelve RCM simulations up to the end of the 21st century. Though there is considerable variation in the changes of the extreme value distributions among the RCM simulations, common tendencies can be identified. In the summer season, the dispersion coefficient increases, while there is hardly any change in the location parameter and the shape parameter. As a consequence, there is almost no change in the 2-year quantile, but as the return period gets longer there is a considerable increase due to the increase in the dispersion coefficient. The increase in large quantiles (on average about 15% for the 50-year quantile) is different from the change in mean summer precipitation, which decreases in the majority of the RCM simulations. In the winter season, there is an increase in the location parameter, almost no change in the dispersion coefficient, and a slight decrease in the shape parameter. The increase in the location parameter implies an increase of the quantiles at short return periods. However, the effect of the increase in the location parameter is counterbalanced by the decrease in the shape parameter. As a result there is almost

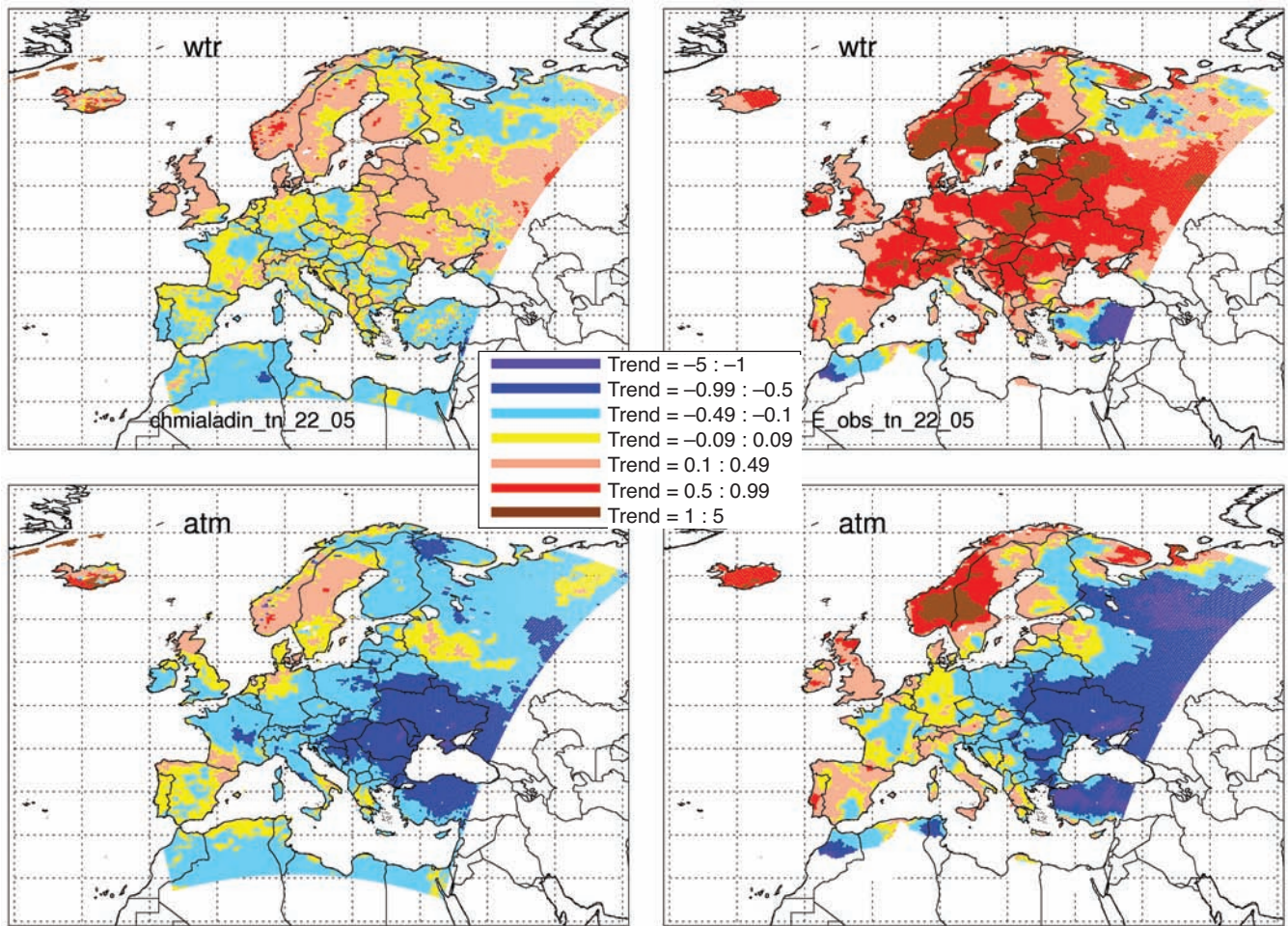


Figure 8.9: Evaluation of trends in extreme minimum temperatures in the period 1961–2000 in the CHMI-ALADIN RCM (Lister and Jones, 2009). The trends (°C per decade) in the 5th percentile of the minimum temperatures (TN05) in the ERA40-driven RCM simulation (left panels) are compared with those in the E-OBS data (right panels) for the winter (upper row) and autumn (lower row) seasons.

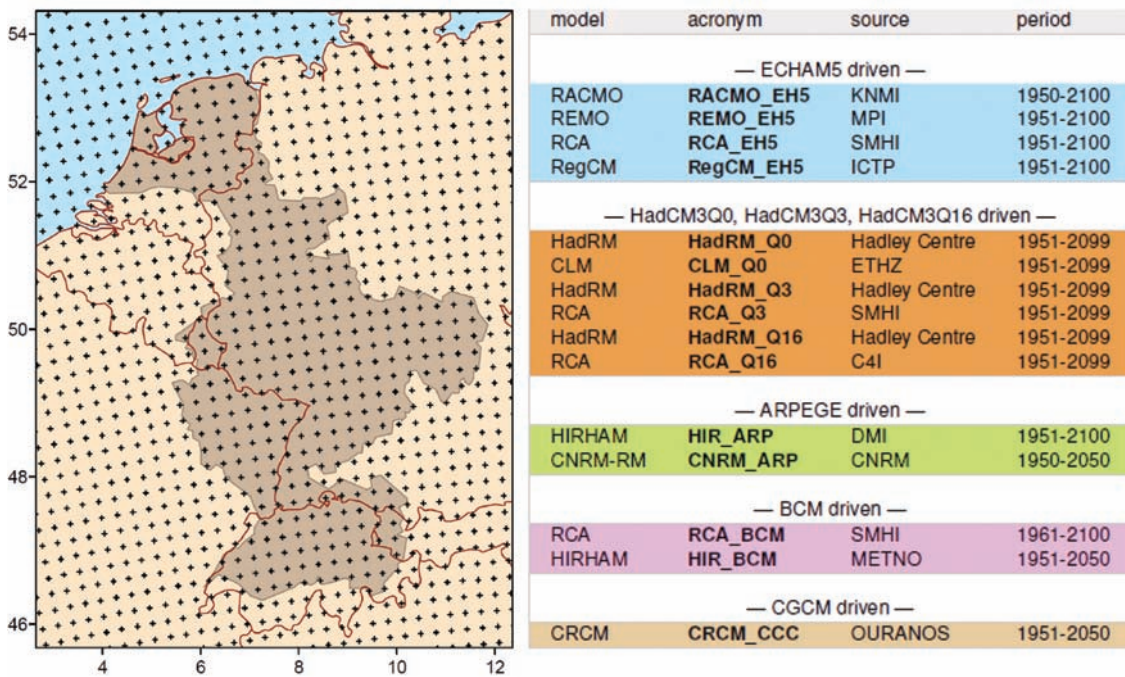


Figure 8.10: The Rhine Basin and the RCM simulations with driving ESM used in the study of precipitation extremes in Figure 8.11.

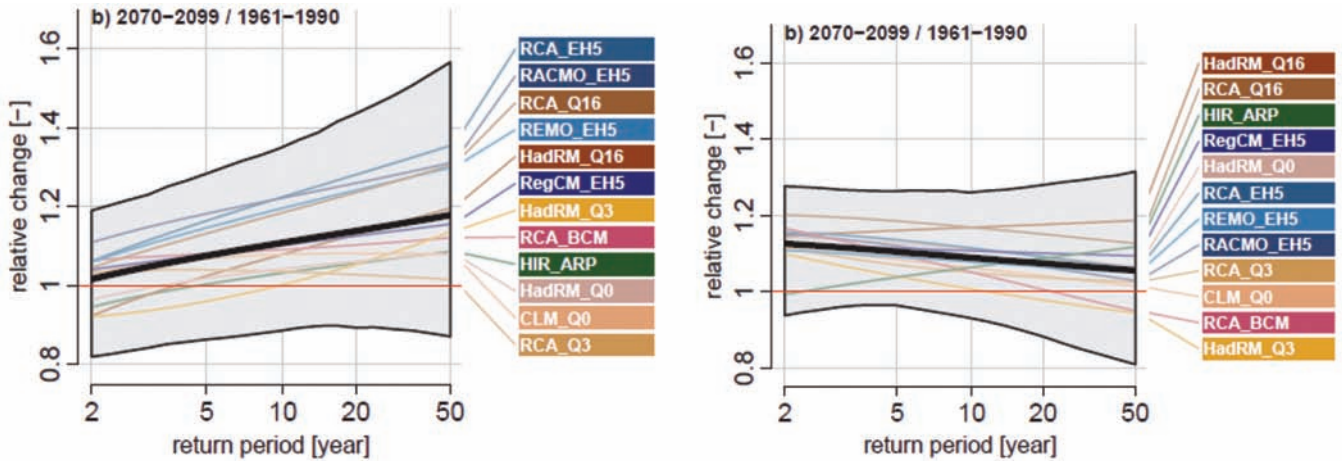


Figure 8.11: Projected changes in precipitation extremes for the Rhine Basin between the periods 1961–1990 and 2070–2099 (Hanel and Buishand, 2009a). Shown are the basin-average relative changes of various quantiles as derived from the changes of the GEV parameters. Left: relative changes in the quantiles of 1-day precipitation maxima in the summer season (JJA). Right: relative changes in the quantiles of 5-day maxima in the winter season (DJF). The thin coloured lines in the figures represent the area-average change for the individual RCMs, the thick black line is the overall mean change. The envelopes indicate the 5th percentile of the minimum and the 95th percentile of the maximum relative basin-average change in 500 bootstrap samples.

no change of large quantiles despite the clear increase in mean winter precipitation in most RCM simulations. The uncertainty of the relative changes in the quantiles, as indicated by the envelope in Figure 8.11, is quite large. This is partly due to the influence of natural variability on the estimated changes.

For the Netherlands, the distributions of the 1-hour and 1-day annual maximum precipitation amounts in eight transient RCM simulations were compared with those from a high-quality radar dataset (Hanel and Buishand, 2009b). The performance of the RCM simulations turned out to be much worse for the hourly precipitation extremes than for the daily extremes. For instance, for the hourly maxima the majority of the RCM simulations underestimate the location parameter by 30–40% with respect to the radar data, whereas the relative bias is no more than 10% for the daily maxima.

Kostopoulou et al. (2009a, 2009b) studied the ability of the ENSEMBLES transient RCM simulations to reproduce extreme climate indices in the eastern Mediterranean region. The evaluation has been initially implemented between the station and the nearest-gridded observed (E-OBS) data at selected sites from the eastern Mediterranean, and then extended to several RCM simulations. The E-OBS dataset satisfactorily reproduced temperature climate indices for most study sites. As expected, the reproduction of precipitation indices was less accurate, in particular for locations with complex topography. Therefore, in some cases it became necessary to use an average of several neighbouring grid points in order to obtain a better representation of the single-site climatic regime. Extreme climate indices were subsequently calculated from ENSEMBLES regional model data and their reliability was assessed against those obtained from the E-OBS dataset. The results varied greatly between sites. In some cases all models performed adequately, while for other sites some models did better than others.

8.6.4 Drought indices

In order to evaluate drought, an optimised objective classification of ‘critical dry’ circulation patterns (CPs), responsible for major droughts and low river flow periods in south-west Germany has been developed based on fuzzy rules (Bárdossy, 2009). An objective function based upon temporal differences of daily low flows was defined for optimisation purposes. The optimisation was done for different numbers of CPs. Finally, circulation patterns were classified into seventeen classes. Objective CP-MSLP-anomalies have been calculated for the period 1990–1999. These anomalies have been compared with the MSLP anomalies of the so-called ‘Grosswetterlagen’, which have been discussed in connection with major historical droughts. The objective drought CP anomalies are quite similar to those from the ‘Grosswetterlagen’. As an illustration of their usage, maps of a CP-based wetness index have been calculated for 172 grid cells (25 km x 25 km) in the German part of the Rhine Basin for all seventeen CPs. The new CP classification system for droughts has been analysed by observing the occurrence frequencies of the identified critical dry CPs in the study area for historical droughts 1959, 1976, 1991, 2003. In addition, the new drought CPs have been evaluated for RCM simulations (both ERA40- and ESM-driven) for the control period 1960–1991 and the period 2001–2100. For the latter, the A1B scenario runs of RACMO2, REMO and HadRM3 (the standard version as well as the versions with high and low climate sensitivity) were considered. Results for RACMO2 and REMO are very similar, probably due to the same driving ESM (ECHAM5). Frequencies of the combined drought CPs show significant increasing trends for summer for the transient A1B runs of RACMO2 and REMO and do not show any significant change for the three HadRM3 transient runs.

8.7 Quality of impact models

The quality of impact models when forced with downscaled reanalysis data and hindcasts was evaluated through the use of application-specific verification datasets. The evaluation has focused on the seasonal time-scale, considering both Europe and Africa. This work is closely related to RT6. An illustration of the evaluation results is presented below for seasonal forecasts of Malaria. Other results are described in Section 9 together with the impact models.

8.7.1 Malaria forecasts

Seasonal forecast performance was evaluated for malaria prediction in Botswana. The results were obtained by driving the Liverpool malaria model (LMM) with rainfall and temperature forecasts from ENSEMBLES and comparing forecast total malaria incidence for November forecast months 4–6 (February, March and April) with a published malaria index for Botswana for the period 1980–2001 (Figure 8.12; Thomson et al., 2005). A comparison with earlier DEMETER results and with the malaria model driven by ‘observations’ (ERA-40 reanalysis) has also been made. Overall, the multi-model results for ENSEMBLES show a small improvement from DEMETER, despite a reduction in the number of models from seven to five. Low-malaria events are forecast with the highest skill, although high-malaria events are also forecast skilfully.

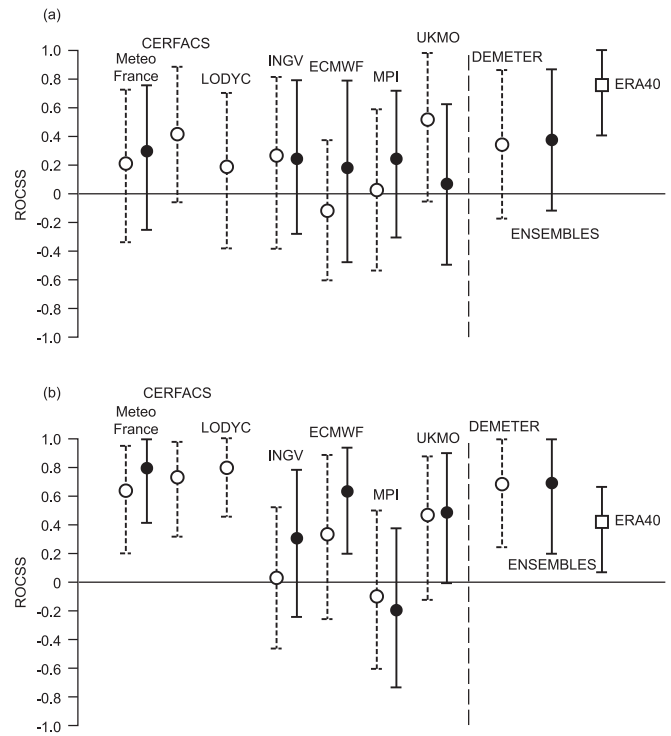


Figure 8.12: ENSEMBLES seasonal forecast performance for malaria prediction in Botswana, for (a) high-malaria events (above the upper tercile) and (b) low-malaria events (below the lower tercile). Single-model results are given on the left of the dashed line, multi-model results on the right. ROC skill score (ROCSS) measures performance relative to climatology: a score of 0 indicates no improvement over a simple climatological forecast. Results were obtained by driving the Liverpool malaria model (LMM) with rainfall and temperature forecasts from ENSEMBLES and comparing forecast total malaria incidence for November forecast months 4–6 (February, March and April) with a published malaria index for Botswana for the period 1980–2001 (Thomson et al., 2005). ENSEMBLES results are shown as solid black circles, with whiskers representing 95% confidence intervals in the ROCSS estimate by 999 bootstrap samples. For comparison, results are also shown for the corresponding model from DEMETER. The hollow squares on the right-hand side show the corresponding scores for the malaria model driven by ‘observations’ (ERA-40 reanalysis).

References

ENSEMBLES publications are highlighted as bold text.

- Alessandri A, Gualdi S, Polcher J, Navarra A, 2007. Effects of land–surface–vegetation on the boreal summer surface climate of a GCM. *Journal of Climate* 20, 255–278.
- Bárdossy A, 2009. Circulation pattern classification and its use in hydrology. *Physics and Chemistry of Earth*, submitted.
- Begert M, Zenkussen E, Häberli C, Appenzeller C, Klok L, 2008. An automated procedure to detect discontinuities: performance assessment and application to a large European climate data set. *Meteorologische Zeitschrift* 17, 663–672.
- Bellucci A, Gualdi S, Navarra A, 2009. The double-ITCZ syndrome in coupled general circulation models: the role of large-scale vertical circulation regimes. *Journal of Climate*, accepted.
- Bony S, Colman R, Kattsov VM, Allan RP, Bretherton CS, Dufresne J-L, Hall A, Hallegatte S, Holland MM, Ingram W, Randall DA, Soden BJ, Tselioudis G, Webb MJ, 2006. How well do we understand and evaluate climate change feedback processes? *Journal of Climate* 19, 3445–3482.
- Braconnot P, Hourdin F, Bony S, Dufresne J-L, Grandpeix JY, Marti O, 2007. Impact of different convective cloud schemes on the simulation of the tropical seasonal cycle in a coupled ocean-atmosphere model. *Climate Dynamics* 29, 501–520.
- Cagnazzo C, Manzini E, 2009. Impact of the stratosphere on the winter tropospheric teleconnections between ENSO and the North Atlantic and European region. *Journal of Climate* 22, 1223–1238.
- Cherchi A, Navarra A, 2007. Sensitivity of the Asian summer monsoon to the horizontal resolution: differences between AMIP-type and coupled model experiments. *Climate Dynamics* 28, 273–290.
- Dufresne J-L, Bony S, 2008. An assessment of the primary sources of spread of global warming estimates from coupled atmosphere–ocean models. *Journal of Climate* 21, 5135–5144.
- Frei C, Schöll R, Fukutome S, Schmidli J, Vidale PL, 2006. Future change of precipitation extremes in Europe: intercomparison of scenarios from regional climate models. *Journal of Geophysical Research* 111, D06105, doi:10.1029/2005JD005965.
- Giorgetta MA, Manzini E, Roeckner E, Esch M, Bengtsson L, 2006. Climatology and forcing of the quasi-biennial oscillation in the MAECHAM5 model. *Journal of Climate* 19, 3882–3901.
- Goulet L, Duvel JP, 2000. A new approach to detect and characterize intermittent atmospheric oscillations: Application to the intraseasonal oscillation. *Journal of the Atmospheric Sciences* 57, 2397–2416.
- Guilyardi E, Braconnot P, Jin F-F, Kim ST, Kolasinski M, Li T, Musat I, 2009. Atmosphere feedbacks during ENSO in a coupled GCM with a modified atmospheric convection scheme. *Journal of Climate*, doi:10.1175/2009JCLI2815.1.
- Hanel M, Buishand TA, 2009a. Evaluation of precipitation extremes in an ensemble of transient regional climate model simulations for the Rhine basin. *Climate Dynamics*, submitted.
- Hanel M, Buishand TA, 2009b. On the value of hourly precipitation extremes in regional climate model simulations. *Geophysical Research Letters*, submitted.
- Hanel M, Buishand TA, Ferro CAT, 2009. A nonstationary index flood model for precipitation extremes in transient regional climate model simulations. *Journal of Geophysical Research* 114, D15107, doi:10.1029/2009JD011712.
- Haylock MR, Hofstra N, Klein Tank AMG, Klok EJ, Jones PD, New M, 2008. A European daily high-resolution gridded dataset of surface temperature and precipitation. *Journal of Geophysical Research* 113, D20119, doi:10.1029/2008JD10201.
- Hofstra N, Haylock MR, New M, Jones PD, Frei C, 2008. Comparison of six methods for the interpolation of daily European climate data. *Journal of Geophysical Research* 113, D21110, doi:10.1029/2008JD010100.
- Hofstra N, Haylock M, New M, Jones PD, 2009a. Testing E-OBS European high-resolution gridded dataset of daily precipitation and surface temperature. *Journal of Geophysical Research*, doi:10.1029/2009JD011799.
- Hofstra N, New M, McSweeney C, 2009b. The influence of interpolation and station network density on the distribution and extreme trends of climate variables in gridded data. *Climate Dynamics*, in press.
- IPCC, 2007. *Climate Change 2007: The Physical Science Basis*. Contribution of Working Group I to the Fourth Assessment Report of the Intergovernmental Panel on Climate Change (S Solomon, D Qin, M Manning, Z Chen, M Marquis, KB Averyt, M Tignor, HL Miller, eds). Cambridge University Press, Cambridge, UK and New York, 996 pp.
- Klok EJ, Klein Tank AMG, 2008. Updated and extended European dataset of daily climate observations. *International Journal of Climatology* 29, 1182–1191.
- Kostopoulou E, Tolika K, Tegoulas I, Giannakopoulos C, Somot S, Anagnostopoulou C, Maheras P, 2009a. Evaluation of a regional climate model using in situ temperature observations over the Balkan Peninsula. *Tellus A* 61, 357–370.
- Kostopoulou E, Giannakopoulos C, Hatzaki M, Founda D, Flocas H, 2009b. On the comparison of extreme climate indices from observed and simulated data in the eastern Mediterranean basin. In: *European Geosciences Union General Assembly*, Vienna, Austria.
- Lister D, Jones PD, 2009. CRU, publication in preparation.
- Navarra A, Gualdi S, Masina S, Behera S, Luo J-J, Masson S, Guilyardi E, Delecluse P, Yamagata T, 2008. Atmospheric horizontal resolution affects tropical climate variability in coupled models. *Journal of Climate* 21, 730–750.
- Pall P, Arnold J, Kotlarski S, Bosshard T, Schär C, 2009. Evaluation of heavy Alpine precipitation in ENSEMBLES regional climate models. In preparation.
- Roeckner E, Brokopf R, Esch M, Giorgetta M, Hagemann S, Kornbluh L, Manzini E, Schlese U, Schulzweida U, 2006. Sensitivity of simulated climate to horizontal and vertical resolution in the ECHAM5 atmosphere model. *Journal of Climate* 19, 3771–3791.
- Terray P, Dominiak S, 2005. Indian Ocean sea surface temperature and El Niño–Southern Oscillation: a new perspective. *Journal of Climate* 18, 1351–1368.
- Thomson M, Mason S, Phindela T, Connor S, 2005. Use of rainfall and sea surface temperature monitoring for

- malaria early warning in Botswana. *American Journal of Tropical Medicine and Hygiene*, 73, 214-221.
- Turner AG, Slingo JM, 2009a. Uncertainties in future projections of extreme precipitation in the Indian monsoon region. *Atmospheric Science Letters* 10, 152–158.
- Turner AG, Slingo JM, 2009b. Subseasonal extremes of precipitation and active-break cycles of the Indian summer monsoon in a climate change scenario. *Quarterly Journal of the Royal Meteorological Society* 133, 1143–1157.
- Webb MJ, Senior CA, Sexton DMH, Ingram WJ, Williams KD, Ringer MA, McAvaney BJ, Colman R, Soden BJ, Gudgel R, Knutson T, Emori S, Ogura T, Tsushima Y, Andronova N, Li B, Musat I, Bony S, Taylor KE, 2006. On the contribution of local feedback mechanisms to the range of climate sensitivity in two GCM ensembles. *Climate Dynamics* 27, 17–38.
- Weigel AP, Liniger MA, Appenzeller C, 2008. Can multi-model combination really enhance the prediction skill of probabilistic ensemble forecasts? *Quarterly Journal of the Royal Meteorological Society* 134, 241–260.
- Weigel AP, Liniger MA, Appenzeller C, 2009. Seasonal ensemble forecasts: are recalibrated single models better than multimodels? *Monthly Weather Review* 137, 1460–1479.
- Xavier PK, Duvel J-P, Braconnot P, Doblus-Reyes FJ, 2009. An evaluation metric for intraseasonal variability in climate models. *Journal of Climate*, submitted.

9 Assessments of climate change impacts

[Research Theme 6]

A. Morse (Liverpool University), C. Prentice (Bristol University), T. Carter (SYKE)

Introduction

Climate change impacts in Research Theme 6 were assessed in three areas:

- The integration of process models of impacts on the natural and managed global environment into Earth System Models (Section 9.1);
- Modelling the impacts of extreme weather events and applying probabilistic climate projections to evaluate impact risks (Section 9.2);
- Maximizing skill in the impacts models driven by seasonal-to-decadal scale forecasting (Section 9.3).

Many of the results presented in Sections 9.2 and 9.3 are preliminary – studies are still ongoing, and so far few have been published in peer reviewed literature.

9.1 The integration of process models of impacts on the natural and managed global environment into Earth system models

9.1.1 Introduction

Global-scale models for the impacts of environmental changes on ecosystems – also known as dynamic global vegetation models (DGVMs) – play two roles in climate research. DGVMs can perform *offline* simulations, driven by climate observations and climate model outputs, to assess impacts on ecosystems and ecosystem services. The latter include freshwater supply, which is strongly influenced by ecosystem processes such as tree–grass competition, and physiological effects of CO₂ that are not represented in conventional hydrological models. DGVMs can also be coupled *online* into climate models, allowing a consistent simulation of the global carbon and water cycles including feedbacks to climate. ENSEMBLES has used DGVMs in both roles.

In terms of model developments, the Lund–Potsdam–Jena (LPJ) offline modelling framework (Sitch et al., 2003) has been radically enhanced. The version called LPJmL simulates the human-modified landscape including arable crops, managed forests, grazing and fire. The DGVM components of the Hadley Centre and IPSL climate models, which can be run either offline or online, have also been upgraded to include human-influenced aspects of ecosystems. The models have been exercised using ENSEMBLES climate model outputs, and the online models have been used as fully embedded components in the RT2a stream 2 model runs.

The research results reported here were influenced by two recent scientific developments. First, the C4MIP project (Friedlingstein et al., 2006) showed that the climate–carbon cycle feedback is subject to large differences between models (see also Section 8). This result was highlighted in the IPCC Working Group I Fourth Assessment (Denman et al., 2007). The resulting uncertainties have been shown to be at least as large as those for climate change itself (Booth et al., 2009). This implies an urgent need to subject the carbon cycle components of models to critical testing, with a view to reducing the uncertainties. Second, IPCC Working Group II has brought the limitations of traditional regional impacts analysis into sharp focus. The publication of the AR4 coincided with a major upswing in government-level interest in quantifying climate impacts. The lack of quantitative, global information on impacts has been perceived as a significant obstacle to progress in climate policy. In response to these challenges, two new research strands were developed: a focus on benchmarking and evaluation of models with the emphasis on carbon, water and energy exchanges at the land surface; and a means to depict quantitative information about climate impacts as a probabilistic global risk analysis. The impacts of climate and CO₂ changes on water resources have been a cross-cutting theme, and a major component both of the risk analysis and of the quantitative assessment of climate impacts.

9.1.2 Model developments

ENSEMBLES has supported many new model developments. All have shared a common goal, to move from modelling the world as if all vegetation were natural, to approximating the real-world vegetation, including land use. These developments are world-leading for DGVMs. The most advanced model in this respect is LPJmL which now includes process-based treatments of arable cultivation (eleven crop types, including irrigation), forestry management (see Deliverable 6.1 at: <http://www.ensembles-eu.org/deliverables.html>), rangelands, and freshwater use and management (Bondeau et al., 2007; Rost et al., 2008a) (Figure 9.1).

Crops have also been included in the Hadley Centre and IPSL climate models. In the Hadley Centre model, ENSEMBLES has supported the implementation of an innovative generic crop model in the land surface modelling framework, allowing investigation of climate feedbacks from land-use changes (including irrigation) as well as impacts of simulated climate changes on crop productivity. This work has been paralleled by implementation of crop models in the IPSL model.

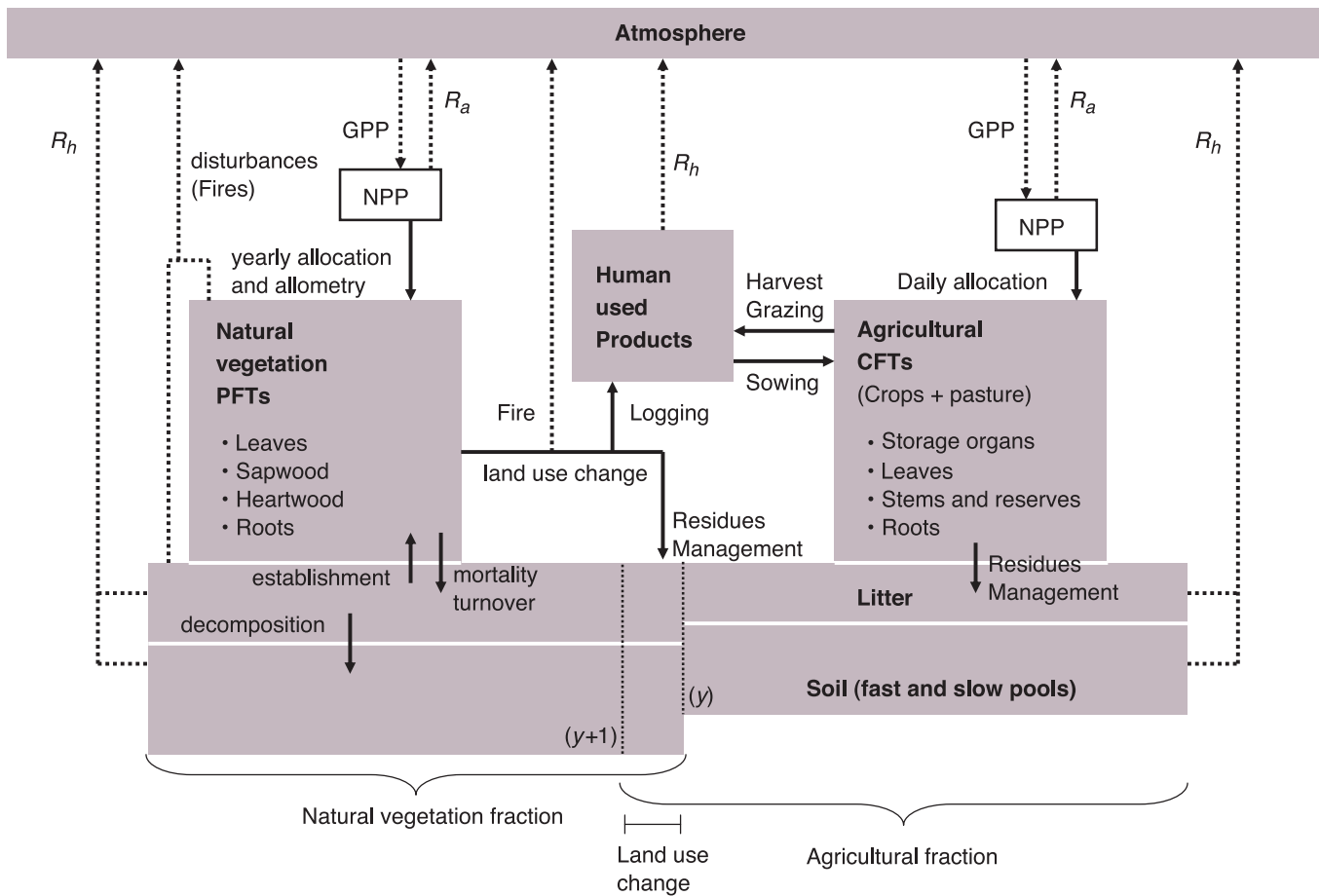


Figure 9.1: Schematic representation of processes in LPJmL (Bondeau et al., 2007).

A process-based representation of fire–vegetation interactions (Thonicke et al., 2009) is included in the LPJ model versions called LPX and LPJ-GUESS. Fire effects can be modelled in a natural way in LPJ-GUESS as it includes more detailed representations of woody population dynamics, distinguishing different age and size classes of woody plants. The fire-enabled version of LPJ-GUESS performs well at the European scale, capturing the potential natural vegetation of the Mediterranean region, in particular, better than previous model versions. A comparable process-based fire regime model has been developed for the Hadley Centre HadCM3LC climate model (see Deliverable 6.6 at: <http://www.ensembles-eu.org/deliverables.html>). The fire model in HadCM3LC was optimised to improve the simulation of burnt area in comparison with satellite data in the GFED database (<http://www.geo.vu.nl/~gwerf/GFED.htm>). The fire model was coupled to the atmospheric component of the carbon cycle module within the climate model. Initial results show spatial and temporal patterns of fire behaviour which are plausible at a global scale (Figure 9.2), but with some regional biases. These are largely due to biases in the climate model, but biases in the modelled vegetation may also be involved.

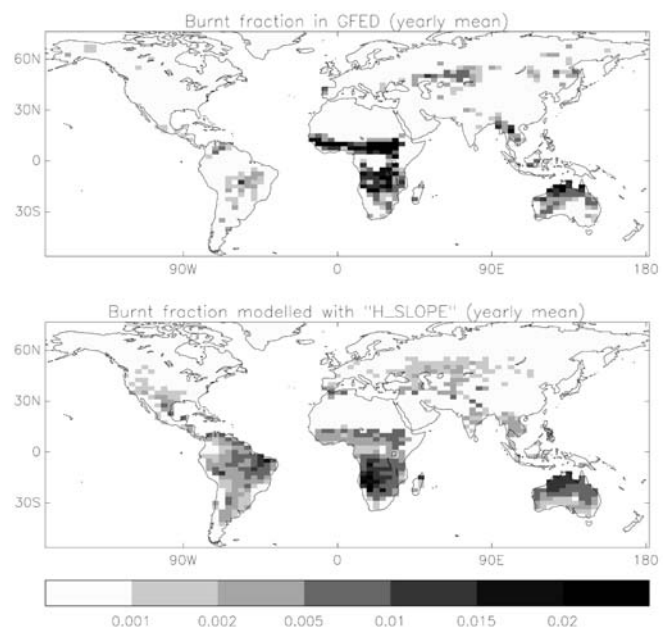


Figure 9.2: Annual mean burnt area fraction of grid cells: observed (GFED database) and modelled (online optimised HadCM3LC model).

A dynamic representation of plant–grazer interactions in LPJ-GUESS was developed, and is undergoing testing. Theoretical analysis has clarified key features of grazing dynamics for modelling, including a proof that ‘grazing optimisation’ (higher plant productivity being achieved with mammalian herbivores rather than without) is possible in model ecosystems.

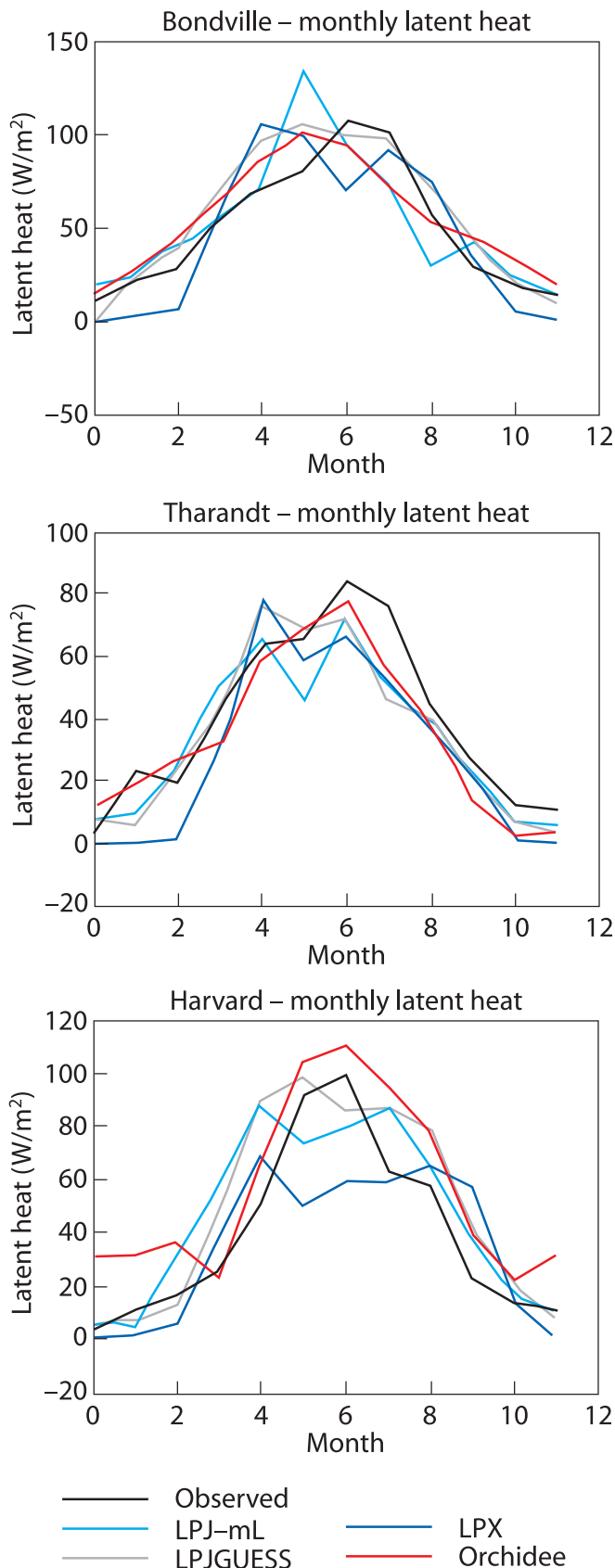


Figure 9.3: Comparison of the seasonal cycle of modelled and observed latent heat flux, for selected FLUXNET measurement sites.

9.1.3 Model benchmarking and evaluation

Offline evaluation

A new protocol has been implemented for offline model evaluation. A pre-industrial spin-up of the model is followed by a historical simulation (1901–2006) driven by gridded observed climate data and atmospheric CO₂ concentration. Three members of the LPJ model family (LPJmL, LPJ-GUESS and LPX), the Hadley Centre land-surface model (JULES), and the IPSL land-surface model (ORCHIDEE) have participated. Standard benchmarks have been defined for the carbon and water cycles and for the fraction of absorbed photosynthetically active radiation, a remotely sensed quantity which links the two cycles.

An initial offline evaluation by Sitch et al. (2008) used earlier variants of the same three models: LPJ (Gerten et al., 2004), ORCHIDEE (Krinner et al., 2005), and TRIFFID (a forerunner of JULES; Cox, 2001). Figures 9.3 and 9.4 show examples of unpublished data–model comparison results for the new water cycle benchmarks. Figure 9.3 compares seasonal cycles of latent heat flux at selected FLUXNET measurement sites (Blyth et al., 2009), indicating generally good agreement but suggesting too large a decrease in simulated evapotranspiration during the summer months in some sites and models.

Figure 9.4 compares seasonal cycles of river discharge from major river basins (data from Fekete et al., 2002). For this comparison, values of monthly runoff simulated on a grid-cell basis have been used as input to the TRIP hydrological routing scheme, so that the analysis takes account of lags in water transport. This comparison is important for evaluation of the models' ability to simulate large-scale changes in freshwater supply. Interpretation has to take account of extractions, not included in the models, which account for the general oversimulation of the flows for (most notably) the Congo, Parana, Nile and Niger catchments. The seasonal patterns are well simulated for the most part.

Figure 9.5 illustrates the model benchmark for seasonal cycles of CO₂ concentration, using LPX as an example. Monthly net ecosystem exchanges are propagated to the stations by transport matrices obtained from the TM2 atmospheric transport model with prescribed wind fields. The CO₂ measurement stations illustrated span a range of latitudes. Greater seasonal cycle amplitudes are seen in the northern high latitudes than in lower (or southern) latitudes (Heimann et al., 1998) because of the large temperature seasonality across the large boreal land masses (Heimann et al., 1998). The comparison shows the model's ability to capture the amplitude and timing of these signals.

Online evaluation

Two sets of coupled climate-carbon cycle model simulations from the Hadley Centre were evaluated, and two from IPSL, against the seasonal cycle of CO₂ during 1980–2005 (Cadule et al., 2009). In 'HC1', the Hadley Centre coupled climate-carbon cycle model was forced by emissions of CO₂ only, as in the C4MIP intercomparison (Friedlingstein et al., 2006). 'HC2', from Jones et al. (2003), includes interactive sulphate aerosols.

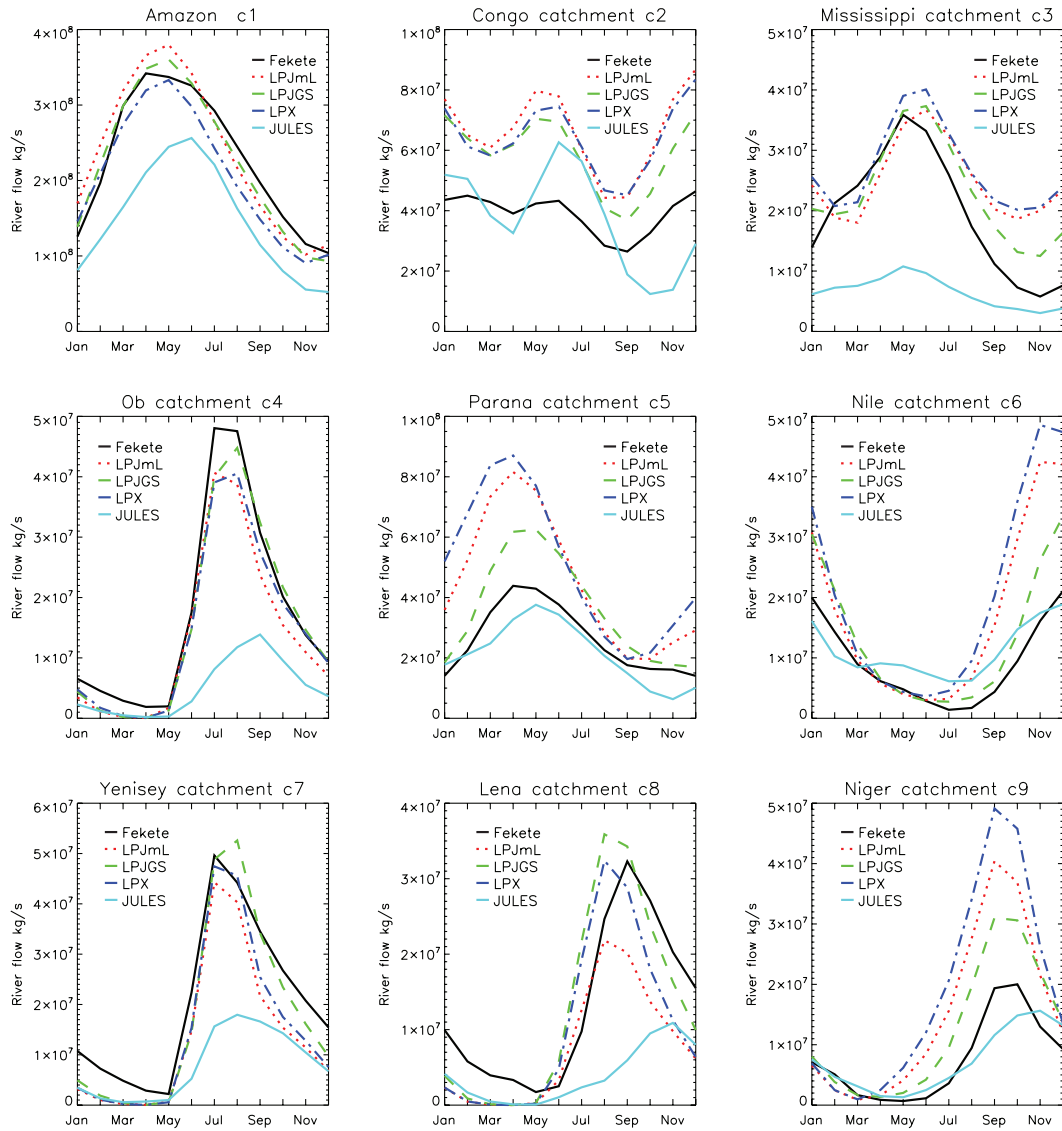


Figure 9.4: Comparison of the seasonal cycle of modelled and observed river discharge, for nine of the world's largest river basins.

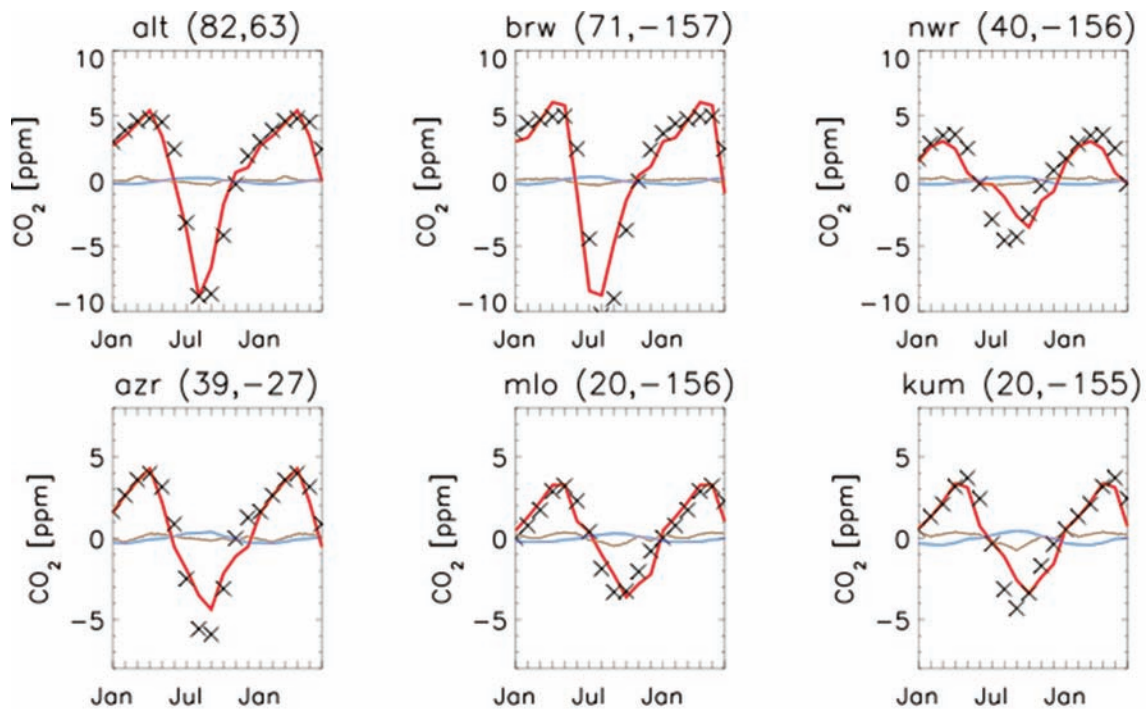


Figure 9.5: Comparison of modelled (LPX, red curve) and observed (crosses) seasonal cycles of atmospheric CO₂ concentration at different latitudes. The blue curves indicate the prescribed ocean component; the brown curves indicate the prescribed fossil fuel component.

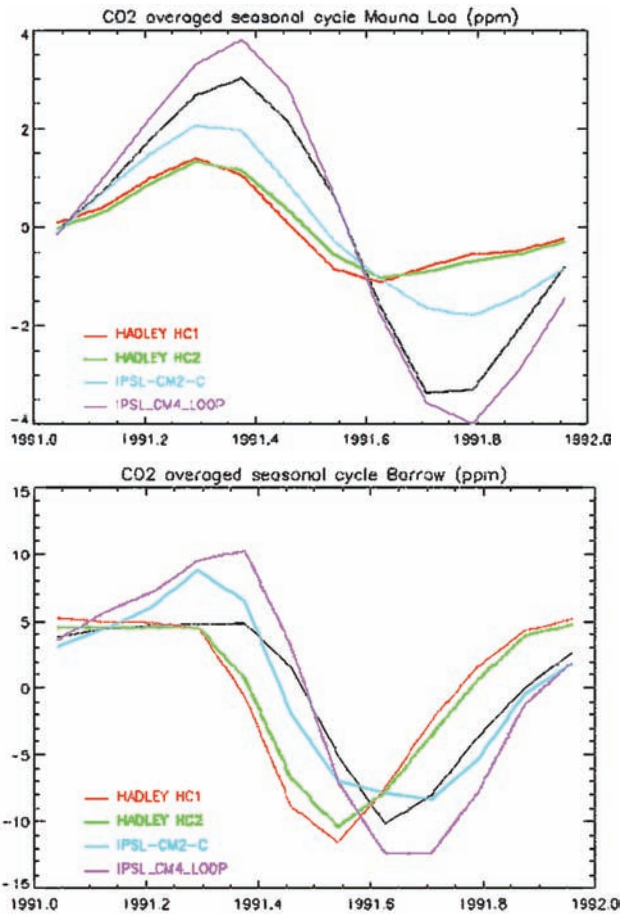


Figure 9.6: Mean seasonal cycle of CO_2 at Mauna Loa, Hawaii (top) and Point Barrow, Alaska (bottom): observed, and as simulated by coupled climate-carbon cycle models.

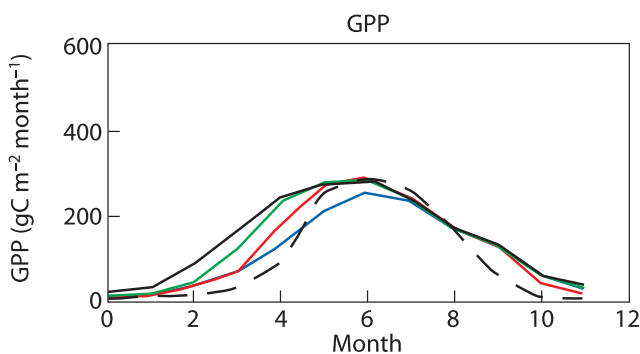


Figure 9.7: Sensitivity of simulated seasonal gross primary production (GPP) at Harvard forest to the representation of phenology in JULES. Dashed line: GPP as measured. Black: JULES with phenology off. Green: standard JULES phenology. Red: parameters set to delay the onset of greening. Blue: parameters set to reduce the rate of leaf growth in spring.

The IPSL model followed the C4MIP protocol. The versions used were IPSL-CM2-C and IPSL_CM4_LOOP ('LOOP') (Friedlingstein et al., 2006). LOOP contains the ORCHIDEE (Krinner et al., 2005) land model, while IPSL-CM2-C uses a simpler land carbon cycle model.

Figure 9.6 shows simulated versus observed seasonal cycles at Mauna Loa, Hawaii and Point Barrow, Alaska ('mlo' and 'brw' in Figure 9.5). The Hadley Centre models simulate too small an amplitude but the correct phase of the seasonal cycle at Mauna

Loa (Figure 9.6; Cadule et al., 2009), whereas at Barrow the simulated amplitude is good but the phase is poor – in particular, the spring drawdown of CO_2 happens too early. LOOP tends to generally overestimate the amplitude of the seasonal cycle at monitoring stations, but the phase is in better agreement with observations.

Further (offline) studies applying JULES at individual FLUXNET sites led to improvements in leaf seasonality in the Hadley model which are now implemented in JULES. Figure 9.7 illustrates these improvements using the Harvard forest FLUXNET site (see Harvard in Figure 9.3) as a test case.

River flows produced by the TRIP river routing scheme have also been evaluated in successive versions of the Hadley Centre model (Falloon et al., 2007). The coupled models have surprisingly good overall skill in predicting river flows, successfully capturing the latitudinal patterns as well as seasonal cycles for the world's largest river basins.

9.1.4 Global risk analysis using LPJmL

A method of mapping probabilistic impacts information was developed by Scholze et al. (2006) and further elaborated for a preliminary (see Deliverable 6.12 at: <http://www.ensembles-eu.org>) and final global risk analysis. In the results shown here, the LPJmL model was forced with the projected climatic patterns from seventeen general circulation models (i.e., the ENSEMBLES RT2a stream 1 ensemble), interpolated to a $1.0^\circ \times 1.0^\circ$ global grid and normalised to the observed CRU TS2.1 climatology (1961–1990 period).

It was found that global warming by 2°C will have important impacts on many biospheric and hydrological processes. For example, carbon stores (in vegetation and soil) and net primary production (NPP) in these model runs consistently increase by 20–30% due primarily to the CO_2 fertilisation effect, and also to regionally increased precipitation and increased temperature in high-latitude regions. On the other hand, carbon losses in heterotrophic respiration increase as well (driven partly by the higher NPP and partly by the additional stimulation of decomposition at higher temperatures), and the incidence of fire (with associated carbon loss) increases dramatically. Total river runoff tends to increase, at global and continental scales, in a warmer world. However, this increase is geographically restricted to high northern latitudes and some tropical regions. Runoff decreases are expected in mid-latitudes, which could potentially pose serious threats to regional water security. The key quantitative results from the global risk analysis are summarised in Figure 9.8.

The model results can be used in a variety of ways to illustrate the risks of different degrees of global warming. For example, Figure 9.9 shows the increase in risk of increasing or decreasing freshwater supplies between climate change scenarios giving a 3°C global warming, compared with scenarios giving a 2°C warming. This result shows starkly the increasing risks of freshwater scarcity with increasing degrees of climate change for many Mediterranean-type and other subtropical regions.

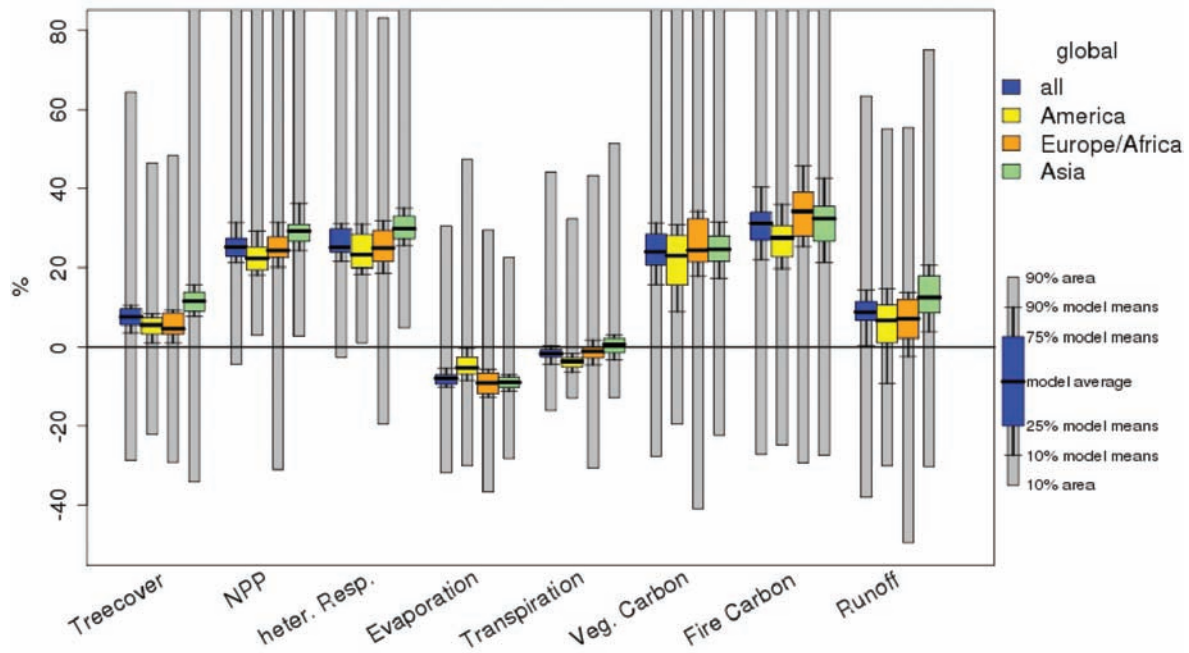


Figure 9.8: Summary of the global risk analysis using LPJmL for 2° mean global warming. Changes are shown as percentages relative to 1971–2000, at times when mean global warming reaches 2°.

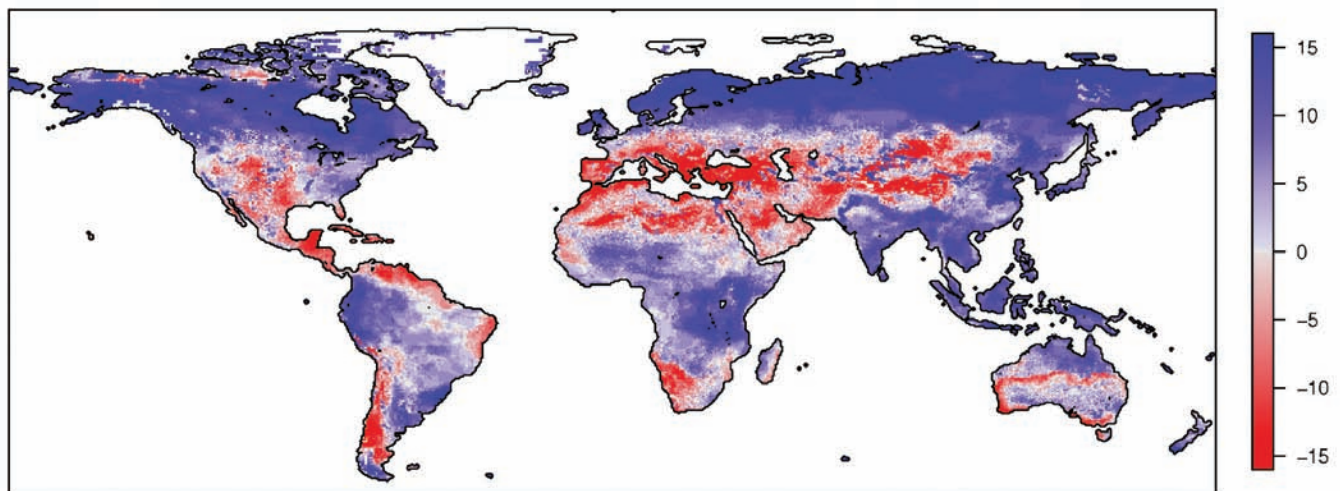


Figure 9.9: Number of scenarios showing a further increase or decrease in freshwater runoff for 3°C global warming, as compared to 2°C.

9.1.5 Assessment of climate impacts: some examples

Offline analyses

LPJmL was used to estimate the global carbon and water balance throughout the 20th century, along with the effects of anthropogenic land-use changes. It was found, for example, that land-cover and land-use changes increased global runoff by 1.7% over the past century, while irrigation decreased discharge by 0.3%. In some regions these effects exceeded the effects of precipitation trends.

An important finding of this work is that the majority of global food production relies on so-called ‘green water’, i.e., the precipitation water stored in the soil and used by plants. ‘Blue water’, the water withdrawn from rivers, reservoirs and groundwater for irrigation, is an important resource only in

intensively irrigated regions. These findings highlight an important principle: that any comprehensive assessment of freshwater resources and scarcity must include the green water resource. Estimates of future increases in food production also need to account for the potential of better water management in non-irrigated agriculture (Rost et al., 2008a, 2008b).

Online analyses

Hadley Centre coupled model runs were used to assess the impacts of climate change on ecosystem services including net primary production (NPP) and water supply (see ENSEMBLES Deliverable 6.18 at <http://www.ensembles-eu.org/deliverables.html>). A perturbed-physics climate model ensemble was used, consisting of 44 versions of the HadSM3 model (a model version with a ‘slab’ ocean which is faster to run than the fully coupled model). The versions differ in the values assigned to key meteorological parameters. HadSM3 includes a land surface

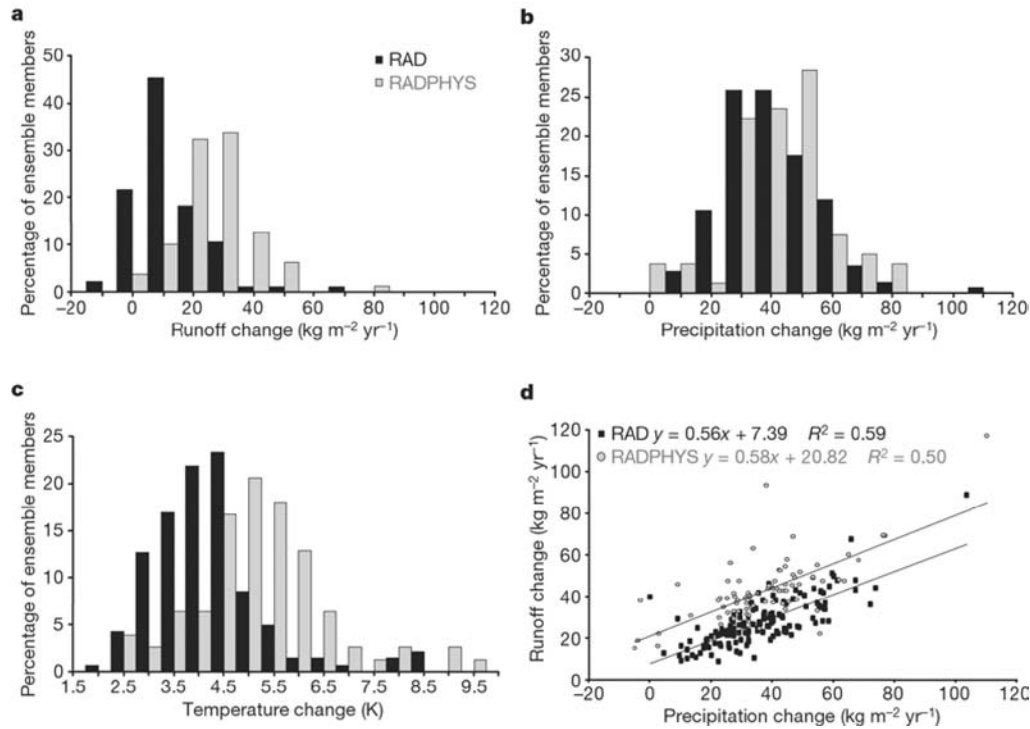


Figure 9.10: Impact of physiological forcing on global mean runoff, precipitation and temperature: (a) frequency distribution of simulated changes in global mean runoff due to doubling of CO₂ in a large climate model ensemble, with physiological forcing included (RADPHYS) and excluded (RAD); (b) as for (a) but for precipitation over land; (c) as for (a) but for near-surface air temperature over land; (d) global mean runoff changes versus global land mean precipitation changes.

scheme that is a forerunner of JULES: it simulates plant physiological processes, but not changing vegetation types. The parameters determining the physiological response of NPP to changes in atmospheric CO₂ were *not* varied within the ensemble, so the ensemble provides information about the uncertainties in climate change itself. The ensemble design was also used to highlight the relative importance of plant physiological responses to CO₂ (Phys) and plant responses to physical drivers of climate (Rad) in determining NPP, runoff and precipitation over land. To separate the physiological and climatic effects, a further ensemble of simulations was performed in which the plant physiological calculations in the doubled-CO₂ simulations used the control (pre-industrial) CO₂ concentration. Results are presented in Betts et al. (2007).

The ensemble-mean NPP response to climate change was an increase in global mean NPP of about 0.2 kg C m⁻² yr⁻¹. Most regions showed an increase. The boreal forests, India and China showed increases of about 0.3 kg C m⁻² yr⁻¹, the temperate agricultural regions 0.2 kg C m⁻² yr⁻¹, and the tropical forests of Africa and South East Asia 0.6 kg C m⁻² yr⁻¹ and above. Central and western Amazonia showed a mean NPP increase of up to 0.3 kg C m⁻² yr⁻¹. However, the mean NPP decreased by about 0.1 kg C m⁻² yr⁻¹ along the southern coast of the Mediterranean, across the Middle East, and in south-west Africa. NPP also decreased along the north-eastern coast of South America, by as much as 0.3 kg C m⁻² yr⁻¹ in some areas. The *range* of regional NPP response across the ensemble was especially large in Amazonia, where the 5–95% percentile range was over 0.9 kg C m⁻² yr⁻¹. This range reflects very large uncertainties in the precipitation changes simulated in that region, ranging from a small drying in the north-east and a wetting in the rest of the basin, to a major drying extending across most of the basin.

These results suggest that although a global mean increase in NPP under doubled-CO₂ climate change seems likely, the climate-related uncertainty in regional NPP change is larger than the mean change in many regions.

The physiological effect of doubled CO₂ concentrations on plant transpiration increases simulated global mean runoff by 6% relative to pre-industrial levels (Betts et al., 2007). This is an important increase, comparable in magnitude to the effect of radiatively forced climate change on transpiration. Assessments of the effect of increasing carbon dioxide concentrations on the hydrological cycle that only consider radiative forcing will therefore tend to underestimate future increases in runoff and overestimate decreases.

Figure 9.10 shows a range of effects of the ‘antitranspirant’ property of CO₂ on the global hydrological cycle. These include increased land precipitation but also increased warming, which is probably caused by a combination of reduced transpiration and increased vegetation cover.

9.1.6 Lessons learned and future research directions

The work done in Research Theme 6 has shown the potential for DGVMs (offline or online) to provide a credible regional to global-scale modelling capability for the managed terrestrial biosphere, and (in online mode) for the potential effects of land-use changes on climate. This work has established the participating DGVMs as world leaders in modelling real-world ecosystems, and will allow an enormous range of questions to be answered regarding the implications of land use. The online

models include a consistent treatment of carbon, water and energy cycle feedbacks that can be exploited, for example, to analyse potential unintended consequences of measures designed for climate mitigation.

Another important lesson from the impacts analyses is the sensitivity of runoff, and therefore freshwater supplies (especially in regions already under water stress), to changes in atmospheric CO₂ concentration as well as changes in climate. A first-order prediction from these analyses is that freshwater resources may be less limited than previously assumed under future global warming scenarios (although there is nevertheless an increased risk of drought in certain regions). A further consequence is that the practice of assessing the climate-forcing potential of all greenhouse gases in terms of their radiative forcing potential, relative to CO₂, does *not* accurately reflect the relative effects of different greenhouse gases on freshwater supply. This point reinforces arguments based on other grounds, such as the very different lifetimes of different greenhouse gases, for a more differentiated analysis of future emissions trajectories aimed at climate stabilisation which does not rely on the problematic concept of CO₂ ‘equivalent’.

Finally, the benchmarking work (both offline and online) provides an optimistic message with regard to uncertainties in the land-surface component of Earth system models, as it has shown that deficient aspects of models can be pinpointed and corrected. The power of setting up benchmarks has been demonstrated for key large-scale properties of the carbon, water and energy cycles based on observations (both ground- and space-based) and the huge importance of continued high-precision monitoring of seasonal cycles, interannual variability and long-term trends in the atmosphere. When the C4MIP results were published, most of the land carbon cycle models involved had never been subjected to this kind of evaluation. The evaluation tests that have been set up within this project should provide an international benchmark test which, in future, all land surface models will be expected to comply with. Future work in this direction should further widen the scope of these evaluations and, in the long run, aim to establish a closer cooperation between the modelling and observational communities.

9.2 Impacts of extreme weather events and evaluating the risks of impact

9.2.1 Introduction

The climate model projections conducted during the ENSEMBLES project are described in earlier sections of this report. One objective of these new model runs has been to deliver probabilistic projections of future climate (an Ensemble Prediction System), accounting for a range of uncertainties in modelling of the climate system. This section describes some of the opportunities and challenges offered by such climate projections for studying the impacts of climate change. Researchers focused their efforts on alternative methods of applying climate projections to allow future impacts to be considered in terms of risk. Most policy makers are familiar with decision making under uncertainty, and approaches for addressing adaptation to climate change make repeated reference to methods of risk assessment.

Impacts have been studied using a range of mathematical models for estimating how climate change may affect agricultural crops, water resources, energy demand, forests, permafrost, human health and infrastructure. Some models are mechanistic, describing processes such as plant growth, leaching of soils and runoff; while others are statistically based, such as for permafrost or forest fire. The models operate at spatial scales ranging from site, through river basin, to national and European, and at time resolutions ranging from sub-daily through to annual. The analysis of impacts comprised two main groups of studies applying ENSEMBLES climate projections¹ (Figure 9.11).

1. Impacts of changes in climatic variability and extreme weather events.
2. A response surface approach for assessing risks of impacts.

9.2.2 Impacts of changes in climatic variability and extremes

Some of the most damaging and costly impacts of climate change are expected to be manifest through extreme weather events. These are weather occurrences such as heavy rainfall, drought, severe cold, heatwaves and storms that can result in damage to natural ecosystems, forests, agriculture, infrastructure or human health and welfare. Extreme events, by definition, are rare, but in a changing climate their frequency and/or intensity may alter. Impact models have been used in ENSEMBLES to define the nature of these extreme events in different sectors under present-day climate, and then to evaluate how these may change in the future, using projections from the latest generation of Global and Regional Climate Models (Figure 9.11).

Five examples are presented here:

1. property damage due to wind-storms in western and central Europe;
2. effects of climate warming on potential energy demand for space heating and cooling in the Mediterranean;
3. forest fire risk in Fennoscandia;
4. forest damage due to low temperature and pests in Sweden;
5. potential impacts of extreme weather in Poland.

The results obtained in each of these examples are critically dependent on daily or sub-daily time-scale information from climate models, and each example highlights new insights gained by applying ENSEMBLES climate simulations.

Property damage due to wind storms

The GCM and RCM scenario simulations produced in RT2A and RT2B were analysed with respect to future changes in wind-storm risk and related loss potentials. In most simulations, as well as in the ensemble mean of multi-model simulations, increased extreme wind speeds were found over northern parts of central and western Europe under increased greenhouse gas forcing. Decreased values of extreme wind speeds were projected for southern Europe. Storm loss potentials were calculated by applying a storm loss regression model.

¹ The results presented in this section are preliminary – studies are still ongoing, and so far few have been published. For this reason, and to aid readability, references are not included in this section.

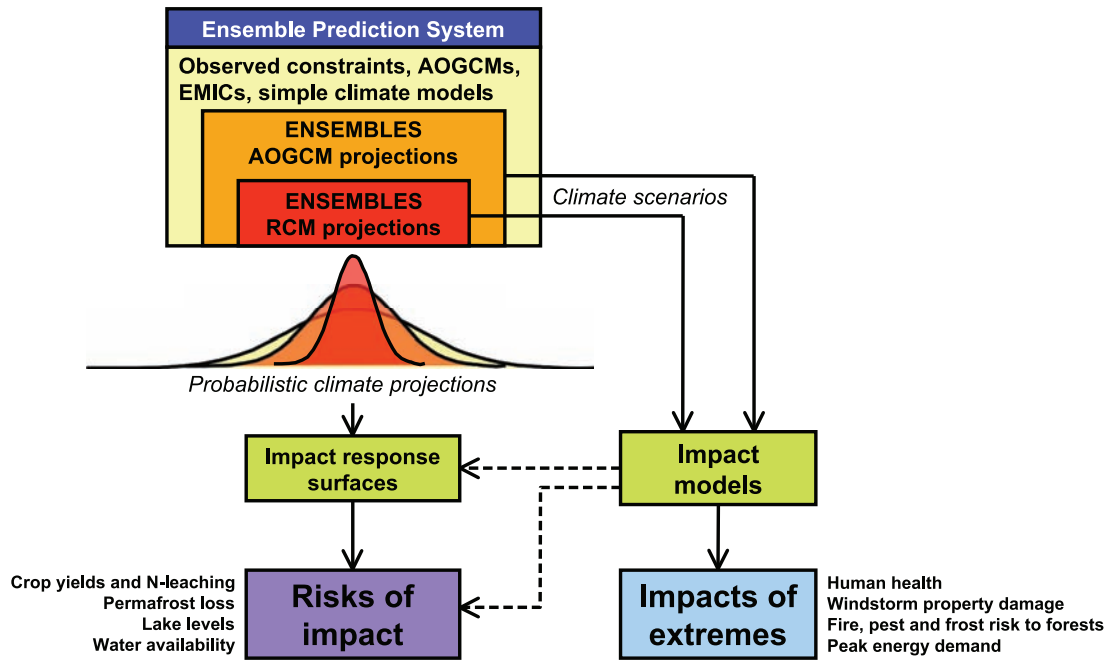


Figure 9.11: Two methods of impact assessment using outputs from the Ensemble Prediction System: either using model-based scenarios applied to impact models for estimating impacts of extreme events or using probabilistic projections combined with impact response surfaces for evaluating impact risks. Impacts illustrated in this report are listed alongside the respective method applied.

Consistent with the changes in extreme wind speeds, higher storm losses were estimated for western and particularly for central Europe, assuming that no adaptation to the changed wind climate takes place (Figure 9.12).

Uncertainties in the range of changes in loss potential are accounted for by using two different measures. First, the standard deviation of the change signals across the different climate model simulations have been computed (parentheses in Figure 9.12), revealing values of the same order as the mean changes for most regions considered. However, as an uncertainty measure, the standard deviation is strongly influenced by outliers. An alternative measure of uncertainty considers the arbitrariness of the multi-model ensembles used in

the study. There are numerous combinations of model outputs that might have been selected as ensembles among the nine GCM and eight RCM simulations, in addition to the nine-member and eight-member ensembles represented in Table 5.1. For example, if only eight of the nine GCMs had been chosen as ensembles, there are nine possible combinations of these; selecting ensembles of seven GCMs from nine gives 36 possible combinations, and so on. Overall there are 511 possible ensemble combinations comprising between one and nine GCM members. Consideration of the signals from all of these combinations results in a relatively symmetrical distribution of possible change signals around the ensemble mean and further allows for the construction of probabilistic information about the range of expected changes (Figure 9.13). For example,

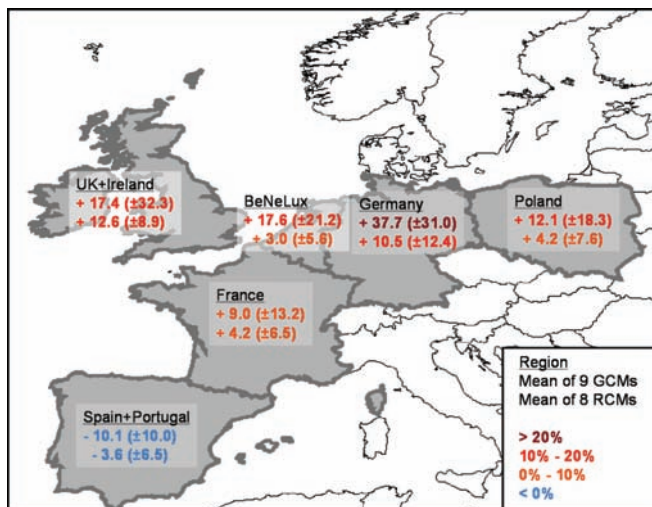


Figure 9.12: Relative changes (%) of mean annual storm loss potential based on nine GCM (upper row) and eight RCM (bottom row) simulations for the end of the 21st century (2071–2100) relative to recent climate conditions (1961–2000), assuming the SRES A1B emissions scenario. Values in parentheses are inter-model standard deviations.

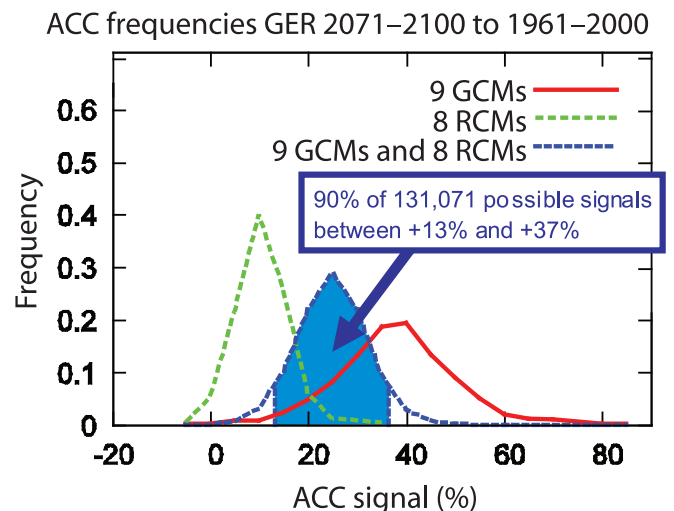


Figure 9.13: Anthropogenic climate change (ACC) signal in storm loss potential over Germany by 2071–2100 relative to 1961–2000 under an A1B emissions scenario, expressed probabilistically based on ensembles comprising all possible combinations of available ENSEMBLES simulations by GCMs (red curve), RCMs (green dotted curve) and all models (blue dotted curve).

extending this analysis to include additionally the eight RCM simulations produces 131,071 different sub-ensembles based on seventeen individual model simulations. Using this distribution, as calculated for grid boxes over Germany for the end of the 21st century, a mean increase in loss potential of 25% can be estimated, with a 90% confidence interval of between +13% and +37%.

Note, however, that these probabilities are conditional on the range of GCM projections provided in the ENSEMBLES project. This range of projections is not as wide, for example, as the range sampled in the IPCC Fourth Assessment Report, which considered around twenty GCMs and three emissions scenarios (IPCC, 2007). Furthermore, the ensembles formed using both GCM and RCM outputs cannot all be regarded as independent, as some of the RCM simulations made use of boundary conditions provided by one of the GCMs.

Potential energy demand for space heating and cooling in the Mediterranean

In the Mediterranean region under present-day conditions the maximum values of energy consumption are related to cold weather in winter (for heating) and hot weather in summer (for cooling). With higher temperatures under a changing climate, it would therefore be logical to expect decreased heating demand during the colder part of the year and increased cooling demand in the warmer part. This hypothesis has been examined using daily temperature outputs from simulations conducted in ENSEMBLES with six Regional Climate Models (RCMs)

assuming the A1B emissions scenario. Simulated temperatures representing the present (for 1960–1989) and the future (2021–2050) were extracted for the Mediterranean region at a horizontal resolution of 25 × 25 km. See ENSEMBLES Deliverable 6.19 at www.ensembles-eu.org/deliverables.html; Giannakopoulos et al., 2009.

A measure that is commonly used as a proxy for energy demand is *accumulated temperature*. This can be defined as the difference in mean daily temperature from a threshold or base temperature at which energy consumption is at a minimum. During the warmer part of the year, temperatures commonly exceed a base temperature above which cooling is activated. By accumulating the daily exceedances during a given period, an indication of total energy demand can be estimated for that period (cooling degree days or CDD). Similarly, the sum of daily temperature departures *below* a temperature threshold is a useful proxy for heating demand in the colder part of the year (heating degree days or HDD). In this study, based on earlier work in southern Europe, 15°C is used as the base temperature for estimating HDD, and 25°C as the corresponding threshold for CDD.

Figure 9.14 presents changes in annual CDD and HDD up to 2021–2050. An increase in cooling requirement is indicated in all regions, with large increases over southern Spain, eastern Greece and western Turkey, and the largest increases over Cyprus and North Africa. Smaller changes are estimated for Sardinia, Corsica and the Aegean Islands (Figure 9.14a). In contrast, heating demand declines over much of the region (Figure 9.14b), but less so in the coastal regions that do not currently experience cold winters.

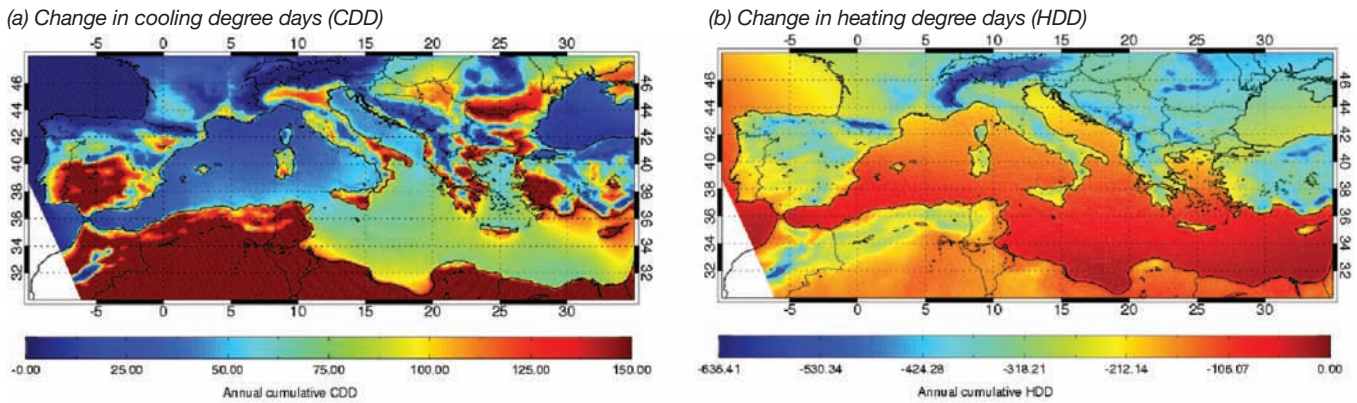


Figure 9.14: Projected change in potential annual energy demand between 1960–1989 and 2021–2050 for (a) cooling and (b) heating, based on accumulated temperature (°Cd).

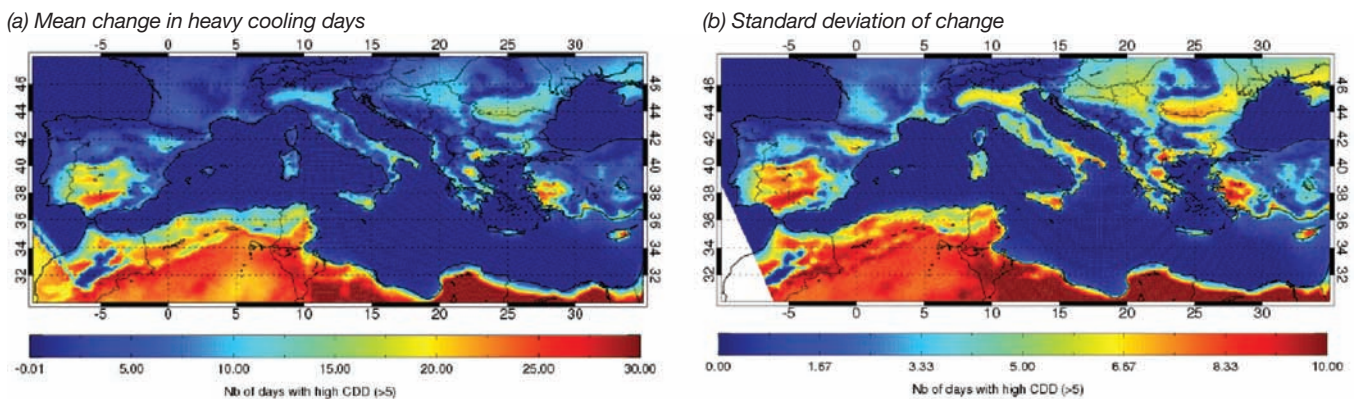


Figure 9.15: Mean change in the number of days with a large cooling demand (>5°Cd) between the baseline and 2021–2050 periods (a) and inter-model standard deviation of the changes (b).

Another dimension of cooling demand is illustrated in Figure 9.15, which shows mean change in the number of days requiring cooling of more than 5°C by 2021–2050 (Figure 9.15a) as well as the standard deviation of the changes as a measure of inter-model spread (Figure 9.15b). Over North Africa, more than one additional month of heavy cooling would be required, while over parts of southern Spain and Italy, eastern Greece, western Turkey and Cyprus, 20 more days would be needed. In both cases this represents more than a doubling compared with today, suggesting a need to plan for additional generating capacity to meet the extra demand. The inter-model standard deviation is considerably smaller than the mean change in most regions, implying that the signal of change is fairly robust.

Forest fire risk in Fennoscandia

Fire is one of the dominant forms of disturbance in the boreal forest and in the transition zone between forest and tundra. During most of the year there is no risk of forest fire, due to the extended presence of snow cover and the increased moisture of the surface during autumn. However, from May until August there are periods when the forest fire risk is high. The climate changes anticipated for the boreal zone in the future could influence both fire frequency and severity, as summers become warmer and evaporation increases.

An assessment of the fire danger rating has been conducted applying the Finnish Forest Fire Index (FFI). In computing the index, the volumetric moisture of a 60 mm thick surface layer is estimated using precipitation and potential evaporation data. The surface moisture is scaled to FFI values that vary between 1 and 6; where index values above 4 (corresponding to a volumetric moisture of 20%) represent a high forest fire risk, while an index value above 5 corresponds to a very high fire danger. Projections from a 100-year simulation with the SMHI-RCA Regional Climate Model starting from 2001 were used for determining future changes in fire danger over Finland, Sweden and the Baltic region, focusing on the fire season, April–September. In addition, sixteen locations have been selected and further statistical analyses have been performed in order to obtain the regional and temporal variation in fire danger. Time-series of the annual number of days with FFI above 4 and 5 have been studied both for these stations and using gridded data for the entire region.

Based on the analysis, a distinct trend towards an increased danger of fire can be observed. For all sixteen stations, the projected change in fire risk index by 2100 is statistically significant at the 95% confidence level. The number of days with very high fire risk is estimated to almost double during this century under the A2 emissions scenario (Figure 9.16, left). The changes indicated for a B2 emissions scenario are slightly moderated (Figure 9.16, right). The largest increases are registered for the northernmost stations (north of latitude 65°N).

Forest damage due to low temperature and pests in Sweden

Regional climate projections provide information on changes in temperature and precipitation regimes, including the frequency and severity of extreme events. The changes can alter the basic conditions for tree growth and the risk of large-scale ecosystem disturbance. Norway spruce, which is an economically important forest tree species in northern and central Europe, has two main vulnerabilities related to weather: frost damage after bud burst, and spruce bark beetle attacks following wind-storm damage. Both these damage types are related to specific weather situations rather than general climatic conditions, and an ensemble approach is useful in order to increase the sample size of weather situations and to obtain a measure of model variation.

In a warmer climate, the spring onset of vegetation processes begins earlier in the season when the sun is still low. Thus the earlier budburst exposes trees to an increased risk of radiation frost during long nights as well as winter cold air outbreaks, in some geographical areas actually increasing the frost risk despite generally warmer winters (Figure 9.17). See also case study in Section 6.6.4.

The spruce bark beetle can kill millions of trees during large outbreaks, which occur after wind-storm damage that produces ample breeding substrates. Warm weather conditions allow for a rapid development of the new generation. A warmer climate can therefore lead to increased frequency of late summer swarming, producing a second generation in southern Scandinavia and a third generation in central Europe (Figure 9.18).

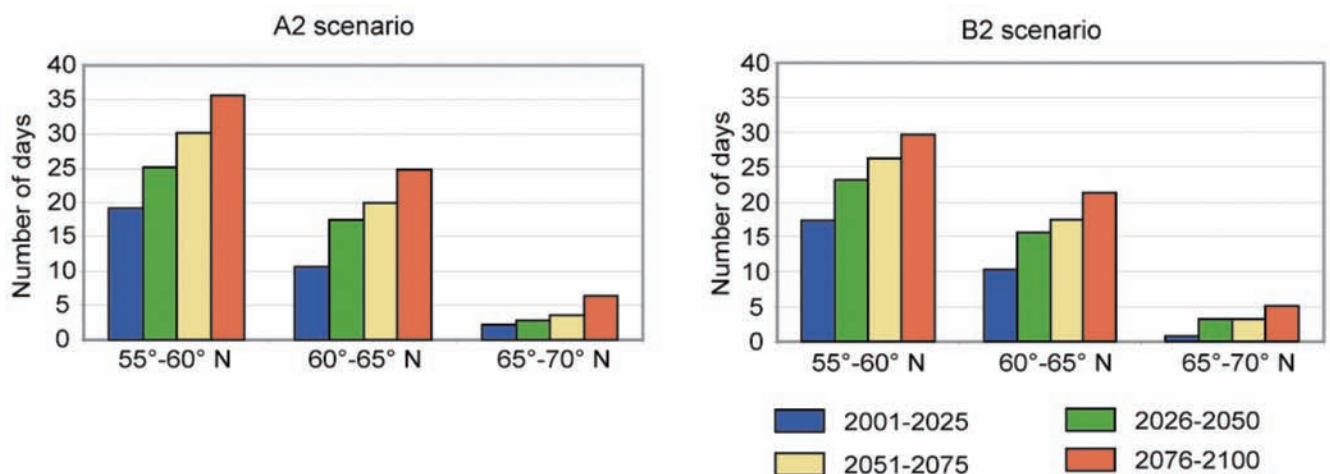


Figure 9.16: Number of days with very high forest fire risk projected for northern Europe during the 21st century. Results for latitudinal zones are averages from station data.

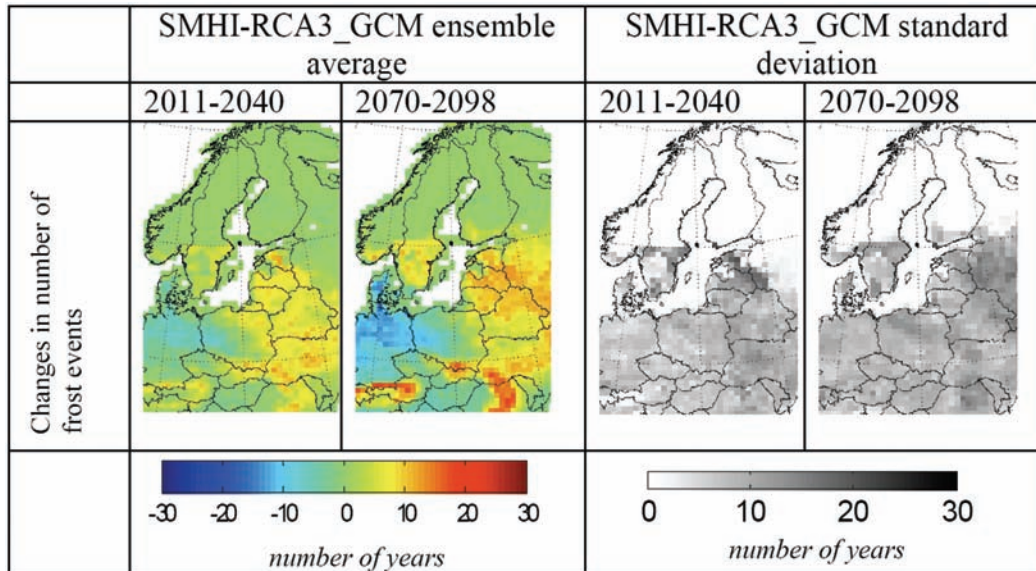


Figure 9.17: Projected changes in frequency of frost events after onset of vegetation processes for the periods 2011–2040 and 2070–2098 compared to the reference period 1961–1990, based on climate projections from one Regional Climate Model (SMHI-RCA3) nested in seven Global Climate Models.

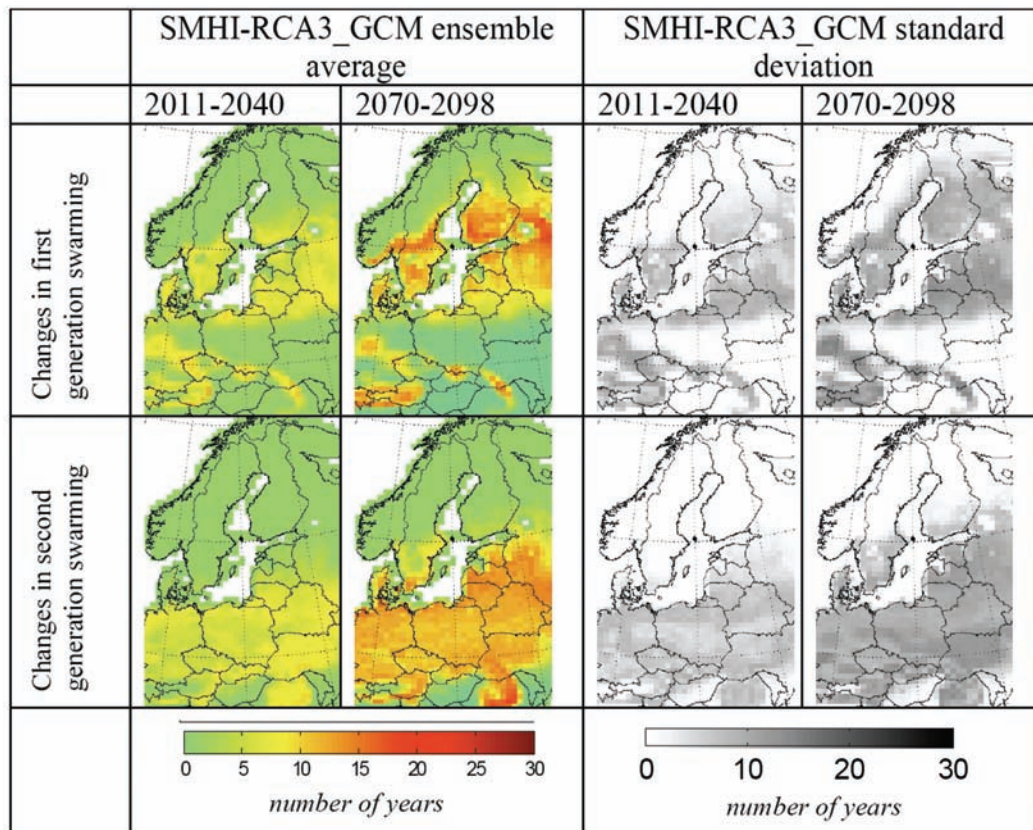


Figure 9.18: Projected changes in swarming frequency of the first and second generation of spruce bark beetle for the periods 2011–2040 and 2070–2098 compared to the reference period 1961–1990, based on climate projections from one Regional Climate Model (SMHI-RCA3) nested in seven Global Climate Models.

Potential impacts of changes in extreme weather on crop yields, water resources and health in Poland

The Institute for Agricultural and Forest Environment of the Polish Academy of Sciences used projections from six ENSEMBLES Regional Climate Model simulations to quantify selected extreme-weather indices for Poland, of importance for the agricultural, water and health sectors, for two time horizons

– a reference period (1961–1990) and a future period (2061–2090). Climate changes, and in particular increases in temperature and changes in rainfall, have strong impacts on agriculture in Poland, and crop yield depends critically on water availability during the plant development phase. For two important crops, potatoes and wheat, decreases in yield are projected for most of the country. The national means of change in yield are: –2.175 t/ha and –0.539 t/ha, respectively.

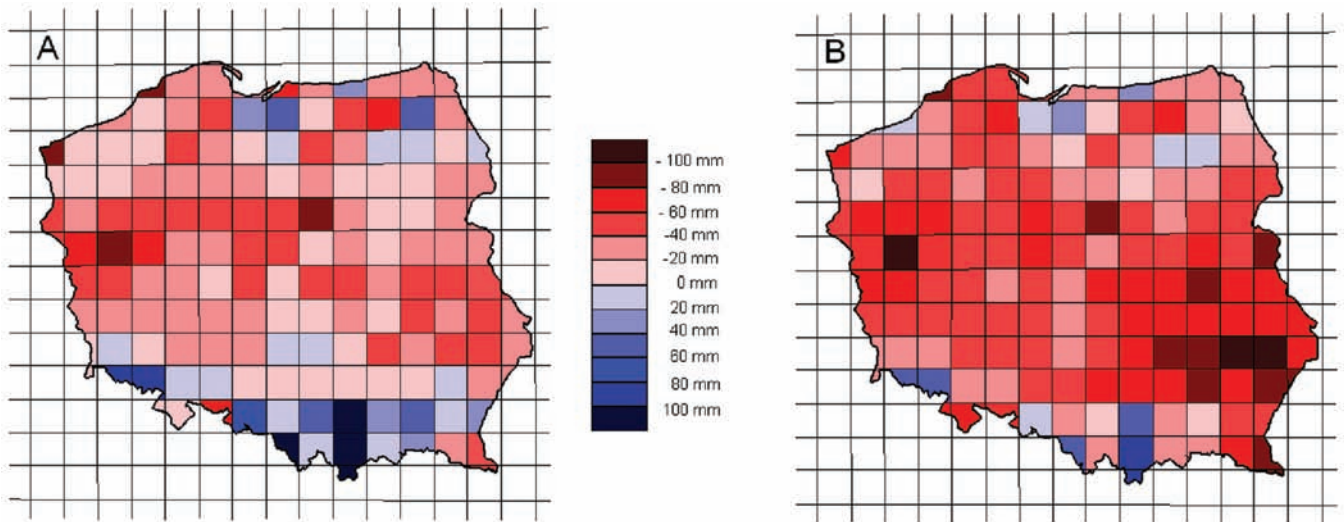


Figure 9.19: Changes in climatic water balance in summer in Poland: for the period 1961–1990 (a) versus the period 2061–2090 (b).

Increasing water deficit problems are projected in Poland under a changing climate. Already, in the present climate, during summer evapotranspiration exceeds precipitation over most of the country, hence the water storage (in surface water bodies, groundwater and soil) is depleted (Figure 9.19a). Summer precipitation deficit is projected to increase considerably in the future (Figure 9.19b), so that the additional water supplies (above precipitation) needed to realise the full potential for crop production are estimated to increase by half between the reference and future time periods (not shown).

As regards climate and health, the value of a composite index (computed as the product of the number of senior discomfort days recording a high heat index and the number of senior citizens aged 65 years or more) is projected to increase between two- and six-fold in 100 years. This is an effect of both increase in the number of senior discomfort days (nearly four times) and the number of senior citizens (over two times).

9.2.3 Assessing risks of impacts

A major novelty of the ENSEMBLES multi-model projections is that they offer a framework for generating probabilistic projections of future climate. This involves fitting a probability density function (PDF) to a large ensemble of individual projections of a given climate variable (Figure 9.11). For example, PDFs have been produced in the ENSEMBLES project for representing uncertainties among multi-model simulations with Regional Climate Models (RCMs) and with Atmosphere–Ocean General Circulation Models (AOGCMs). PDFs representing a wider set of uncertainties across climate models of varied complexity and incorporating observational constraints are also available in ENSEMBLES from the UKCP09 (UKCP, 2009) project of the UK Met Office Hadley Centre (MOHC), subsequently referred to as ‘MOHC ENSEMBLES probabilistic projections’, cf. Section 3.2.2.

A straightforward way to evaluate impacts is to run an impact model with each of the climate projections used to create the PDFs and then to determine the risk of impact on the basis of ensemble

impact outcomes (Figure 9.11, lower dashed arrow). However, given the large number of ensemble projections required for such a procedure, this may be precluded on practical grounds, especially for more complex impact models. An alternative method is to construct an impact response surface from a sensitivity analysis of the impact model with respect to key climatic variables (Figure 9.11, upper dashed arrow) and to superimpose onto this a probabilistic representation of projected changes in these same climatic variables. If the significance of an impact is judged relative to an impact threshold (i.e., some level of impact deemed unacceptable by a decision maker), then the risk of this threshold being exceeded can be estimated as the proportion of the superimposed climate PDF in the exceedance zone.

Five examples are presented to illustrate the response surface approach:

1. changes in exceedance of high or low lake water levels in Fennoscandia;
2. changes in water availability in large European river catchments;
3. the disappearance of permafrost features in northern Fennoscandia;
4. changes in durum wheat yields in the Mediterranean region;
5. estimates of nitrogen leaching and wheat yields in different regions of Europe.

Exceedance of low lake water levels in Fennoscandia

Critical thresholds for hydrological systems vary between basins. Although river discharge is generally the most important variable for consideration, time and space scales, and local topography play important roles. For Nordic conditions, with many lakes, water level can also be a critical factor. This is of particular consequence for the large natural lakes where outflows are nowadays regulated for optimal use of the water as a resource. Excessively high lake levels are a concern for flooding, while low levels pose a threat to availability and quality of water supply, and navigation. The specifics of each hydrological basin must ideally be taken into account in resolving where critical thresholds lie.

The city of Stockholm is centred at the outflow point where Lake Mälaren flows into the Baltic Sea. This large lake is a major source of drinking water and a means of transport for cities along its shores. A critical threshold for the lake was identified in terms of low water level. This was set to ‘50 consecutive days with water levels equal to or below 4.15 m’, the level where both navigation becomes difficult and the intake of water for local water supply can be inhibited. It also represents a higher risk for saltwater intrusion from the Baltic Sea.

Although there is already a risk of low water levels in today’s climate, this could increase considerably with a changing climate, as seen in the threshold response in Figure 9.20. Although annual precipitation shows a slight increase, summer precipitation is projected to decrease. This basin is therefore particularly sensitive to how seasonal precipitation changes are represented in creating response surfaces. Note that the results shown here are preliminary and do not take into account the full range of the ENSEMBLES simulations.

Water availability in large European river catchments

We analysed the risk of societal vulnerability thresholds of water availability being exceeded in eighteen major river basins in Europe under climate change projections from six RCMs for the year 2100 under the A1B scenario. Vulnerability thresholds were based on high flow (Q_{20}) and low flow (Q_{80}) indicators as well as indicators of water stress (withdrawal to availability – w.t.a.; water availability index – w.a.i.). These, together with projected climate changes for each basin, are superimposed onto response surfaces of water availability (Figure 9.21). The vulnerability classification is based on the absolute number of climate modelling projections under which the above described thresholds are violated in 2100.

The most vulnerable basins in Europe are the Tiber and Vistula basins because both the low flow threshold and water stress thresholds are violated under all of the climate scenario simulations. For example, the Vistula and Tiber fall into the

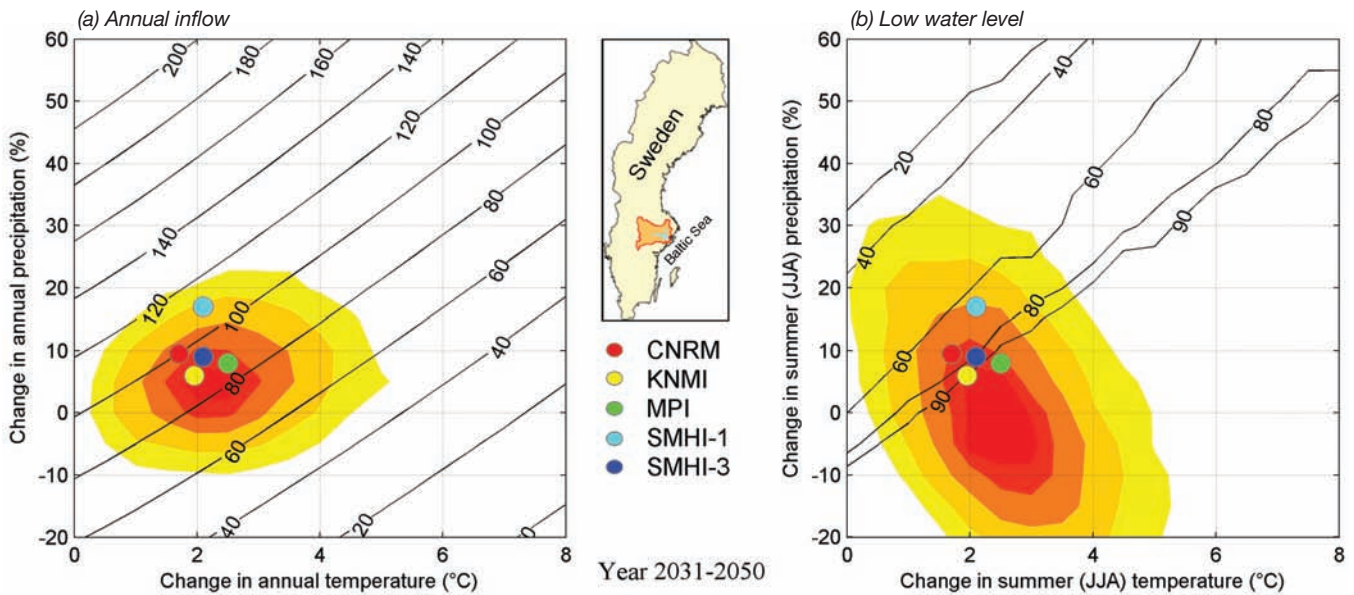


Figure 9.20: Impact response surfaces for Lake Mälaren in Sweden: (a) mean annual inflow to the lake as a percentage of present day inflow; (b) likelihood (in percent) of summer water level below the target operating threshold for a consecutive period of 50 days. Climate projections are depicted as probability density plots for the period 2031–2050 based on the MOHC ENSEMBLES probabilistic projections. The coloured area encloses approximately 90% of all projected outcomes. Also shown are projections from five RCM simulations (coloured dots). Impact response surfaces were created from some 300 simulations using the HBV hydrological model.

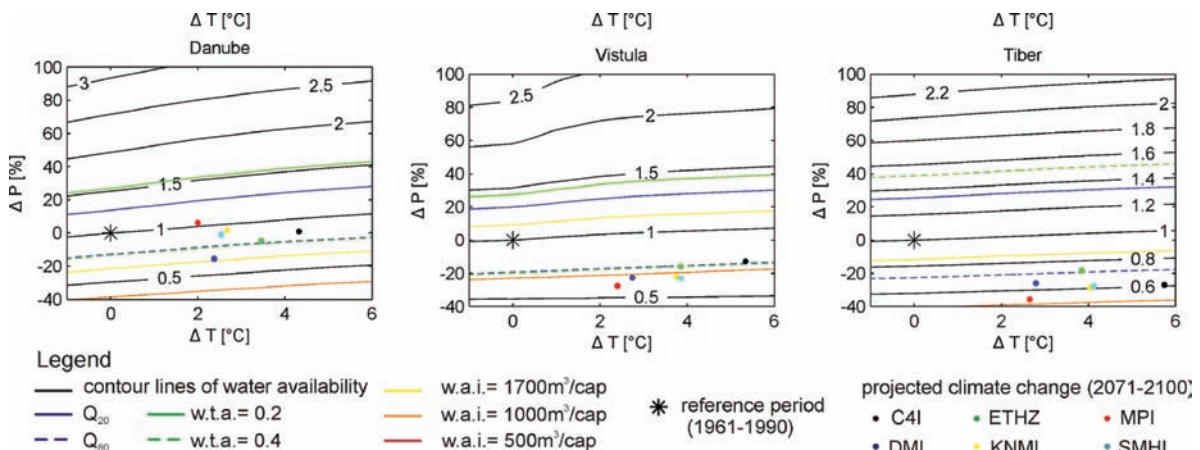


Figure 9.21: Response surfaces of water availability for three European catchments with societal vulnerability thresholds and RCM projections of climate change for 2071–2100 under the A1B scenario.

second highest (medium) water stress class, based on the w.a.i. The Danube Basin might be facing lower water availability in the future, as projected by five of the six RCMs. In general, southern European basins suffer from decreasing availability, while northern basins have to cope with increasing water availability, even violating high flow thresholds (not shown). Climate change projections for the central European basins are scattered around the '1'-line, showing both projections of increase as well as decrease of water availability.

Risk of palsa mire disappearance in Fennoscandia

Palsas are mounds with a permanently frozen core that occur at the edge of the permafrost zone across the circumpolar north. They are ecologically valuable for birds, representing a priority habitat listed by the EU Habitats Directive. There is evidence that they are already disappearing and this is presumed to be due to observed regional warming.

Figure 9.22a is an impact response surface showing the area climatically suitable for palsas with respect to changes in two key climate variables, mean annual temperature and mean annual precipitation, relative to the 1961–1990 observed climate. A critical threshold of impact was selected as the total disappearance of suitable area for palsas (white area in Figure 9.22a).

Scatter plots of projected mean annual temperature and precipitation change over Fennoscandia for the A1B emissions scenario were produced from the MOHC ENSEMBLES probabilistic projections and presented as climate surfaces for 20-year periods at decadal intervals throughout the 21st century. These were then superimposed on the impact response surface (Figure 9.22a). The climate surface falling in the area beyond the -100% isoline represents the risk of total disappearance of palsas at different time periods in the future. Figure 9.22b indicates that it is *likely* ($>66\%$) that all suitable areas will disappear by the end of the 21st century under the A1B emissions scenario.

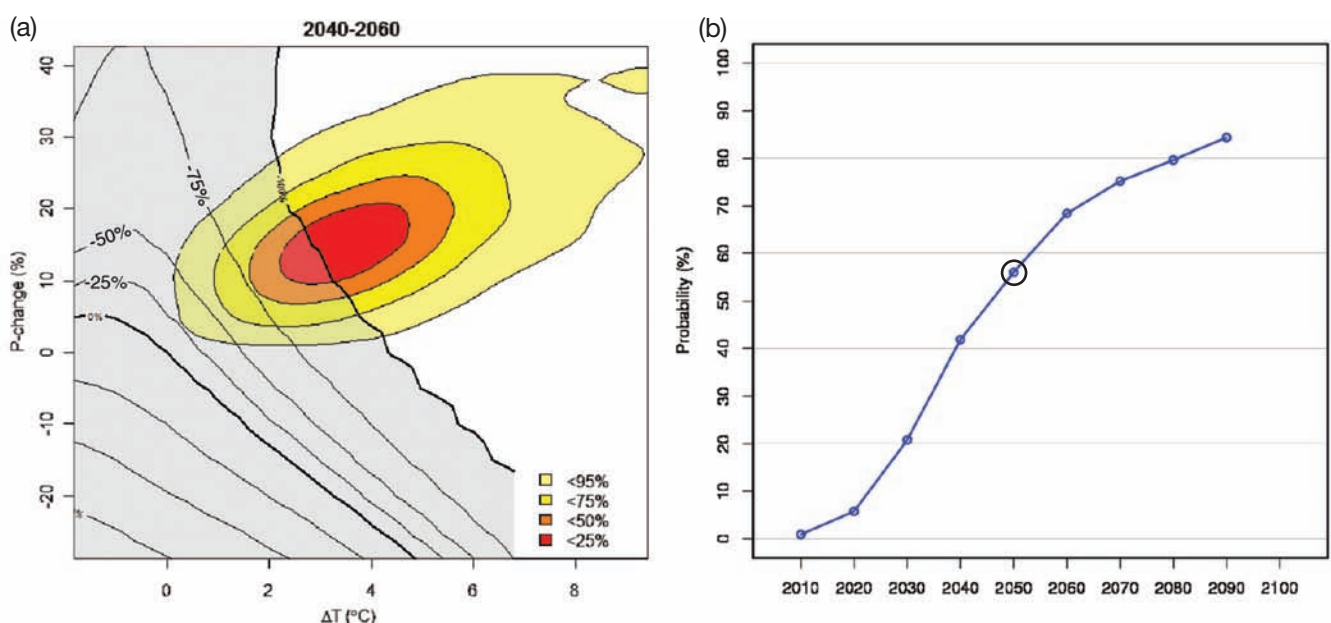


Figure 9.22: (a) Impact response surface showing modelled percentage change in area of suitability for palsa mires in Fennoscandia as a function of changes in mean annual temperature and precipitation relative to 1961–1990 (isolines). A joint PDF of future climate by the period 2040–2060 (coloured areas) is superimposed, about half of which lies in the area exceeding the -100% isoline (i.e., complete loss of palsa mire suitability). (b) Probability of complete loss of palsa suitability at different future time periods. The value for 2040–2060 taken from (a) is circled.

Risk of wheat yield shortfall in the Mediterranean region

Durum wheat is a rain-fed crop that it is widely cultivated over the Mediterranean Basin. Projected climate changes in this region, in particular rising temperature and decreasing rainfall, may seriously compromise durum wheat yields, thus representing a serious threat for the cultivation of such a typical Mediterranean crop.

A wheat simulation model (SIRIUS Quality) was used to create yield response surfaces with respect to variations in mean annual temperature and mean annual precipitation for each climate model grid box in the region. 10,000 projections of the same climate variables, sampled from the joint PDF for the A1B scenario from the MOHC ENSEMBLES probabilistic projections, were overlaid on the yield response surfaces to estimate the future yield distribution at each grid box. A critical yield threshold was defined as the 20th percentile of yields estimated for present-day climate, and the future risk of yield shortfall was estimated as the relative frequency of yields projected to fall below this threshold according to the climate projections. Baseline climate in the region was represented using the ENSEMBLES E-OBS 25 km interpolated daily observational dataset for the period 1961–1990.

Figure 9.23 depicts the change in risk of yield shortfall for four 20-year periods in the future under climate projected for the A1B scenario compared with the present-day. Green areas indicate a decreased risk of shortfall; pink and red areas show an increased risk. In contrast to previous studies suggesting that the beneficial effects of elevated atmospheric CO_2 concentration over the next few decades would outweigh the detrimental effects of the early stages of climatic warming and drying, the results here are of more concern (Figure 9.23a). They indicate declining risk over only a few small areas at the northern fringes of the Mediterranean zone. For the majority of the case study area, there is increased risk of

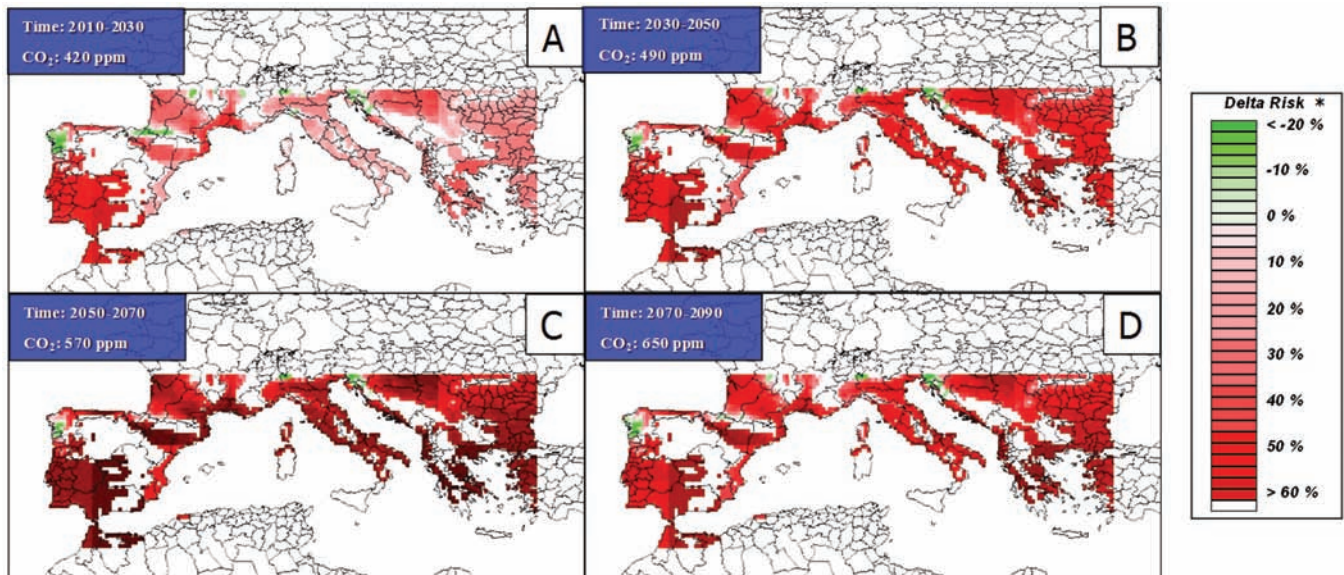


Figure 9.23: Spatial plots of changes in durum wheat risk of yield shortfall by: (a) 2010-2030, (b) 2031-2050, (c) 2051-2070 and (d) 2071-2090, relative to the baseline (1961-1990). Shortfall is defined as yields below the 20th percentile yield calculated for the present-day period 1990-2010.

yield shortfall, which becomes more severe as the century progresses, reaching a maximum by mid-century (Figure 9.23b,c) before declining somewhat towards the end of the century (Figure 13d). Note that there are some local gaps in coverage of both observed and projected climate (e.g. over Sardinia, and parts of southern Italy). These, and areas above 700m elevation, where durum wheat is rarely cultivated, were excluded from the analysis and are indicated as white areas on the maps.

A probabilistic assessment of climate change impacts on wheat yield and nitrogen leaching

Climatic conditions have a high impact on both crop yields and nutrient losses from arable land. To assess the effects of future climate change on crop yields and nitrate leaching, detailed simulation under predicted future climatic conditions has been conducted. Continuous winter wheat grown on two soil types – sandy (S) and sandy loam (SL) – under conditions representa-

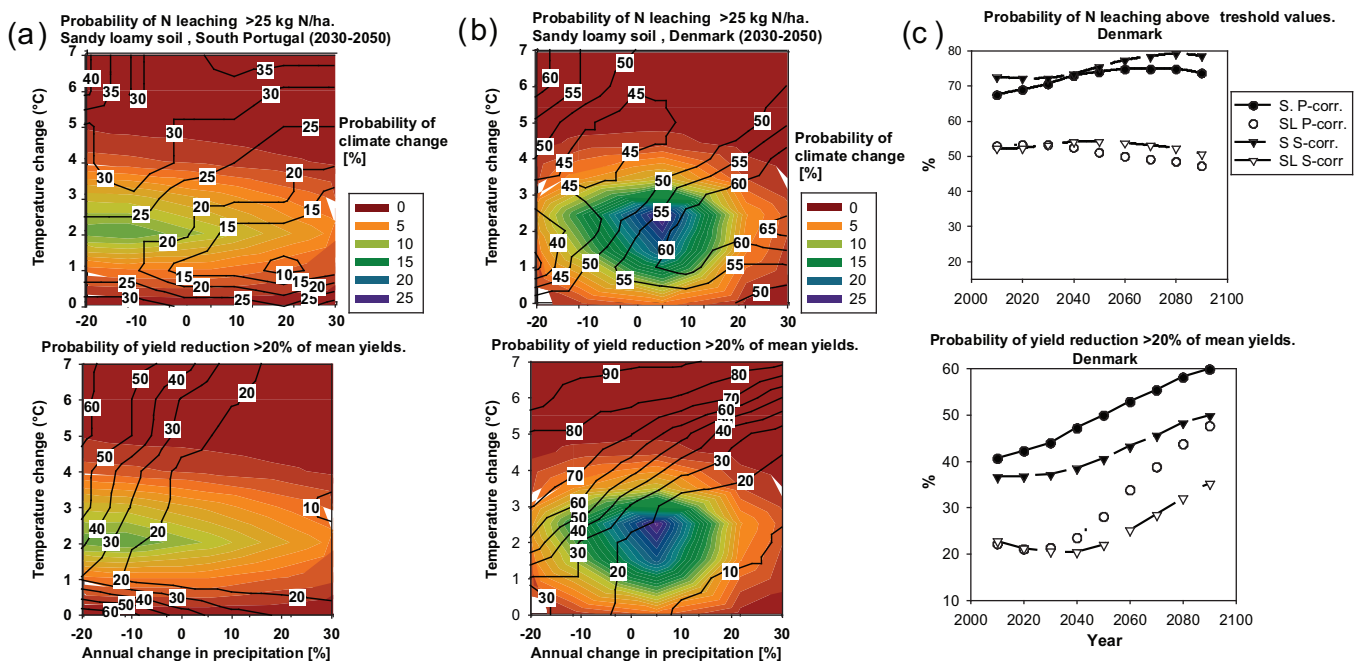


Figure 9.24: DAISY model simulated probability response functions (isolines) of N leaching above threshold values (upper panels) and probability response functions of yield reduction >20% of mean yields (lower panels) calculated for south Portugal (a) and Denmark (b). Coloured contours show the relative probability of climate change outcomes calculated for binned classes of changes in temperature (1°C intervals) and precipitation (10% intervals) and then interpolated. (c) Calculated cumulative probability of N leaching above 25 and 40 kg N/ha for a sandy loam and sandy soil, respectively, and yield reduction >20% of average yields. Calculations are for decadal intervals from 2010 to 2090 and for combinations of soil type – sand (S) and sandy loam (SL) – and methods to change precipitation – proportional (P-corr.) and seasonal correction (S-corr.).

tive of Denmark and southern Portugal were simulated using the crop, soil, nitrogen simulation model DAISY. The model was used to provide response functions for effects of changes in annual temperature and rainfall on grain yield and nitrate leaching. Two different methods were tested to obtain daily values of rainfall changes; either a straightforward correction method where the same correction is applied to all days in the year, or a seasonal correction where seasonal patterns in rainfall change for the specific site are used to estimate the correction for rainfall change. To obtain a measure of the predicted climate effect on N leaching and yields, a cumulative probability of N leaching above arbitrary threshold values (25 kg N/ha for sandy loamy soils and 40 kg N/ha for sandy soils) and the cumulative probability of an arbitrary reduction in yield of >20% were calculated for each combination of soil, climate data and region. The results were combined with future climate projections for the years 2000–2100 using PDFs obtained in the MOHC ENSEMBLES probabilistic projections.

In Figure 9.24a,b, examples of PDFs representing the probability of climate change for the years 2030–2050 are superimposed on impact response functions calculated with the DAISY model for N leaching (upper panels) and yield reduction (lower panels) for southern Portugal (a) and Denmark (b). Figure 9.24c shows the calculated cumulative probability for N leaching (upper panel) and yield reduction (lower panel) for the years 2010–2090 in Denmark. Each point in Figure 9.24c is calculated by combining PDFs describing the probability of climate change with the DAISY response functions from Figure 9.24b. In general, the responses to climate change of both N losses and yields are different in the two regions. For southern Portugal (not shown) the probability of N leaching above threshold values is almost unchanged under future climate conditions, whereas for Denmark (Figure 9.24c) an increase for the sandy soils and a slight decrease for sandy loamy soils are obtained. The probability of a yield reduction exceeding 20% is seen to increase for sandy soils in Denmark during the whole period. The lowest risk of yield shortfall was found for sandy loam soils, which is believed to be due to the higher root zone capacity of this soil type, which reduces periods with plant water stress, and thereby minimises the effect of periods with low precipitation.

9.3 Impact modelling at seasonal to decadal time-scales

9.3.1 Introduction

The research here¹ builds on pioneering work started in DEMETER, introducing a wider range of impacts to the utilisation of multi-model ensemble prediction systems at seasonal scale in preparation for time-scales beyond this. Many operational activities, for example energy demand, insurance risk, health risk and agricultural yield, have a significant operational need for forecasts of risk, demand or yield for the forthcoming season. In Europe it may be information in terms of relative frequency of winter storms or cold spells during the

winter, whereas in the tropics, especially Africa, it may be the amount of rain in the forthcoming rainy season. The rains lead to impacts on crop yield and thus food security and also impact on the relative risk of disease, especially from vector-borne diseases such as malaria.

We also transferred techniques used with seasonal-scale forecasts to work with longer climate time-scales. An example is the use of a probabilistic approach to represent model uncertainty with the RCM data for animal health impacts in Europe. Much effort has been focused on post-processing activity including downscaling, dressing and weighting, and this has involved interaction with other Research Themes within the project

We have a strong emphasis on building integrated modelling systems that are validated with current climate observations, developed as reanalysis, used to drive the impacts models forming control runs before using future climate projection runs. The majority of the work has focused on using the seasonal ensemble prediction system outputs but with the knowledge exchange to the model runs using the RCM datasets.

We also see the importance of the portability of an impacts model, e.g., between seasonal scale and climate change time-scales – the Liverpool malaria model (LMM) has now been developed to work with a range driving datasets from different climate modelling systems.

By using impacts models that make use of daily data from the ensemble prediction systems, we capture the dynamics of the climate in a way that is not possible when using monthly or annual mean values. By dynamic we suggest that the frequency and timing of meteorological events have a profound influence on environmental and biological systems when run on a seasonal basis. It is clear, in some regions, that skill is being impacted through these dynamics as well as through mean prediction at seasonal or annual scales.

9.3.2 Research results

In Figure 9.25 it is shown how multi-model ensemble seasonal hindcasts developed in ENSEMBLES have been incorporated into an operational crop yield forecasting system for wheat and other crops in Emilia-Romagna, Italy.

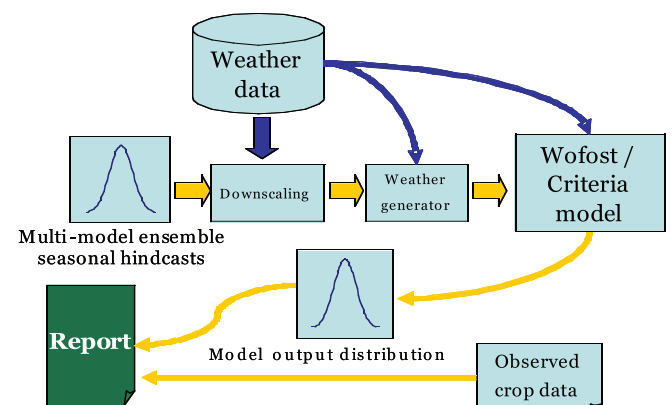


Figure 9.25: How multi-model ensemble seasonal hindcasts developed in ENSEMBLES were incorporated into an operational crop yield forecasting system.

¹ The results presented in this section are preliminary – studies are still ongoing, and so far few have been published. For this reason, and to aid readability, references are not included in this section.

Crop modelling – tropics

This example shows the use of DEMETER seasonal forecasts in crop yield models for groundnuts in Gujarat. In Figure 9.26 note how closely the modelled yield distribution captures the observed crop yield. For planning purposes it is important to show the full range of modelled outcomes to inform the planning process, as even a relatively small chance of a very low crop yield, below a locally determined threshold, may require special contingency and planning action based on experience of past performance of the integrated modelling system.

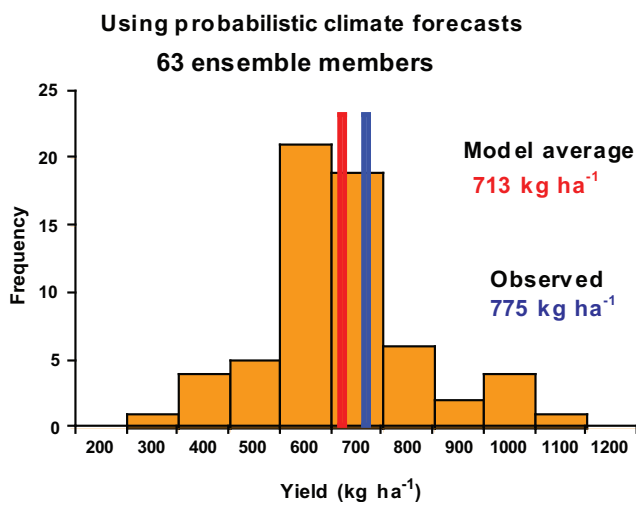


Figure 9.26: Use of the DEMETER multi-model ensemble for groundnut yield in Gujarat, 1998 (from Challinor et al., 2005).

Crop modelling – Europe

The system shown for Emilia-Romagna adapted and developed an operational crop forecasting system (seen in Figure 9.26) to use downscaled ENSEMBLES seasonal forecasts. Downscaling was used so that the spatial resolution of the datasets was as close as possible to the plot area, as opposed to the several-hundred-kilometre resolution of the seasonal forecast model outputs. This example investigates the reduction in soil moisture under a field of cultivated kiwi fruit. The models driven by seasonal forecast prediction and actual weather observations are compared with the measured soil moisture. It can be seen in Figure 9.27 that the spread of the seasonal forecast-driven crop model reproduces a distribution of soil moisture levels that captures both the observation-driven and weather station model-driven results. These early results are promising and the system may have some skill in the region. Further work extending the dataset back for 20 years will allow skill scores to be computed between the weather station control run and ensembles forecast.

The ENSEMBLES project has shown that it has utility in crop modelling both in Europe and in the Indian subcontinent. The ability of governments in both regions to have access to a prediction of crop yields is important for both food security and for the use in intervention, storage and planning purposes.

Winter wind storms – Europe

Winter wind storms are a major risk in Europe, especially for insurance companies who need to assess their level of risk for both commercial and regularity purposes. Figure 9.28 shows the extended winter (October–April) storm frequency between a series of modelled datasets. There are model resolution differences between the data in (b) and (d), which have a lower resolution than those from the newer model system which is the core of the ENSEMBLES system in (c) and the reanalysis in

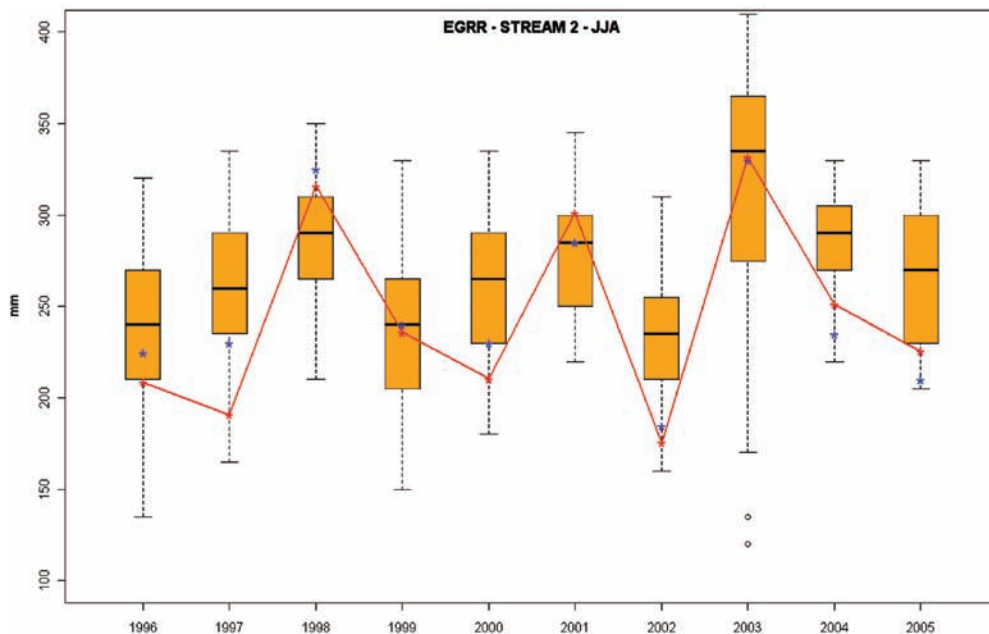


Figure 9.27: The comparison between actual tensiometer-based irrigation data (red line) for kiwi fruit at Brisighella (180 m asl), Emilia-Romagna, Italy, and the assessment of irrigation water needs (box and whiskers), computed using downscaled ENSEMBLES seasonal hindcasts for the JJA period as input for the CRITERIA water balance model of ARPA Emilia-Romagna, for the years 1996–2005. The multi-model runs use five models, nine members, and five weather generator replicates (225 member replicates). Blue stars represent the irrigation need computed by the model using actual weather data.

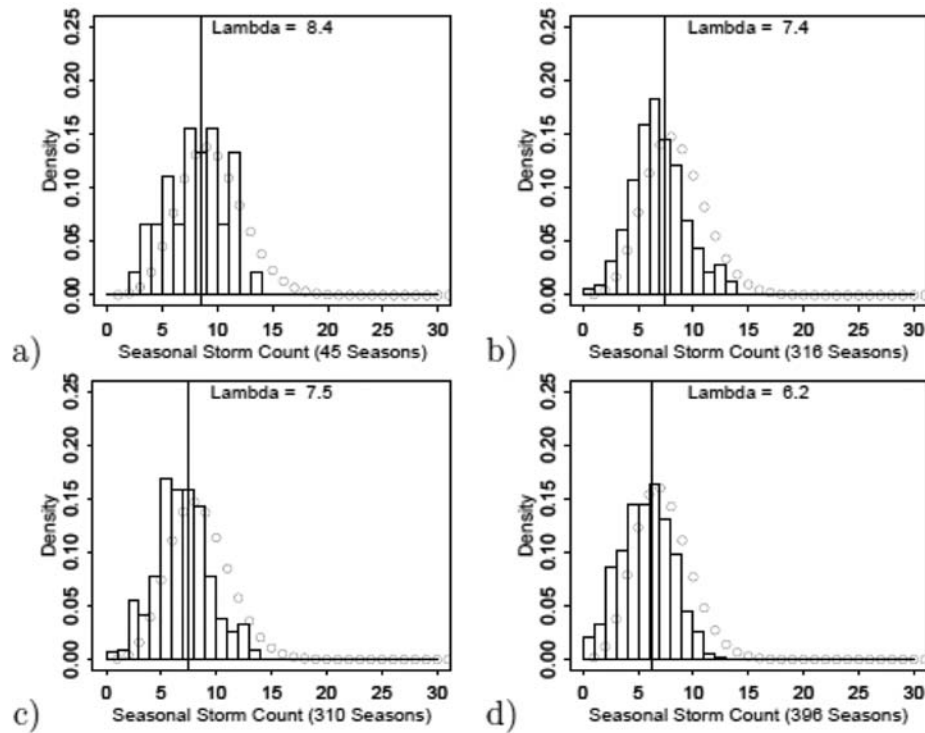


Figure 9.28: The extended winter (October–April) storm frequency between a series of modelled datasets: (a) the ERA-40 reanalysis data, (b) the ECMWF operational seasonal forecasting System-2, (c) the latest ECMWF operational System 3, (d) the DEMETER hindcasts.

(a). The model physics also have a role, with similar model physics in (a), (b) and (d), whereas the newer data in (c) have revised model physics. The differences in the distributions show that direct comparison of modelled wind-storm climatologies should not be made, but instead calibration techniques need to be developed. This has led to the development of calibration techniques which show how to apply development work undertaken with research model datasets to operational forecasts.

Forecasting interannual malaria risk

Through ENSEMBLES there has been continued development of the dynamic malaria model for use with seasonal-scale EPS. The insights gained have also started to be used for the application of EPS to other diseases not discussed here. The malaria model has used it to test both a series of weighting studies and to test ensemble dressing techniques. The weighting studies show that, on the whole, the multi-model ensemble performs as well as any model weighted ensemble combination. The ensemble dressing used a range of dressing techniques, originally developed by a partner within the consortium; however, the ensemble dressing work remains inconclusive, as the improvement in model skill is marginal – but on the other hand, the dressed ensemble was not found to lose skill either! The main problem is that to calibrate a once-per-season event such as the seasonal malaria risk, the number of events in the model archive is too small to effectively refit the distribution using techniques that were developed for the much more plentiful daily maximum temperature analysis.

Further efforts have been undertaken to show the probabilistic output of the malaria model in a decision-maker recognisable format. In Figure 9.29, the annual probability of exceeding the

threshold for the upper tercile event is shown. Years where the event was observed are shown by the solid bars. The decision maker is encouraged, given the performance of the model for their region, to decide what probability of the event would trigger a response and how this probability threshold would have led to hits, misses and false alarms over previous years. This example is for malaria forecasts in Botswana.

Major improvements have been seen in the quality of the seasonal forecasts in ENSEMBLES for use in West Africa over what was observed with the DEMETER dataset. Grid points that have high interannual variability in modelled malaria incidence, i.e., potential epidemic zones in the model are selected using NCEP reanalysis-driven runs of the Liverpool malaria model. The geographical position of these zones should be (1) consistent between each of the seasonal forecast models and the reanalysis control run and (2) that, when verified against the reanalysis-driven runs, have some skill above climatology. The results shown in Figure 9.30 indicate that the majority of these grid points are skilful. In practice, this shows that the integrated malaria model system has the potential to give a lead time of 4–6 months from issue. Such a system could contribute to an early warning system, giving some indication of those zones that might have a higher than average epidemic transmission risk in the forthcoming rainy season. An early warning system would also contain local knowledge of typical transmission patterns and recent intervention programmes.

The work in West Africa was undertaken as a joint initiative between EMSEMBLES and the FP6 AMMA (African Monsoon Multidisciplinary Analysis) project.

The ENSEMBLES project also provided RCM runs for a large domain across Africa at 50 km resolution as part of its

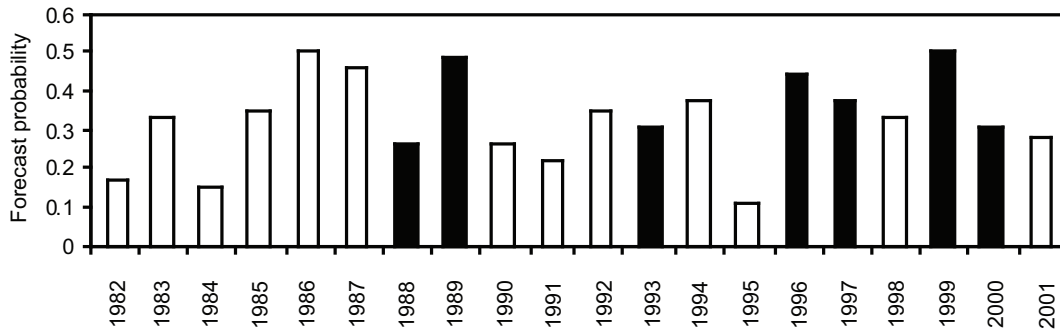


Figure 9.29: The annual probability of exceeding the threshold for the upper tercile event. The solid columns are where the event is observed.

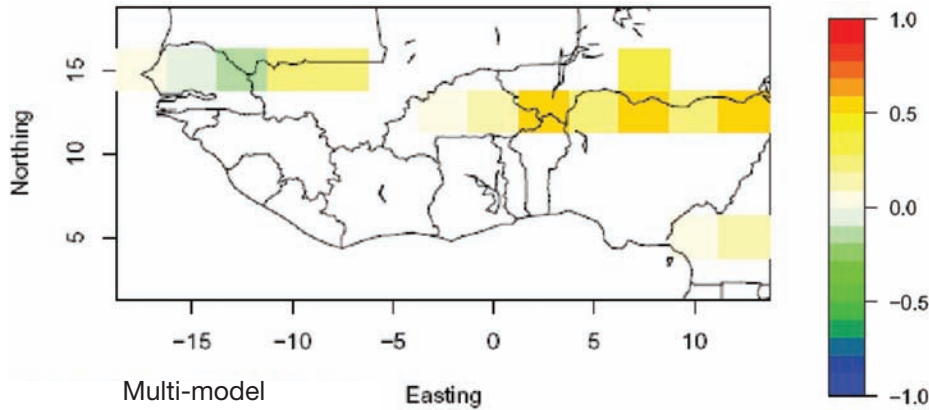


Figure 9.30: Skill of ENSEMBLES-driven Liverpool malaria model (LMM) incidence for the above upper tercile event, as measured by ROCSS relative to the ROCSS of the persistence-type control run (where positive) for grid points categorised as epidemic (mean monthly incidence >1/100 people, CV>0.5) according to NCEP-driven incidence. May forecast months 4–6 (ASO) 1971–2005 for all ensemble members of the ENSEMBLES multi-model.

collaboration with FP6 AMMA. The LMM was successfully adapted to run with the daily RCM data. At present only the current climate control runs have been completed. The RCMs use ERAINTERIM reanalysis for their boundary conditions and the coarser resolution ERAINTERIM and NCEP reanalysis-driven LMM runs are shown for comparison with the RCM-driven outputs in Figure 9.31. Initial (non-bias-corrected) results show a good comparison between the RCM-driven runs and a fair comparison with the reanalysis datasets and known areas of malaria transmission in West Africa.

Spread of emerging animal diseases captured by Regional Climate Model data

This work, co-funded with a spin-off project, in cooperation with veterinary epidemiologists, has advanced the use of Regional Climate Model (RCM) output to run a Ro disease transmission model for the spread of bluetongue disease in sheep and cattle, which has recently emerged in northern Europe. The plots (not shown) of bluetongue risk for the recent climate time-slices using the RCM model runs forced by ERA-40 boundary conditions show a very close comparison with known bluetongue virus outbreaks.

In Figure 9.32 it can be seen that the models predict an increase in bluetongue disease risk over northern Europe (especially the UK), south-eastern France, northern Spain, Italy and Greece for the period 2031–2050. Changes over northern Europe are

mainly related to changes in the bluetongue virus replication rates related to more favourable temperature conditions, whereas over southern Europe the change is mainly related to the spread and increase of the vector, namely the midge, *Culicoides imicola*.

Seasonal forecasts for electricity demand – uses of downscaling

A significant amount of work has been undertaken with the newly developed downscaling portal. The application here is the use of downscaling for catchment regions for the power industry. Generally, in the mid-latitudes, skill from seasonal forecasts is relatively low or current forecasting systems have no skill. Through spatial disaggregation of the datasets and the use of local target data from long-term established weather station sites, it is possible to both improve the skill in the ensemble forecasts and provide datasets at local scales, which thus become useful for impacts studies. The results, produced by the R&D division of a major European power supplier, are reanalysed with an enhancement of skill, depending on variable, location, and season and lead time, as well as the careful choice of downscaling methods and selection of predictors. It is fair to say, however, that the field of downscaling seasonal lead time ensemble prediction systems is still in its infancy. However, the work completed in ENSEMBLES has shown some potential, suggesting that with the ongoing improvement in ensemble seasonal forecasting systems, downscaling will become an important post-processing step. This will be especially the case

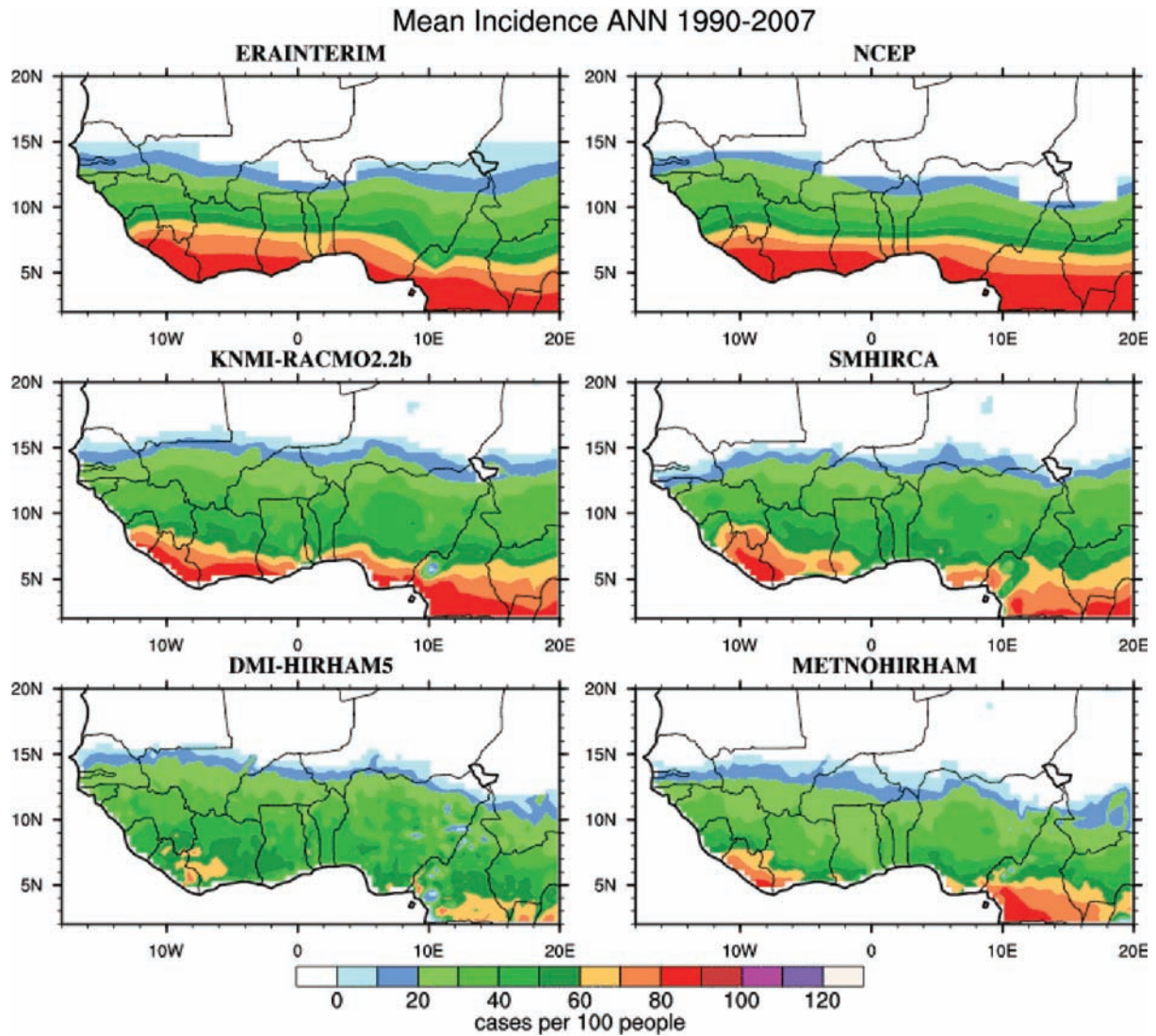


Figure 9.31: Mean annual malaria incidence for 1990–2007 (cases per 100 people) from the Liverpool malaria model (LMM) for West Africa. The LMM is run with ERAINTERIM and NCEP reanalysis (top row) and four RCMs for the ERAINTERIM control runs (middle and lower rows).

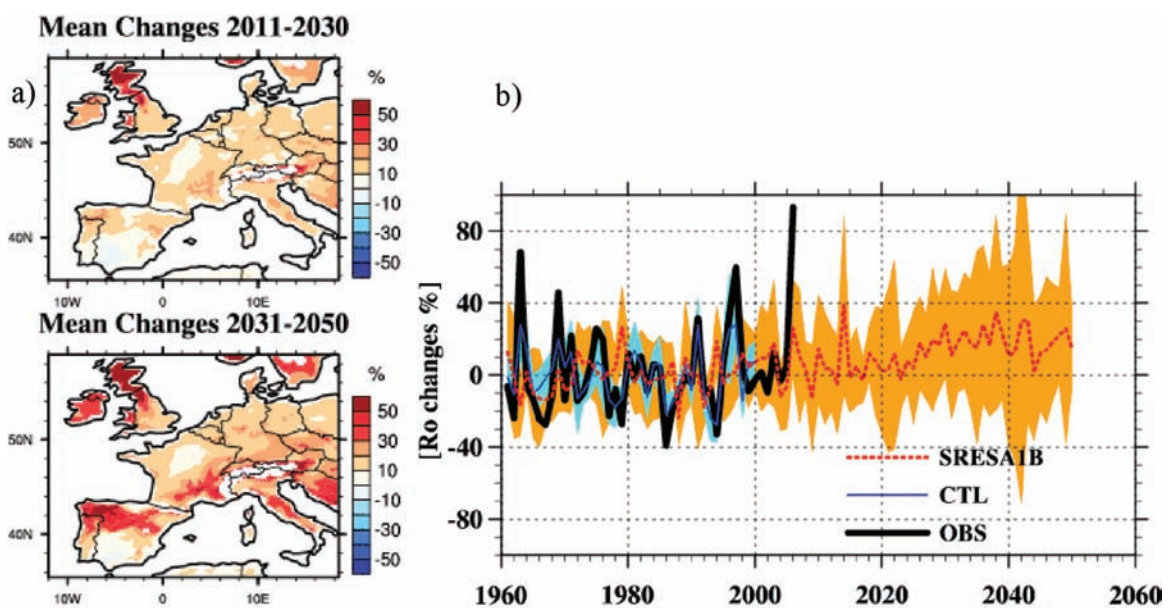


Figure 9.32: (a) Simulated bluetongue disease risk changes over Europe (% , with respect to 1961–2000) for the delimitated summer–autumn season ASO; (b) bluetongue disease risk index for the season ASO over northern Europe (12°W–18.5°E, 48°N–59°N). The gridded ECA observations are displayed in black, the control (CTL) (SRES A1B) multi-model ensemble means are displayed in dark blue (red). The light blue (orange) envelope highlights the multi-model spread in SRES A1B projection runs.

for the use of these data in the mid-latitudes and for impacts studies and its use by industry, e.g., power supply.

The downscaling results shown in Figure 9.33 are for the temperature at 2 m in a series of river basins in France. In general it shows that downscaling makes an improvement in the forecasting of 2 m temperature compared with the raw data prior to downscaling.

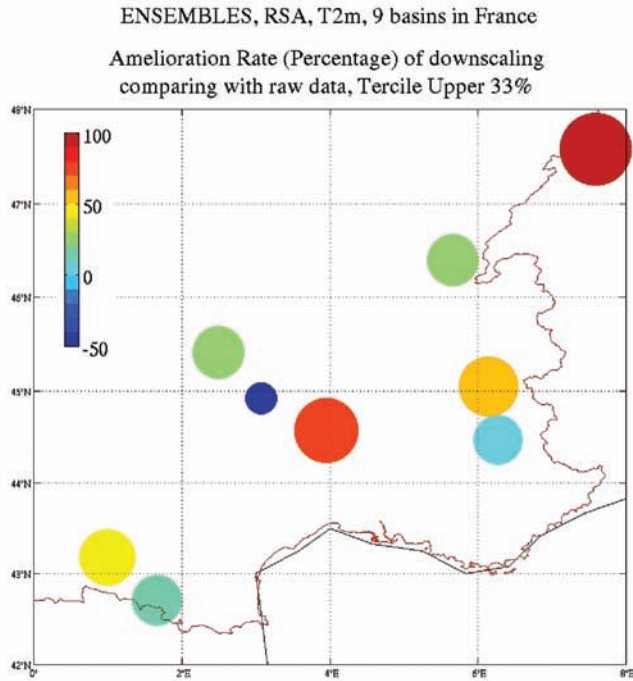


Figure 9.33: The improvement in temperature prediction following downscaling for a series of river basins in France, for the upper tercile event.

9.3.3 Summary impact modelling at seasonal to decadal time-scales

ENSEMBLES has allowed a wide range of impacts groups to work with probabilistic seasonal forecasts. Much work has been undertaken in data post-processing and downscaling. It is possible that these techniques can add to areas that have marginal skill, but where forecasts have no skill they cannot currently be used. The idea of validation of hindcasts against reanalysis control runs is now firmly established. Impacts models can now be moved across climate modelling streams, seasonal EPS to RCMs, and the methods developed and validated at seasonal scales are now being transferred to longer climate-change time-scales within the development of seamless integration of impacts models with a suite of climate prediction and projections models.

As seasonal forecasts improve in future, more user communities will use the approaches and methods developed in ENSEMBLES to utilise the forecasts. Looking forward: the emerging discipline of initial-condition decadal ensemble prediction will also be able to utilise the techniques developed here for seasonal-scale forecasts, and the seasonal impacts communities will be able to map future potential risks over the forthcoming decade. Finally, a number of the impacts models refined through the ENSEMBLES project are now ready for limited-release operational use.

References

ENSEMBLES publications are highlighted as bold text.

- Betts RA, Boucher O, Collins M, Cox PM, Falloon PD, Gedney N, Hemming DL, Huntingford C, Jones CJ, Sexton DMH, Webb MJ, 2007. Projected increase in continental runoff due to plant responses to increasing carbon dioxide. *Nature* 448, 1037–1041**
- Blyth EM, Gash JHC, Lloyd A, Pryor M, Weedon GP, Shuttleworth WJ, 2009. Evaluating the JULES land surface model energy fluxes with FLUXNET data. *Journal of Hydrometeorology*, in press.
- Bondeau A, Smith PC, Zaehle S, Schaphoff S, Lucht W, Cramer W, Gerten D, Lotze-Campen H, Müller C, Reichstein M, Smith B, 2007. Modelling the role of agriculture for the 20th century global terrestrial carbon balance. *Global Change Biology* 13, 679–706.**
- Booth BBB, Jones CD, Collins M, Totterdell IJ, Cox PM, Sitch S, Huntingford C, Betts R, 2009. Global warming uncertainties due to carbon cycle feedbacks exceed those due to CO₂ emissions. *Nature Geoscience*. Submitted.
- Cadule, P, P. Friedlingstein, L. Bopp, S. Sitch, C.D. Jones, P., Ciais, S.L. Piao and P. Peylin. Benchmarking coupled carbon-climate models against long-term atmospheric CO₂ measurements (in revision), *Global Biogeochemical Cycles*.
- Challinor AJ, Slingo J, Wheeler T, Doblus-Reyes F, 2005. Probabilistic hindcasts of crop yield over western India. *Tellus* 57A 498–512.**
- Cox PM, 2001. Description of the ‘TRIFFID’ Dynamic Global Vegetation Model. Hadley Centre Technical Note 24.
- Denman KL, Brasseur G, et al., 2007. Couplings between changes in the climate system and biogeochemistry. In: *Climate Change 2007: The Physical Science Basis. Contribution of Working Group I to the Fourth Assessment Report of the Intergovernmental Panel on Climate Change* (S Solomon, D Qin, M Manning, Z Chen, M Marquis, KB Averyt, M Tignor, HL Miller, eds). Cambridge University Press, Cambridge UK and New York, 499–587.
- Falloon P, Betts R, Bunton C, 2007. New Global River Routing Scheme in the Unified Model. Hadley Centre Technical Note 72.
- Fekete BM, Vörösmarty CJ, Grabs W, 2002. High-resolution fields of global runoff combining observed river discharge and simulated water balances. *Global Biogeochemical Cycles* 16, 1042, doi:10.1029/1999GB001254.
- Friedlingstein P, Cox PM, Betts R, et al., 2006. Climate-carbon cycle feedback analysis: results from the C4MIP model intercomparison. *Journal of Climate* 19, 3337–3353.
- Gerten D, Schaphoff S, Haberlandt U, Lucht W, Sitch S, 2004. Terrestrial vegetation and water balance: hydrological evaluation of a dynamic global vegetation model. *Journal of Hydrology* 286, 249–270.
- Giannakopoulos C, P Hadjinicolaou, C Zerefos G Demosthenous, 2009. Changing energy requirements in the Mediterranean under changing climatic conditions, *Energy* 2009, 2(4), 805–815; doi:10.3390/en20400805.**
- Heimann M, Esser G, Haxeltine A, Kaduk J, Kicklighter DW, Knorr W, Kohlmaier GH, McGuire AD, Melillo J, Moore B III, Otto RD, Prentice IC, Sauf W, Schloss A, Sitch S, Wittenberg U, Würth G, 1998. Evaluation of terrestrial carbon cycle models through simulations of the seasonal cycle of atmospheric CO₂: first results of a model intercomparison study. *Global Biogeochemical Cycles* 12, 1–24.
- IPCC, 2007. *Climate Change 2007: The Physical Science Basis. Contribution of Working Group I to the Fourth Assessment Report of the Intergovernmental Panel on Climate Change* (S Solomon, D Qin, M Manning, Z Chen, M Marquis, KB Averyt, M Tignor, HL Miller, eds). Cambridge University Press, Cambridge, UK and New York, 996 pp.
- Jones CD, Cox PM, Essery RLH, Roberts DL, Woodage MJ, 2003. Strong carbon cycle feedbacks in a climate model with interactive CO₂ and sulphate aerosols. *Geophysical Research Letters* 30, 1479, doi:10.1029/2003GL016867.
- Krinner G, Viovy N, de Noblet-Ducoudré N, Ogée J, Polcher J, Friedlingstein P, Ciais P, Sitch S, Prentice IC, 2005. A dynamic global vegetation model for studies of the coupled atmosphere–biosphere system. *Global Biogeochemical Cycles* 19, GB1015, doi:10.1029/2003GB002199.
- Rost S, Gerten D, Bondeau A, Lucht W, Rohwer J, Schaphoff S, 2008b. Agricultural green and blue water consumption and its influence on the global water system. *Water Resources Research* 44, W09405, doi:10.1029/2007WR006331.**
- Rost S, Gerten D, Heyder U, 2008a. Human alterations of the terrestrial water cycle through land management. *Advances in Geosciences* 18, 43–50.**
- Scholze M, Knorr W, Arnell NW, Prentice IC, 2006. A climate change risk analysis for world ecosystems. *Proceedings of the National Academy of Sciences* 103, 13116–13120.**
- Sitch S, Huntingford C, Gedney N, Levy PE, Lomas M, Piao S, Betts R, Ciais P, Cox P, Friedlingstein P, Jones CD, Prentice IC, Woodward FI, 2008. Evaluation of the terrestrial carbon cycle, future plant geography and climate-carbon cycle feedbacks using five Dynamic Global Vegetation Models (DGVMs). *Global Change Biology* 14, 1–25.**
- Sitch S, Smith B, Prentice IC, Arneth A, Bondeau A, Cramer W, Kaplan JO, Levis S, Lucht W, Sykes MT, Thonicke K, Venevsky S, 2003. Evaluation of ecosystem dynamics, plant geography and terrestrial carbon cycling in the LPJ dynamic vegetation model. *Global Change Biology* 9, 161–185.
- Thonicke K, Spessa A, Prentice IC, Harrison SP, Dong L, Carmona-Moreno C, 2009. The influence of vegetation, fire spread and fire behaviour on global biomass burning and trace gas emissions: results from a process-based model. In revision.
- UKCP09, 2009. UK Climate Projections, UK Climate Impacts Programme. Available at: http://www.ukcip.org.uk/index.php?option=com_content&task=view&id=163&Itemid=287

10 Scenarios and policy implications

[Research Theme 7]

F. Bosello (FEEM), S. Kovats (LSHTM)

10.1 Research aims

The links between climate and socio-economic systems are numerous and extremely complex. Trying to summarise all the multifaceted aspects, a two-way relationship can be identified: anthropogenic activities affect climate dynamics through greenhouse gas emissions and increased CO₂ concentration; while climate change affects social and economic dynamics through a set of impacts (which are generally adverse, but sometimes also positive) on human activities, and thus on human welfare. This nexus is not static, but concerns two systems in constant evolution and constant interaction.

The aim of Research Theme 7 (RT7) is to shed some light on these mechanisms. More specifically it aims:

- to produce, analyse critically, and provide to climatologists within the ENSEMBLES project a set of emission scenarios consistent with possible future socio-economic evolutions;
- to describe and quantify the major impacts that anthropogenic climate change can exert on social and economic systems. Due to its importance, particular emphasis is placed on health aspects; however, a more general indication of the climate change vulnerability of different world regions is also provided;
- finally, to assess the feedback (expressed as percentage change in emissions) that the climate-impacted economic system generates on the climate system.

10.2 Critical assessment of the IPCC scenarios

The emissions scenarios of the Intergovernmental Panel on Climate Change (IPCC) are commonly used for research into climate change, estimates of the impacts of climate change, and as a background for analysing greenhouse gas emission reduction policies. The SRES scenarios (Nakicenovic and Swart, 2000), the latest set of IPCC scenarios, were also used as the basis of the scenarios of the Millennium Ecosystem Assessment (2005) and national scenarios, e.g., in the UK (UKCIP, 2001).

There are four base scenarios: A1, A2, B1 and B2. The A scenarios place more emphasis on economic growth, the B scenarios on environmental protection; the 1 scenarios assume more globalisation, the 2 scenarios more regionalisation. The A1 scenario has three variants: A1B, A1FI and A1T.

10.2.1 IPCC scenarios, main assumptions and criticalities

The SRES scenarios have been criticised (Castles and Henderson, 2003a, 2003b; Castles, 2004; Henderson, 2005) with respect to many aspects: accounting methods, the absence of validation of the models used to generate the scenarios, and the lack of updates when new information was available.

One of the most problematic issues, at least for the social sciences, was the use of market exchange rates (MER) rather than the more appropriate purchasing power exchange rates (PPP) to represent homogeneously the wealth of different regions and its evolution. Basically, if measured in PPP, the gap between developed and developing countries is smaller, and thus the rate of GDP convergence between rich and poor, which according to modern growth theory is directly proportional to this gap, is also lower. As a consequence, the use of MER tends to overestimate emission growth from the developing countries and potentially the climate change problem.

However three considerations counterbalance this potential bias.

- Firstly, it is particularly relevant if GDPs converge effectively. While this is an axiom of modern growth theory and, as such, is embedded in IPCC SRES, it is somewhat controversial in the light of 'real data observation'. In addition, that theoretical result is superseded by new growth theory based on the idea that technological progress, one of the main drivers of growth, is endogenous and not exogenous.
- Secondly, the IPCC SRES also assume absolute convergence in energy intensity, which is not supported by observation; with respect to this, they are thus more optimistic in terms of emissions, compensating the upward bias of emissions seen when assuming GDP convergence.
- Thirdly, the implications of these biases would be more pronounced in regional emissions of greenhouse gases and aerosols than in global emissions, and will thus be less pronounced in terms of greenhouse gas concentrations, and even less so in terms of the global mean temperature and sea level.

In conclusion: the IPCC SRES emissions scenarios are far from perfect. However, they constitute the standard reference, and their quality is no worse, and often better, than alternative emissions scenarios. Moreover, much of the critique is directed at the demographic and economic details of the scenarios. This

may have led to a small upward bias in emissions projection. The range of future greenhouse gas emissions is undisputed, however. It is therefore appropriate that the ENSEMBLES GCMs run the SRES scenarios.

10.2.2 An alternative proposal

Even though using the IPCC SRES can be justified, some attempts can be made to produce a baseline emission scenario which tries to address at least the two main criticisms raised against their economic component: the calibration at MER and a ‘growth engine’ based on exogenous technological change.

A new baseline emission scenario was developed in ENSEMBLES, called E1 (Figure 10.1); this is calibrated with purchasing power exchange rates and uses a ‘new growth’ model to originate dynamics, i.e., it endogenises technical progress. Moreover, it uses a population model to project population dynamics based on more recent information. In this sense, it is superior to the SRES scenarios. The E1 scenario was developed using the IMAGE 2.4 integrated assessment model, which simulates in detail the energy system, land use and carbon cycle (see Section 10.4 for more information).

As can be seen (Figure 10.1), in terms of emissions, the E1 scenario is closest to the B2 scenario until 2020 when it diverges from the SRES envelope, falling continuously until the end of the century when it is down to 1 gigatonne of CO₂ emissions in 2100.

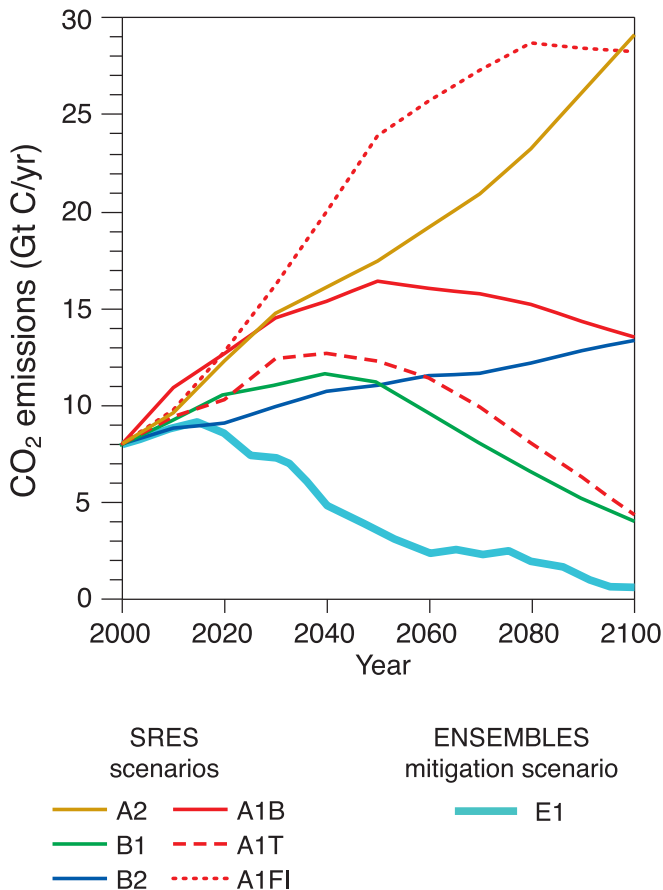


Figure 10.1: Global carbon dioxide emissions (in gigatonnes of carbon per year) according to the E1 scenario and the six SRES marker scenarios.

10.3 ‘Interfacing’ climate change with the socio-economic dimension

Due to its spatial and time scale and the still pervasive role of uncertainty, assessing the socio-economic consequences of climate change is extremely challenging. In particular, it is evident that an economic evaluation cannot be performed independently upon knowledge coming from other domains. It comes into play only after climatic changes have been translated into physical consequences (impacts), which, in their turn, are able to induce a change in human activities. Modelling these interdependences therefore requires an integrated approach (IA), where information coming from different disciplines is merged to provide a comprehensive and internally consistent picture of the problem to be analysed. To treat this complexity, IA models have been developed.

10.3.1 Linking climate change and economics

Notwithstanding modelling differences, basically two approaches are used to provide economic assessments of climate change.

With ‘*direct costing*’, the economic consequences of climate change impacts for major world regional economic systems (but also at a more local level) are defined for the purpose of ‘pricing’ a quantity change – e.g., land loss to sea level rise multiplied by the market value of that land – and then compared to regional GDP. Thereby, reduced form climate change damage functions can be built, linking temperature increase to GDP loss through impacts.

The ‘*indirect or higher-order costing*’ method explicitly models the social and economic reactions triggered within economic systems by climate impacts. This approach depicts the world economy as a system of markets interacting through exchanges of inputs, goods and services responding to changes in relative prices induced by climate shocks. In doing so, the direct cost dimension of climate change merely constitutes the starting point of the investigation. Its final outcome is the welfare implications of climate change, i.e., the situation materialising once the economic system has had the opportunity to adjust, reallocating its scarce resources more efficiently. In other words, market-driven or autonomous socio-economic adaptation is explicitly described.

The socio-economic assessment provided by RT7 follows this second approach. It uses ICES (Intertemporal Computable Equilibrium System), which is a recursive dynamic general equilibrium model. Its general equilibrium structure, in which all markets are interlinked, is tailored to capture and highlight the production and consumption substitution processes in a socio-economic system as a response to a set of climate shocks. These are summarised in Table 10.1. They have been calculated for a climate change scenario of +1.2°C in 2050 with respect to 2000, consistent with the A2 IPCC SRES. They have been obtained by extrapolation and meta-analysis of the existing literature, inputting to reduced-form modules linking temperature change and physical impacts.

Table 10.1: Climate change impacts: inputs for the CGE ICES model.

Climate Change Shocks for 1.2° C temperature increase (2050) percentage change wrt 2001							
Region	Health			Agriculture (land productivity)			Sea Level Rise
	Labour Prod.	Public Exp.	Private Exp.	Wheat	Rice	Cereal Crops	Land Loss
USA	-0.002	-0.196	-0.022	1.650	1.277	-2.190	0.026
EU	0.082	-0.390	-0.015	0.951	1.858	-1.577	0.015
EEFSU	0.104	-0.417	-0.009	5.027	2.784	-1.258	0.008
JPN	0.085	0.043	0.001	0.298	0.996	-2.297	0.073
RoA1	0.097	-0.264	-0.013	10.909	7.938	4.694	0.003
EEx	-0.243	1.307	0.080	4.351	3.525	0.726	0.067
CHIND	0.025	-0.078	-0.001	5.227	3.802	0.692	0.040
RoW	-0.190	1.019	0.094	-1.239	-1.451	-4.197	0.104

Climate Change Shocks for 1.2° C temperature increase (2050) (cont.) percentage change wrt 2001						
Region	Tourism		Energy Demand			
	Mserv Demand	Income transfers*	Coal	Nat Gas	Oil Products	Electricity
USA	-0.82	-68,327.92	104.85	-34.39	-3.15	-2.52
EU	1.08	72,024.59	71.17	-17.78	-18.98	-9.08
EEFSU	-2.34	-11,578.35	98.26	-32.81	-3.03	-0.56
JPN	7.87	281,252.04	99.25	-31.95	-2.71	0.06
RoA1	0.95	11,314.12	14.43	-23.18	-9.68	-10.96
EEx	-5.11	-142,800.34	1.28	0.00	-2.03	6.35
CHIND	-1.27	-6,394.80	64.55	-23.20	-2.06	5.98
RoW	-5.13	-135,489.36	50.13	0.00	-2.55	64.69

* 2001 US\$ million

Source: Our calculations from environmental impacts interface modules.

10.3.2 The specific link between climate change and human health

Among the many impacts of climate change, those on health are particularly important for their immediate and obvious relevance to human well-being, but also because of their implications for health expenditure and for the productivity

of the labour force. For these reasons, dedicated research has been devoted to the investigation of this topic within RT7.

Climate change can affect human health through a wide range of mechanisms and for a range of diseases or health outcomes (deaths, injuries) (see Figure 10.2).

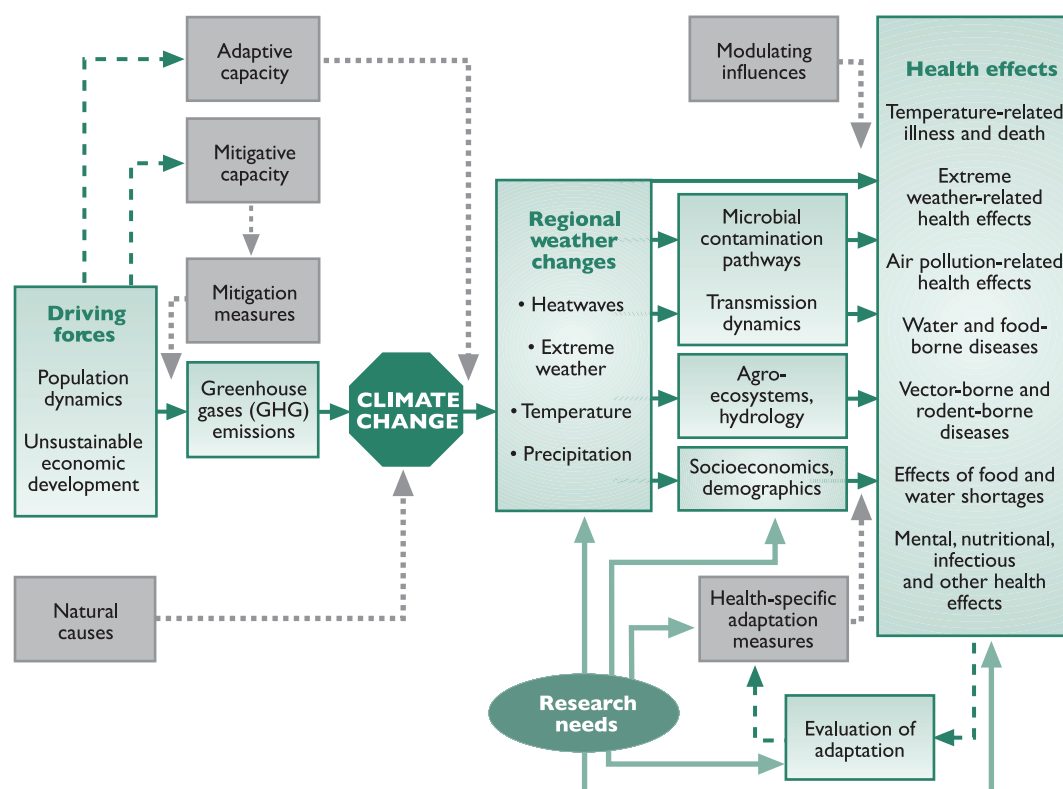


Figure 10.2: The pathways through which climate change can affect human health (McMichael et al., 2003).

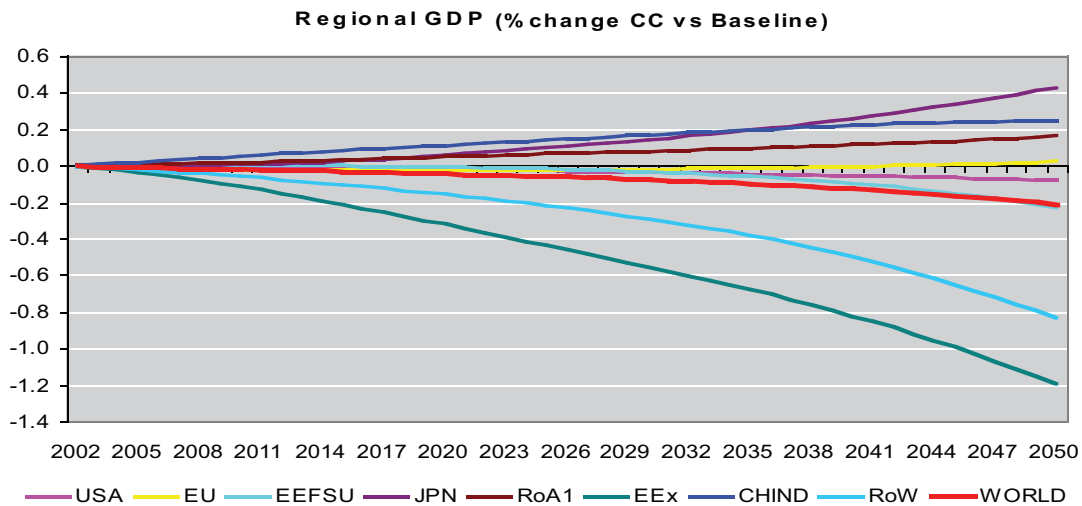


Figure 10.3: Climate change impact on macro-regional GDP. USA, United States of America; EU, Western Europe; EEFSU, Eastern Europe and Former Soviet Union; JPN, Japan; RoA1, Rest of Annex I countries; EEx, Energy exporter countries; CHIND, China and India; ROW, Rest of the world.

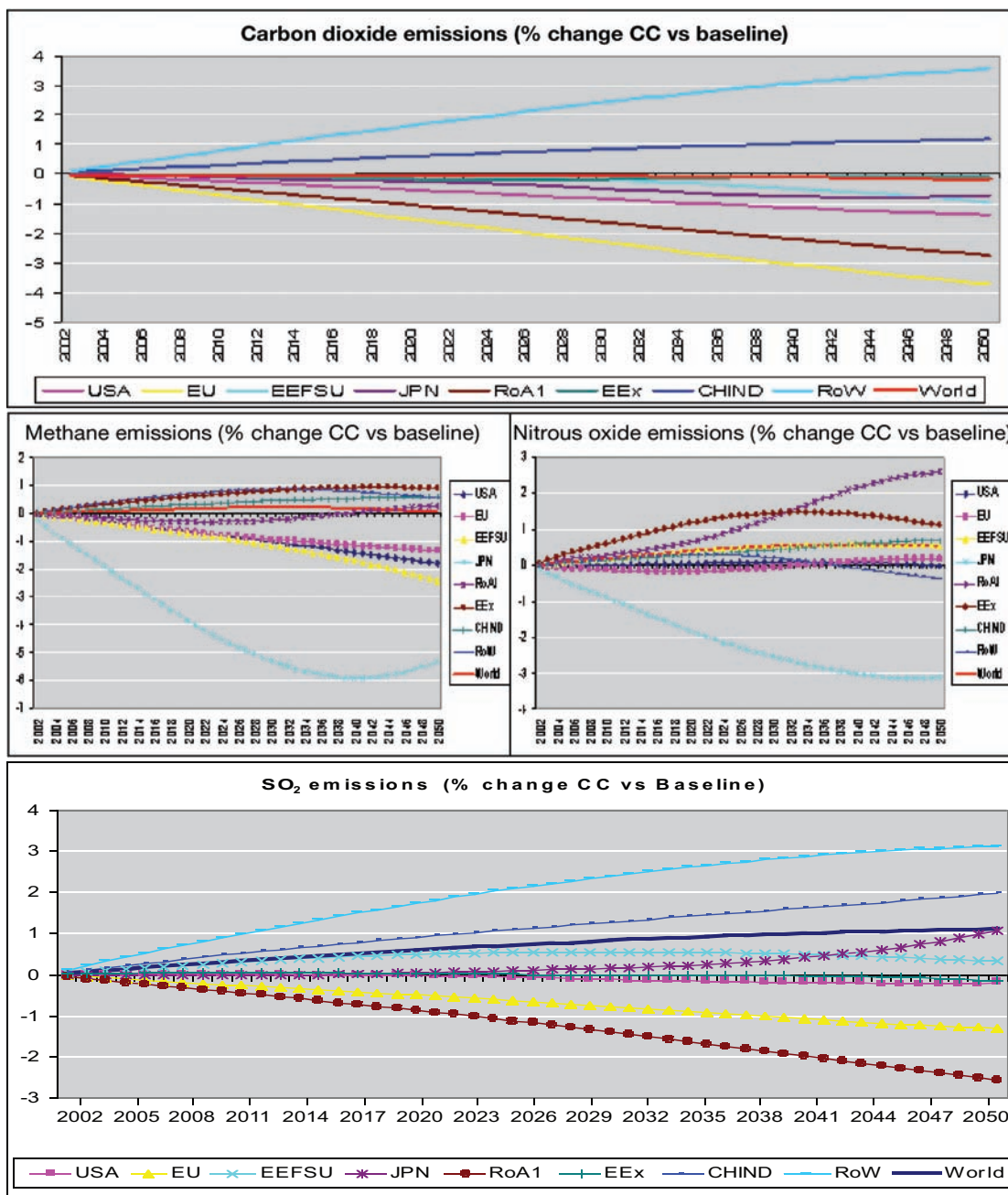


Figure 10.4: Climate change feedback on main GHG emissions as mediated by socio-economic impacts.

Climate variability, as characterised by extreme weather events and interannual variability, is known to affect certain infectious diseases. The impacts of long-term shifts in climate conditions may lead to shifts in the distribution of infectious diseases and areas suitable for food production. The impacts on health will outweigh the benefits, and populations in low-income countries are likely to be worst affected.

10.3.3 Methods for estimating the effects of climate change on human health

Methods for estimating the health effects of climate change are at an early stage of development. Inappropriate assumptions have often been included in integrated assessment models with respect to health outcomes and there is a need to improve the relevant health impact models. Future disease burdens are sensitive to the underlying assumptions about population growth and ageing, and future health status.

Global climate change will increase outdoor and indoor heat loads, and may impair health and productivity for millions of working people. Within RT7 a model has been developed that applies physiological evidence about effects of heat, climate guidelines for safe work environments, climate modelling, and global distributions of working populations to estimate the impact of climate scenarios on future labour productivity. Empirical-statistical models were developed to estimate the direct impact of daily temperature on respiratory and cardiovascular mortality (the direct effects of heat and cold) and on diarrhoeal disease mortality, based on observational studies of exposure-response functions.

10.4 Estimating climate change feedbacks

10.4.1 An integrated economic assessment of climate change impacts

The economic implications of climate change impacts reported by Table 10.1 are summarised in Figure 10.3. For the world as a whole, the impacts jointly considered can impose costs of around 0.2% of GDP in 2050. This global figure conceals important regional differences. While the developed regions and China and India gain slightly, developing regions can lose considerably more, up to 1.2% in countries that are net energy exporters.

In terms of GHG emissions (Figure 10.4), effects can be quite significant regionally, but almost negligible at the global level. Indeed, regional emission changes with opposite signs tend to cancel each other out. Interestingly, there is no direct relationship between GDP changes and emissions: for instance all developed countries increase their GDP, but their CO₂ emissions decline. Albeit with higher production, emissions are driven down by a decreased household energy demand for heating purposes. Conversely, the 'Rest of the world', i.e., developing countries, whose GDP declines, experience an increase in CO₂ emissions due to an increase in coal and electricity demand for cooling purposes. World N₂O and CH₄ emissions increase slightly (with a peak of 1.5% for N₂O). This is linked to agricultural production, which at a global level

increases, fostered by increased agricultural productivity induced by the CO₂ fertilisation effect in mid- to high-latitude regions.

10.4.2 Estimating climate change impacts on health

Climate change is very likely to decrease labour productivity in many regions, even when changes in the labour force are taken into account. Under the simple assumption of no specific adaptation, by the 2080s, the greatest absolute losses of population-based labour work capacity are seen under the A2 scenario in South East Asia, Andean and Central America, and the Caribbean (Figure 10.5). Increased occupational heat exposure due to climate change may significantly impact on labour productivity and costs unless preventive measures are implemented (Kjellstrom et al., 2009).

Climate change will have important effects on temperature-related mortality. Climate change is estimated to increase the temperature-attributable proportion of diarrhoeal disease, but this is in the context of an overall decline in diarrhoeal disease mortality. Climate change will increase heat-related mortality and decrease cold-related mortality. The estimates of changes in attributable cardiovascular mortality are large, due to population ageing and the large burden of cardiovascular disease projected in low- and middle-income countries.

At the global level, low rainfall is a determinant of diarrhoeal disease. That is, the incidence of child diarrhoeal disease is greater in arid and semi-arid areas than in other areas, even after socio-economic factors have been taken into account. The incidence of diarrhoea increased by 4% (95% confidence interval, CI: 1–7%, $p = 0.02$) for each 10 mm/month decline in rainfall (Lloyd et al., 2007).

10.4.3 Climate change, health impacts, and the role of adaptive capacity

Although the interactions involved can be very numerous, complex and subtle (see, e.g., Casman and Dowlatabadi, 2002), climate determines the potential of many infectious diseases to flourish. On the other hand, health care influences the actual incidence of diseases. One would therefore expect that, in a scenario of economic growth, infectious diseases would fall as health care improves (Medlin et al., 2006). Likewise, in a scenario of global warming, one would expect to see infectious diseases spread into new regions and perhaps intensify (McMichael et al., 2001). It is thus extremely important and scientifically challenging to assess the impacts on mortality in a scenario with both climate change and economic development.

This assessment has been performed for sub-Saharan Africa. Scenarios for three determinants of development – per capita income, literacy, and absolute poverty – and for climate change have been used to project the future incidence of malaria, assuming that it changes in proportion to infant mortality. It is shown that deaths from malaria will first increase, because of population growth and climate change, but will then fall, because of development. This pattern is robust to the choice of scenario, parameters, and starting conditions; and also holds for

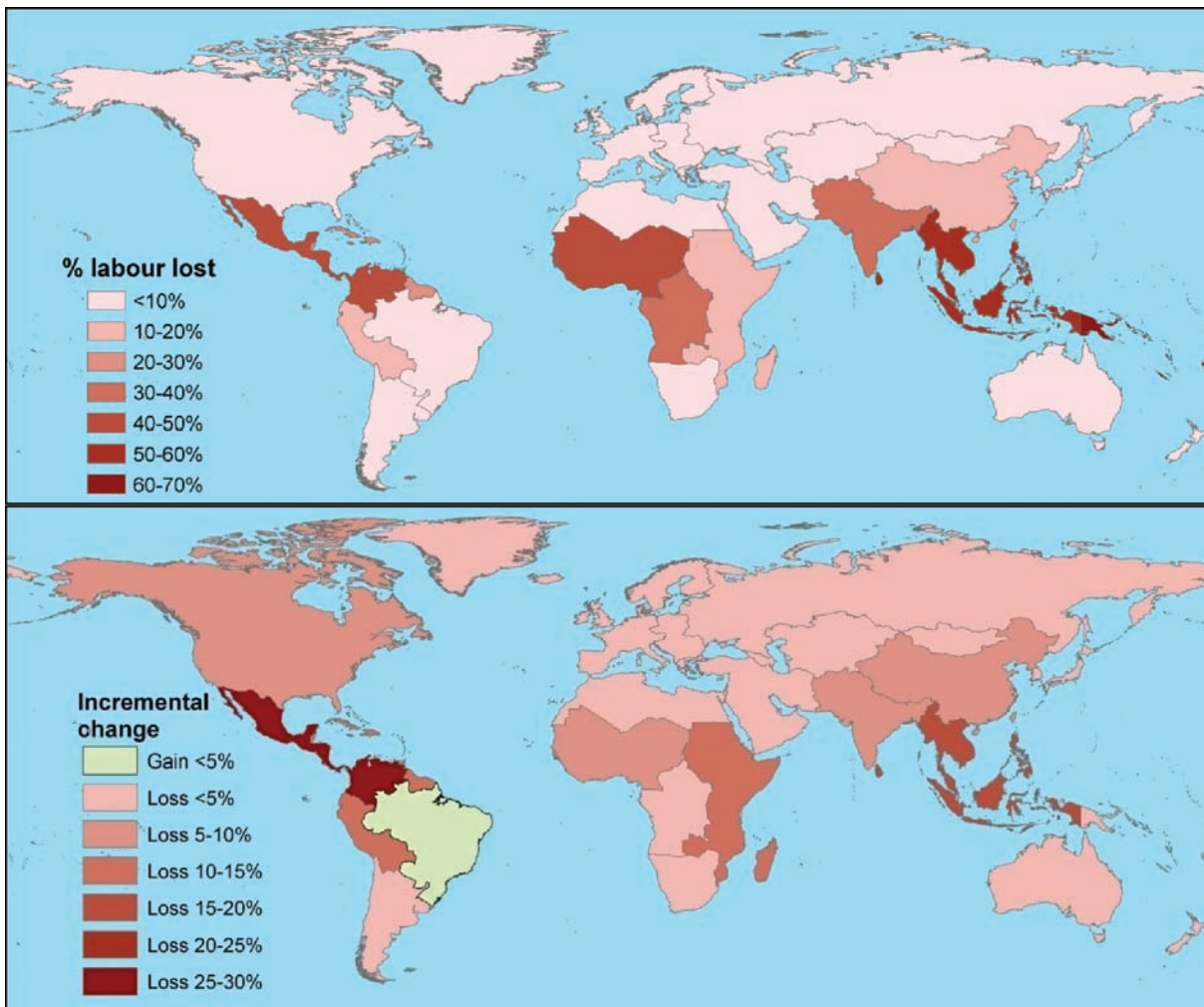


Figure 10.5: Changes in labour productivity (% days lost due to occupational heat exposures) by region in the 2080s, under the A2 climate scenario. Top panel: absolute % days lost due to heat stress, assuming no adaptation. Lower panel: change in % days lost due to changes in both climate and labour profiles, assuming no adaptation, compared to current baseline (1961–1990 climate and 2000 labour profile).

diarrhoea, schistosomiasis and dengue fever. However, the timing and level of the mortality peak is very sensitive to assumptions (Ebi, 2007). In this model climate change is important in the medium term, but is dominated in the long term by development.

10.5 Conclusions and further steps

The ENSEMBLES research has confirmed some important findings already highlighted by 20 years of literature on impacts: anthropogenic activity is relevant in the determination of climate change and climate change can exert relevant impacts on human welfare. These impacts can be huge in their ‘physical’ materialisation (see, for instance, the negative effect on labour productivity), but market-driven adaptation can smooth considerably the final impact on the economic system. However, the apparently low world GDP loss found by the present study should not be a cause of complacency, for the following reasons.

In the light of the still limited set of climatic impacts considered, climate change raises important distributional and equity issues. Higher negative impacts are felt in developing regions, which are poorer and are already facing severe challenges for their development.

Comparing macro-regional losses with the world figure, it is very likely that larger losses can be found simply by increasing the detail of the investigation. This stresses the need to carefully tailor the scope of any climate change impact assessment, as conclusions are scale-dependent.

Considering that the GDP impacts shown are calculated only on a subset of potential adverse effects of climate change (for instance, the possible consequences of increased intensity and frequency of extreme weather events and of biodiversity losses are not included); that the climate scenario is on the low end of the A2 range; that irreversibilities or abrupt climate and catastrophic changes to which adaptation can be only limited are neglected; that the current assessment assumes costless and instantaneous market-driven adjustments; and finally that the world is currently moving on an emissions trajectory leading to a higher temperature increase than that consistent with the A2 scenario, what is proposed here, which is far from negligible anyway, can be taken only as the lowest possible bound for climate change costs. The main implication is that notwithstanding its impact-smoothing potential, market-driven adaptation cannot be the solution to the climate change problem: its distributional and scale consequences need to be addressed with policy-driven mitigation and adaptation strategies.

Interestingly, the feedback of climate change impacts on emission paths themselves is very limited. Indeed even pronounced regional differences tend to compensate for each other, leaving global emission trends almost unchanged.

This work is preliminary and exploratory. Future work could be to extend the set of climate change impacts considered, and to check the robustness of results with respect to different climate change scenarios, different socio-economic scenarios, and different modelling approaches.

10.6 Technical Appendix

Within RT7, two modelling tools have predominantly been used to assess climate change impacts on the economic system and subsequently the implied feedback on emissions. These are the FUND model (Tol, 2006) and the ICES model (Eboli et al., 2009).

The Climate Framework for Uncertainty, Negotiation and Distribution (FUND) is an integrated assessment model of climate change. It links scenarios and simple models of population, technology, economics, emissions, atmospheric

chemistry, climate, sea level, and impacts with the main purpose of performing cost–benefit and cost-effectiveness analyses of greenhouse gas emission reduction policies and supporting game-theoretic investigations into international environmental agreements. The model runs in time-steps of 1 year from 1950 to 2200, and distinguishes nine major world regions. The FUND model is particularly well suited to studying long-term dynamics in economic growth and can embed different assumptions concerning endogenous technical progress.

The Intertemporal Computable Equilibrium System (ICES) model is a recursive dynamic general equilibrium model for the world economy. Its general equilibrium structure, in which all markets are interlinked by domestic and international trade of factors of production, goods and services, is tailored to capture and highlight the production and consumption substitution processes triggered in a socio-economic system by different ‘perturbations’ including those generated by climate shocks. Exploiting this feature, the model has been used within RT7 to highlight autonomous socio-economic adaptation and feedback effects on anthropogenic emissions. The model was calibrated in 2001 and provides regional detail for eight world macro-regions and seventeen production sectors. It runs from 2001 to 2050 in yearly steps.

References

ENSEMBLES publications are highlighted as bold text.

- Casman EA, Dowlatabadi H, 2002. Contextual Determinants of Malaria. Resources for the Future Press, Washington, DC.
- Castles I, 2004. Climate work based on unsound economics. Australian Financial Review, 7 February.
- Castles I, Henderson D, 2003a. The IPCC emission scenarios: an economic-statistical critique. *Energy and Environment* 14, 159–185.
- Castles I, Henderson D, 2003b. Economics, emission scenarios and the work of the IPCC. *Energy and Environment* 14, 415–435.
- Ebi K, Tol RSJ, Yohe G, 2007. Infectious disease, development, and climate change: a scenario analysis. *Environment and Development Economics* 12, 687–706.**
- Eboli F, Parrado R, Roson R, 2009. Climate Change Feedback on Economic Growth: Explorations with a Dynamic General Equilibrium Model. FEEM Note di Lavoro, 43.091**
- Henderson D, 2005. The treatment of economic issues by the Intergovernmental Panel on Climate Change. *Energy and Environment* 16, 321–326.
- Kjellstrom T, Kovats RS, Lloyd SJ, Holt T, Tol RSJ, 2009. The direct impact of climate change on regional labour productivity. Archives of Environmental and Occupational Health, in press.**
- Lloyd S, Kovats RS, Armstrong B (2007) Global cross-sectional study of the association between diarrhoea morbidity, weather and climate. *Climate Research*, 34(2): 119-127.**

- McMichael A, Githeko A, Akhtar R, Carcavallo P, Gubler D, Haines A, Kovats RS, Martens P, Patz J, Sasaki A, 2001. Human health. In: *Climate Change 2001: Impacts, Adaptation, and Vulnerability. Contribution of Working Group II to the Third Assessment Report of the Intergovernmental Panel on Climate Change* (JJ McCarthy, OF Canziani, NA Leary, DJ Dokken, KS White, eds). Cambridge University Press, Cambridge, UK.
- McMichael AJ, Campbell-Lendrum DH, Corvalán CF, Ebi KL, Githeko A, Scheraga JD, Woodward A (eds), 2003. *Climate Change and Health: Risks and Responses*. WHO, Geneva.
- Medlin CA, Chowdhury M, Jamison DT, Measham AR, 2006. Improving the health of populations: lessons of experience. In: *Disease Control Priorities in Developing Countries*, 2nd edn (DT Jamison, JG Breman, AR Measham, G Alleyne, M Claeson, DB Evans, P Jha, A Mills, P Musgrove, eds). Oxford University Press, Oxford.
- Millennium Ecosystem Assessment, 2005. *Ecosystems and Human Well-Being: Scenarios*. Island Press, Washington, DC.
- Nakicenovic N, Swart RJ, 2000. *Emissions Scenarios 2000: Special Report of the Intergovernmental Panel on Climate Change*. Cambridge University Press, Cambridge, UK.
- Tol RSJ, 2006. *The Climate Framework for Uncertainty, Negotiation and Distribution (FUND), Technical Description, Version 2.8* [available at <http://www.mi.uni-hamburg.de/fileadmin/fnu-files/models-data/fund/technical.pdf>].
- UKCIP, 2001. *Socio-economic Scenarios for Climate Change Impact Assessments: A Guide to their Use in the UK Climate Impacts Programme*. UKCIP, Oxford.

Appendix 1: Examples of ENSEMBLES climate descriptions and projections

Introduction

This Appendix gives illustrative examples of some of the spatial output climate descriptions from the project. These examples are a small subset of the many existing time-slice plots produced so

far, some of which have already been published in peer-reviewed journals. Those shown here have been chosen specifically to show the projected evolution of European and global climate over this century. To illustrate the climate baseline, plots of the 1961-1990 climate produced from the E-OBS data set are also shown.

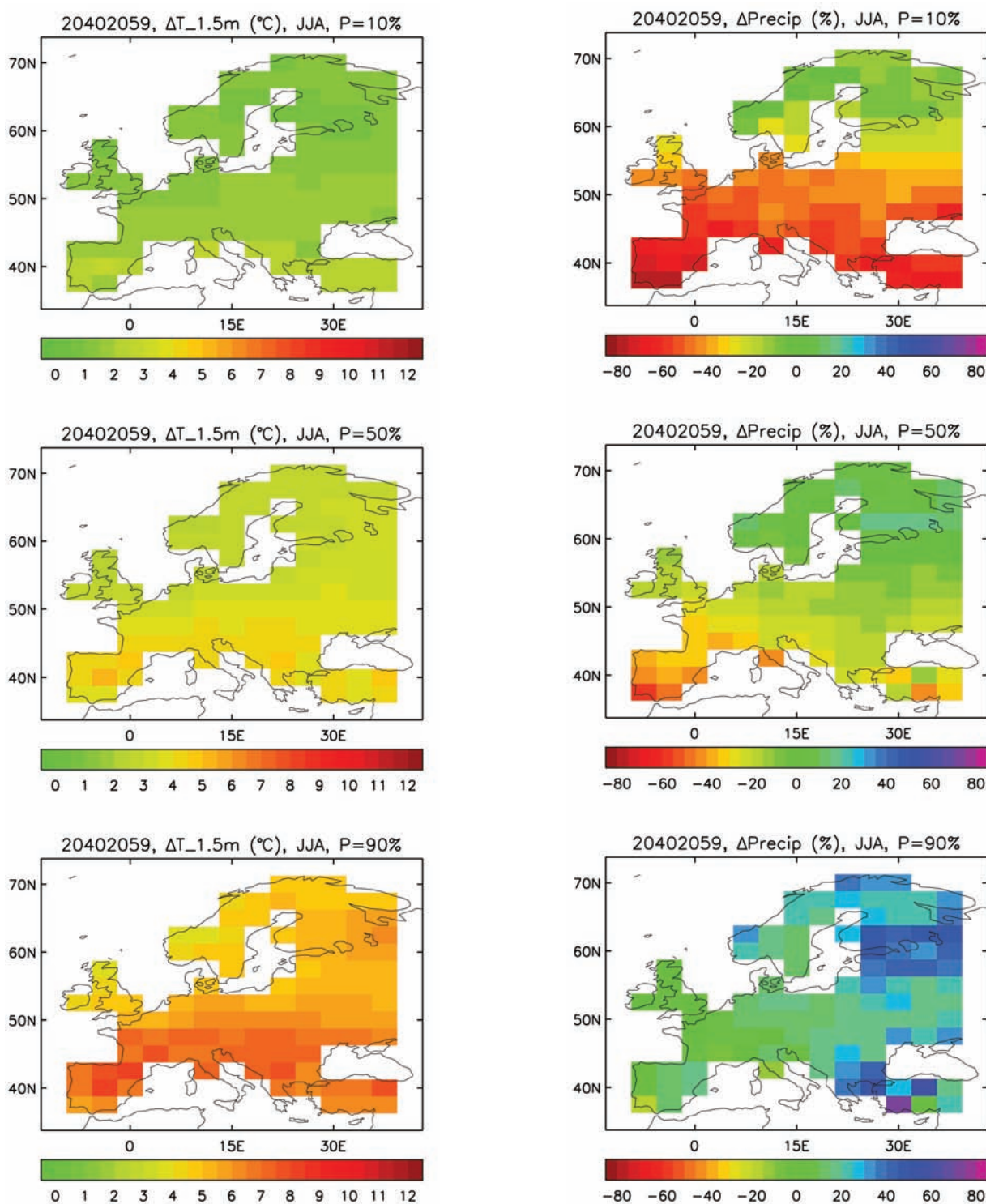


Figure A1.1: The ENSEMBLES probabilistic projections for Europe under the A1B emission scenario from the perturbed physics 'grand ensemble'. The maps show the 10%, 50% (median) and 90% percentiles (top, middle and bottom rows respectively) of (left) European surface temperature change and (right) European percentage precipitation change, for the summer season for the twenty year period 2040–2059 relative to the 1961–1990 baseline period. [RT1]

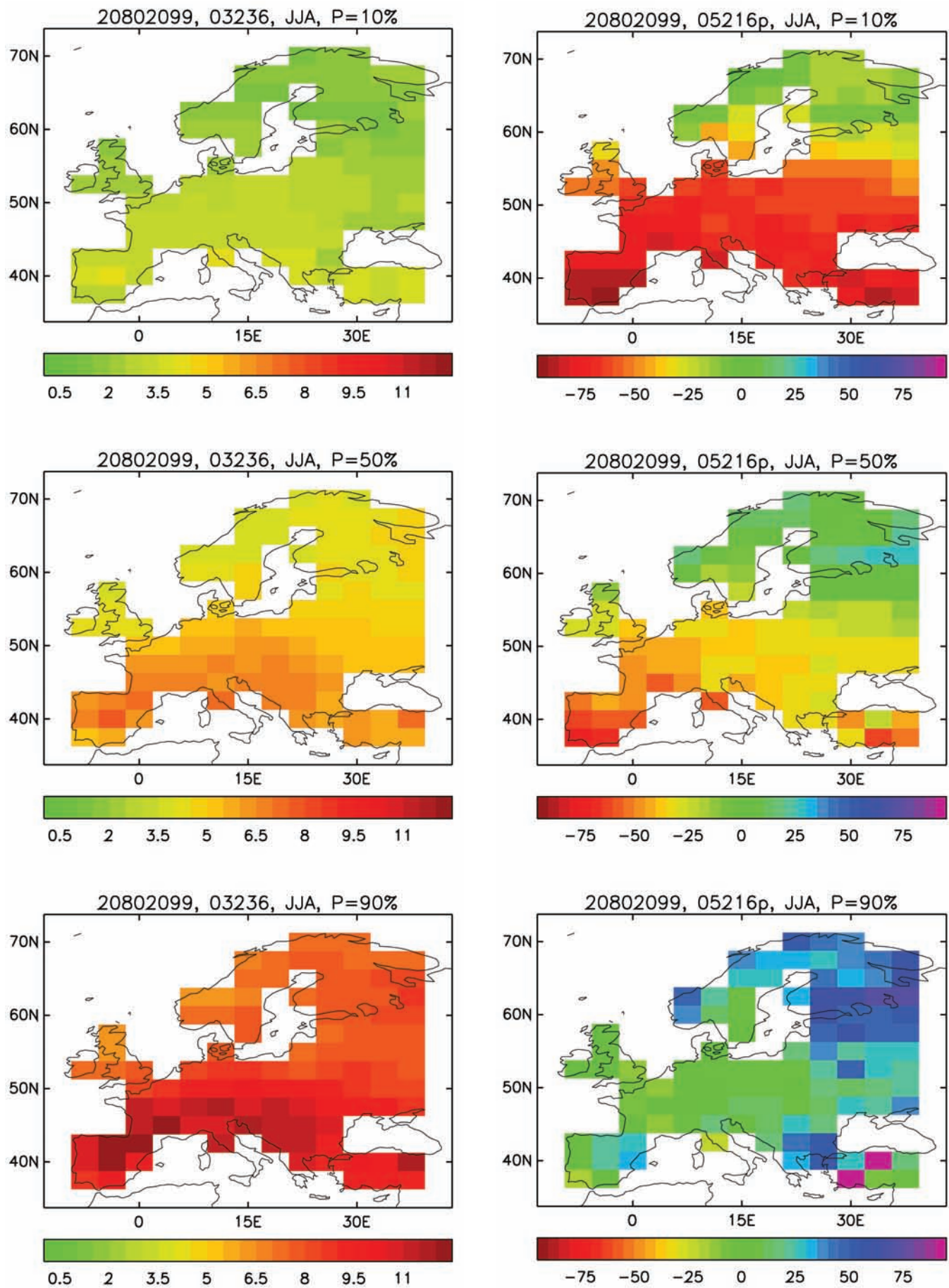


Figure A1.2: The ENSEMBLES probabilistic projections for Europe under the A1B emission scenario from the perturbed physics 'grand ensemble'. The maps show the 10%, 50% (median) and 90% percentiles (top, middle and bottom rows respectively) of (left) European surface temperature change and (right) European percentage precipitation change, for the **summer season** for the twenty year period 2080–2099 relative to the 1961–1990 baseline period. [RT1]

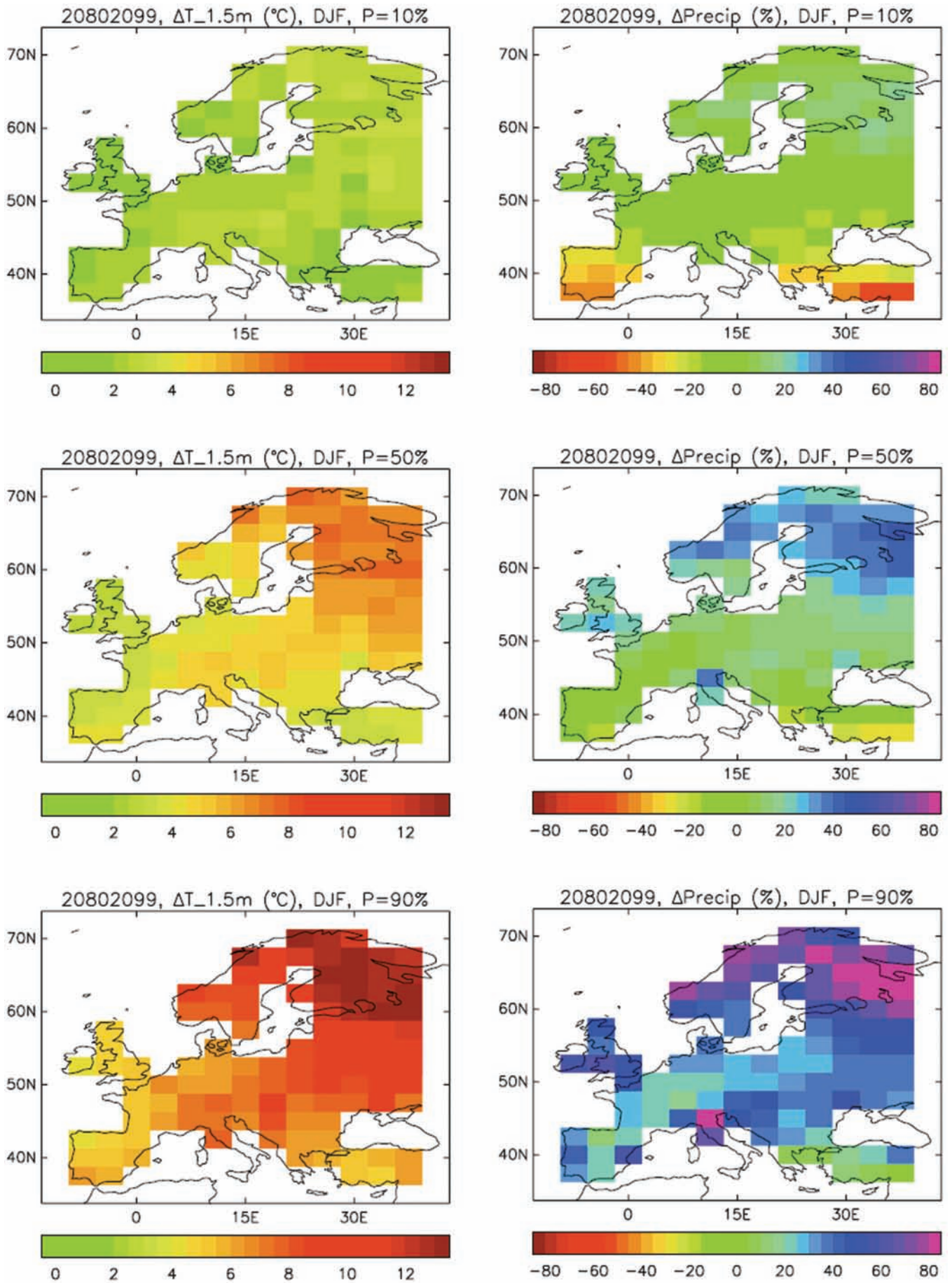


Figure A1.3: The ENSEMBLES probabilistic projections for Europe under the A1B emission scenario from the perturbed physics 'grand ensemble'. The maps show the 10%, 50% (median) and 90% percentiles (top, middle and bottom rows respectively) of (left) European surface temperature change and (right) European percentage precipitation change, for the **winter season** for the twenty year period 2080–2099 relative to the 1961–1990 baseline period. [RT1]

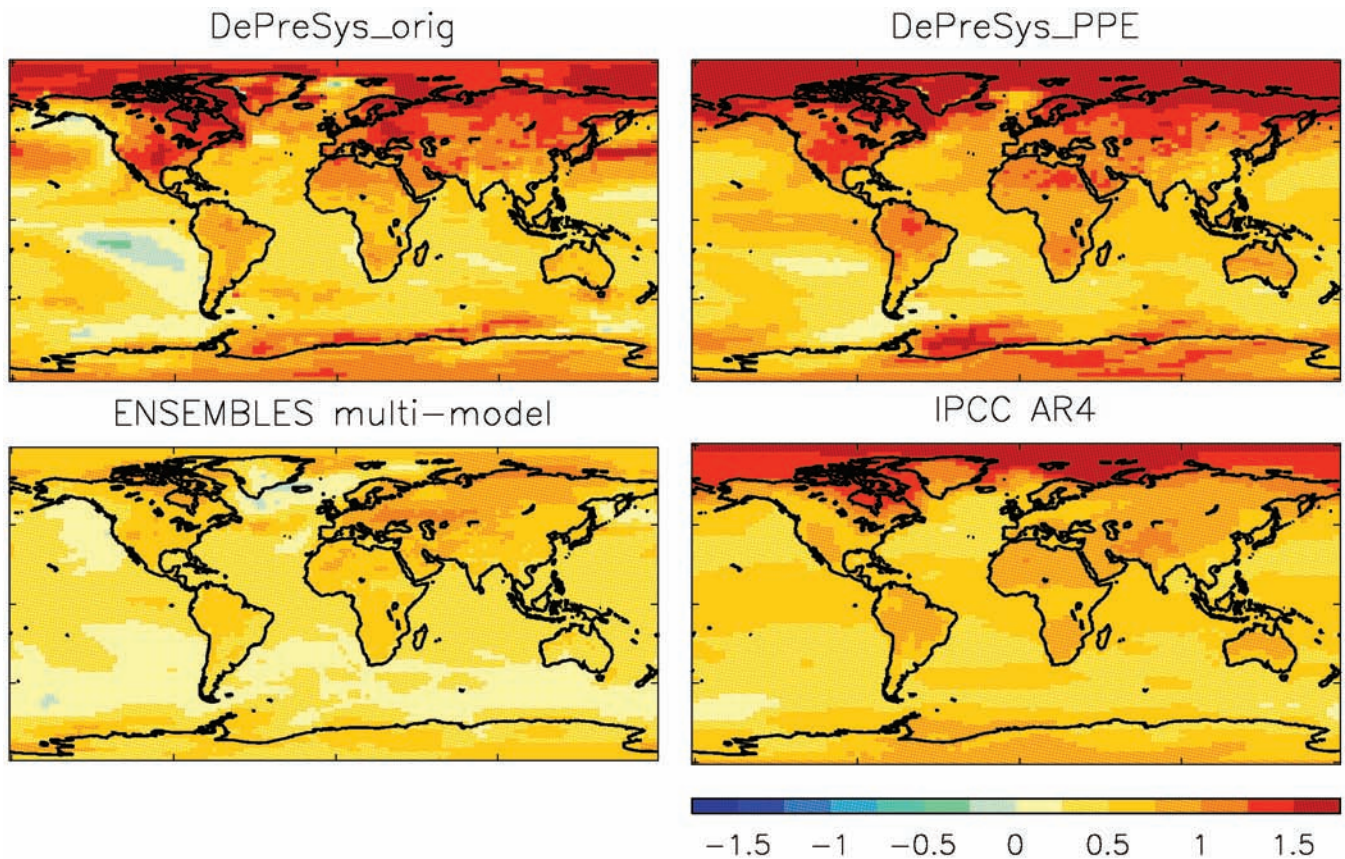


Figure A1.4: Projected surface temperature anomalies (K) for December 2010 to November 2015, relative to 1961–2001, from initialised ensemble-mean projections of the original DePreSys single-model system of Smith et al. (2007) (top left), and the DePreSys perturbed parameter (top right) and multi-model (bottom left) projections from ENSEMBLES, all started from November 2005. The bottom right panel shows the ensemble mean of uninitialised multi-model climate change projections from the IPCC AR4 assessment. The ensemble means are created from 9, 12, 10 and 22 simulations respectively. [RT1]

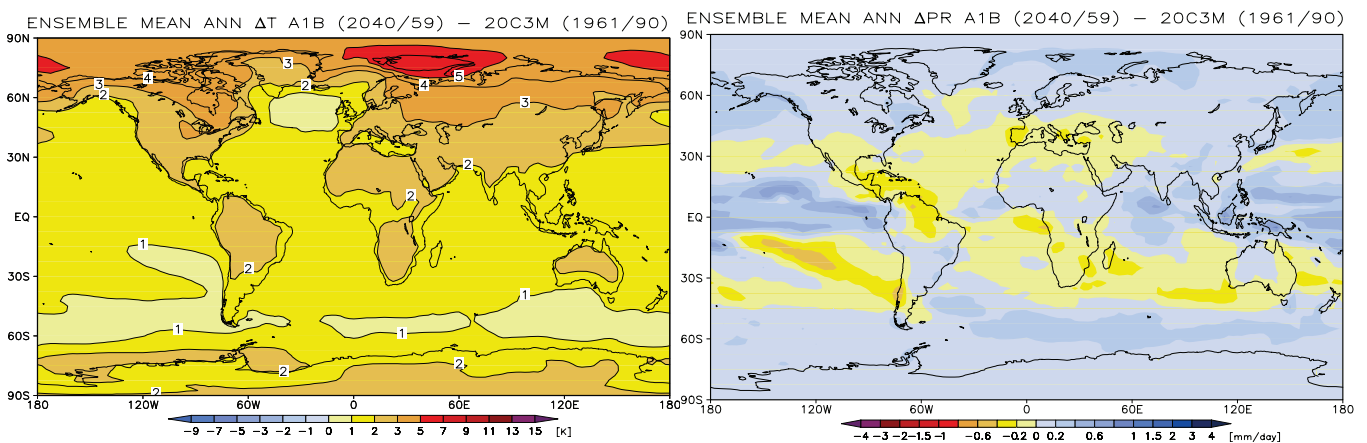


Figure A1.5: Projected changes under the A1B scenario, multi-model ensemble mean from the stream 1 GCM simulations for the twenty year period 2040–2059 relative to the 1961–1990 mean. Left panel is annual mean surface air temperature change (K) and the right panel is precipitation change in mm/day. [RT2A]

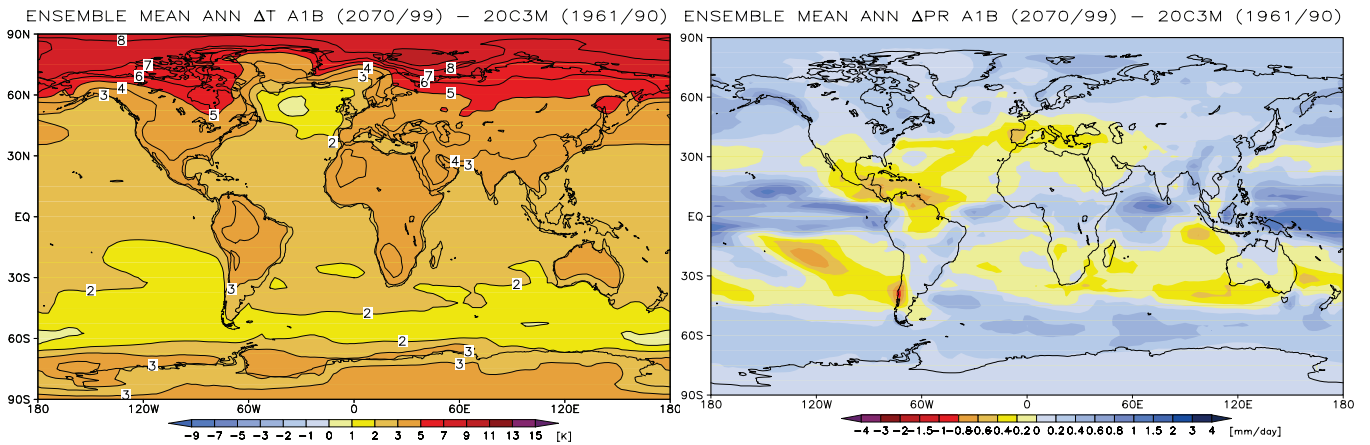


Figure A1.6: Projected changes under the A1B scenario, multi-model ensemble mean from the stream 1 GCM simulations for the period 2070–2099 relative to the 1961–1990 mean. Left panel is annual mean surface air temperature change (K) and the right panel is precipitation change in mm/day. [RT2A]

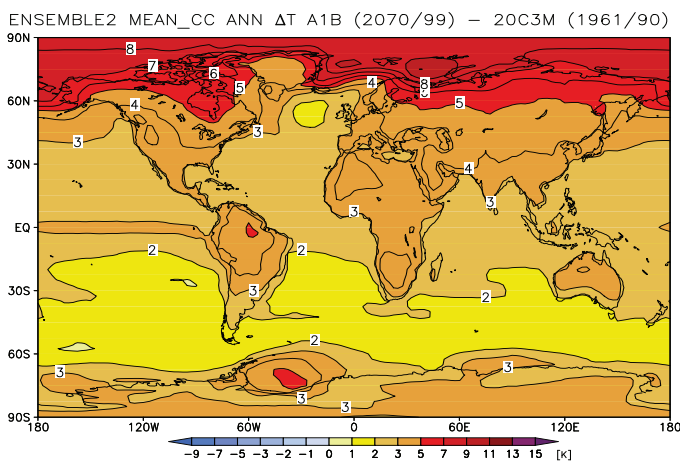


Figure A1.7: Annual mean surface air temperature change (K) projected under the A1B scenario for the period 2070–2099 relative to the 1961–1990 mean, using the multi-model ensemble mean of the stream 2 simulations run with GCMs that actively model carbon cycle feedbacks. [RT2A]

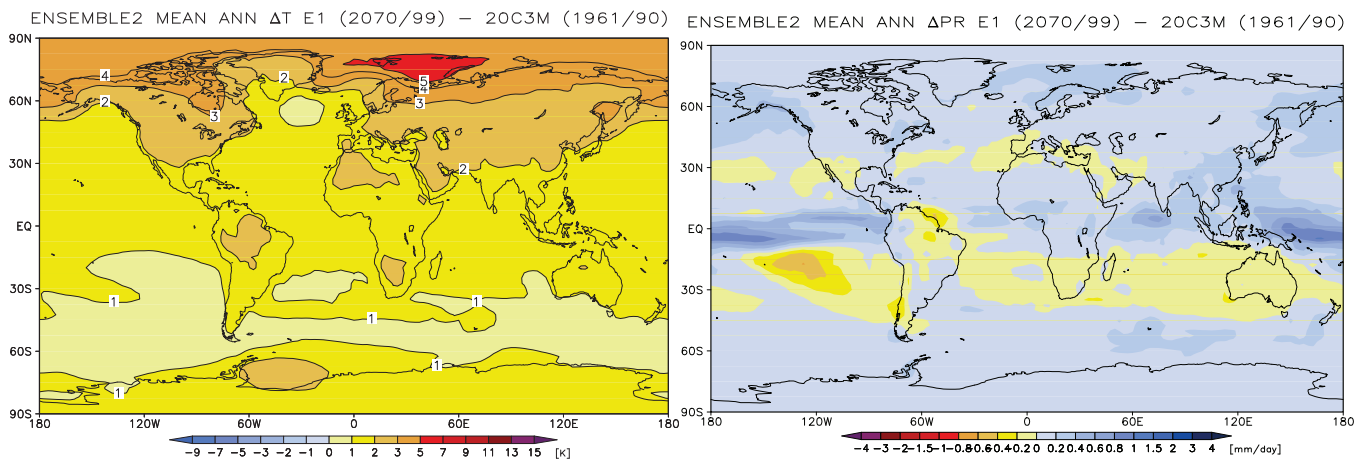


Figure A1.8: Projected changes under the E1 mitigation scenario, multi-model ensemble mean of the stream 2 GCM simulations for the period 2070–2099 relative to the 1961–1990 mean. Left panel is annual mean surface air temperature change (K) and the right panel is precipitation change in mm/day. [RT2A]

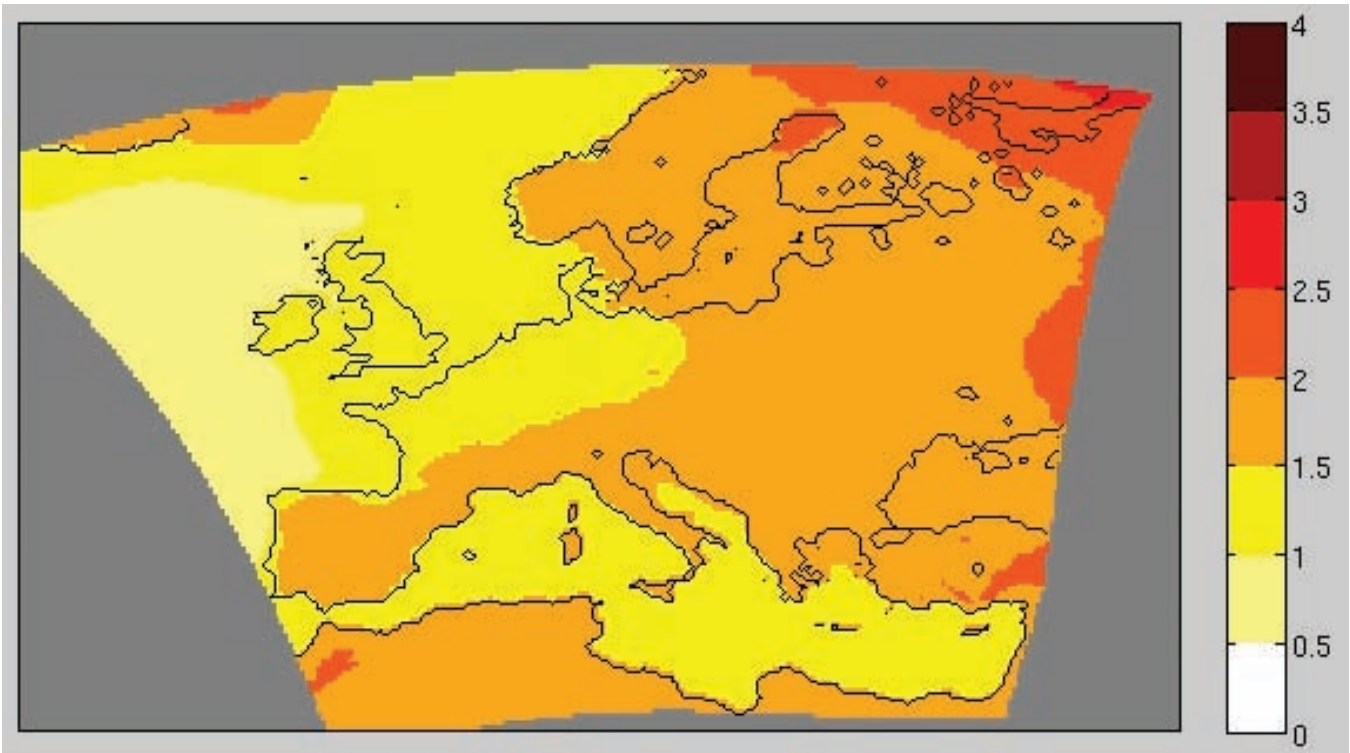


Figure A1.9: Projected changes in annual mean surface air temperature (K) under the A1B scenario, multi-model ensemble mean of RCM simulations for the time period 2021–2050 relative to the 1961–1990 mean. [RT2B]

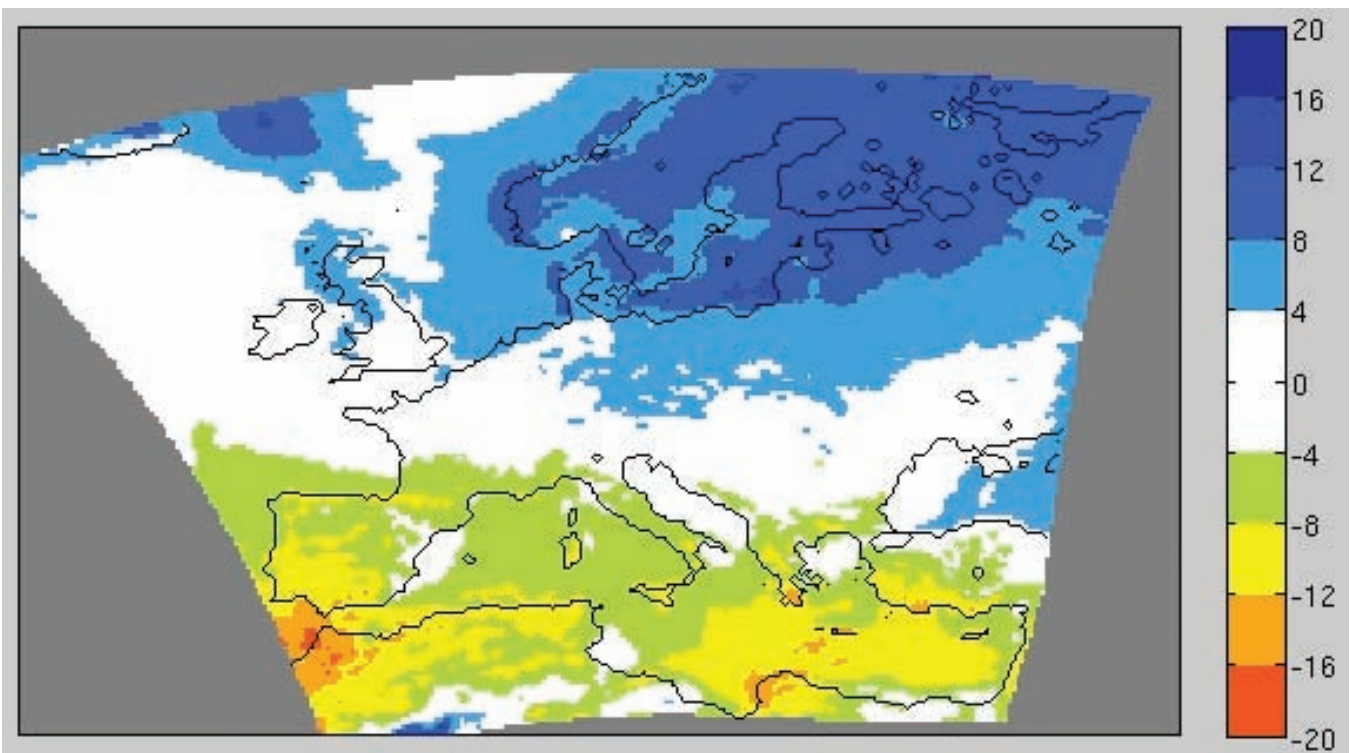


Figure A1.10: Projected changes in annual precipitation (%) under the A1B scenario, multi-model ensemble mean of RCM simulations for the time period 2021–2050 relative to the 1961–1990 mean. [RT2B]

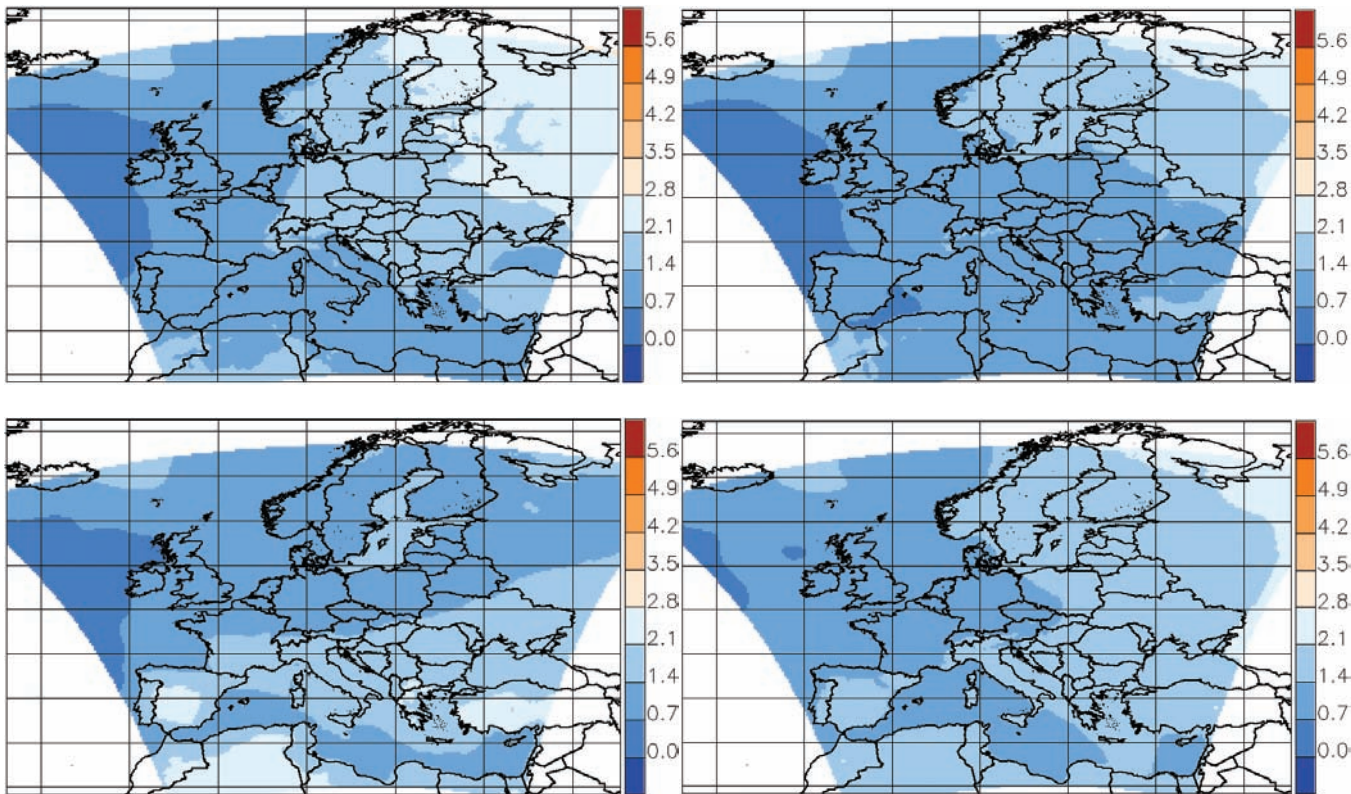


Figure A1.11: Projected changes in seasonal mean surface air temperature (K) under the A1B scenario, multi-model ensemble mean of RCM simulations for the time period 2021–2050 relative to 1961–1990 seasonal means. Top left panel is DJF, top right is MAM, bottom left is JJA, bottom right is SON. [RT2B]

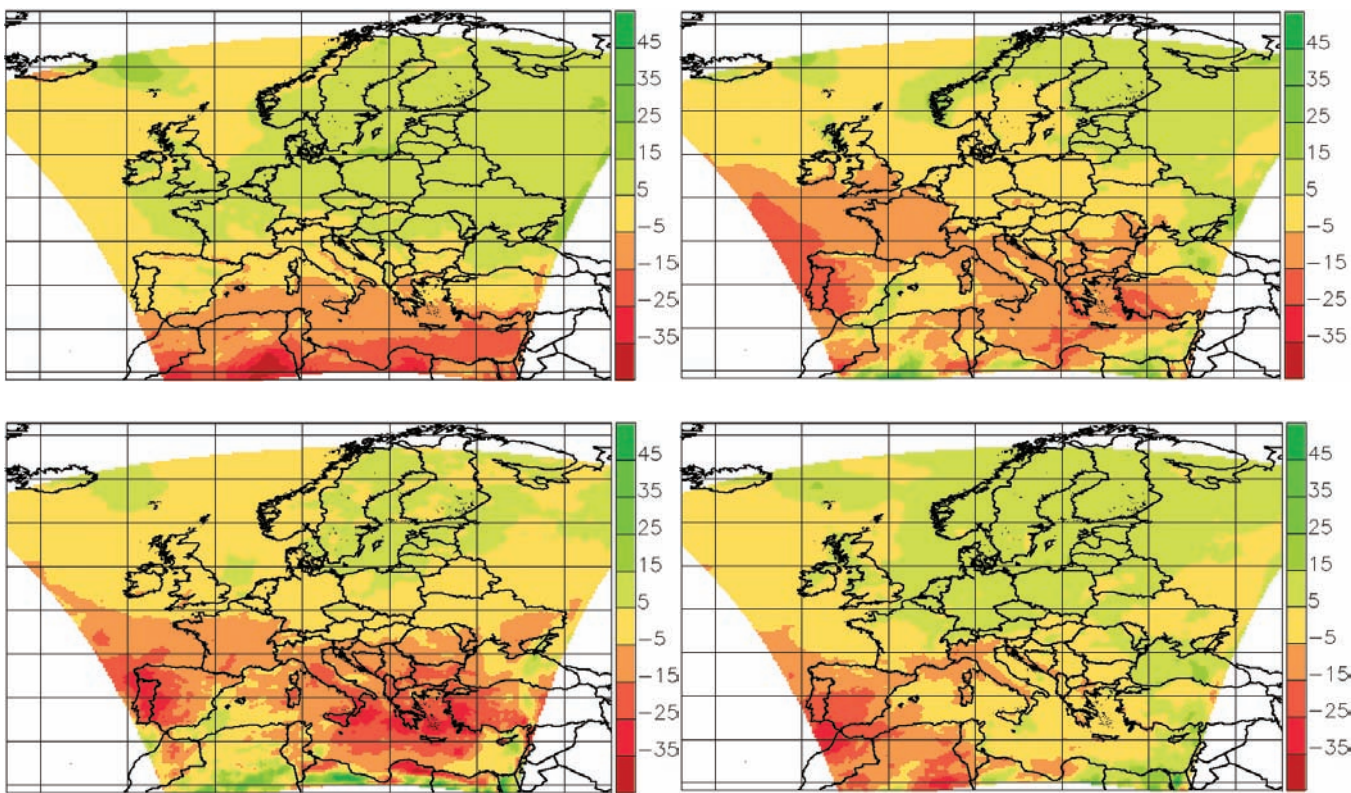


Figure A1.12: Projected changes in seasonal precipitation (%) under the A1B scenario, multi-model ensemble mean of RCM simulations for the time period 2021–2050 relative to 1961–1990 seasonal means. Top left panel is DJF, top right is MAM, bottom left is JJA, bottom right is SON. [RT2B]

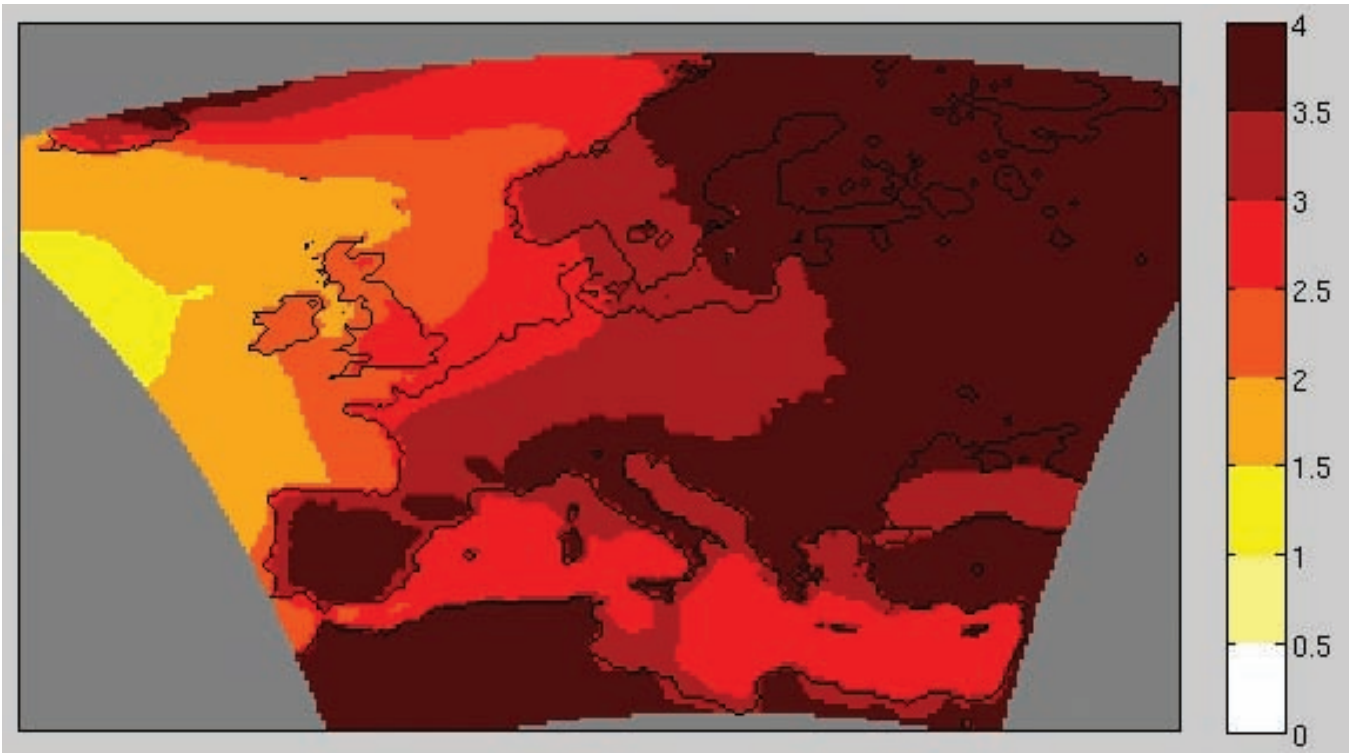


Figure A1.13: Projected changes in annual mean surface air temperature (K) under the A1B scenario, multi-model ensemble mean of RCM simulations for the time period 2071–2100 relative to the 1961–1990 mean. [RT2B]

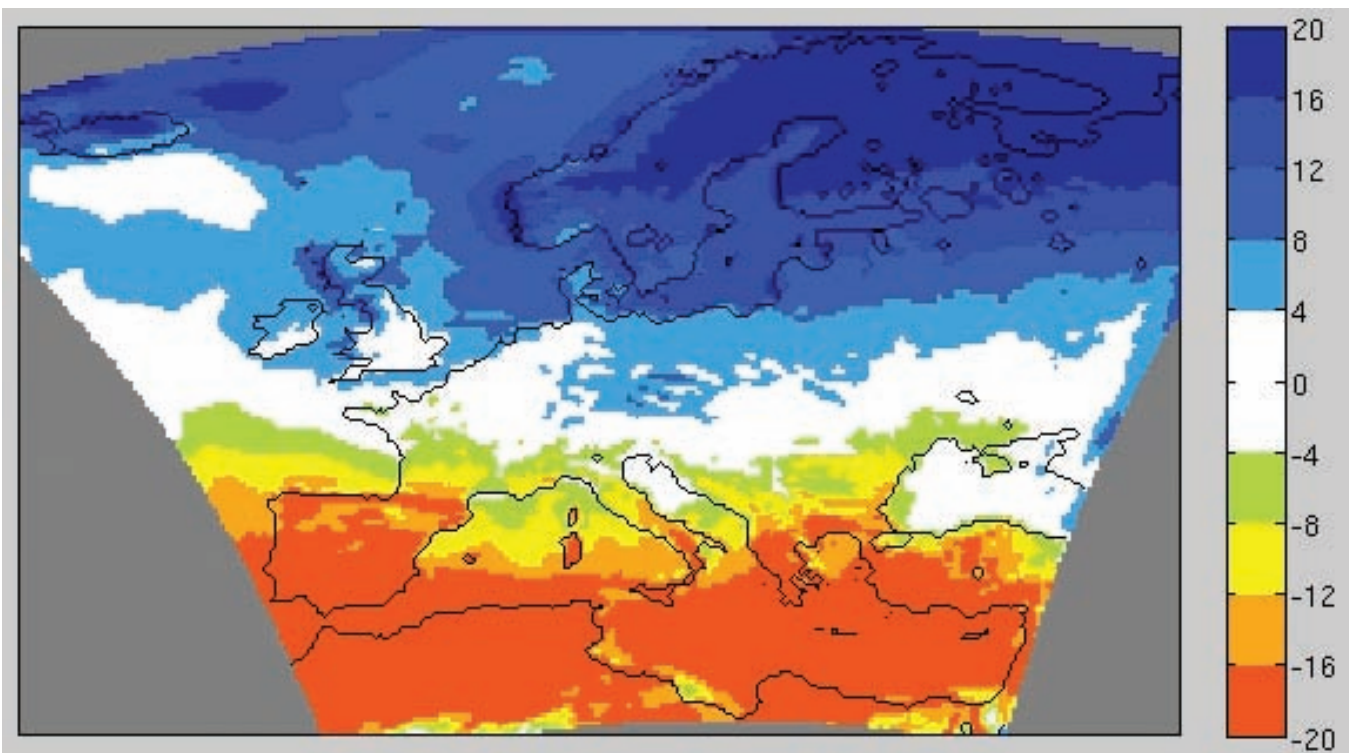


Figure A1.14: Projected changes in annual precipitation (%) under the A1B scenario, multi-model ensemble mean of RCM simulations for the time period 2071–2100 relative to the 1961–1990 mean. [RT2B]

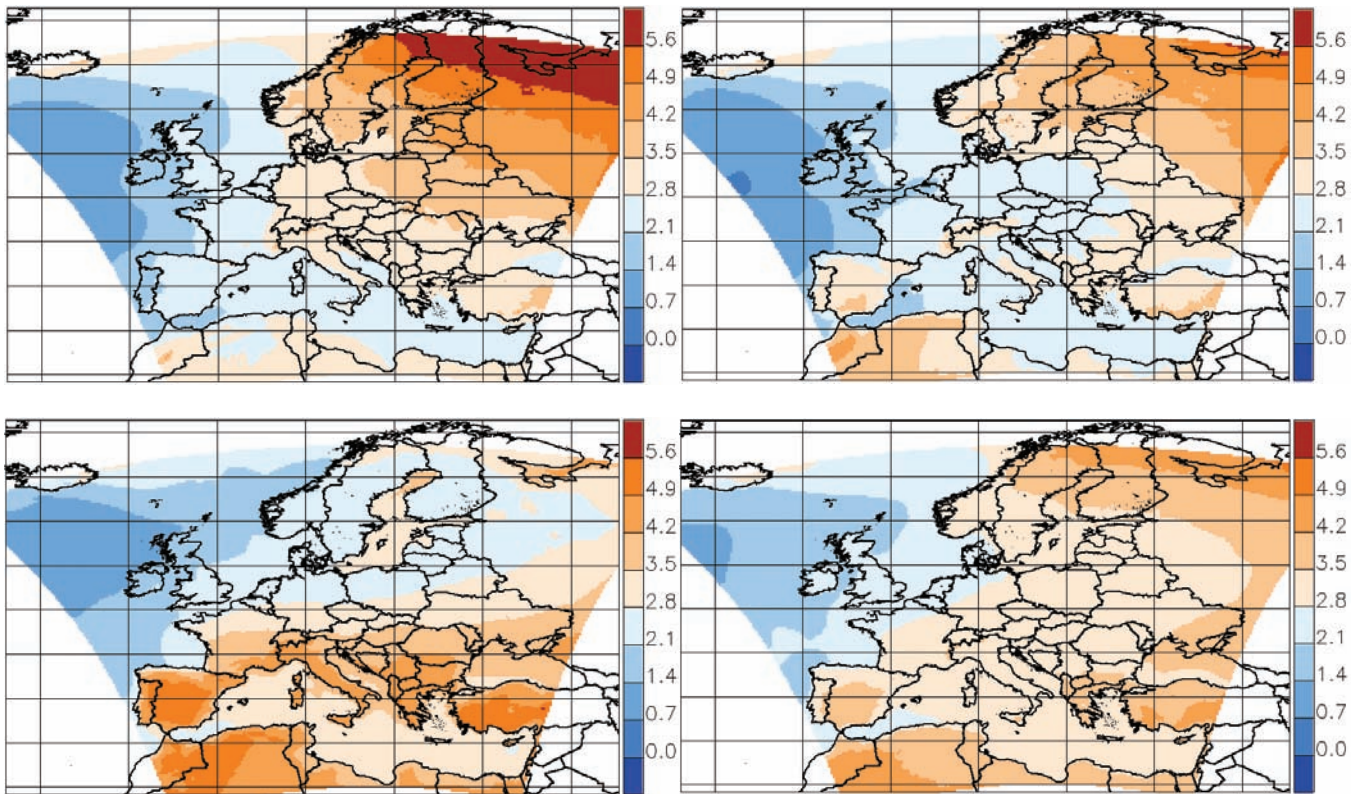


Figure A1.15: Projected changes in seasonal mean surface air temperature (K) under the A1B scenario, multi-model ensemble mean of RCM simulations for the time period 2071–2100 relative to 1961–1990 seasonal means. Top left panel is DJF, top right is MAM, bottom left is JJA, bottom right is SON. [RT2B]

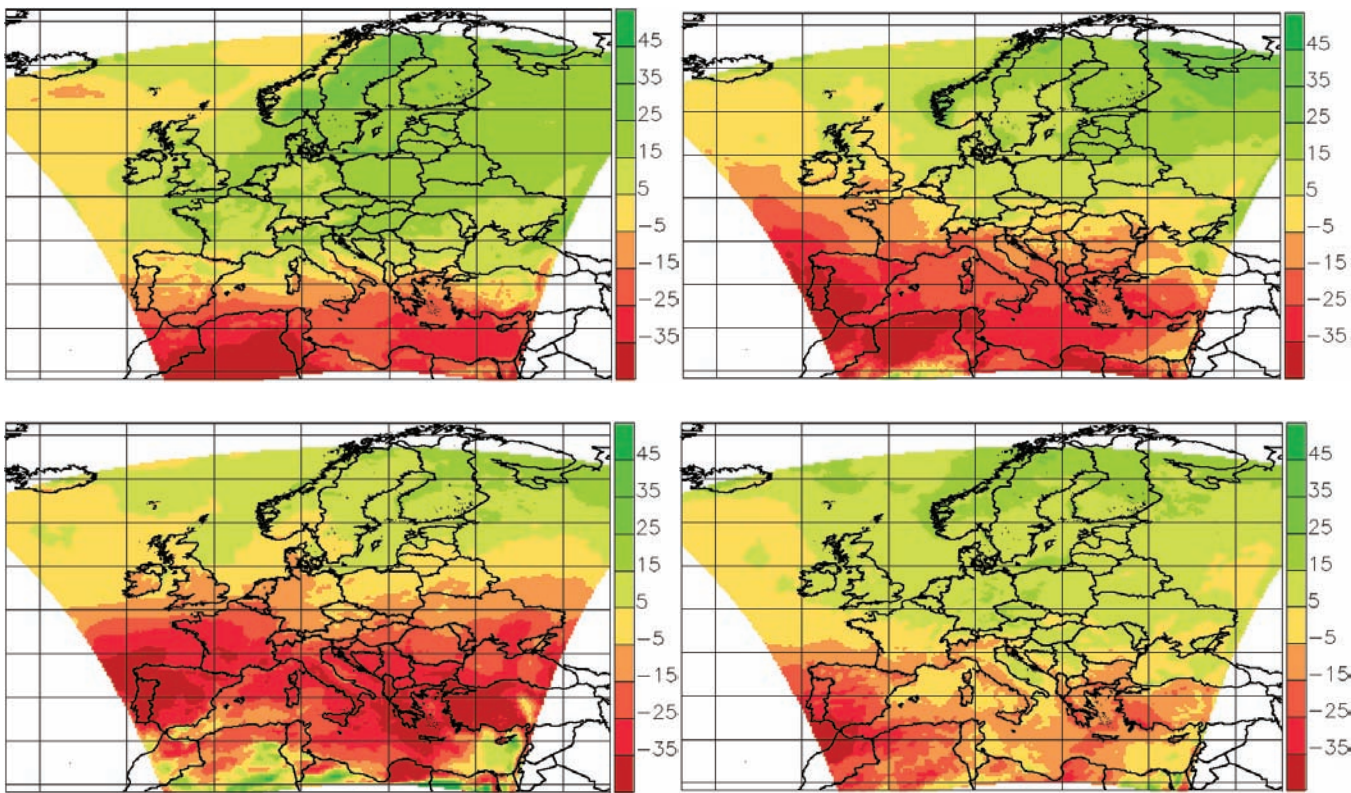


Figure A1.16: Projected changes in seasonal precipitation (%) under the A1B scenario, multi-model ensemble mean of RCM simulations for the time period 2071–2100 relative to 1961–1990 seasonal means. Top left panel is DJF, top right is MAM, bottom left is JJA, bottom right is SON. [RT2B]

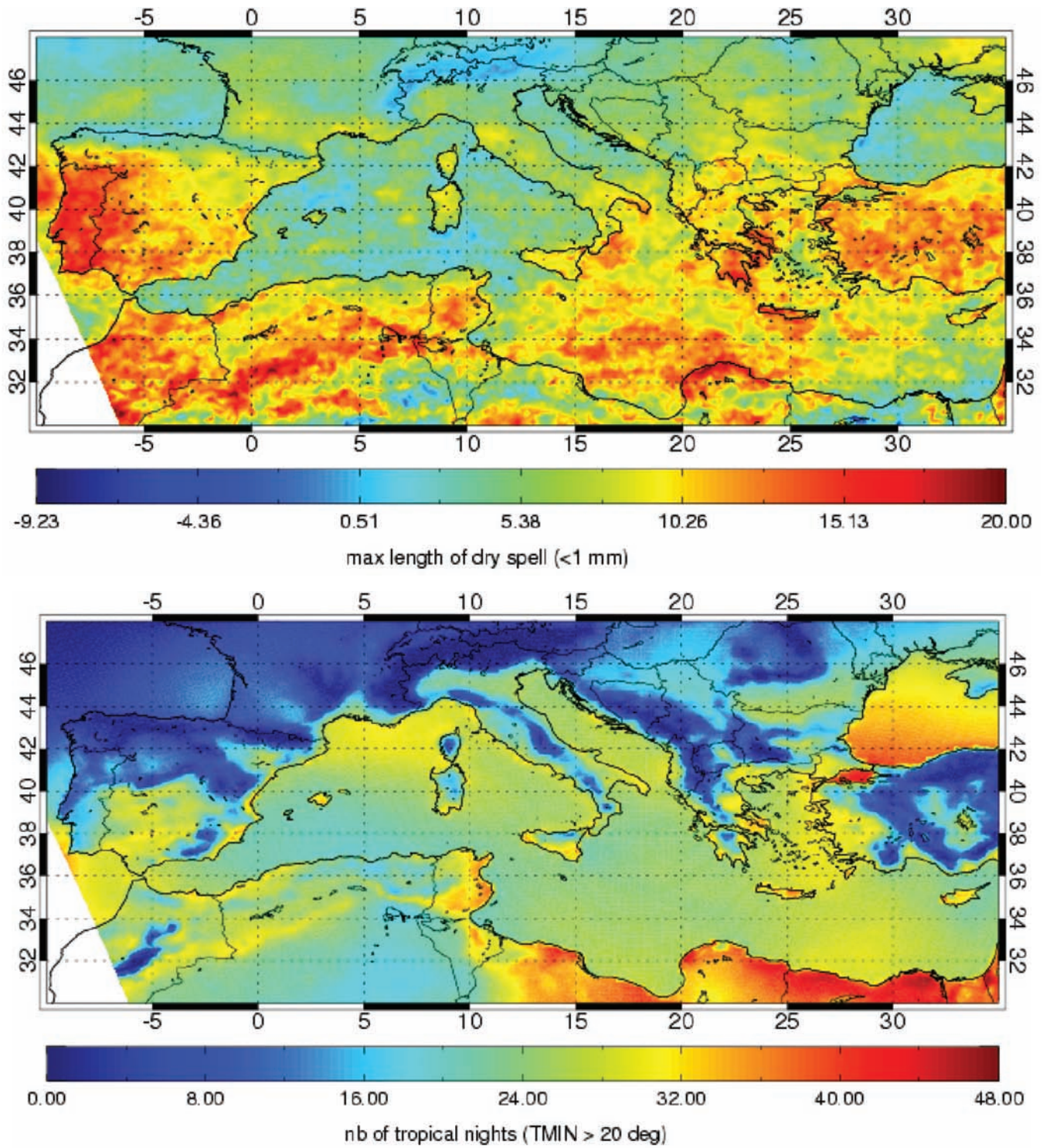


Figure A1.17: Projected change in the difference of maximum dry spell length (top) and differences in the number of nights with the minimum temperature exceeding 20°C (bottom), for the Mediterranean region under the A1B scenario, multi-model ensemble mean of six RCM simulations for the time period 2021–2050 relative to the 1961–1990 mean. [RT2B]

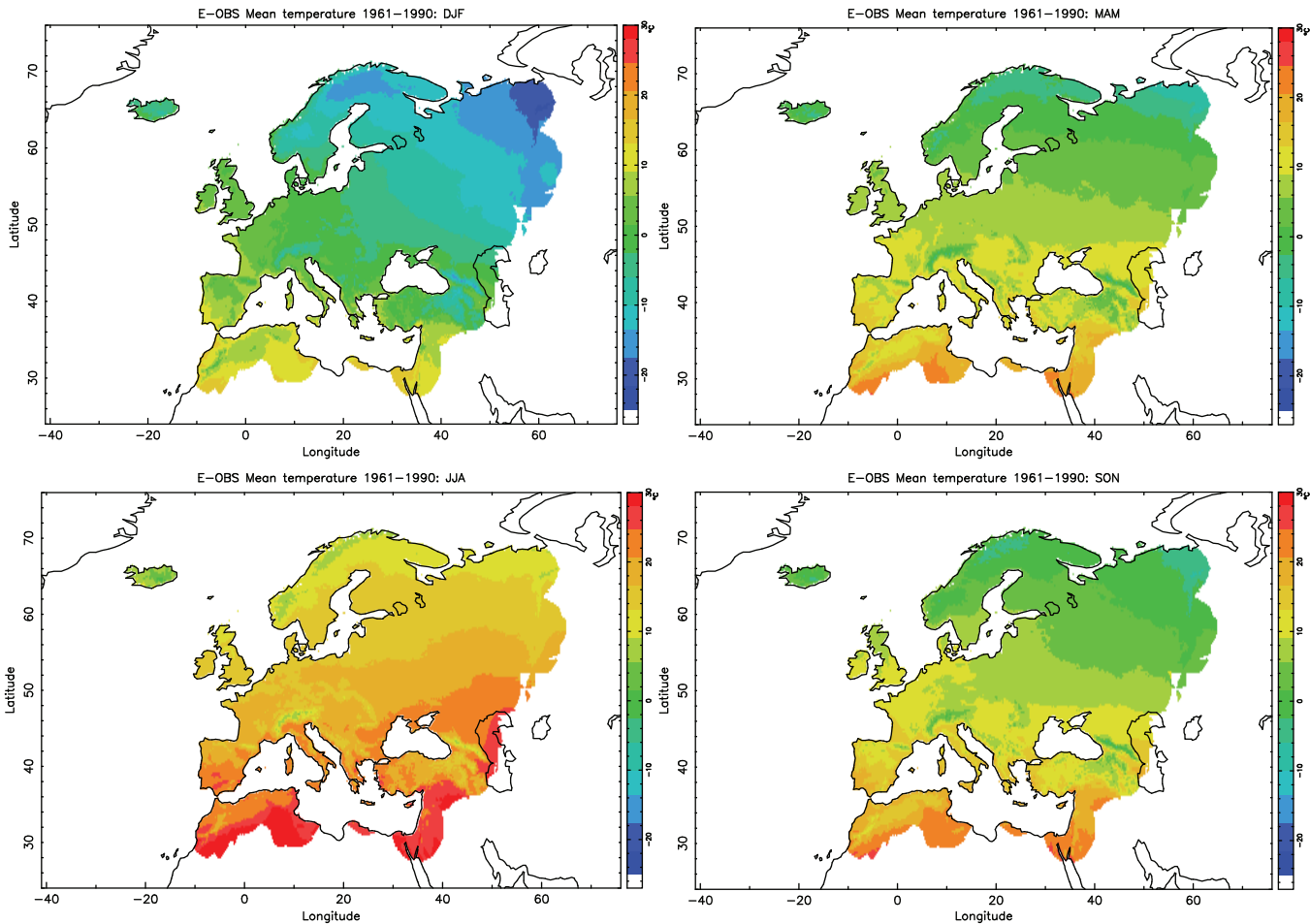


Figure A1.18: Gridded climate observations of mean seasonal temperature (K) for the period 1961–90. Top left panel is DJF, top right is MAM, bottom left is JJA, bottom right is SON. [RT5]

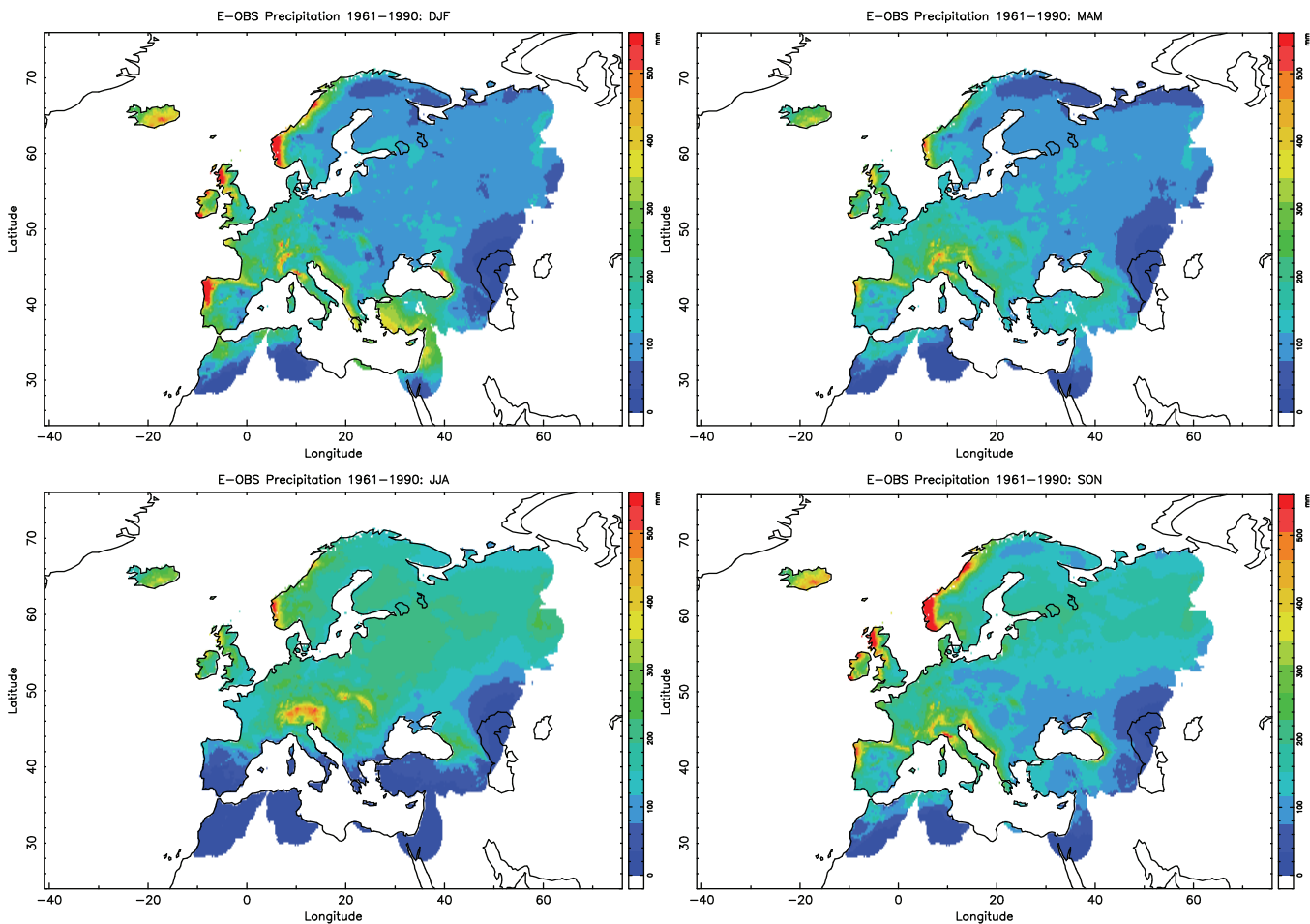


Figure A1.19: Gridded climate observations of mean seasonal rainfall (mm) for the period 1961–90. Top left panel is DJF, top right is MAM, bottom left is JJA, bottom right is SON. [RT5]

Ensemble-based global-scale quantification of terrestrial biospheric and hydrological climate change impacts [RT6]

The LPJmL dynamic global vegetation and water balance model (Bondeau et al., 2007; Rost et al., 2008a) has been applied to quantify impacts of climate change upon key terrestrial biospheric and hydrological processes by the end of this century under a suite of climate change scenarios from RT2 (Heyder et al., 2009). These impact simulations have been carried out on a $1^\circ \times 1^\circ$ global grid over land, driven by climate projections from seventeen bias-corrected general circulation models (GCMs) under forcing from the SRES A2 emission scenario (see Randall et al., 2007). Direct physiological and structural responses of plants to rising CO_2 concentration (taken from http://www.ipcc-data.org/ddc_co2.html) are dynamically accounted for in the simulations (Leipprand and Gerten, 2006; Rost et al., 2008b). Only potential natural vegetation is considered. For each output variable and grid cell, the ensemble

mean and the inter-model standard deviation of average annual values have been calculated for the period 2069–2098.

Selected results of this analysis are plotted below as a series of global maps showing the differences between 2069–2098 and 1961–1990 long-term annual averages of water fluxes (runoff, plant transpiration, soil evaporation), carbon storage (in the vegetation as well as in the soil), carbon fluxes (net primary production, heterotrophic soil respiration), and vegetation distribution (tree cover). The dotted areas in each map represent regions where the projected average change exceeds the inter-model standard deviation in 2069–2098, indicating high agreement between the different climate change scenarios (small standard deviation and/or strong change in ensemble average). The broad regional patterns of change are briefly interpreted in relation to each other. A more complete account of results based on impact metrics that account for concurrent changes in the individual processes shown will be given in a forthcoming publication (Heyder et al., 2009).

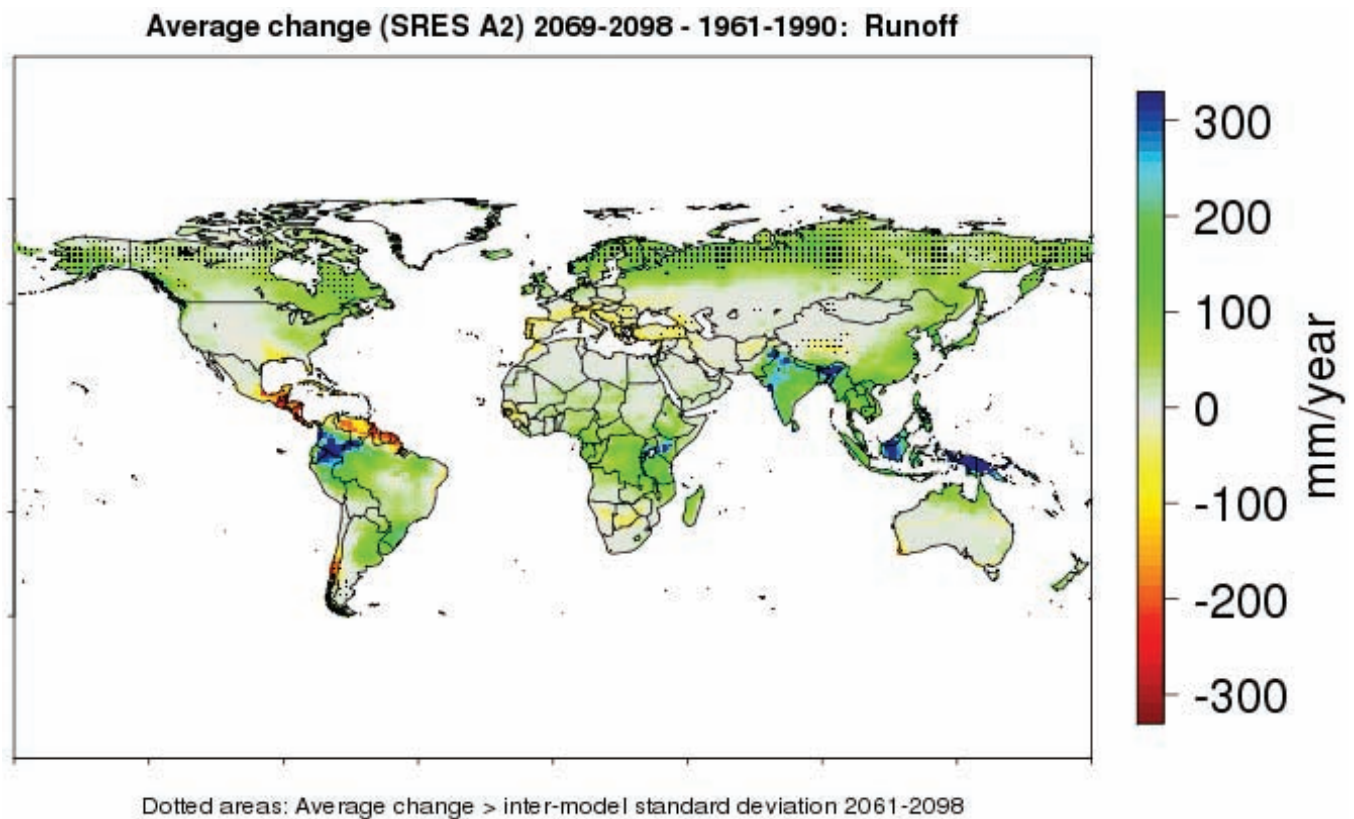
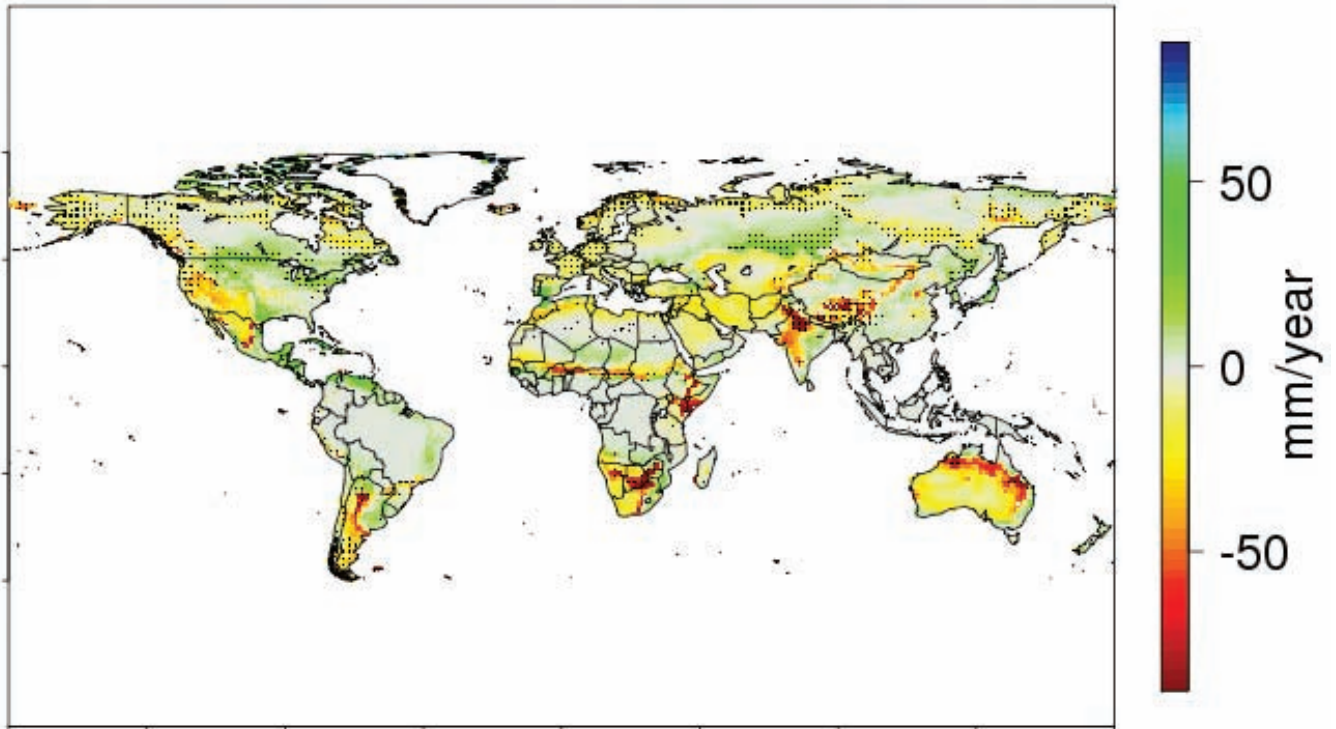


Figure A1.20. Projected changes (in mm yr^{-1}) in average annual surface and subsurface runoff. Note the high agreement among models in terms of runoff increase for high northern latitudes in response to increasing precipitation in all GCMs; and the relatively consistent decrease in runoff in parts of eastern Europe, the Near East, and parts of central Asia (dotted areas).

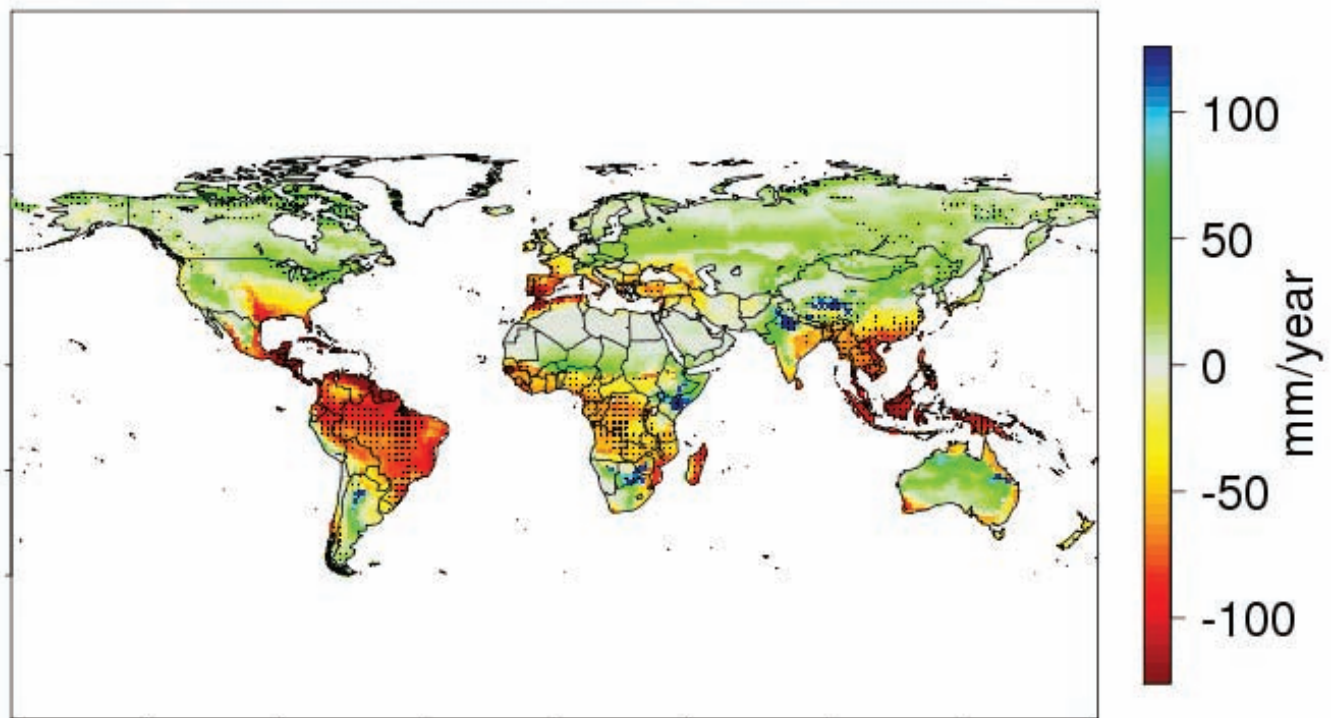
Average change (SRES A2) 2069-2098 - 1961-1990: Evaporation



Dotted areas: Average change > inter-model standard deviation 2061-2098

Figure A1.21. The projected changes (in mm yr^{-1}) in average annual soil evaporation show a pronounced regional pattern, with decreases particularly in northern Australia, western India, the Sahel, and parts of southern Africa. These changes basically mirror the changes in vegetation and transpiration patterns (see below).

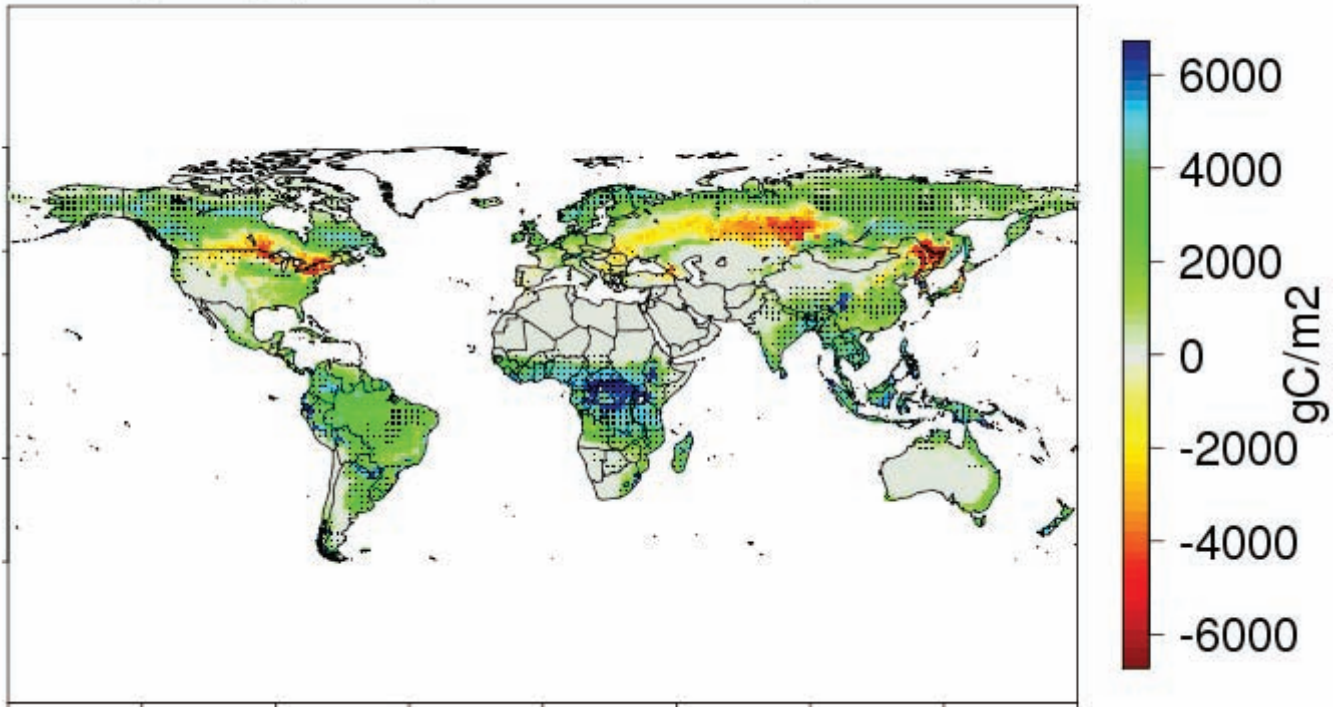
Average change (SRES A2) 2069-2098 - 1961-1990: Transpiration



Dotted areas: Average change > inter-model standard deviation 2061-2098

Figure A1.22. Simulated changes (in mm yr^{-1}) in average annual transpiration by plants. Considerable decreases occur, especially in the tropics (mostly due to the physiological CO_2 effect that reduces the aperture of plants' stomata and thus decreases transpiration, but also due to less precipitation especially in northern South America in some of the climate models). Increases in dry regions are mostly related to structural plant responses to rising CO_2 , i.e., boosted net primary production and extended vegetation cover (see below) which apparently increases regional transpiration more than the physiological CO_2 effect decreases it. Transpiration increases in the sub-Arctic zone result from the temperature-driven northward migration of the tree line.

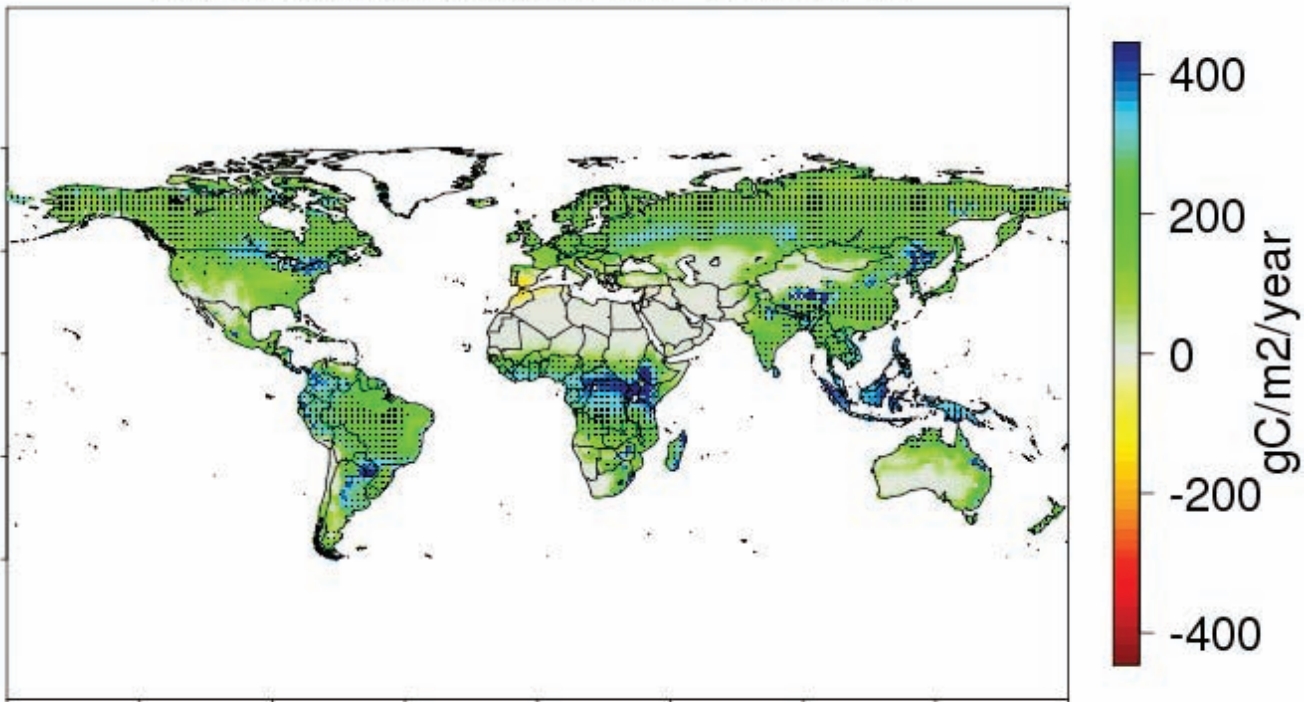
Average change (SRES A2) 2069-2098 - 1961-1990: Vegetation Carbon



Dotted areas: Average change > inter-model standard deviation 2061-2098

Figure A1.23. Projected changes (in g C m^{-2}) in average annual vegetation carbon. Structural forest changes (shifts from evergreen to summer-green) and regional forest die-backs in the temperate/boreal transition zone (see below) could lead to declining carbon stocks (Fischlin et al., 2007); in most other regions, carbon stocks are projected to increase with increasing net primary production (see below).

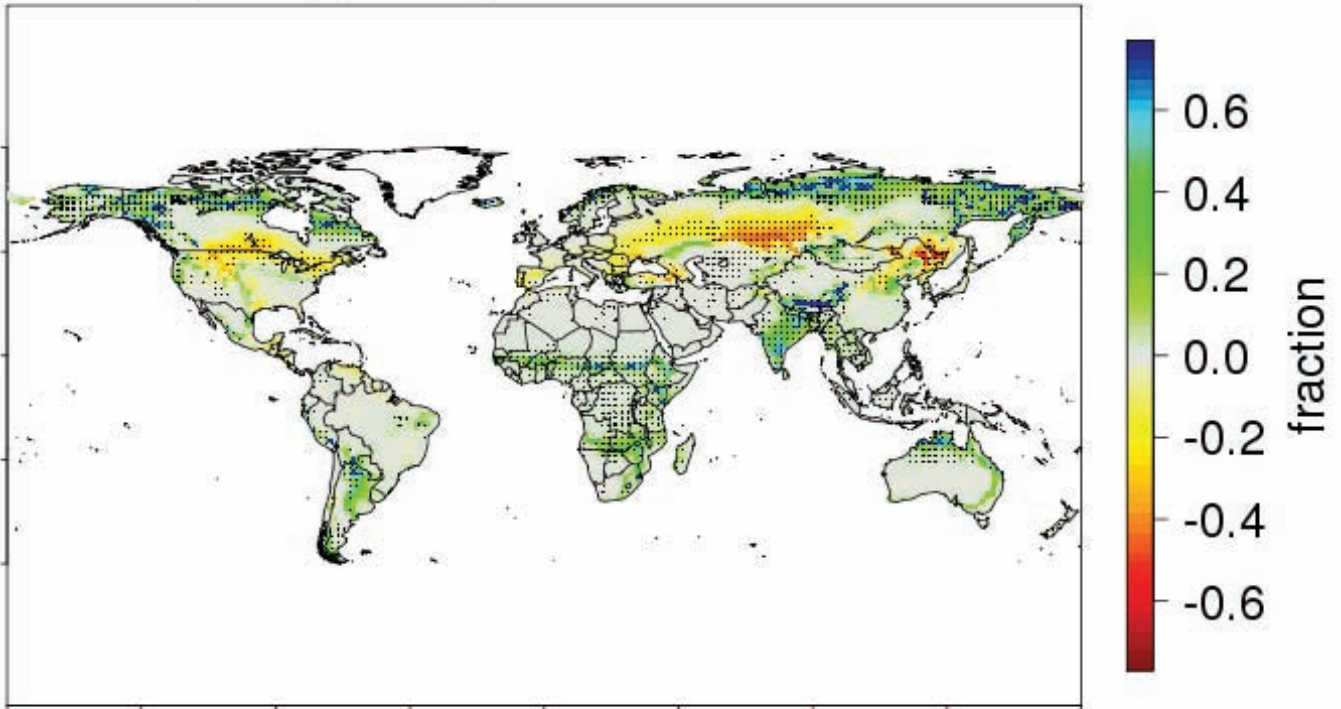
Average change (SRES A2) 2069-2098 - 1961-1990: NPP



Dotted areas: Average change > inter-model standard deviation 2061-2098

Figure A1.24. The simulated changes (in $\text{g C m}^{-2} \text{ yr}^{-1}$) in net primary production (NPP) demonstrate increases almost everywhere due to structural CO_2 fertilisation effects. Though generally supported by observational evidence, this effect is somewhat overestimated for regions that will be nutrient-limited in the future (Leipprand and Gerten, 2006). Decreases in NPP are simulated for the Mediterranean area and some other regions, where the CO_2 fertilisation effect is not able to buffer the effect of declining precipitation.

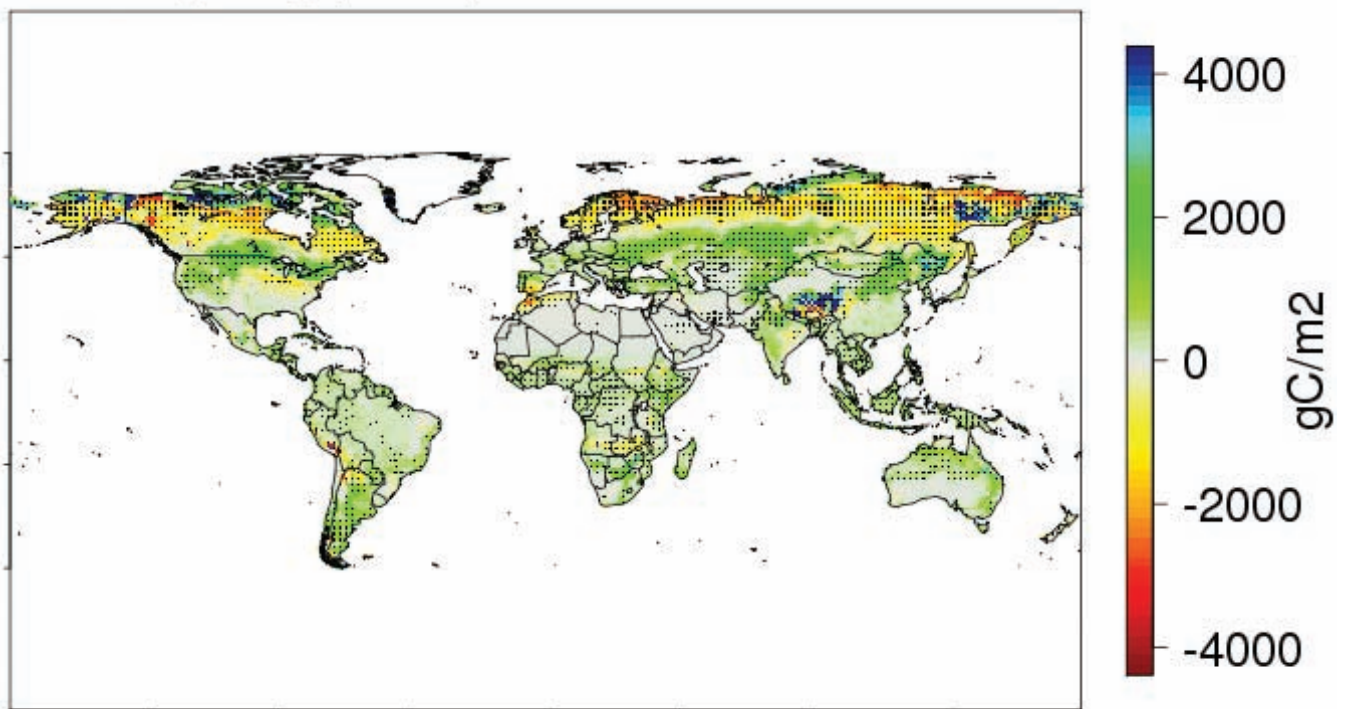
Average change (SRES A2) 2069-2098 - 1961-1990: Tree Cover



Dotted areas: Average change > inter-model standard deviation 2061-2098

Figure A1.25. Projected changes in tree cover (expressed as fraction per grid cell). Note in particular the significant declines in the southern boreal zone, which is attributable primarily to increasing heat stress (see also Schaphoff et al., 2006; Fischlin et al., 2007).

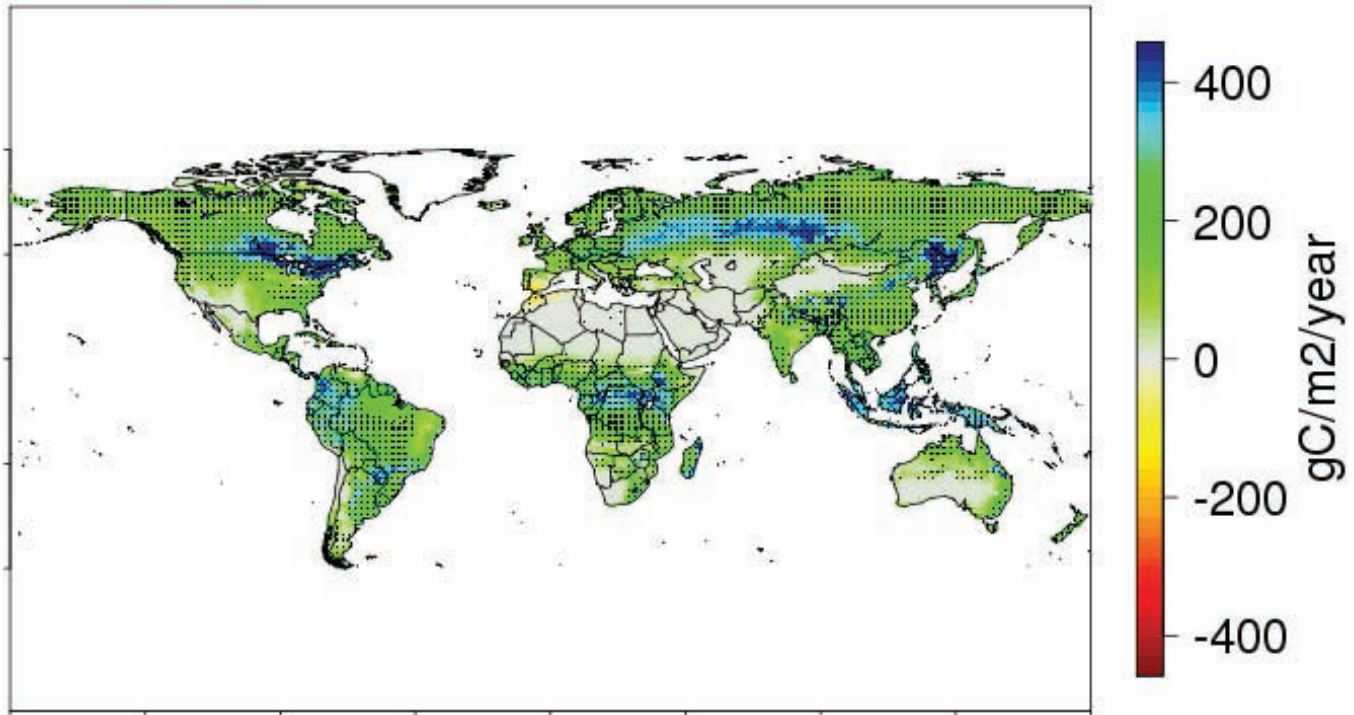
Average change (SRES A2) 2069-2098 - 1961-1990: Soil Carbon



Dotted areas: Average change > inter-model standard deviation 2061-2098

Figure A1.26. Projected changes (in $g\ C\ m^{-2}$) in soil carbon, demonstrating in particular a strong decrease in the boreal zone where higher temperatures lead to increased decomposition rates (see below).

Average change (SRES A2) 2069-2098 - 1961-1990: Heterotrophic Resp.



Dotted areas: Average change > inter-model standard deviation 2061-2098

Figure A1.27. Projected changes (in $\text{g C m}^{-2} \text{ yr}^{-1}$) in soil respiration. Increases occur almost everywhere due to a combination of increased biomass inputs to the soil through increased NPP and temperature-induced increases in decomposition rates, especially in the boreal zone. Since respiration increases more strongly than NPP in the latter region, the global terrestrial biosphere turns from a net carbon sink to a net carbon source under some climate scenarios (see Schaphoff et al., 2006).

References

- Bondeau A, Smith PC, Zaehle S, Schaphoff S, Lucht W, Cramer W, Gerten D, Lotze-Campen H, Müller C, Reichstein M, Smith B, 2007. Modelling the role of agriculture for the 20th century global terrestrial carbon balance. *Global Change Biology* 13, 679–706.
- Fischlin A, Midgley GF, Price JT, Leemans R, Gopal B, Turley C, Rounsvell MDA, Dube OP, Tarazona J, Velichko AA, 2007. Ecosystems, their properties, goods, and services. In: *Climate Change 2007: Impacts, Adaptation and Vulnerability* (IPCC, ed.). Cambridge University Press, Cambridge, UK, 211–272.
- Heyder U, Lucht W, Gerten D, 2009. Risks of change in biospheric features under multi-model projections of climate change. In preparation.
- Leipprand A, Gerten D, 2006. Global effects of doubled atmospheric CO_2 content on evapotranspiration, soil moisture, and runoff under potential natural vegetation. *Hydrological Sciences Journal* 51, 171–185.
- Randall DA, et al., 2007. Climate models and their evaluation. In: *Climate Change 2007: The Physical Science Basis. Contribution of Working Group I to the Fourth Assessment Report of the Intergovernmental Panel on Climate Change* (IPCC, ed.). Cambridge University Press, Cambridge, UK, 589–662.
- Rost S, Gerten D, Bondeau A, Lucht W, Rohwer J, Schaphoff S, 2008a. Agricultural green and blue water consumption and its influence on the global water system. *Water Resources Research* 44, W09405, doi:10.1029/2007WR006331.
- Rost S, Gerten D, Heyder U, 2008b. Human alterations of the terrestrial water cycle through land management. *Advances in Geosciences* 18, 43–50.
- Schaphoff S, Lucht W, Gerten D, Sitch S, Cramer W, Prentice IC, 2006. Terrestrial biosphere carbon storage under alternative climate projections. *Climatic Change* 74, 97–122.
- Smith DM, Cusack S, Colman AW, Folland CK, Harris GR, Murphy JM, 2007. Improved surface temperature prediction for the coming decade from a global climate model. *Science* 317, 796–799.

Appendix 2: ENSEMBLES datasets

Introduction

The ENSEMBLES project has generated a vast (>60 terabytes) resource base of data, which is all digital and stored on internet archives. This Appendix describes these datasets – where to find them, what they consist of, and other supporting information. All data are made freely available for academic, educational and commercial use, but use must be acknowledged by inclusion of the following statement: ‘*The ENSEMBLES data used in this work was funded by the EU FP6 Integrated Project ENSEMBLES (Contract number 505539), whose support is gratefully acknowledged.*’ Please see the ENSEMBLES data policy document for more information: http://ensembles-eu.metoffice.com/docs/Ensembles_Data_Policy_261108.pdf.

The following dataset descriptions cover the daily gridded observational datasets (RT5), the seasonal to decadal predictions for streams 1 and 2 (RT1 and RT2A), the global climate change simulations for streams 1 and 2 (RT2A), the regional simulations for the ERA-40 period (RT3), the regional climate change simulations, the quick-look analyses (RT2B), and the statistical downscaling (RT2B).

Daily gridded observational datasets [RT5]

Gridded observational datasets of daily precipitation and temperature have been developed on the basis of a European network of high-quality station series. The datasets cover the period from 1950 to 2008. They are made available on a 0.25 and 0.5 degree regular latitude–longitude grid, as well as on a 0.22 and 0.44 degree rotated pole grid. The grid is the same as the Climatic Research Unit monthly datasets for the globe. The rotated grid is the same as used in many ENSEMBLES Regional Climate Models. As well as ‘best estimate’ values, separate files are provided containing 95% confidence intervals, and surface elevation. A description can be found in Haylock et al. (2008). Note that these datasets are strictly for use in non-commercial research and non-commercial education projects only. They are available from: <http://eca.knmi.nl/download/ensembles/ensembles.php>

For more details contact Albert Klein Tank:
Albert.Klein.Tank@knmi.nl

Reference: Haylock MR, Hofstra N, Klein Tank AMG, Klok EJ, Jones PD, New M, 2008. A European daily high-resolution gridded dataset of surface temperature and precipitation for 1950–2006. *Journal of Geophysical Research* 113, doi:10.1029/2008JD010201.

Seasonal to decadal simulations [RT1 and RT2A]

The seasonal to decadal (s2d) experiments comprise two sets of simulations: the stream 1 and stream 2 simulations. For both streams, coordinated forecast experiments over seasonal, interannual and decadal timescales have been performed. Three

different approaches were pursued to represent model uncertainties: the multi-model approach, the perturbed physical parameter approach and the stochastic physics approach. The data are available through the MARS server at ECMWF. For more information on the scope of the experiments as well as results look at: http://www.ecmwf.int/research/EU_projects/ENSEMBLES/data/index.html.

For more details contact Francisco J. Doblas-Reyes:
Francisco.Doblas-Reyes@ecmwf.int

Centennial simulations [RT2A]

Centennial simulations using climate models from European modelling groups (CNRM, DMI, FUB, INGV, IPSL, METO-HC, MPIMET, NERSC) produced a set of state-of-the-art benchmark simulations during the first phase of ENSEMBLES (stream 1). A set of multi-model simulations were produced over the period 1860–2000 to simulate the longer-term climate anomalies observed during the 20th century in response to a prescribed set of anthropogenic forcings only and also with the addition of natural forcings. A multi-model set of coupled simulations over the 21st century has been produced with the three scenarios of aerosol and GHG forcings proposed by IPCC (scenarios A2, A1B and B1) in order to produce a projection of the future climate with a better estimate of the uncertainties due to model formulation, initial state of the climate system, and scenario choice.

Results of most of the RT2A climate scenarios are stored in the WCRP CMIP3 archive at PCMDI, from where they were used in the IPCC AR4 assessment (see http://www-pcmdi.llnl.gov/ipcc/about_ipcc.php). High temporal resolution (daily and 6-hourly) results from the RT2A multi-decadal simulations are available on the CERA database, run by the Model&Data group at the Max-Planck Institute for Meteorology (<http://www.mad.zmaw.de/projects-at-md/ensembles/>).

Improved model versions, some including new components for the carbon cycle and aerosols, have run a new set of simulations taking into account land-use change, as observed or computed by a recent version of the IMAGE integrated assessment model. In addition to an A1B scenario, a new stabilisation scenario to 450 ppm of CO₂-equivalent, developed in collaboration with RT7, was used for the stream 2 climate change simulations. A subset of the stream 2 data is stored at the CERA database in Hamburg.

For more details about CERA contact Heinz-Dieter Hollweg:
Heinz-Dieter.Hollweg@zmaw.de

The probabilistic projections produced by the Met Office Hadley Centre and commonly referred to as the ‘grand ensemble’ are also available online. The data are supplied in numerical form in terms of 10,000 distribution sample points per grid box. Rockel, northern Europe, Mediterranean and Europe regions are also defined. The data are available from http://ensembles-eu.metoffice.com/secure/RT6_data_230609/data_for_RT6.html.

Regional simulations driven by ERA-40 reanalysis data [RT3]

The ENSEMBLES RT3 simulations with the ERA-40 reanalysis as boundary conditions are available on the RT3/RT2B archive at <http://ensemblesrt3.dmi.dk>. Up to 130 fields are available from each simulation, covering the period 1951–2002. The data are available through an OpenDAP interface, which allows sub-windows and sub-periods to be selected for download. Institutes, models and contact persons are listed below:

C4I	RCA	Ray McGrath
CHMI	ALADIN	Petr Štěpánek
CNRM	ALADIN	Michel Déqué
DMI	HIRHAM	Ole B. Christensen
ETHZ	CLM	Christoph Schär
GKSS	CLM	Burkhardt Rockel
HC	HadRM	Erasmus Buonomo
ICTP	RegCM	Filippo Giorgi
INM	RCA	Bartolomé Orfila
KNMI	RACMO	Erik van Meijgaard
METNO	HIRHAM	Jan Erik Haugen
MPI	REMO	Daniela Jacob
SMHI	RCA	Erik Kjellström
UCLM	PROMES	Manuel de Castro
OURANOS	CRCM	Dominique Paquin

For more details contact Ole Bøssing Christensen: obc@dmi.dk

Regional climate change simulations and quick-look analysis [RT2B]

RT2B formed Part 2 of the ENSEMBLES model engine, i.e., the regional component (RT2A forms Part 1, the global component). It constructed and analysed probabilistic high-resolution regional climate scenarios and seasonal–decadal hindcasts. An ensemble of regional climate change scenarios using as many GCM-RCM combinations as possible was constructed and is described in Table A2.1. These simulations are available on the RT3/RT2B archive at <http://ensemblesrt3.dmi.dk>

Quick-look analysis [RT2B]

A quick-look analysis has been set up in order to provide very fast information on the RCM scenarios results. For 2 m temperature, precipitation and evaporation, area means for the eight Rockel regions are available on a monthly basis by each modelling partner for their transient runs on 25 km horizontal resolution. MPI-M has computed yearly means, seasonal means and annual cycles for each decade and produced plots showing time-series of the results of all ENSEMBLES RCMs.

Statistical downscaling [RT2B]

Statistical downscaling (SDS) was conducted by ten ENSEMBLES partners in RT2B using a range of different

Table A2.1: ENSEMBLES GCM-RCM Matrix of RCM simulations at 25 km resolution. Those simulations and institutes marked with an asterisk (*) are non-contractual runs. For the METO-HC GCM, there are standard (std), low and high sensitivity runs.

RCM	GCM	ERA40	METO-HC, Std	METO-HC, Low	METO-HC, High	MPIMET	IPSL	CNRM	NERSC	CGCM3	Total
METO-HC <i>HadRM</i>		1961–2002	1951–2100	1951–2100*	1951–2100*	1951–2100					4
MPIMET <i>REMO</i>		1961–2002				1951–2100	1951–2050*				2
CNRM <i>ALADIN</i>		1961–2002						1951–2050			1
DMI <i>HIRHAM</i>		1961–2002				1951–2100*		1951–2100	1951–2100*		3
ETH <i>CLM</i>		1961–2002	1951–2100								1
KNMI <i>RACMO</i>		1961–2002				1951–2100					1
ICTP <i>RegCM</i>		1961–2002				1951–2100					1
SMHI <i>RCA3</i>		1961–2002		1951–2100*		1951–2100*			1951–2100		3
UCLM <i>PROMES</i>		1961–2002	1951–2050	1951–2050							1
C4I <i>RCA3</i>		1961–2002			1951–2100*	1951–2050*					2
GKSS <i>CLM</i>		1961–2002					1951–2050*				1
Met.No <i>HIRHAM</i>		1961–2002	1951–2050						1951–2050*		1
CHMI <i>ALADIN</i>		1961–2002						1951–2050*			1
OURANOS* <i>CRCM</i>		1961–2002								1951–2050*	1
EC* <i>GEMLAM</i>		1961–2002									
VMGO* <i>VMGO</i>			1951–2050*								1
Total			3	3	2	7	2	3	3	1	25

methods. Most groups downscaled GCM simulations, but C4I applied SDS to RCM outputs.

For each group (ARPA-SIM, FIC, GKSS, IAP, KNMI, NIHWM, NMA, UEA) and downscaling method, the following information is provided: predictands and predictors, brief description of method and reference, source of predictors, region(s)/predictand datasets which have been downscaled, and a brief outline of how uncertainties are addressed and/or probabilistic projections derived. A summary of the information available is shown in Table A2.2.

This table does not list the methods implemented in the ENSEMBLES web-based downscaling service developed by the University of Cantabria (UC) (www.meteo.unican.es/ensembles). This service is intended as a useful and friendly service for end-users with limited experience in the technical issues associated

with statistical downscaling. It allows downscaling of ENSEMBLES seasonal–decadal hindcasts as well as climate change simulations. It also incorporates a data access tool which provides easy access to reanalysis data and a number of ENSEMBLES data outputs.

Dynamically downscaled hindcast simulations undertaken by INM in RT2B are available at:
http://www.ecmwf.int/research/EU_projects/ENSEMBLES/data/index.html

Access to RT2B SDS outputs is through the Regional Scenarios Portal, which also provides access to many other relevant datasets and background information: <http://www.cru.uea.ac.uk/projects/ensembles/ScenariosPortal/>

For more details contact Clare Goodess: c.goodess@uea.ac.uk

Table A2.2: Summary of statistical downscaling methods used in RT2B. Note that methods implemented in the ENSEMBLES web-based downscaling service (www.meteo.unican.es/ensembles) are not listed. ACC: Anthropogenic Climate Change runs to 2100; s2d: seasonal to decadal hindcasts.

ENSEMBLES partner	Variables to be downscaled	Method	ENSEMBLES runs to be downscaled	Region(s) where downscaling will be applied
ARPA-SIM	Daily Precipitation, Tmin, Tmax	Regression, conditioned by circulation - canonical correlation analysis (CCA)	ACC GCM runs	N-Italy
ARPA-SIM	Daily Precipitation, Tmin, Tmax	Multiple linear regression –Model Output Statistics + BLUE	Stream 1 s2d runs	Italy
FIC	Daily precipitation and temperatures. Wind and humidity will be tested.	Two-step analogue method	ACC GCM runs RT2B RCMs later	Europe – ENSEMBLES gridded observations
GKSS	Marine surface wind	Conditional stochastic weather generator	ACC GCM runs	Germany/Netherlands
IAP	Daily temperature (& daily precipitation?)	Regression, conditioned by circulation	ACC GCM runs	ECA&D European stations
IAP	Daily temperature	Multilayer perceptron neural network	ACC GCM runs	ECA&D European stations
IAP	Precipitation, Tmin and Tmax, solar radiation	Conditional stochastic weather generator	ACC GCM runs	ECA&D European stations
IAP	Daily temperature (& daily precipitation?)	Multiple linear regression	ACC GCM runs	ECA&D European stations
KNMI	Multi-site (sub)daily RCM precipitation (and temperature)	Nearest-neighbour resampling	ACC GCM runs	River Rhine catchment
NIHWM	Temperature, precipitation, drought indices, river discharge	Conditional stochastic weather generator	ACC GCM runs	Danube basin
NMA	Daily precipitation	Mixture between two-state first order Markov chain and CCA	ACC GCM runs Possibly RCM runs	Southern Romania
UEA	Daily precipitation, Tmax, Tmin, vapour pressure, wind speed, sunshine duration, relative humidity, reference PET	Stochastic weather generator	Change factors taken from RT2B RCM runs	7 mainland European stations, plus 3–4 UK stations.

Appendix 3: ENSEMBLES partners and affiliates

ENSEMBLES partners

	Partner name	Country
1	Met Office, Hadley Centre for Climate Prediction and Research	UK
2	Météo-France, Centre National de Recherches Météorologiques	France
3	Centre National de la Recherche Scientifique (inc. IPSL, LMD, LSCE, LGGE)	France
4	Danish Meteorological Institute	Denmark
5	European Centre for Medium-Range Weather Forecasts	UK
6	International Institute for Applied Systems Analysis	Austria
7	Istituto Nazionale di Geofisica e Vulcanologia	Italy
8	Royal Netherlands Meteorological Institute	Netherlands
9	University of Bristol	UK
10	MPG represented by Max-Planck-Institut für Meteorologie (comprises two institutions: MPIMET and MPIMET.MD)	Germany
11	National Observatory of Athens	Greece
12	Swedish Meteorological and Hydrological Institute	Sweden
13	University of East Anglia	UK
14	Universität Hamburg	Germany
15	CGAM, University of Reading	UK
16	Agenzia Regionale per la Prevenzione e l'Ambiente dell'Emilia-Romagna, Servizio Idro Meteorologico	Italy
17	Aristotle University of Thessaloniki	Greece
18	Bureau of Meteorology Research Centre	Australia
19	Société Civile CERFACS	France
20	Czech Hydrometeorological Institute	Czech Republic
21	Center for International Climate and Environmental Research, Oslo	Norway
22	CLIMPACT	France
23	Consiglio Nazionale Delle Ricerche	Italy
24	Charles University, Prague, Faculty of Mathematics and Physics	Czech Republic
25	Department of Agronomy and Land Management, University of Florence	Italy
26	<i>Deutscher Wetterdienst (resigned in Year 4)</i>	Germany
27	Electricité de France	France
28	École Normale Supérieure, Paris	France
29	Swiss Federal Institute of Technology Zurich	Switzerland
30	Fondazione Eni Enrico Mattei	Italy
31	Fundacion para la Investigacion del Clima	Spain
32	Finnish Meteorological Institute	Finland
33	University of Applied Sciences Stuttgart	Germany
34	Freie Universität Berlin	Germany
35	GKSS Forschungszentrum Geesthacht GmbH	Germany
36	Ústav fyziky atmosféry AV ČR	Czech Republic
37	The Abdus Salam International Centre for Theoretical Physics	Italy
38	Instituto Nacional de Meteorologia	Spain
39	The Trustees of Columbia University in the City of New York	USA
40	University of Stuttgart	Germany
41	Joint Research Centre of the European Community	Italy
42	London School of Economics	UK
43	London School of Hygiene and Tropical Medicine	UK
44	Norwegian Meteorological Institute	Norway
45	Federal Office of Meteorology and Climatology	Switzerland
46	Nansen Environmental and Remote Sensing Center	Norway
47	National Institute of Hydrology and Water Management	Romania
48	National Meteorological Administration	Romania
49	Research Centre for Agricultural and Forest Env't, Polish Academy of Sciences	Poland
50	Potsdam Institute for Climate Impact Research	Germany
51	Société de Mathématiques et de Sciences Humaines	France

52	Finnish Environment Institute	Finland
53	Universidad de Cantabria	Spain
54	Université Catholique de Louvain	Belgium
55	Universidad de Castilla La Mancha	Spain
56	University of Oslo	Norway
57	Lunds Universitet	Sweden
58	Universität Kassel	Germany
59	University of Liverpool	UK
60	Chancellor Masters and Scholars of Oxford University	UK
61	<i>WINFORMATICS (Resigned in Year 1)</i>	UK
62	Université Joseph Fourier	France
63	Met Éireann (Community Climate Change Consortium for Ireland)	Ireland
64	Universität Bern (previously IUKB)	Switzerland
65	Leibniz-Institut für Meereswissenschaften (previously IfM)	Germany
66	University of Geneva (previously University of Fribourg)	Switzerland
67	Planbureau voor de Leefomgeving (previously RIVM and MNP)	Netherlands
68	University of Aarhus (previously DIAS)	Denmark

ENSEMBLES affiliates

	Institute name	Country
1	University of Copenhagen	Denmark
2	University of Exeter	UK
3	FAO	Italy
4	WHO	Italy
5	University of Zurich	Switzerland
6	ESSC	USA
7	University of Ireland	Ireland
8	NCAR	USA
9	FRGCG	Japan
10	University of Tokyo (CSSR)	Japan
11	National Institute of Earth Sciences	Japan
12	SINTEF Energy Research	Norway
13	OURANOS	Canada
14	CRCMD	Canada
15	Climate Analysis Group	Canada
16	National Academy of Sciences of Ukraine	Ukraine
17	University of Newcastle	UK
18	Proudman Oceanographic Laboratory	UK
19	IBIMET Institute	Italy
20	Institute of Atmospheric Physics (IAP)	China
21	University College London	UK
22	Instituto Geofísico Infante D Luiz, University of Lisbon	Portugal
23	Consejería de Medio Ambiente de Andalucía	Spain
24	CEH (WATCH project)	UK
25	NEA (Nordic CES Project)	Iceland
26	Katholieke Universiteit Leuven	Belgium
27	Agrarian Technological Institute of Castilla y León (ITACyL)	Spain
28	King's College London (FREE - HydroClimate.org)	UK
29	Dept. Física General y de la Atmosfera Ciencias Físicas, Universidad de Salamanca	Spain
30	International Commission for the Hydrology of the Rhine Basin (CHR)	Netherlands

Appendix 4: Contributors

The following people kindly submitted material or reviewed this report and the section authors gratefully acknowledge their contributions by naming them in this appendix.

J. Alcamo (UNEP and University of Kassel)
M. Allen (Oxford University)
J. Andréasson (SMHI)
C. Appenzeller (MeteoSwiss)
L. Bärring (Lund University and SMHI)
M. Baylis (University of Liverpool)
J. Beersma (KNMI)
M. Begert (Meteo Swiss)
A. Bellucci (INGV)
M. Beniston (University of Geneva)
R. Betts (Met Office)
M. Bindi (University of Florence)
E. Blyth (CEH)
C. Børgesen (University of Aarhus)
S. Bony (IPSL)
A. Busuioc (NMA)
P. Cadule (LSCE)
C. Caminade (University of Liverpool)
H. Caspary (FTS-STU)
A. Challinor (University of Leeds)
O. Christensen (DMI)
A.S. Cofiño (University of Cantabria)
U. Cubasch (FUB)
P. Della-Marta (PartnerRe Reinsurance and MeteoSwiss)
M. Déqué (Météo-France)
E. Diez (Instituto Nacional de Meteorología)
F. Doblas-Reyes (ECMWF)
M. Donat (Freie Universität Berlin)
H. Douville (CNRM)
L. Dubus (EDF)
R. Ferrise (University of Florence)
T. Fichefet (UCL)
J. Fisher (University of Oxford)
P. Foster (University of Bristol)
P. Friedlingstein (LSCE and University of Bristol)
S. Fronzek (SYKE)
D. Gerten (PIK)
C. Giannakopoulos (National Observatory of Athens)
M. Giorgetta (MPIMET)
F. Giorgi (ICTP)
P. Graham (SMHI)
N. Groll (GKSS)
H. Guis (CIRAD)
J.M. Gutiérrez (University of Cantabria)
G. Harris (Met Office)
T. Hickler (Lund University)
I. Hoeschel (FUB)
H-D. Hollweg (MPI)
H. Huebener (FUB)
T. Johns (Met Office)
A. Jones (University of Liverpool)
A.M. Jönsson (Lund University)
N. Keenleyside (ifM)
E. Kendon (Met Office)
E. Kjellström (SMHI)
E. Kostopoulou (NOA)
S. Kotlarski (ETH)
Z. Kundzewicz (Polish Academy of Sciences)
G.C. Leckebusch (Freie Universität Berlin)
M. Liniger (MeteoSwiss)
D. Lister (UEA)
P. Lorenz (MPI)
N. MacKellar (DMI)
C. Mares (NIHWM)
I. Mares (NIHWM)
V. Marletto (ARPA-SIM)
W. May (DMI)
F. Niehörster (Free University of Berlin)
M. Nogaj (EDF)
J. Olesen (University of Aarhus)
B. Orfila (Instituto Nacional de Meteorología)
P. Pardeep (ETHZ)
V. Pavan (ARPA-SIMC)
J. Polcher (LMD)
Z. Qu (EDF)
S. Rauscher (ICTP)
J. Ribalaygua (Fundacion para la Investigacion del Clima)
P. Rogel (CERFACS)
S. Rost (PIK)
J-F. Royer (CNRM)
E. Sanchez (UCLM)
S. Schubert (MPIMET-MD)
F. Selten (KNMI)
T. Semmler (C4I)
S. Sitch (University of Leeds)
D. Smith (Met Office)
S. Somot (Météo-France)
M. Szwed (Polish Academy of Sciences)
F. Tomei (ARPA-SIM)
R. Tomozeiu (ARPA-SIMC)
A. Turner (University of Reading)
E. van den Besselaar (KNMI)
E. van Meijgaard (KNMI)
G.J. van Oldenborgh (KNMI)
D. van Vuuren (PBL)
A. Venäläinen (Finnish Meteorological Institute)
G. Villani (ARPA-SIM)
A. Weisheimer (ECMWF)
A. Weigel (Meteo Swiss)
M. Weiß (University of Kassel)
F. Wetterhall (King's College, University of London)
T. Wheeler (University of Reading)

The ENSEMBLES project was funded by the European Commission to research climate change and its impacts in Europe. The research was conducted between September 2004 and December 2009 by a Consortium of 66 research institutes, mostly from Europe. The Consortium was led by the Met Office Hadley Centre.

The three main integrated results were that ENSEMBLES:

- developed an ensemble prediction system for climate change based on state-of-the-art, high-resolution, global and regional Earth system models developed in Europe, validated against quality-controlled, high-resolution gridded datasets for Europe, and produced an objective probabilistic estimate of uncertainty in future climate at seasonal to decadal, and up to centennial time-scales;
- quantified and reduced the uncertainty in the representation of physical, chemical, biological and human-related feedbacks in the Earth system (including water resource, land use and carbon cycle feedbacks);
- maximised the exploitation of the results by linking the outputs of the ensemble prediction system to a range of applications, including agriculture, health, energy, water resources and insurance.

This report summarises the research methods developed in the project as well as the results arising from their application.



ENSEMBLES was funded by the European Commission under the 6th Framework Programme Priority: Global Change and Ecosystems



Met Office
Hadley Centre for Climate Prediction and Research
FitzRoy Road, Exeter EX1 3PB, UK
www.ensembles-eu.org